DOT/FAA/PM-86/7,II

Program Engineering
and Maintenance Service
Washington, D.C. 20591

PM
86
7,II

COPY 1

Investigations for Improving Operational Reliability and Maintainability of Instrument Landing System Components

Volume II, Figures and Illustrations

Richard H. McFarland
Walter D. Phipps
Larry D. Brady
Jeff Dennis
Joe D. Longworth

AUG 21 1986

Avionics Engineering Center
Department of Electrical and Computer Engineering
Ohio University
Athens, Ohio 45701

February 1986

This Document is available to the public through the National Technical Information Service, Springfield, Virginia 22161.

U.S. Department of Transportation
Federal Aviation Administration

NOTICE

This document is disseminated under the sponsorship of the Department of Transportation in the interest of information exchange. The United States Government assumes no liability for the contents or use thereof.

Technical Report Documentation Page

1. Report No.	2. Government Accession No.	3. Recipient's Catalog No.
DOT/FAA/PM-86/7, II		

4. Title and Subtitle	5. Report Date
INVESTIGATIONS FOR IMPROVING OPERATIONAL RELIABILITY AND MAINTAINABILITY OF ILS COMPONENTS VOLUME II, FIGURES AND ILLUSTRATIONS	February 1986
	6. Performing Organization Code
7. Author(s) R. H. McFarland, W. D. Phipps, L. D. Brady, Jeff Dennis, and J. D. Longworth	8. Performing Organization Report No. OU/AEC/EER 79-1
9. Performing Organization Name and Address Avionics Engineering Center Department of Electrical and Computer Engineering Ohio University Athen, Ohio 45701	10. Work Unit No. (TRAIS)
	11. Contract or Grant No. DTFA01-83-C-20025
12. Sponsoring Agency Name and Address U. S. Department of Transportation Federal Aviation Administration Program Engineering and Maintenance Service Washington, D. C. 20591	13. Type of Report and Period Covered Final Report Feb. 1983 - Feb. 1986
	14. Sponsoring Agency Code

15. Supplementary Notes

16. Abstract

Evaluations and performance analysis are presented for Dallas-Fort Worth, TX; Wheeling, WV.; Bristol, TN,; Parkersburg, WV.; Pontiac, MI.; and DeKalb-Peachtree, GA. An investigation of anomalous performance of the glide slope at Lambert-St. Louis is reported. An analysis of Instrument Landing System (ILS) Reference Datum Heights (RDH) is reported, as well as the results of an investigation of glide slope critical areas. A study into the feasibility of developing ground-based checking techniques for validating the Sideband Reference (SBR) glide slope is presented, as well as an assessment of the current standards and tolerances used to qualify glide slope structures. In addition, a proposed methodology for mathematical model validation is discussed.

17. Key Words	18. Distribution Statement
ILS, Critical Areas, Glide Slope, Reference Datum Height, Anomalies, Mathematical Modeling, Ground Monitoring	This document is available to the U. S. public through the National Technical Information Service, Springfield, Virginia 22161

19. Security Classif. (of this report)	20. Security Classif. (of this page)	21. No. of Pages	22. Price
Unclassified	Unclassified	344	

Form DOT F 1700.7 (8-72) Reproduction of completed page authorized

English/Metric Conversion Factors

Length

From \ To	Cm	m	Km	in	ft	s mi	nmi
Cm	1	0.01	1×10^{-5}	0.3937	0.0328	6.21×10^{-6}	5.39×10^{-6}
m	100	1	0.001	39.37	3.281	0.0006	0.0005
Km	100,000	1000	1	39370	3281	0.6214	0.5395
in	2.540	0.0254	2.54×10^{-5}	1	0.0833	1.58×10^{-5}	1.37×10^{-5}
ft	30.48	0.3048	3.05×10^{-4}	12	1	1.89×10^{-4}	1.64×10^{-4}
S mi	160,900	1609	1.609	63360	5280	1	0.8688
nmi	185,200	1852	1.852	72930	6076	1.151	1

Area

From \ To	Cm^2	m^2	Km^2	in^2	ft^2	S mi^2	nmi^2
Cm^2	1	0.0001	1×10^{-10}	0.1550	0.0011	3.86×10^{-11}	5.11×10^{-11}
m^2	10,000	1	1×10^{-6}	1550	10.76	3.86×10^{-7}	5.11×10^{-7}
Km^2	1×10^{10}	1×10^{6}	1	1.55×10^{9}	1.08×10^{7}	0.3861	0.2914
in^2	6.452	0.0006	6.45×10^{-10}	1	0.0069	2.49×10^{-10}	1.88×10^{-10}
ft^2	929.0	0.0929	9.29×10^{-8}	144	1	3.59×10^{-8}	2.71×10^{-8}
S mi^2	2.59×10^{10}	2.59×10^{6}	2.590	4.01×10^{9}	2.79×10^{7}	1	0.7548
nmi^2	3.43×10^{10}	3.43×10^{6}	3.432	5.31×10^{9}	3.70×10^{7}	1.325	1

Volume

From \ To	Cm^3	Liter	m^3	in^3	ft^3	yd^3	fl oz	fl pt	fl qt	gal
Cm^3	1	0.001	1×10^{-6}	0.0610	3.53×10^{-5}	1.31×10^{-6}	0.0338	0.0021	0.0010	0.0002
liter	1000	1	0.001	61.02	0.0353	0.0013	33.81	2.113	1.057	0.2642
m^2	1×10^{6}	1000	1	61,000	35.31	1.308	33,800	2113	1057	264.2
in^3	16.39	0.0163	1.64×10^{-5}	1	0.0006	2.14×10^{-5}	0.5541	0.0346	2113	0.0043
ft^3	28,300	28.32	0.0283	1728	1	0.0370	957.5	59.84	0.0173	7.481
yd^3	765,000	764.5	0.7646	46700	27	1	25900	1616	807.9	202.0
fl oz	29.57	0.2957	2.96×10^{-5}	1.805	0.0010	3.87×10^{-5}	1	0.0625	0.0312	0.0078
fl pt	473.2	0.4732	0.0005	28.88	0.0167	0.0006	16	1	0.5000	0.1250
fl qt	946.3	0.9463	0.0009	57.75	0.0334	0.0012	32	2	1	0.2500
gal	3785	3.785	0.0038	231.0	0.1337	0.0050	128	8	4	1

Mass

From \ To	g	Kg	oz	lb	ton
g	1	0.001	0.0353	0.0022	1.10×10^{-6}
Kg	1000	1	35.27	2.205	0.0011
oz	28.35	0.0283	1	0.0625	3.12×10^{-5}
lb	453.6	0.4536	16	1	0.0005
ton	907,000	907.2	32,000	2000	1

Temperature

$$^{\circ}C = 5/9\ (^{\circ}F - 32)$$

$$^{\circ}F = 9/5\ (^{\circ}C) + 32$$

LIST OF FIGURES

Figure		Page No.
2-1	Plot of the "as found" St. Louis 30R CAT II glide slope structure. Digitized and plotted from computer data.	1
2-2	Plot of measured structure for the St. Louis 30R CAT II glide slope left of centerline approach. Digitized and plotted from computer data.	2
2-3	Plot of structure measurement for the St. Louis 30R CAT I glide slope. Digitized and plotted from computer data.	3
2-4	Comparison of the measured and modeled St. Louis 30R CAT II glide slope structure with the Mark 1E monitor tower in place.	4
2-5	Comparison of the measured and modeled Mark 1E glide slope structure with the Mark 1E monitor tower in place.	5
2-6	Plot of the measured glide slope structure for the St. Louis 30R CAT II facility with the Mark 1E monitor tower removed. Digitized and plotted from computer data.	6
2-7	View of the null reference glide slope site serving runway 18R, DFW, January 4, 1984.	7
2-8	Ground-based radio telemetering theodolite used by Ohio University to provide the reference for the flight measurements on the 18R glide slope at DFW.	7
2-9	Mini-Lab Mark IIIa used by Ohio University in a Beechcraft Model A-36 to collect flight data.	8
2-10	Level run recording showing the vertical structure of the glide slope facility at runway 18R, Dallas-Fort Worth.	9
2-11	Low approach recording showing path structure of glide slope facility at runway 18R, Dallas-Fort Worth.	10
2-12	Level run recording showing vertical structure of glide slope facility at Wheeling, WV.	11
2-13	Low approach recording showing path structure of glide slope facility at Wheeling, WV.	12
2-14	View of the tree line running parallel to runway at Wheeling, WV.	13

LIST OF FIGURES (continued)

Figure		Page No.
2-15	View of the glide slope facility at Wheeling, WV.	13
2-16	Low approach recording made in line with the row of trees alongside the runway at Wheeling, WV.	14
2-17	Low approach recording for runway 18 at Greenville, SC.	15
2-18	Low approach recording showing improved glide slope path structure for runway 18 at Greenville, SC.	16
2-19	Differential amplifier trace representing glide slope path for the "as-found" conditions at Bristol, TN.	17
2-20	Differential amplifier trace representing improved glide slope path structure at Bristol, TN.	18
2-21	Low approach recording showing final glide slope path structure at Bristol, TN.	19
2-22	Low approach recording showing the "as-found" glide slope path structure at DeKalb-Peachtree.	20
2-23	Low approach recording showing the improved glide slope path structure at DeKalb-Peachtree.	21
2-24	Far-field monitoring site near the Pontiac middle marker.	22
2-25	Receiving and recording systems used for data collection.	23
2-26	2 1/2 ton truck used as equipment shelter for data collection at the far-field monitoring site.	23
2-27	Polar plot of relative field intensity level for half-wave dipole radiating elements.	24
2-28	Polar plot of relative field intensity level for FA-8976 radiating elements.	25
2-29	Polar plot of relative field intensity level for GRN-27 radiating elements.	26
2-30	Overall dimensions of scattering plates used to simulate specific aircraft.	27
2-31	Grid locations of scatterer aircraft for which an approach is calculated.	28

LIST OF FIGURES (continued)

Figure		Page No.
2-32	Typical CDI plot.	29
2-33	Contour map of predicted peak CDI perturbations in ILS Zone 2 for a C-440.	30
2-34	Critical area map for CAT II/III tolerances relating to R-500 aircraft. R-500 fuselage is perpendicular to runway centerline with tail away from the runway. Null reference glide slope, directional antennas.	31
2-35	Contours of peak CDI values produced in ILS Zone 2 for an R-500. R-500 fuselage is perpendicular to runway centerline, with tail away from the runway. Null reference glide slope, directional antennas.	32
2-36	Contours of peak CDI values produced between ILS Point B and ILS Point C for an R-500. R-500 fuselage is perpendicular to runway centerline, with tail away from runway. Null reference glide slope, directional antennas.	33
2-37	Contours of peak CDI values produced between ILS Point C and threshold for an R-500. R-500 fuselage is perpendicular to runway centerline, with tail away from runway. Null reference glide slope, directional antennas.	34
2-38	Contours of peak CDI values produced between ILS Point C and threshold for an R-500. R-500 fuselage is parallel to runway centerline, with tail towards the mast. Null reference glide slope, directional antennas.	35
2-39	Critical area map for CAT I tolerances relating to C-440 aircraft. C-440 fuselage is perpendicular to runway centerline with tail away from the runway. Null reference glide slope, directional antennas.	36
2-40	Critical area map for CAT II/III tolerances relating to C-440 aircraft. C-440 fuselage is perpendicular to runway centerline with tail away from the runway. Null reference glide slope, directional antennas.	37
2-41	Contours of peak CDI values produced in ILS Zone 2 for a C-440. C-440 fuselage is perpendicular to runway centerline, with tail away from the runway. Null reference glide slope, directional antennas.	38

LIST OF FIGURES (continued)

Figure		Page No.
2-42	Contours of peak CDI values produced between ILS Point B and ILS Point C for a C-440. C-440 fuselage is perpendicular to runway centerline, with tail away from runway. Null reference glide slope, directional antennas.	39
2-43	Contours of peak CDI values produced between ILS Point C and threshold for a C-440. C-440 fuselage is perpendicular to runway centerline, with tail away from runway. Null reference glide slope, directional antennas.	40
2-44	Critical area map for CAT I tolerances relating to C-440 aircraft. C-440 fuselage is parallel to runway centerline with tail towards the mast. Null reference glide slope, directional antennas.	41
2-45	Critical area map for CAT II/III tolerances relating to C-440 aircraft. C-440 fuselage is parallel to runway centerline with tail towards the mast. Null reference glide slope, directional antennas.	42
2-46	Contours of peak CDI values produced in ILS Zone 2 for a C-440. C-440 fuselage is parallel to runway centerline, with tail towards the mast. Null reference glide slope, directional antennas.	43
2-47	Contours of peak CDI values produced between ILS Point B and ILS Point C for a C-440. C-440 fuselage is parallel to runway centerline, with tail towards the mast. Null reference glide slope, directional antennas.	44
2-48	Contours of peak CDI values produced between ILS Point C and threshold for a C-440. C-440 fuselage is parallel to runway centerline, with tail towards the mast. Null reference glide slope, directional antennas.	45
2-49	Critical area map for CAT I tolerances relating to DC-9 aircraft. DC-9 fuselage is perpendicular to runway centerline with tail away from the runway. Null reference glide slope, directional antennas.	46
2-50	Critical area map for CAT II/III tolerances relating to DC-9 aircraft. DC-9 fuselage is perpendicular to runway centerline with tail away from the runway. Null reference glide slope, directional antennas.	47

LIST OF FIGURES (continued)

Figure		Page No.
2-51	Contours of peak CDI values produced in ILS Zone 2 for a DC-9. DC-9 fuselage is perpendicular to runway centerline, with tail away from the runway. Null reference glide slope, directional antennas.	48
2-52	Contours of peak CDI values produced between ILS Point B and ILS Point C for a DC-9. DC-9 fuselage is perpendicular to runway centerline, with tail away from runway. Null reference glide slope, directional antennas.	49
2-53	Contours of peak CDI values produced between ILS Point C and threshold for a DC-9. DC-9 fuselage is perpendicular to runway centerline, with tail away from runway. Null reference glide slope, directional antennas.	50
2-54	Critical area map for CAT I tolerances relating to DC-9 aircraft. DC-9 fuselage is parallel to runway centerline with tail towards the mast. Null reference glide slope, directional antennas.	51
2-55	Critical area map for CAT II/III tolerances relating to DC-9 aircraft. DC-9 fuselage is parallel to runway centerline with tail towards the mast. Null reference glide slope, directional antennas.	52
2-56	Contours of peak CDI values produced in ILS Zone 2 for a DC-9. DC-9 fuselage is parallel to runway centerline, with tail towards the mast. Null reference glide slope, directional antennas.	53
2-57	Contours of peak CDI values produced between ILS Point B and ILS Point C for a DC-9. DC-9 fuselage is parallel to runway centerline, with tail towards the mast. Null reference glide slope, directional antennas.	54
2-58	Contours of peak CDI values produced between ILS Point C and threshold for a DC-9. DC-9 fuselage is parallel to runway centerline, with tail towards the mast. Null reference glide slope, directional antennas.	55
2-59	Critical area map for CAT I tolerances relating to B-727 aircraft. B-727 fuselage is perpendicular to runway centerline with tail away from the runway. Null reference glide slope, directional antennas.	56

LIST OF FIGURES (continued)

Figure		Page No.
2-60	Critical area map for CAT II/III tolerances relating to B-727 aircraft. B-727 fuselage is perpendicular to runway centerline with tail away from the runway. Null reference glide slope, directional antennas.	57
2-61	Contours of peak CDI values produced in ILS Zone 2 for a B-727. B-727 fuselage is perpendicular to runway centerline, with tail away from the runway. Null reference glide slope, directional antennas.	58
2-62	Contours of peak CDI values produced between ILS Point B and ILS Point C for a B-727. B-727 fuselage is perpendicular to runway centerline, with tail away from runway. Null reference glide slope, directional antennas.	59
2-63	Contours of peak CDI values produced between ILS Point C and threshold for a B-727. B-727 fuselage is perpendicular to runway centerline, with tail away from runway. Null reference glide slope, directional antennas.	60
2-64	Critical area map for CAT I tolerances relating to B-727 aircraft. B-727 fuselage is parallel to runway centerline with tail towards the mast. Null reference glide slope, directional antennas.	61
2-65	Critical area map for CAT II/III tolerances relating to B-727 aircraft. B-727 fuselage is parallel to runway centerline with tail towards the mast. Null reference glide slope, directional antennas.	62
2-66	Contours of peak CDI values produced in ILS Zone 2 for a B-727. B-727 fuselage is parallel to runway centerline, with tail towards the mast. Null reference glide slope, directional antennas.	63
2-67	Contours of peak CDI values produced between ILS Point B and ILS Point C for a B-727. B-727 fuselage is parallel to runway centerline, with tail towards the mast. Null reference glide slope, directional antennas.	64
2-68	Contours of peak CDI values produced between ILS Point C and threshold for a B-727. B-727 fuselage is parallel to runway centerline, with tail towards the mast. Null reference glide slope, directional antennas.	65

LIST OF FIGURES (continued)

Figure		Page No.
2-69	Critical area map for CAT I tolerances relating to B-747 aircraft. B-747 fuselage is perpendicular to runway centerline with tail away from the runway. Null reference glide slope, directional antennas.	66
2-70	Critical area map for CAT II/III tolerances relating to B-747 aircraft. B-747 fuselage is perpendicular to runway centerline with tail away from the runway. Null reference glide slope, directional antennas.	67
2-71	Contours of peak CDI values produced in ILS Zone 2 for a B-747. B-747 fuselage is perpendicular to runway centerline, with tail away from the runway. Null reference glide slope, directional antennas.	68
2-72	Contours of peak CDI values produced between ILS Point B and ILS Point C for a B-747. B-747 fuselage is perpendicular to runway centerline, with tail away from runway. Null reference glide slope, directional antennas.	69
2-73	Contours of peak CDI values produced between ILS Point C and threshold for a B-747. B-747 fuselage is perpendicular to runway centerline, with tail away from runway. Null reference glide slope, directional antennas.	70
2-74	Critical area map for CAT I tolerances relating to B-747 aircraft. B-747 fuselage is parallel to runway centerline with tail towards the mast. Null reference glide slope, directional antennas.	71
2-75	Critical area map for CAT II/III tolerances relating to B-747 aircraft. B-747 fuselage is parallel to runway centerline with tail towards the mast. Null reference glide slope, directional antennas.	72
2-76	Contours of peak CDI values produced in ILS Zone 2 for a B-747. B-747 fuselage is parallel to runway centerline, with tail towards the mast. Null reference glide slope, directional antennas.	73
2-77	Contours of peak CDI values produced between ILS Point B and ILS Point C for a B-747. B-747 fuselage is parallel to runway centerline, with tail towards the mast. Null reference glide slope, directional antennas.	74

LIST OF FIGURES (continued)

Figure		Page No.
2-78	Contours of peak CDI values produced between ILS Point C and threshold for a B-747. B-747 fuselage is parallel to runway centerline, with tail towards the mast. Null reference glide slope, directional antennas.	75
2-79	Contours of peak CDI values produced in ILS Zone 2 for an R-500. R-500 fuselage is perpendicular to runway centerline, with tail away from the runway. Sideband reference glide slope, directional antennas.	76
2-80	Contours of peak CDI values produced between ILS Point B and ILS Point C for an R-500. R-500 fuselage is perpendicular to runway centerline, with tail away from runway. Sideband reference glide slope, directional antennas.	77
2-81	Contours of peak CDI values produced between ILS Point C and threshold for an R-500. R-500 fuselage is perpendicular to runway centerline, with tail away from runway. Sideband reference glide slope, directional antennas.	78
2-82	Contours of peak CDI values produced between ILS Point B and ILS Point C for an R-500. R-500 fuselage is parallel to runway centerline, with tail towards the mast. Sideband reference glide slope, directional antennas.	79
2-83	Contours of peak CDI values produced between ILS Point C and threshold for an R-500. R-500 fuselage is parallel to runway centerline, with tail towards the mast. Sideband reference glide slope, directional antennas.	80
2-84	Critical area map for CAT I tolerances relating to C-440 aircraft. C-440 fuselage is perpendicular to runway centerline with tail away from the runway. Sideband reference glide slope, directional antennas.	81
2-85	Critical area map for CAT II/III tolerances relating to C-440 aircraft. C-440 fuselage is perpendicular to runway centerline with tail away from the runway. Sideband reference glide slope, directional antennas.	82
2-86	Contours of peak CDI values produced in ILS Zone 2 for a C-440. C-440 fuselage is perpendicular to runway centerline, with tail away from the runway. Sideband reference glide slope, directional antennas.	83

Figure		Page No.
2-87	Contours of peak CDI values produced between ILS Point B and ILS Point C for a C-440. C-440 fuselage is perpendicular to runway centerline, with tail away from runway. Sideband reference glide slope, directional antennas.	84
2-88	Contours of peak CDI values produced between ILS Point C and threshold for a C-440. C-440 fuselage is perpendicular to runway centerline, with tail away from runway. Sideband reference glide slope, directional antennas.	85
2-89	Critical area map for CAT I tolerances relating to C-440 aircraft. C-440 fuselage is parallel to runway centerline with tail towards the mast. Sideband reference glide slope, directional antennas.	86
2-90	Critical area map for CAT II/III tolerances relating to C-440 aircraft. C-440 fuselage is parallel to runway centerline with tail towards the mast. Sideband reference glide slope, directional antennas.	87
2-91	Contours of peak CDI values produced in ILS Zone 2 for a C-440. C-440 fuselage is parallel to runway centerline, with tail towards the mast. Sideband reference glide slope, directional antennas.	88
2-92	Contours of peak CDI values produced between ILS Point B and ILS Point C for a C-440. C-440 fuselage is parallel to runway centerline, with tail towards the mast. Sideband reference glide slope, directional antennas.	89
2-93	Contours of peak CDI values produced between ILS Point C and threshold for a C-440. C-440 fuselage is parallel to runway centerline, with tail towards the mast. Sideband reference glide slope, directional antennas.	90
2-94	Critical area map for CAT II/III tolerances relating to DC-9 aircraft. DC-9 fuselage is perpendicular to runway centerline with tail away from the runway. Sideband reference glide slope, directional antennas.	91
2-95	Contours of peak CDI values produced in ILS Zone 2 for a DC-9. DC-9 fuselage is perpendicular to runway centerline, with tail away from the runway. Sideband reference glide slope, directional antennas.	92

LIST OF FIGURES (continued)

Figure		Page No.
2-96	Contours of peak CDI values produced between ILS Point B and ILS Point C for a DC-9. DC-9 fuselage is perpendicular to runway centerline, with tail away from runway. Sideband reference glide slope, directional antennas.	93
2-97	Contours of peak CDI values produced between ILS Point C and threshold for a DC-9. DC-9 fuselage is perpendicular to runway centerline, with tail away from runway. Sideband reference glide slope, directional antennas.	94
2-98	Critical area map for CAT I tolerances relating to DC-9 aircraft. DC-9 fuselage is parallel to runway centerline with tail towards the mast. Sideband reference glide slope, directional antennas.	95
2-99	Critical area map for CAT II/III tolerances relating to DC-9 aircraft. DC-9 fuselage is parallel to runway centerline with tail towards the mast. Sideband reference glide slope, directional antennas.	96
2-100	Contours of peak CDI values produced in ILS Zone 2 for a DC-9. DC-9 fuselage is parallel to runway centerline, with tail towards the mast. Sideband reference glide slope, directional antennas.	97
2-101	Contours of peak CDI values produced between ILS Point B and ILS Point C for a DC-9. DC-9 fuselage is parallel to runway centerline, with tail towards the mast. Sideband reference glide slope, directional antennas.	98
2-102	Contours of peak CDI values produced between ILS Point C and threshold for a DC-9. DC-9 fuselage is parallel to runway centerline, with tail towards the mast. Sideband reference glide slope, directional antennas.	99
2-103	Critical area map for CAT II/III tolerances relating to B-727 aircraft. B-727 fuselage is perpendicular to runway centerline with tail away from the runway. Sideband reference glide slope, directional antennas.	100
2-104	Contours of peak CDI values produced in ILS Zone 2 for a B-727. B-727 fuselage is perpendicular to runway centerline, with tail away from the runway. Sideband reference glide slope, directional antennas.	101

LIST OF FIGURES (continued)

Figure		Page No.
2-105	Contours of peak CDI values produced between ILS Point B and ILS Point C for a B-727. B-727 fuselage is perpendicular to runway centerline, with tail away from runway. Sideband reference glide slope, directional antennas.	102
2-106	Contours of peak CDI values produced between ILS Point C and threshold for a B-727. B-727 fuselage is perpendicular to runway centerline, with tail away from runway. Sideband reference glide slope, directional antennas.	103
2-107	Critical area map for CAT I tolerances relating to B-727 aircraft. B-727 fuselage is parallel to runway centerline with tail towards the mast. Sideband reference glide slope, directional antennas.	104
2-108	Critical area map for CAT II/III tolerances relating to B-727 aircraft. B-727 fuselage is parallel to run-centerline with tail towards the mast. Sideband reference glide slope, directional antennas.	105
2-109	Contours of peak CDI values produced in ILS Zone 2 for a B-727. B-727 fuselage is parallel to runway centerline, with tail towards the mast. Sideband reference glide slope, directional antennas.	106
2-110	Contours of peak CDI values produced between ILS Point B and ILS Point C for a B-727. B-727 fuselage is parallel to runway centerline, with tail towards the mast. Sideband reference glide slope, directional antennas.	107
2-111	Contours of peak CDI values produced between ILS Point C and threshold for a B-727. B-727 fuselage is parallel to runway centerline, with tail towards the mast. Sideband reference glide slope, directional antennas.	108
2-112	Critical area map for CAT I tolerances relating to B-747 aircraft. B-747 fuselage is perpendicular to runway centerline with tail away from the runway. Sideband reference glide slope, directional antennas.	109
2-113	Critical area map for CAT II/III tolerances relating to B-747 aircraft. B-747 fuselage is perpendicular to runway centerline with tail away from the runway. Sideband reference glide slope, directional antennas.	110

LIST OF FIGURES (continued)

Figure		Page No.
2-114	Contours of peak CDI values produced in ILS Zone 2 for a B-747. B-747 fuselage is perpendicular to runway centerline, with tail away from the runway. Sideband reference glide slope, directional antennas.	111
2-115	Contours of peak CDI values produced between ILS Point B and ILS Point C for a B-747. B-747 fuselage is perpendicular to runway centerline, with tail away from runway. Sideband reference glide slope, directional antennas.	112
2-116	Contours of peak CDI values produced between ILS Point C and threshold for a B-747. B-747 fuselage is perpendicular to runway centerline, with tail away from runway. Sideband reference glide slope, directional antennas.	113
2-117	Critical area map for CAT I tolerances relating to B-747 aircraft. B-747 fuselage is parallel to runway centerline with tail towards the mast. Sideband reference glide slope, directional antennas.	114
2-118	Critical area map for CAT II/III tolerances relating to B-747 aircraft. B-747 fuselage is parallel to runway centerline with tail towards the mast. Sideband reference glide slope, directional antennas.	115
2-119	Contours of peak CDI values produced in ILS Zone 2 for a B-747. B-747 fuselage is parallel to runway centerline, with tail towards the mast. Sideband reference glide slope, directional antennas.	116
2-120	Contours of peak CDI values produced between ILS Point B and ILS Point C for a B-747. B-747 fuselage is parallel to runway centerline, with tail towards the mast. Sideband reference glide slope, directional antennas.	117
2-121	Contours of peak CDI values produced between ILS Point C and threshold for a B-747. B-747 fuselage is parallel to runway centerline, with tail towards the mast. Sideband reference glide slope, directional antennas.	118
2-122	Contours of peak CDI values produced in ILS Zone 2 for an R-500. R-500 fuselage is perpendicular to runway centerline, with tail away from the runway. Capture effect glide slope, directional antennas.	119

LIST OF FIGURES (continued)

Figure		Page No.
2-123	Contours of peak CDI values produced between ILS Point B and ILS Point C for an R-500. R-500 fuselage is perpendicular to runway centerline, with tail away from runway. Capture effect glide slope, directional antennas.	120
2-124	Contours of peak CDI values produced between ILS Point C and threshold for an R-500. R-500 fuselage is perpendicular to runway centerline, with tail away from runway. Capture effect glide slope, directional antennas.	121
2-125	Contours of peak CDI values produced between ILS Point C and threshold for an R-500. R-500 fuselage is parallel to runway centerline, with tail towards the mast. Capture effect glide slope, directional antennas.	122
2-126	Critical area map for CAT I tolerances relating to C-440 aircraft. C-440 fuselage is perpendicular to runway centerline with tail away from the runway. Capture effect glide slope, directional antennas.	123
2-127	Critical area map for CAT II/III tolerances relating to C-440 aircraft. C-440 fuselage is perpendicular to runway centerline with tail away from the runway. Capture effect glide slope, directional antennas.	124
2-128	Contours of peak CDI values produced in ILS Zone 2 for a C-440. C-440 fuselage is perpendicular to runway centerline, with tail away from the runway. Capture effect glide slope, directional antennas.	125
2-129	Contours of peak CDI values produced between ILS Point B and ILS Point C for a C-440. C-440 fuselage is perpendicular to runway centerline, with tail away from runway. Capture effect glide slope, directional antennas.	126
2-130	Contours of peak CDI values produced between ILS Point C and threshold for a C-440. C-440 fuselage is perpendicular to runway centerline, with tail away from runway. Capture effect glide slope, directional antennas.	127
2-131	Critical area map for CAT I tolerances relating to C-440 aircraft. C-440 fuselage is parallel to runway	128

Figure		Page No.
	centerline with tail towards the mast. Capture effect glide slope, directional antennas.	
2-132	Critical area map for CAT II/III tolerances relating to C-440 aircraft. C-440 fuselage is parallel to runway centerline with tail towards the mast. Capture effect glide slope, directional antennas.	129
2-133	Contours of peak CDI values produced in ILS Zone 2 for a C-440. C-440 fuselage is parallel to runway centerline, with tail towards the mast. Capture effect glide slope, directional antennas.	130
2-134	Contours of peak CDI values produced between ILS Point B and ILS Point C for a C-440. C-440 fuselage is parallel to runway centerline, with tail towards the mast. Capture effect glide slope, directional antennas.	131
2-135	Contours of peak CDI values produced between ILS Point C and threshold for a C-440. C-440 fuselage is parallel to runway centerline, with tail towards the mast. Capture effect glide slope, directional antennas.	132
2-136	Critical area map for CAT II/III tolerances relating to DC-9 aircraft. DC-9 fuselage is perpendicular to runway centerline with tail away from the runway. Capture effect glide slope, directional antennas.	133
2-137	Contours of peak CDI values produced in ILS Zone 2 for a DC-9. DC-9 fuselage is perpendicular to runway centerline, with tail away from the runway. Capture effect glide slope, directional antennas.	134
2-138	Contours of peak CDI values produced between ILS Point B and ILS Point C for a DC-9. DC-9 fuselage is perpendicular to runway centerline, with tail away from runway. Capture effect glide slope, directional antennas.	135
2-139	Contours of peak CDI values produced between ILS Point C and threshold for a DC-9. DC-9 fuselage is perpendicular to runway centerline, with tail away from runway. Capture effect glide slope, directional antennas.	136

Figure		Page No.
2-140	Critical area map for CAT I tolerances relating to DC-9 aircraft. DC-9 fuselage is parallel to runway centerline with tail towards the mast. Capture effect glide slope, directional antennas.	137
2-141	Critical area map for CAT II/III tolerances relating to DC-9 aircraft. DC-9 fuselage is parallel to runway centerline with tail towards the mast. Capture effect glide slope, directional antennas.	138
2-142	Contours of peak CDI values produced in ILS Zone 2 for a DC-9. DC-9 fuselage is parallel to runway centerline, with tail towards the mast. Capture effect glide slope, directional antennas.	139
2-143	Contours of peak CDI values produced between ILS Point B and ILS Point C for a DC-9. DC-9 fuselage is parallel to runway centerline, with tail towards the mast. Capture effect glide slope, directional antennas.	140
2-144	Contours of peak CDI values produced between ILS Point C and threshold for a DC-9. DC-9 fuselage is parallel to runway centerline, with tail towards the mast. Capture effect glide slope, directional antennas.	141
2-145	Critical area map for CAT II/III tolerances relating to B-727 aircraft. B-727 fuselage is perpendicular to runway centerline with tail away from the runway. Capture effect glide slope, directional antennas.	142
2-146	Contours of peak CDI values produced in ILS Zone 2 for a B-727. B-727 fuselage is perpendicular to runway centerline, with tail away from the runway. Capture effect glide slope, directional antennas.	143
2-147	Contours of peak CDI values produced between ILS Point B and ILS Point C for a B-727. B-727 fuselage is perpendicular to runway centerline, with tail away from runway. Capture effect glide slope, directional antennas.	144
2-148	Contours of peak CDI values produced between ILS Point C and threshold for a B-727. B-727 fuselage is perpendicular to runway centerline, with tail away from runway. Capture effect glide slope, directional antennas.	145

LIST OF FIGURES (continued)

Figure		Page No.
2-149	Critical area map for CAT I tolerances relating to B-727 aircraft. B-727 fuselage is parallel to runway centerline with tail towards the mast. Capture effect glide slope, directional antennas.	146
2-150	Critical area map for CAT II/III tolerances relating to B-727 aircraft. B-727 fuselage is parallel to runway centerline with tail towards the mast. Capture effect glide slope, directional antennas.	147
2-151	Contours of peak CDI values produced in ILS Zone 2 for a B-727. B-727 fuselage is parallel to runway centerline, with tail towards the mast. Capture effect glide slope, directional antennas.	148
2-152	Contours of peak CDI values produced between ILS Point B and ILS Point C for a B-727. B-727 fuselage is parallel to runway centerline, with tail towards the mast. Capture effect glide slope, directional antennas.	149
2-153	Contours of peak CDI values produced between ILS Point C and threshold for a B-727. B-727 fuselage is parallel to runway centerline, with tail towards the mast. Capture effect glide slope, directional antennas.	150
2-154	Critical area map for CAT II/III tolerances relating to B-747 aircraft. B-747 fuselage is perpendicular to runway centerline with tail away from the runway. Capture effect glide slope, directional antennas.	151
2-155	Contours of peak CDI values produced in ILS Zone 2 for a B-747. B-747 fuselage is perpendicular to runway centerline, with tail away from the runway. Capture effect glide slope, directional antennas.	152
2-156	Contours of peak CDI values produced between ILS Point B and ILS Point C for a B-747. B-747 fuselage is perpendicular to runway centerline, with tail away from runway. Capture effect glide slope, directional antennas.	153
2-157	Contours of peak CDI values produced between ILS Point C and threshold for a B-747. B-747 fuselage is perpendicular to runway centerline, with tail away from runway. Capture effect glide slope, directional antennas.	154

LIST OF FIGURES (continued)

Figure		Page No.
2-158	Critical area map for CAT I tolerances relating to B-747 aircraft. B-747 fuselage is parallel to runway centerline with tail towards the mast. Capture effect glide slope, directional antennas.	155
2-159	Critical area map for CAT II/III tolerances relating to B-747 aircraft. B-747 fuselage is parallel to runway centerline with tail towards the mast. Capture effect glide slope, directional antennas.	156
2-160	Contours of peak CDI values produced in ILS Zone 2 for a B-747. B-747 fuselage is parallel to runway centerline, with tail towards the mast. Capture effect glide slope, directional antennas.	157
2-161	Contours of peak CDI values produced between ILS Point B and ILS Point C for a B-747. B-747 fuselage is parallel to runway centerline, with tail towards the mast. Capture effect glide slope, directional antennas.	158
2-162	Contours of peak CDI values produced between ILS Point C and threshold for a B-747. B-747 fuselage is parallel to runway centerline, with tail towards the mast. Capture effect glide slope, directional antennas.	159
2-163	Critical area map for CAT I tolerances relating to B-727 aircraft. B-727 fuselage is parallel to runway centerline with tail towards the mast. Null reference glide slope, dipole antennas.	160
2-164	Critical area map for CAT II/III tolerances relating to B-727 aircraft. B-727 fuselage is parallel to runway centerline with tail towards the mast. Null reference glide slope, dipole antennas.	161
2-165	Contours of peak CDI values produced in ILS Zone 2 for a B-727. B-727 fuselage is parallel to runway centerline, with tail towards the mast. Null reference glide slope, dipole antennas.	162
2-166	Contours of peak CDI values produced between ILS Point B and ILS Point C for a B-727. B-727 fuselage is parallel to runway centerline, with tail towards the mast. Null reference glide slope, dipole antennas.	163

LIST OF FIGURES (continued)

Figure		Page No.
2-167	Contours of peak CDI values produced between ILS Point C and threshold for a B-727. B-727 fuselage is parallel to runway centerline, with tail towards the mast. Null reference glide slope, dipole antennas.	164
2-168	Critical area map for CAT I tolerances relating to B-727 aircraft. B-727 fuselage is parallel to runway centerline with tail towards the mast. Null reference glide slope, 2-lambda antennas.	165
2-169	Critical area map for CAT II/III tolerances relating to B-727 aircraft. B-727 fuselage is parallel to runway centerline with tail towards the mast. Null reference glide slope, 2-lambda antennas.	166
2-170	Contours of peak CDI values produced in ILS Zone 2 for a B-727. B-727 fuselage is parallel to runway centerline, with tail towards the mast. Null reference glide slope, 2-lambda antennas.	167
2-171	Contours of peak CDI values produced between ILS Point B and ILS Point C for a B-727. B-727 fuselage is parallel to runway centerline, with tail towards the mast. Null reference glide slope, 2-lambda antennas.	168
2-172	Contours of peak CDI values produced between ILS Point C and threshold for a B-727. B-727 fuselage is parallel to runway centerline, with tail towards the mast. Null reference glide slope, 2-lambda antennas.	169
2-173	Copy of flight record 4-12A made on a low approach to runway 18R made Ohio University in January, 1984.	170
2-174	Example of how a low RDH is produced by a decrease of the path angle in ILS Zone 2.	171
2-175	Positioning of theodolite.	172
2-176	Test geometry for calculations.	173
2-177	Digitized Flight Recording for a Low Approach to runway 18R. Data taken by Ohio University, January 4, 1984, Run No. 4-12A.	174
2-178	Topographic map of glide slope critical area terrain for DFW runway 18R.	175

LIST OF FIGURES (continued)

Figure		Page No.
2-179	Coordinates of terrain profile system.	176
2-180	Isometric drawing of the three-dimensional terrain profile showing the three depressions in the first Fresnel zone.	177
2-181	Simulated differential amplifier trace for the terrain profile in figure 2-180.	178
2-182	Comparison of actual and simulated differential amplifier recordings. The actual data is taken from Run 4-12A by Ohio University. The simulated trace is for the terrain profile shown in figure 2-180.	179
2-183	CDI trace showing the effect of decreasing depth of depression at Y=900' to 598.85' MSL.	180
2-184	CDI trace showing the effect of decreasing depth of depression at Y=900' to 599.85' MSL.	181
2-185	CDI trace showing the effect of decreasing depth of depression at Y=900' to 600.85' MSL.	182
2-186	CDI trace showing the effect of decreasing depth of depression at Y=900' to 601.85' MSL.	183
2-187	CDI trace showing the effect of decreasing depth of depression at Y=900' to 602.85' MSL.	184
2-188	Sensitivity of RDH to depth of depression at Y=900'.	185
2-189	Sensitivity of ARDH to depth of depression at Y=900'.	186
2-190	CDI trace showing the effect of decreasing depth of depression at Y=1242' to 599.85' MSL.	187
2-191	CDI trace showing the effect of decreasing depth of depression at Y=1242' to 600.85' MSL.	188
2-192	CDI trace showing the effect of decreasing depth of depression at Y=1242' to 601.85' MSL.	189
2-193	CDI trace showing the effect of decreasing depth of depression at Y=1242' to 602.85' MSL.	190
2-194	Sensitivity of RDH to depth of depression at Y=1242'.	191
2-195	Sensitivity of ARDH to depth of depression at Y=1242'.	192

LIST OF FIGURES (continued)

Figure		Page No.
2-196	CDI trace showing the effect of decreasing depth of depression at Y=1600' to 598.85' MSL.	193
2-197	CDI trace showing the effect of decreasing depth of depression at Y=1600' to 599.85' MSL.	194
2-198	CDI trace showing the effect of decreasing depth of depression at Y=1600' to 600.85' MSL.	195
2-199	CDI trace showing the effect of decreasing depth of depression at Y=1600' to 601.85' MSL.	196
2-200	CDI trace showing the effect of decreasing depth of depression at Y=1600' to 602.85' MSL.	197
2-201	Sensitivity of RDH to depth of depression at Y=1600'.	198
2-202	Sensitivity of ARDH to depth of depression at Y=1600'.	199
2-203	Isometric drawing of the modified terrain profile simulating grading of area between antennas and taxiway W-19.	200
2-204	Differential amplifier recording for the terrain profile in figure 27. Antenna heights adjusted for 3 degree path angle.	201
2-205	CDI trace showing the effect of decreasing depth of depression at Y=900' to 598.85' MSL for modified profile.	202
2-206	CDI trace showing the effect of decreasing depth of depression at Y=900' to 599.85' MSL for modified profile.	203
2-207	CDI trace showing the effect of decreasing depth of depression at Y=900' to 600.85' MSL for modified profile.	204
2-208	CDI trace showing the effect of decreasing depth of depression at Y=900' to 601.85' MSL for modified profile.	205
2-209	CDI trace showing the effect of decreasing depth of depression at Y=900' to 602.85' MSL for modified profile.	206
2-210	Sensitivity of RDH to depth of depression at Y=900' for modified profile.	207
2-211	Sensitivity of ARDH to depth of depression at Y=900' for modified profile.	208

LIST OF FIGURES (continued)

Figure		Page No.
2-212	CDI trace showing the effect of decreasing depth of depression at Y=1242' to 599.85' MSL for modified profile.	209
2-213	CDI trace showing the effect of decreasing depth of depression at Y=1242' to 600.85' MSL for modified profile.	210
2-214	CDI trace showing the effect of decreasing depth of depression at Y=1242' to 601.85' MSL for modified profile.	211
2-215	CDI trace showing the effect of decreasing depth of depression at Y=1242' to 602.85' MSL for modified profile.	212
2-216	Sensitivity of RDH to depth of depression at Y=1242' for modified profile.	213
2-217	Sensitivity of ARDH to depth of depression at Y=1242' for modified profile.	214
2-218	CDI trace showing the effect of decreasing depth of depression at Y=1600' to 598.85' MSL for modified profile.	215
2-219	CDI trace showing the effect of decreasing depth of depression at Y=1600' to 599.85' MSL for modified profile.	216
2-220	CDI trace showing the effect of decreasing depth of depression at Y=1600' to 600.85' MSL for modified profile.	217
2-221	CDI trace showing the effect of decreasing depth of depression at Y=1600' to 601.85' MSL for modified profile.	218
2-222	CDI trace showing the effect of decreasing depth of depression at Y=1600' to 602.85' MSL for modified profile.	219
2-223	Sensitivity of RDH to depth of depression at Y=1600' for modified profile.	220
2-224	Sensitivity of ARDH to depth of depression at Y=1600' for modified profile.	221
2-225	CDI trace showing the effects of decreasing the depth of the depression at Y=900' to 599.85' MSL and the depth of the depression at Y=1600' to 602.85' MSL.	222
2-226	Topographic map of proposed glide slope critical area terrain at runway 9R, Chicago O'Hare International Airport.	223

LIST OF FIGURES (continued)

Figure		Page No.
2-227	Two-dimensional terrain profile representing the critical area terrain shown in figure 2-226.	224
2-228	Sample of input data file for mathematical model OUGS.	225
2-229	Simulated differential amplifier recording for the terrain profile shown in figure 2-227.	226
2-230	Simulated differential amplifier recording for the terrain profile shown in figure 2-227, with Category I tolerances applied.	227
2-231	Examples of the shapes of irregular terrain considered.	228
2-232	Example of a sensitivity curve produced by varying location of a hill 10 feet in duration (w) and 10 feet high (h).	229
2-233	Three-dimensional approximation of a terrain depression formed by two-dimensional reflecting plates.	230
2-234	Profiles of the shapes of irregular terrain considered initially for sensitivity analysis.	231
2-235	Simulated differential amplifier recordings for the shapes of irregular terrain shown in figure 2-234 and of the dimensions shown, for a null-reference glide slope.	232
2-236	Example of a terrain profile which is used as an input to the simulation.	233
2-237	Example of an input for the mathematical model OUGS.	234
2-238	Flow chart of the procedure used in the sensitivity analysis.	235
2-239	Comparison of sensitivity curves for triangular- and trapezoidal-shaped profiles of irregular terrain.	236
2-240	Simulated differential amplifier recordings for a triangular-shaped elevation of 10' duration and 10' high, located at 600' to 1000' from the antenna mast.	237
2-241	Simulated differential amplifier recordings for a triangular-shaped elevation of 10' duration and 10' high, located at 1100' to 1500' from the antenna mast.	238

LIST OF FIGURES (continued)

Figure		Page No.
2-242	Simulated differential amplifier recordings for a triangular-shaped elevation of 10' duration and 10' high, located at 1600' to 2000' from the antenna mast.	239
2-243	Simulated differential amplifier recordings for a triangular-shaped elevation of 10' duration and 10' high, located at 2100' to 2500' from the antenna mast.	240
2-244	Simulated differential amplifier recordings for a triangular-shaped elevation of 10' duration and 10' high, located at 2600' to 3000' from the antenna mast.	241
2-245	Simulated differential amplifier recordings for a triangular-shaped elevation of 10' duration and 10' high, located at 3100' to 3500' from the antenna mast.	242
2-246	Simulated differential amplifier recordings for a triangular-shaped elevation of 10' duration and 10' high, located at 3600' to 4000' from the antenna mast.	243
2-247	Simulated differential amplifier recordings for a triangular-shaped elevation of 10' duration and 10' high, located at 4100' to 4500' from the antenna mast.	244
2-248	Simulated differential amplifier recordings for a triangular-shaped elevation of 10' duration and 10' high, located at 4600' to 5000' from the antenna mast.	245
2-249	Comparison of sensitivity curves produced by a trapezoidal-shaped elevation, 10' in duration and 10' high, for distances of the antenna mast along centerline from threshold of 800', 1000', an 1200'.	246
2-250	Comparison of sensitivity curves produced by a trapezoidal-shaped elevation, 10' in duration and 10' high, for path angles of 2.7, 3.0, and 3.3 degrees.	247
2-251	Illustration of the uniform, laterally sloping terrain in the plane containing the glide slope antenna mast.	248
2-252	Comparison of various heights at threshold for an ideal glide slope site, with the antennas located as shown, for a path angle of 3.0 degrees.	249
2-253	Illustration of the effects of uniform, longitudinally upsloping terrain on the reference datum heights.	250

LIST OF FIGURES (continued)

Figure		Page No.
2-254	Sensitivity curves for deviation of RDH and ARDH from the ideal values, for an elevation with a duration of 10' and a height of 2, 4, 6, 8, and 10'.	251
2-255	Sensitivity curves for deviation of RDH and ARDH from the ideal values, for an elevation with a duration of 20' and a height of 2, 4, 6, 8, and 10'.	252
2-256	Sensitivity curves for deviation of RDH and ARDH from the ideal values, for a depression with a duration of 10' and a height of 2, 4, 6, 8, and 10'.	253
2-257	Sensitivity curves for deviation of RDH and ARDH from the ideal values, for a depression with a duration of 20' and a height of 2, 4, 6, 8, and 10'.	254
2-258	Two terrain profiles of a finite region of upsloping terrain considered to examine the effects of terrain following the upslope.	255
2-259	Simulated differential amplifier recordings for terrain profiles shown in figure 2-258, showing the independence of the trace (and reference datum heights) on the terrain following the upslope.	256
2-260	Sensitivity curves for deviation of RDH and ARDH from the ideal values, for a depression with a duration of 100' and a height of 5, 10, 15, and 20'.	257
2-261	Sensitivity curves for deviation of RDH and ARDH from the ideal values, for a depression with a duration of 200' and a height of 5, 10, 15, and 20'.	258
2-262	Sensitivity curves for deviation of RDH and ARDH from the ideal values, for a depression with a duration of 300' and a height of 5, 10, 15, and 20'.	259
2-263	Sensitivity curves for deviation of RDH and ARDH from the ideal values, for a depression with a duration of 400' and a height of 5, 10, 15, and 20'.	260
2-264	Sensitivity curves for deviation of RDH and ARDH from the ideal values, for depressions with durations of 100, 200, 300, 400 and 500', showing how increasing durations of terrain depressions affect the reference datum heights.	261
2-265	Flight recording made on a level run at Wheeling, WV before removal of trees.	262

LIST OF FIGURES (continued)

Figure		Page No.
2-266	Differential amplifier recording made on a low approach at Wheeling, WV before removal of trees, showing marginal CAT I tolerance and an RDH of 76'.	263
2-267	Picture of the tree line after cutting at Wheeling, WV. The sideband reference glide slope is located 250' off centerline and the row of trees is located approximately 300' off centerline.	264
2-268	Differential amplifier recording made on a low approach at Wheeling, WV in line with the long row of trees to the east of the runway centerline.	265
2-269	Differential amplifier recording made on a low approach at Wheeling, WV after removal of the row of trees. The structure is clearly improved (see Figure 36) and the RDH of 52' is within applicable tolerances.	266
2-270	Differential amplifier recording made on a low approach to Runway 18 at the Greenville, SC, Downtown Airport.	267
2-271	Differential amplifier recording made on a low approach after advancing the phase of the upper antenna by 20 degrees.	268
2-272	Types of sites encountered in U.S.	269
2-273	Matrix of mean RMS values.	270
2-274	Flowchart of math model validation procedure (2 sheets).	271
2-275	Frequency response of filter used on measured and calculated data.	273
2-276	Sample terrain profile for Tamiami test site.	274
2-277	Sample of digitized RTT information recorded at TMB.	275
2-278	Measured raw CDI and differential CDI traces from aircraft recorder.	276
2-279	Measured CDI trace after digitization and sampling process.	277
2-280	Model calculation.	278
2-281	Digitized measured raw CDI and model output traces.	279

LIST OF FIGURES (continued)

Figure		Page No.
2-282	Filtered, zero-mean, CDI traces; TMB 10-11.	280
2-283	Filtered, zero-mean, CDI traces; TMB 10-12.	281
2-284	Filtered, zero-mean, CDI traces; TMB 10-13.	282
2-285	TMB terrain profile.	283
2-286	LAW terrain profile.	284
2-287	PAJ terrain profile.	285
2-288	Filtered, zero-mean, CDI traces; LAW 26-03.	286
2-289	Filtered, zero-mean, CDI traces; LAW 26-04.	287
2-290	Filtered, zero-mean, CDI traces; LAW 26-05.	288
2-291	Filtered, zero-mean, CDI traces; PAJ 16-08.	289
2-292	Filtered, zero-mean, CDI traces; PAJ 16-10.	290
2-293	Filtered, zero-mean, CDI traces; PAJ 16-11.	291
2-294	SGH terrain profile.	292
2-295	Filtered, zero-mean, CDI traces; SGH 23-19.	293
2-296	Filtered, zero-mean, CDI traces; SGH 23-20.	294
2-297	RDB terrain profile.	295
2-298	Filtered, zero-mean, CDI traces; RDB 25-04.	296
2-299	Filtered, zero-mean, CDI traces; RDB 25-07.	297
2-300	Measured raw CDI and differential CDI traces from aircraft recorder.	298
2-301	Two-dimensional conducting plate approximation to reflecting terrain.	299
2-302	Sample terrain profile.	300
2-303	Example of model input data.	301
2-304	Sample memo file containing data used in validation procedure.	302

LIST OF FIGURES (continued)

Figure		Page No.
2-305	Flowchart of math model validation procedure (2 sheets).	303
2-306	Measured CDI trace after digitization and sampling process.	305
2-307	Sample of digitized RTT information recorded at TMB.	306
2-308	Sample of model input for validation of glide slope.	307
2-309	Model calculation.	308
2-310	Filtered, zero-mean, CDI traces used for model validation.	309
4-1	Test Path 1 (Case 1), glide slope structure for flight simulation which provided a uniform spatial frequency existing throughout ILS Zones 2 and 3. The magnitude shown was that for which Category II limits would be reached.	310
4-2	Test Path 2 (Case 2), the glide slope structure was constructed to provide a slowly decreasing spatial frequency with a maximum fly-down occurring as the threshold of the runway is approached.	311
4-3	Test Path 3 (Case 3), the glide slope structure was constructed to provide a slowly varying path, one which the pilot could be expected to fly ending in a maximum fly-down condition at the runway threshold.	312
5-1	Coordinate system description.	313
5-2	TMB predicted data, normal SBR, X=50', Z=2' to Z=12'.	314
5-3	TMB predicted data, normal SBR, X=250', Z=2' to Z=12'.	315
5-4	TMB predicted data, normal SBR, X=500', Z=2' to Z=12'.	316
5-5	TMB predicted data, normal SBR, X=0' to X=550', Z=10'.	317
5-6	TMB predicted data, dephase U/L , X=50', Z=10'.	318
5-7	TMB predicted data, dephase U/L , X=200', Z=10'.	319
5-8	TMB predicted data, dephase U/L , X=500', Z=10'.	320
5-9	TMB predicted data, dephase U/L , X=500', Z=8'.	321
5-10	TMB measured data, dephase U/L , X=500' Z=8'.	322

LIST OF FIGURES (continued)

Figure		Page No.
5-11	TMB predicted data, dephase CSB/SBO, X=500', Z=8'.	323
5-12	TMB measured data, dephase CSB/SBO, X=500', Z=8'.	324
5-13	TMB measured data, U/L dephase, probe locations.	325
5-14	TMB measured data, CSB/SBO dephase, probe locations.	326
5-15	MGW predicted data, normal SBR, X=200' to X=350',Z=8'.	327
5-16	MGW measured data, normal SBR, X=200' to X=350', Z=8'.	328
5-17	MGW predicted data, dephase U/L, 0 μA locations.	329
5-18	MGW measured data, dephase U/L, probe locations.	330
5-19	MGW predicted data, dephase CSB/SBO, 0 μA locations.	331
5-20	MGW measured data, dephase CSB/SBO, probe locations.	332
5-21	CKB predicted data, normal SBR, X=250' to X=400',Z=8'.	333
5-22	CKB measured data, normal SBR, X=250' to X=400', Z=8'.	334
5-23	CKB predicted data, dephase U/L, 0 μA locations.	335
5-24	CKB measured data, dephase U/L, probe locations.	336
5-25	CKB predicted data, dephase CSB/SBO, 0 μA locations.	337
5-26	BLF predicted data, normal SBR, X=250' to X=400',Z=8'.	338
5-27	BLF measured data, normal SBR, X=250' to X=400', Z=8'.	339
5-28	BLF predicted data, dephase U/L, 0 μA locations.	340
5-29	BLF measured data, dephase U/L, probe locations.	341
5-30	BLF predicted data, dephase CSB/SBO, 0 μA locations.	342
5-31	BLF measured data, dephase CSB/SBO, probe locations.	343
5-32	Photograph of wooden mast used in measurements.	344

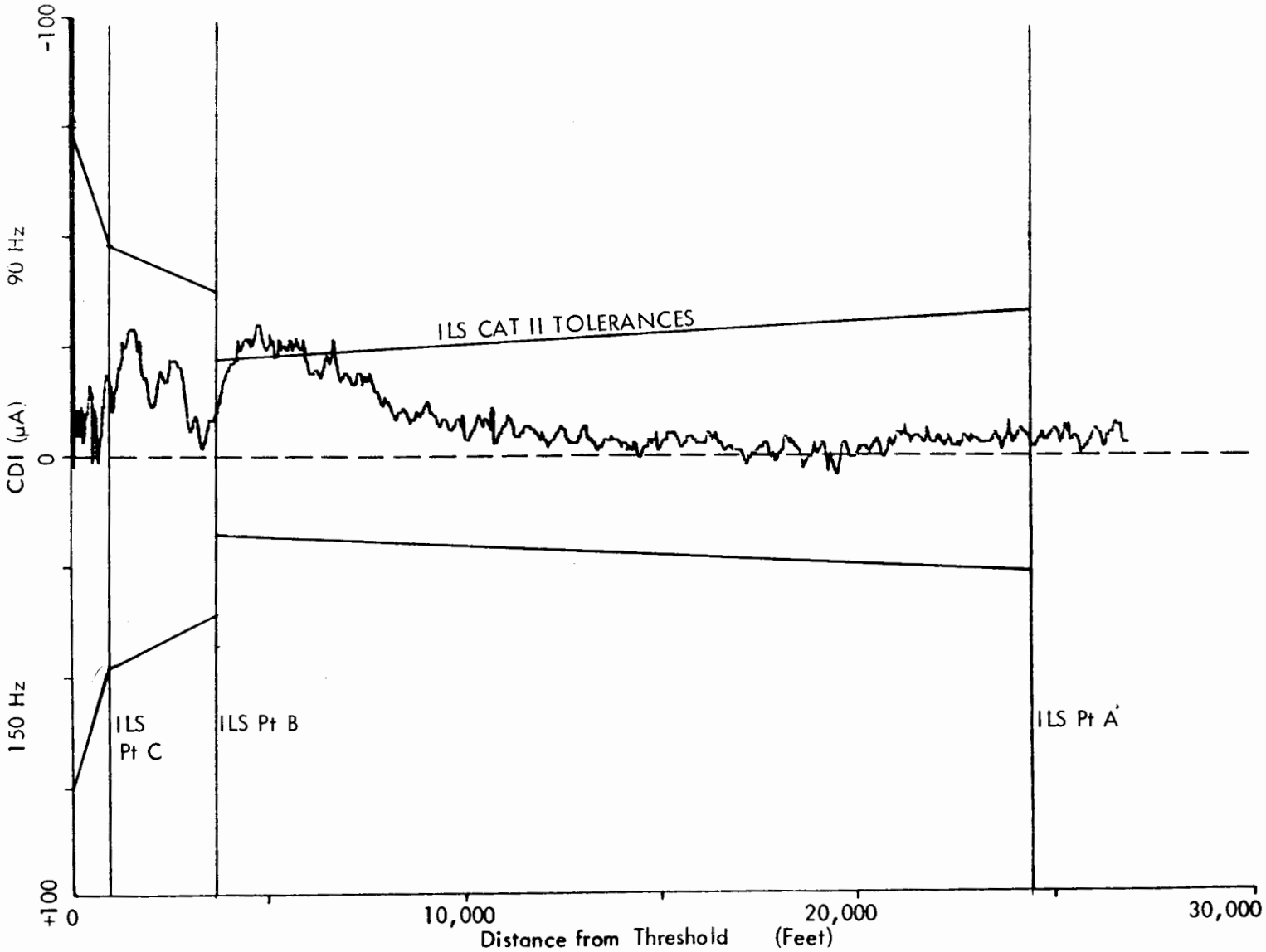

Figure 2-1. Plot of the "as found" St. Louis 30R CAT II glide slope structure. Digitized and plotted from computer data.

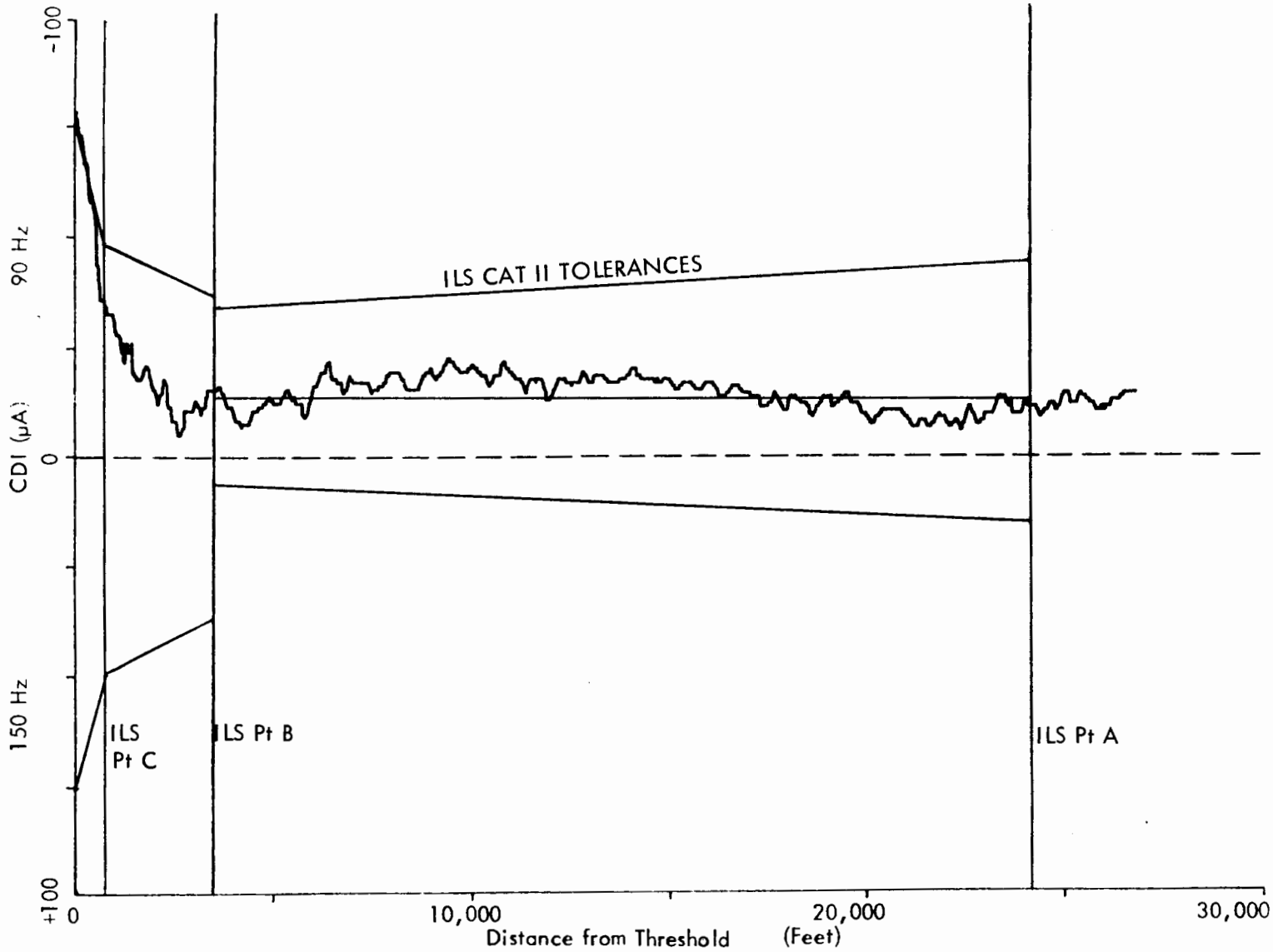

Figure 2-2. Plot of measured structure for the St. Louis 30R CAT II glide slope left of centerline approach. Digitized and plotted from computer data.

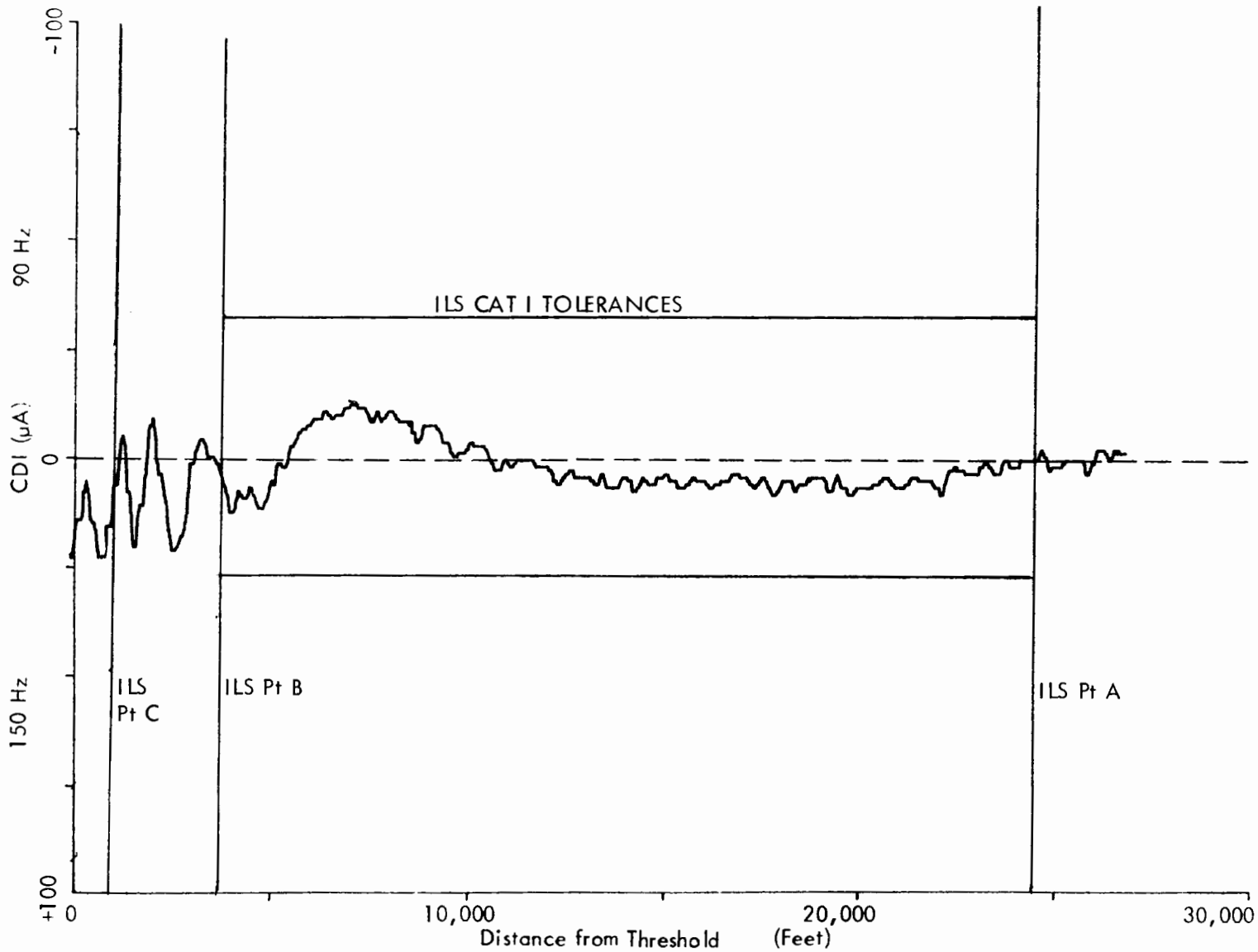

Figure 2-3. Plot of structure measurement for the St. Louis 30R CAT I glide slope. Digitized and plotted from computer data.

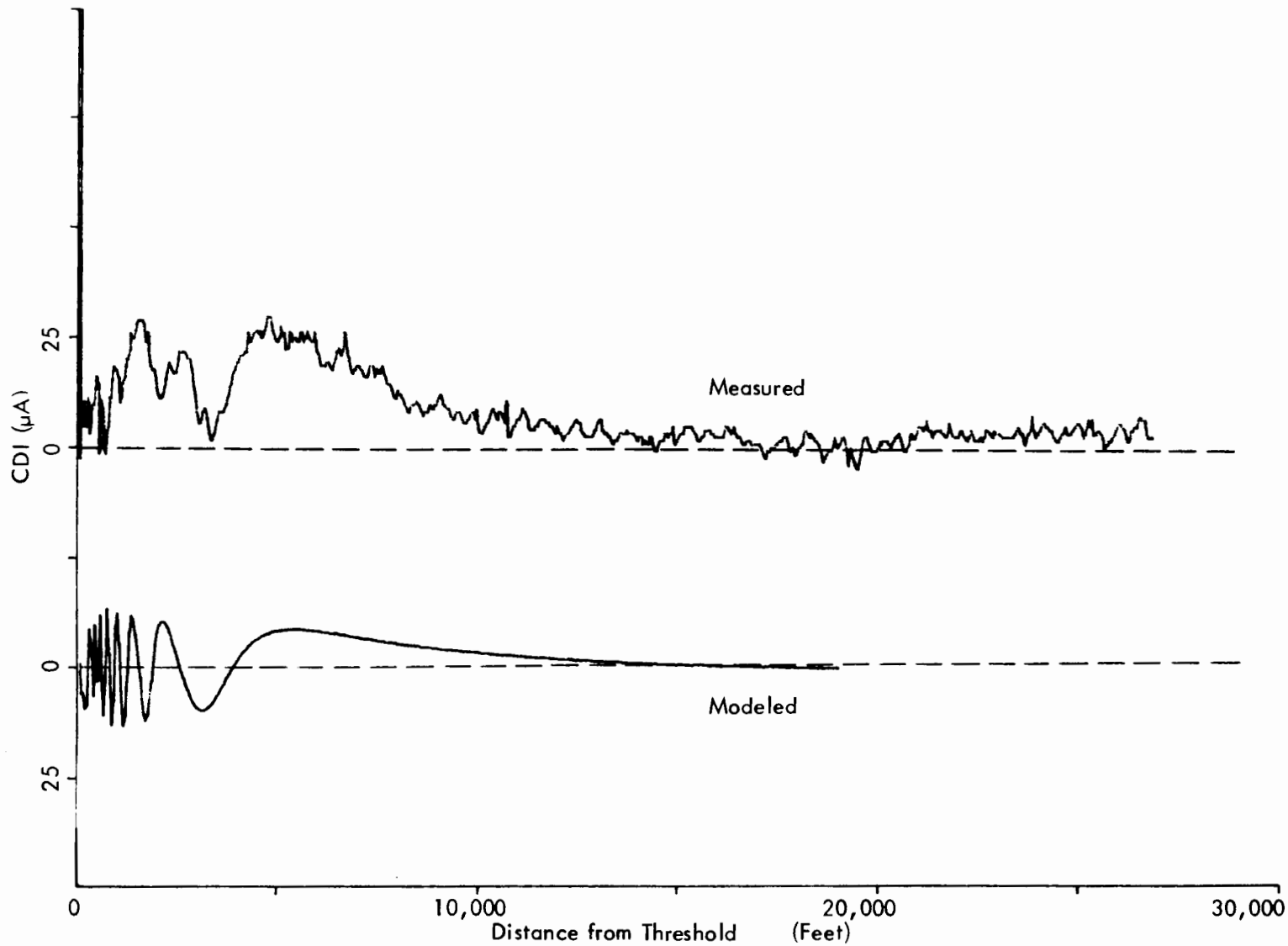

Figure 2-4. Comparison of the measured and modeled St. Louis 30R CAT II glide slope structure with the Mark 1E monitor tower in place.

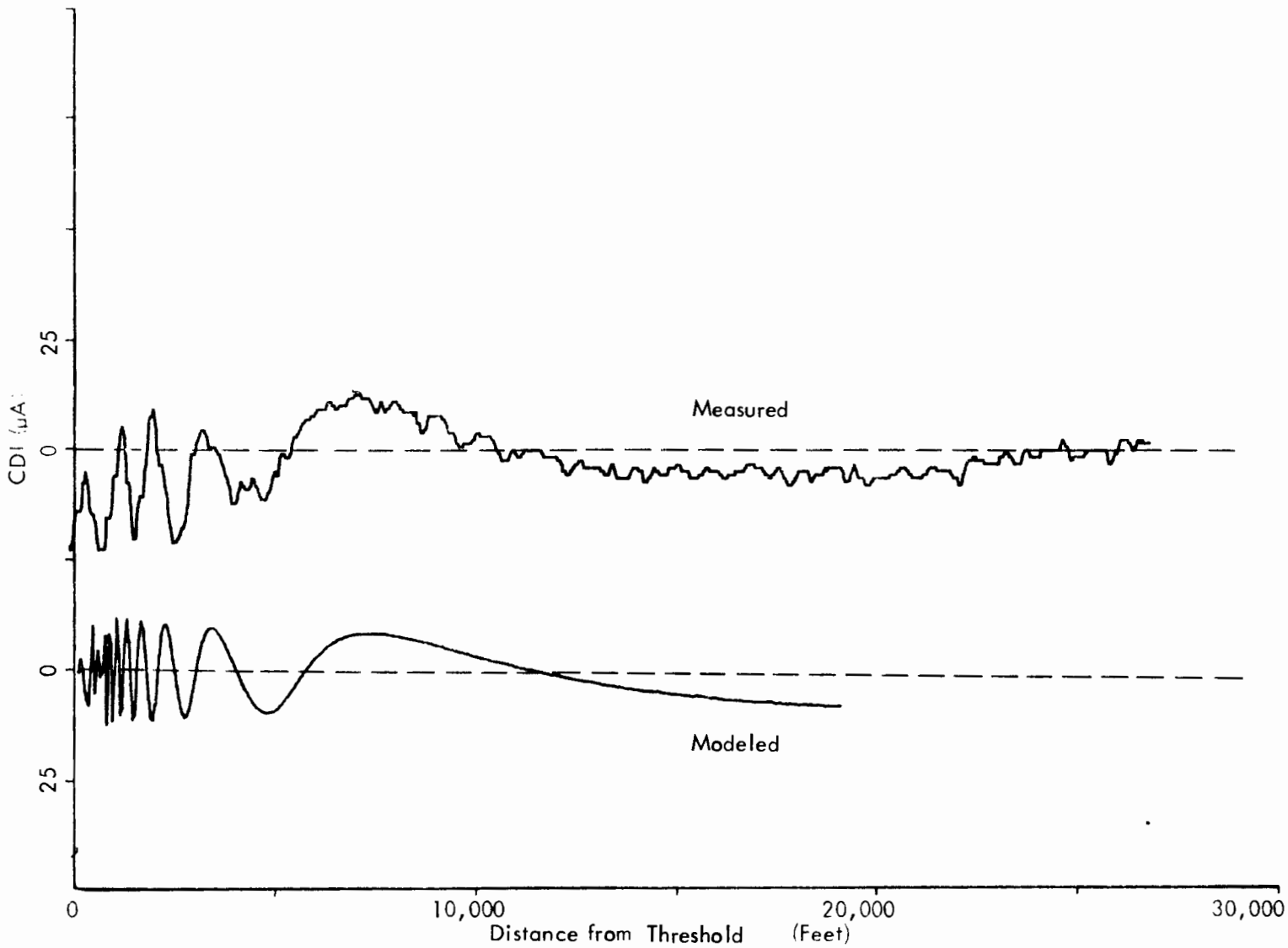

Figure 2-5. Comparison of the measured and modeled Mark 1E glide slope structure with the Mark 1E monitor tower in place.

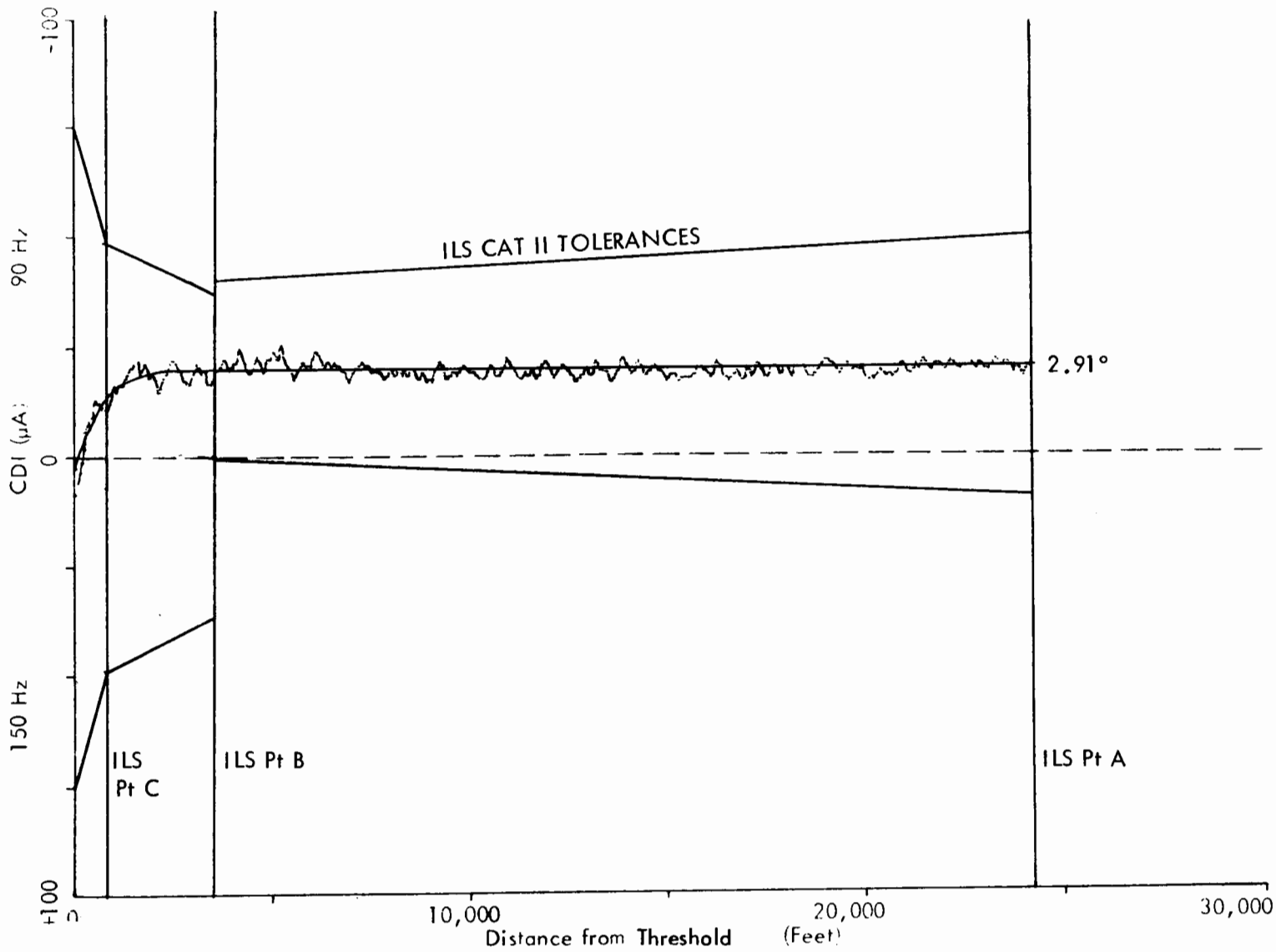

Figure 2-6. Plot of the measured glide slope structure for the St. Louis 30R CAT II facility with the Mark 1E monitor tower removed. Digitized and plotted from computer data.

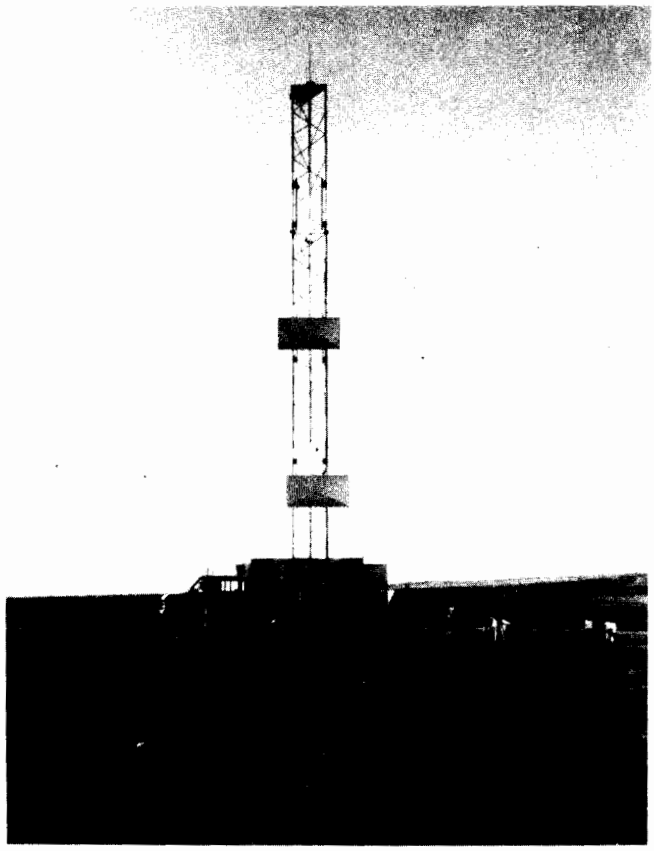

Figure 2-7. View of the null reference glide slope site serving runway 18R, DFW, January 4, 1984.

Figure 2-8. Ground-based radio telemetering theodolite used by Ohio University to provide the reference for the flight measurements on the 18R glide slope at DFW.

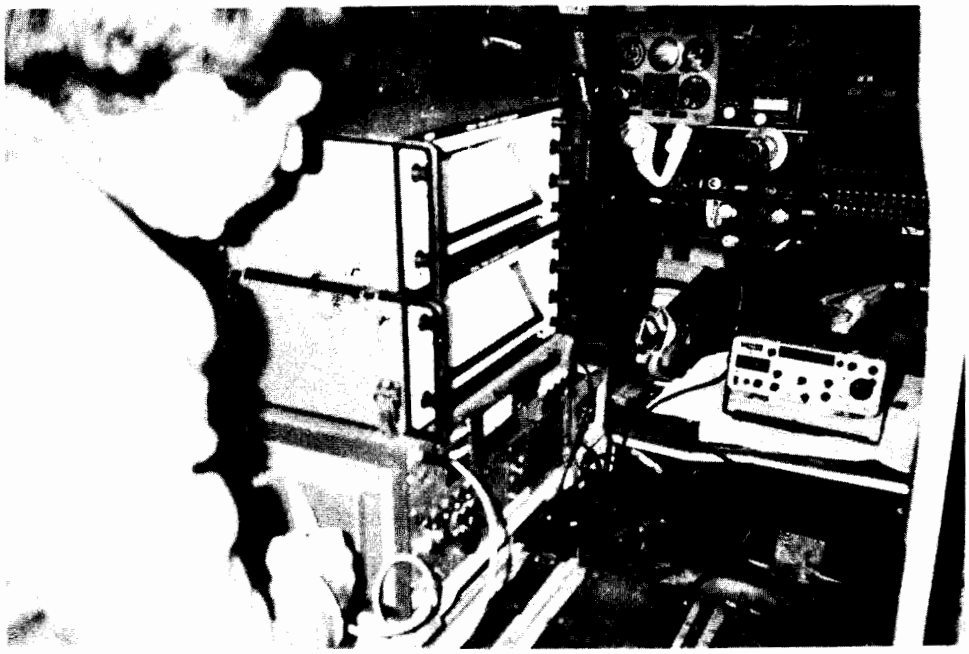

Figure 2-9. Mini-Lab Mark IIIA used by Ohio University in a Beechcraft Model A-36 to collect flight data. Shown on the right is the IFR 401-L ILS calibration transfer standard traceable to the National Bureau of Standards. With this equipment, calibration can be accomplished between data runs in flight.

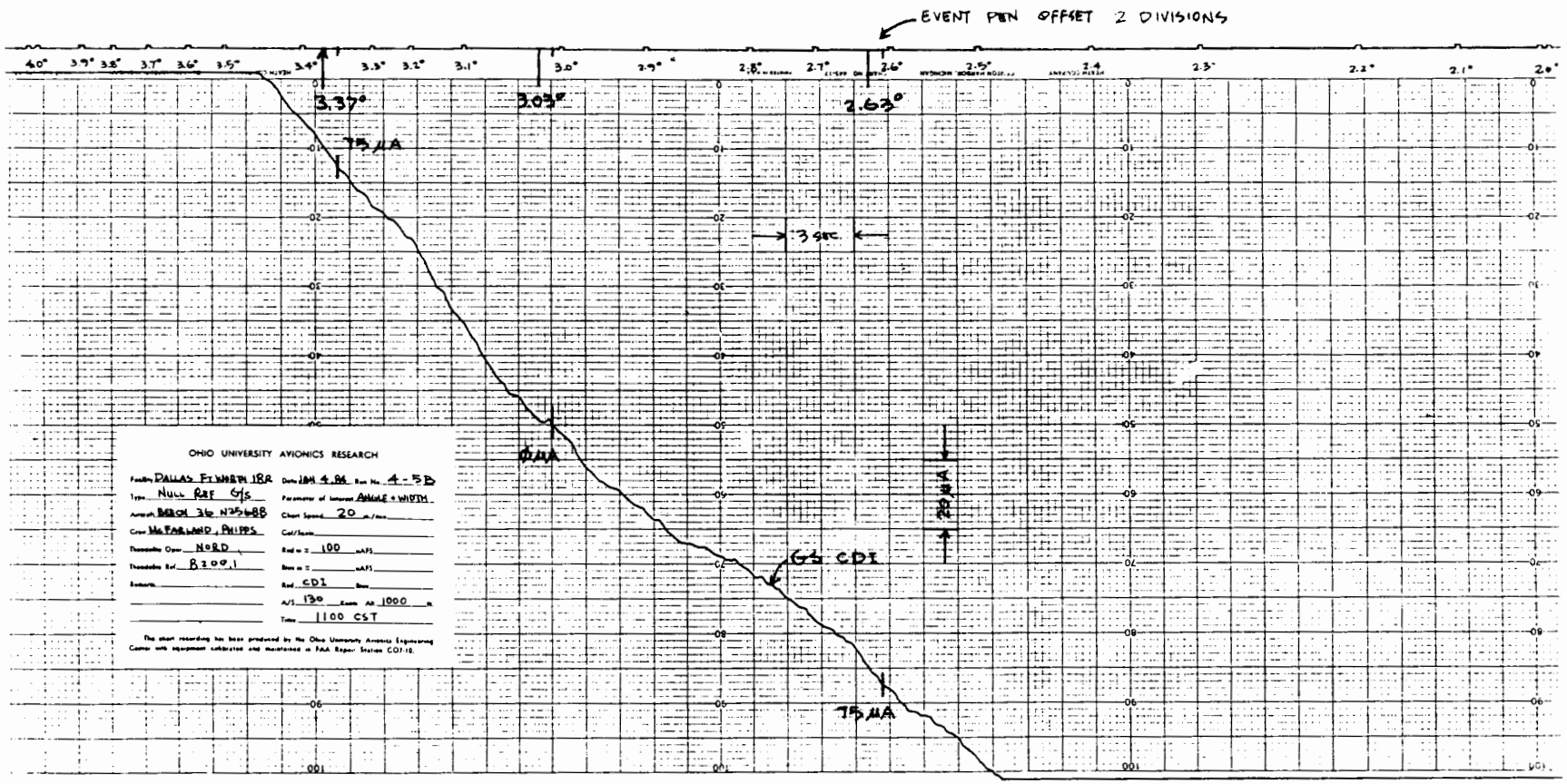

Figure 2-10. Copy of flight recording showing the vertical structure of the glide path. This record was obtained by flying at 1000 feet above the elevation of the glide slope site. A path angle of 3.03 degrees with a width of 0.74 degree and a symmetry of 46:54 are evident.

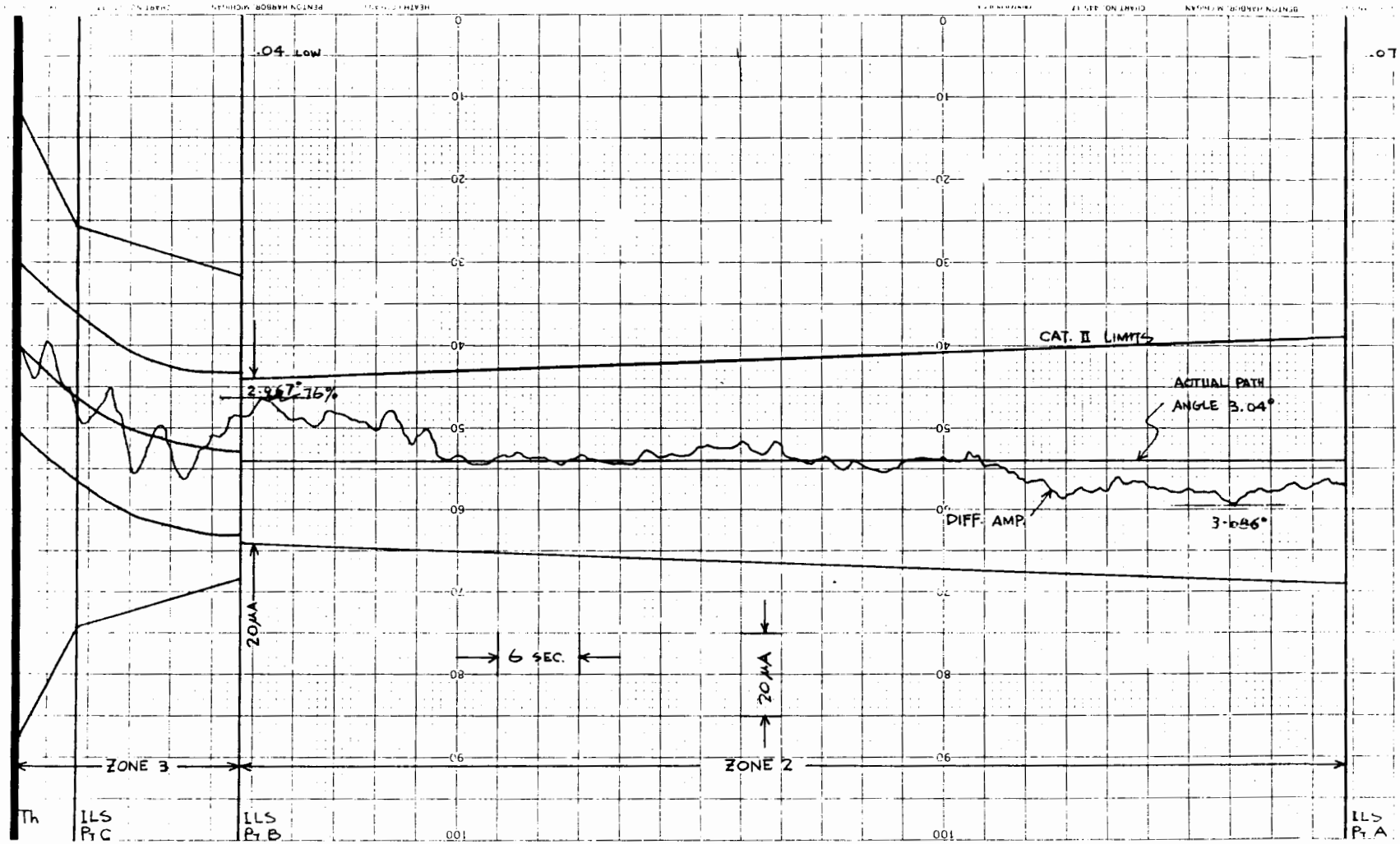

Figure 2-11. Copy of flight record 4-12A made on a low approach to runway 18R. The trace is that of the differential amplifier output which is representative of the path position in space. A maximum of 76 % of the allowable structure tolerance is indicated.

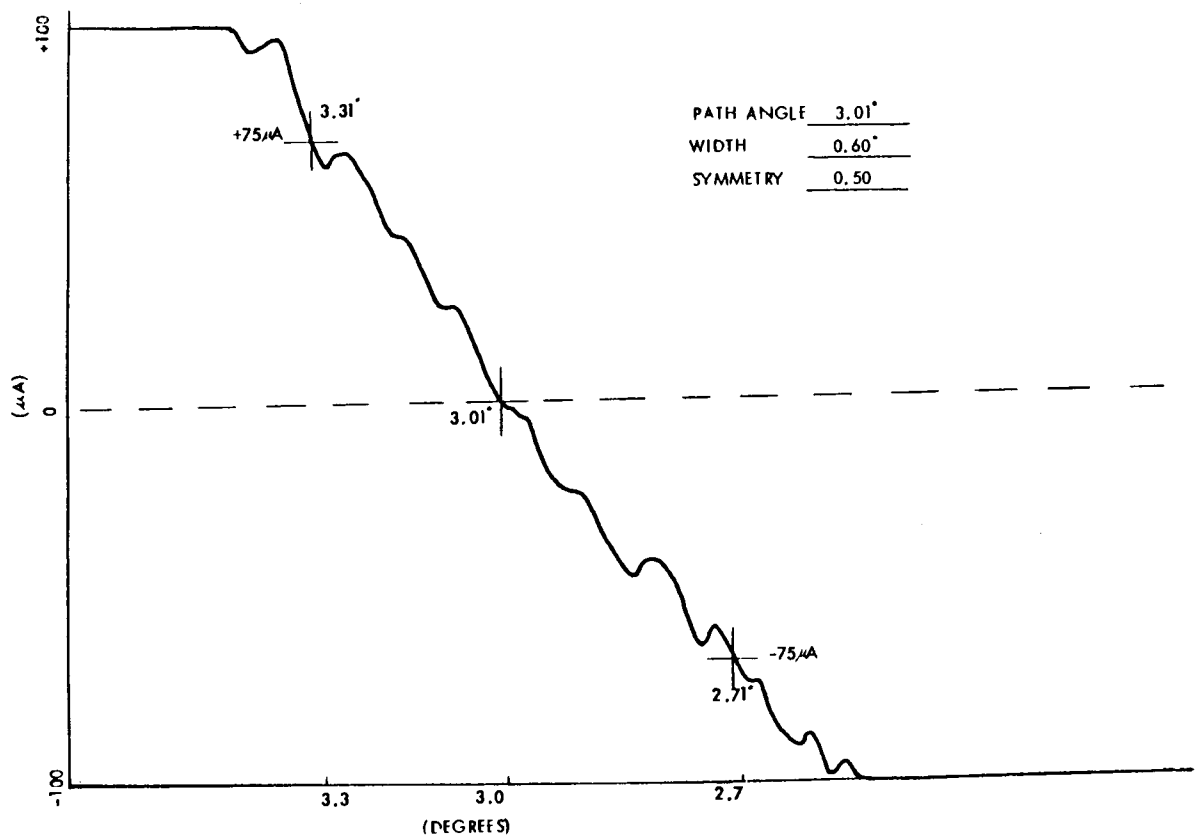

Figure 2-12. Level run recording showing vertical structure of glide slope facility at Wheeling, WV.

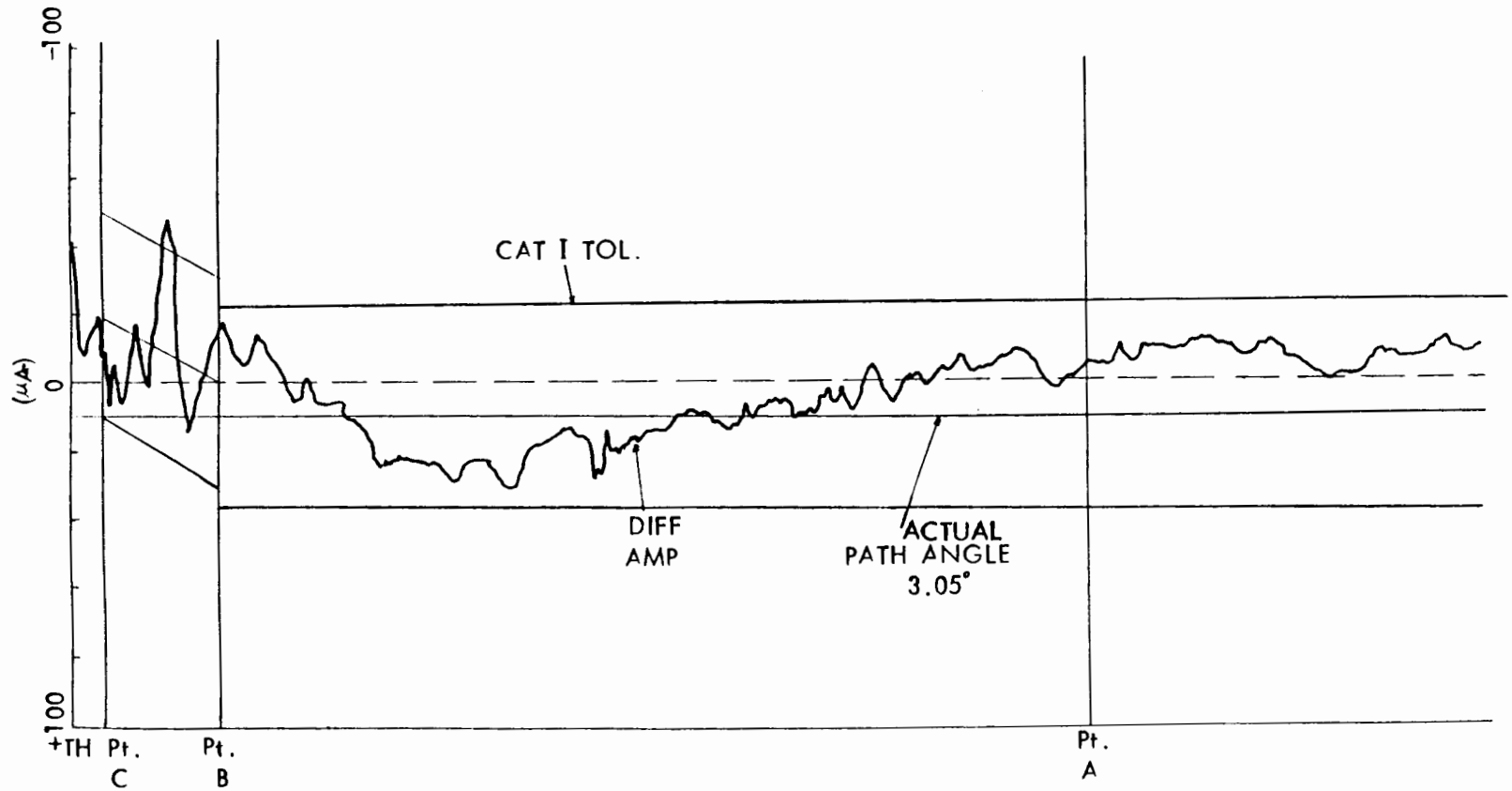

Figure 2-13. Low approach recording showing path structure of glide slope facility at Wheeling, WV.

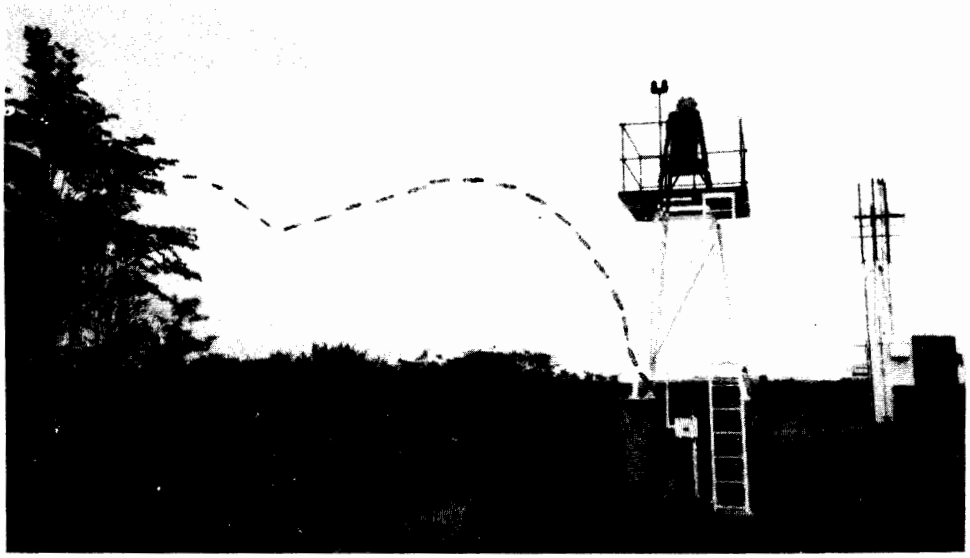

Figure 2-14. View of the tree line running parallel to runway at Wheeling, WV. after cutting. Original tree line profile is shown by dotted line.

Figure 2-15. Additional view of the glide slope facility at Wheeling, WV.

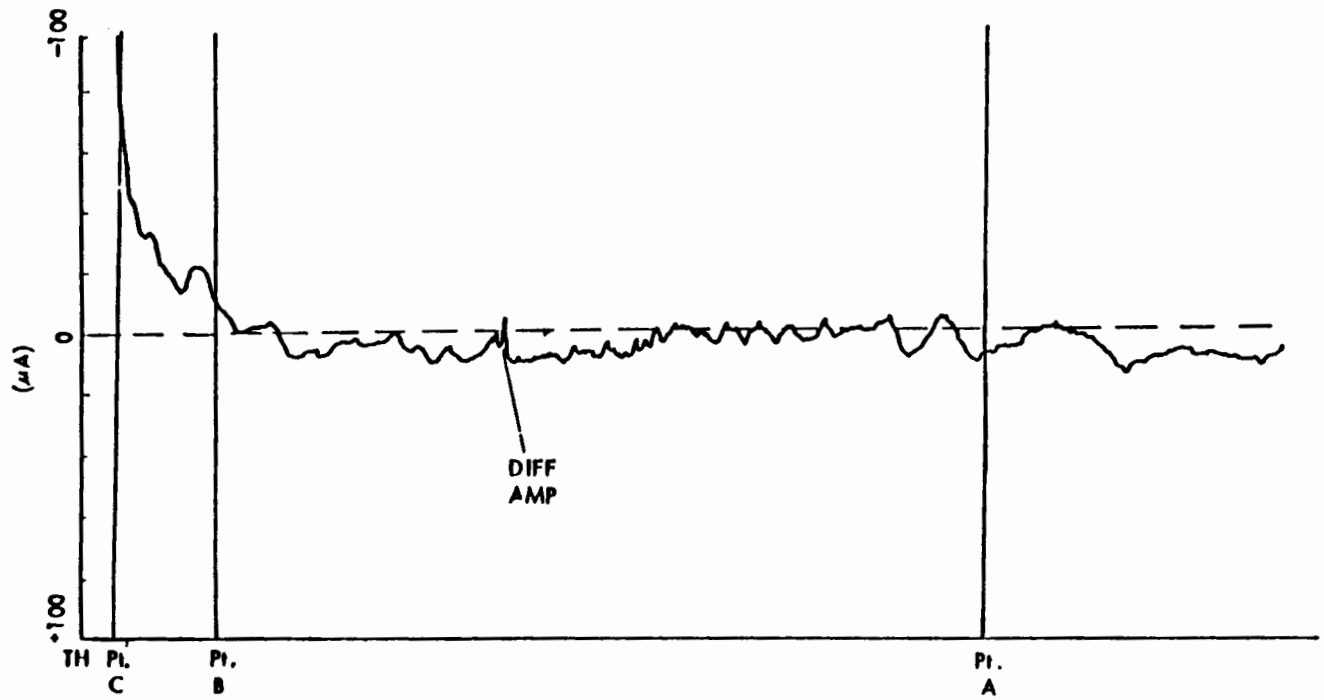

Figure 2-16. Low approach recording made in line with the row of trees alongside the runway at Wheeling, WV.

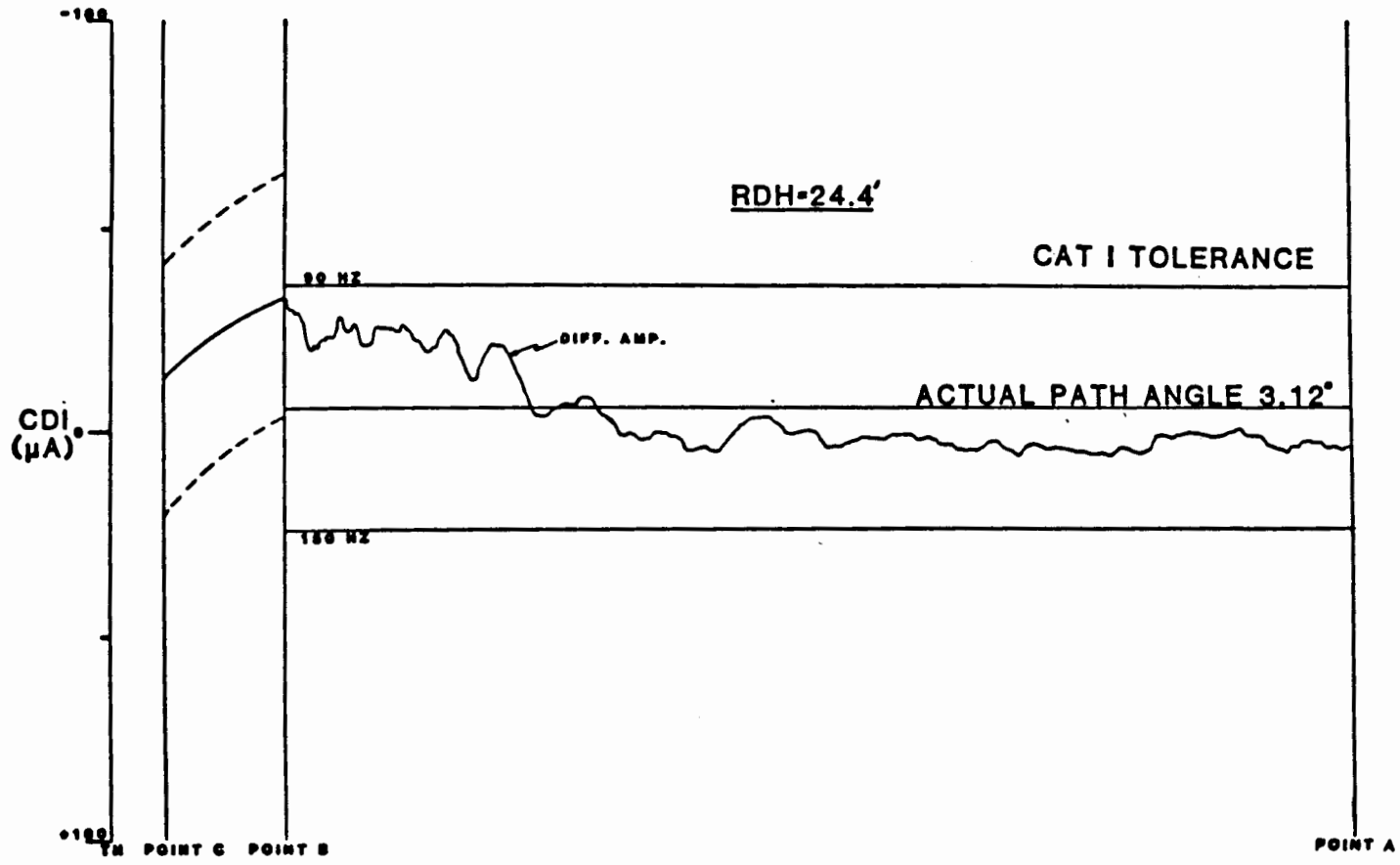

Figure 2-17. Low approach recording for runway 18 at Greenville, SC.

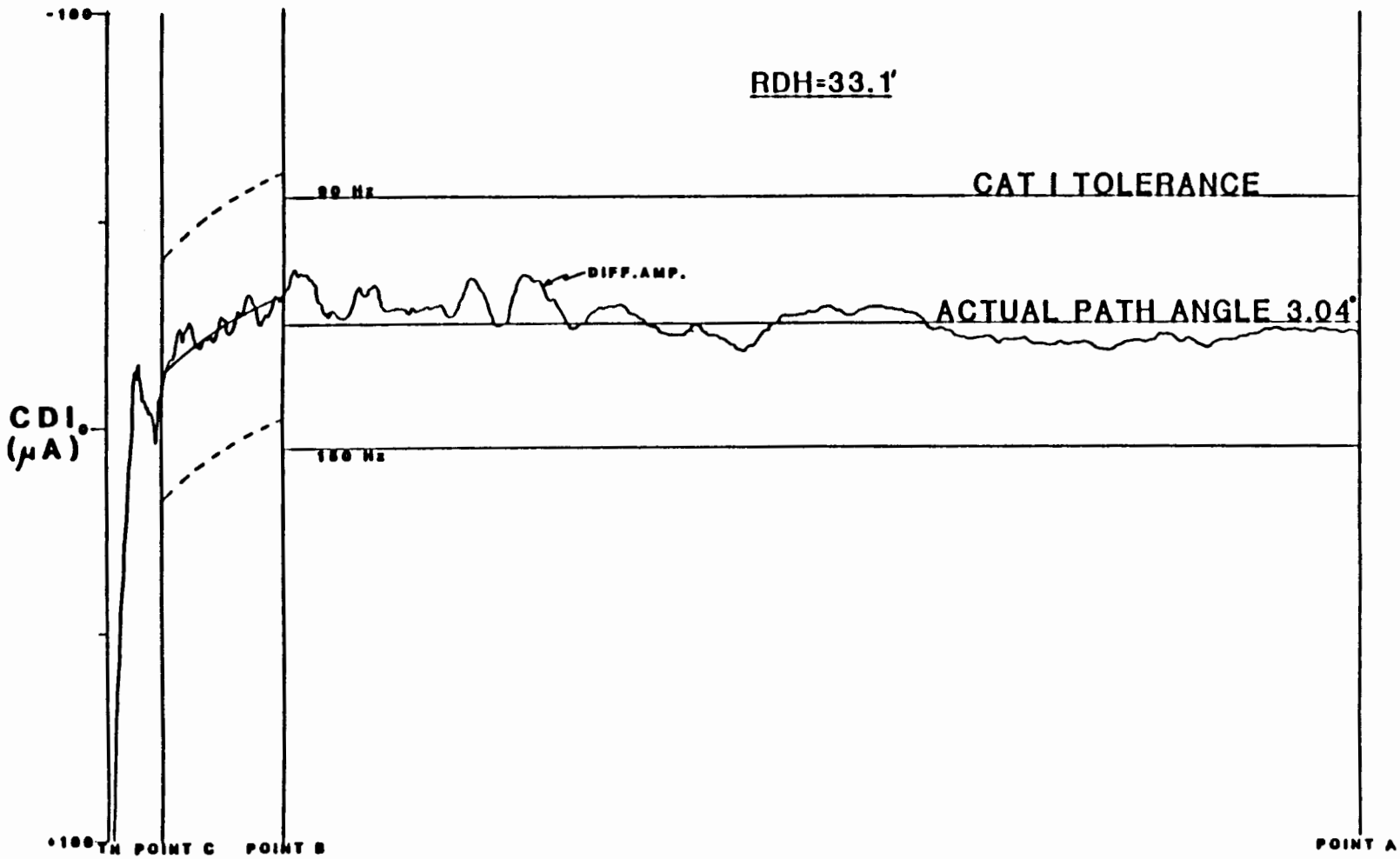

Figure 2-18. Low approach recording showing improved glide slope path structure for runway 18 at Greenville, SC.

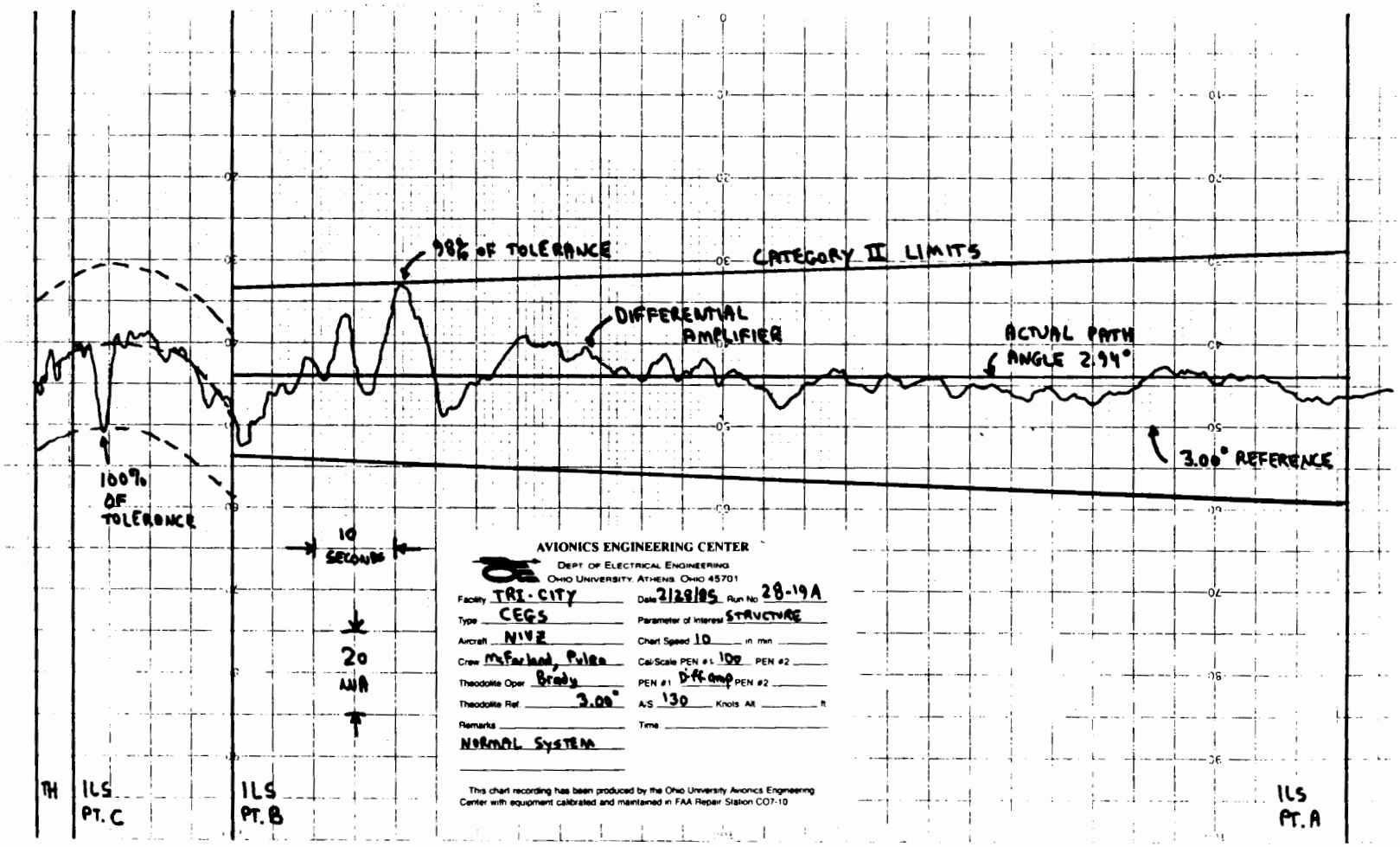

Figure 2-19. Differential amplifier trace representing glide slope path for the "as-found" conditions at Bristol, TN.

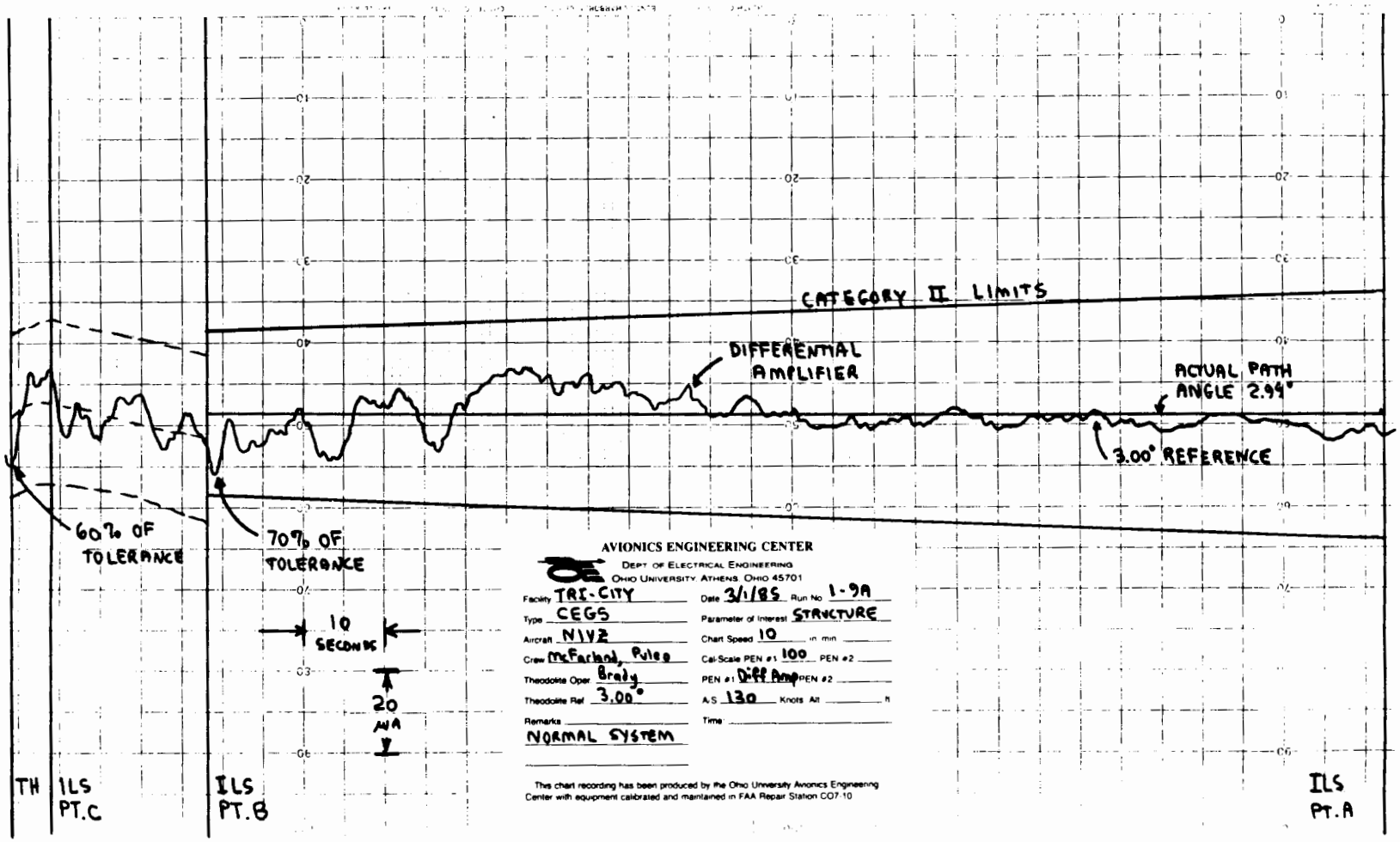

Figure 2-20. Differential amplifier trace representing improved glide slope path structure at Bristol, TN.

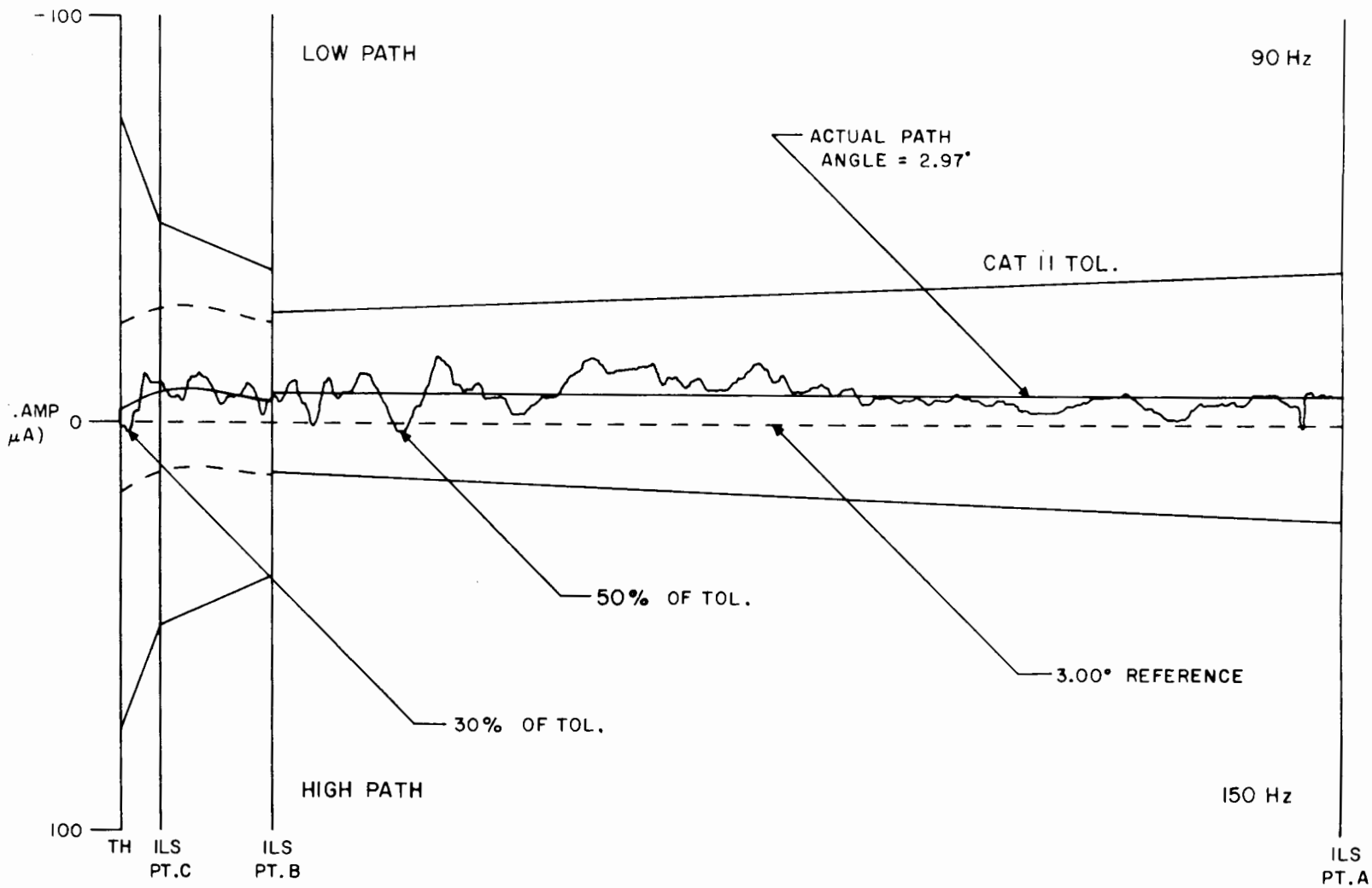

Figure 2-21. Low approach recording showing final glide slope path structure at Bristol, TN.

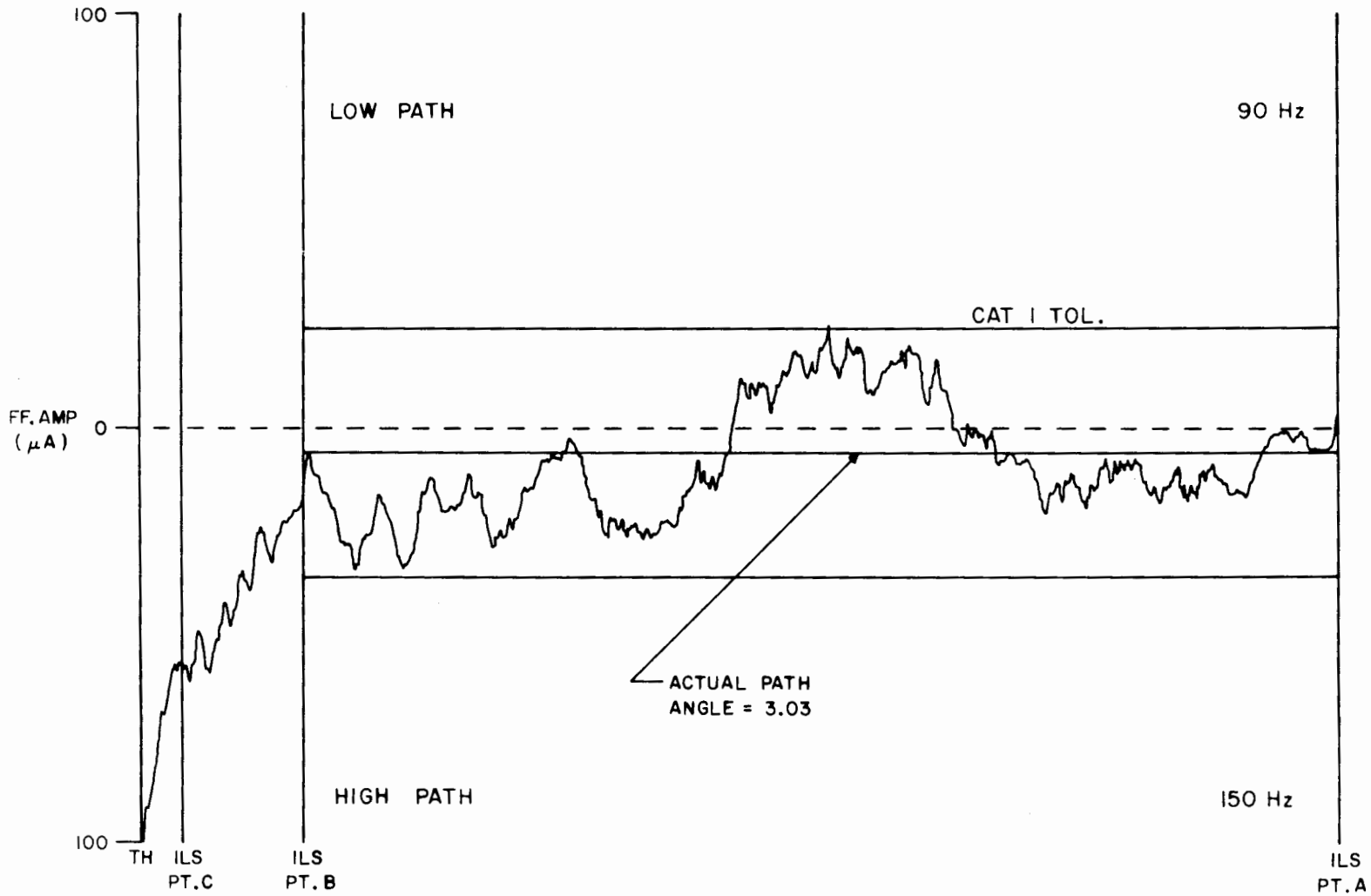

Figure 2-22. Low approach recording showing the "as-found" glide slope path structure at DeKalb-Peachtree.

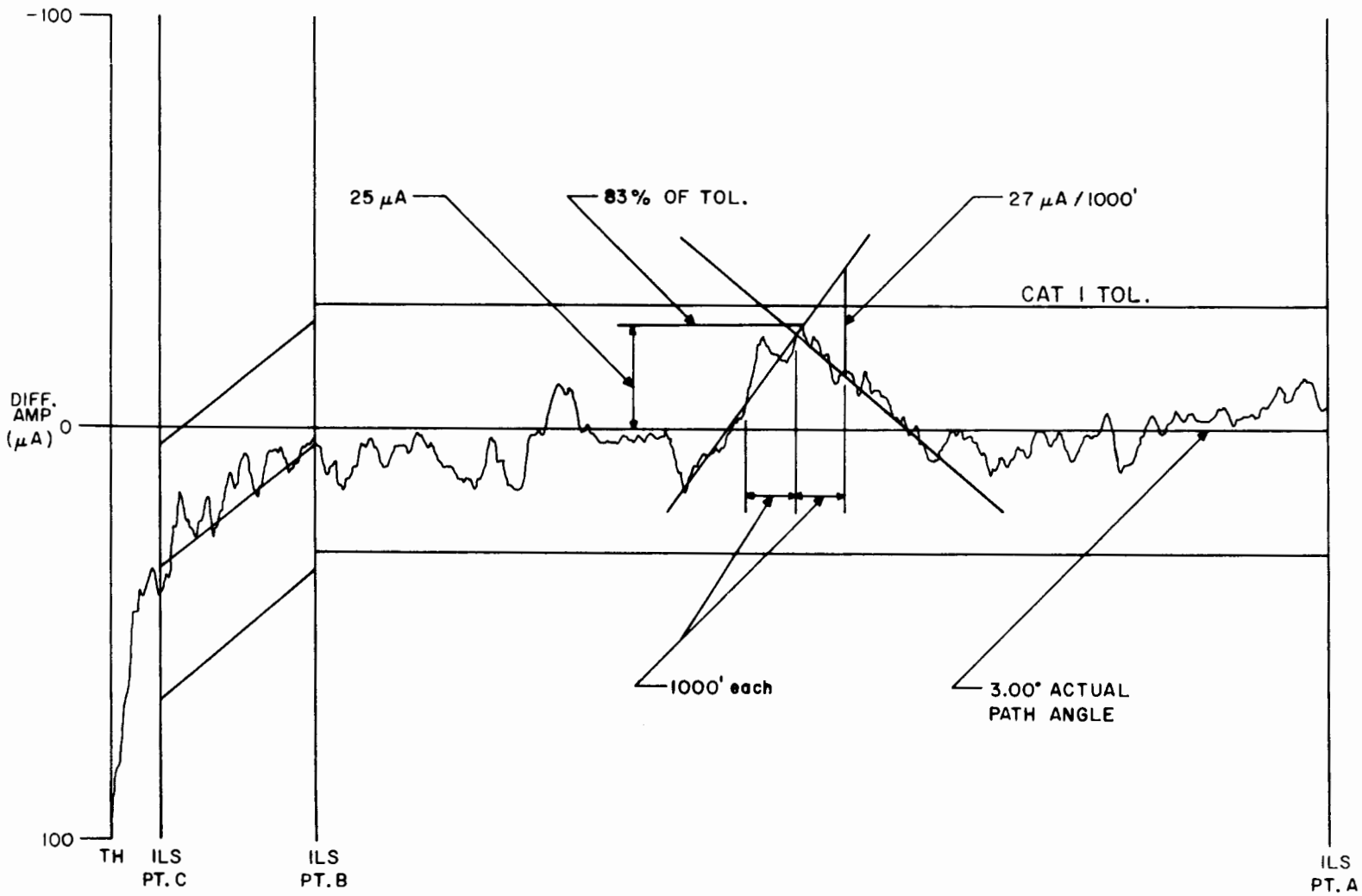

Figure 2-23. Low approach recording showing the improved glide slope path structure at DeKalb-Peachtree.

Figure 2-24. Far-Field monitoring site near the Pontiac middle marker.

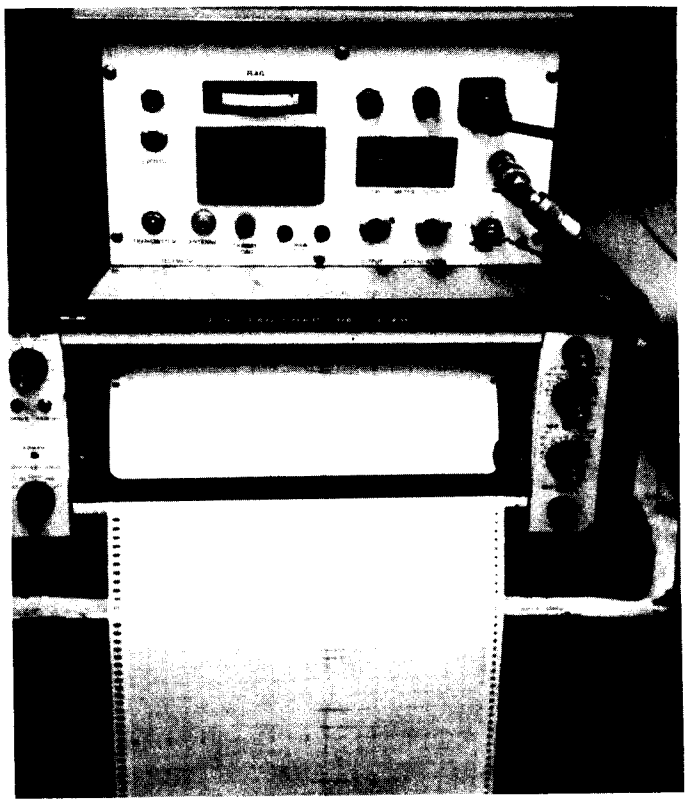

Figure 2-25. Receiving and recording systems used for data collection.

Figure 2-26. Interior of 2½ ton truck used as equipment shelter at the far-field monitoring site.

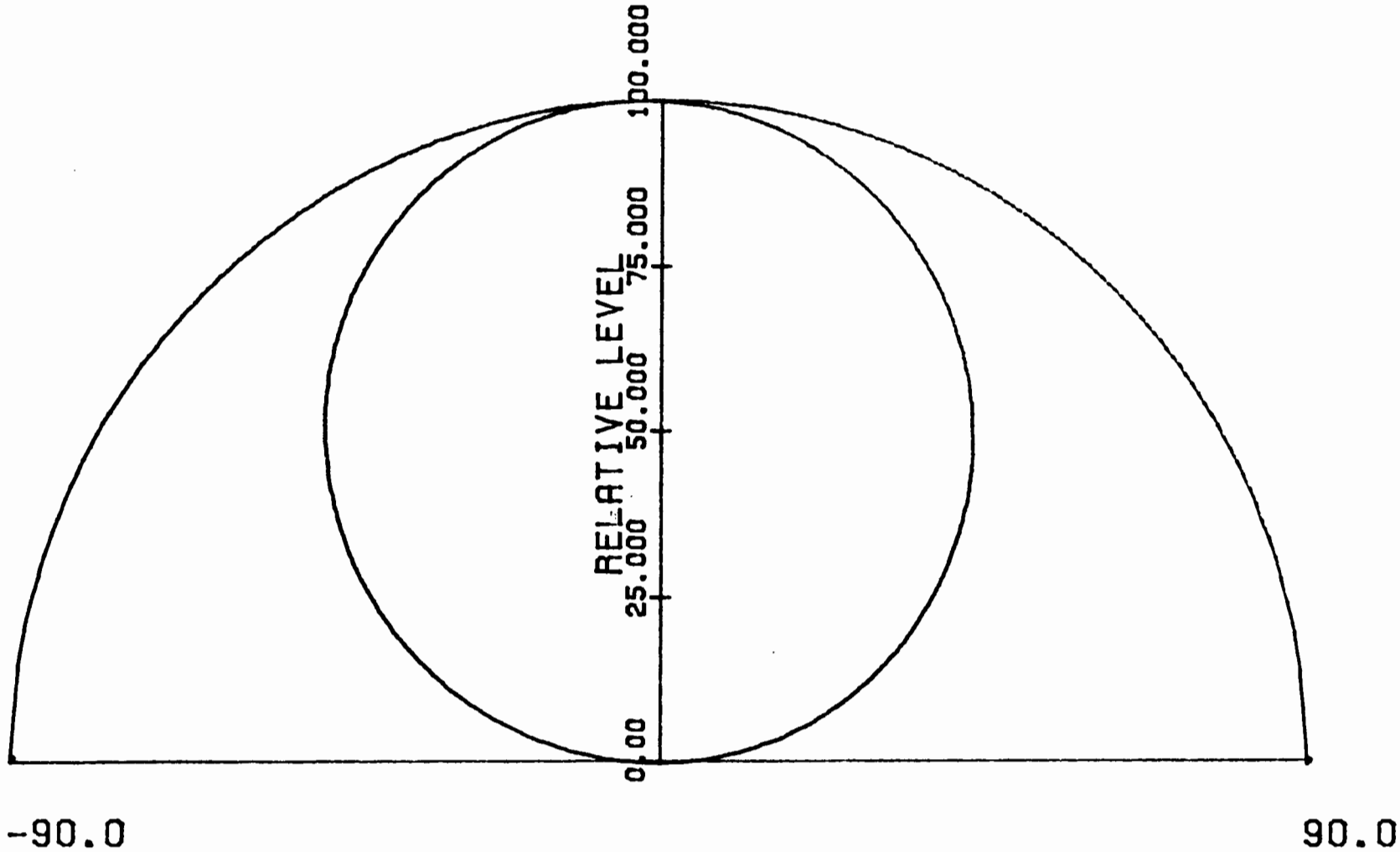

Figure 2-27. Polar plot of relative field intensity level for half-wave dipole radiating elements.

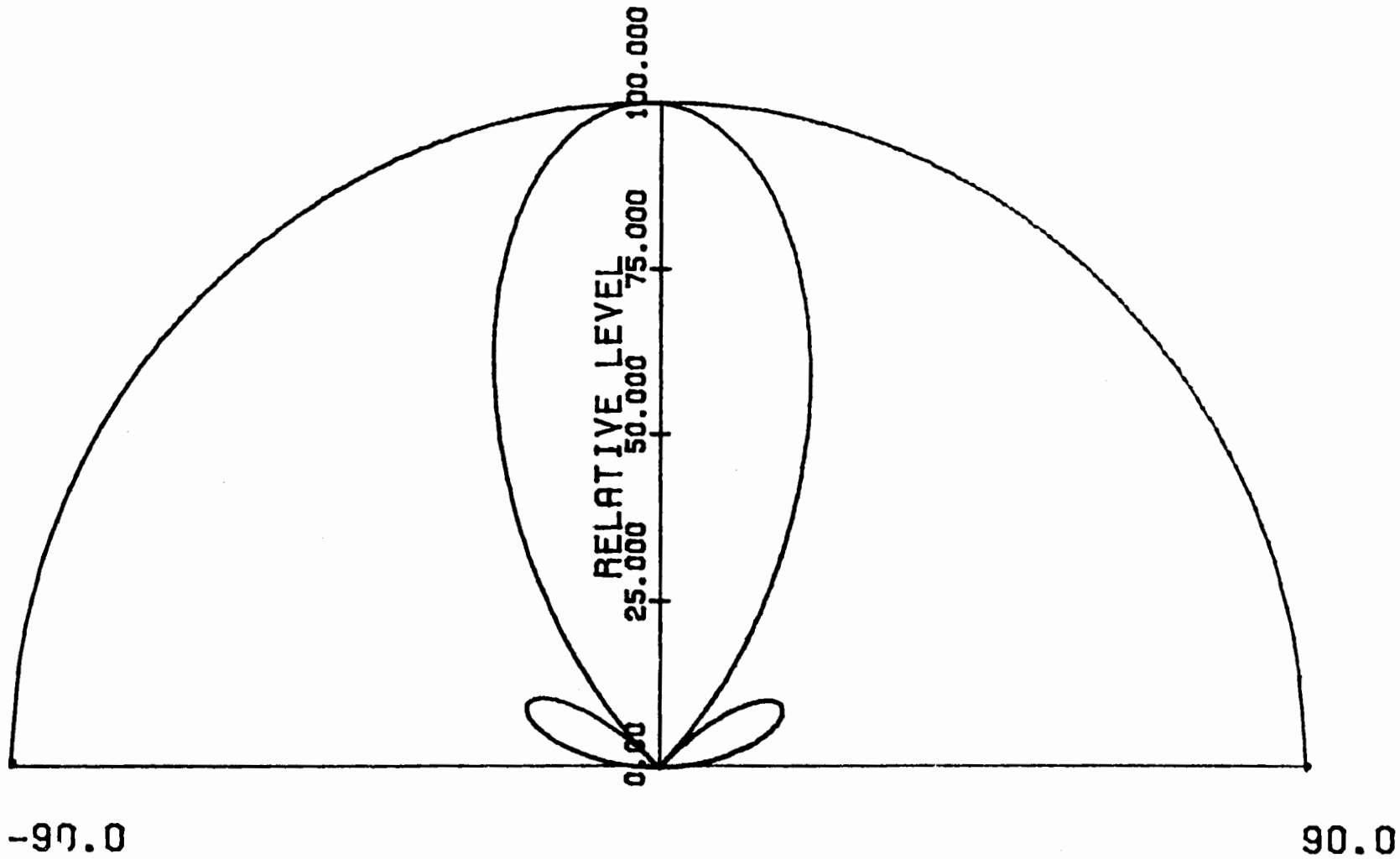

Figure 2-28. Polar plot of relative field intensity level for FA-8976 radiating elements.

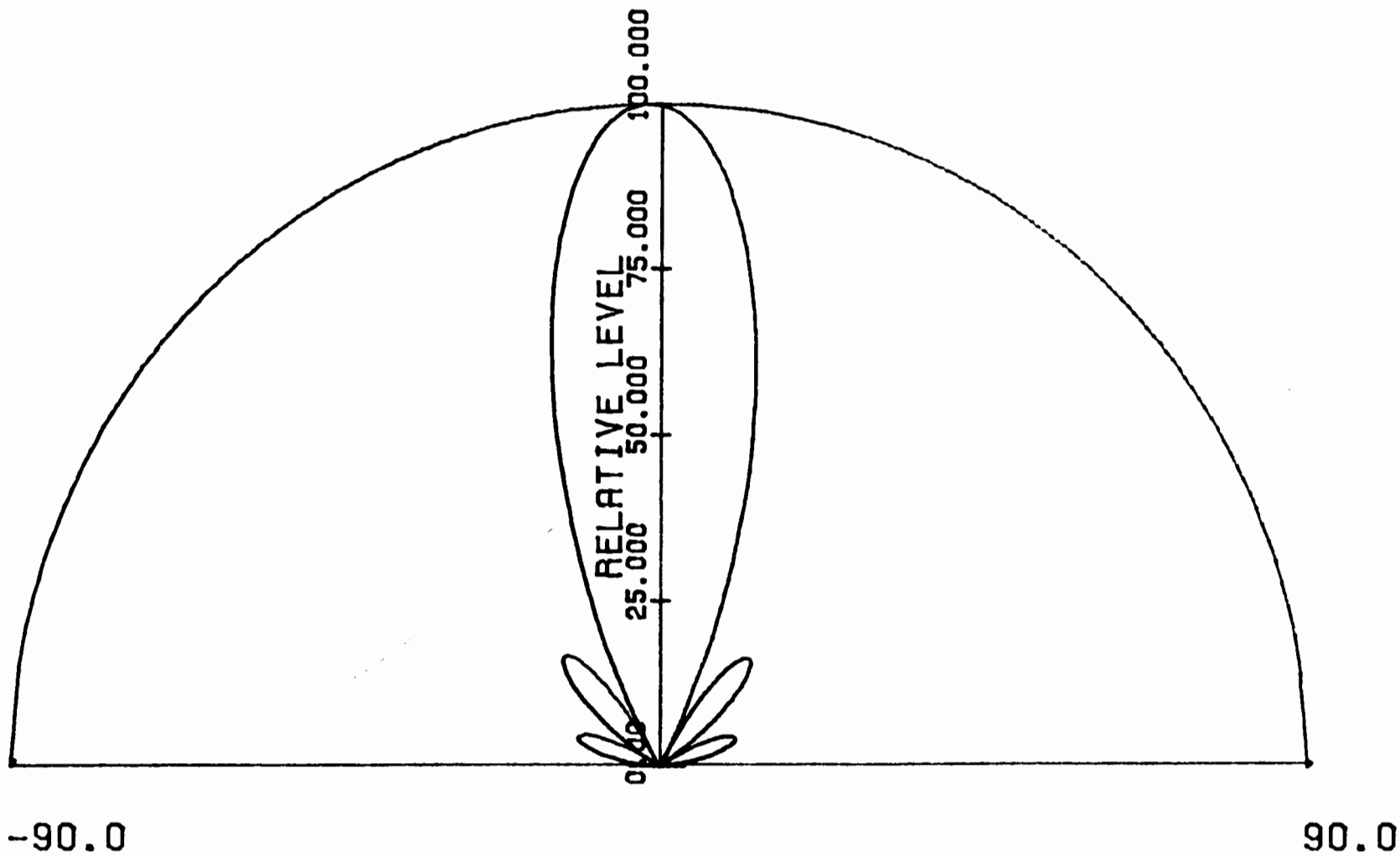

Figure 2-29. Polar plot of relative field intensity level for GRN-27 radiating elements.

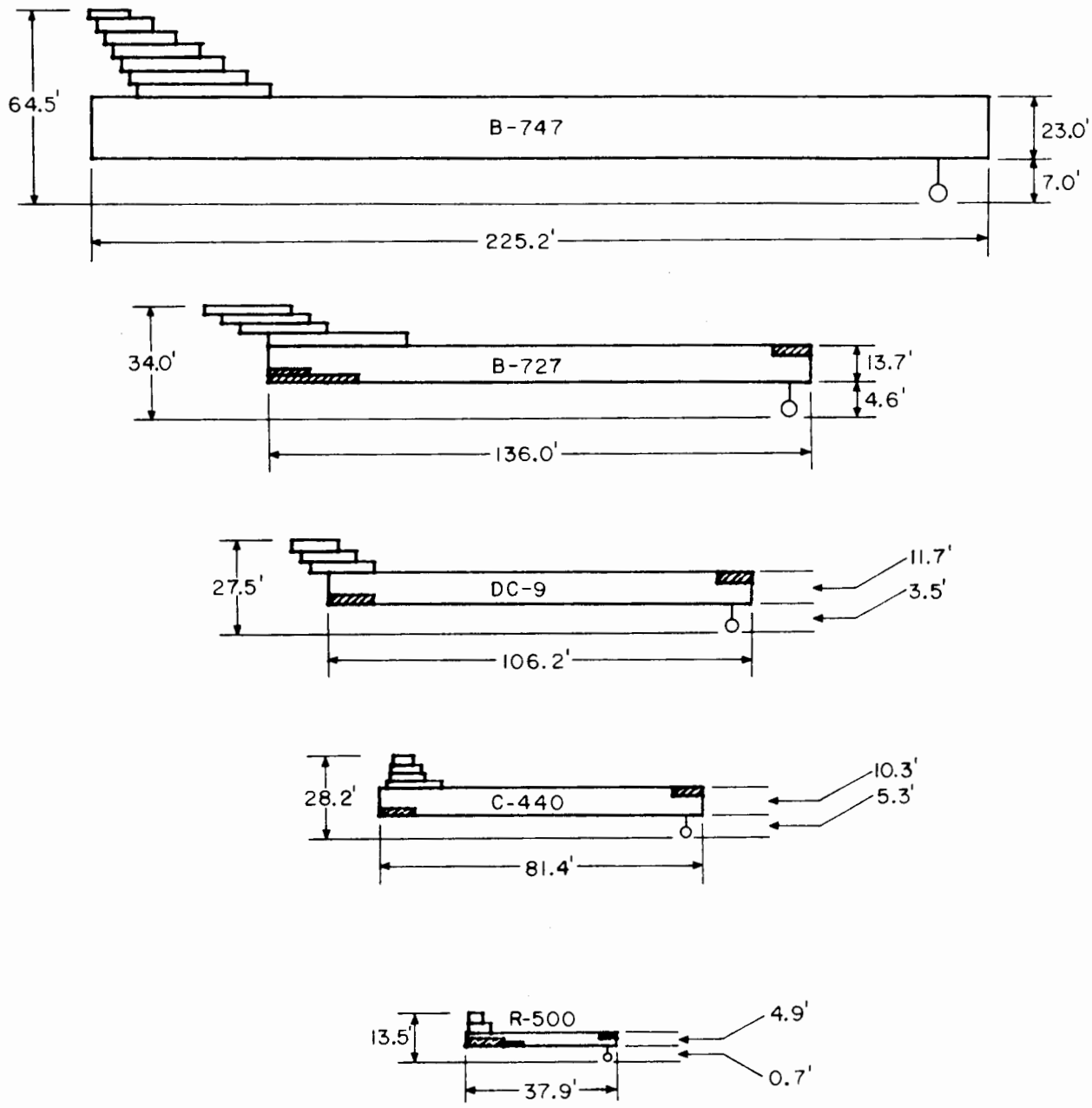

Figure 2-30. Overall dimensions of scattering plates used to simulate specific aircraft.

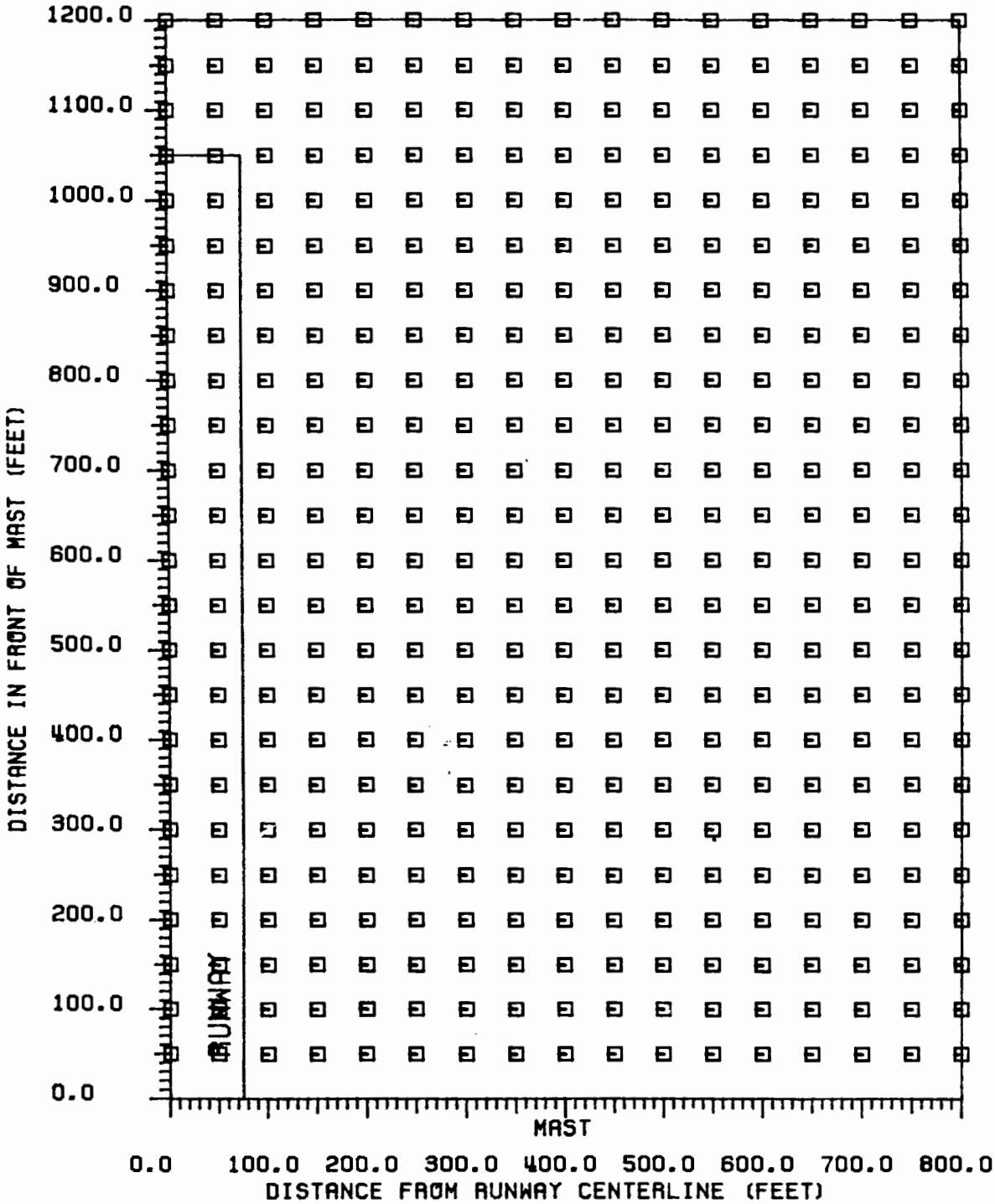

Figure 2-31. Grid locations of scatterer aircraft for which an approach is calculated. The dots are also used to denote out-of-tolerance conditions on the critical areas maps.

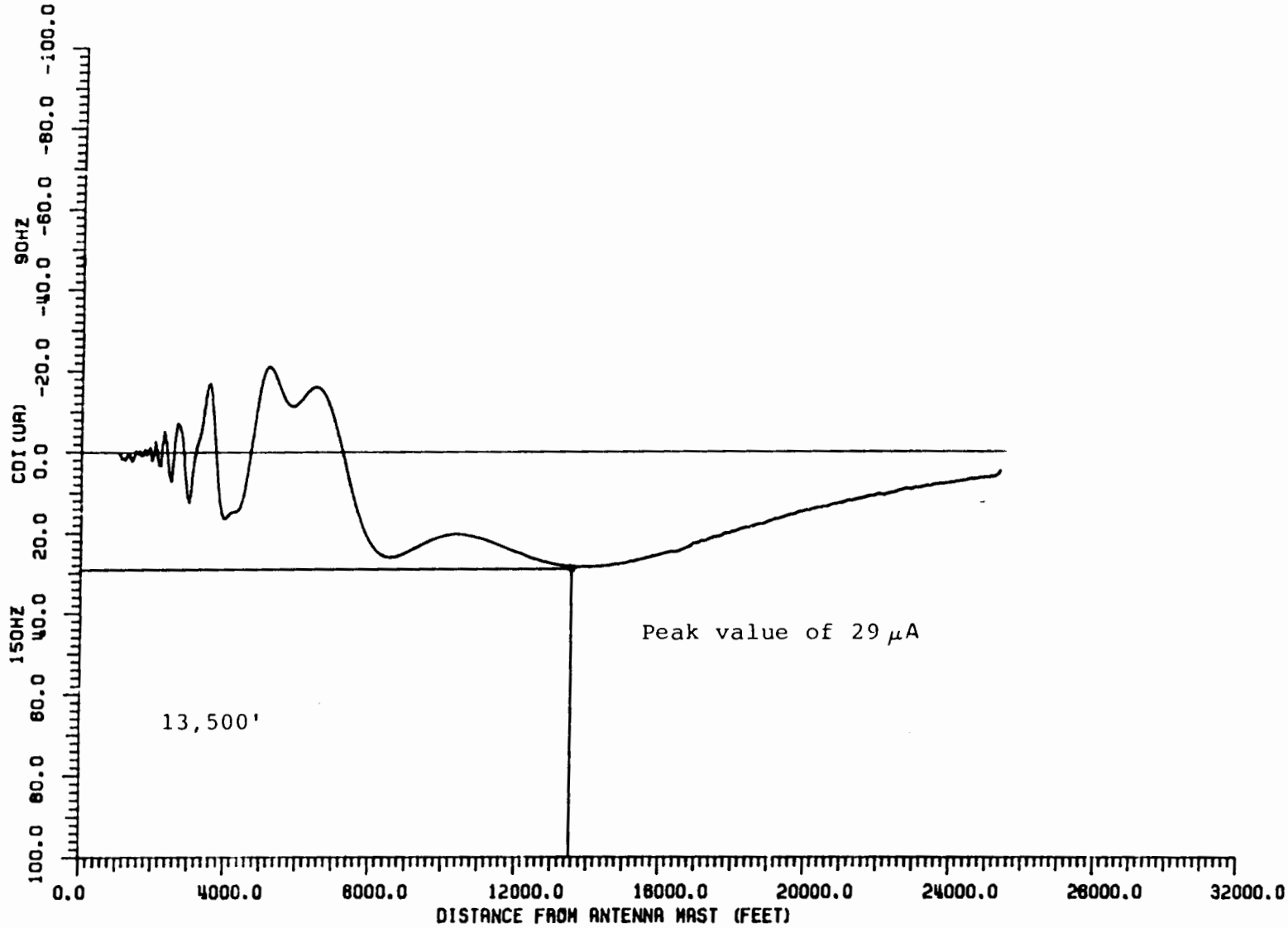

Figure 2-32. Typical CDI plot. Perturbations are caused by a Convair C-440. Orientation is perpendicular to runway centerline with tail away from the runway. Center of fuselage is 500 feet in front of mast, and 450 feet from centerline.

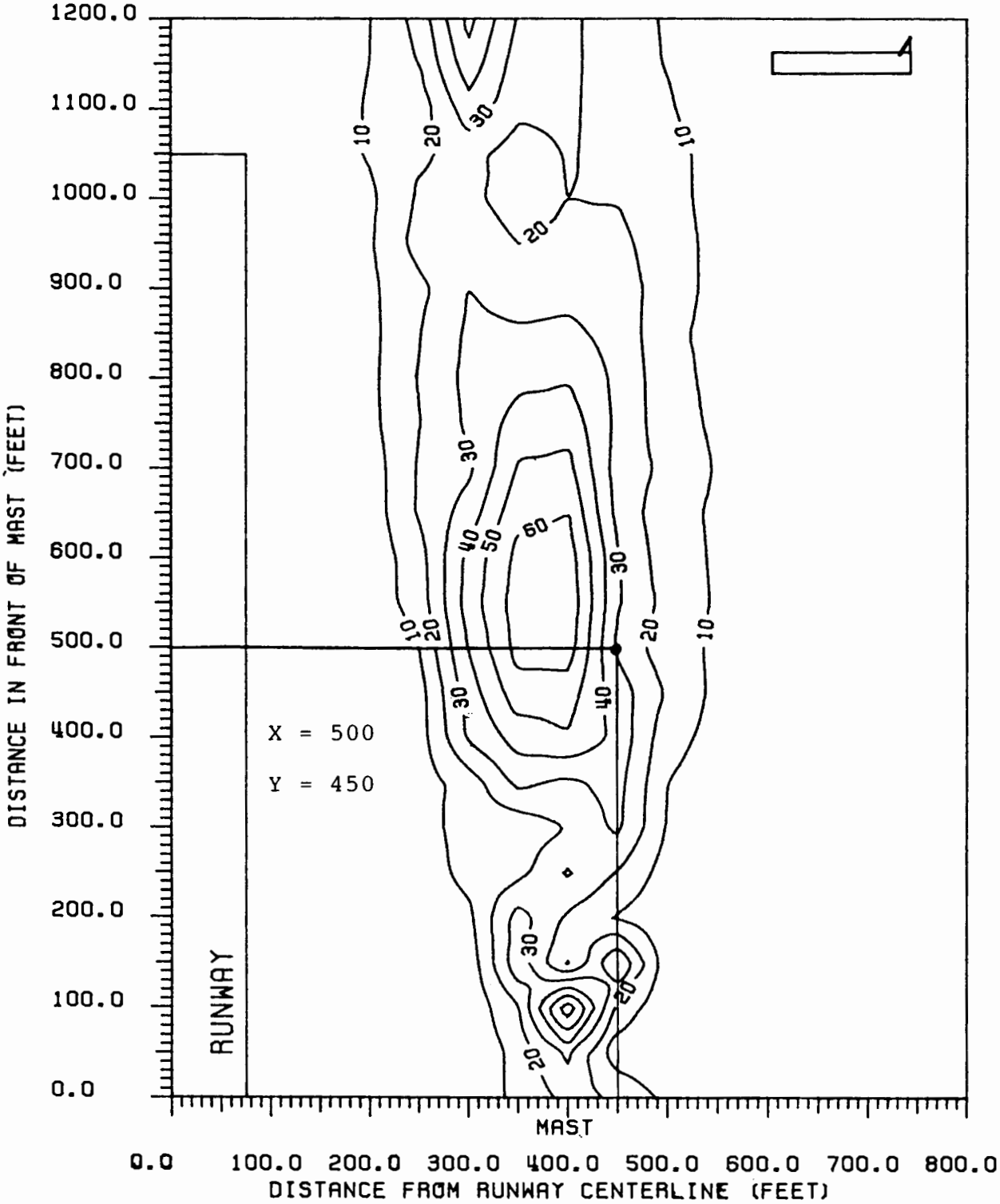

Figure 2-33. Contour map of predicted peak CDI perturbations in ILS Zone 2 for a C-440. C-440 fuselage is perpendicular to runway centerline with tail away from the runway.

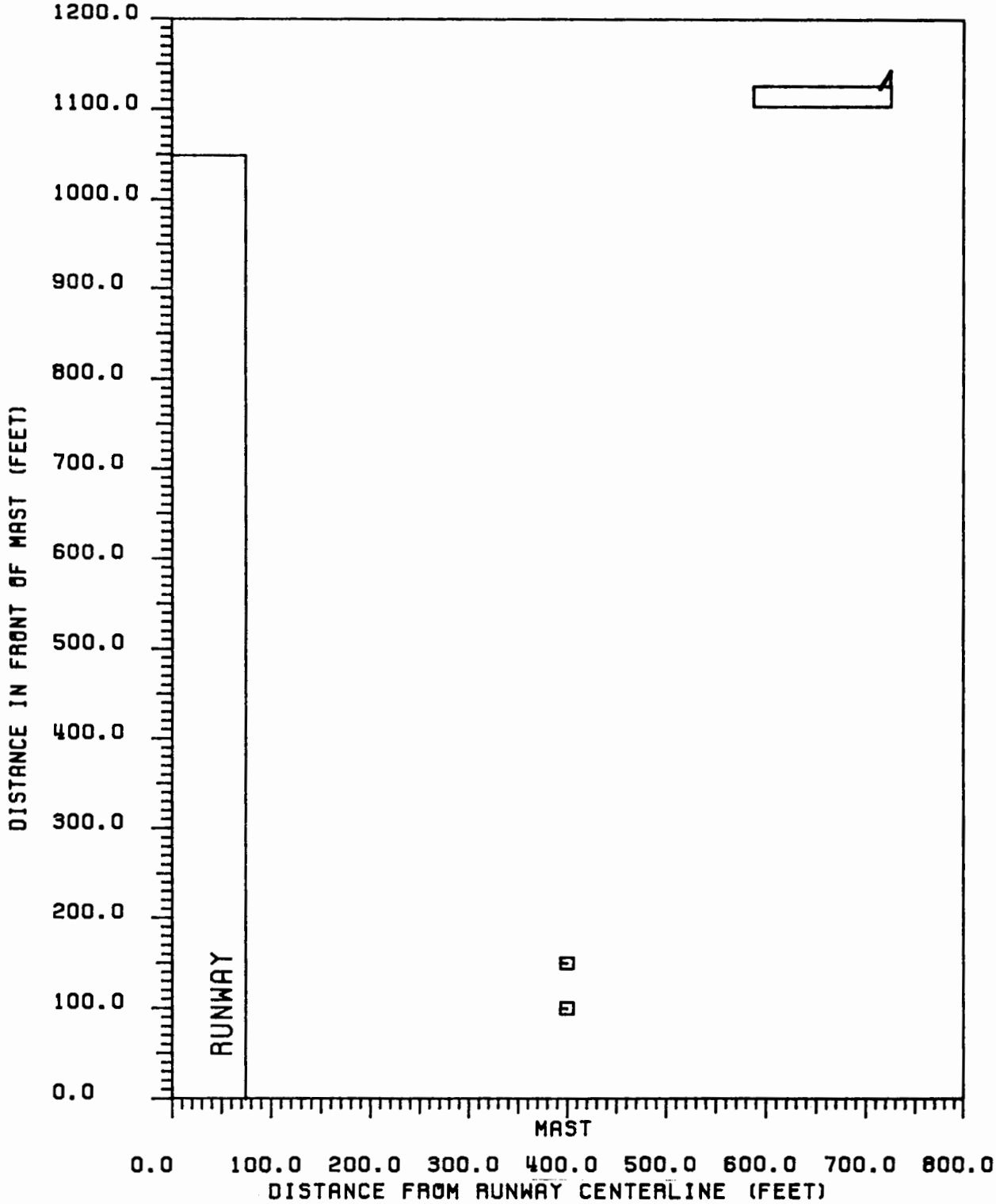

Figure 2-34. Critical area map for CAT II/III tolerances relating to R-500 aircraft. R-500 fuselage is perpendicular to runway centerline with tail away from the runway. Null reference glide slope, directional antennas.

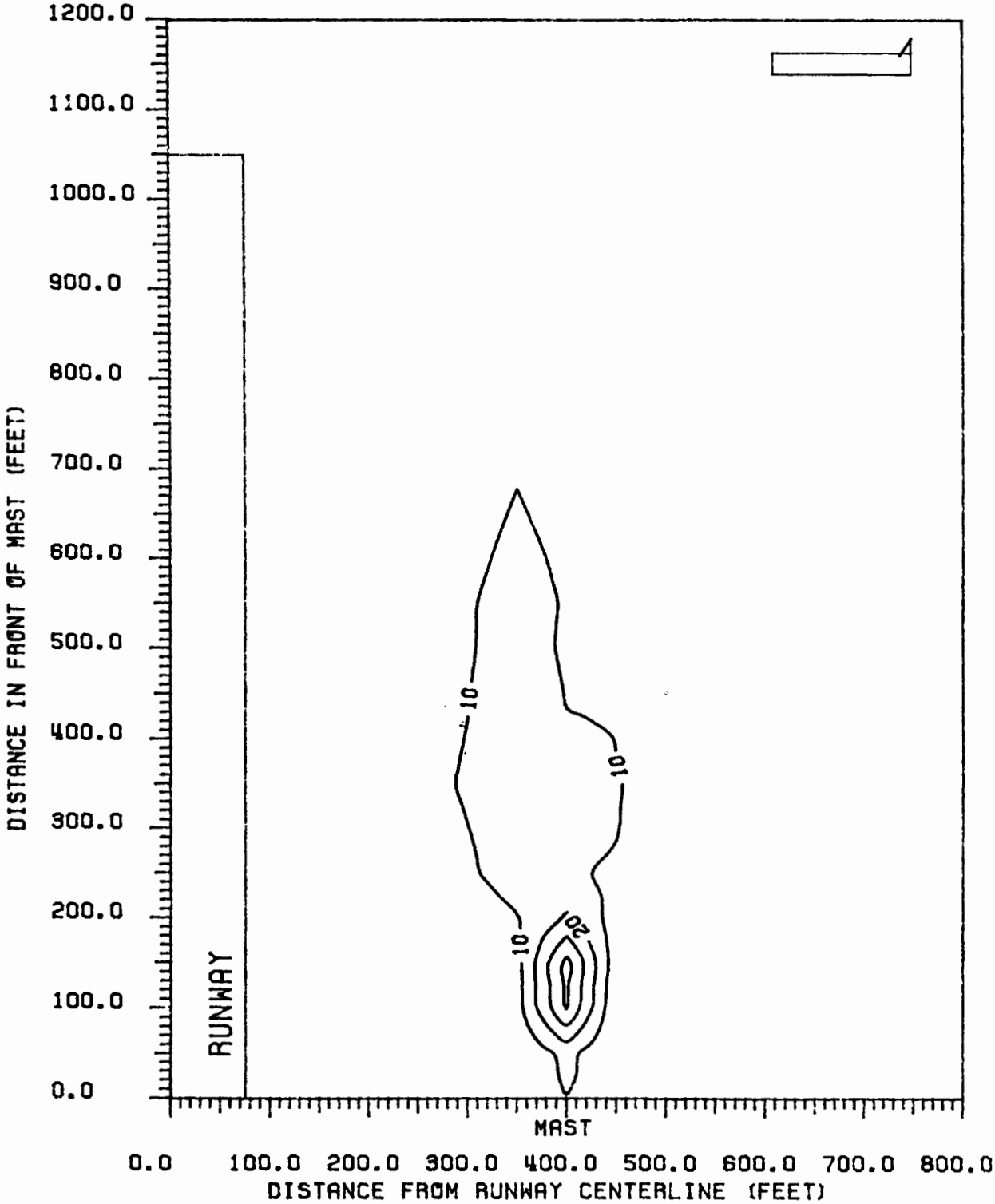

Figure 2-35. Contours of peak CDI values produced in ILS Zone 2 for an R-500. R-500 fuselage is perpendicular to runway centerline, with tail away from the runway. Null reference glide slope, directional antennas.

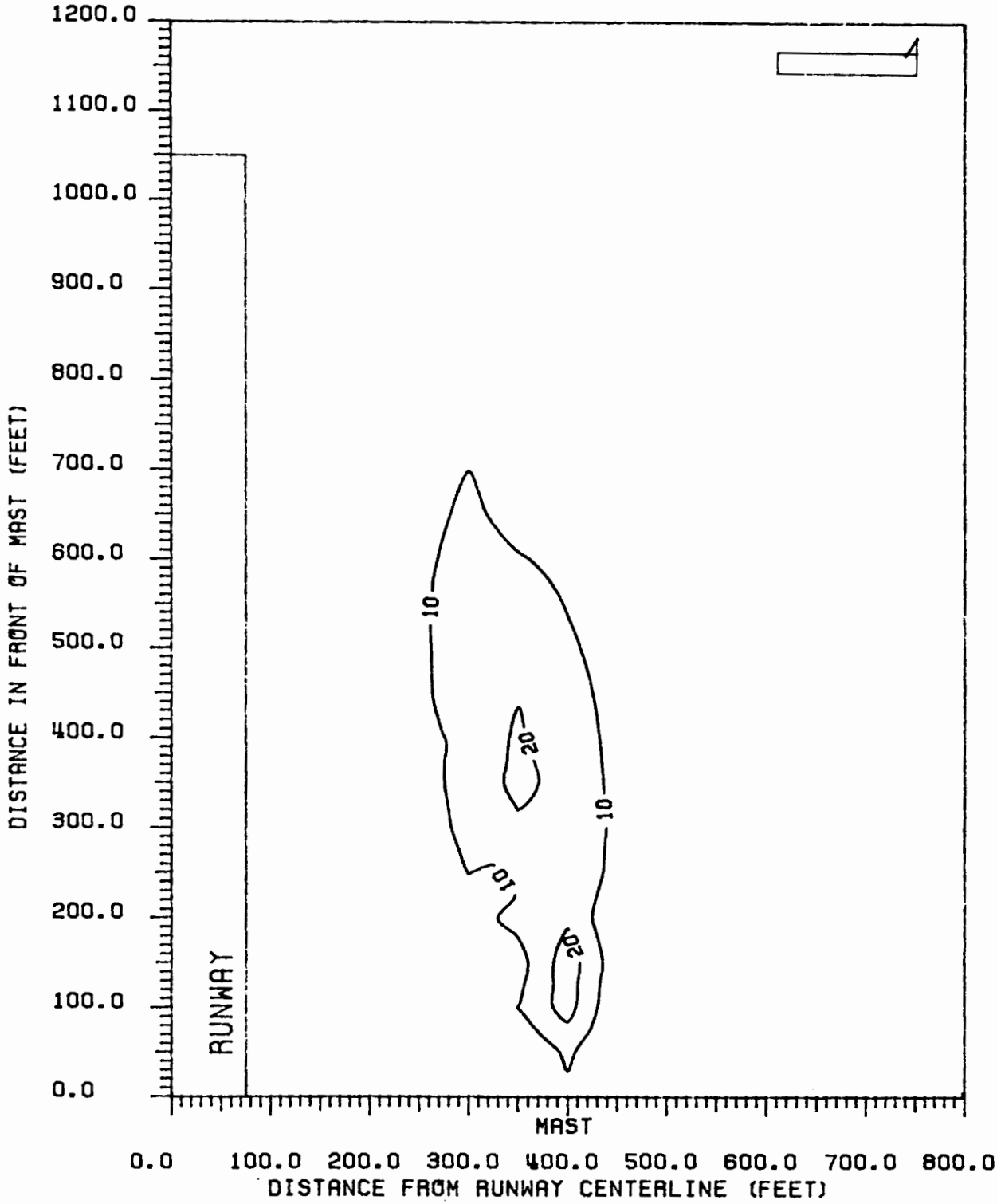

Figure 2-36. Contours of peak CDI values produced between ILS Point B and ILS Point C for an R-500. R-500 fuselage is perpendicular to runway centerline, with tail away from runway. Null reference glide slope, directional antennas.

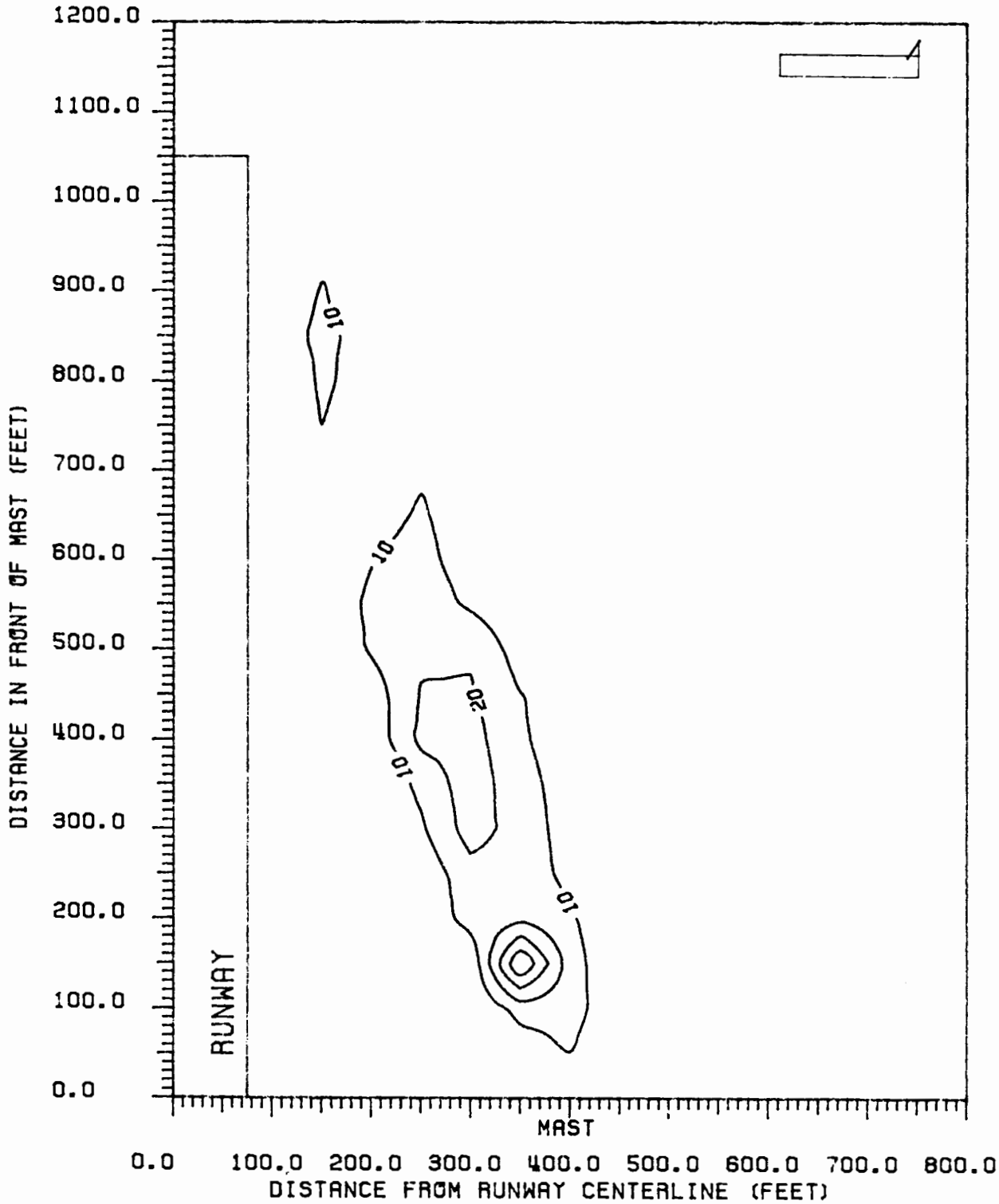

Figure 2-37. Contours of peak CDI values produced between ILS Point C and threshold for an R-500. R-500 fuselage is perpendicular to runway centerline, with tail away from runway. Null reference glide slope, directional antennas.

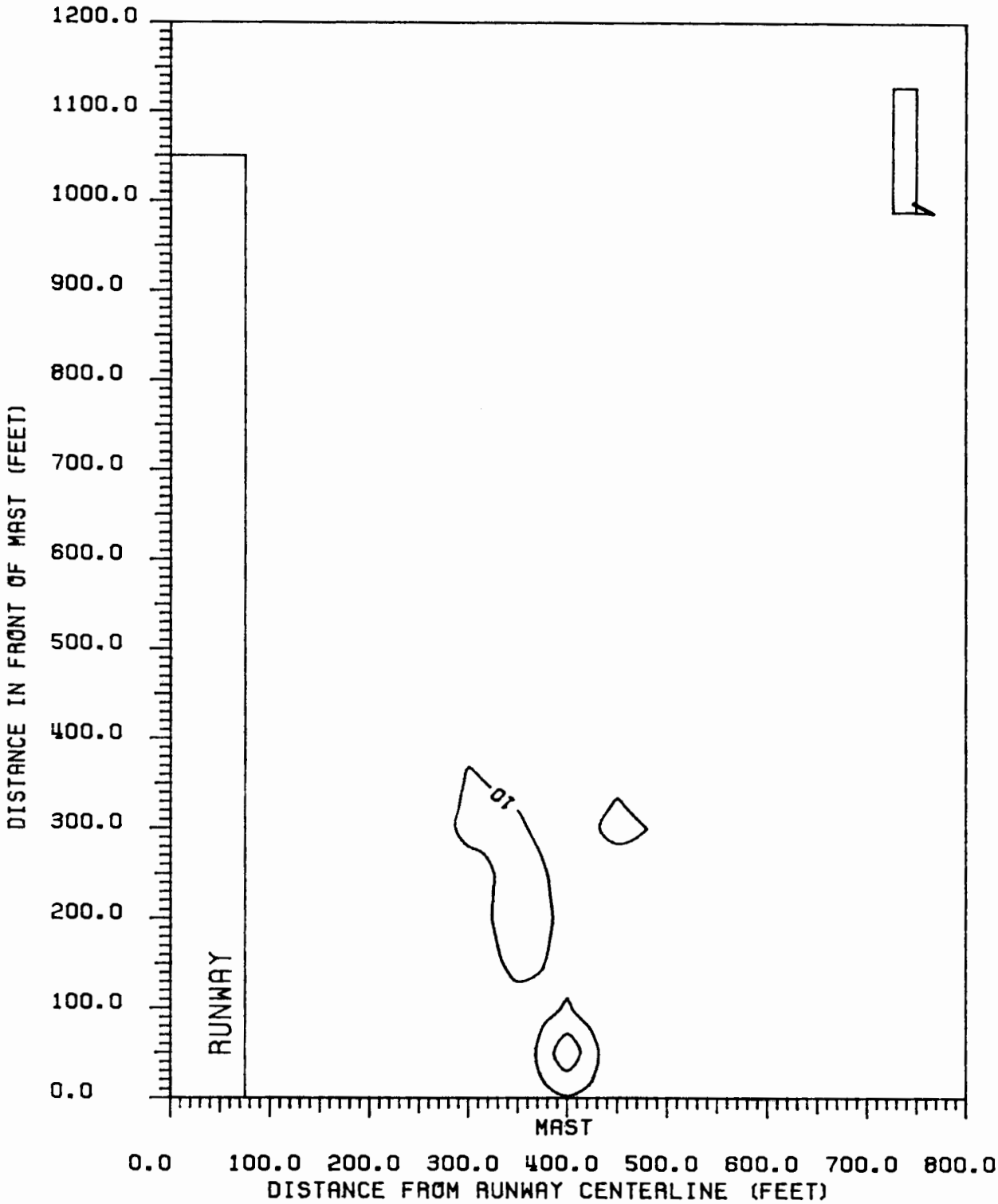

Figure 2-38. Contours of peak CDI values produced between ILS Point C and threshold for an R-500. R-500 fuselage is parallel to runway centerline, with tail towards the mast. Null reference glide slope, directional antennas.

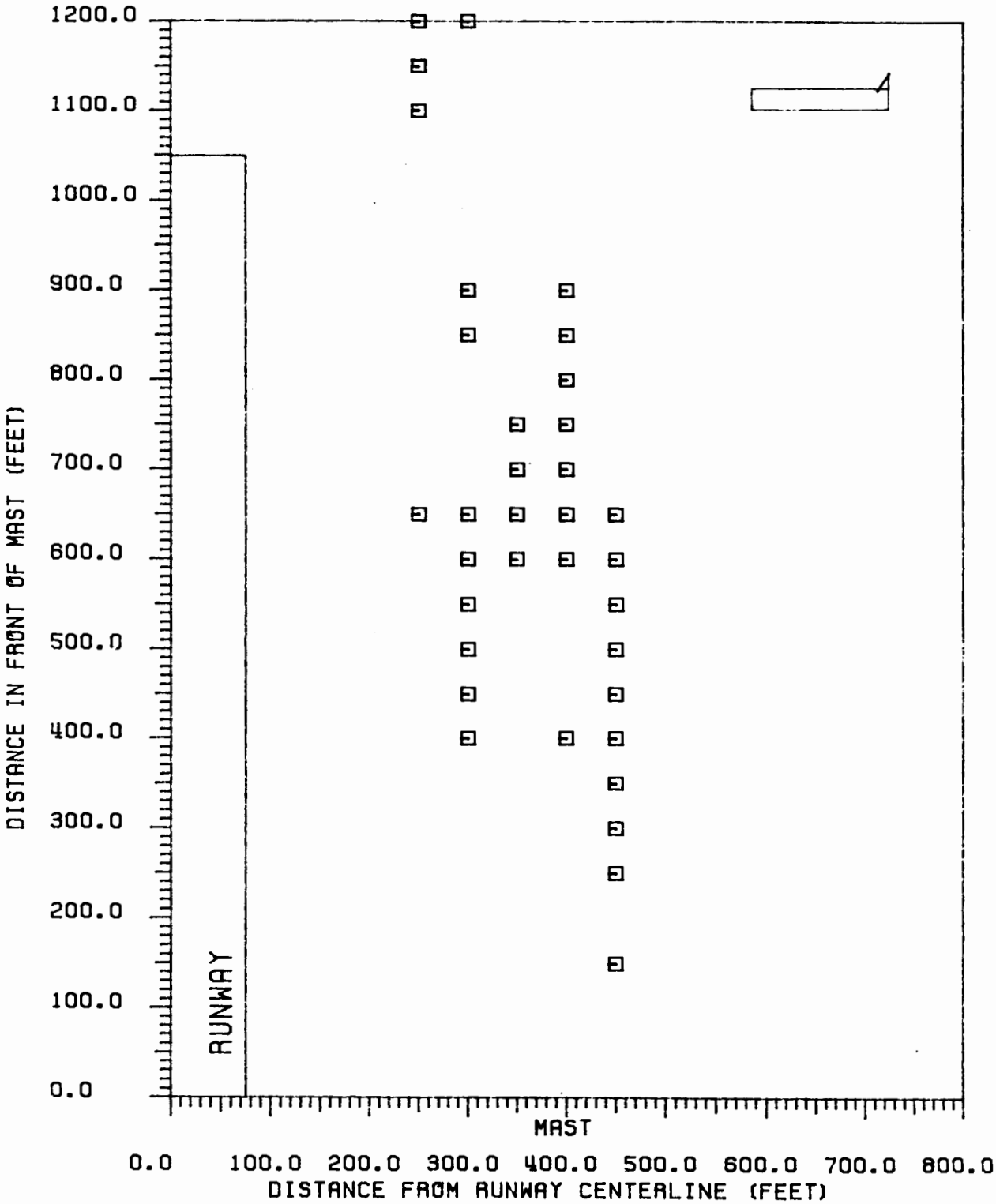

Figure 2-39. Critical area map for CAT I tolerances relating to C-440 aircraft. C-440 fuselage is perpendicular to runway centerline with tail away from the runway. Null reference glide slope, directional antennas.

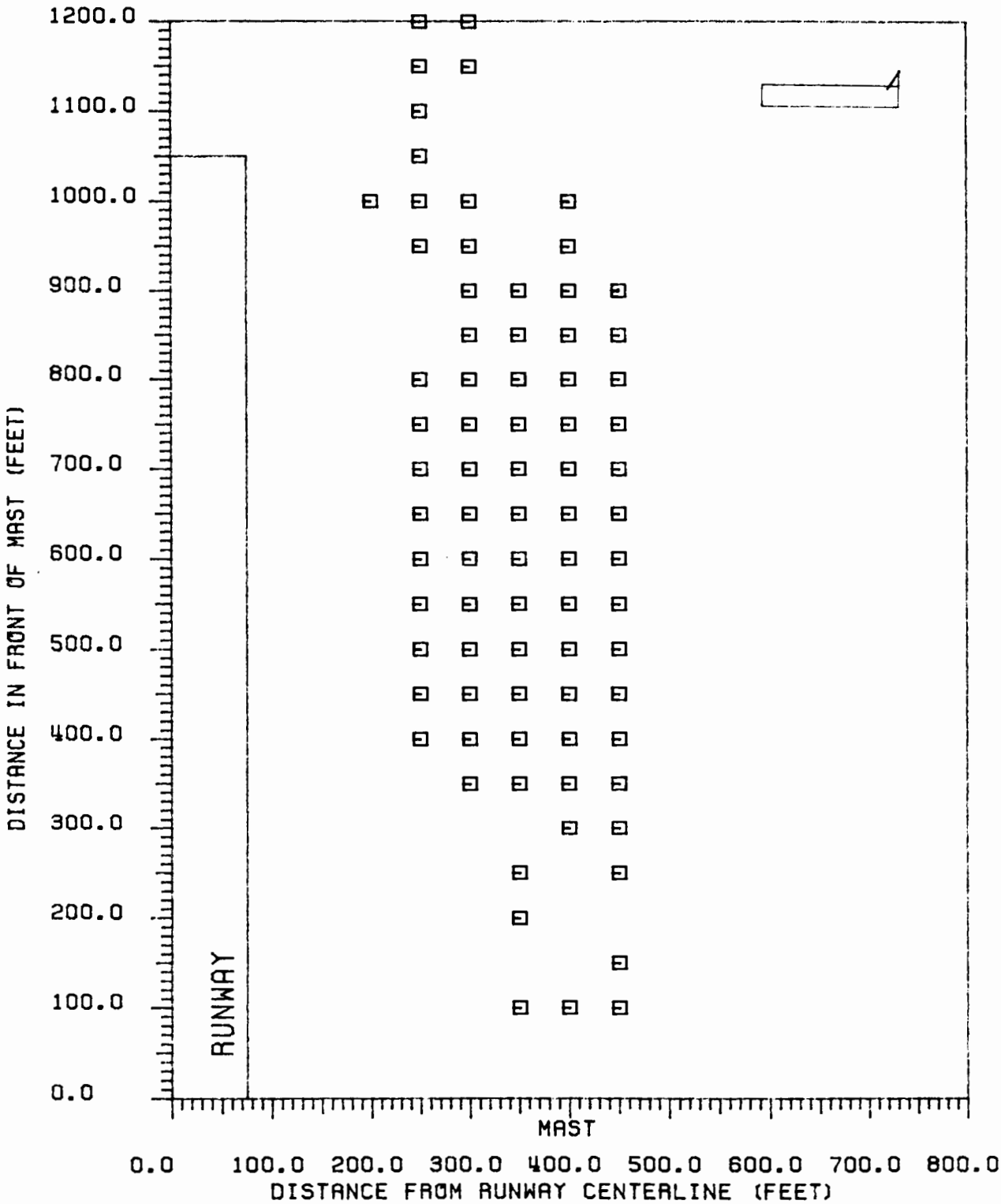

Figure 2-40. Critical area map for CAT II/III tolerances relating to C-440 aircraft. C-440 fuselage is perpendicular to runway centerline with tail away from the runway. Null reference glide slope, directional antennas.

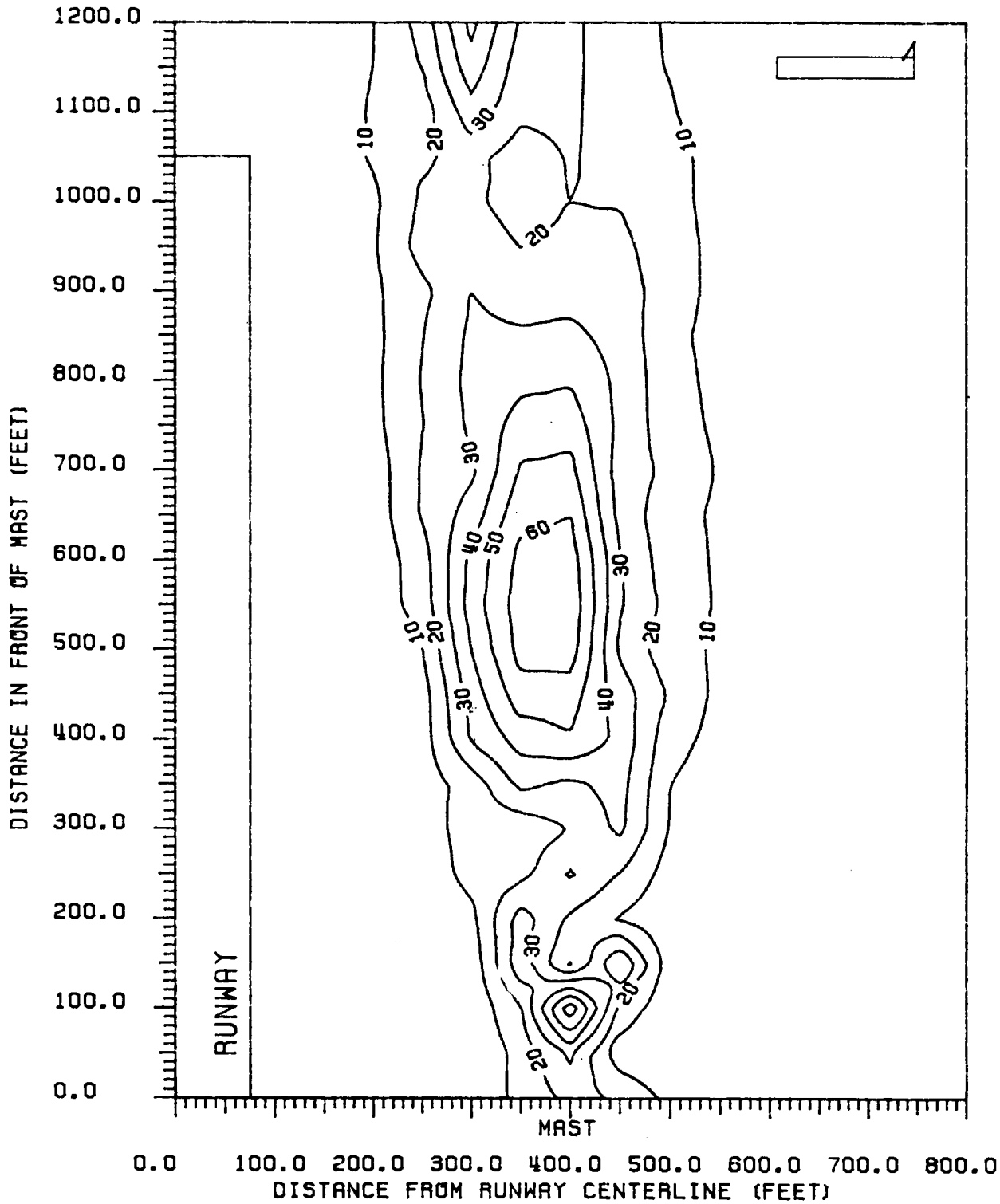

Figure 2-41. Contours of peak CDI values produced in ILS Zone 2 for a C-440. C-440 fuselage is perpendicular to runway centerline, with tail away from the runway. Null reference glide slope, directional antennas.

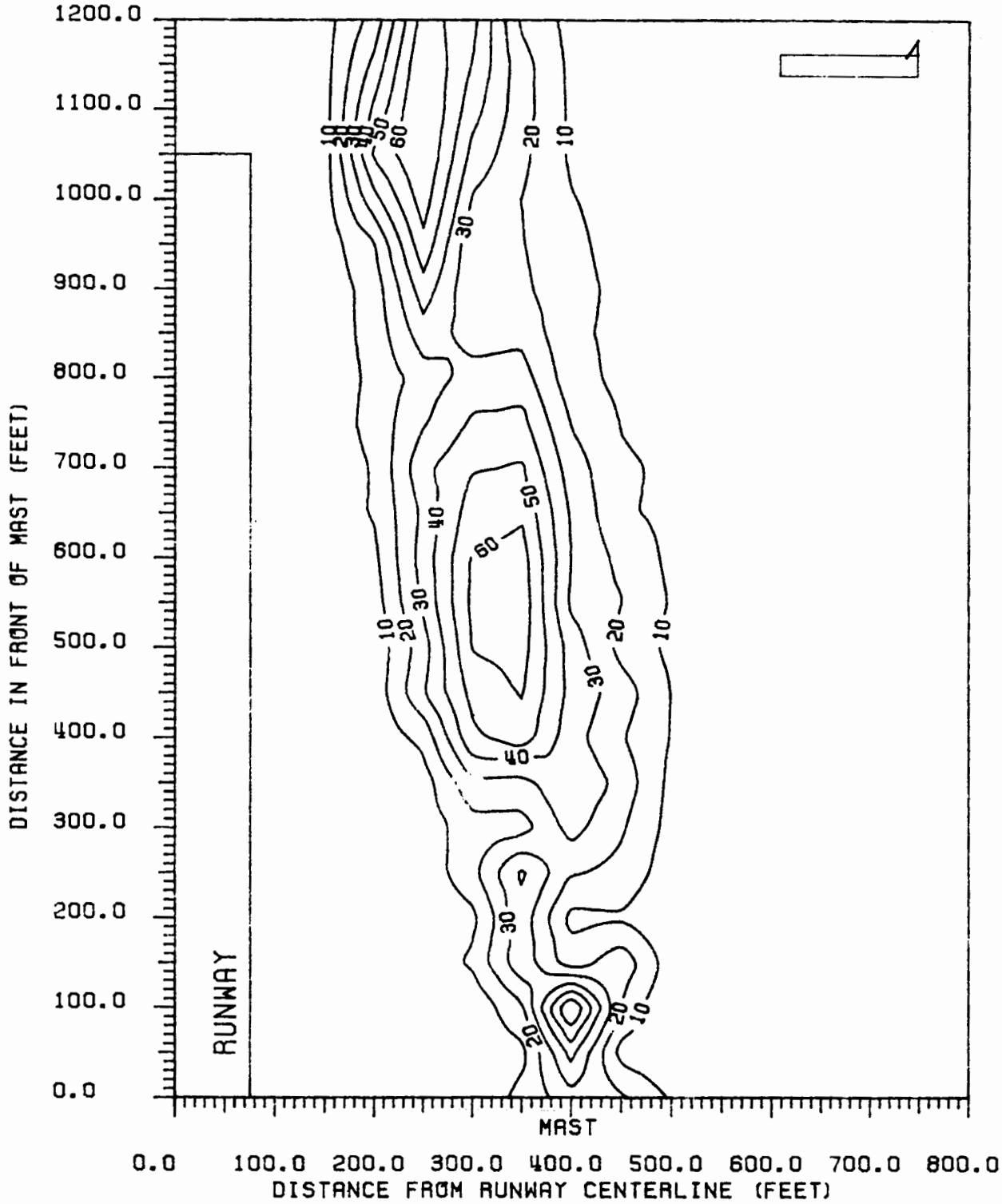

Figure 2-42. Contours of peak CDI values produced between ILS Point B and ILS Point C for a C-440. C-440 fuselage is perpendicular to runway centerline, with tail away from runway. Null reference glide slope, directional antennas.

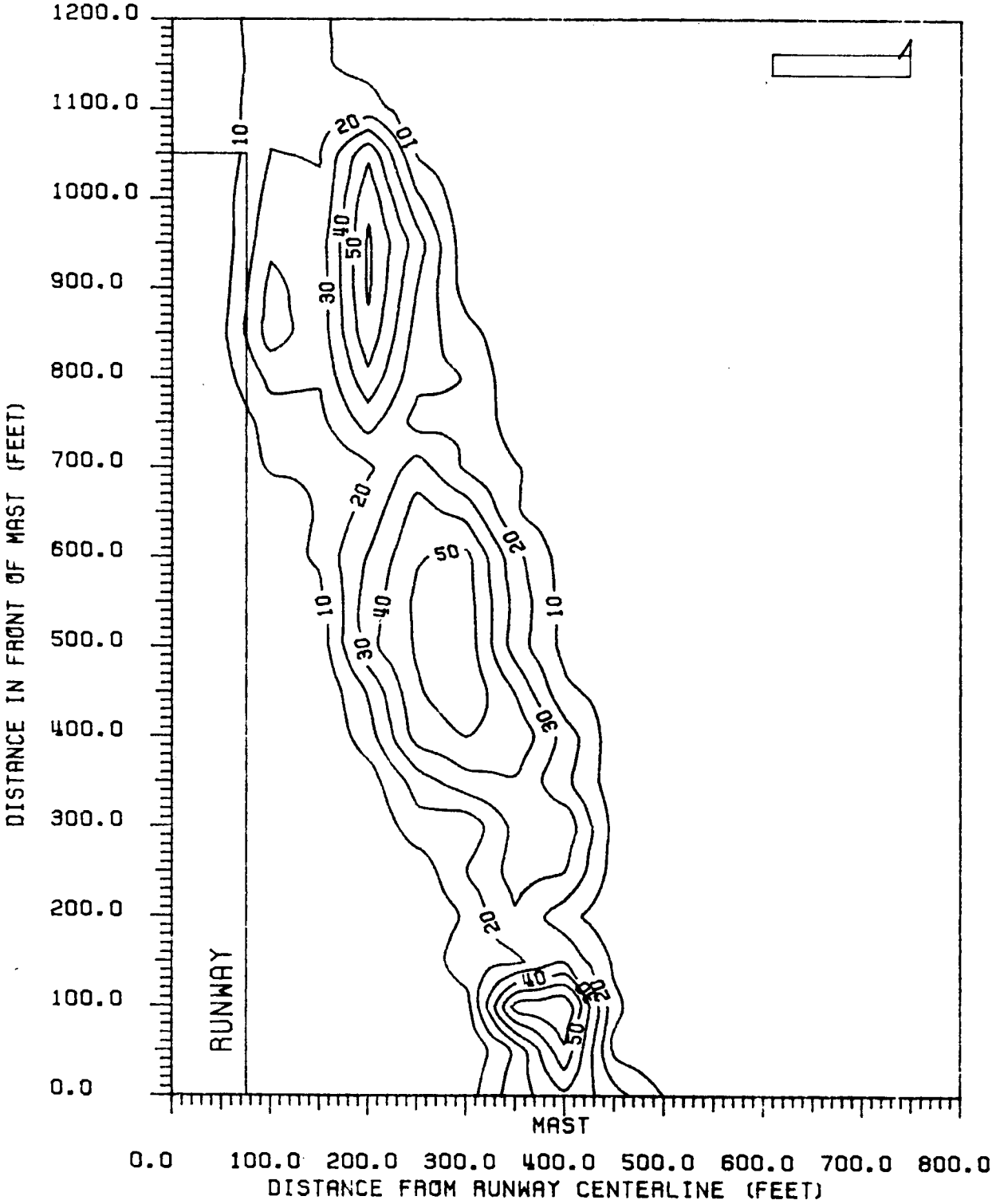

Figure 2-43. Contours of peak CDI values produced between ILS Point C and threshold for a C-440. C-440 fuselage is perpendicular to runway centerline, with tail away from runway. Null reference glide slope, directional antennas.

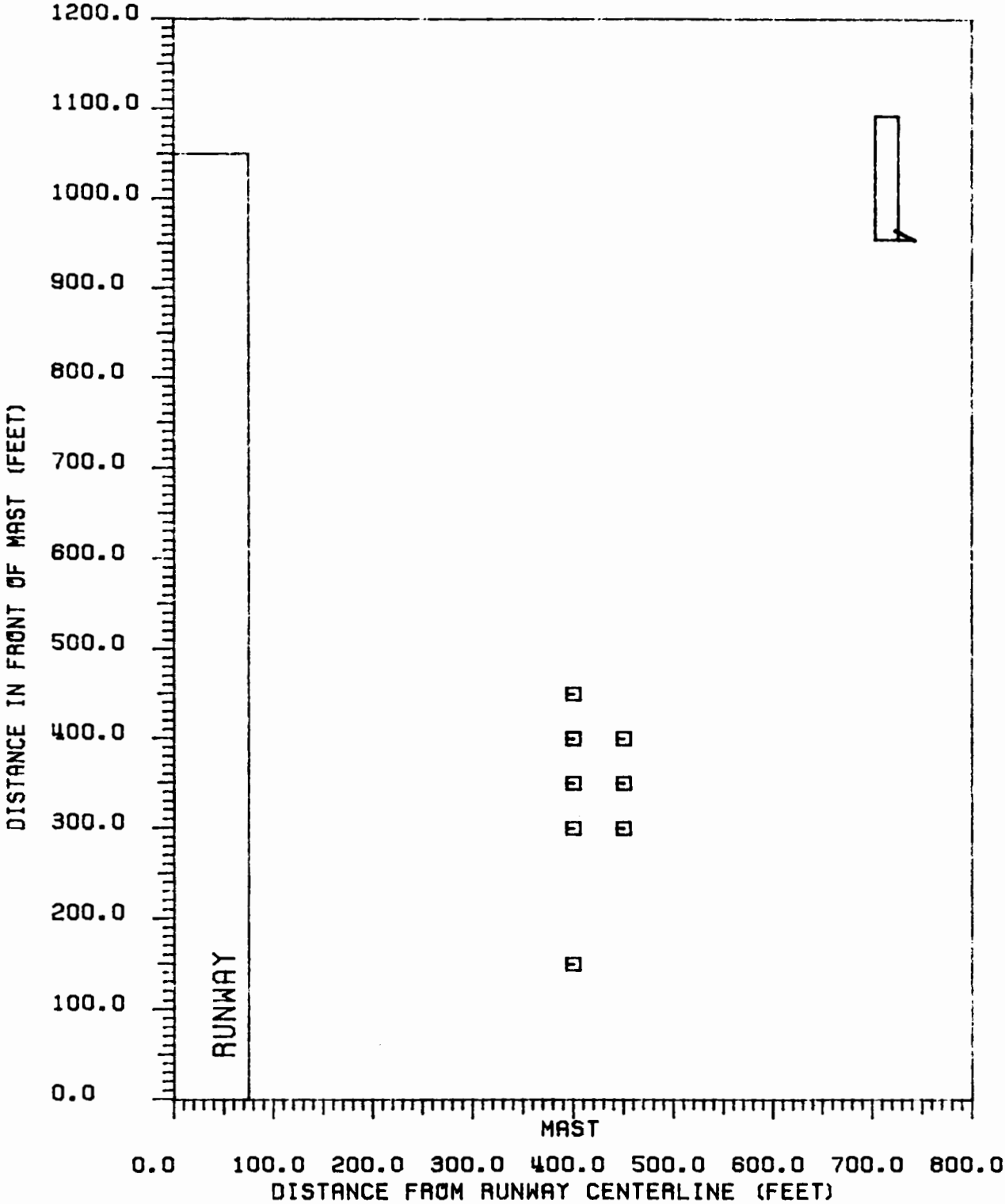

Figure 2-44. Critical area map for CAT I tolerances relating to C-440 aircraft. C-440 fuselage is parallel to runway centerline with tail towards the mast. Null reference glide slope, directional antennas.

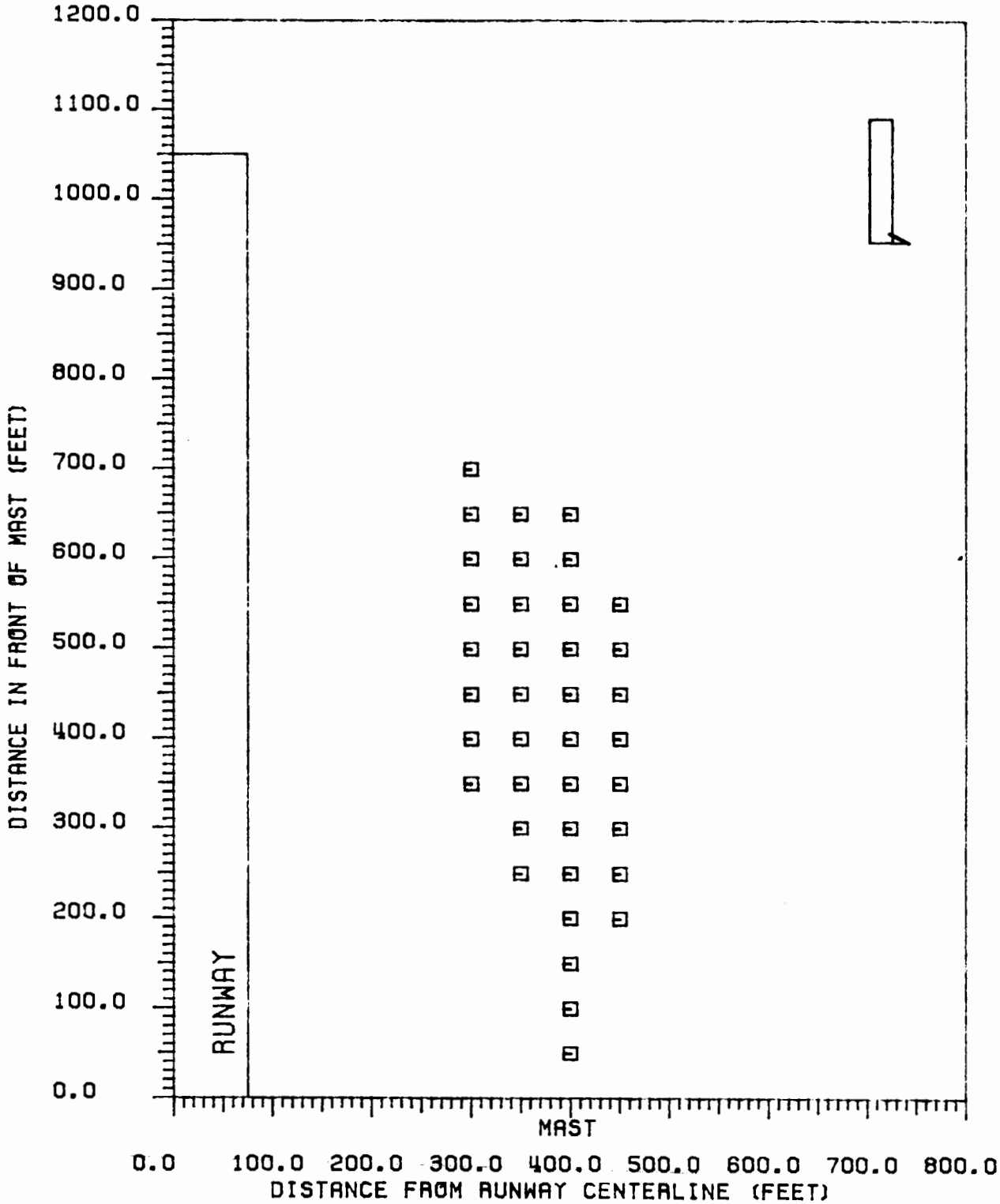

Figure 2-45. Critical area map for CAT II/III tolerances relating to C-440 aircraft. C-440 fuselage is parallel to runway centerline with tail towards the mast. Null reference glide slope, directional antennas.

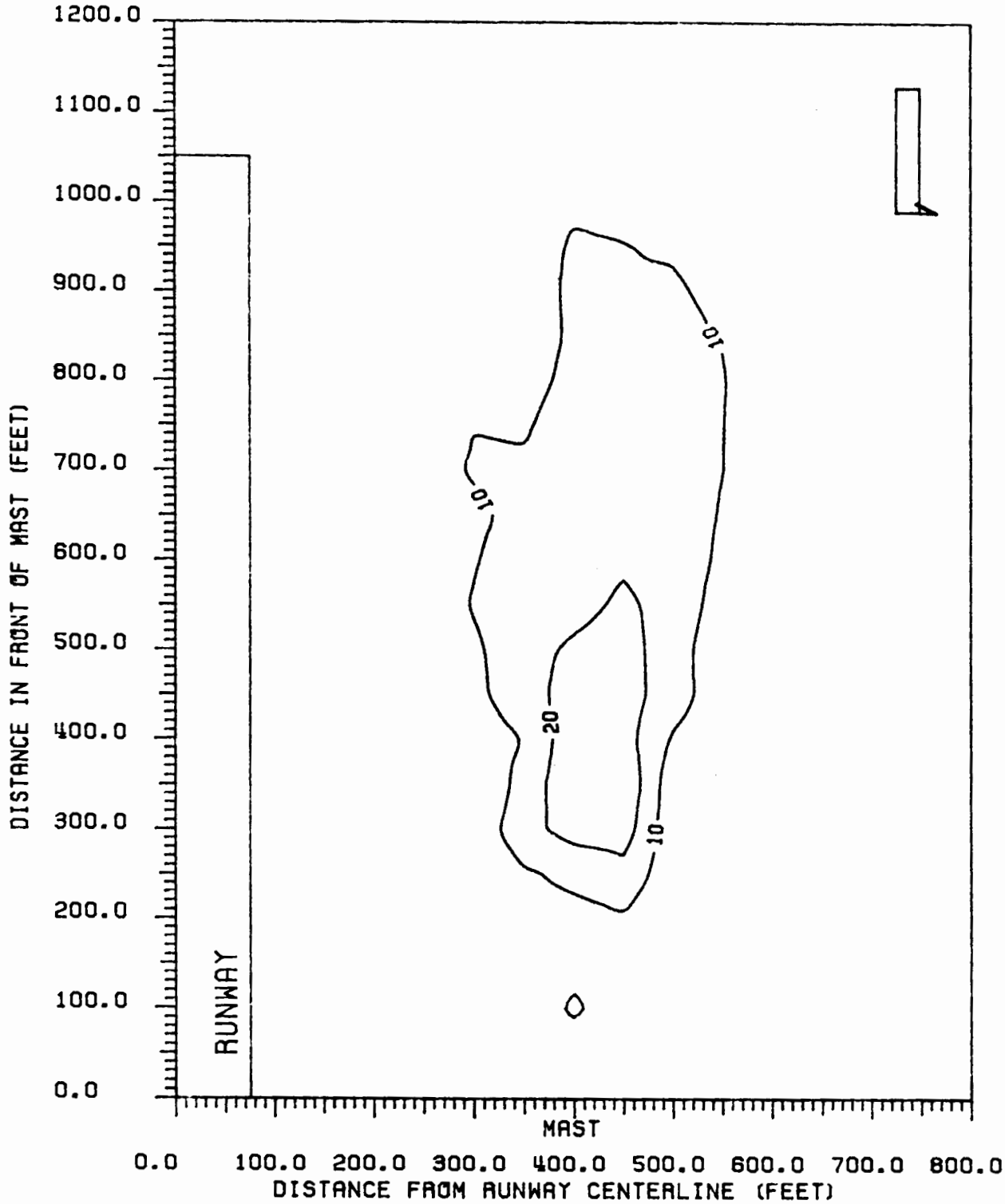

Figure 2-46. Contours of peak CDI values produced in ILS Zone 2 for a C-440. C-440 fuselage is parallel to runway centerline, with tail towards the mast. Null reference glide slope, directional antennas.

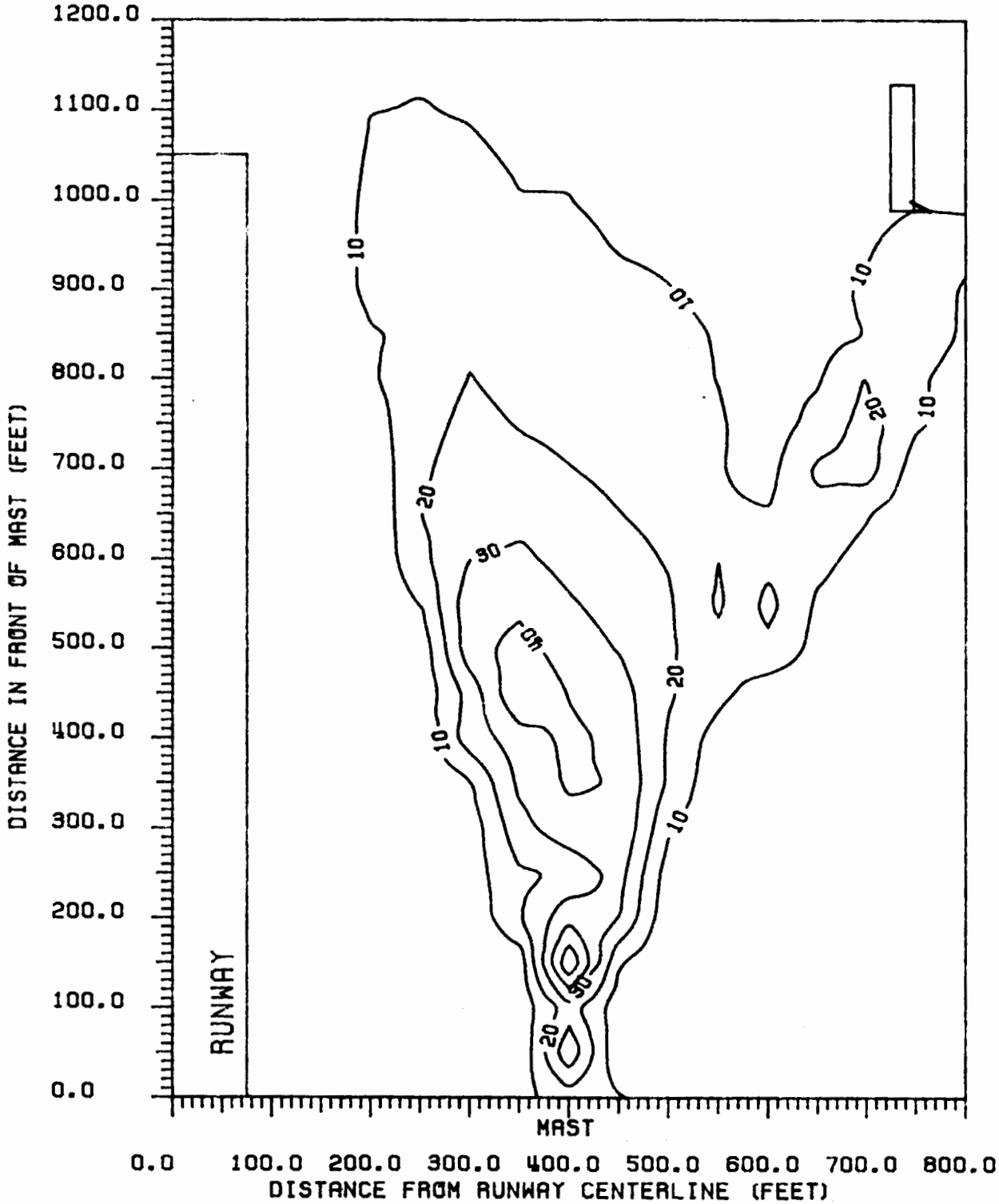

Figure 2-47. Contours of peak CDI values produced between ILS Point B and ILS Point C for a C-440. C-440 fuselage is parallel to runway centerline, with tail towards the mast. Null reference glide slope, directional antennas.

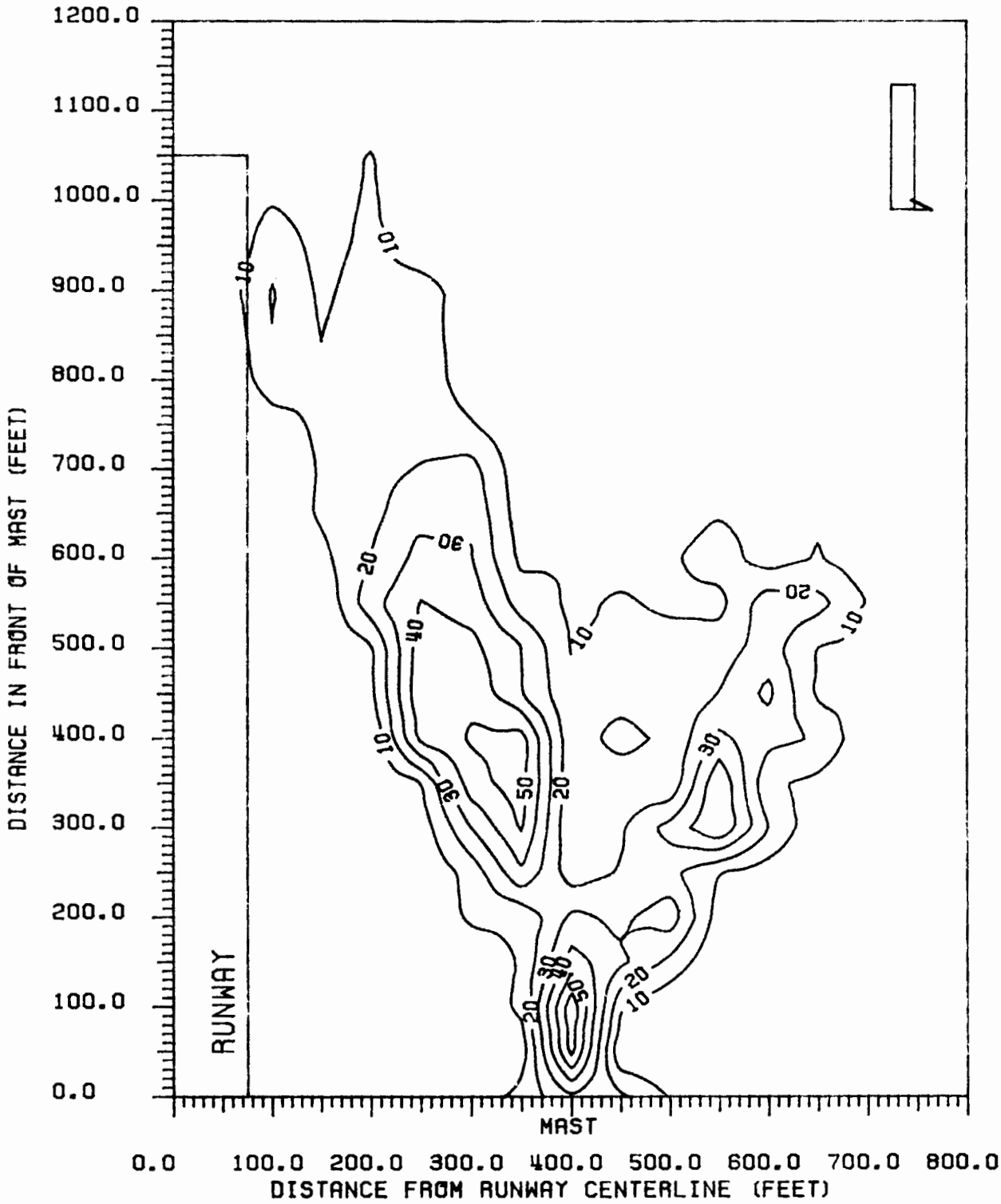

Figure 2-48. Contours of peak CDI values produced between ILS Point C and threshold for a C-440. C-440 fuselage is parallel to runway centerline, with tail towards the mast. Null reference glide slope, directional antennas.

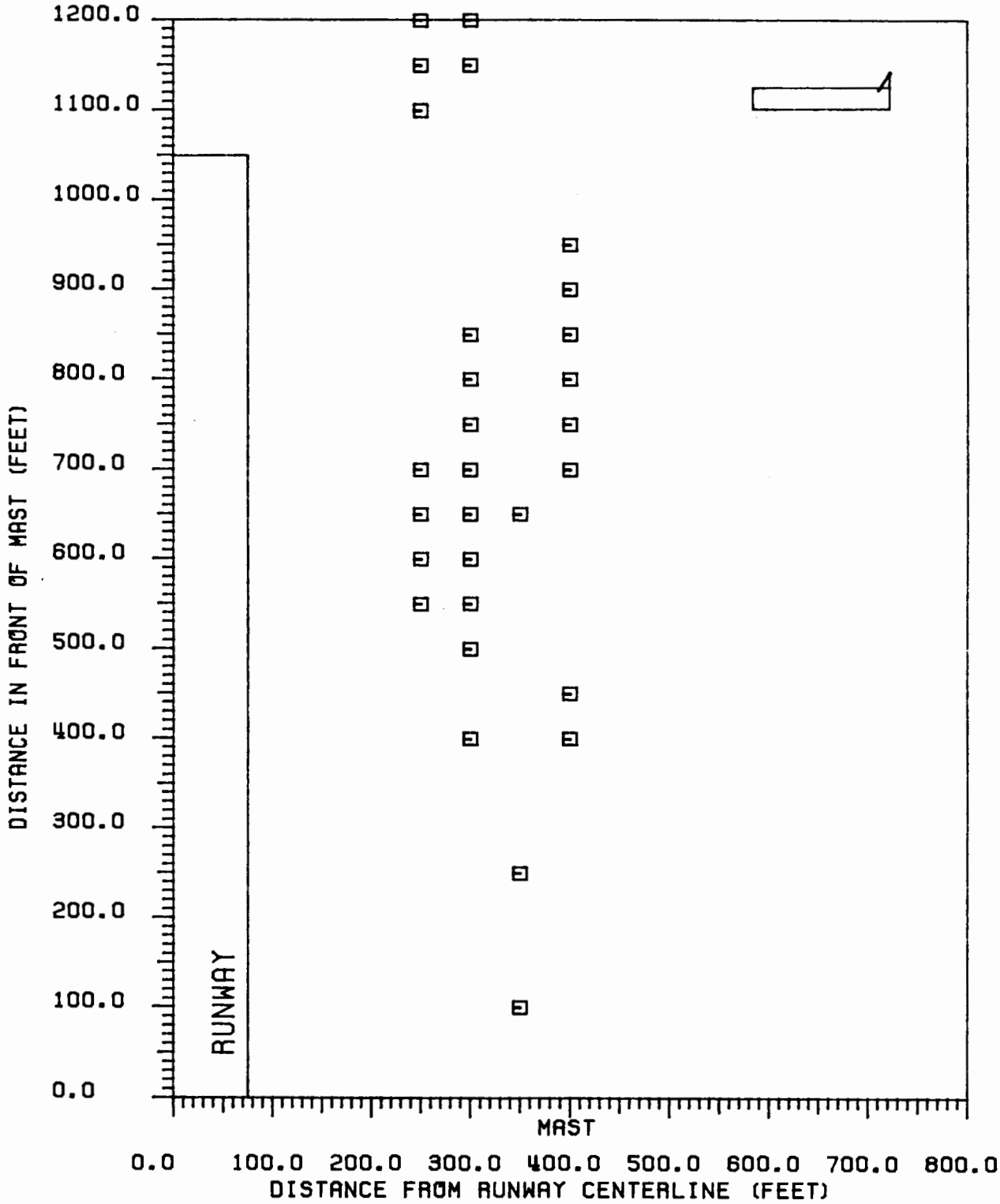

Figure 2-49. Critical area map for CAT I tolerances relating to DC-9 aircraft. DC-9 fuselage is perpendicular to runway centerline with tail away from the runway. Null reference glide slope, directional antennas.

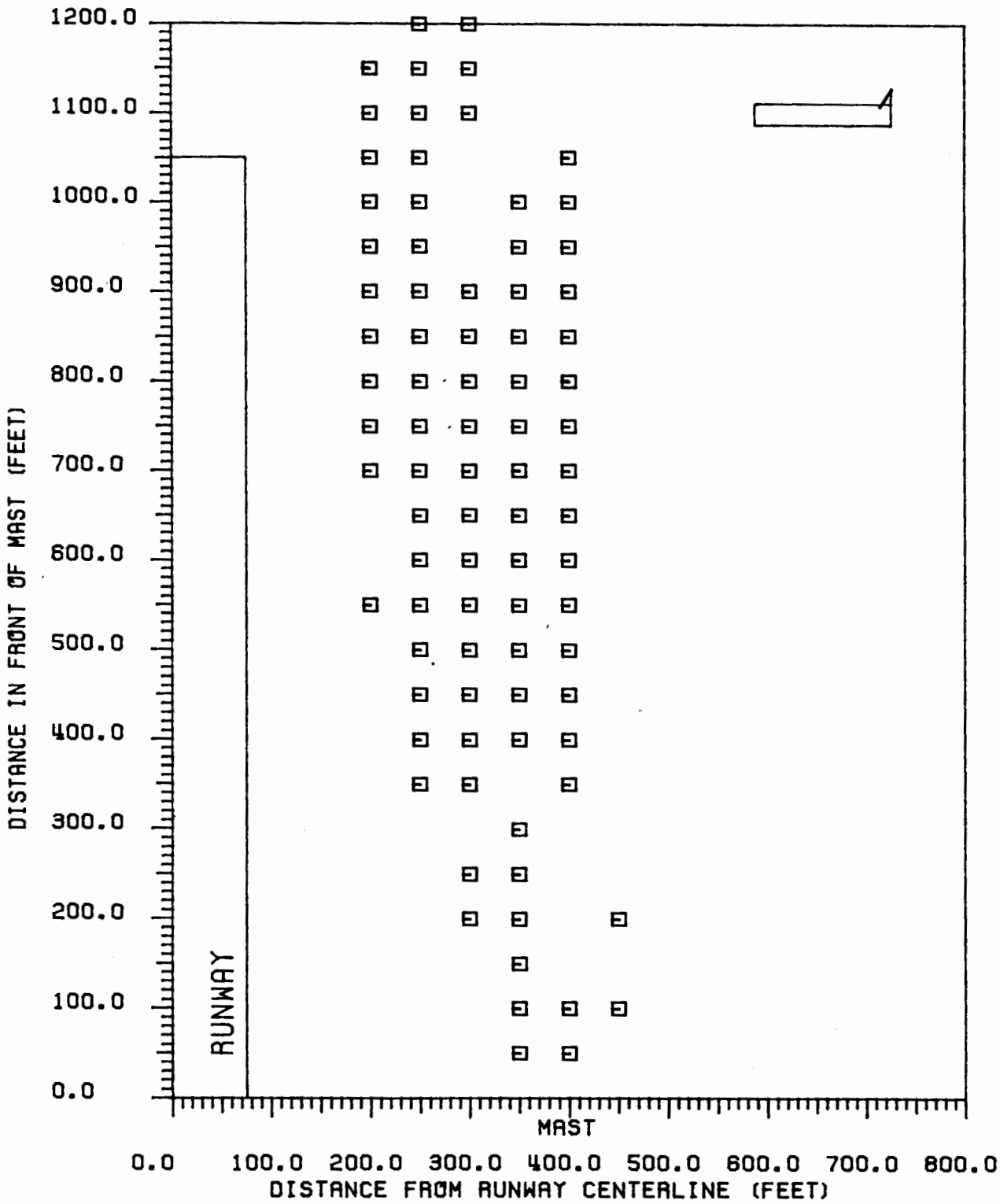

Figure 2-50. Critical area map for CAT II/III tolerances relating to DC-9 aircraft. DC-9 fuselage is perpendicular to runway centerline with tail away from the runway. Null reference glide slope, directional antennas.

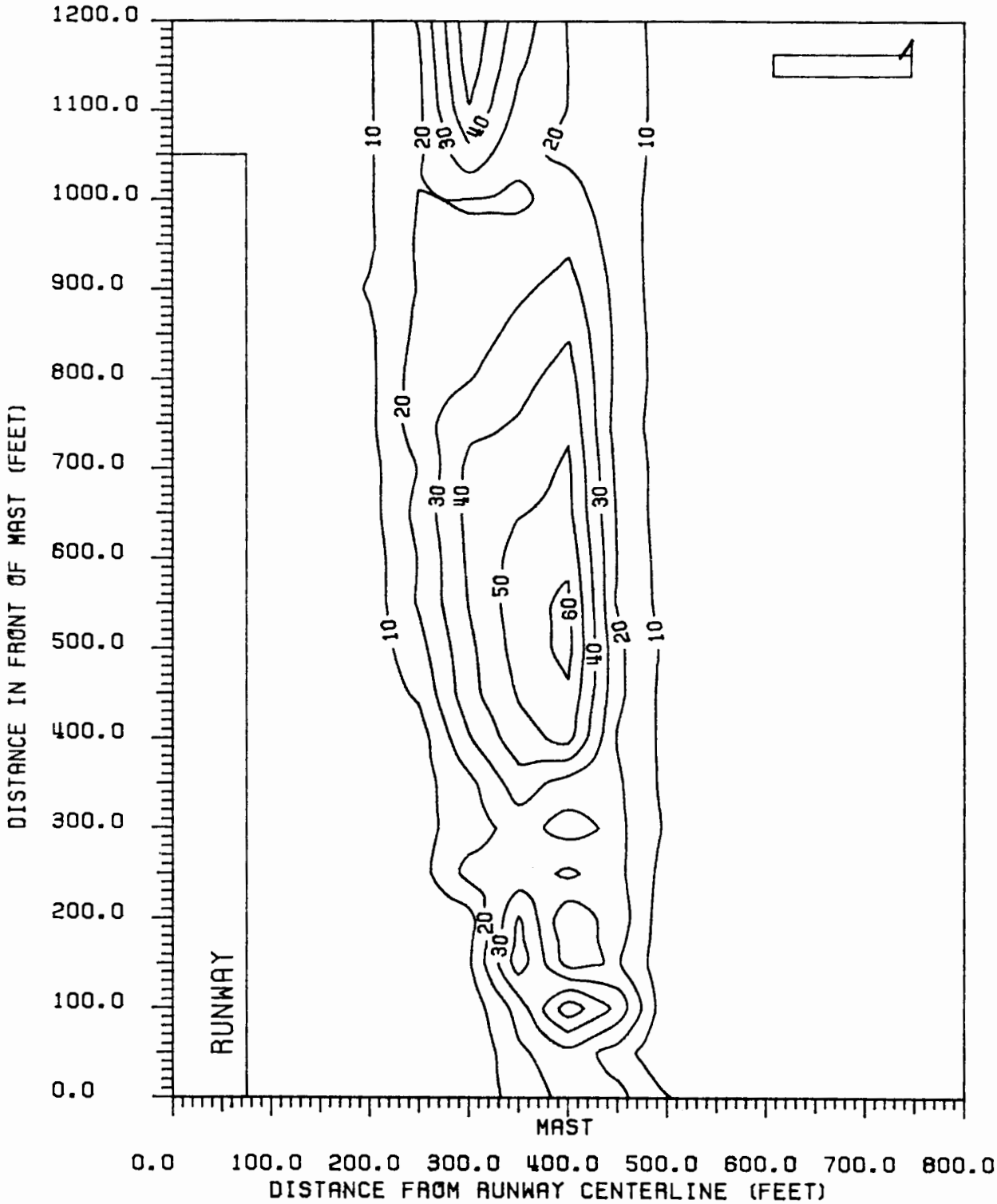

Figure 2-51. Contours of peak CDI values produced in ILS Zone 2 for a DC-9. DC-9 fuselage is perpendicular to runway centerline, with tail away from the runway. Null reference glide slope, directional antennas.

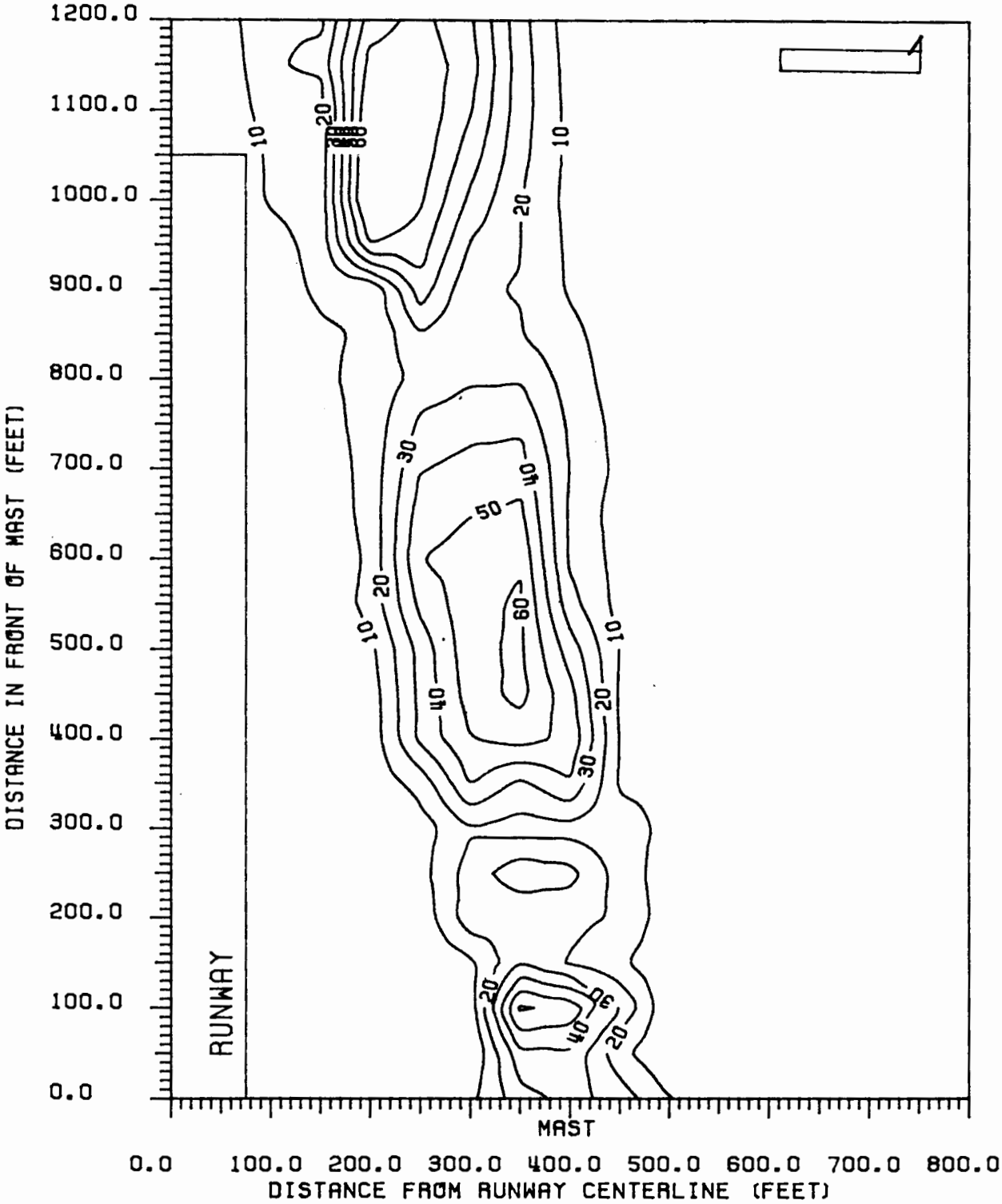

Figure 2-52. Contours of peak CDI values produced between ILS Point B and ILS Point C for a DC-9. DC-9 fuselage is perpendicular to runway centerline, with tail away from runway. Null reference glide slope, directional antennas.

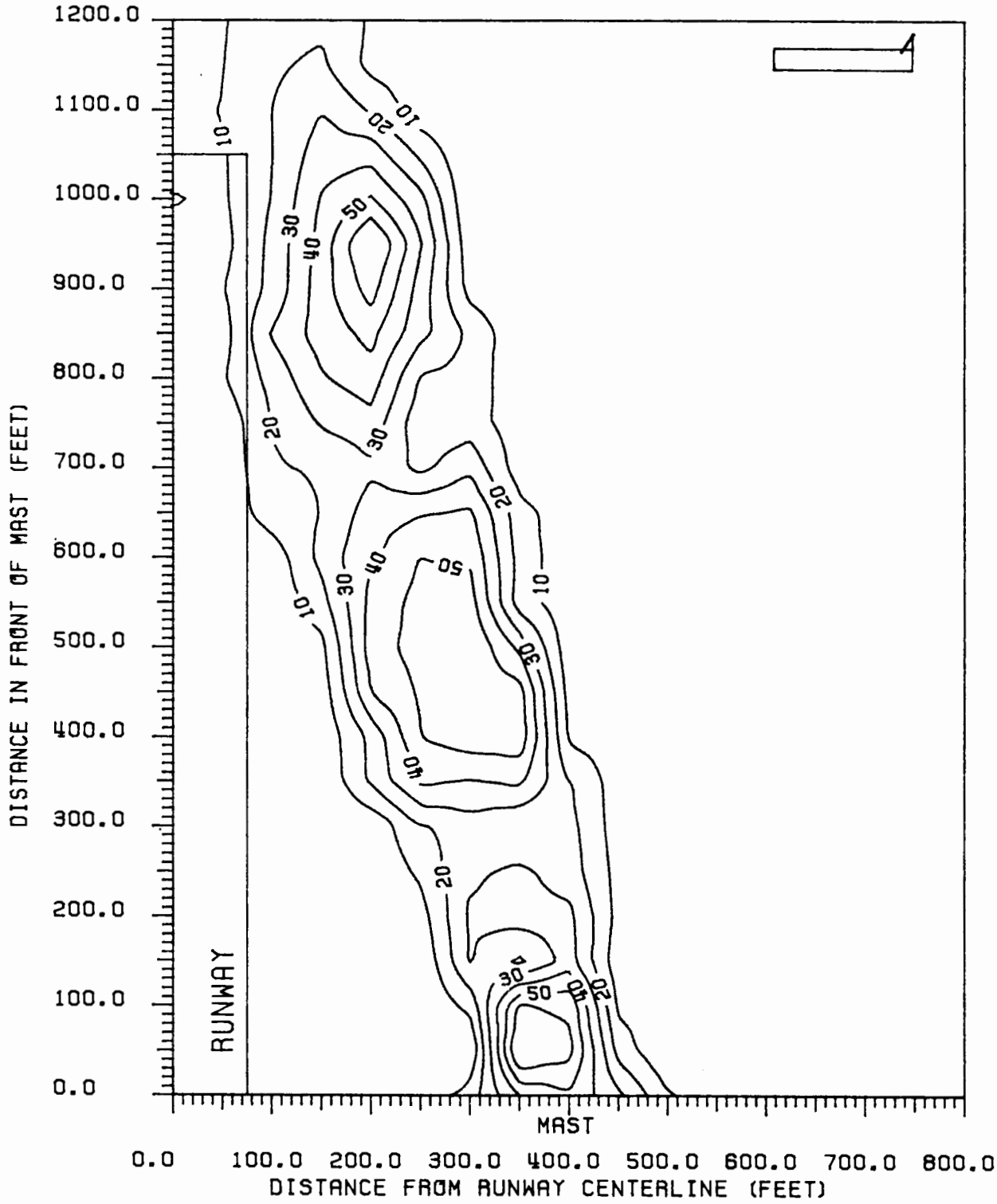

Figure 2-53. Contours of peak CDI values produced between ILS Point C and threshold for a DC-9. DC-9 fuselage is perpendicular to runway centerline, with tail away from runway. Null reference glide slope, directional antennas.

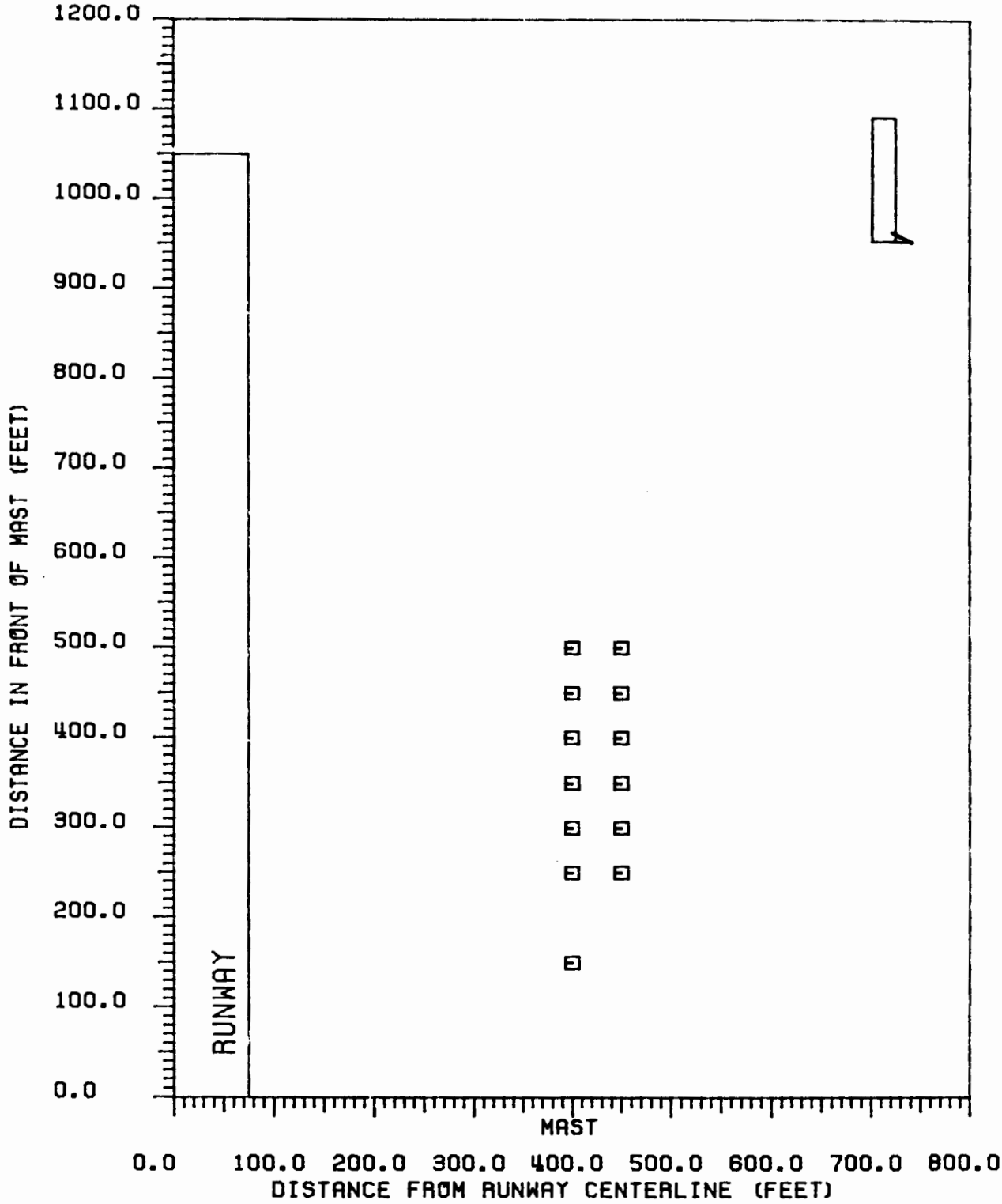

Figure 2-54. Critical area map for CAT I tolerances relating to DC-9 aircraft. DC-9 fuselage is parallel to runway centerline with tail towards the mast. Null reference glide slope, directional antennas.

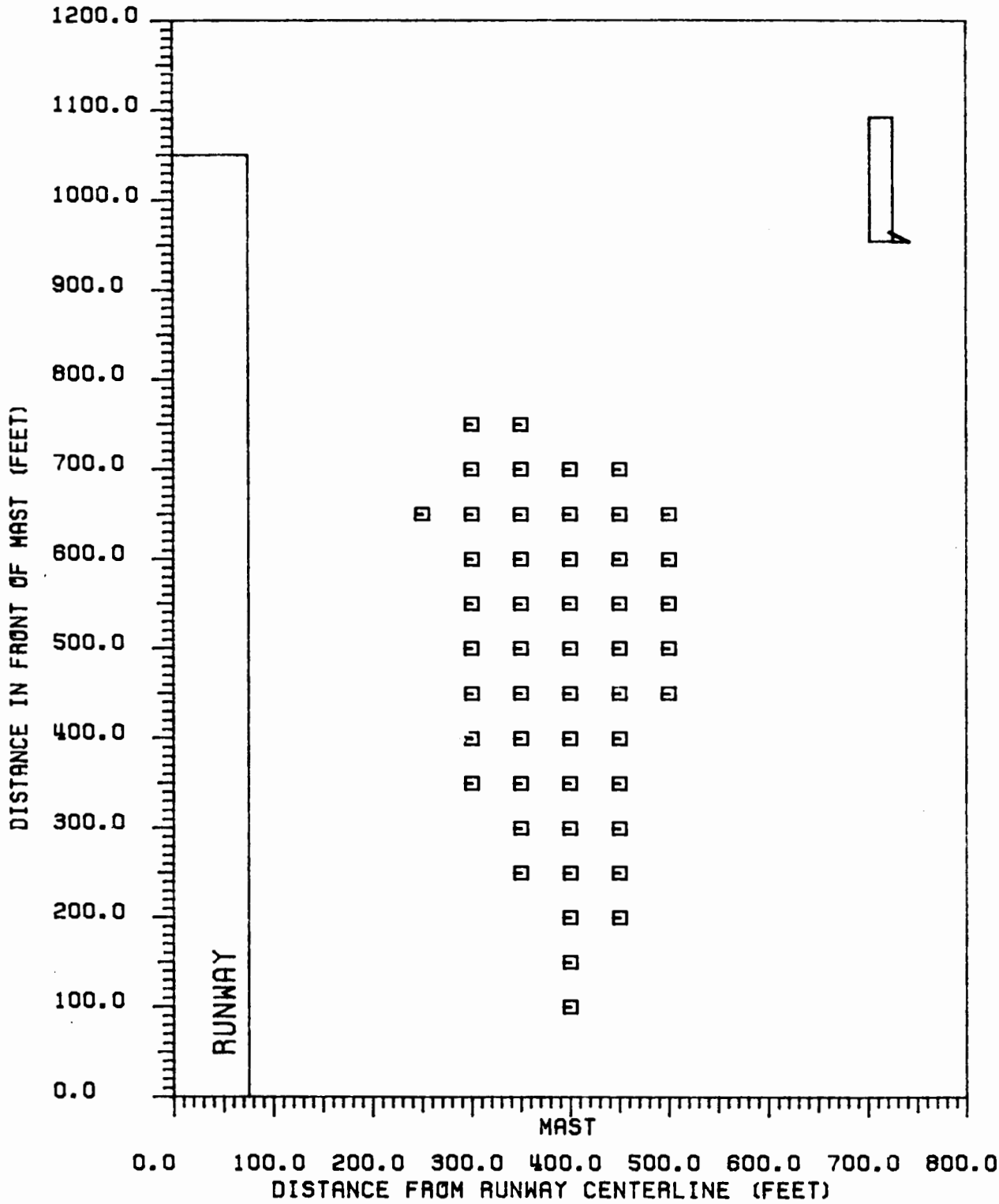

Figure 2-55. Critical area map for CAT II/III tolerances relating to DC-9 aircraft. DC-9 fuselage is parallel to runway centerline with tail towards the mast. Null reference glide slope, directional antennas.

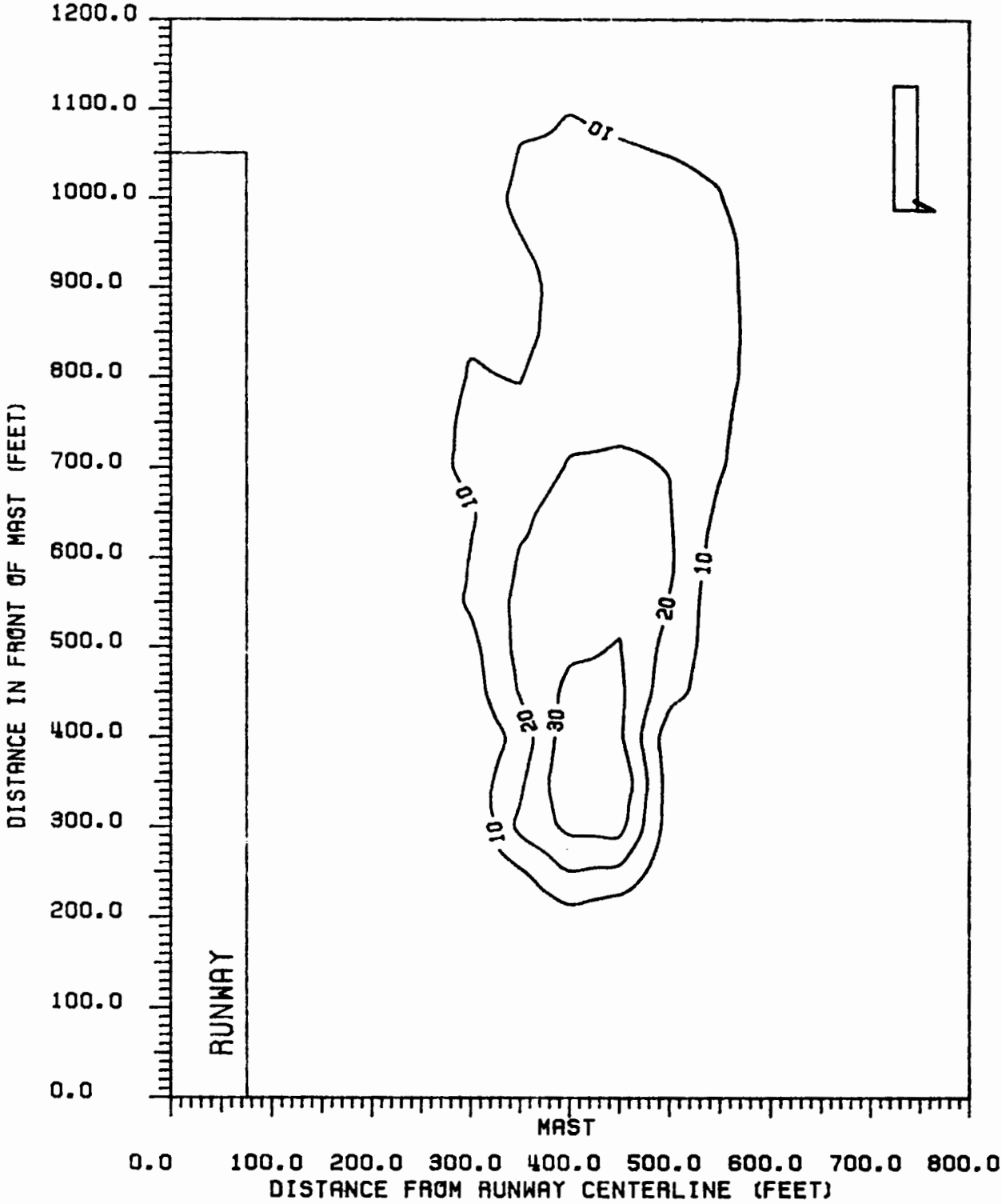

Figure 2-56. Contours of peak CDI values produced in ILS Zone 2 for a DC-9. DC-9 fuselage is parallel to runway centerline, with tail towards the mast. Null reference glide slope, directional antennas.

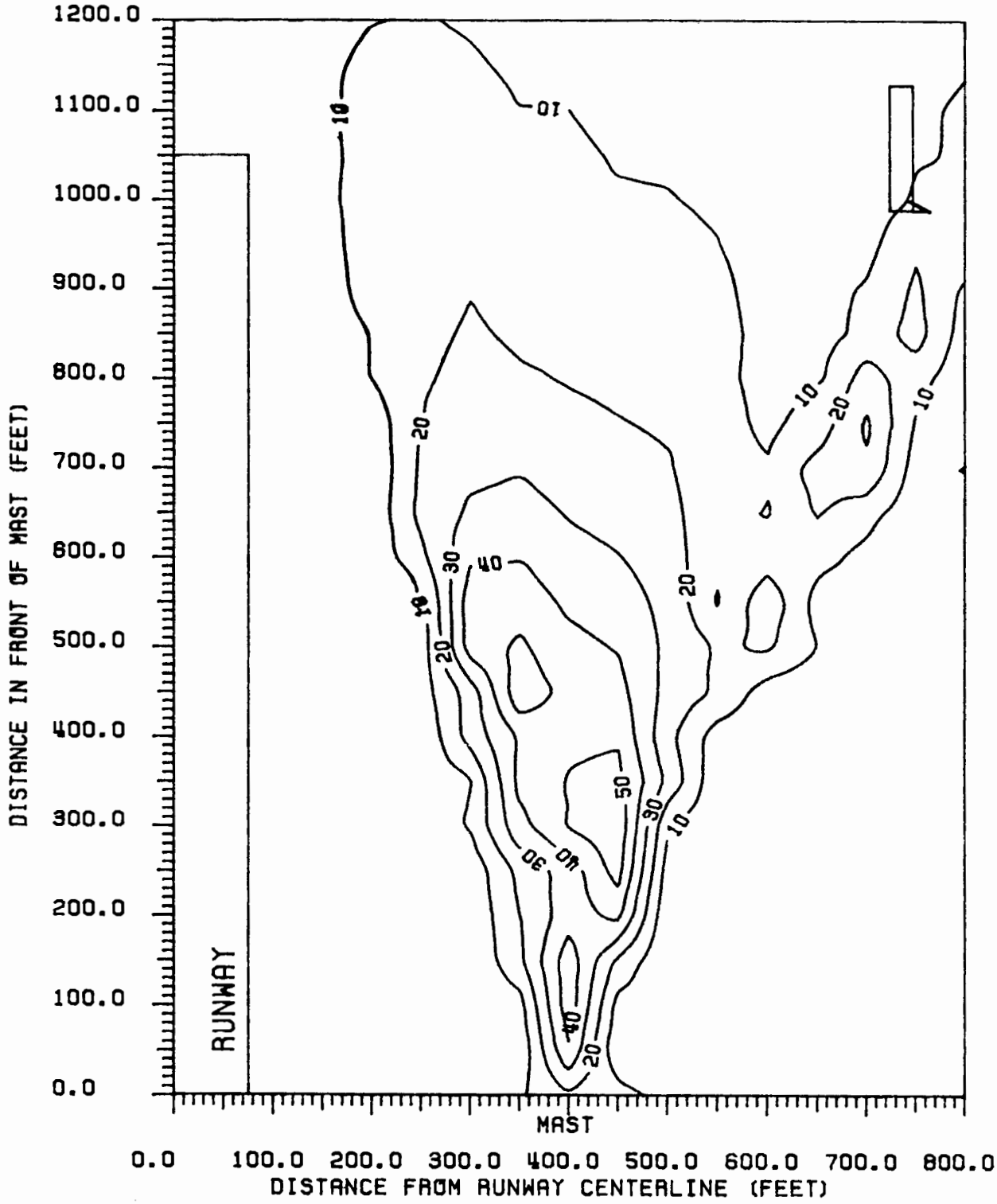

Figure 2-57. Contours of peak CDI values produced between ILS Point B and ILS Point C for a DC-9. DC-9 fuselage is parallel to runway centerline, with tail towards the mast. Null reference glide slope, directional antennas.

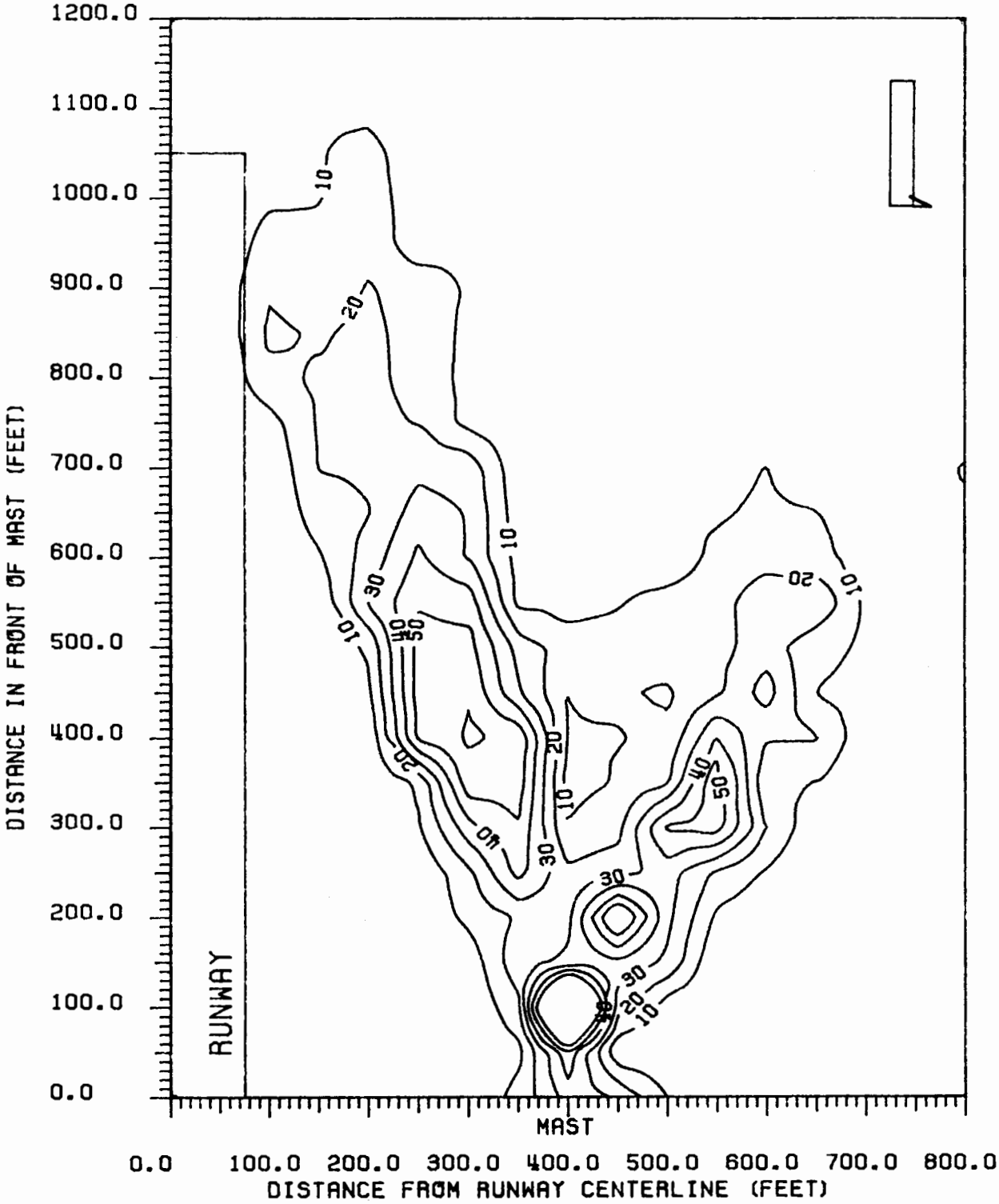

Figure 2-58. Contours of peak CDI values produced between ILS Point C and threshold for a DC-9. DC-9 fuselage is parallel to runway centerline, with tail towards the mast. Null reference glide slope, directional antennas.

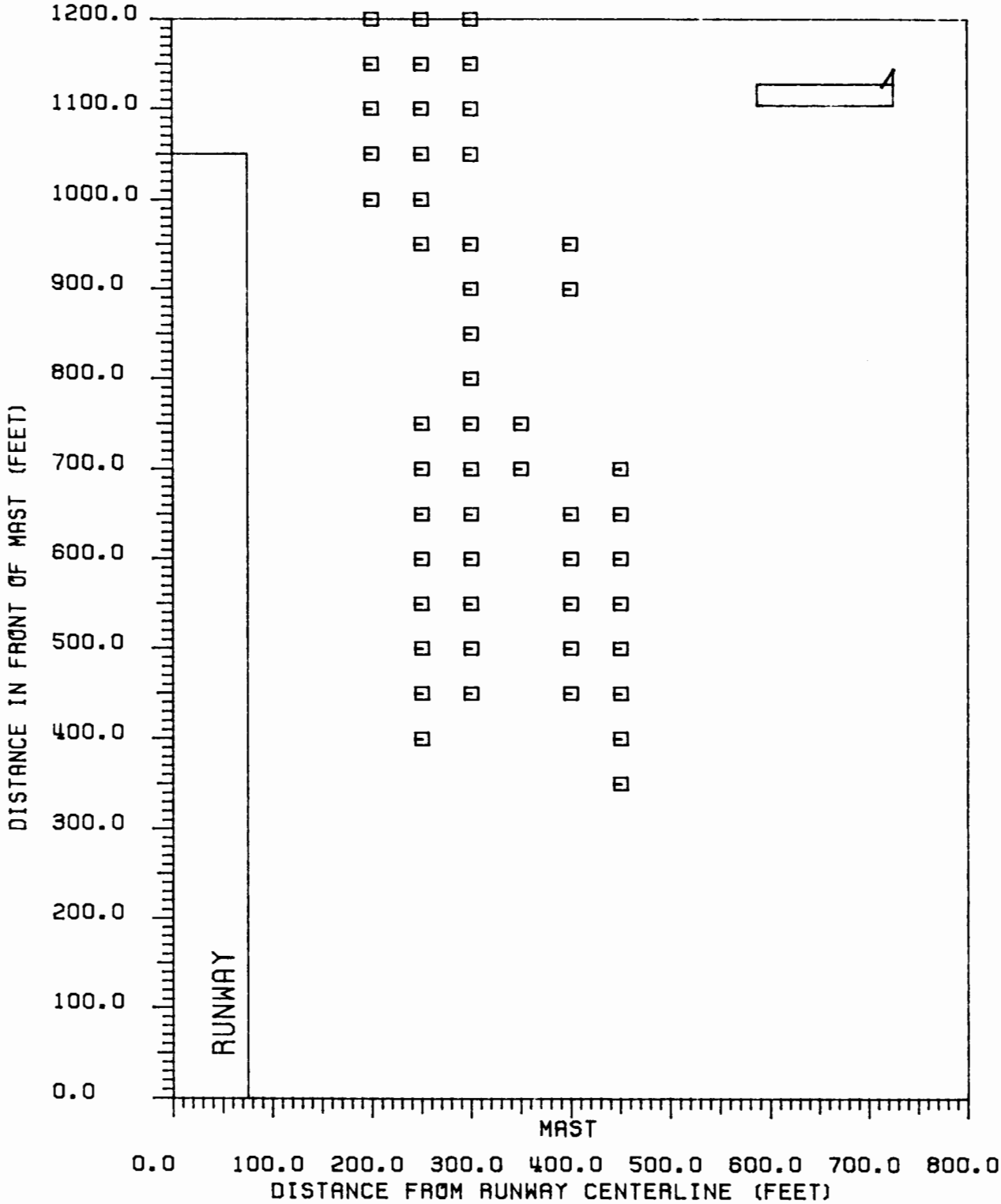

Figure 2-59. Critical area map for CAT I tolerances relating to B-727 aircraft. B-727 fuselage is perpendicular to runway centerline with tail away from the runway. Null reference glide slope, directional antennas.

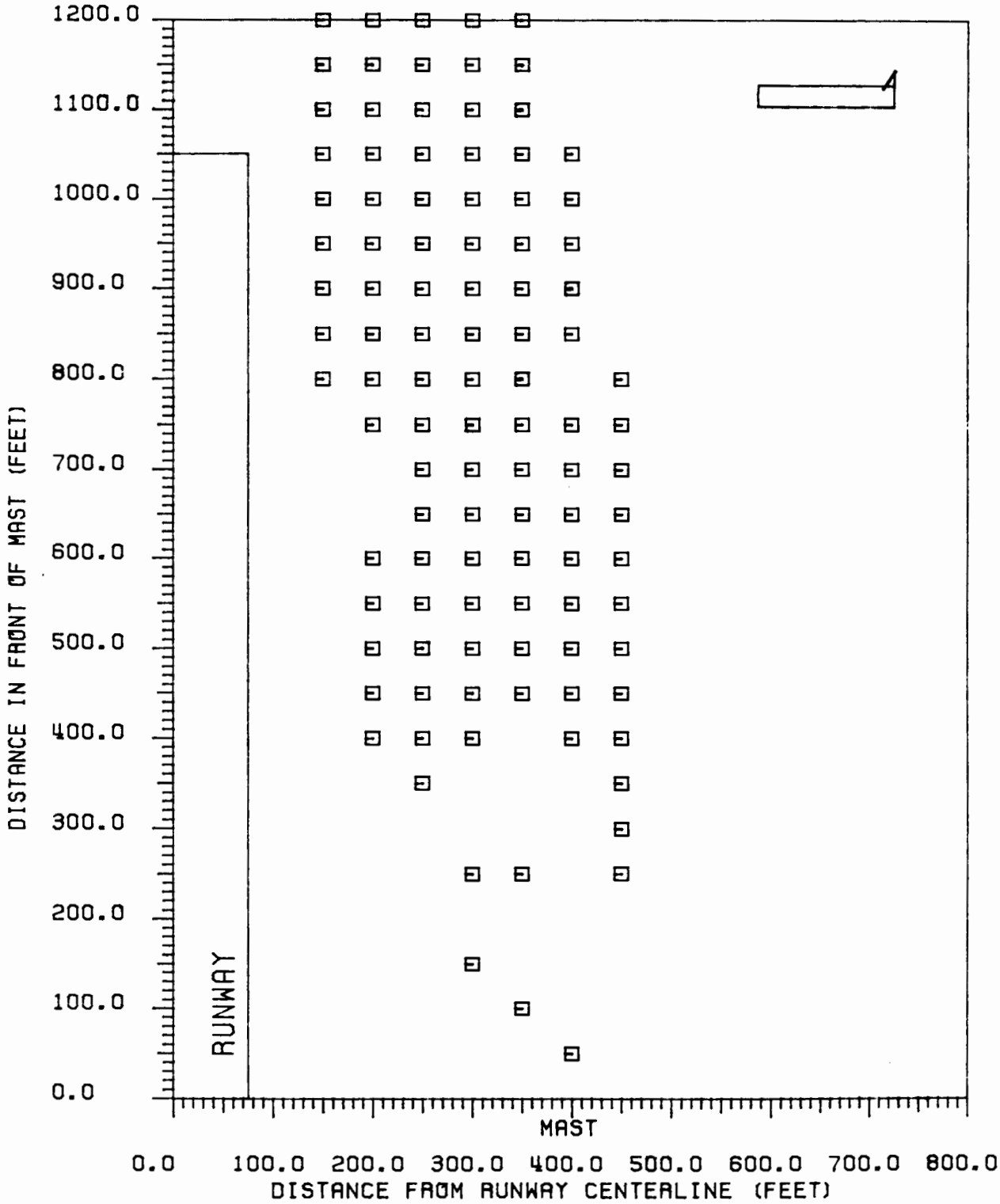

Figure 2-60. Critical area map for CAT II/III tolerances relating to B-727 aircraft. B-727 fuselage is perpendicular to runway centerline with tail away from the runway. Null reference glide slope, directional antennas.

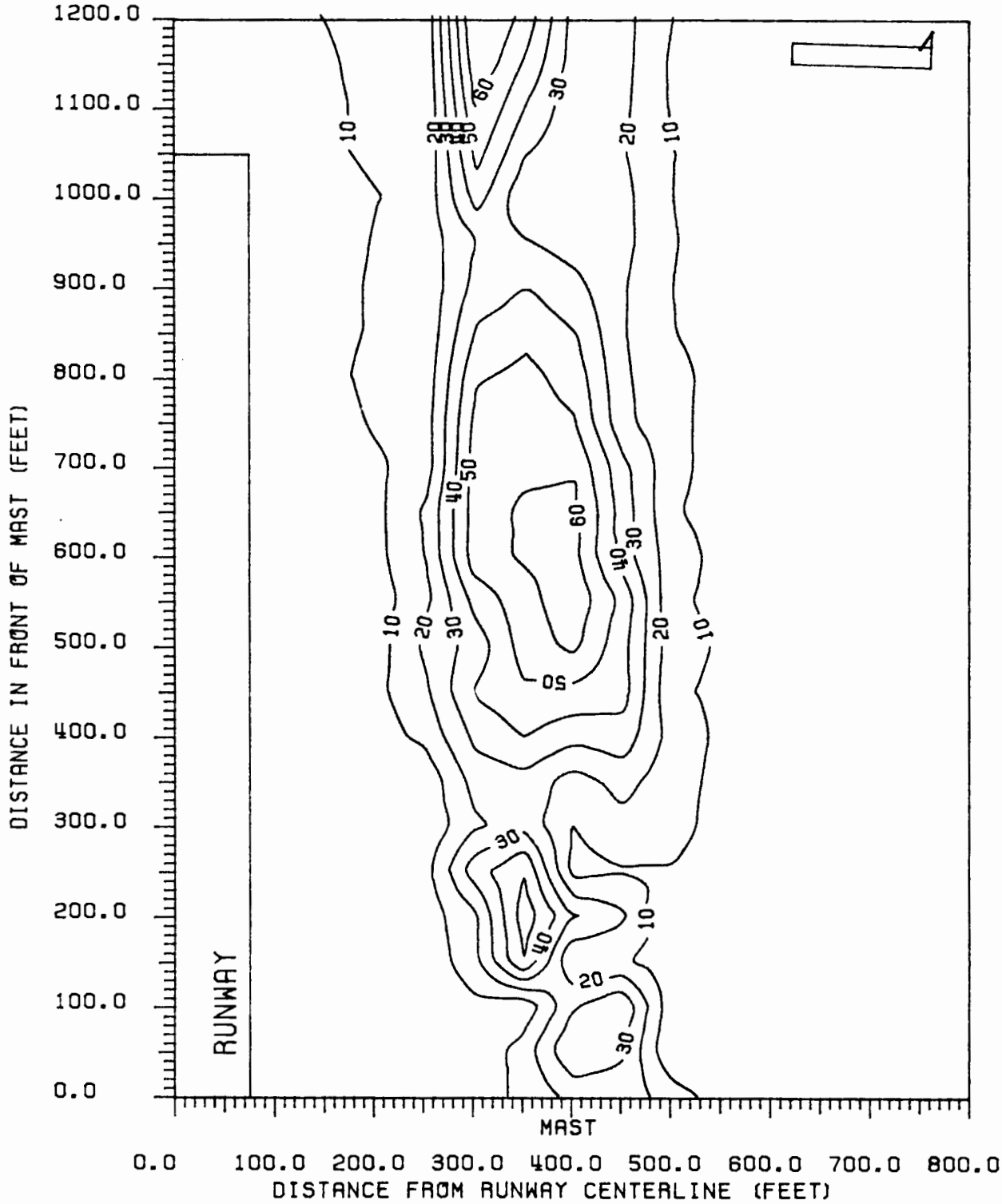

Figure 2-61. Contours of peak CDI values produced in ILS Zone 2 for a B-727. B-727 fuselage is perpendicular to runway centerline, with tail away from the runway. Null reference glide slope, directional antennas.

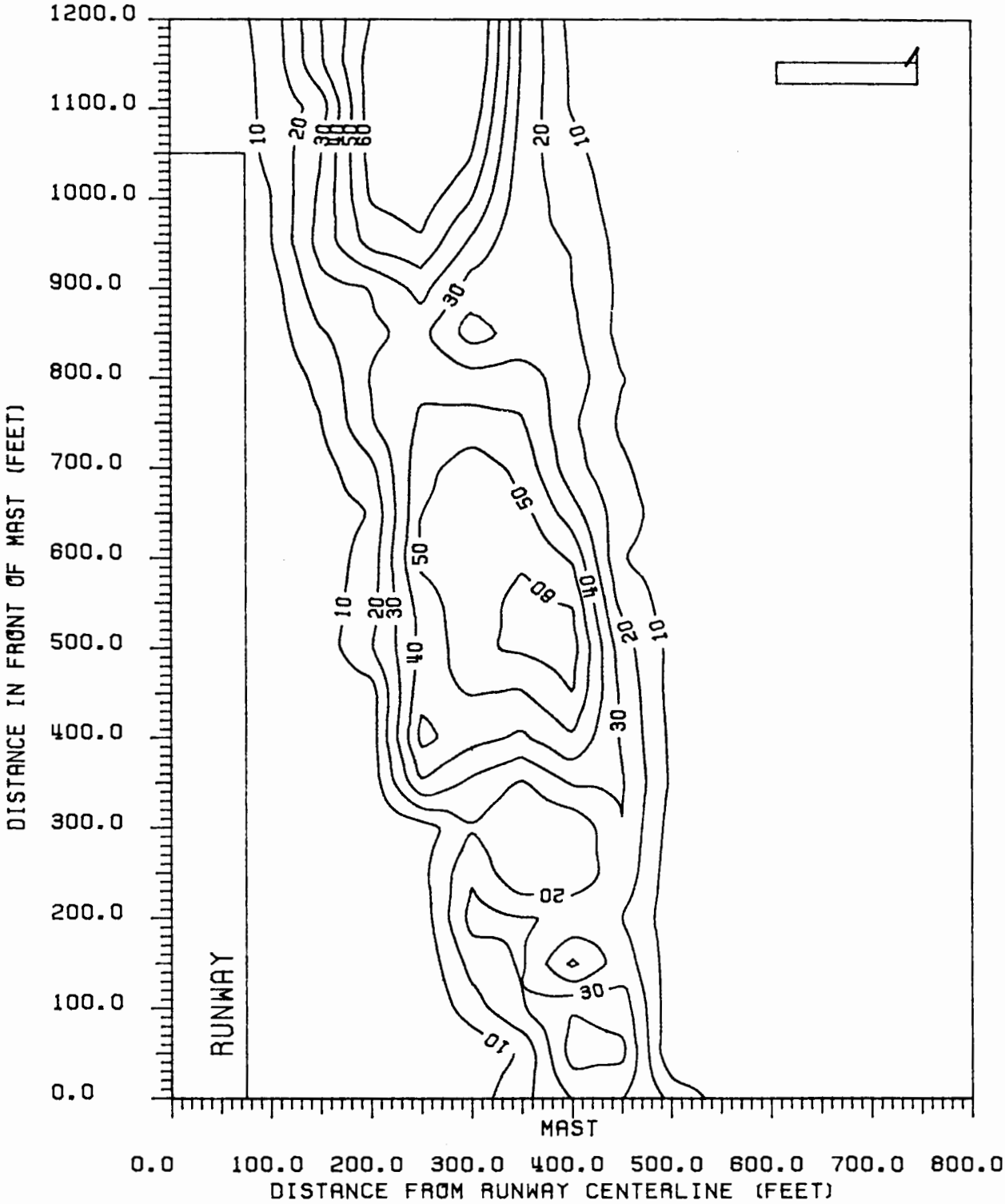

Figure 2-62. Contours of peak CDI values produced between ILS Point B and ILS Point C for a B-727. B-727 fuselage is perpendicular to runway centerline, with tail away from runway. Null reference glide slope, directional antennas.

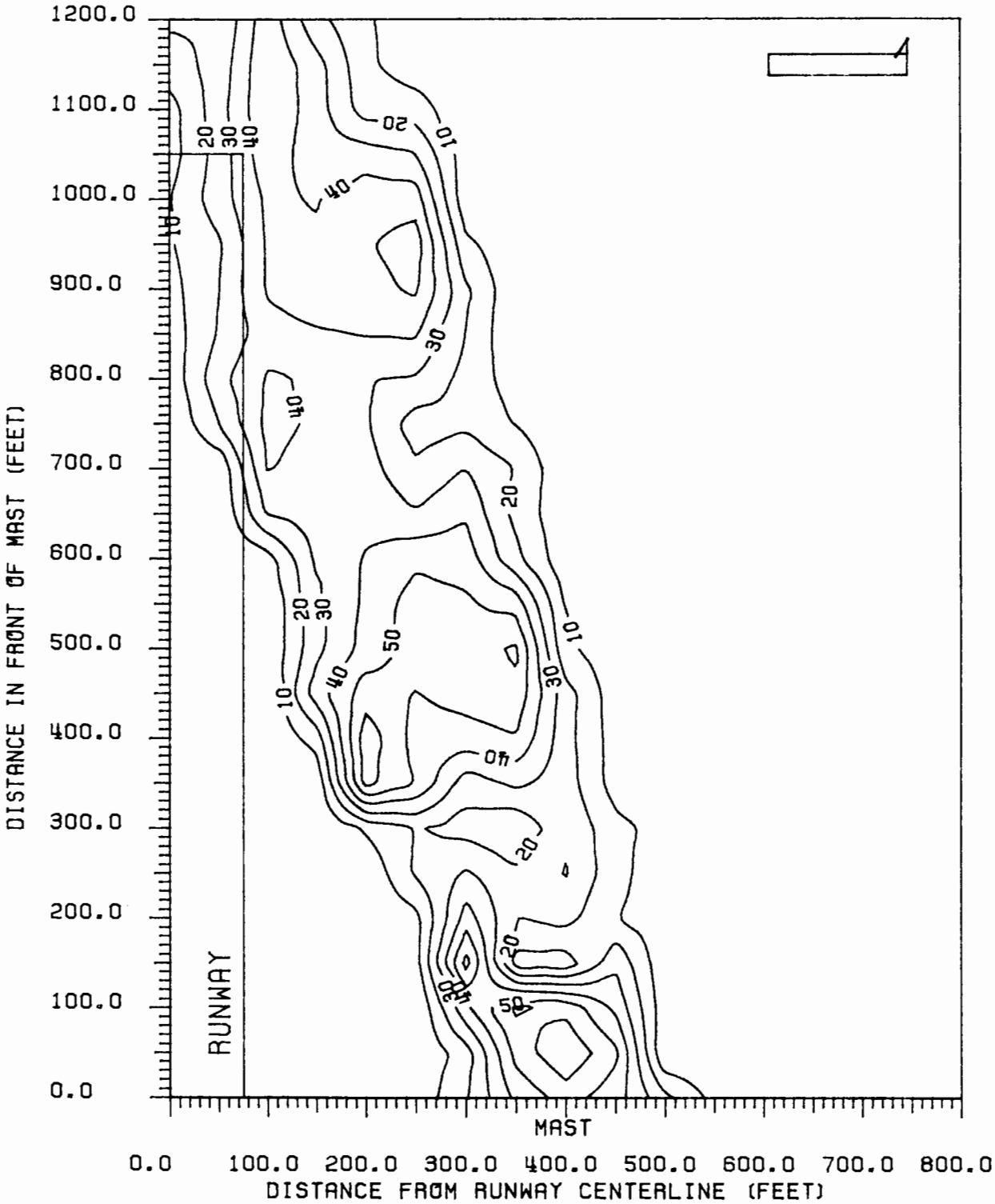

Figure 2-63. Contours of peak CDI values produced between ILS Point C and threshold for a B-727. B-727 fuselage is perpendicular to runway centerline, with tail away from runway. Null reference glide slope, directional antennas.

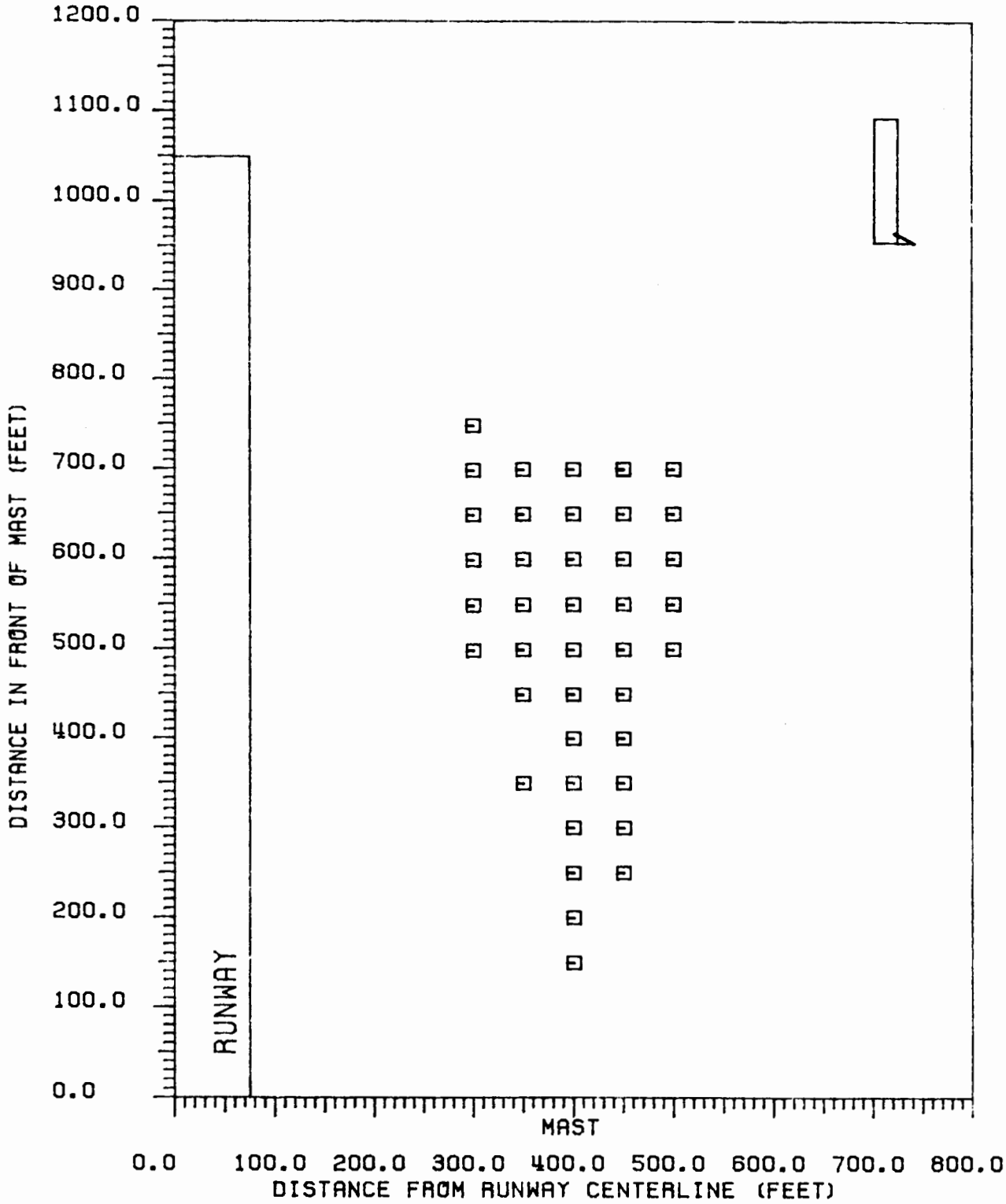

Figure 2-64. Critical area map for CAT I tolerances relating to B-727 aircraft. B-727 fuselage is parallel to runway centerline with tail towards the mast. Null reference glide slope, directional antennas.

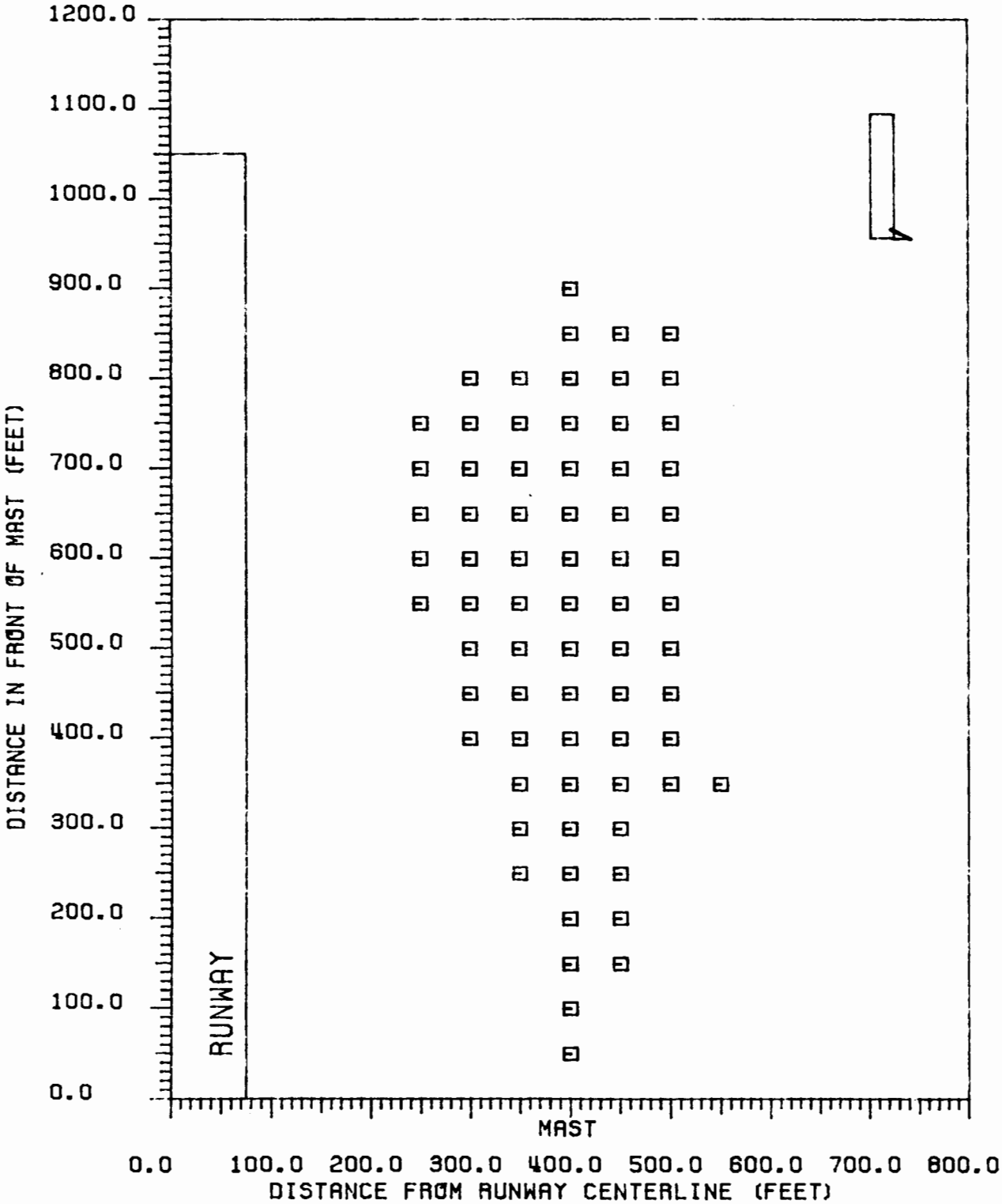

Figure 2-65. Critical area map for CAT II/III tolerances relating to B-727 aircraft. B-727 fuselage is parallel to runway centerline with tail towards the mast. Null reference glide slope, directional antennas.

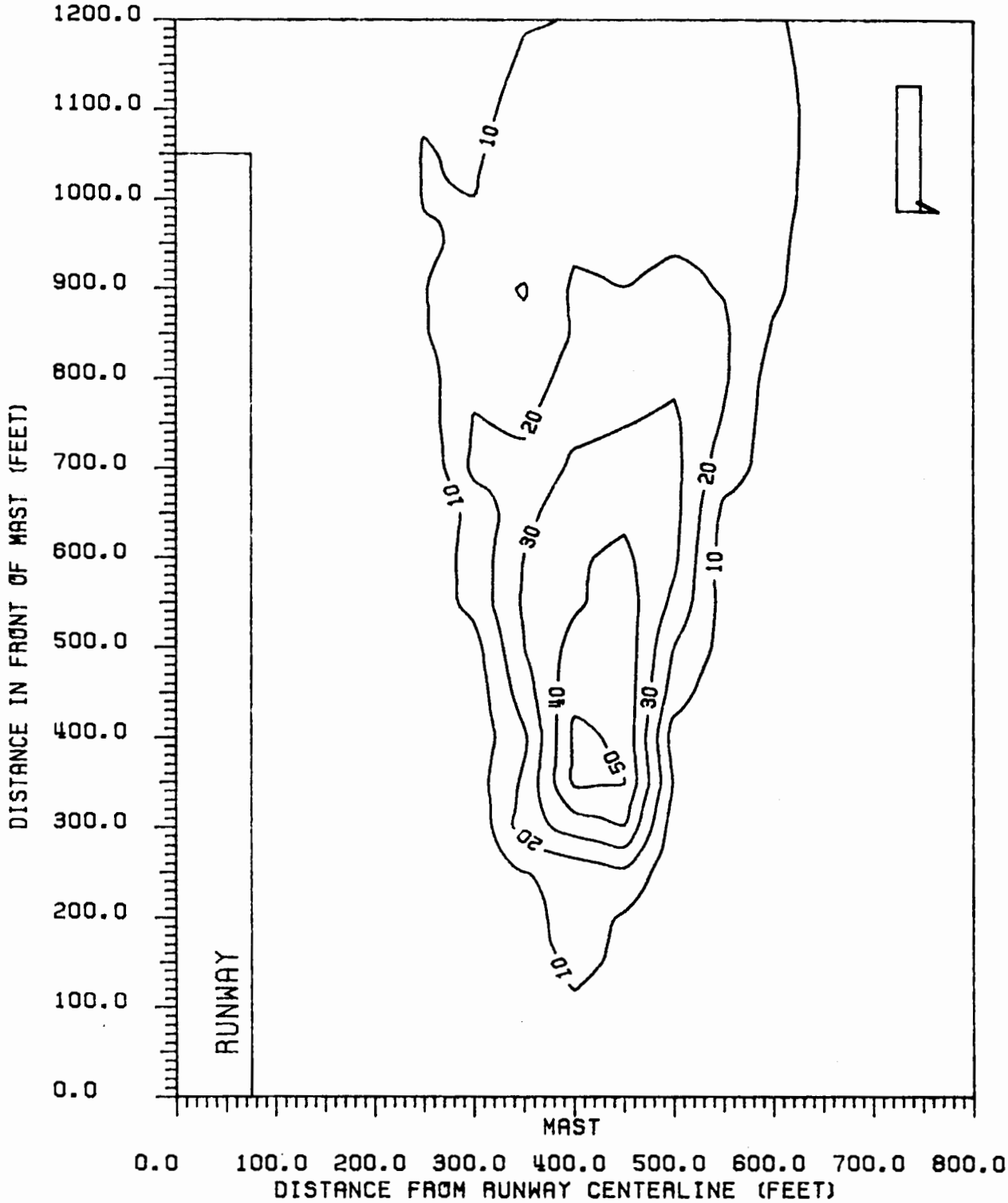

Figure 2-66. Contours of peak CDI values produced in ILS Zone 2 for a B-727. B-727 fuselage is parallel to runway centerline, with tail towards the mast. Null reference glide slope, directional antennas.

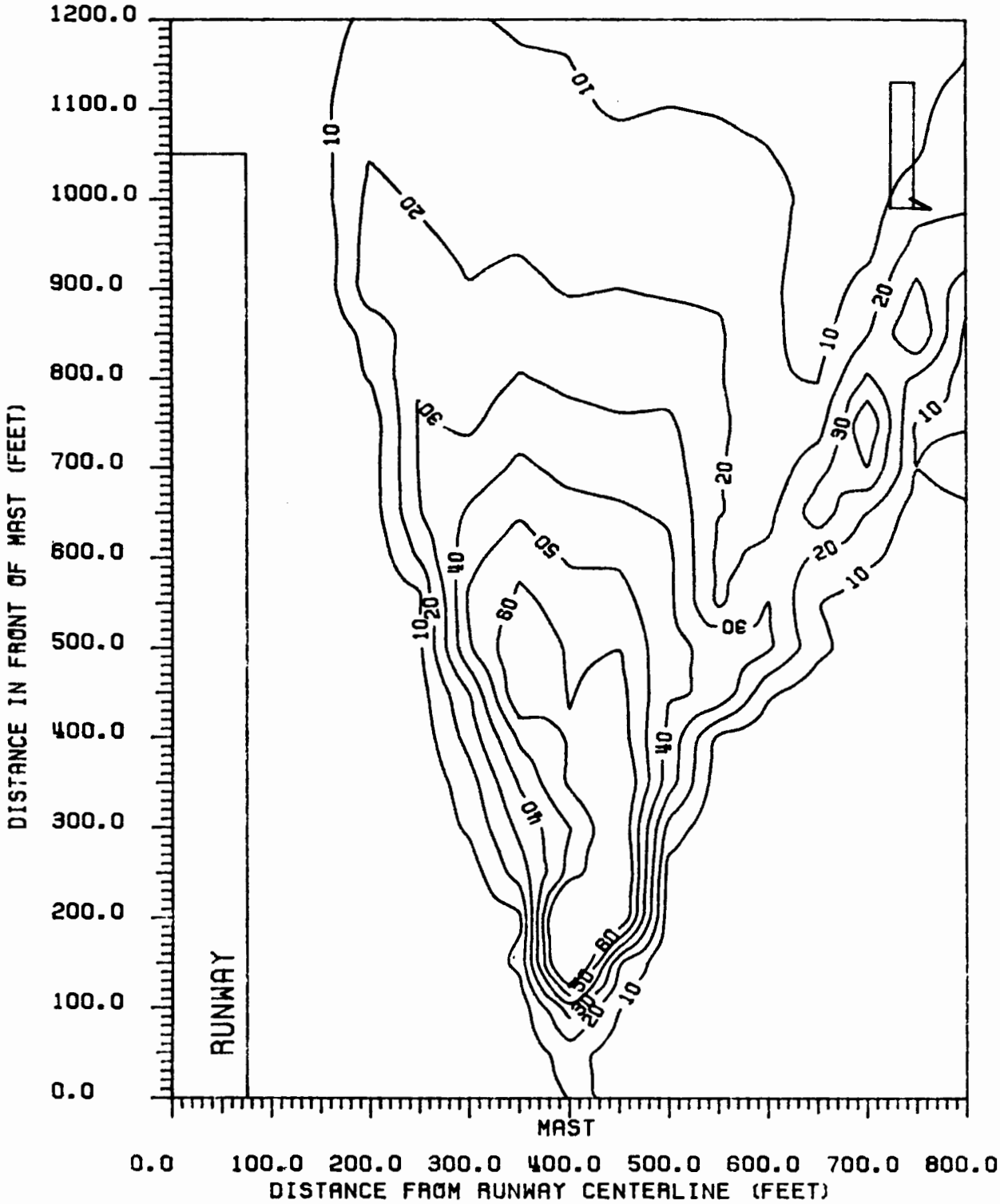

Figure 2-67. Contours of peak CDI values produced between ILS Point B and ILS Point C for a B-727. B-727 fuselage is parallel to runway centerline, with tail towards the mast. Null reference glide slope, directional antennas.

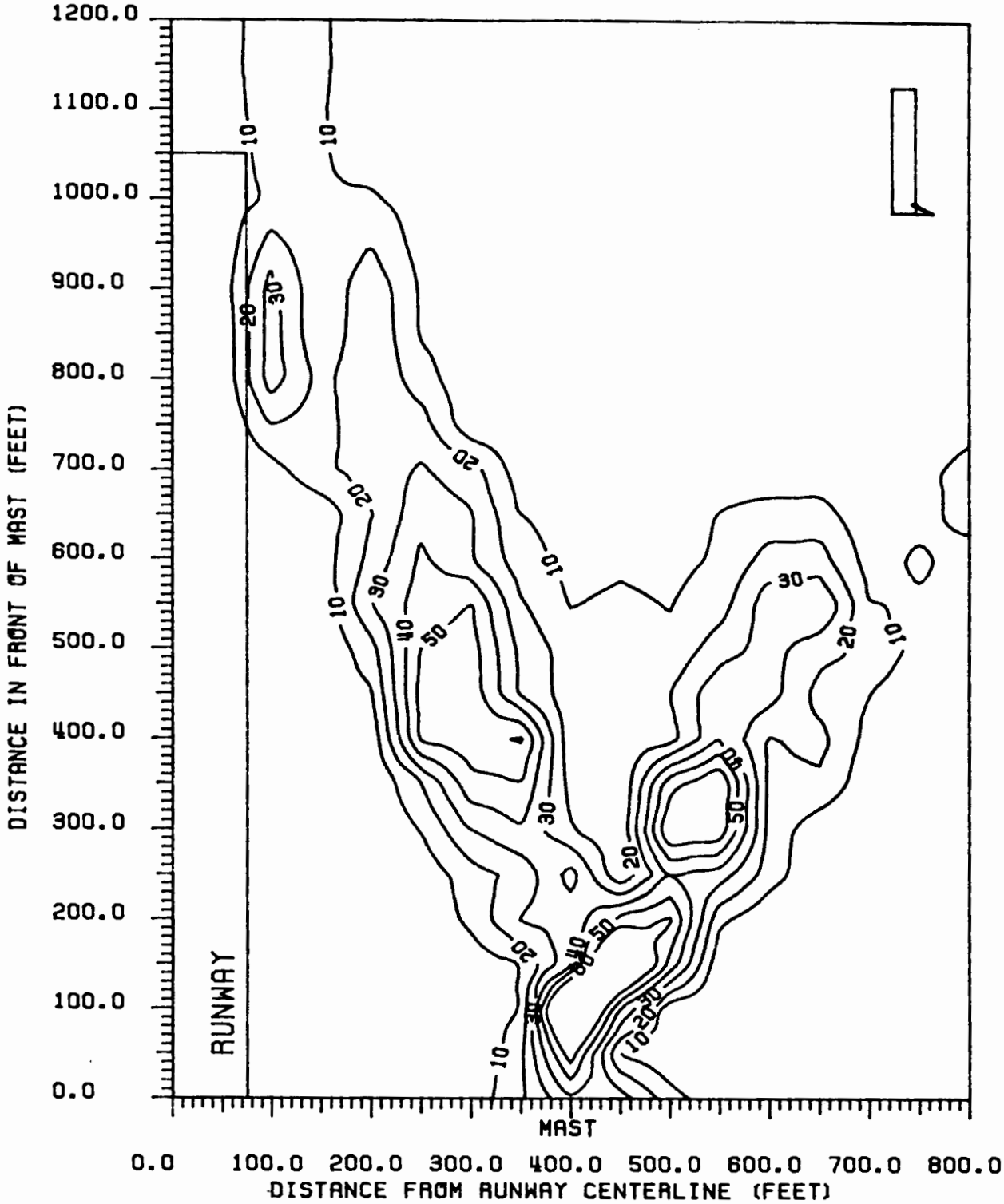

Figure 2-68. Contours of peak CDI values produced between ILS Point C and threshold for a B-727. B-727 fuselage is parallel to runway centerline, with tail towards the mast. Null reference glide slope, directional antennas.

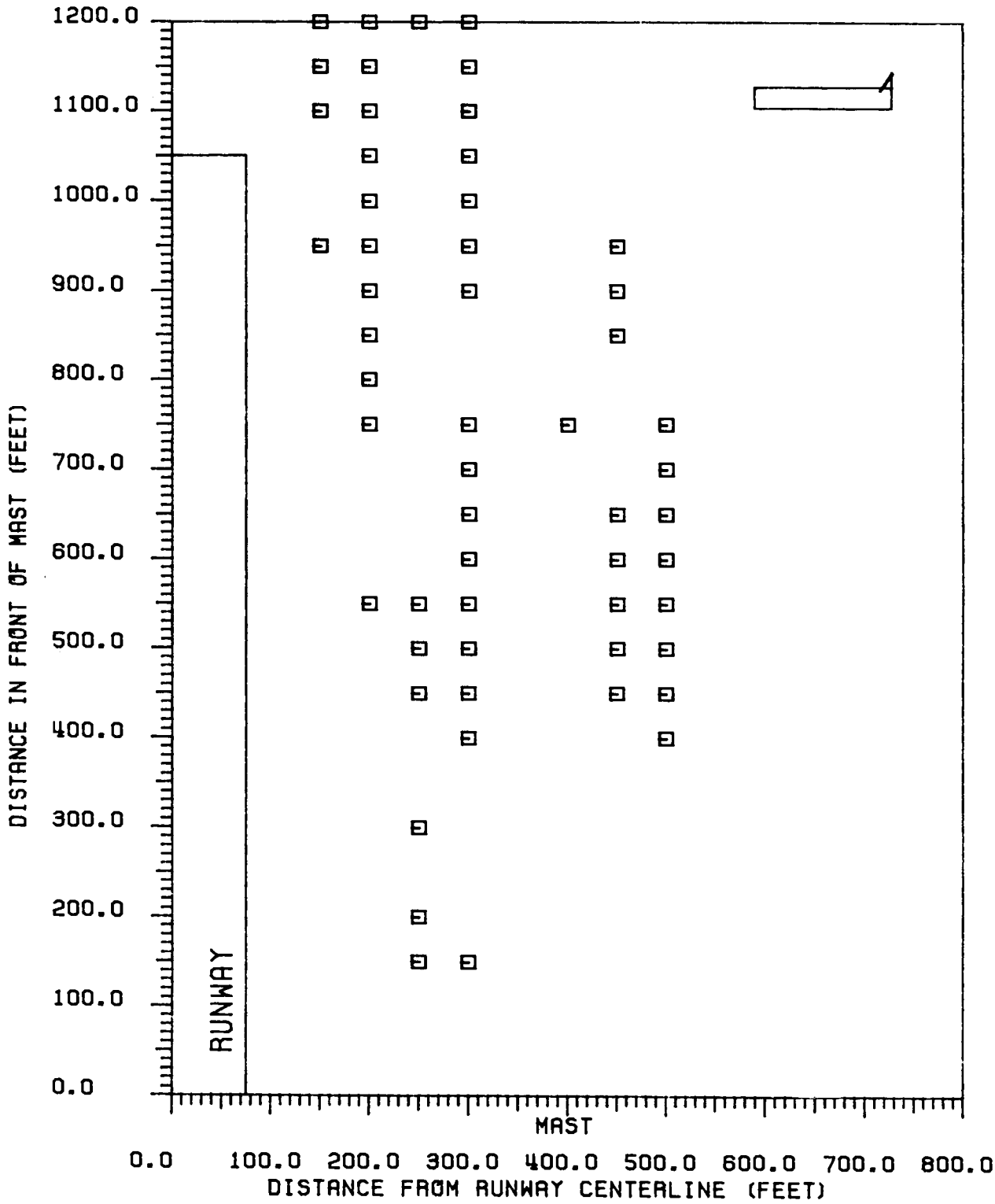

Figure 2-69. Critical area map for CAT I tolerances relating to B-747 aircraft. B-747 fuselage is perpendicular to runway centerline with tail away from the runway. Null reference glide slope, directional antennas.

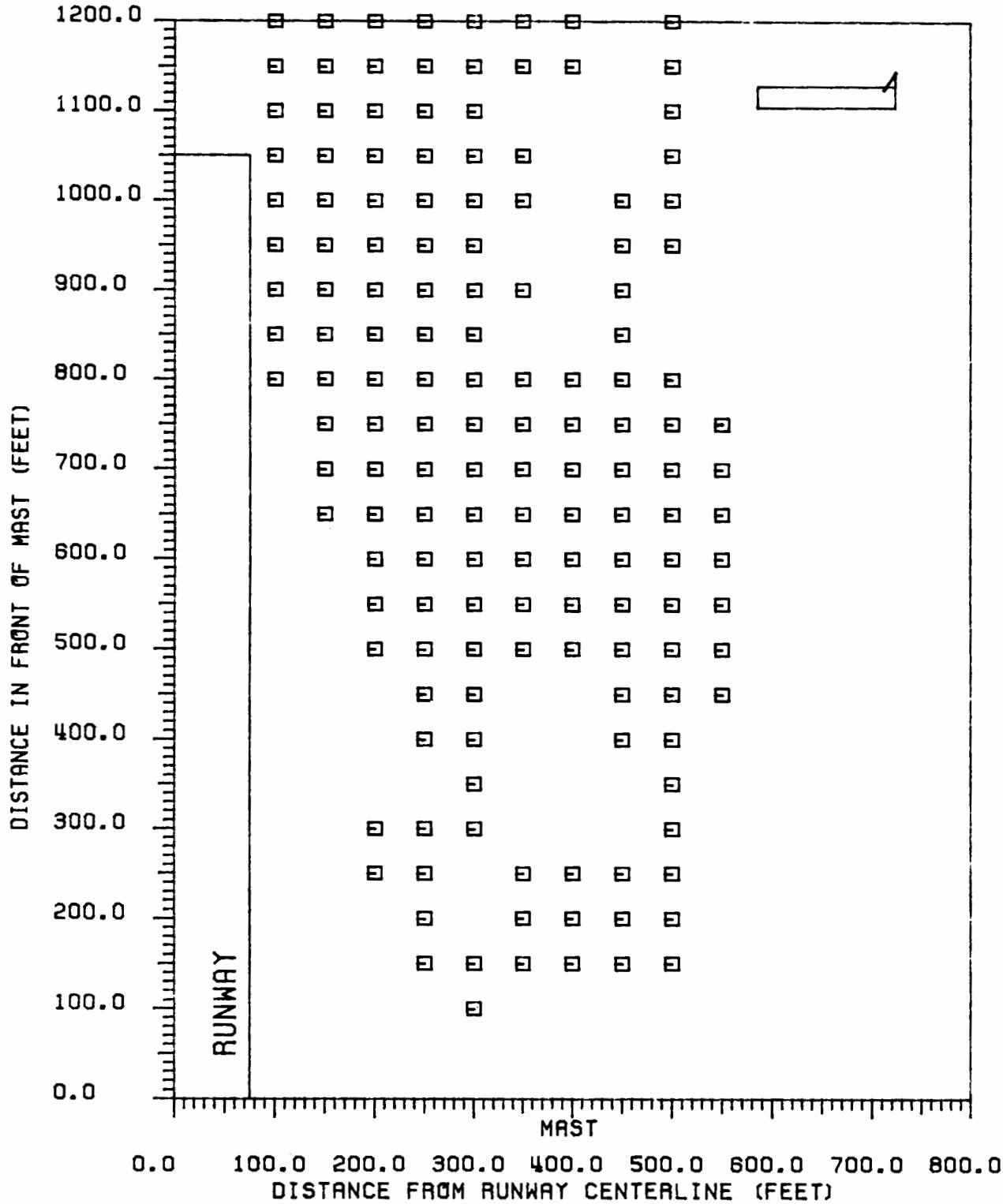

Figure 2-70. Critical area map for CAT II/III tolerances relating to B-747 aircraft. B-747 fuselage is perpendicular to runway centerline with tail away from the runway. Null reference glide slope, directional antennas.

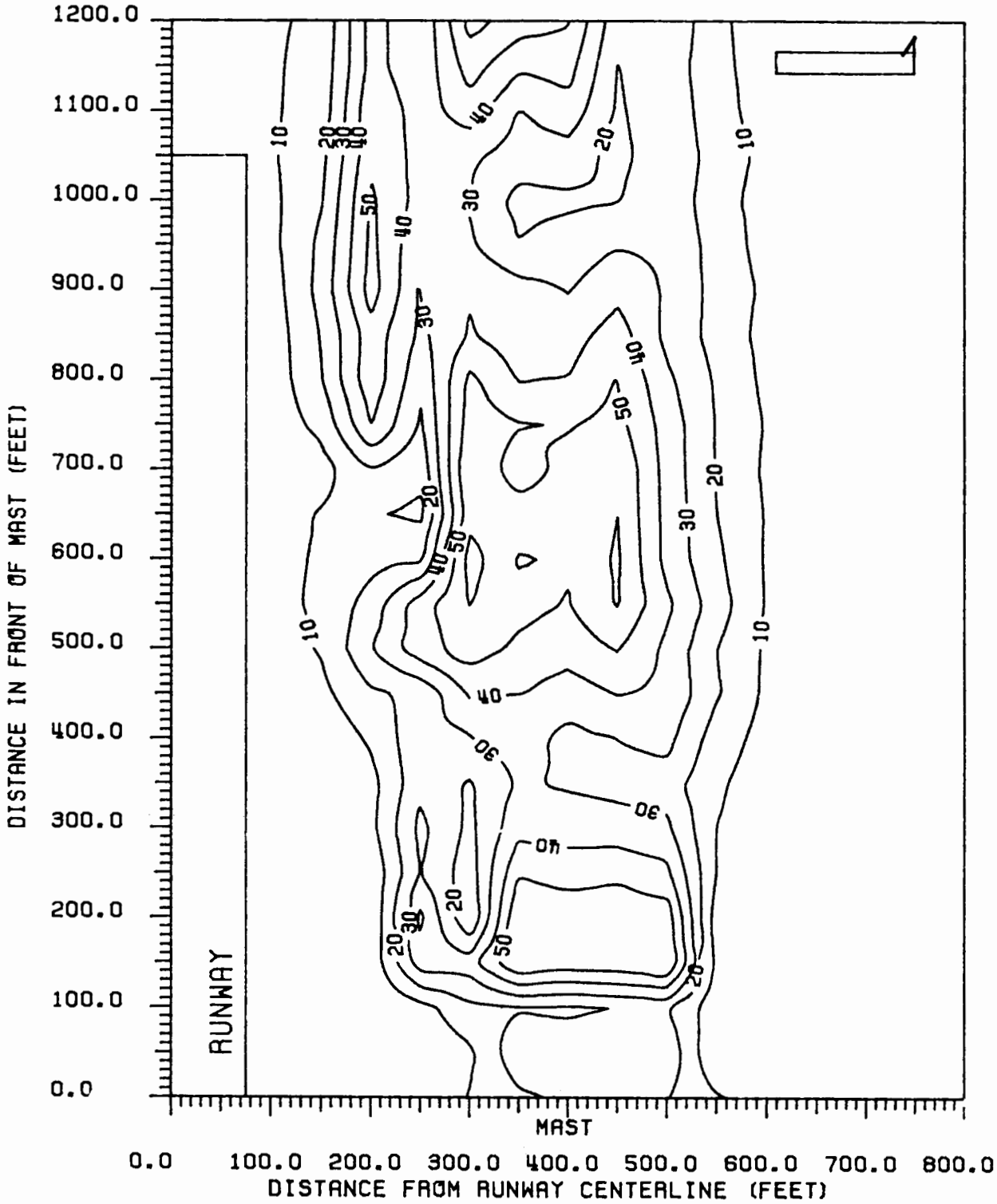

Figure 2-71. Contours of peak CDI values produced in ILS Zone 2 for a B-747. B-747 fuselage is perpendicular to runway centerline, with tail away from the runway. Null reference glide slope, directional antennas.

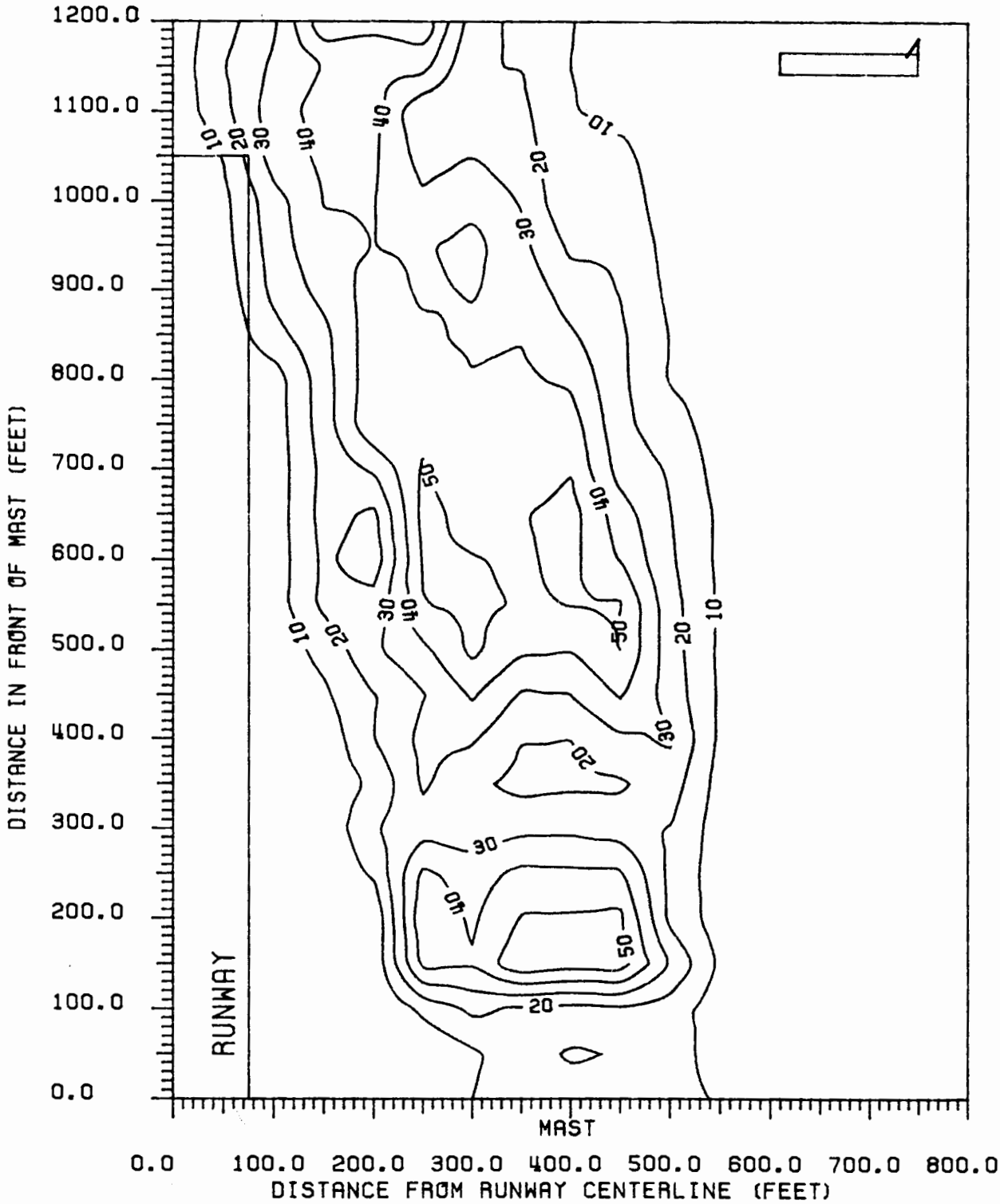

Figure 2-72. Contours of peak CDI values produced between ILS Point B and ILS Point C for a B-747. B-747 fuselage is perpendicular to runway centerline, with tail away from runway. Null reference glide slope, directional antennas.

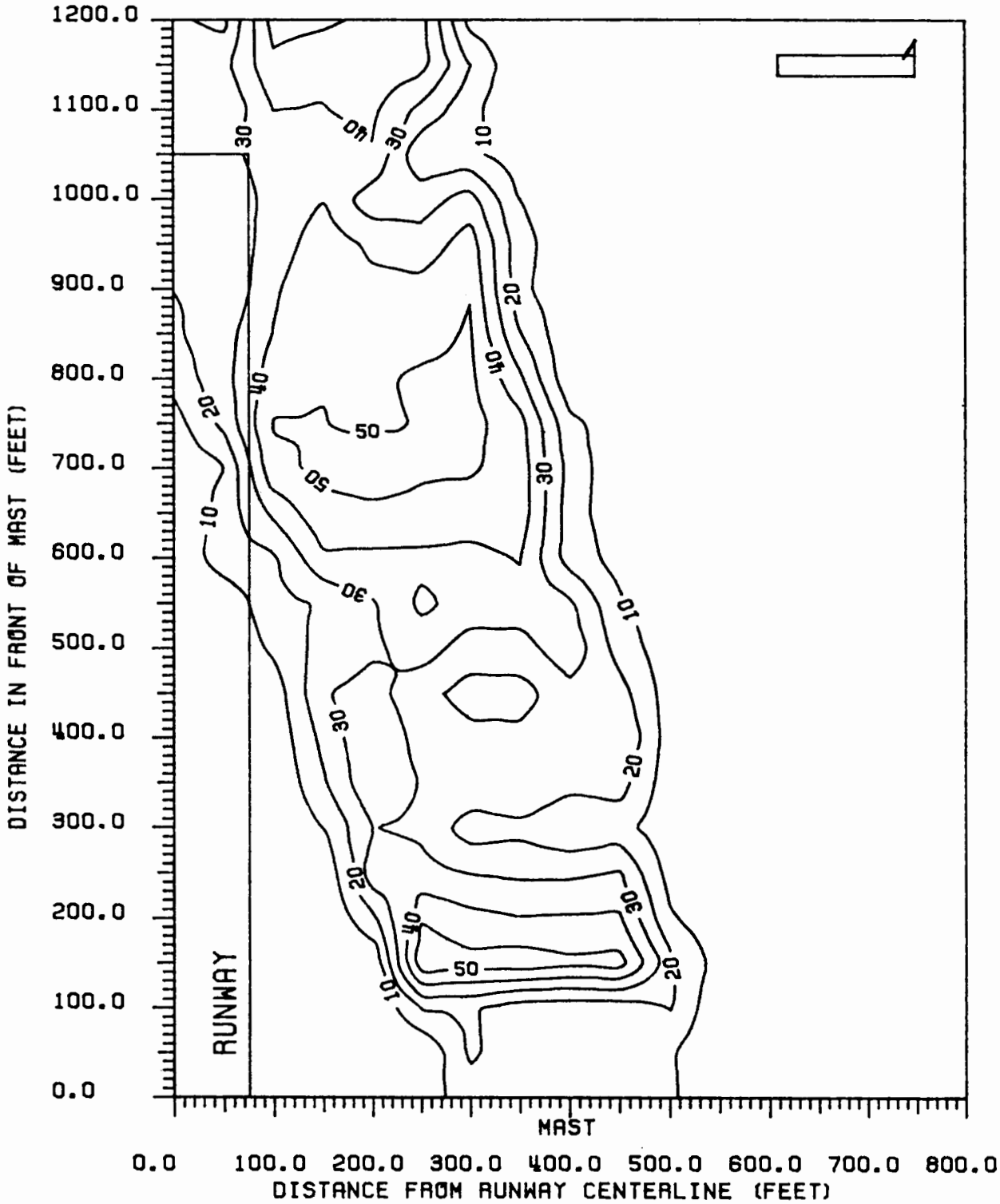

Figure 2-73. Contours of peak CDI values produced between ILS Point C and threshold for a B-747. B-747 fuselage is perpendicular to runway centerline, with tail away from runway. Null reference glide slope, directional antennas.

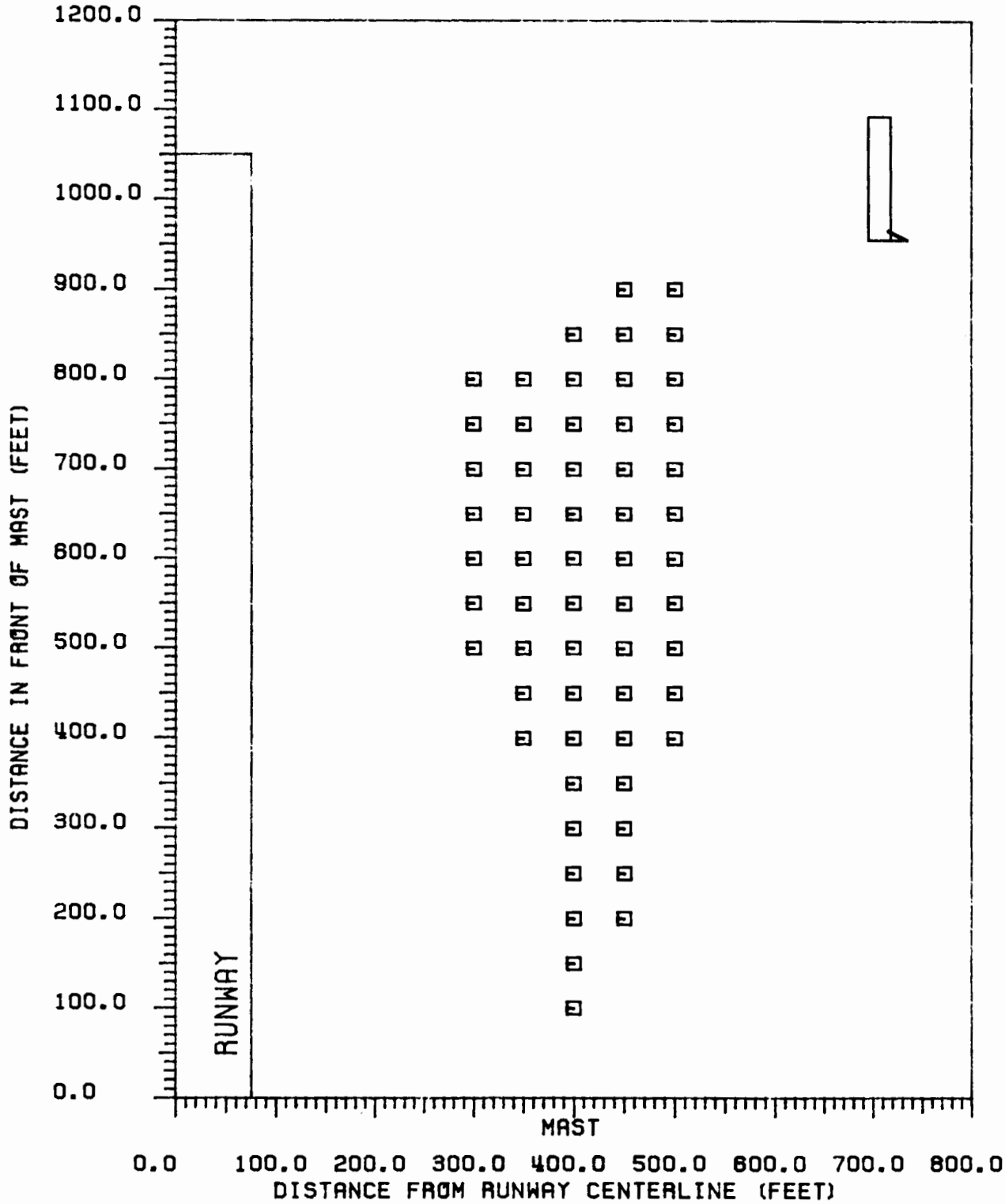

Figure 2-74. Critical area map for CAT I tolerances relating to B-747 aircraft. B-747 fuselage is parallel to runway centerline with tail towards the mast. Null reference glide slope, directional antennas.

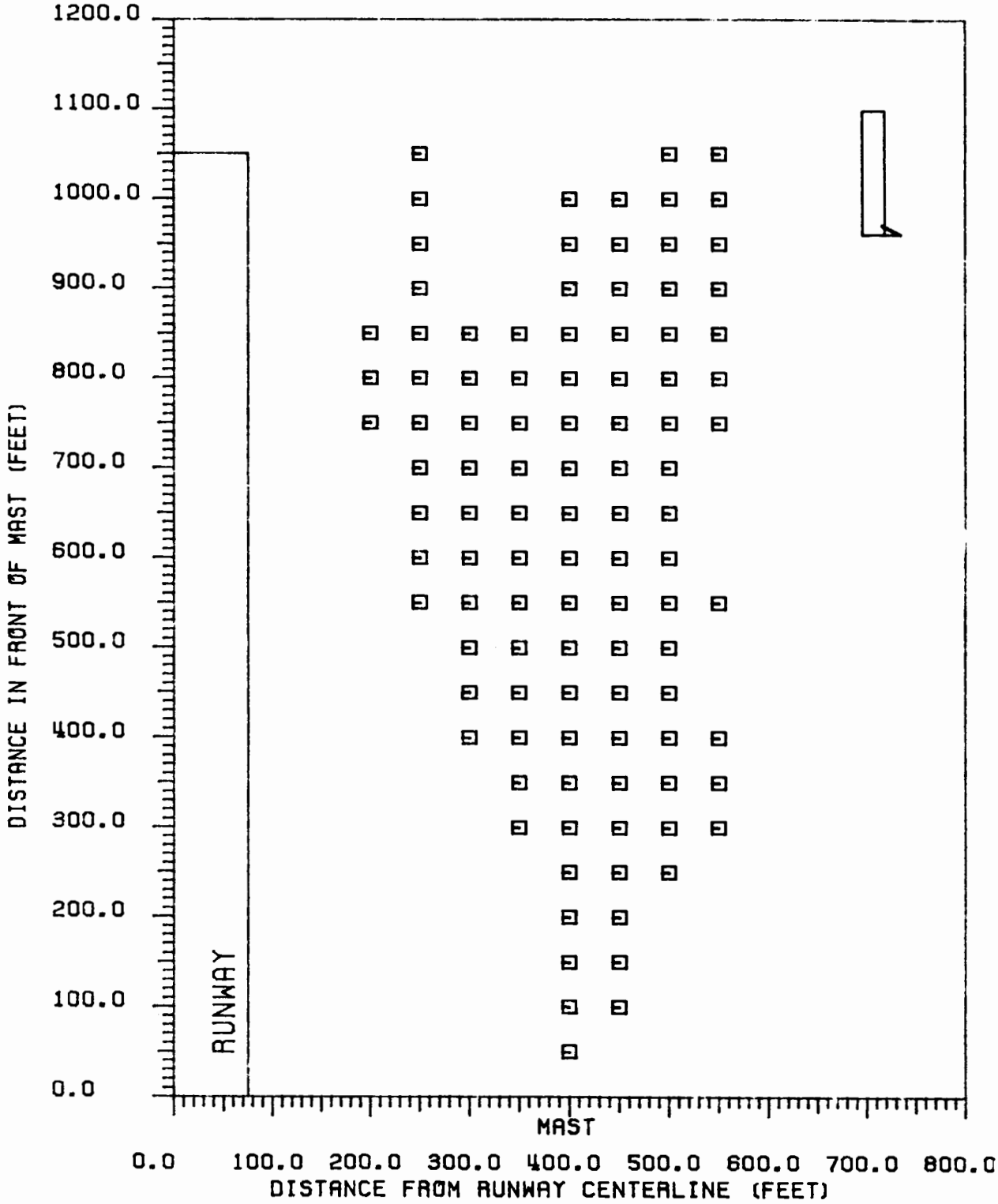

Figure 2-75. Critical area map for CAT II/III tolerances relating to B-747 aircraft. B-747 fuselage is parallel to runway centerline with tail towards the mast. Null reference glide slope, directional antennas.

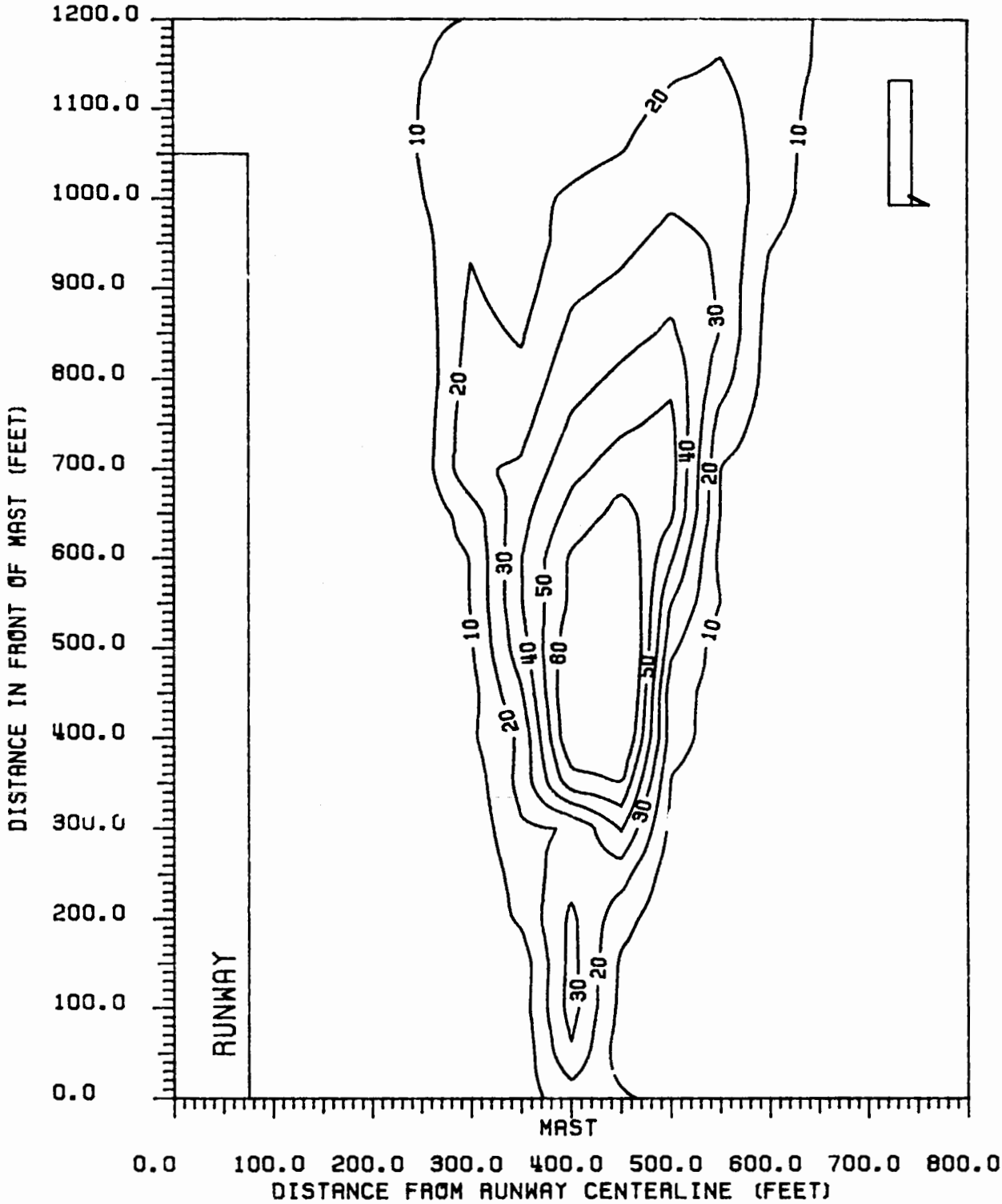

Figure 2-76. Contours of peak CDI values produced in ILS Zone 2 for a B-747. B-747 fuselage is parallel to runway centerline, with tail towards the mast. Null reference glide slope, directional antennas.

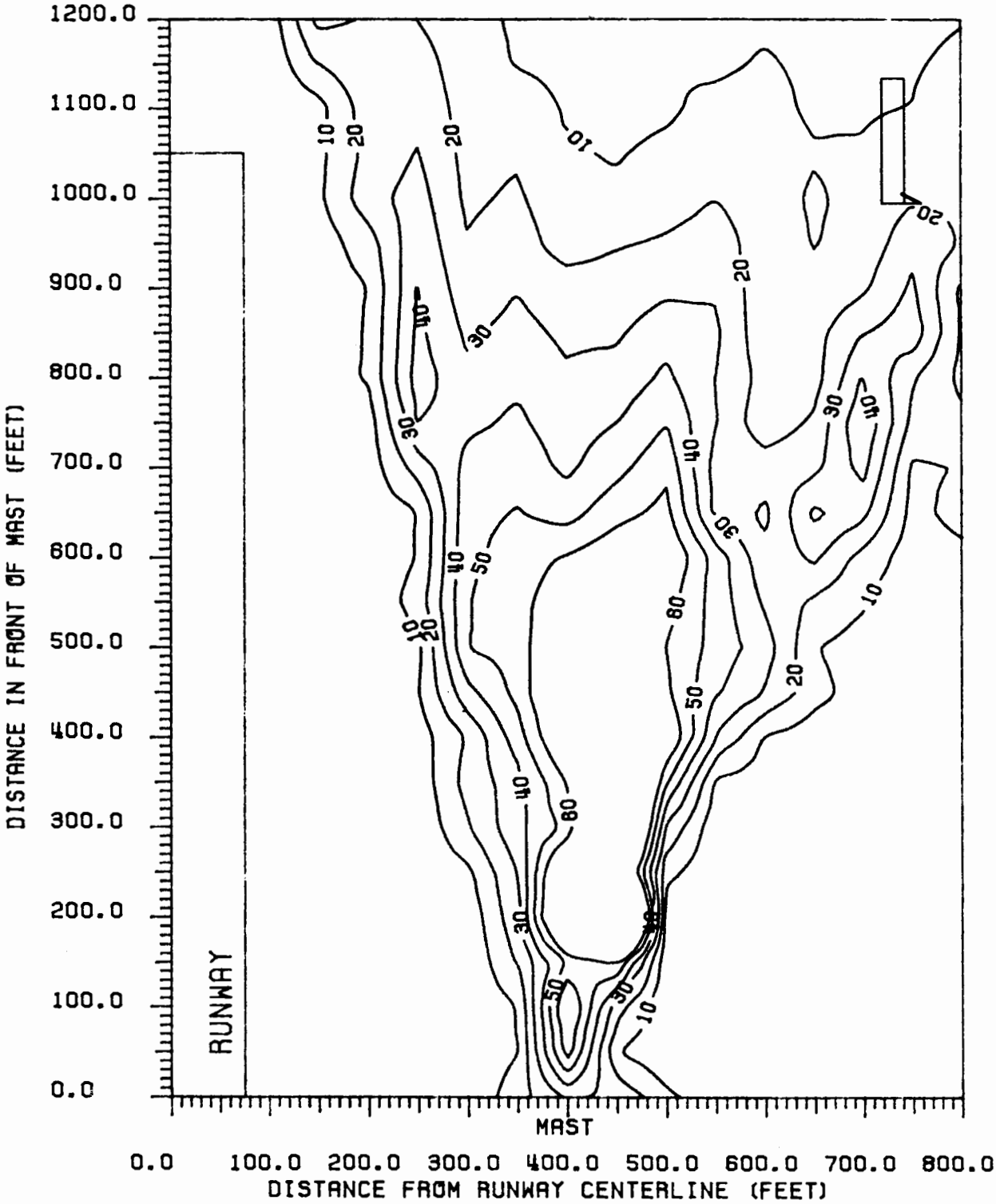

Figure 2-77. Contours of peak CDI values produced between ILS Point B and ILS Point C for a B-747. B-747 fuselage is parallel to runway centerline, with tail towards the mast. Null reference glide slope, directional antennas.

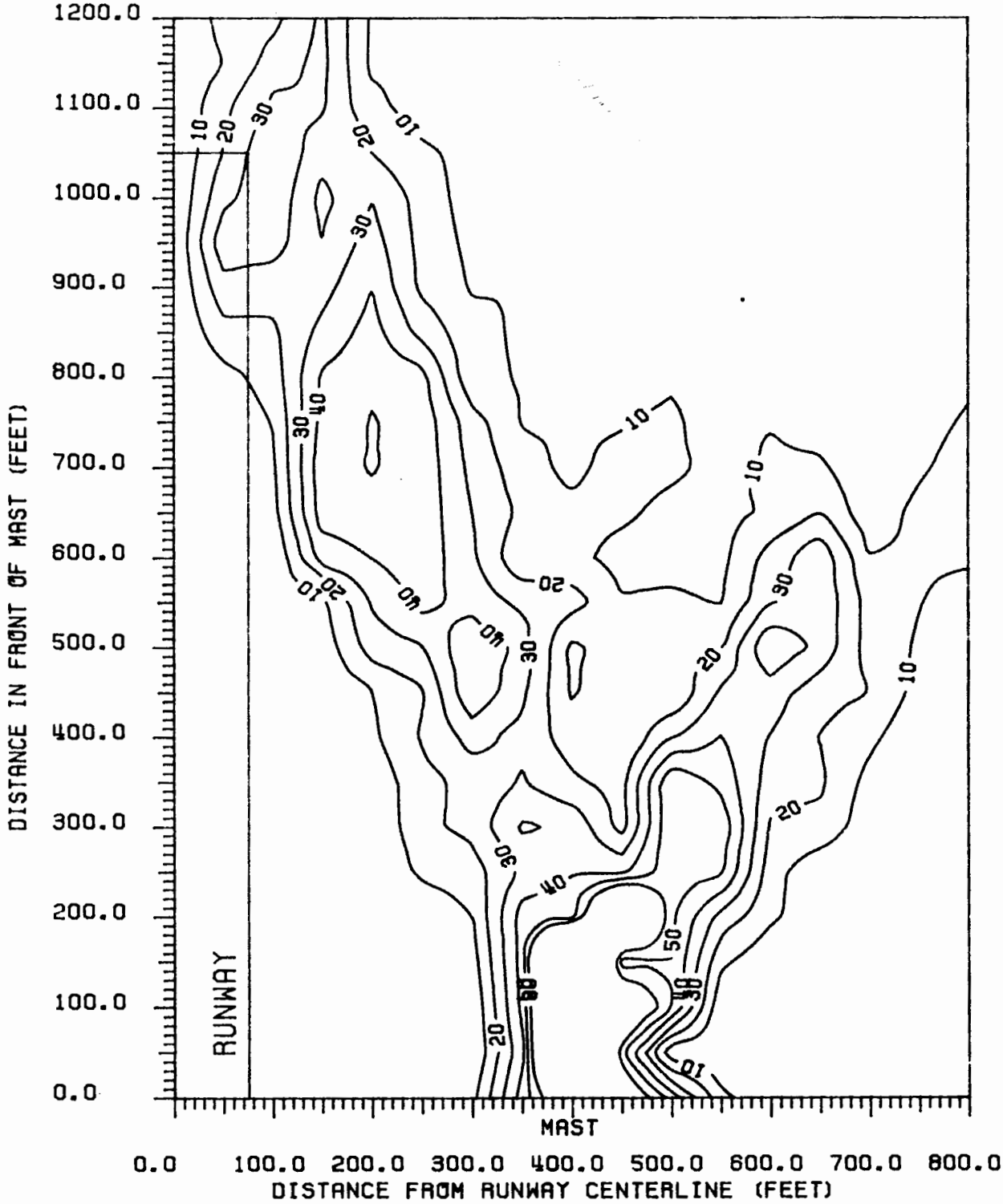

Figure 2-78. Contours of peak CDI values produced between ILS Point C and threshold for a B-747. B-747 fuselage is parallel to runway centerline, with tail towards the mast. Null reference glide slope, directional antennas.

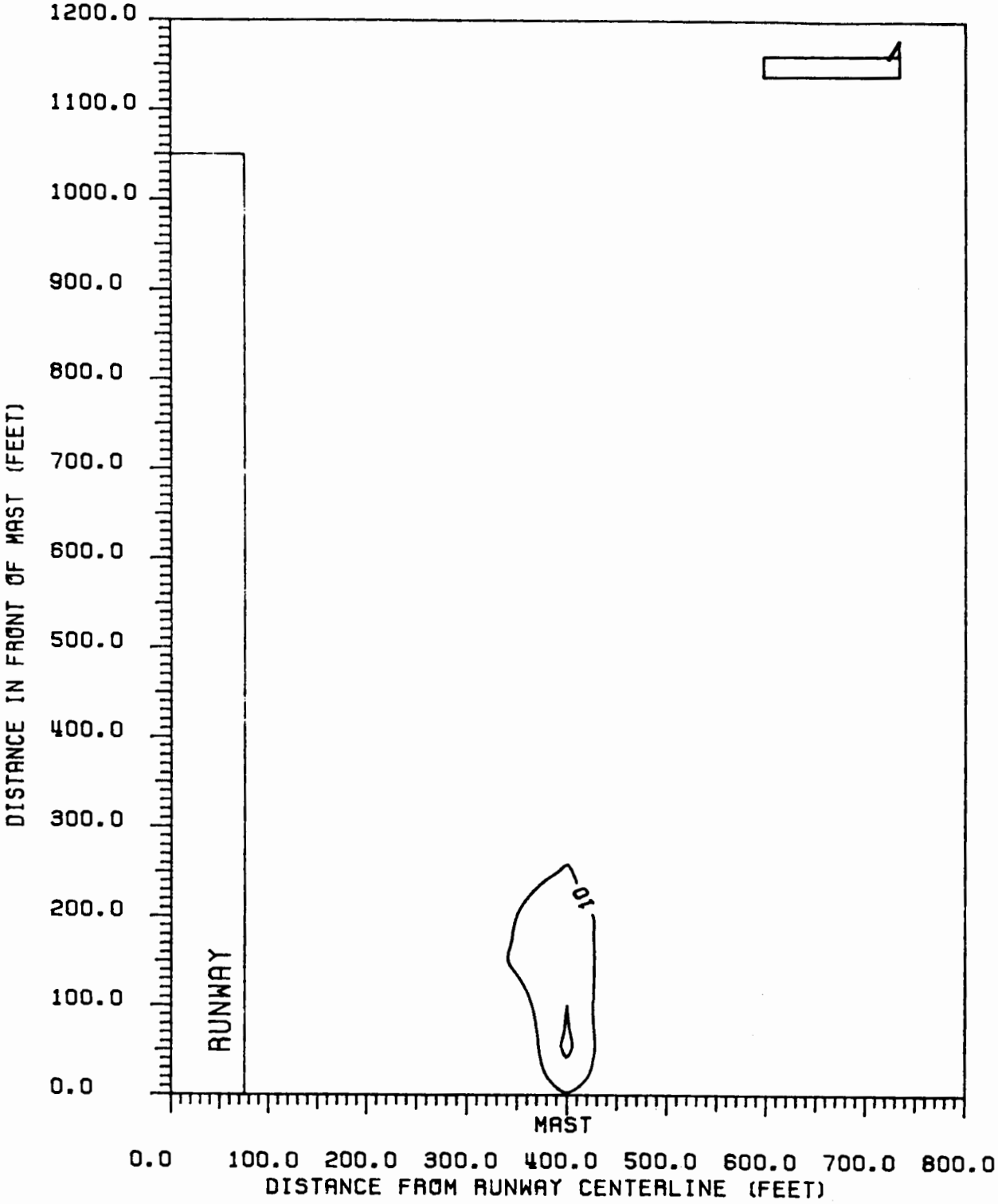

Figure 2-79. Contours of peak CDI values produced in ILS Zone 2 for an R-500. R-500 fuselage is perpendicular to runway centerline, with tail away from the runway. Sideband reference glide slope, directional antennas.

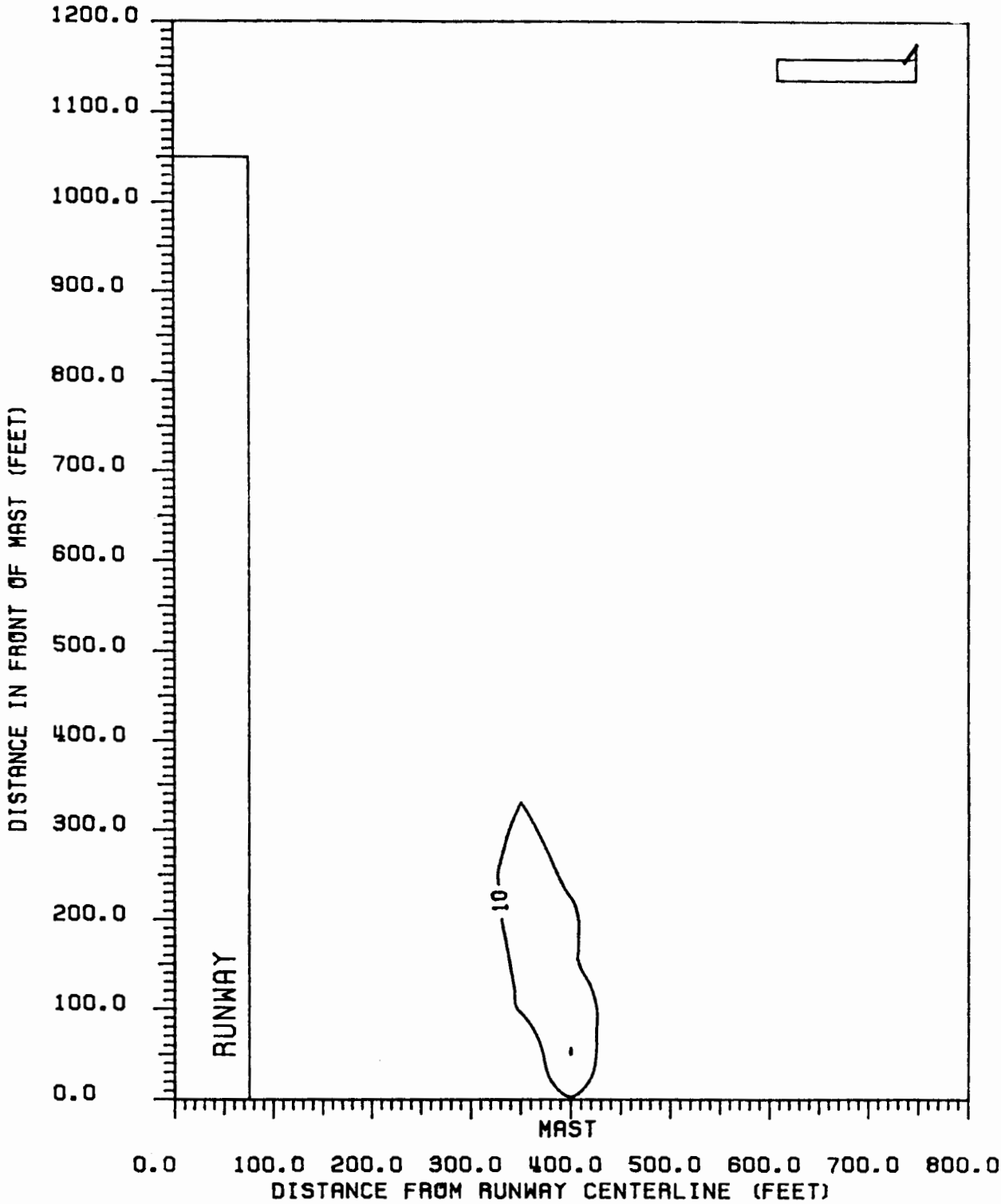

Figure 2-80. Contours of peak CDI values produced between ILS Point B and ILS Point C for an R-500. R-500 fuselage is perpendicular to runway centerline, with tail away from runway. Sideband reference glide slope, directional antennas.

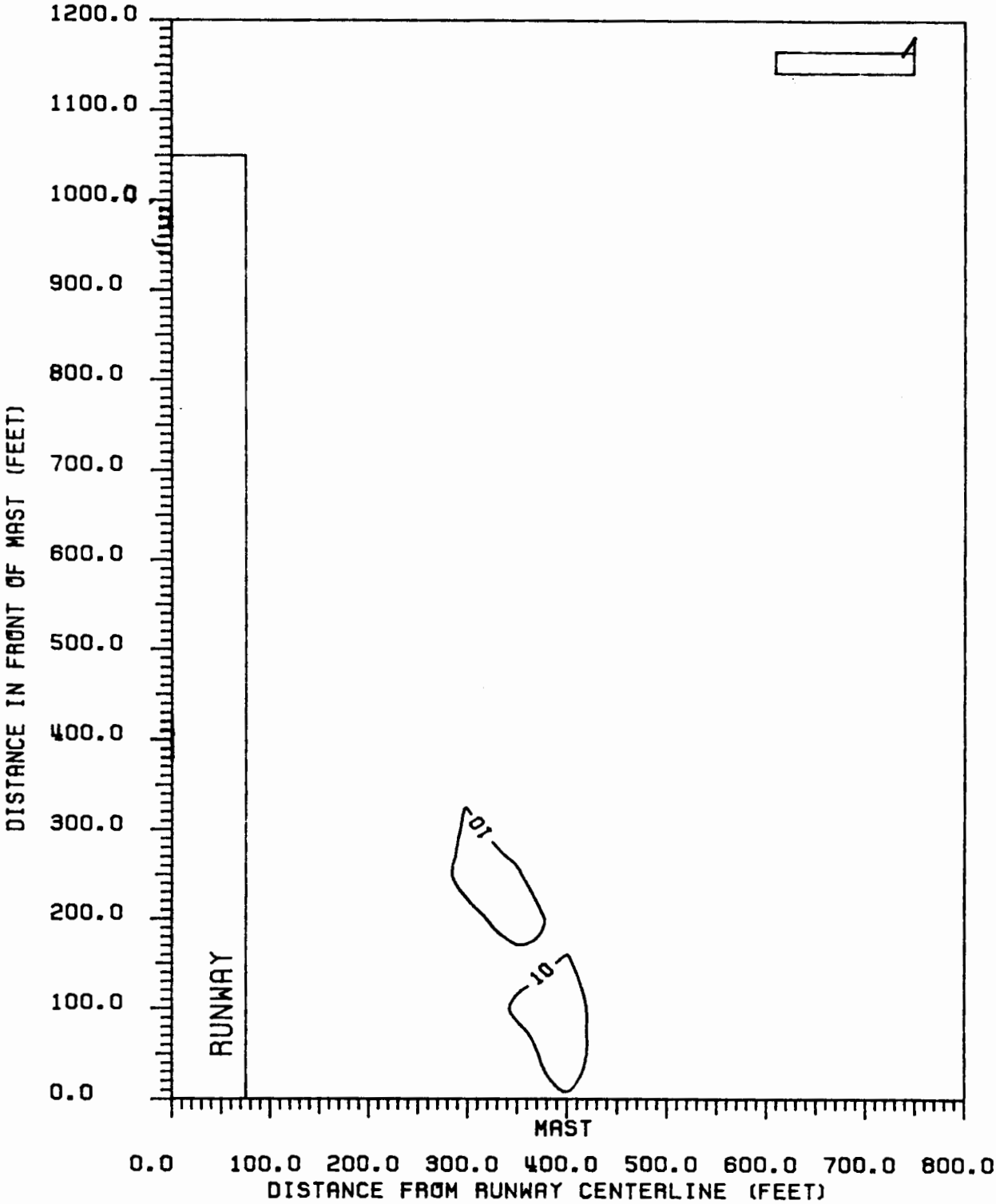

Figure 2-81. Contours of peak CDI values produced between ILS Point C and threshold for an R-500. R-500 fuselage is perpendicular to runway centerline, with tail away from runway. Sideband reference glide slope, directional antennas.

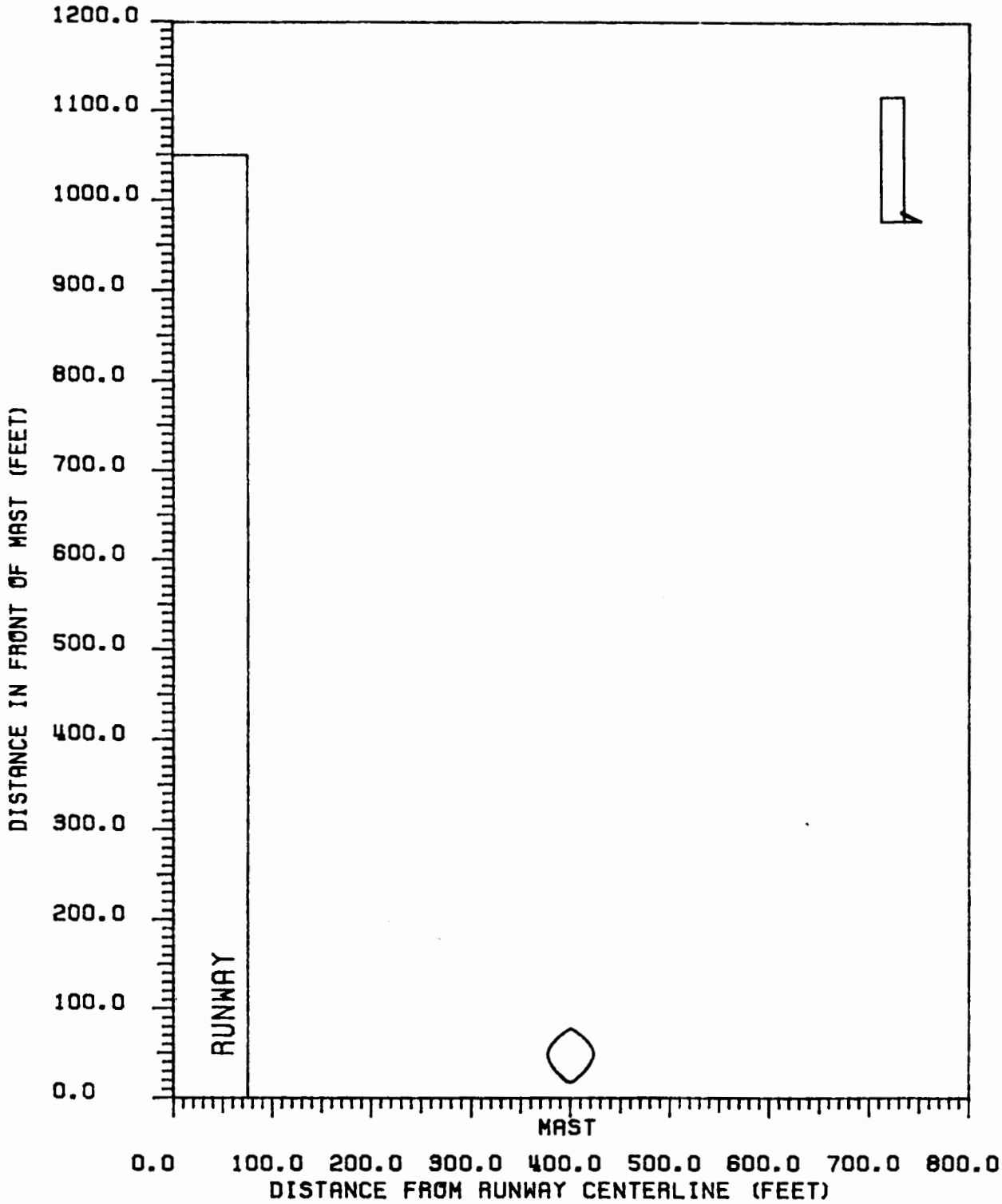

Figure 2-82. Contours of peak CDI values produced between ILS Point B and ILS Point C for an R-500. R-500 fuselage is parallel to runway centerline, with tail towards the mast. Sideband reference glide slope, directional antennas.

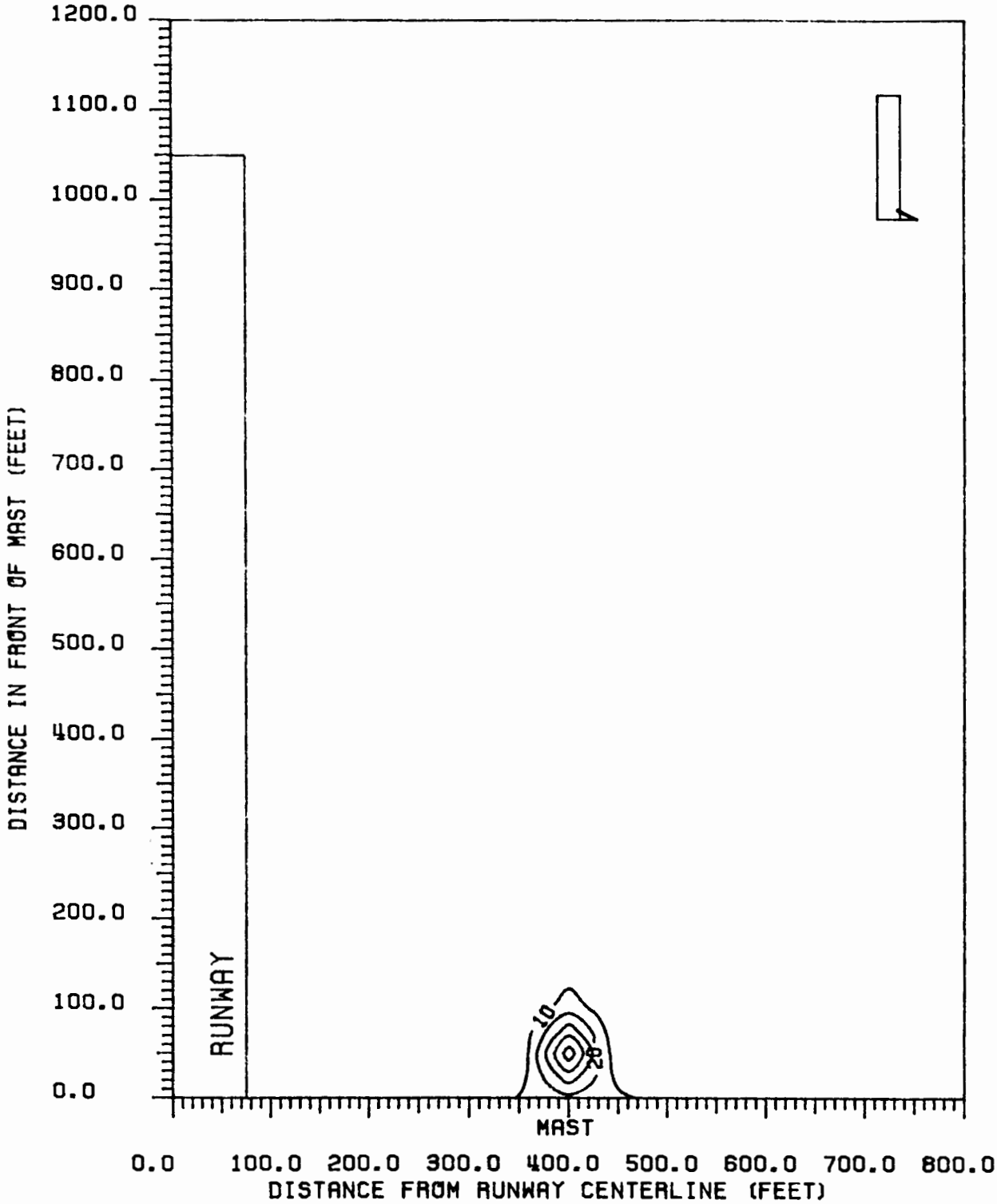

Figure 2-83. Contours of peak CDI values produced between ILS Point C and threshold for an R-500. R-500 fuselage is parallel to runway centerline, with tail towards the mast. Sideband reference glide slope, directional antennas.

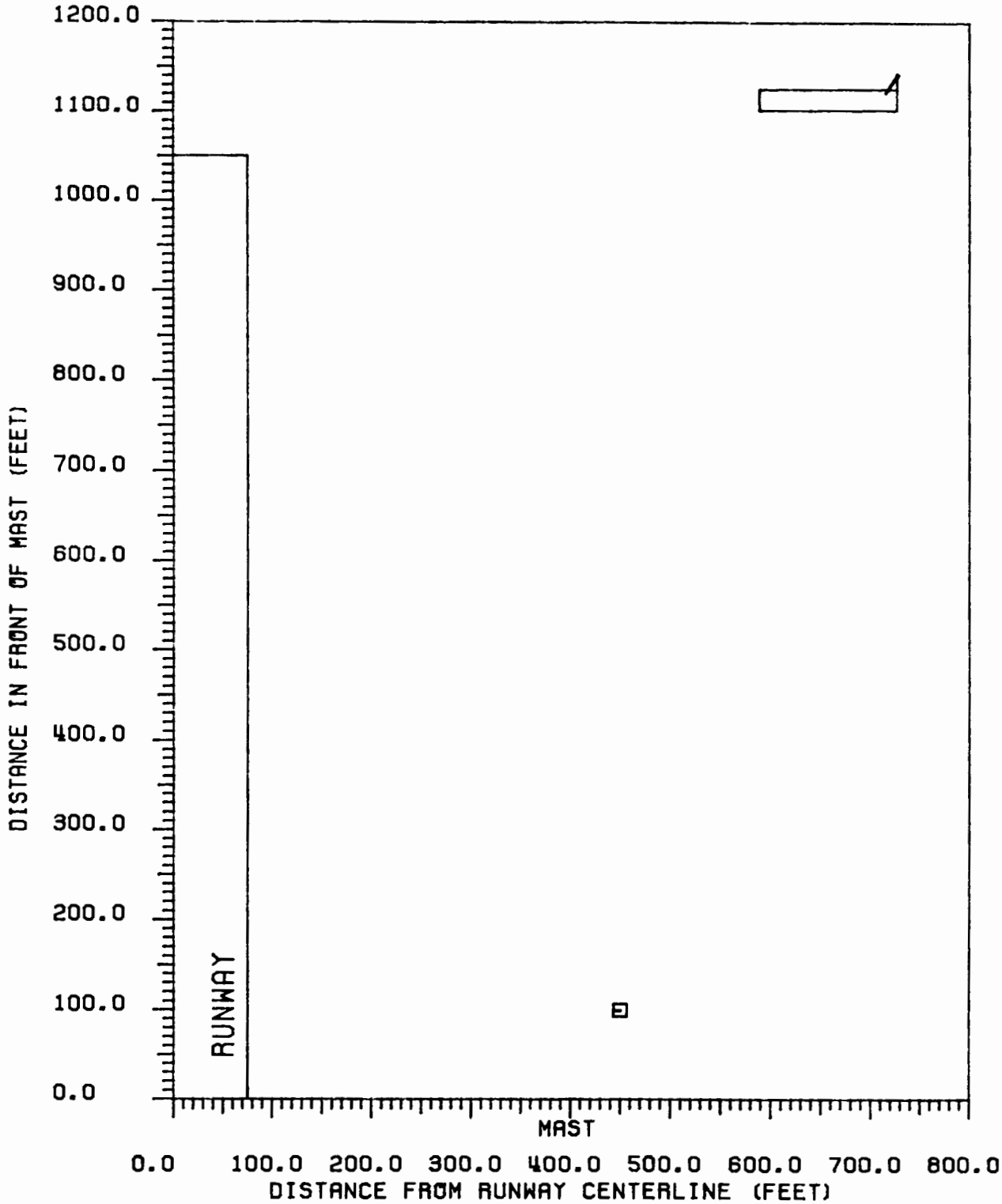

Figure 2-84. Critical area map for CAT I tolerances relating to C-440 aircraft. C-440 fuselage is perpendicular to runway centerline with tail away from the runway. Sideband reference glide slope, directional antennas.

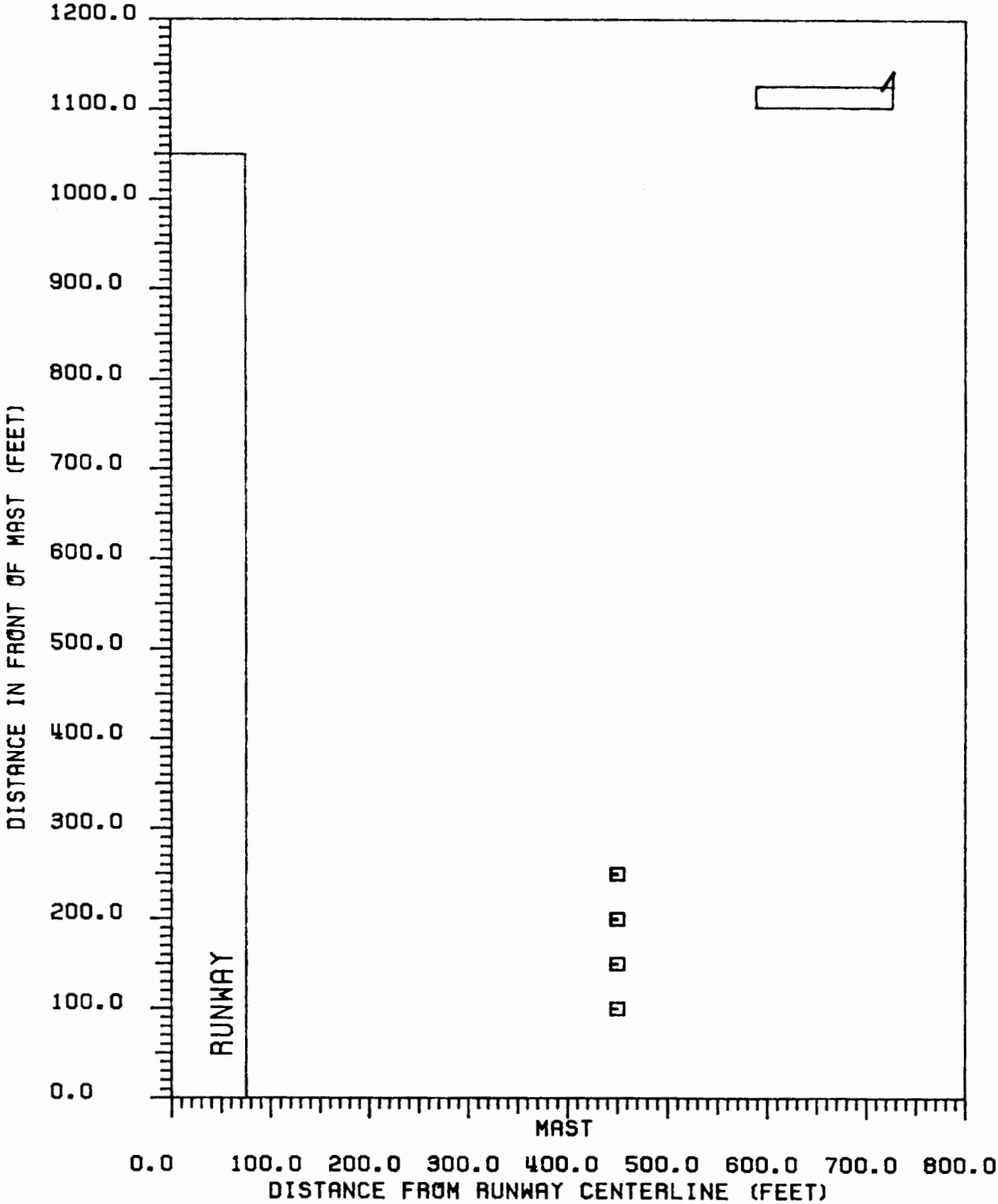

Figure 2-85. Critical area map for CAT II/III tolerances relating to C-440 aircraft. C-440 fuselage is perpendicular to runway centerline with tail away from the runway. Sideband reference glide slope, directional antennas.

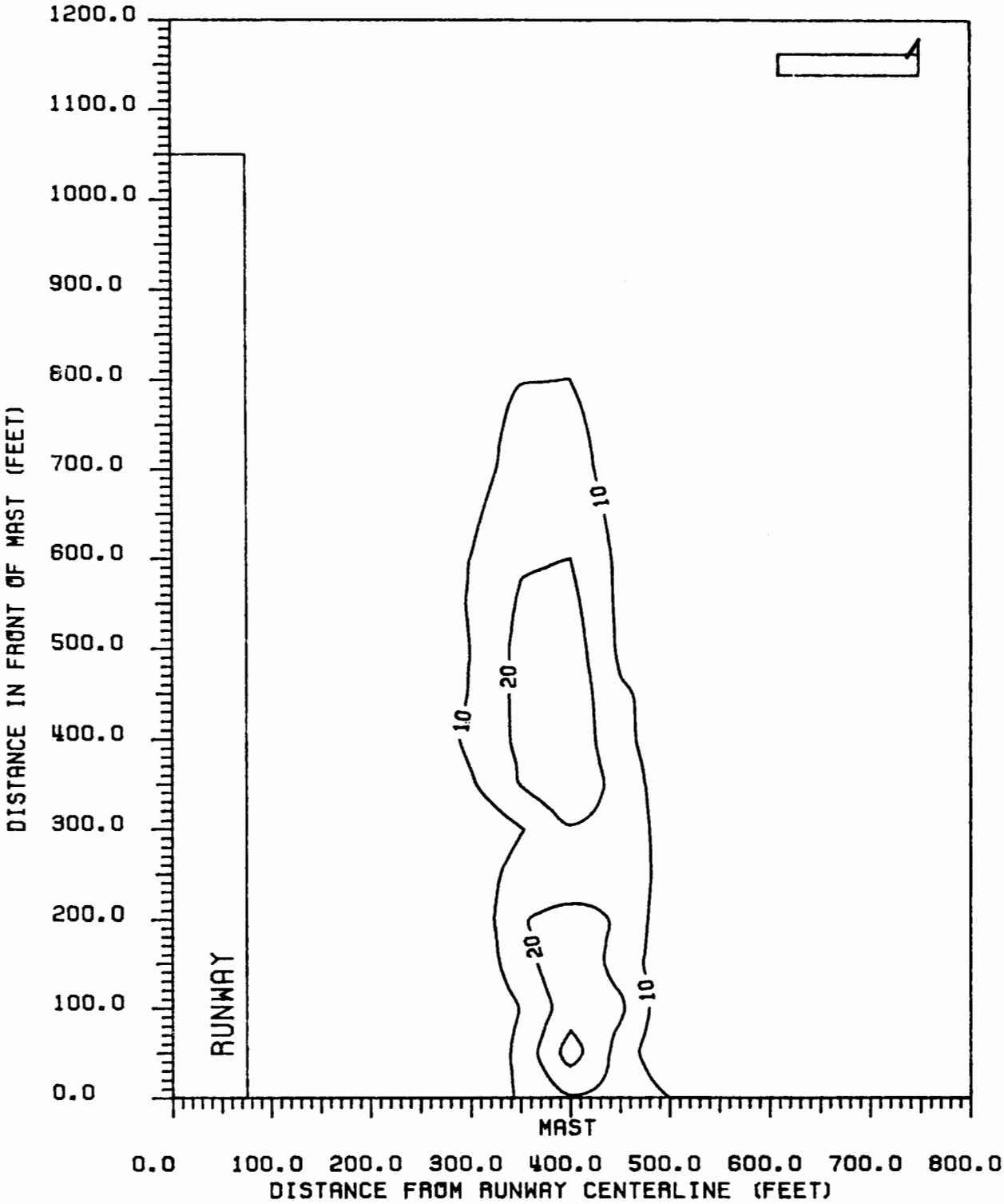

Figure 2-86. Contours of peak CDI values produced in ILS Zone 2 for a C-440. C-440 fuselage is perpendicular to runway centerline, with tail away from the runway. Sideband reference glide slope, directional antennas.

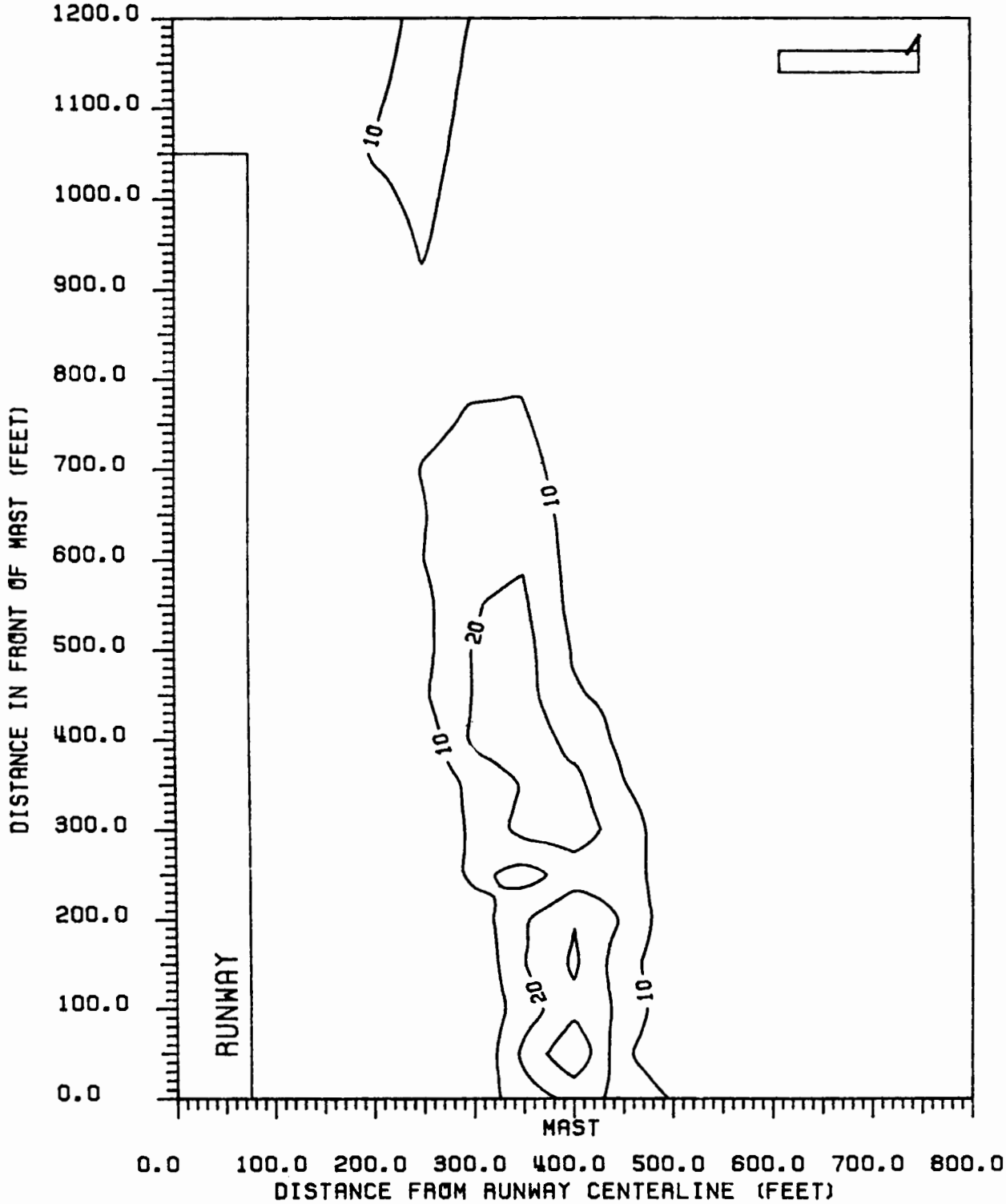

Figure 2-87. Contours of peak CDI values produced between ILS Point B and ILS Point C for a C-440. C-440 fuselage is perpendicular to runway centerline, with tail away from runway. Sideband reference glide slope, directional antennas.

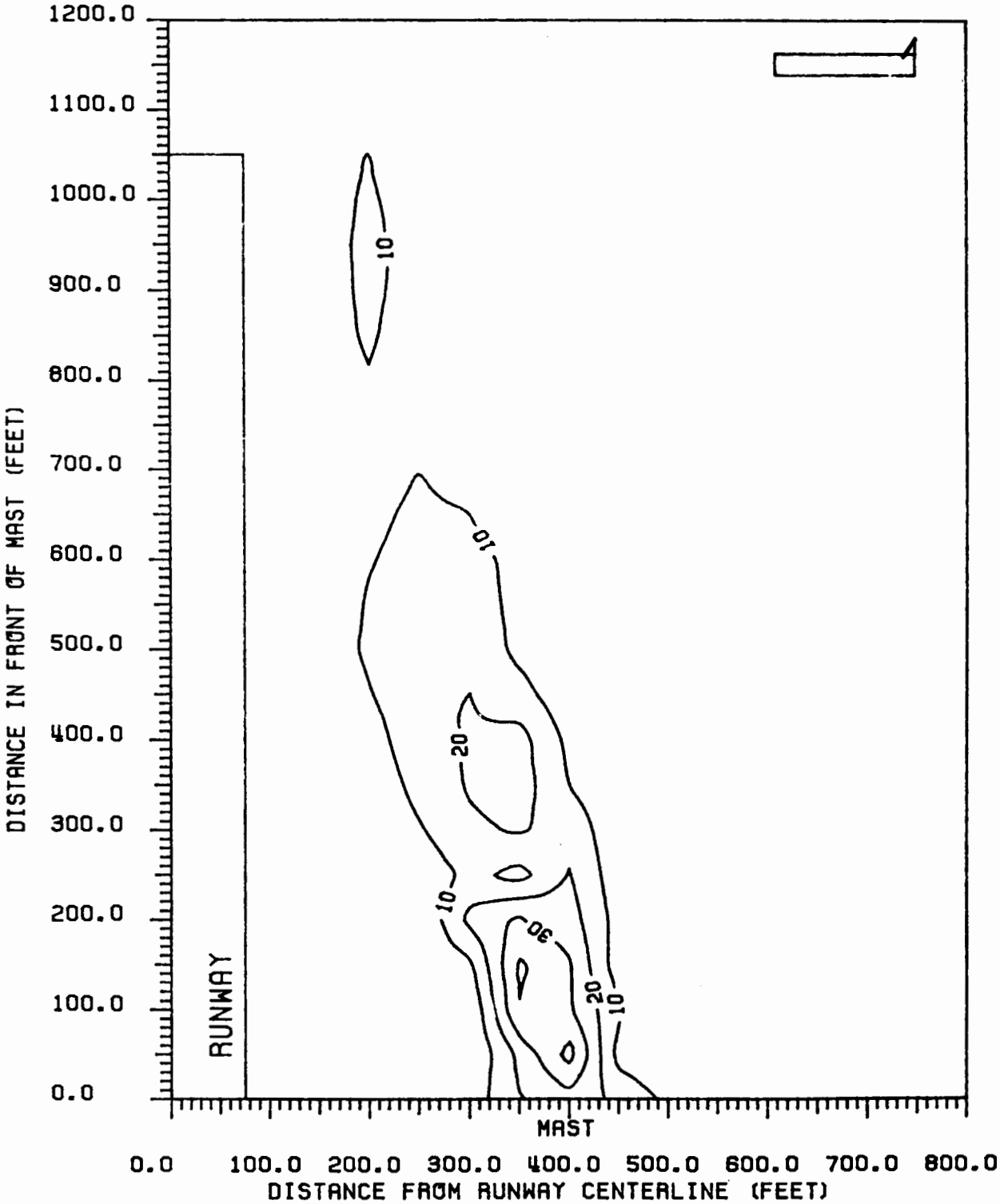

Figure 2-88. Contours of peak CDI values produced between ILS Point C and threshold for a C-440. C-440 fuselage is perpendicular to runway centerline, with tail away from runway. Sideband reference glide slope, directional antennas.

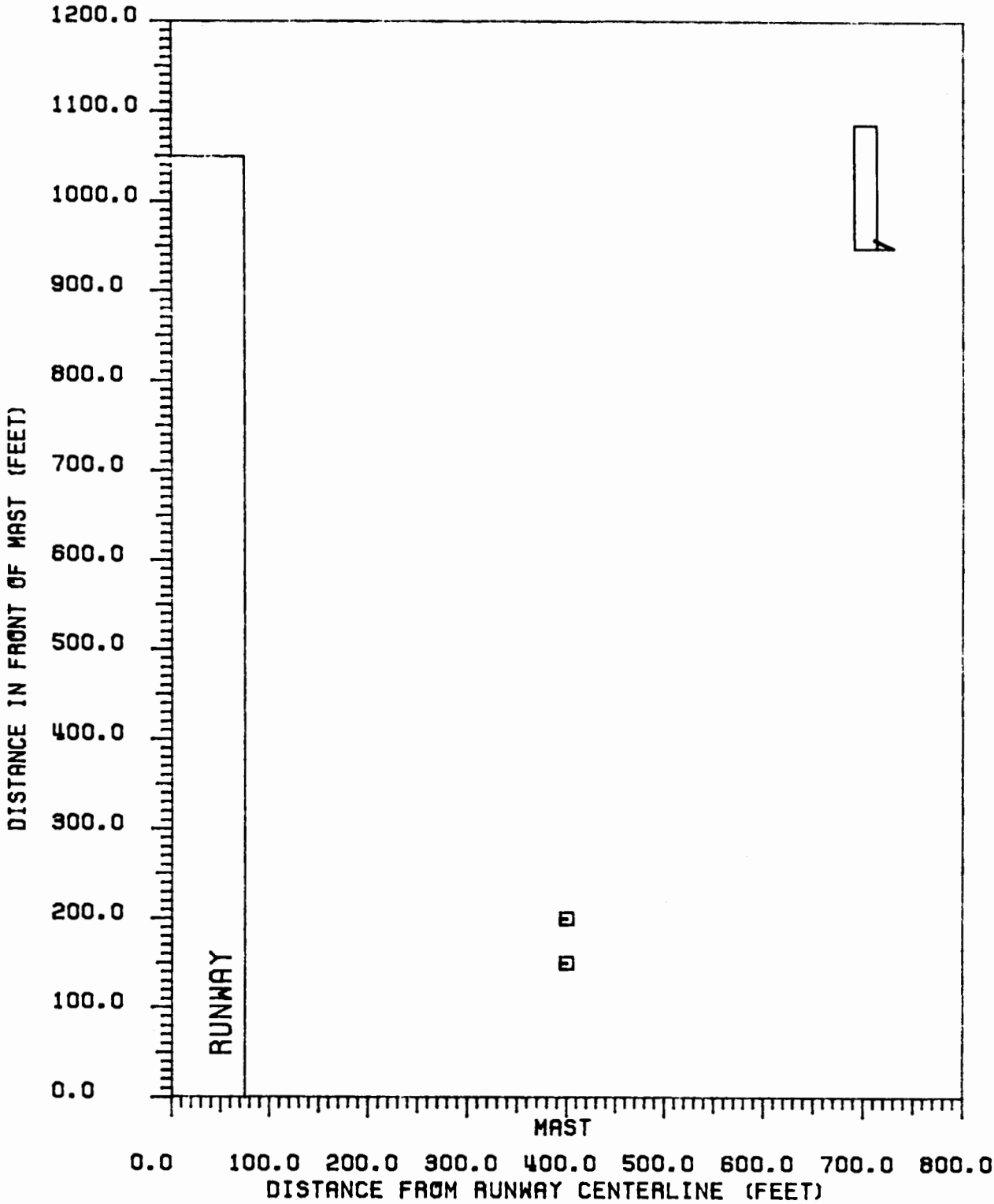

Figure 2-89. Critical area map for CAT I tolerances relating to C-440 aircraft. C-440 fuselage is parallel to runway centerline with tail towards the mast. Sideband reference glide slope, directional antennas.

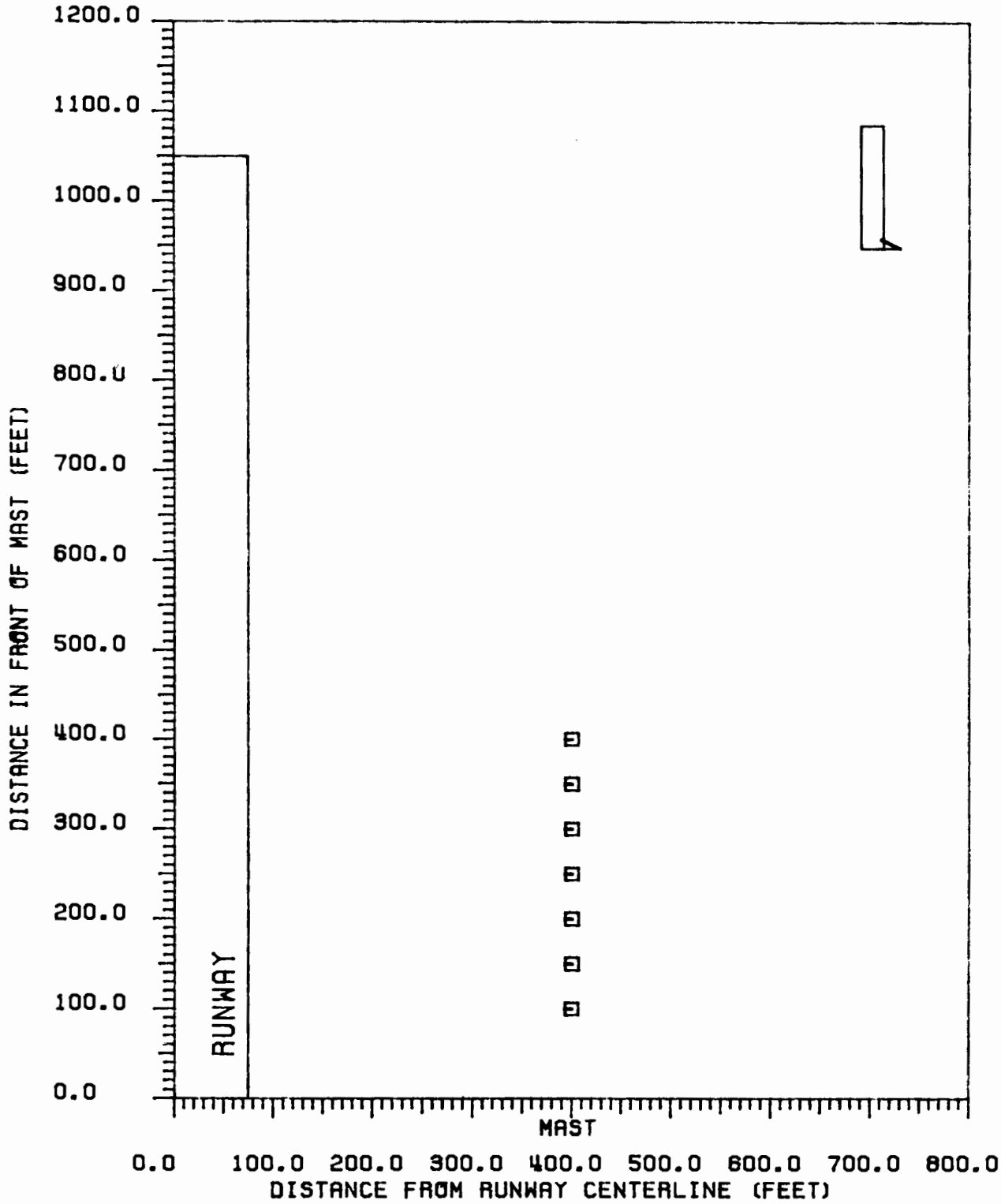

Figure 2-90. Critical area map for CAT II/III tolerances relating to C-440 aircraft. C-440 fuselage is parallel to runway centerline with tail towards the mast. Sideband reference glide slope, directional antennas.

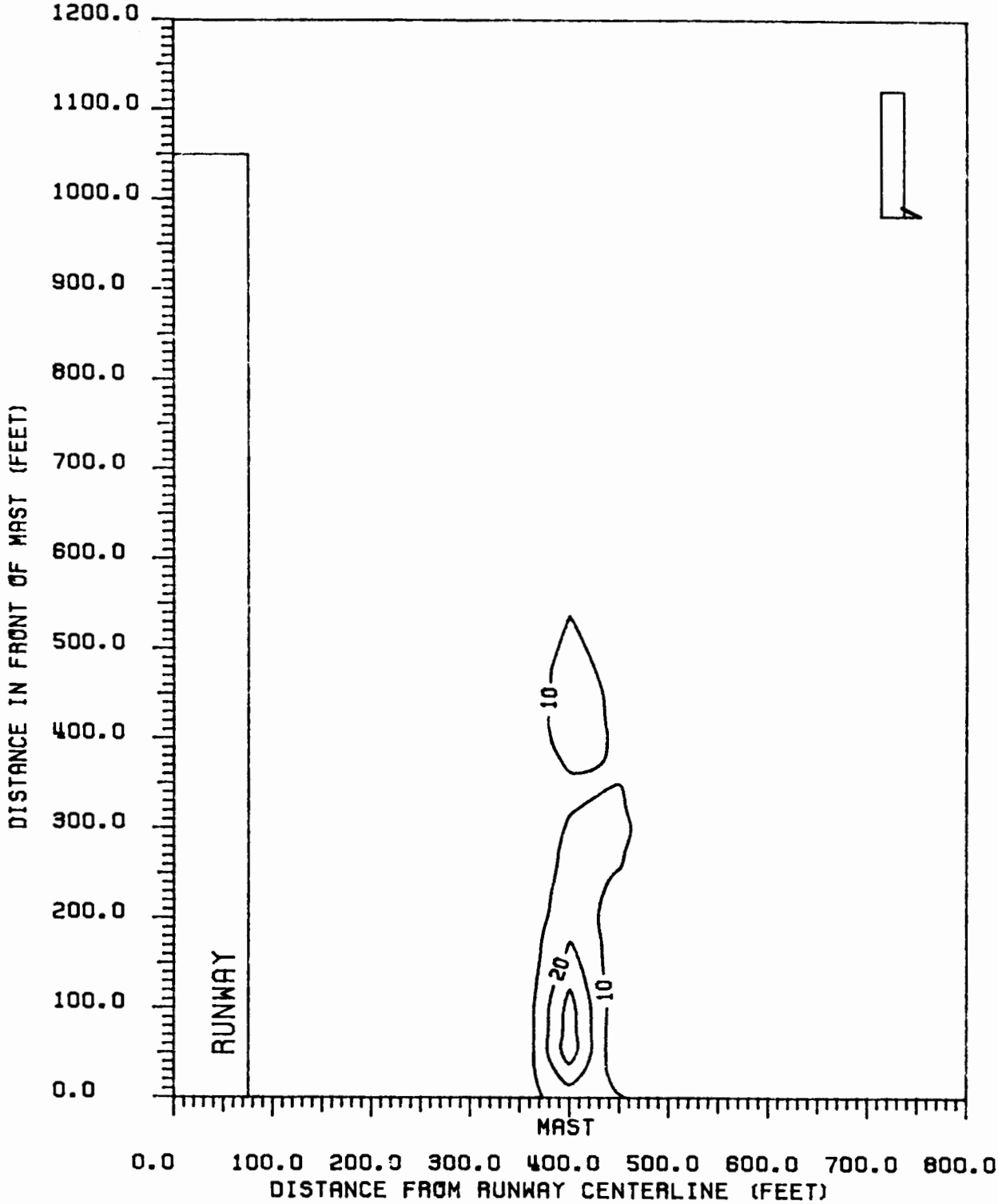

Figure 2-91. Contours of peak CDI values produced in ILS Zone 2 for a C-440. C-440 fuselage is parallel to runway centerline, with tail towards the mast. Sideband reference glide slope, directional antennas.

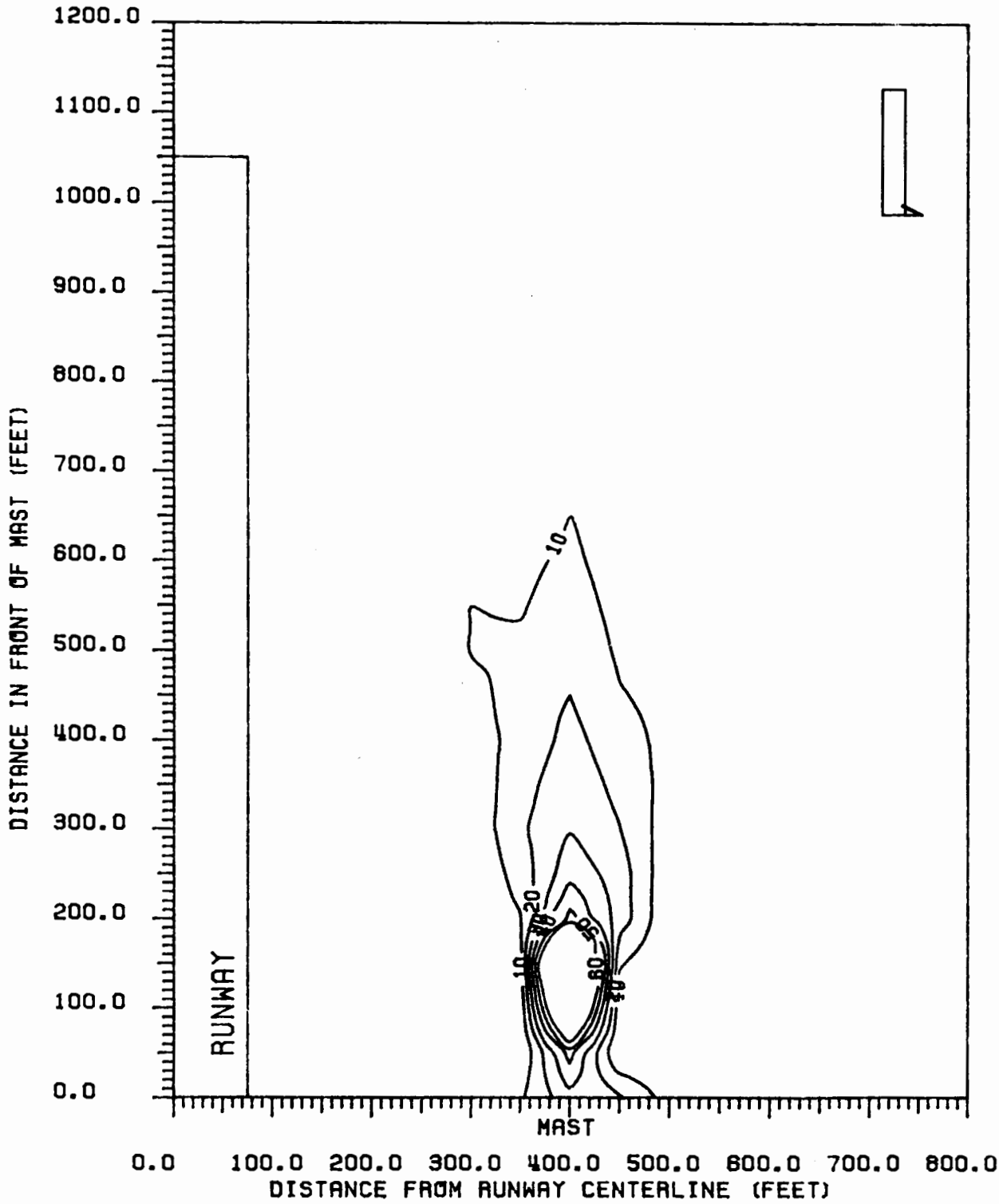

Figure 2-92. Contours of peak CDI values produced between ILS Point B and ILS Point C for a C-440. C-440 fuselage is parallel to runway centerline, with tail towards the mast. Sideband reference glide slope, directional antennas.

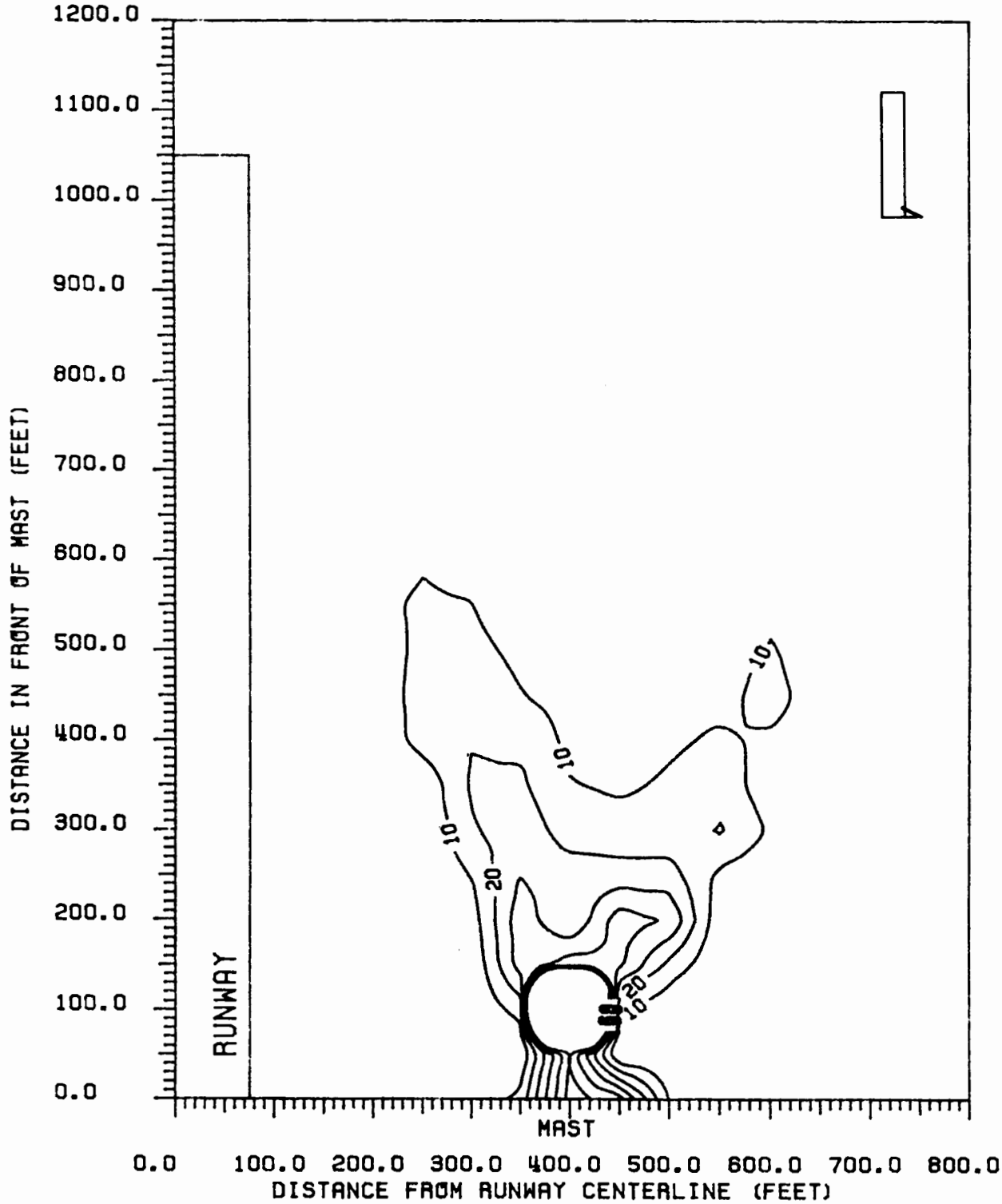

Figure 2-93. Contours of peak CDI values produced between ILS Point C and threshold for a C-440. C-440 fuselage is parallel to runway centerline, with tail towards the mast. Sideband reference glide slope, directional antennas.

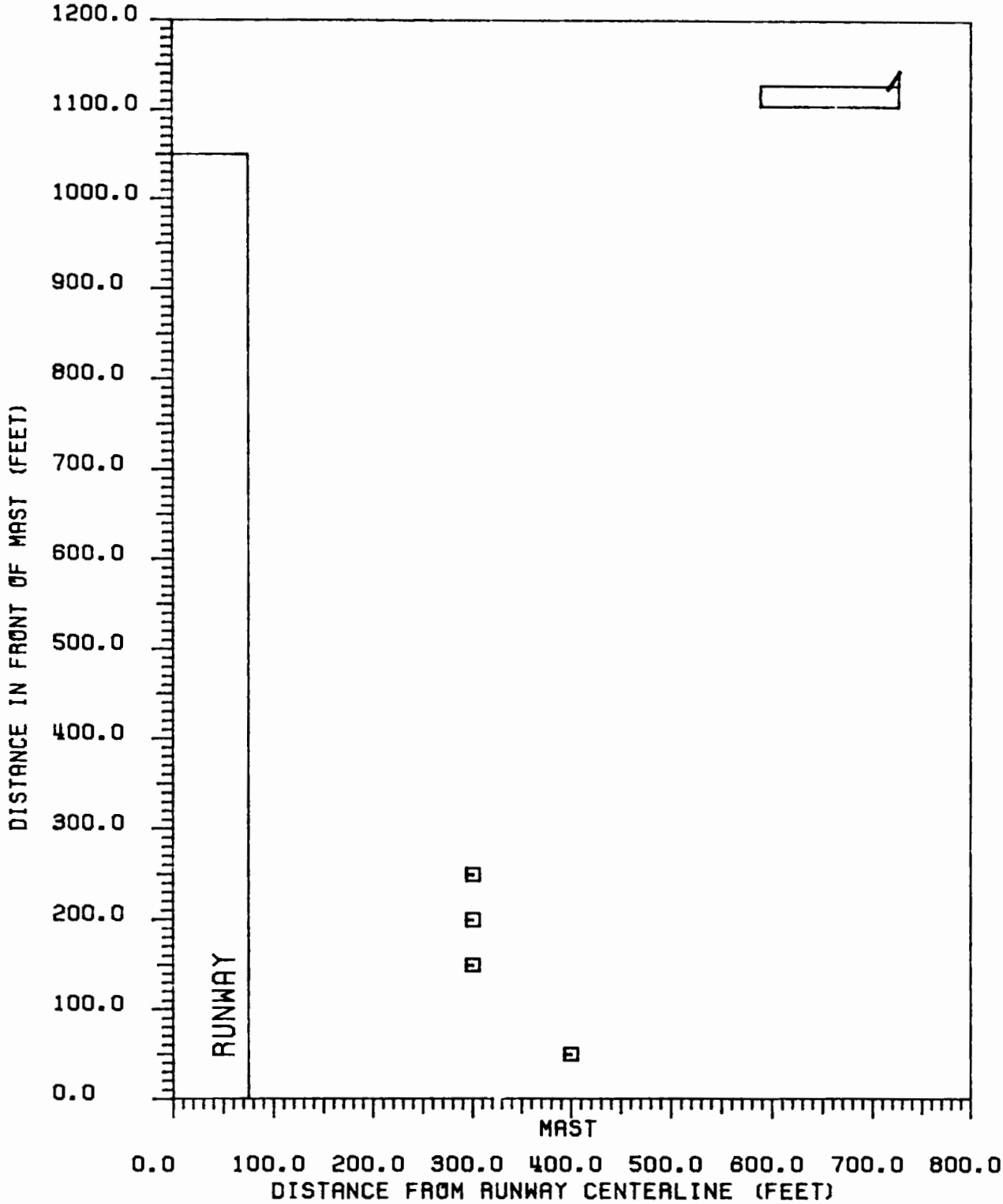

Figure 2-94. Critical area map for CAT II/III tolerances relating to DC-9 aircraft. DC-9 fuselage is perpendicular to runway centerline with tail away from the runway. Sideband reference glide slope, directional antennas.

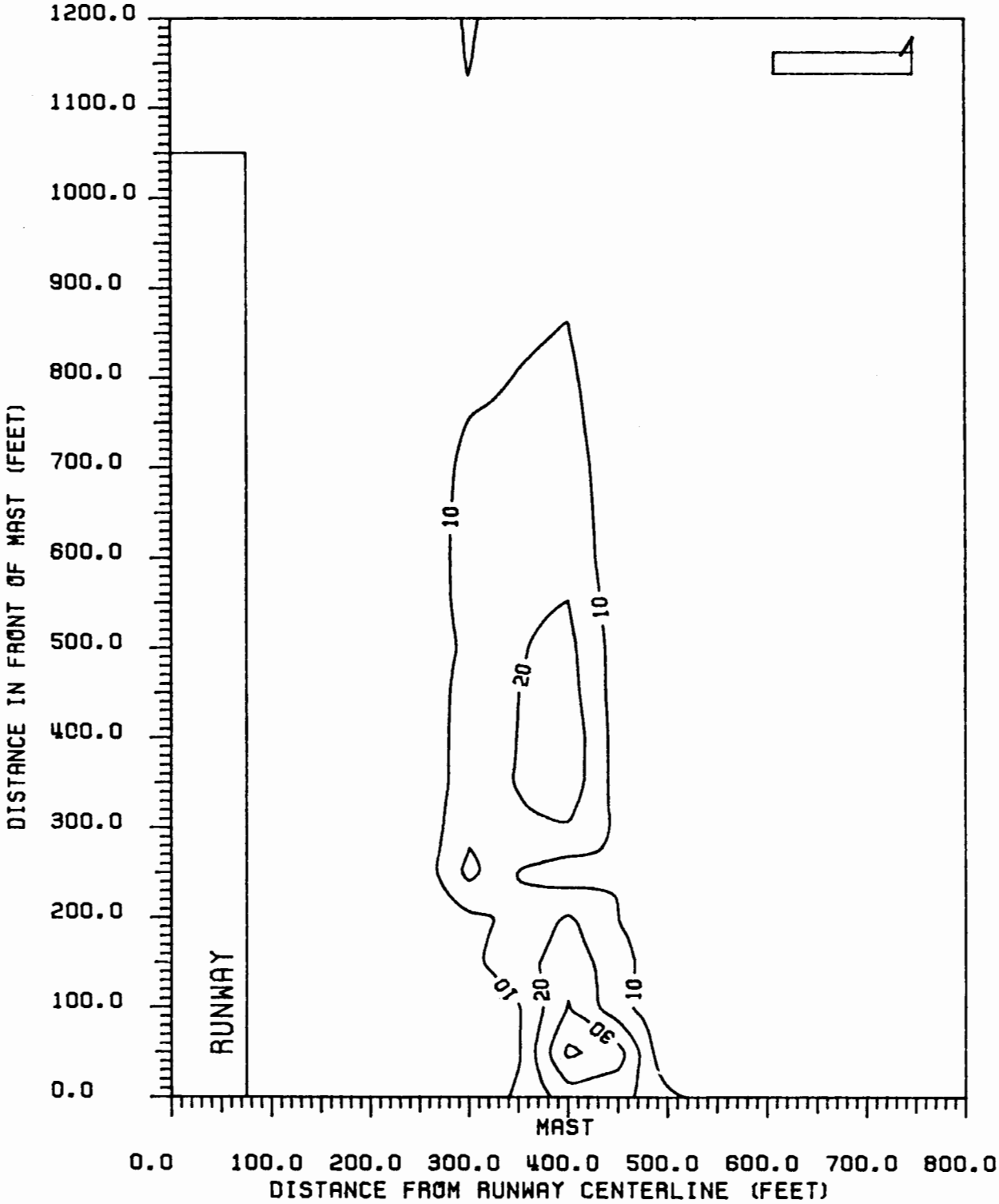

Figure 2-95. Contours of peak CDI values produced in ILS Zone 2 for a DC-9. DC-9 fuselage is perpendicular to runway centerline, with tail away from the runway. Sideband reference glide slope, directional antennas.

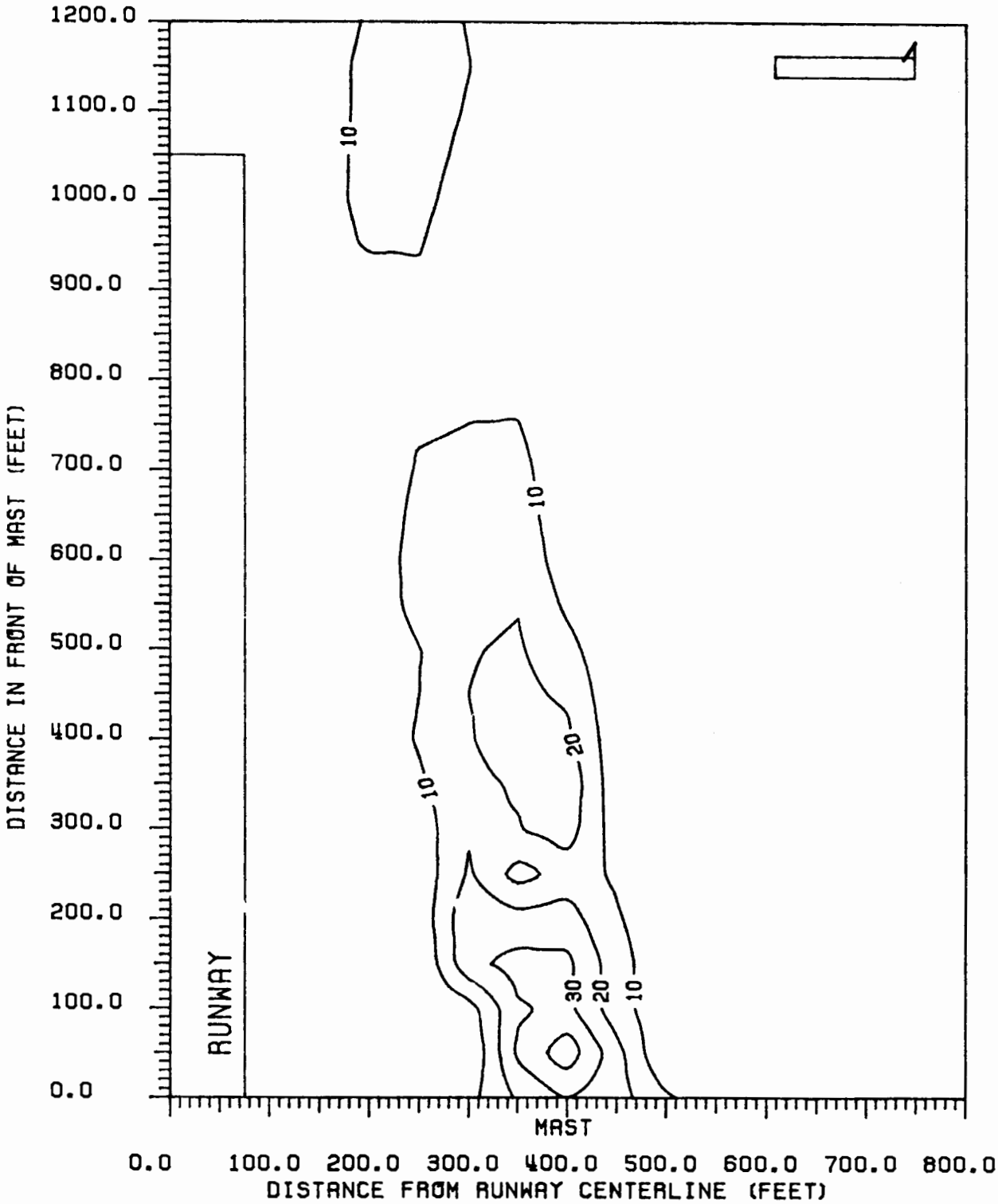

Figure 2-96. Contours of peak CDI values produced between ILS Point B and ILS Point C for a DC-9. DC-9 fuselage is perpendicular to runway centerline, with tail away from runway. Sideband reference glide slope, directional antennas.

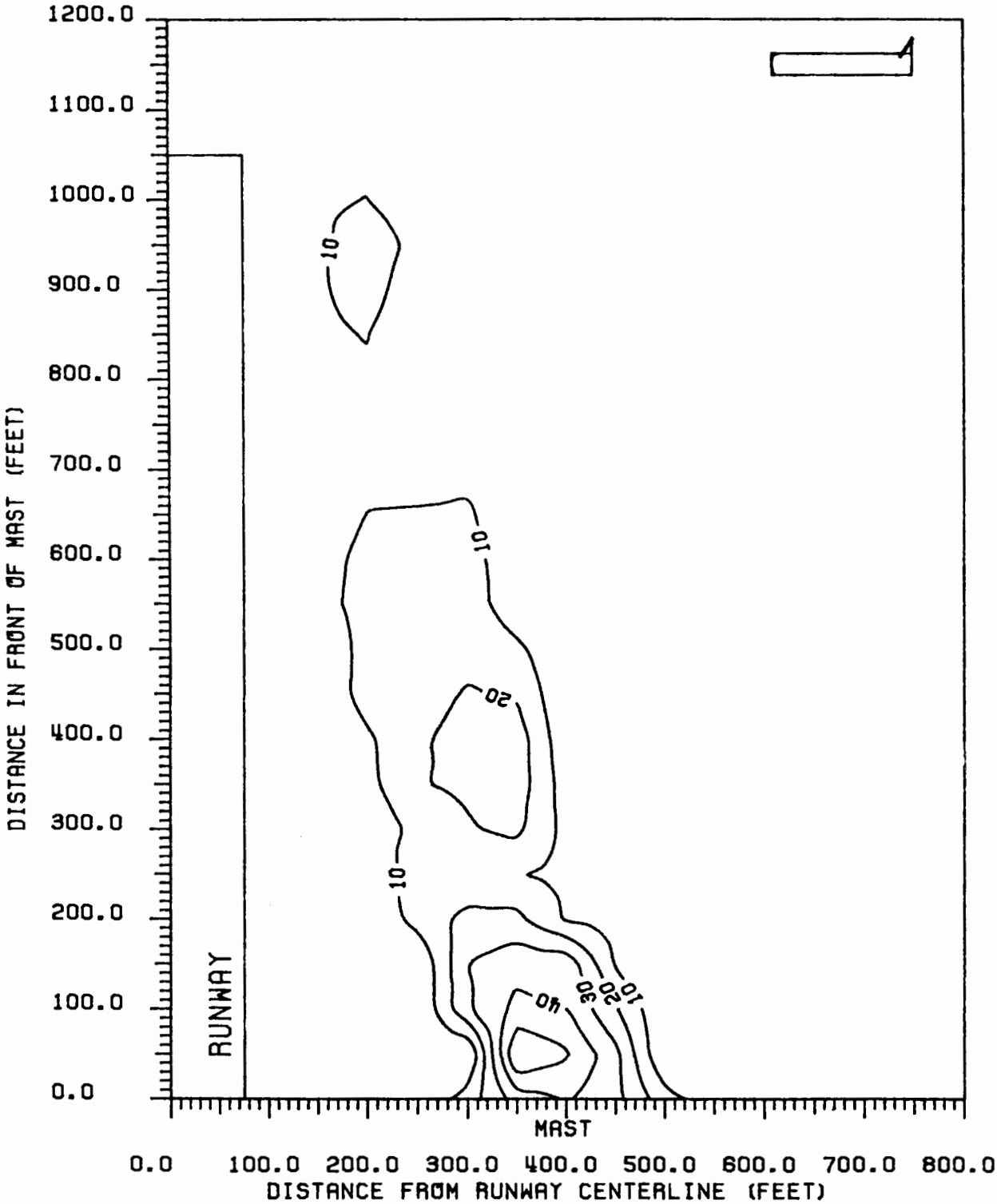

Figure 2-97. Contours of peak CDI values produced between ILS Point C and threshold for a DC-9. DC-9 fuselage is perpendicular to runway centerline, with tail away from runway. Sideband reference glide slope, directional antennas.

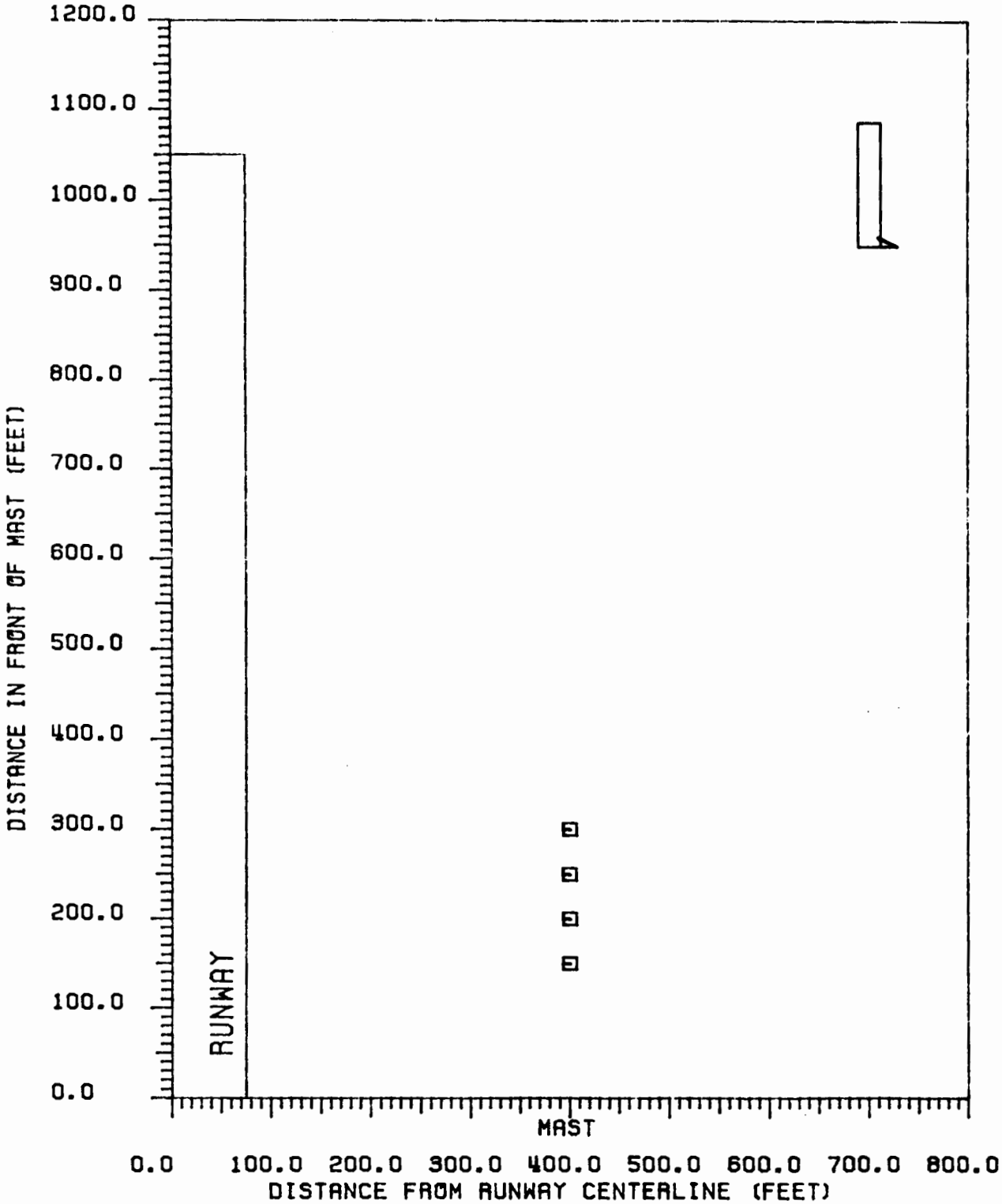

Figure 2-98. Critical area map for CAT I tolerances relating to DC-9 aircraft. DC-9 fuselage is parallel to runway centerline with tail towards the mast. Sideband reference glide slope, directional antennas.

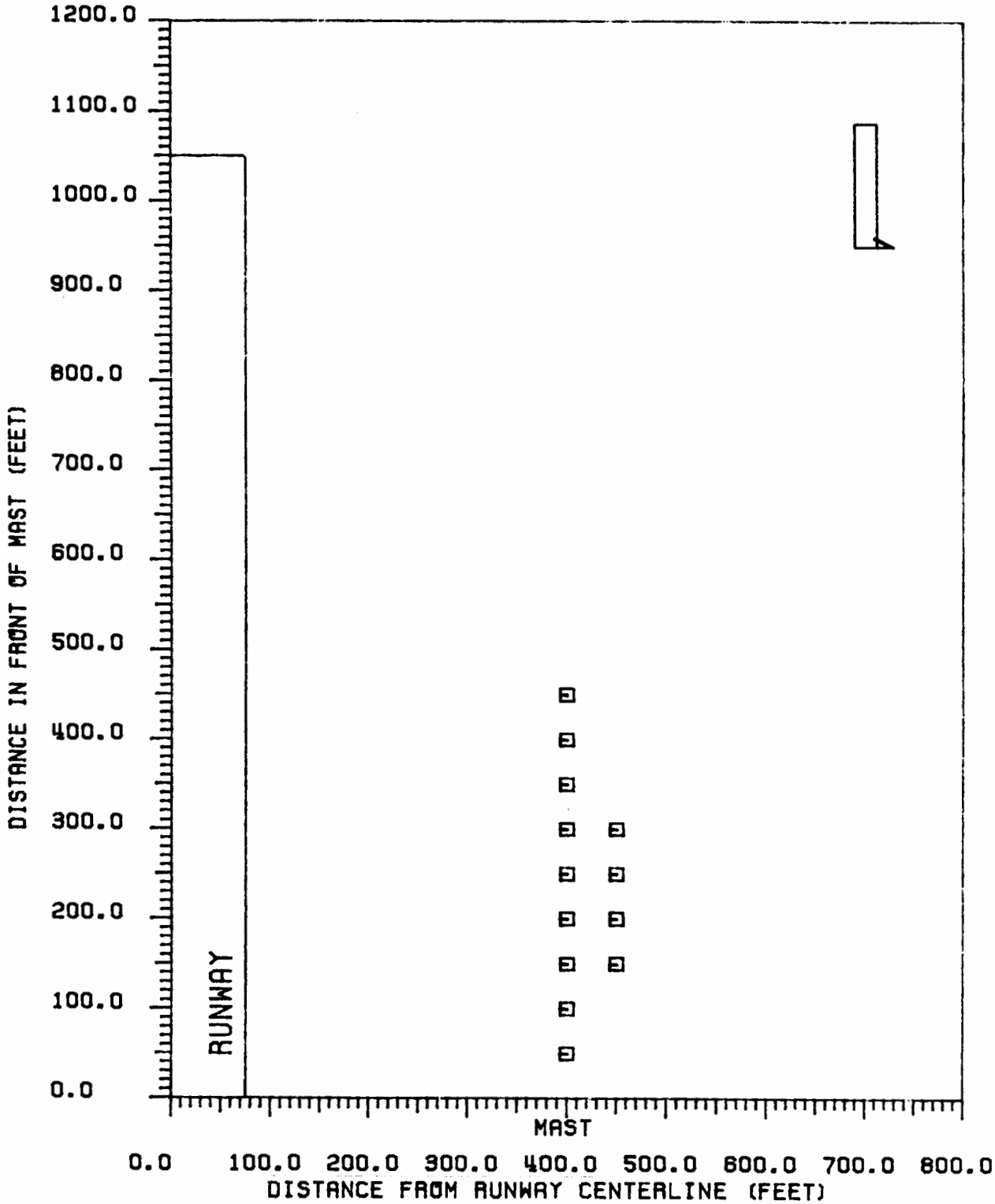

Figure 2-99. Critical area map for CAT II/III tolerances relating to DC-9 aircraft. DC-9 fuselage is parallel to runway centerline with tail towards the mast. Sideband reference glide slope, directional antennas.

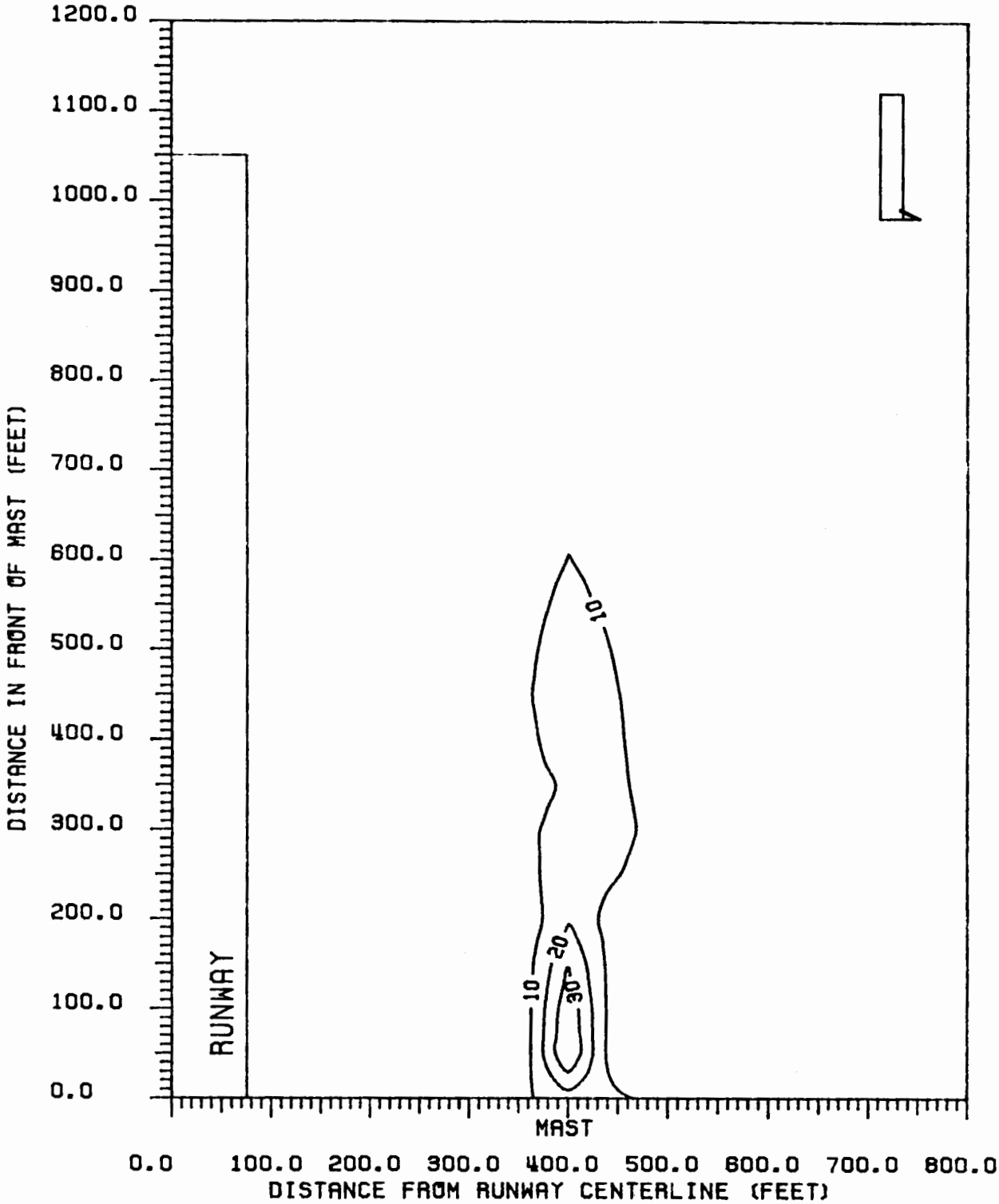

Figure 2-100. Contours of peak CDI values produced in ILS Zone 2 for a DC-9. DC-9 fuselage is parallel to runway centerline, with tail towards the mast. Sideband reference glide slope, directional antennas.

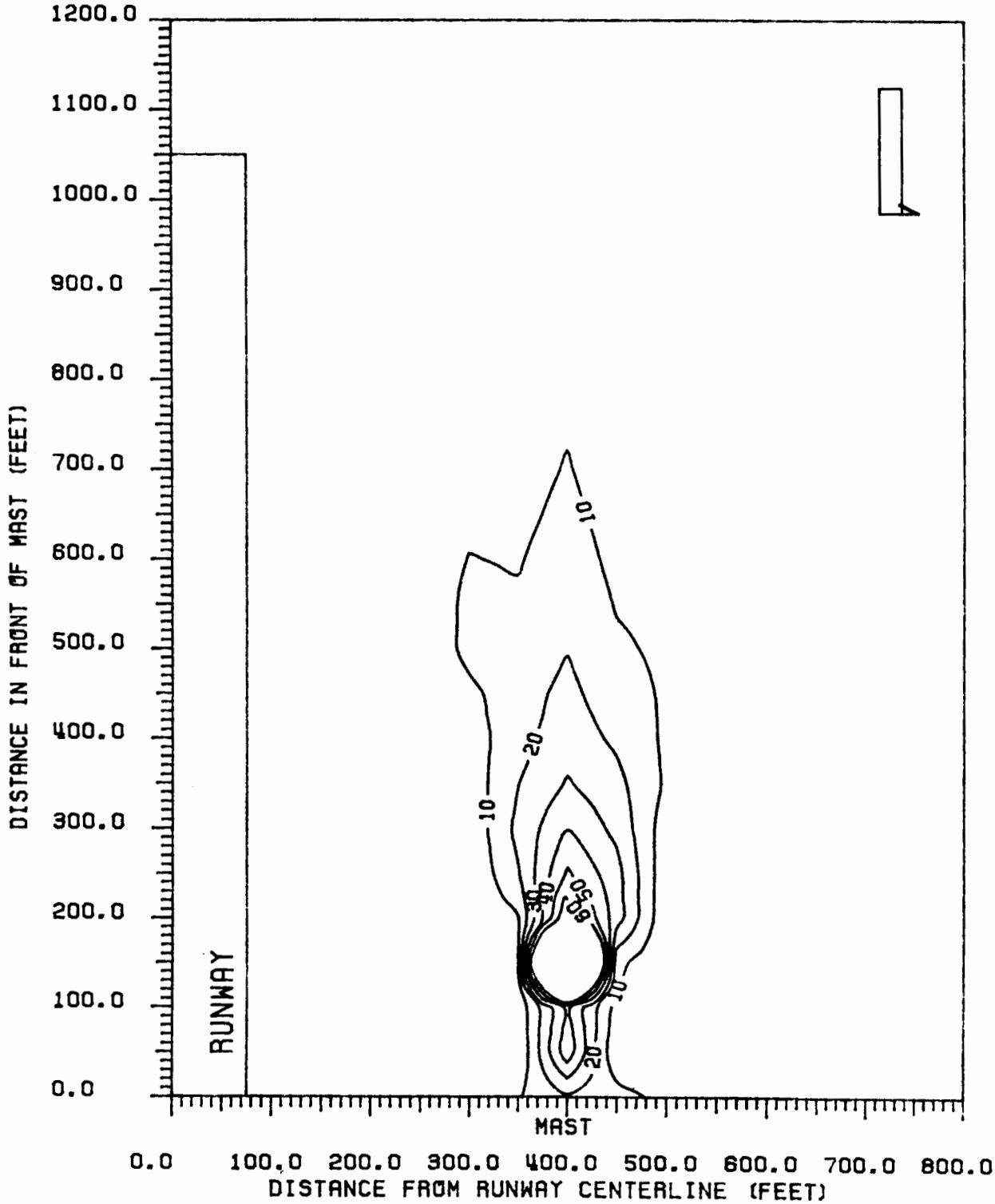

Figure 2-101. Contours of peak CDI values produced between ILS Point B and ILS Point C for a DC-9. DC-9 fuselage is parallel to runway centerline, with tail towards the mast. Sideband reference glide slope, directional antennas.

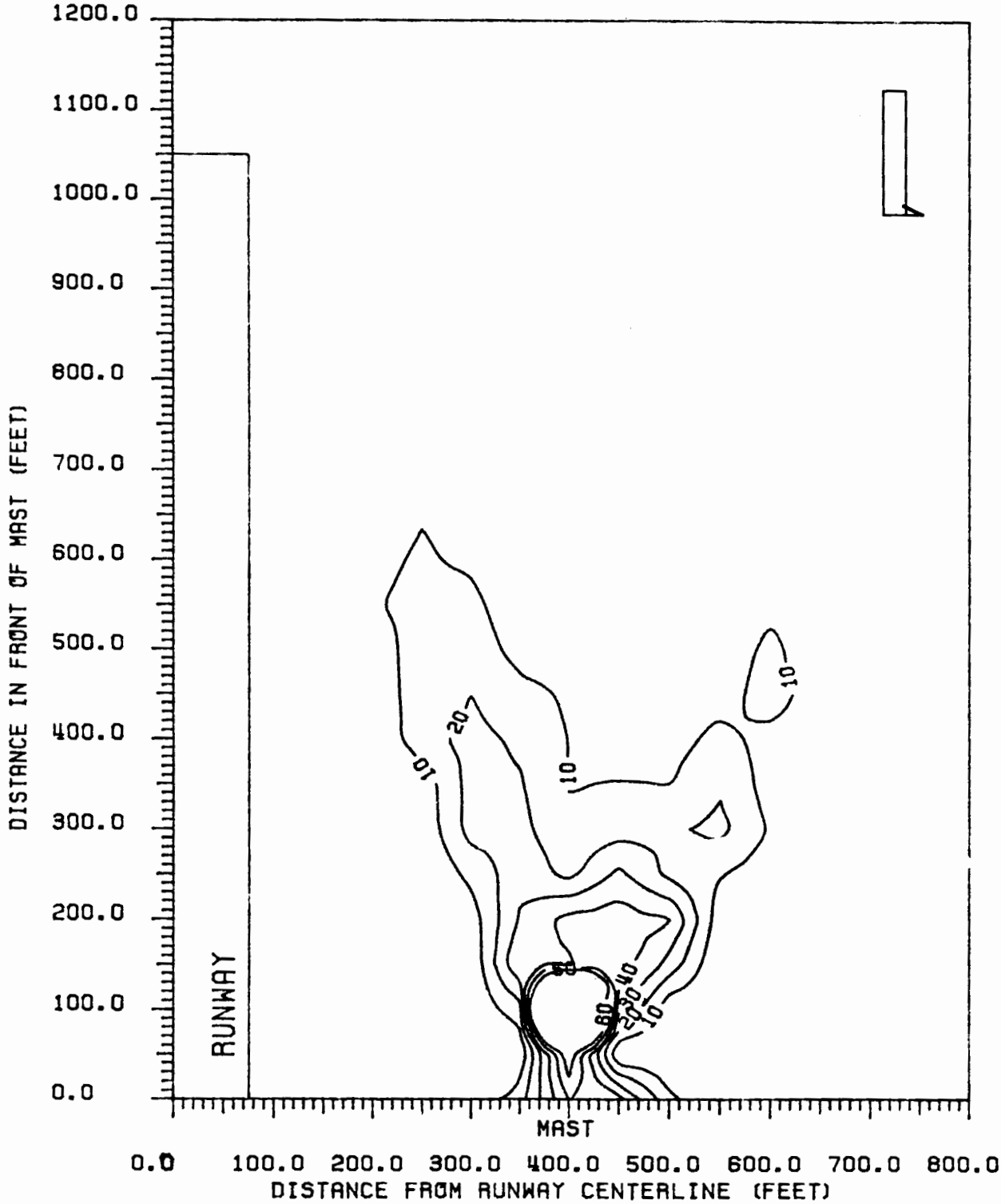

Figure 2-102. Contours of peak CDI values produced between ILS Point C and threshold for a DC-9. DC-9 fuselage is parallel to runway centerline, with tail towards the mast. Sideband reference glide slope, directional antennas.

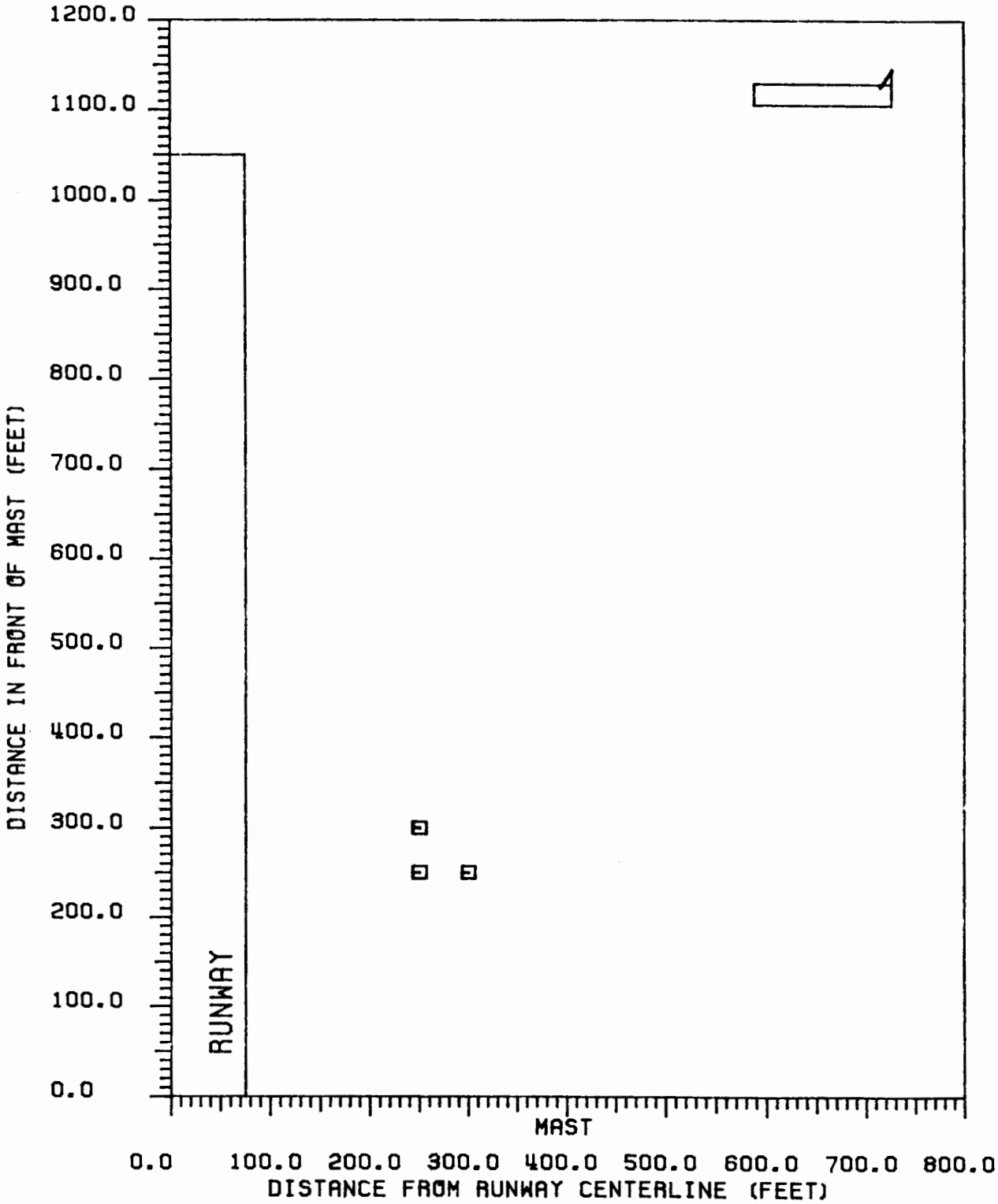

Figure 2-103. Critical area map for CAT II/III tolerances relating to B-727 aircraft. B-727 fuselage is perpendicular to runway centerline with tail away from the runway. Sideband reference glide slope, directional antennas.

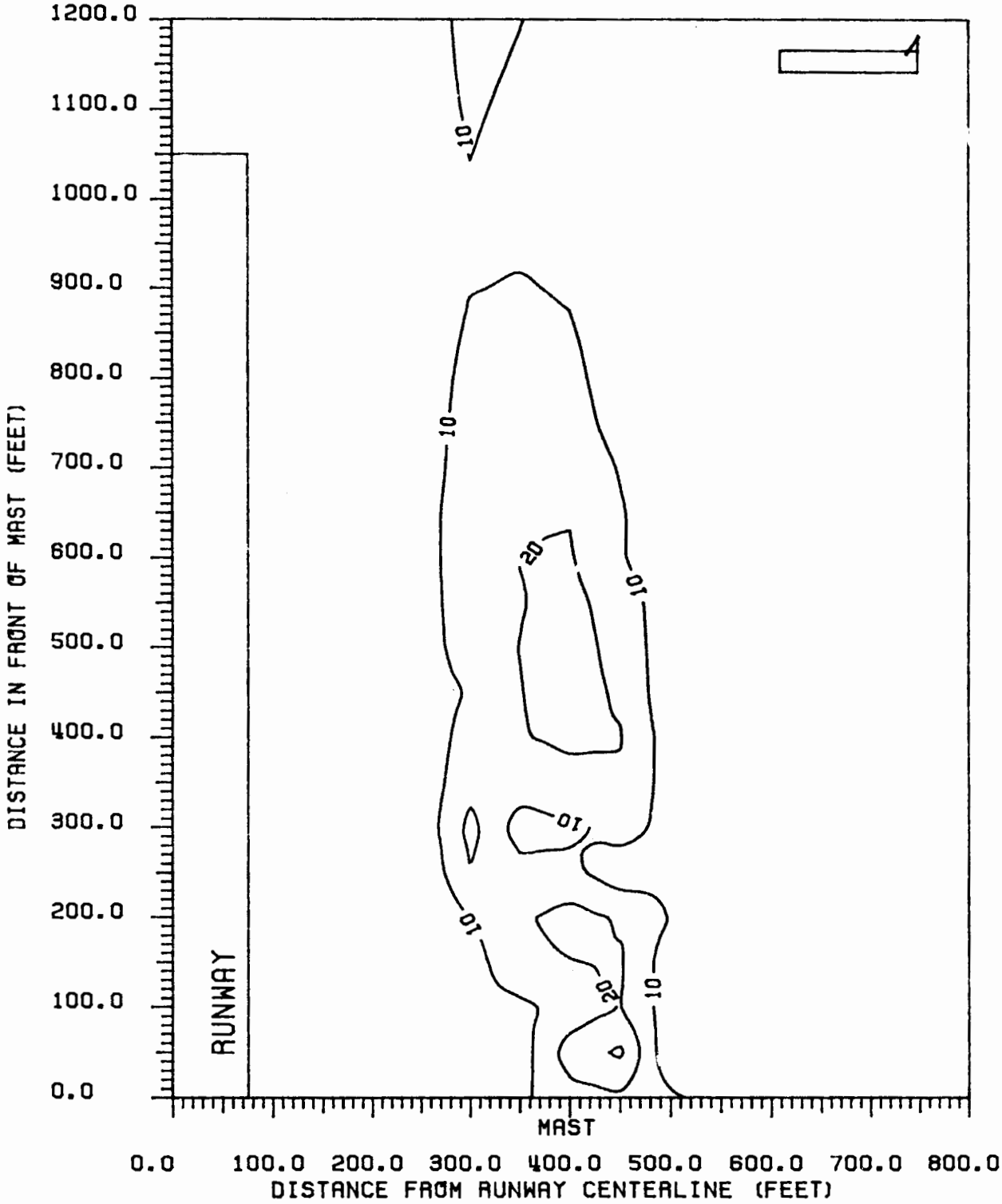

Figure 2-104. Contours of peak CDI values produced in ILS Zone 2 for a B-727. B-727 fuselage is perpendicular to runway centerline, with tail away from the runway. Sideband reference glide slope, directional antennas.

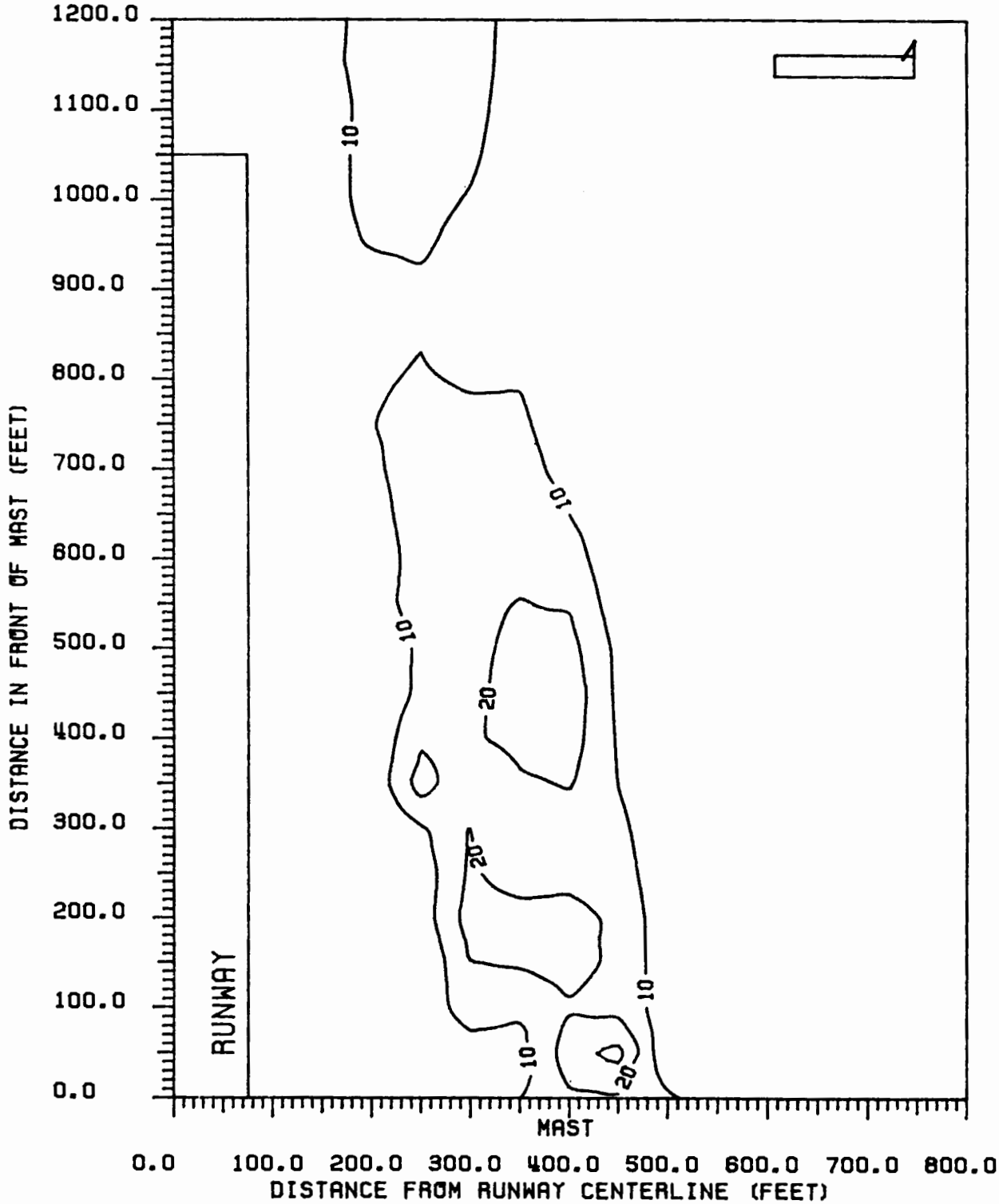

Figure 2-105. Contours of peak CDI values produced between ILS Point B and ILS Point C for a B-727. B-727 fuselage is perpendicular to runway centerline, with tail away from runway. Sideband reference glide slope, directional antennas.

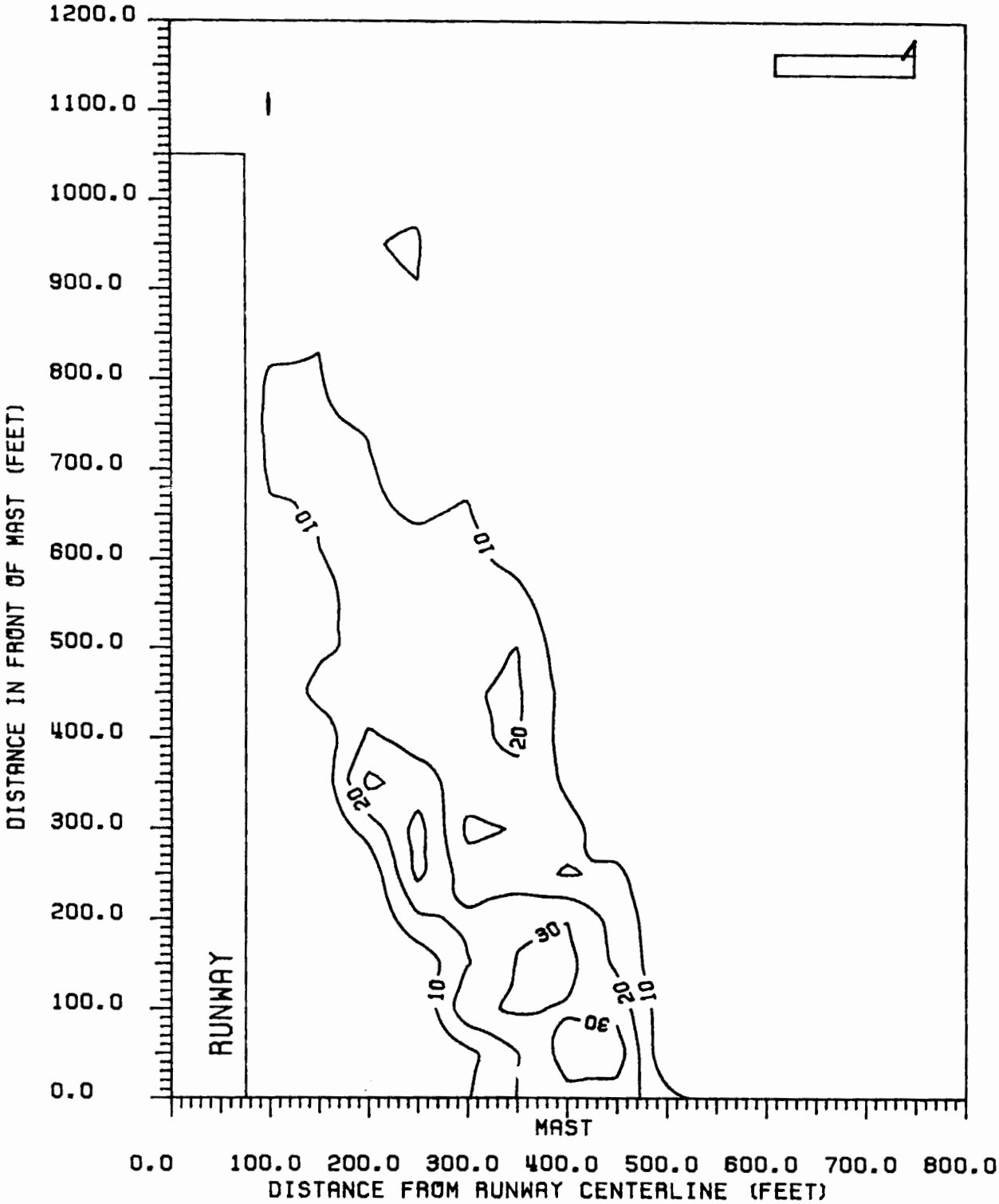

Figure 2-106. Contours of peak CDI values produced between ILS Point C and threshold for a B-727. B-727 fuselage is perpendicular to runway centerline, with tail away from runway. Sideband reference glide slope, directional antennas.

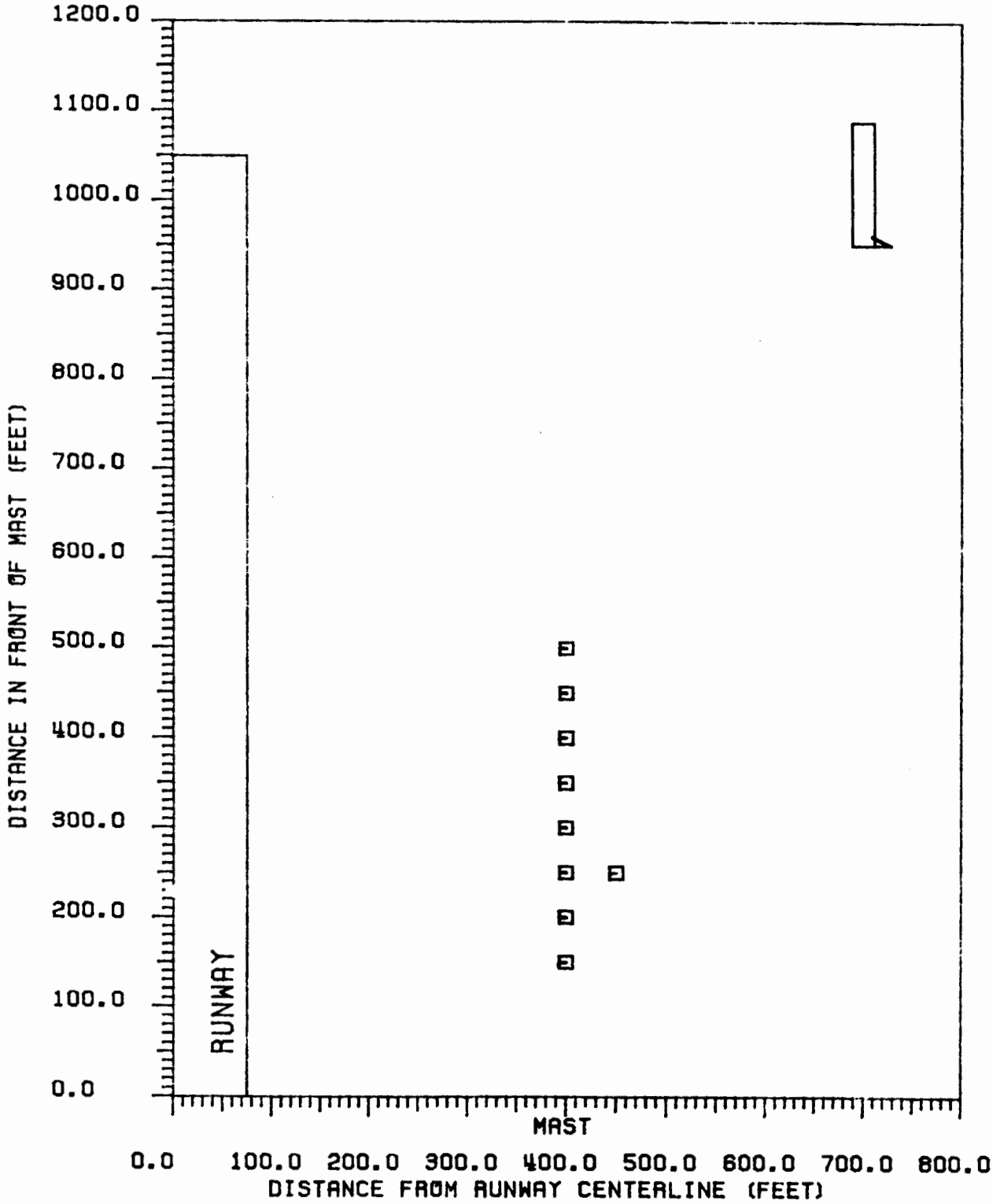

Figure 2-107. Critical area map for CAT I tolerances relating to B-727 aircraft. B-727 fuselage is parallel to runway centerline with tail towards the mast. Sideband reference glide slope, directional antennas.

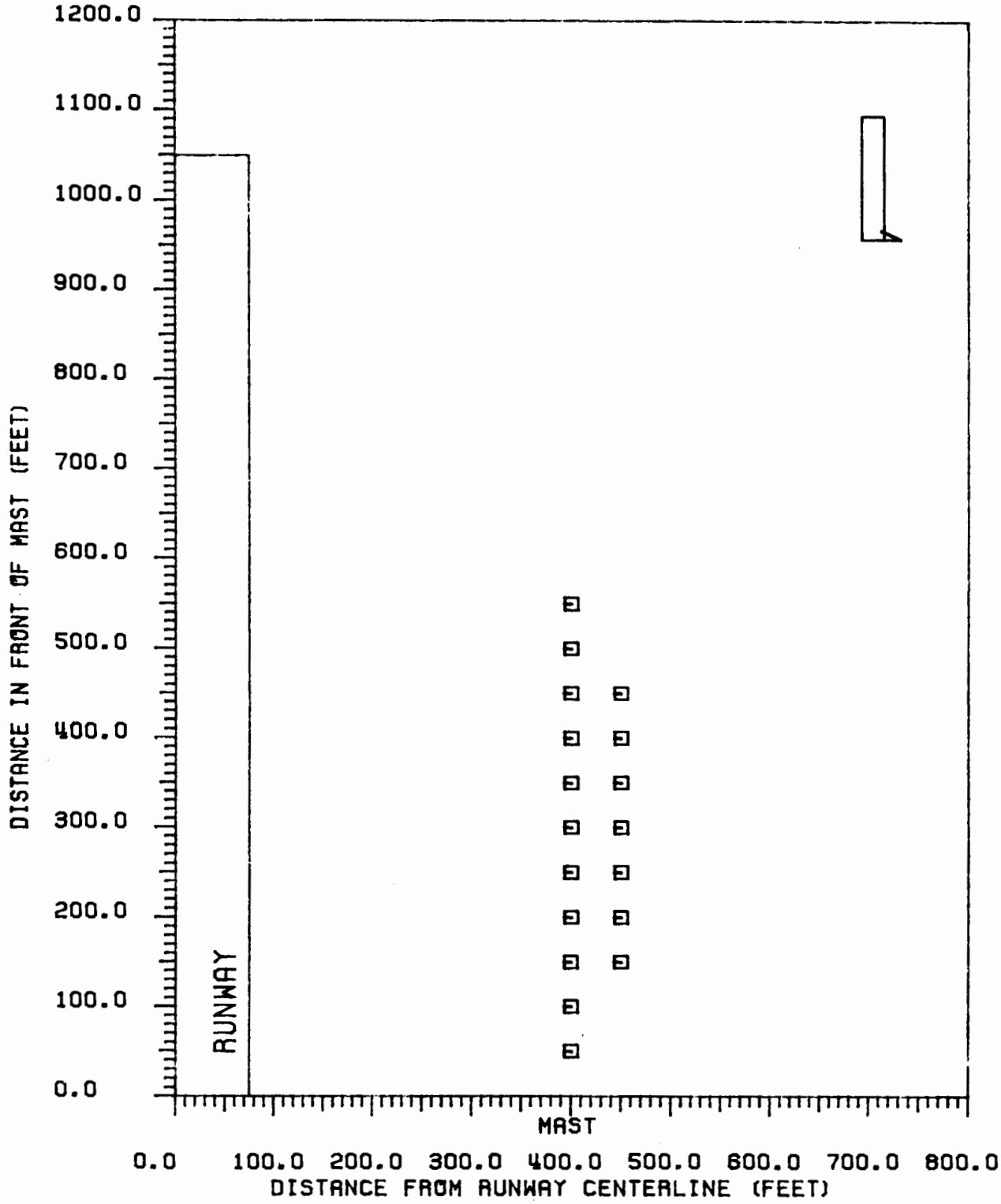

Figure 2-108. Critical area map for CAT II/III tolerances relating to B-727 aircraft. B-727 fuselage is parallel to run-centerline with tail towards the mast. Sideband reference glide slope, directional antennas.

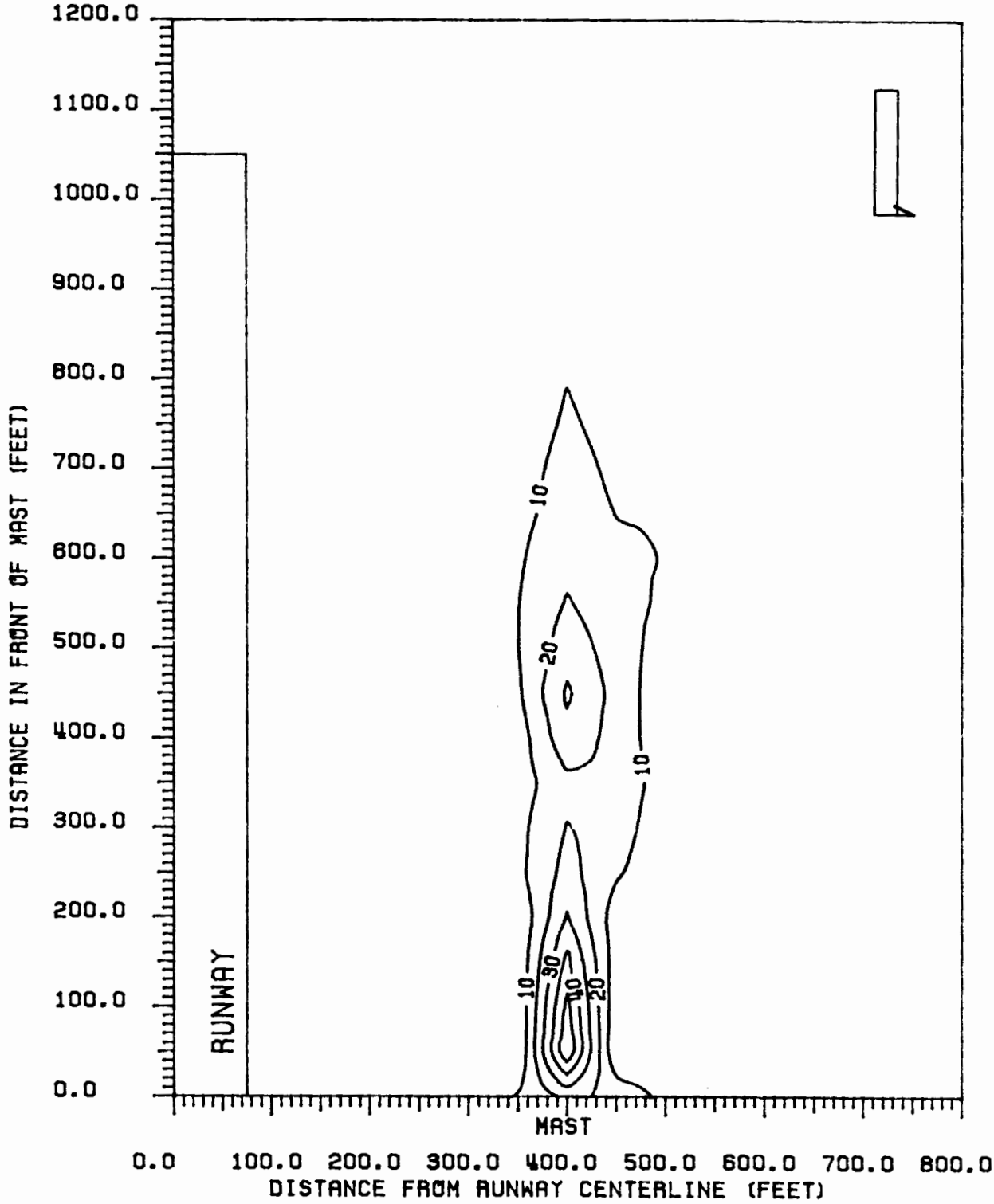

Figure 2-109. Contours of peak CDI values produced in ILS Zone 2 for a B-727. B-727 fuselage is parallel to runway centerline, with tail towards the mast. Sideband reference glide slope, directional antennas.

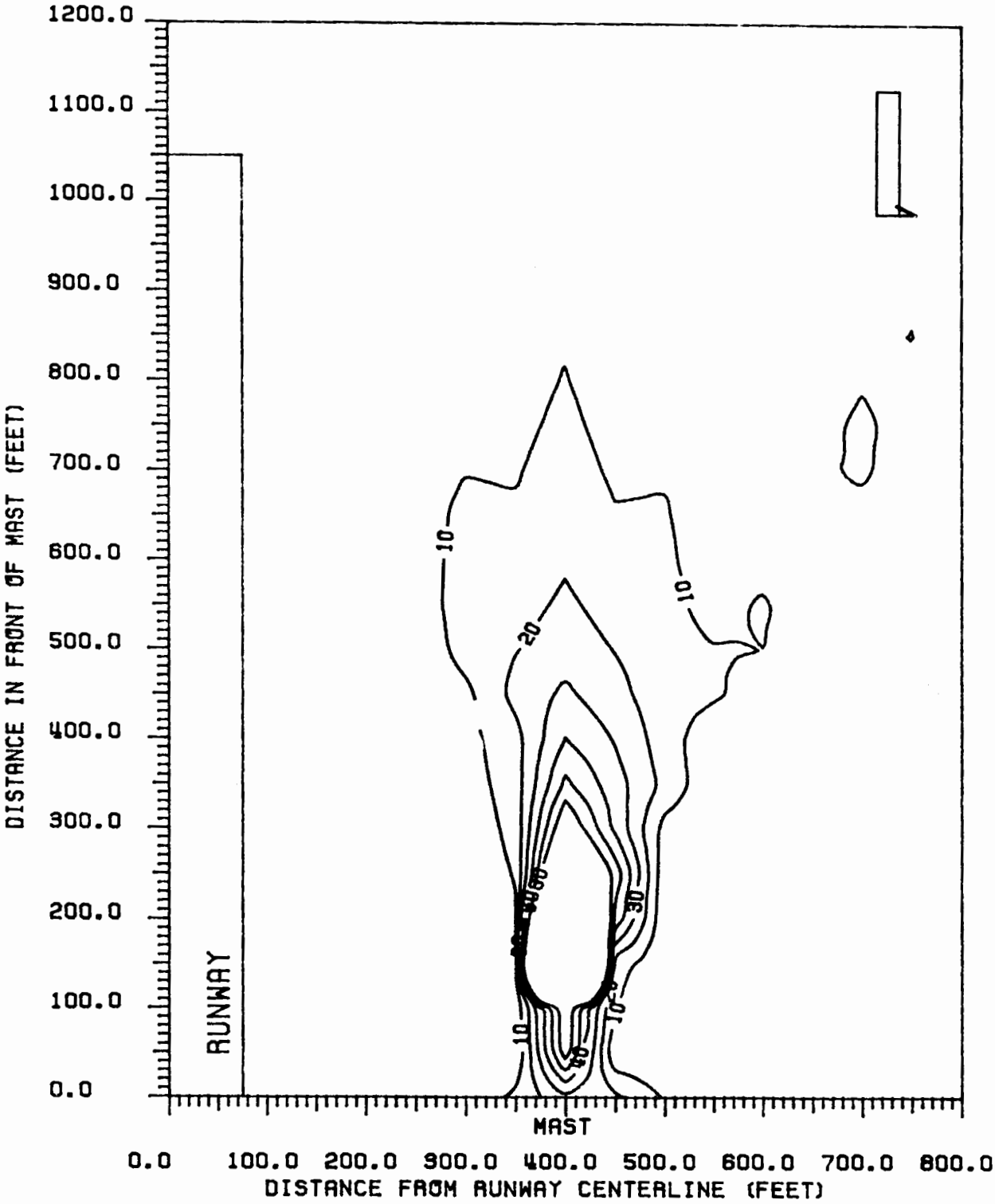

Figure 2-110. Contours of peak CDI values produced between ILS Point B and ILS Point C for a B-727. B-727 fuselage is parallel to runway centerline, with tail towards the mast. Sideband reference glide slope, directional antennas.

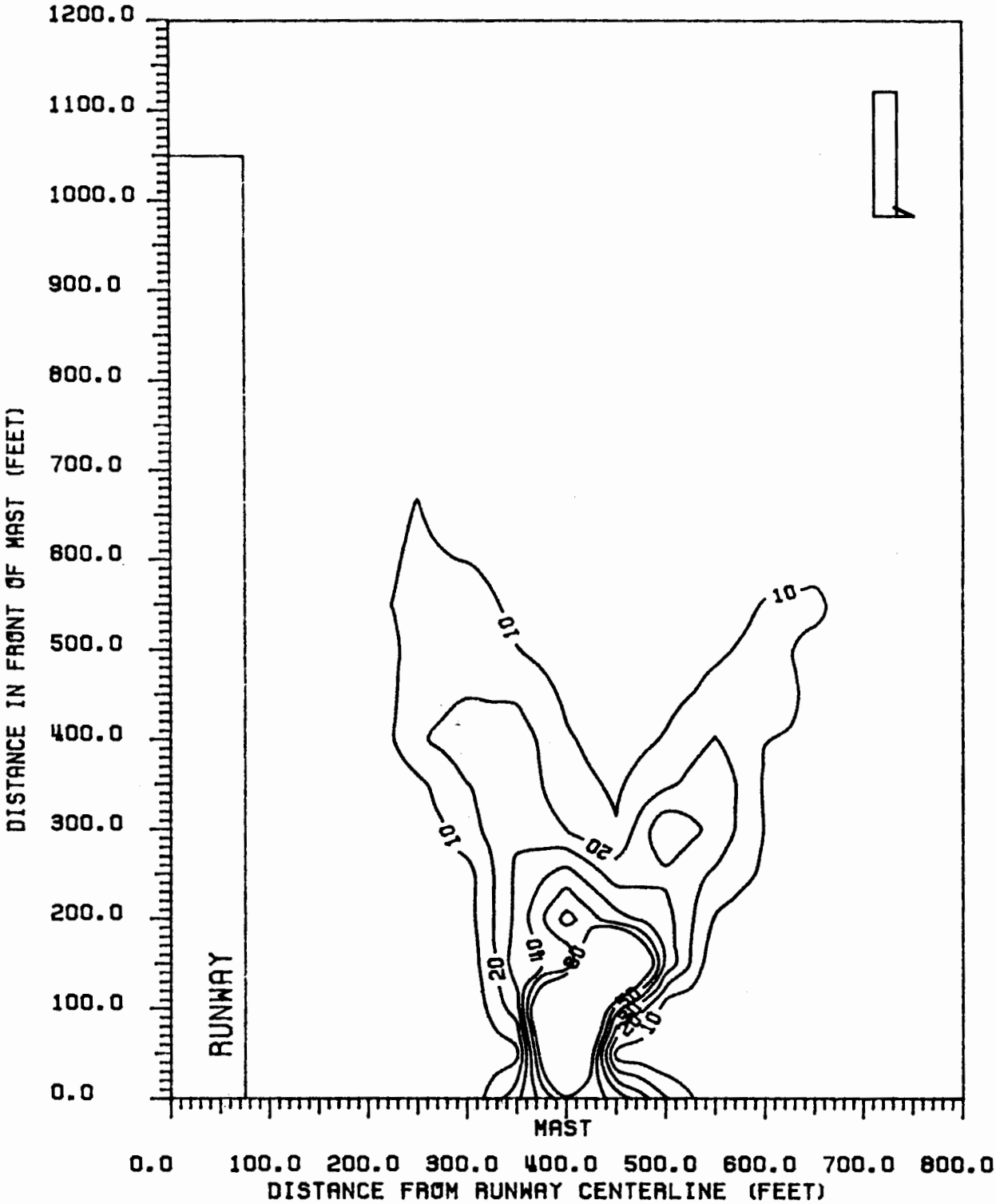

Figure 2-111. Contours of peak CDI values produced between ILS Point C and threshold for a B-727. B-727 fuselage is parallel to runway centerline, with tail towards the mast. Sideband reference glide slope, directional antennas.

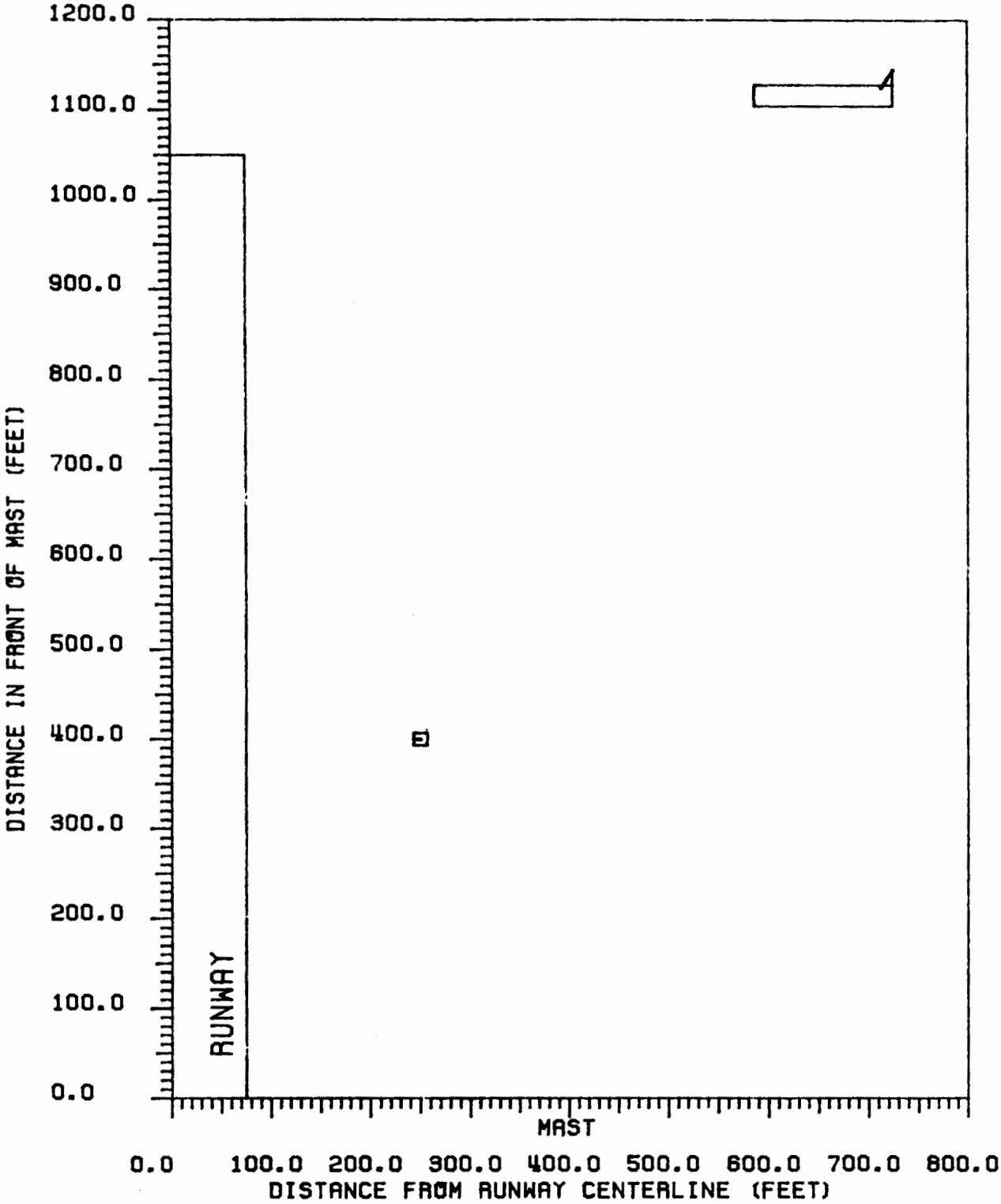

Figure 2-112. Critical area map for CAT I tolerances relating to B-747 aircraft. B-747 fuselage is perpendicular to runway centerline with tail away from the runway. Sideband reference glide slope, directional antennas.

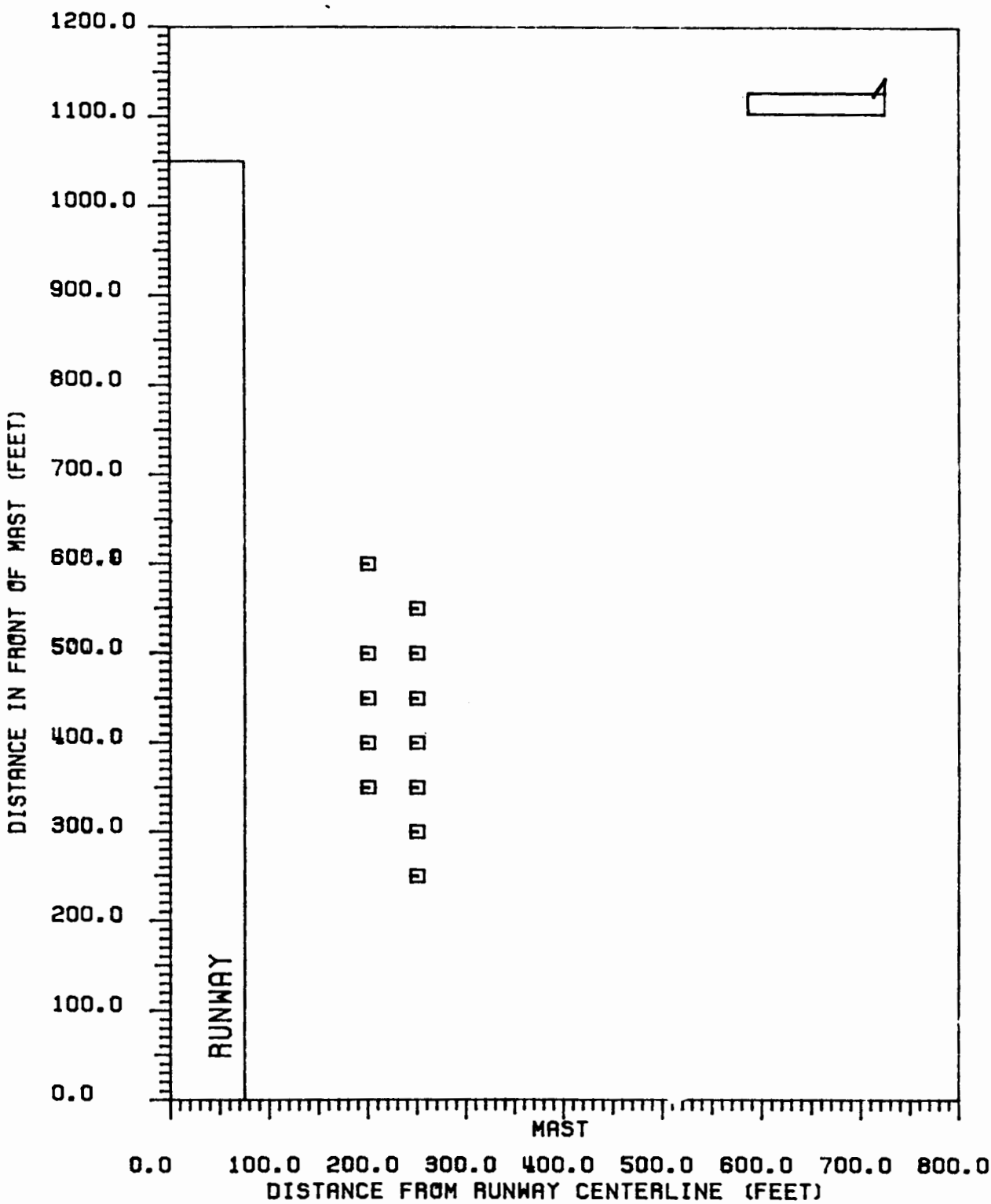

Figure 2-113. Critical area map for CAT II/III tolerances relating to B-747 aircraft. B-747 fuselage is perpendicular to runway centerline with tail away from the runway. Sideband reference glide slope, directional antennas.

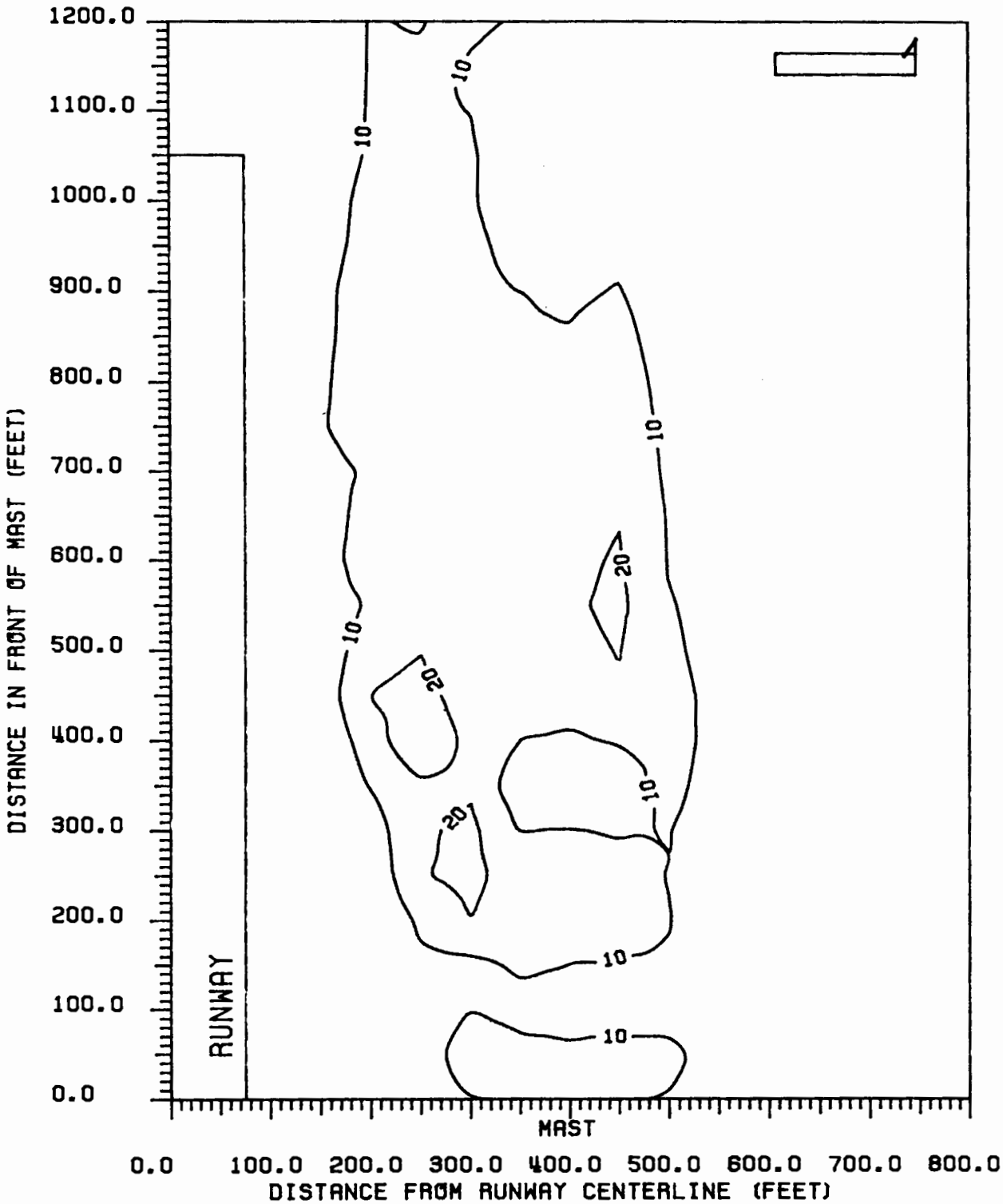

Figure 2-114. Contours of peak CDI values produced in ILS Zone 2 for a B-747. B-747 fuselage is perpendicular to runway centerline, with tail away from the runway. Sideband reference glide slope, directional antennas.

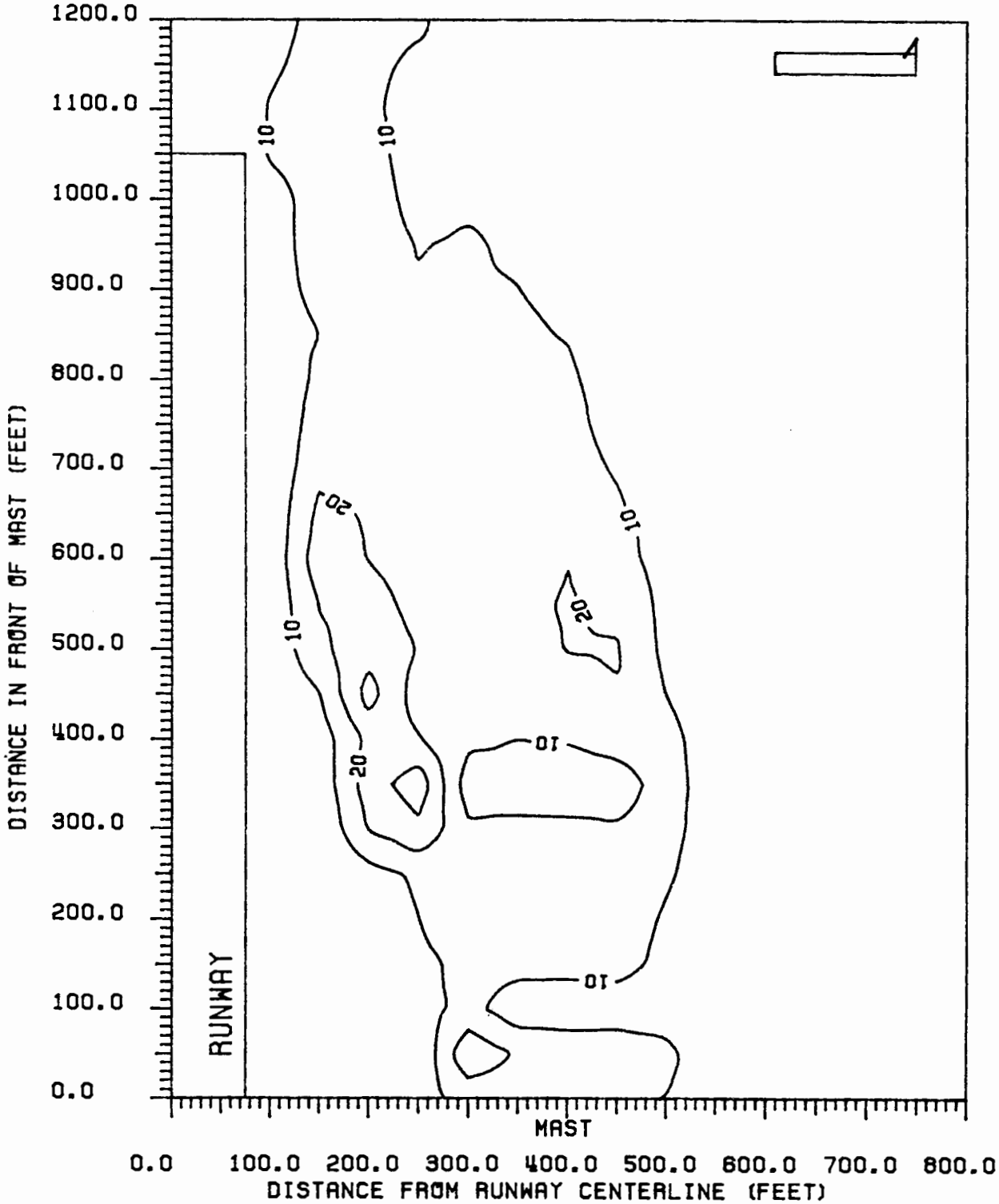

Figure 2-115. Contours of peak CDI values produced between ILS Point B and ILS Point C for a B-747. B-747 fuselage is perpendicular to runway centerline, with tail away from runway. Sideband reference glide slope, directional antennas.

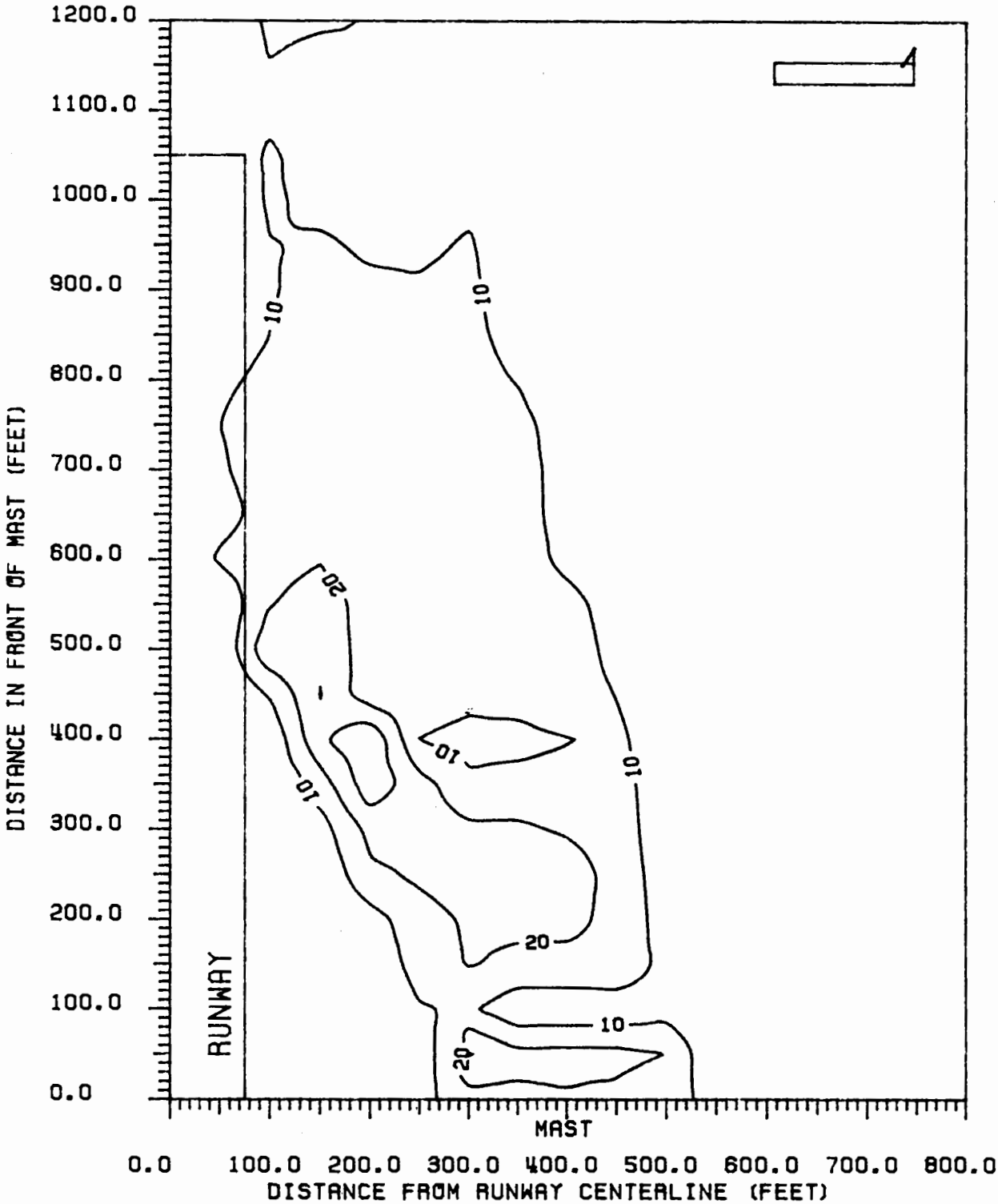

Figure 2-116. Contours of peak CDI values produced between ILS Point C and threshold for a B-747. B-747 fuselage is perpendicular to runway centerline, with tail away from runway. Sideband reference glide slope, directional antennas.

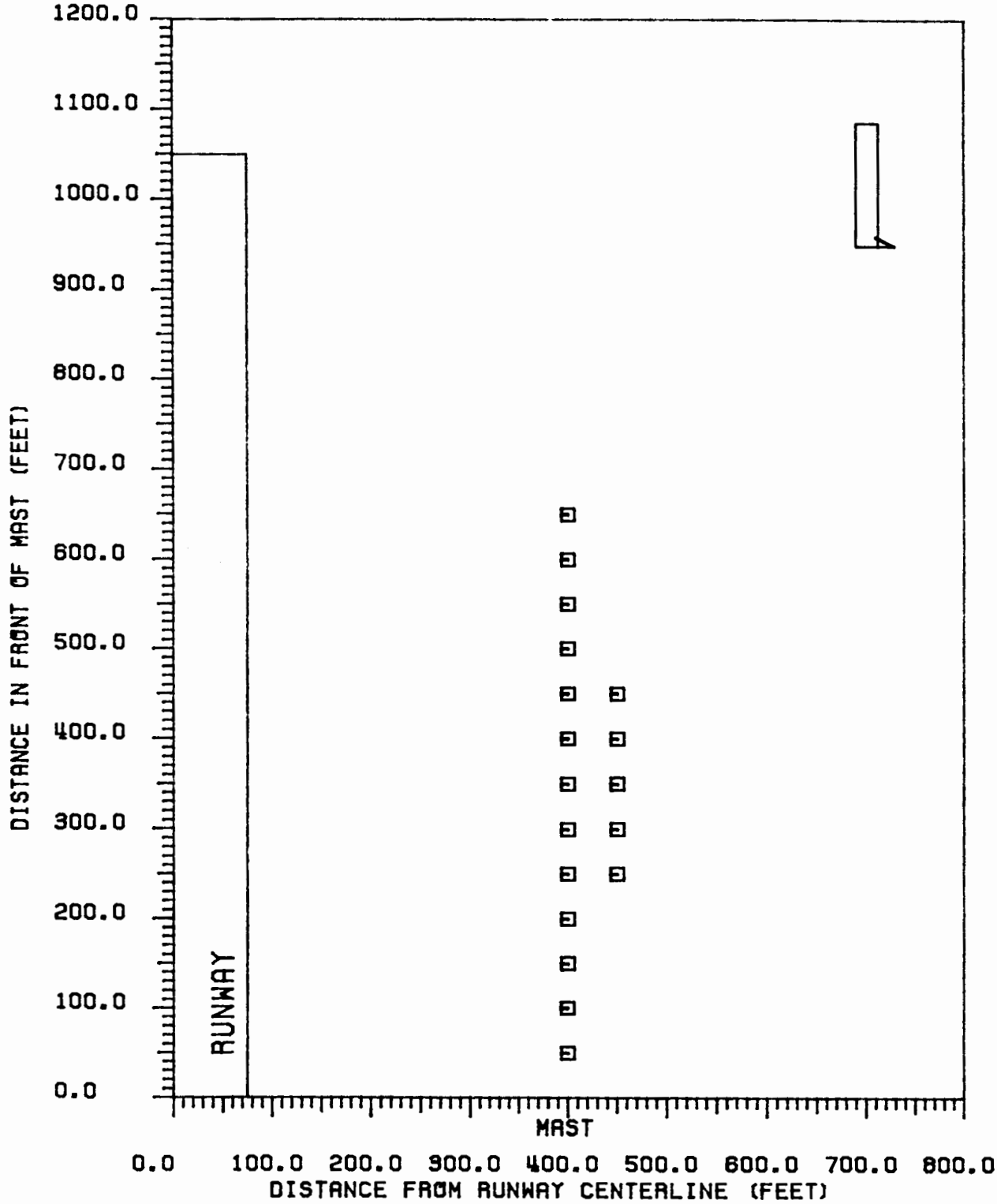

Figure 2-117. Critical area map for CAT I tolerances relating to B-747 aircraft. B-747 fuselage is parallel to runway centerline with tail towards the mast. Sideband reference glide slope, directional antennas.

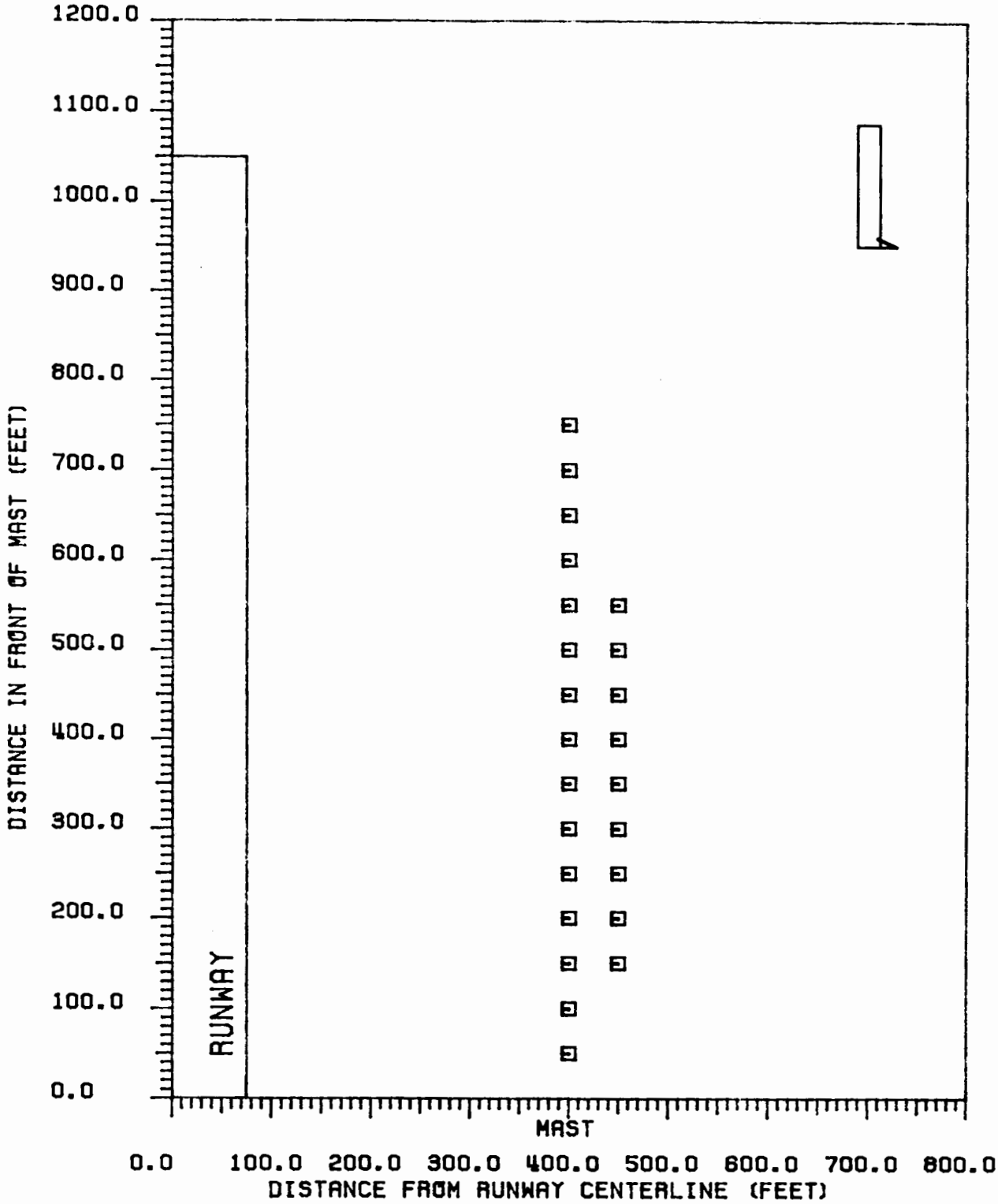

Figure 2-118. Critical area map for CAT II/III tolerances relating to B-747 aircraft. B-747 fuselage is parallel to runway centerline with tail towards the mast. Sideband reference glide slope, directional antennas.

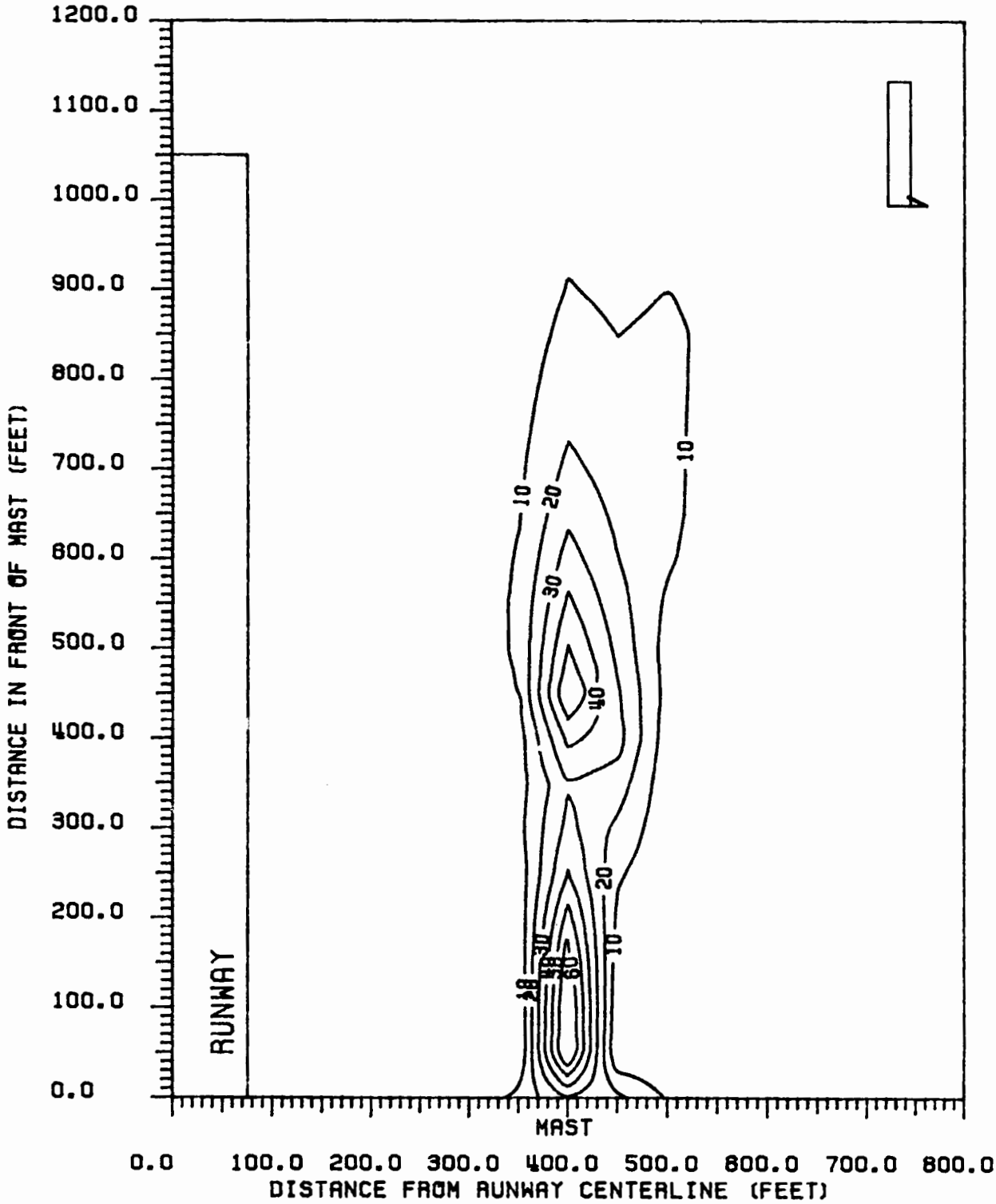

Figure 2-119. Contours of peak CDI values produced in ILS Zone 2 for a B-747. B-747 fuselage is parallel to runway centerline, with tail towards the mast. Sideband reference glide slope, directional antennas.

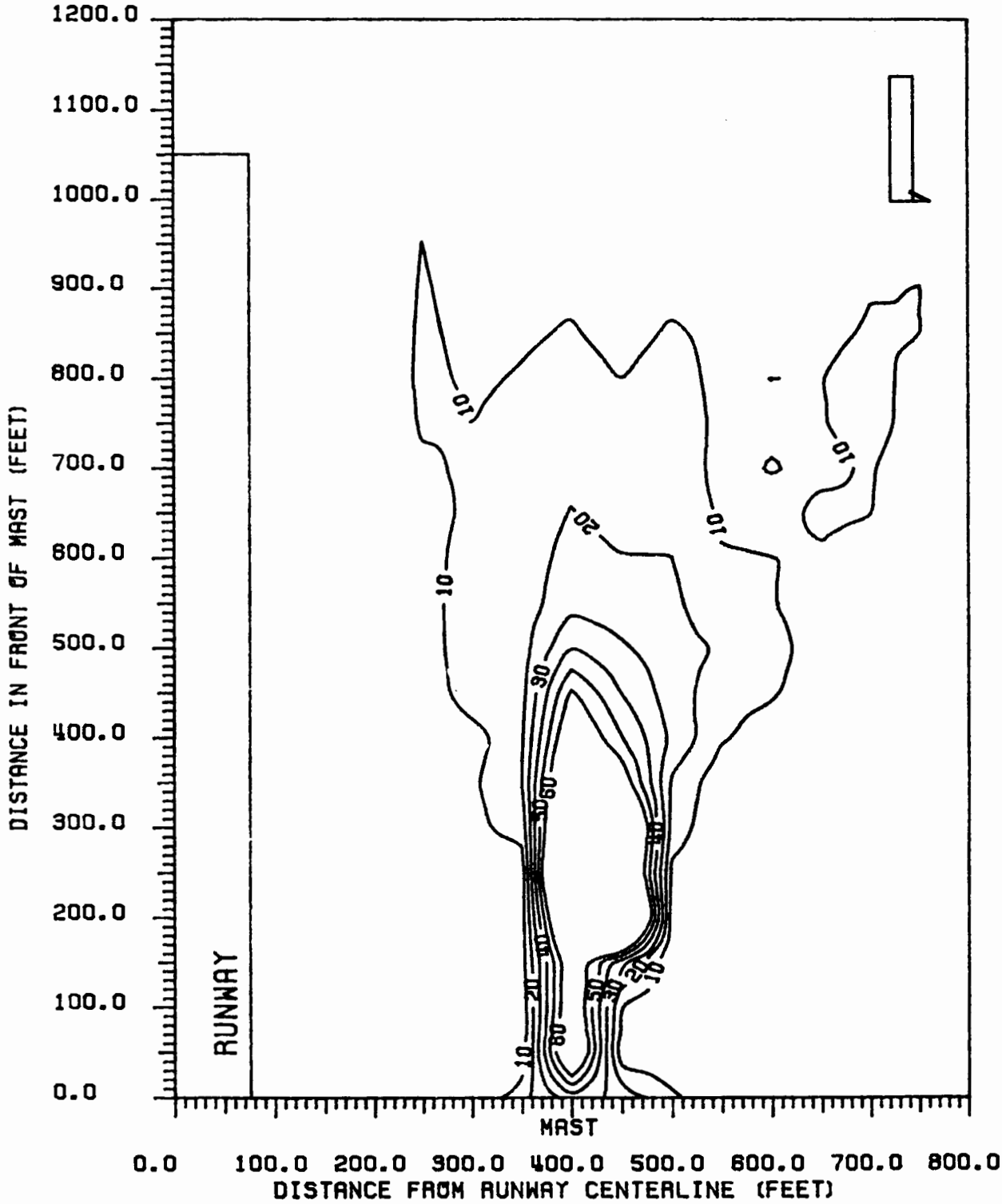

Figure 2-120. Contours of peak CDI values produced between ILS Point B and ILS Point C for a B-747. B-747 fuselage is parallel to runway centerline, with tail towards the mast. Sideband reference glide slope, directional antennas.

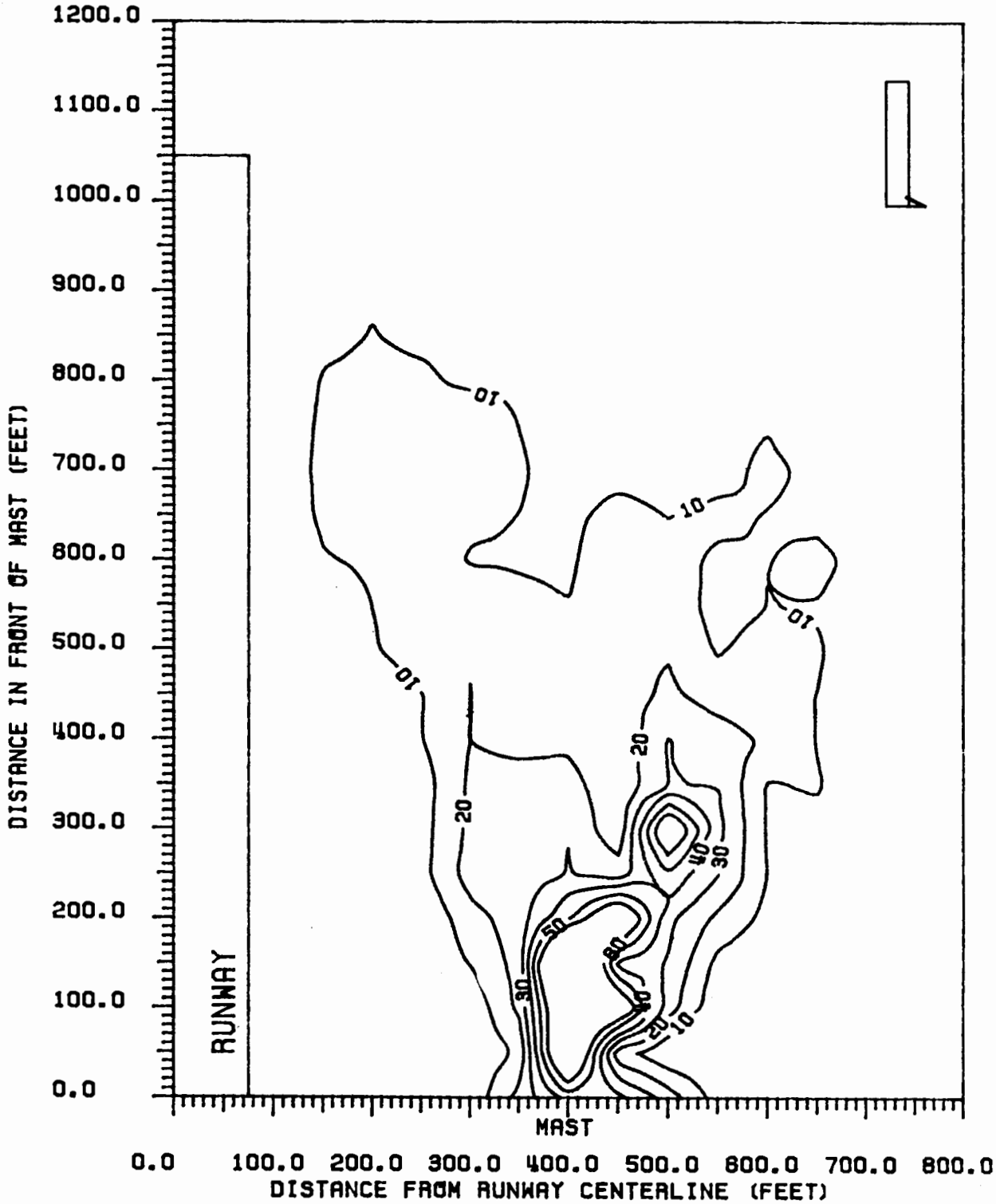

Figure 2-121. Contours of peak CDI values produced between ILS Point C and threshold for a B-747. B-747 fuselage is parallel to runway centerline, with tail towards the mast. Sideband reference glide slope, directional antennas.

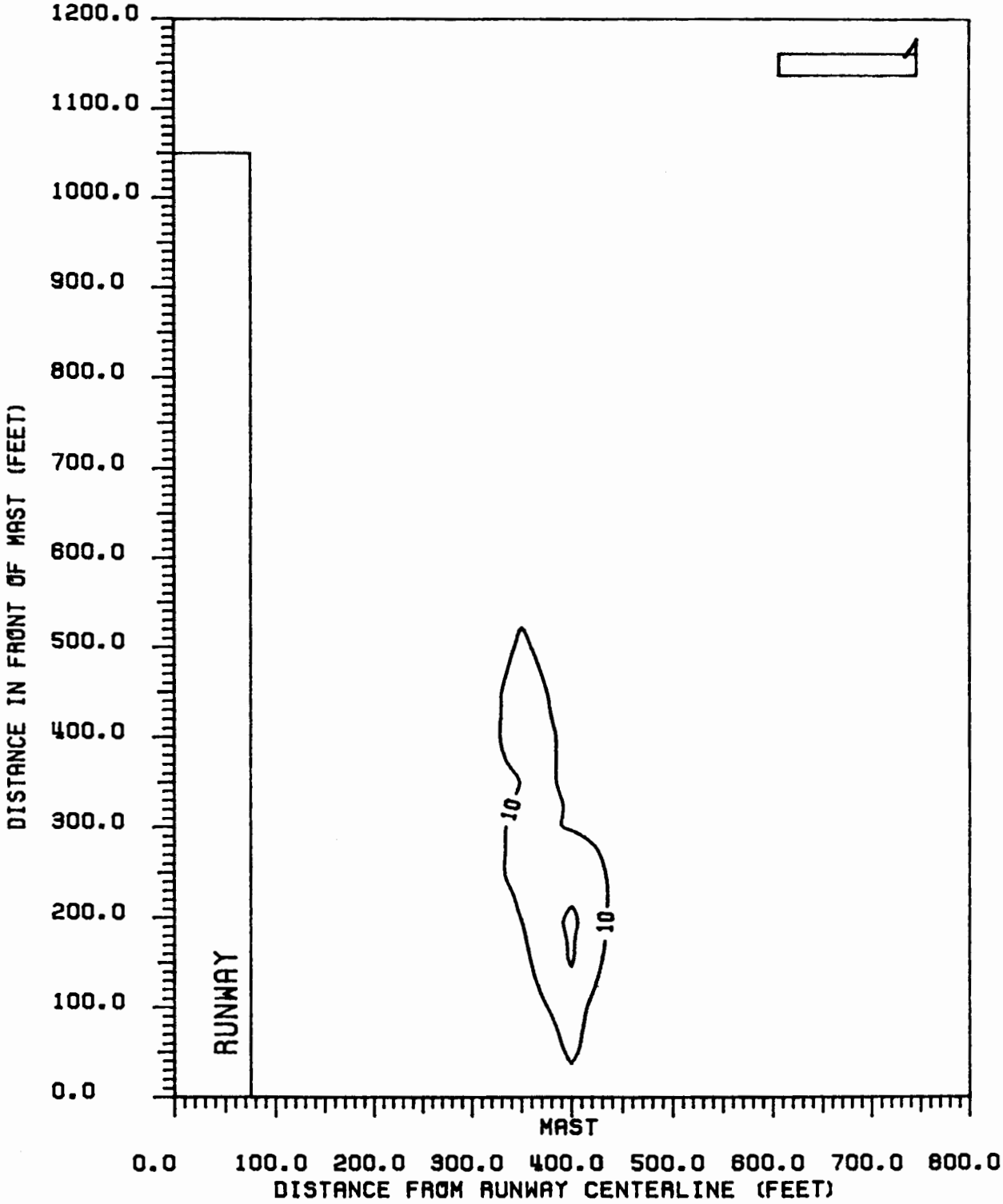

Figure 2-122. Contours of peak CDI values produced in ILS Zone 2 for an R-500. R-500 fuselage is perpendicular to runway centerline, with tail away from the runway. Capture effect glide slope, directional antennas.

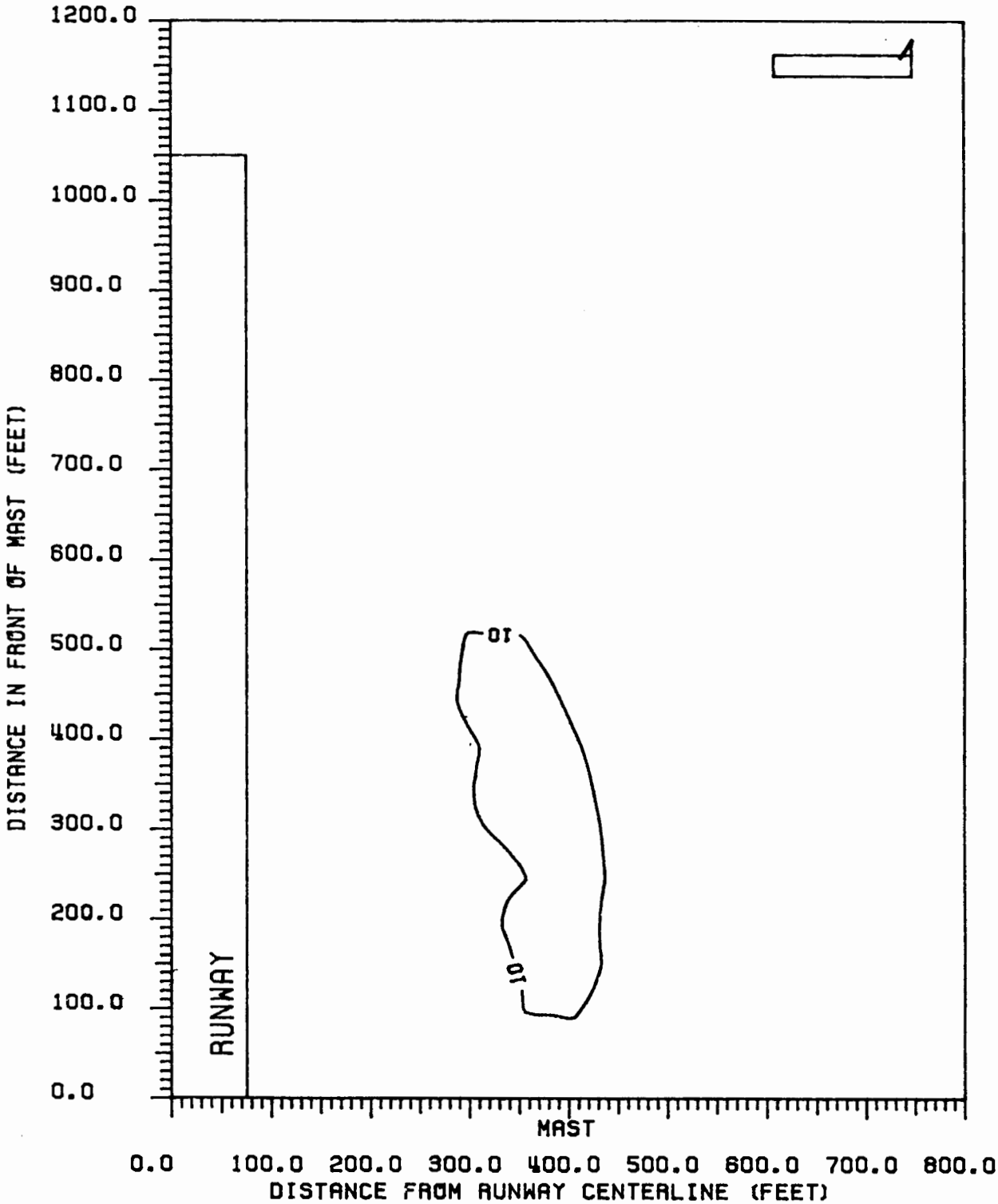

Figure 2-123. Contours of peak CDI values produced between ILS Point B and ILS Point C for an R-500. R-500 fuselage is perpendicular to runway centerline, with tail away from runway. Capture effect glide slope, directional antennas.

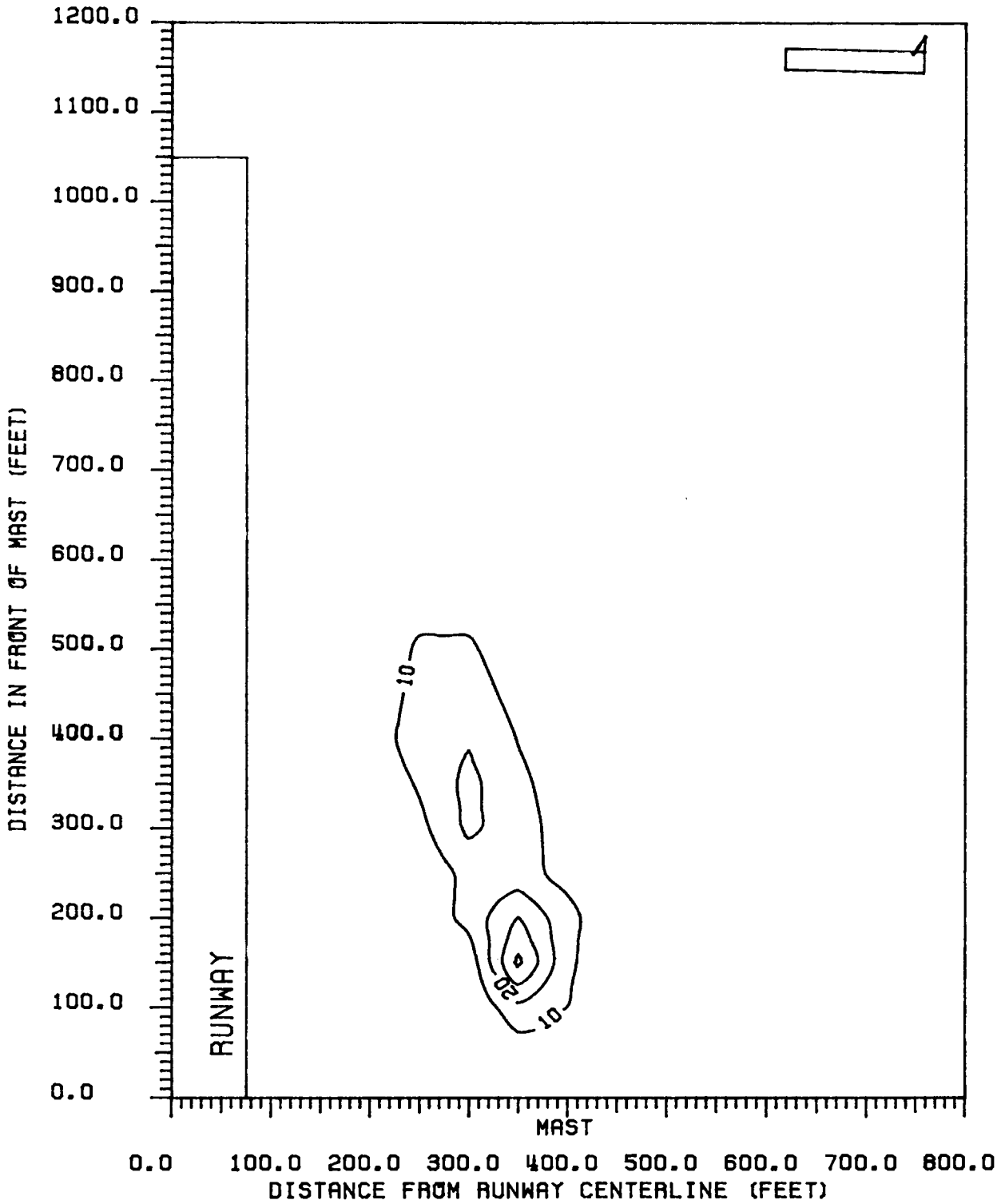

Figure 2-124. Contours of peak CDI values produced between ILS Point C and threshold for an R-500. R-500 fuselage is perpendicular to runway centerline, with tail away from runway. Capture effect glide slope, directional antennas.

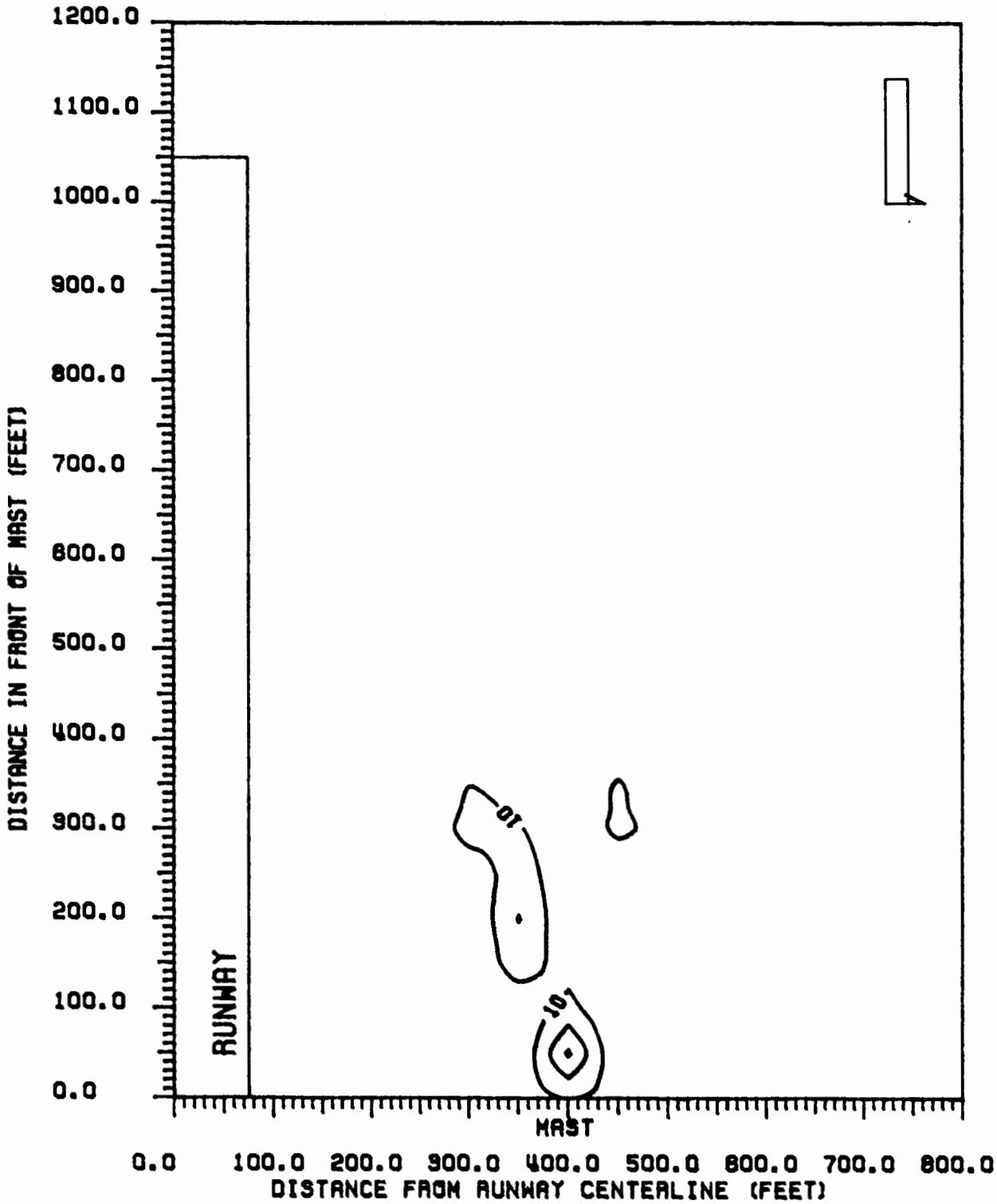

Figure 2-125. Contours of peak CDI values produced between ILS Point C and threshold for an R-500. R-500 fuselage is parallel to runway centerline, with tail towards the mast. Capture effect glide slope, directional antennas.

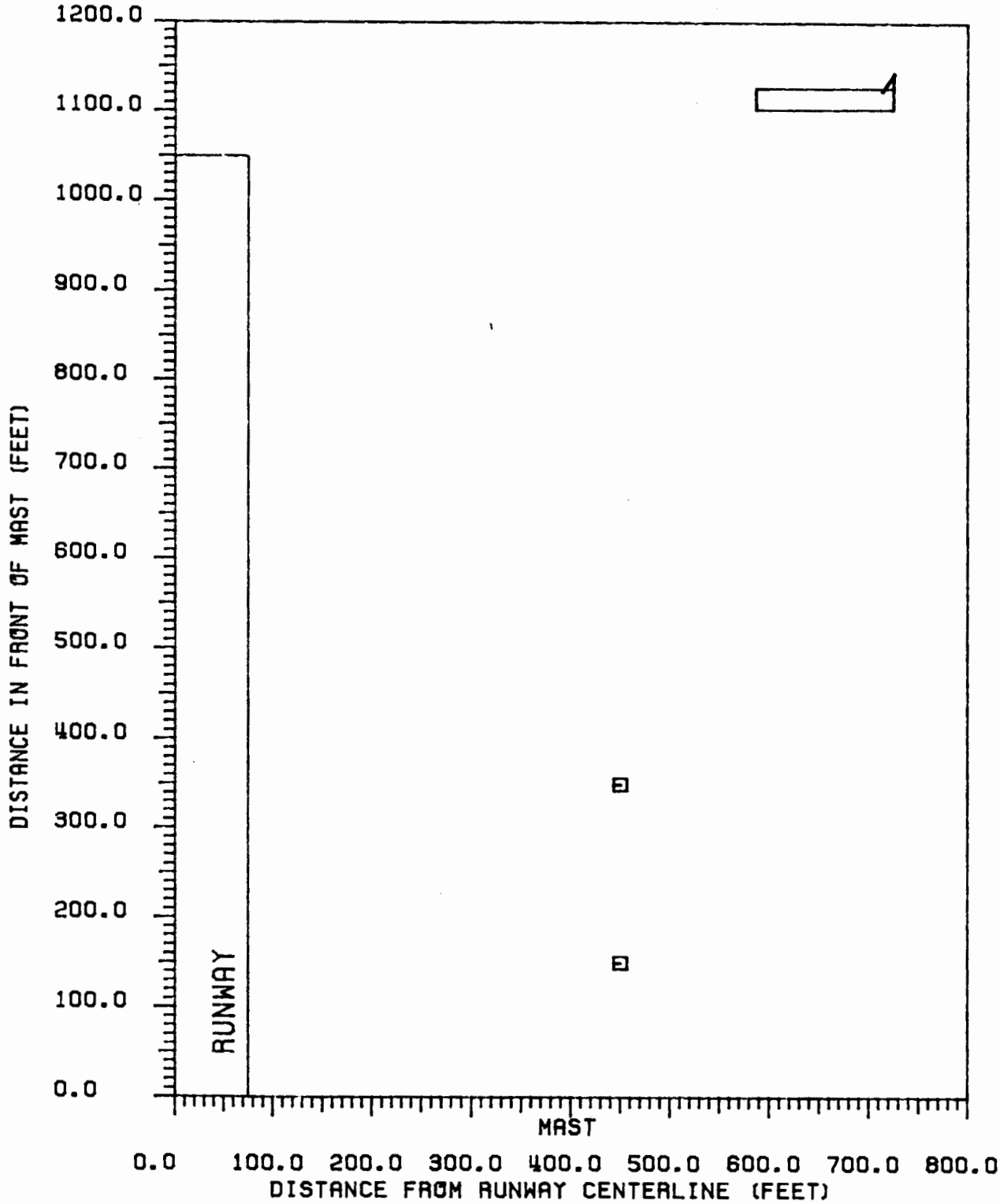

Figure 2-126. Critical area map for CAT I tolerances relating to C-440 aircraft. C-440 fuselage is perpendicular to runway centerline with tail away from the runway. Capture effect glide slope, directional antennas.

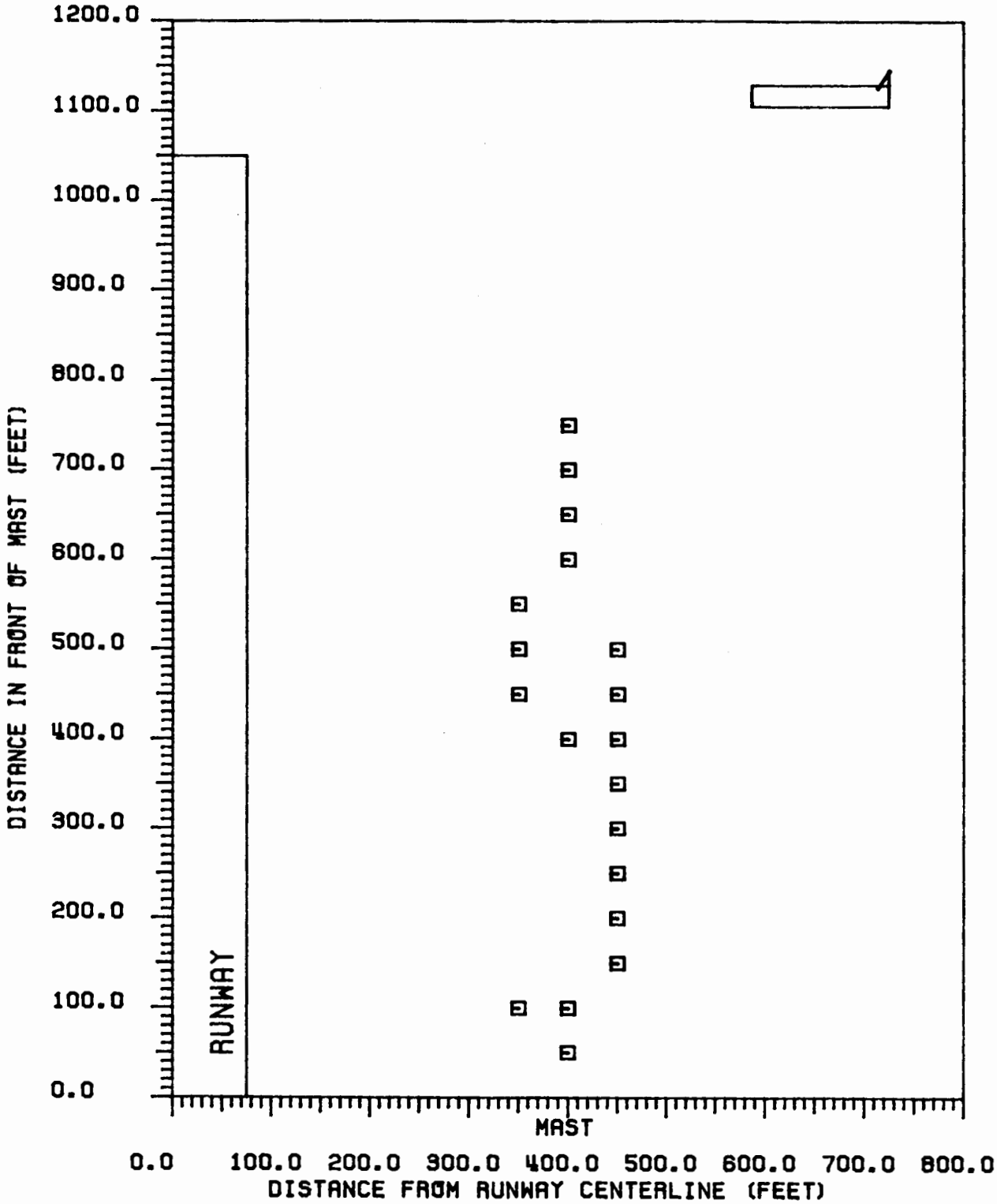

Figure 2-127. Critical area map for CAT II/III tolerances relating to C-440 aircraft. C-440 fuselage is perpendicular to runway centerline with tail away from the runway. Capture effect glide slope, directional antennas.

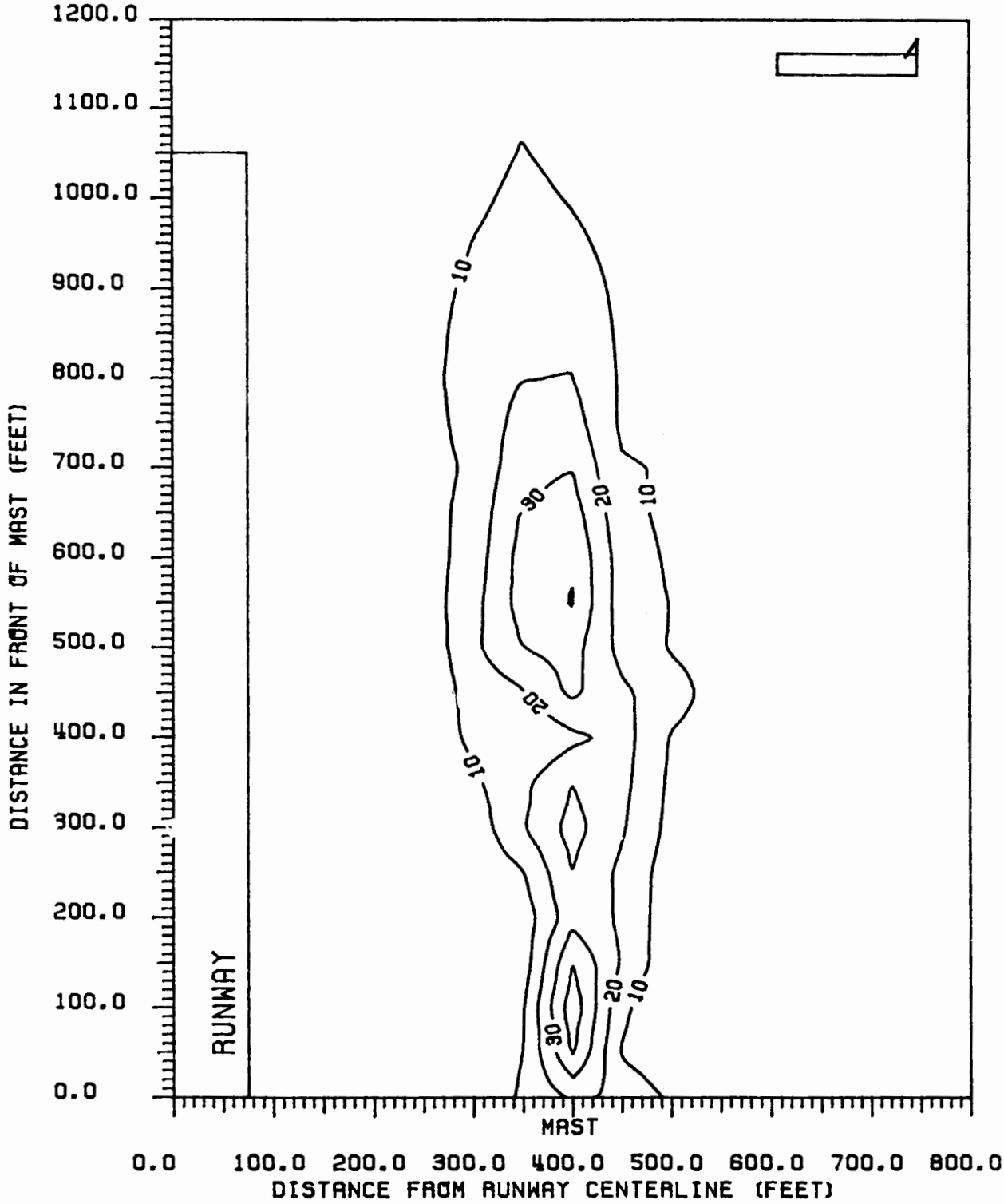

Figure 2-128. Contours of peak CDI values produced in ILS Zone 2 for a C-440. C-440 fuselage is perpendicular to runway centerline, with tail away from the runway. Capture effect glide slope, directional antennas.

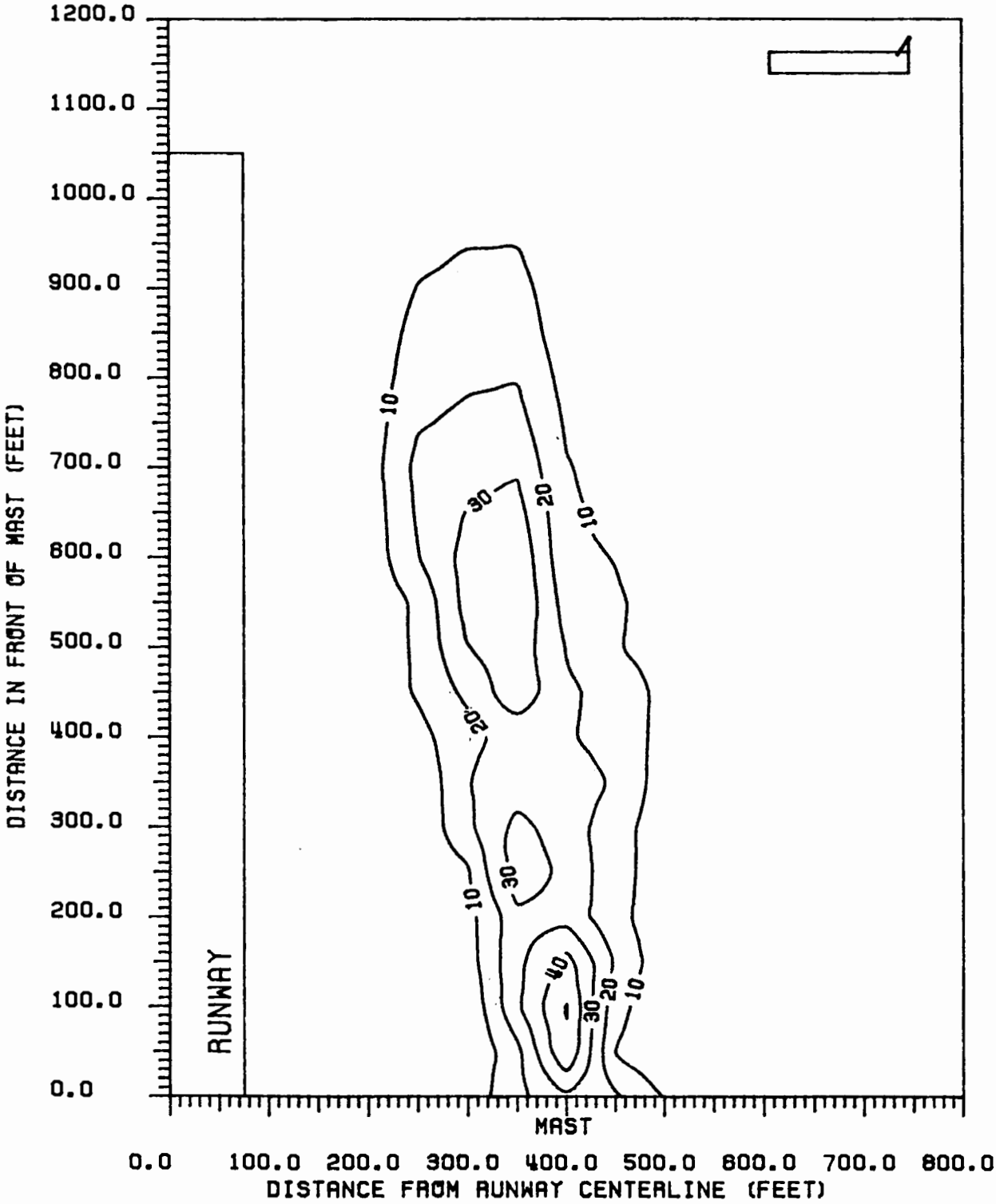

Figure 2-129. Contours of peak CDI values produced between ILS Point B and ILS Point C for a C-440. C-440 fuselage is perpendicular to runway centerline, with tail away from runway. Capture effect glide slope, directional antennas.

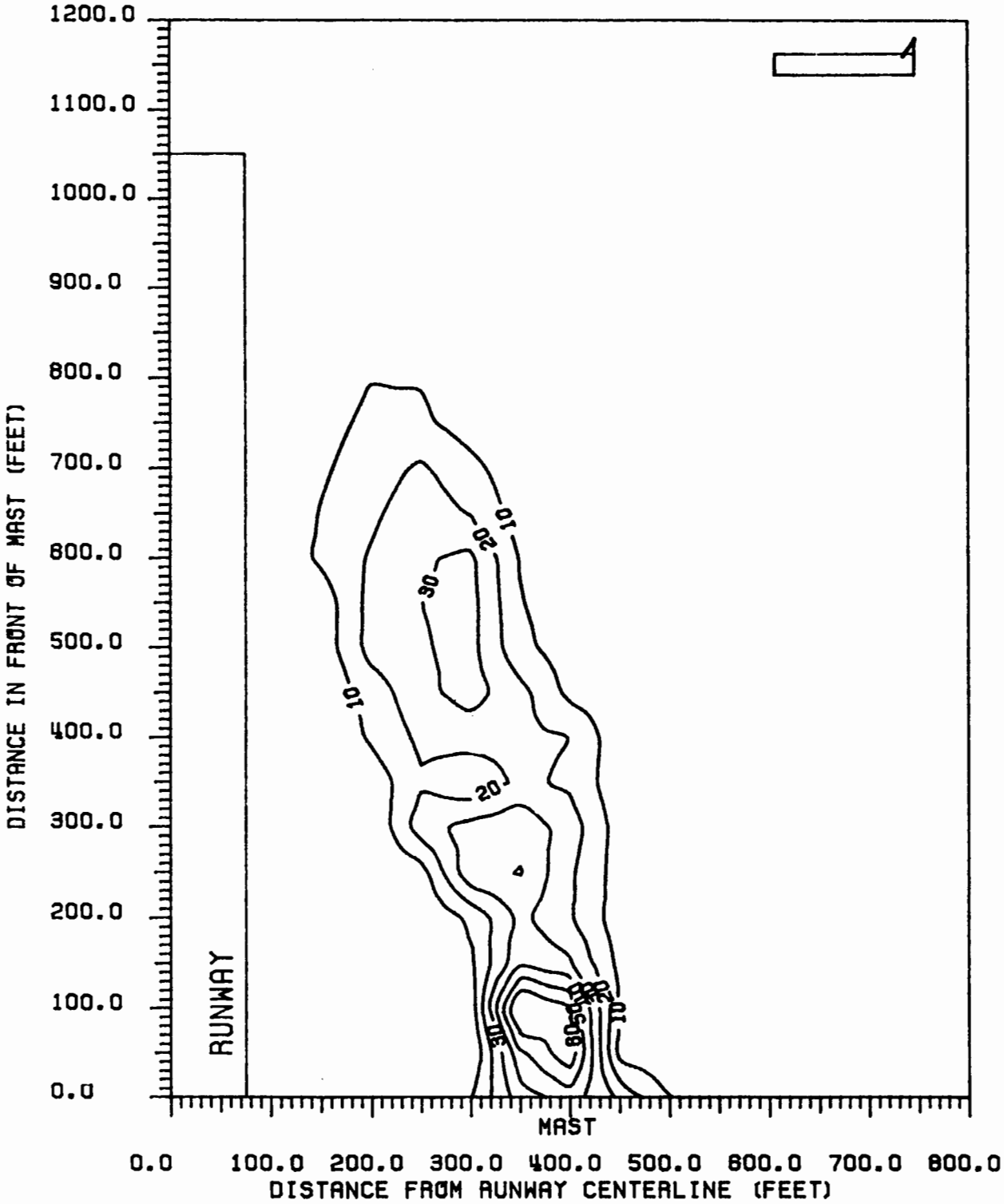

Figure 2-130. Contours of peak CDI values produced between ILS Point C and threshold for a C-440. C-440 fuselage is perpendicular to runway centerline, with tail away from runway. Capture effect glide slope, directional antennas.

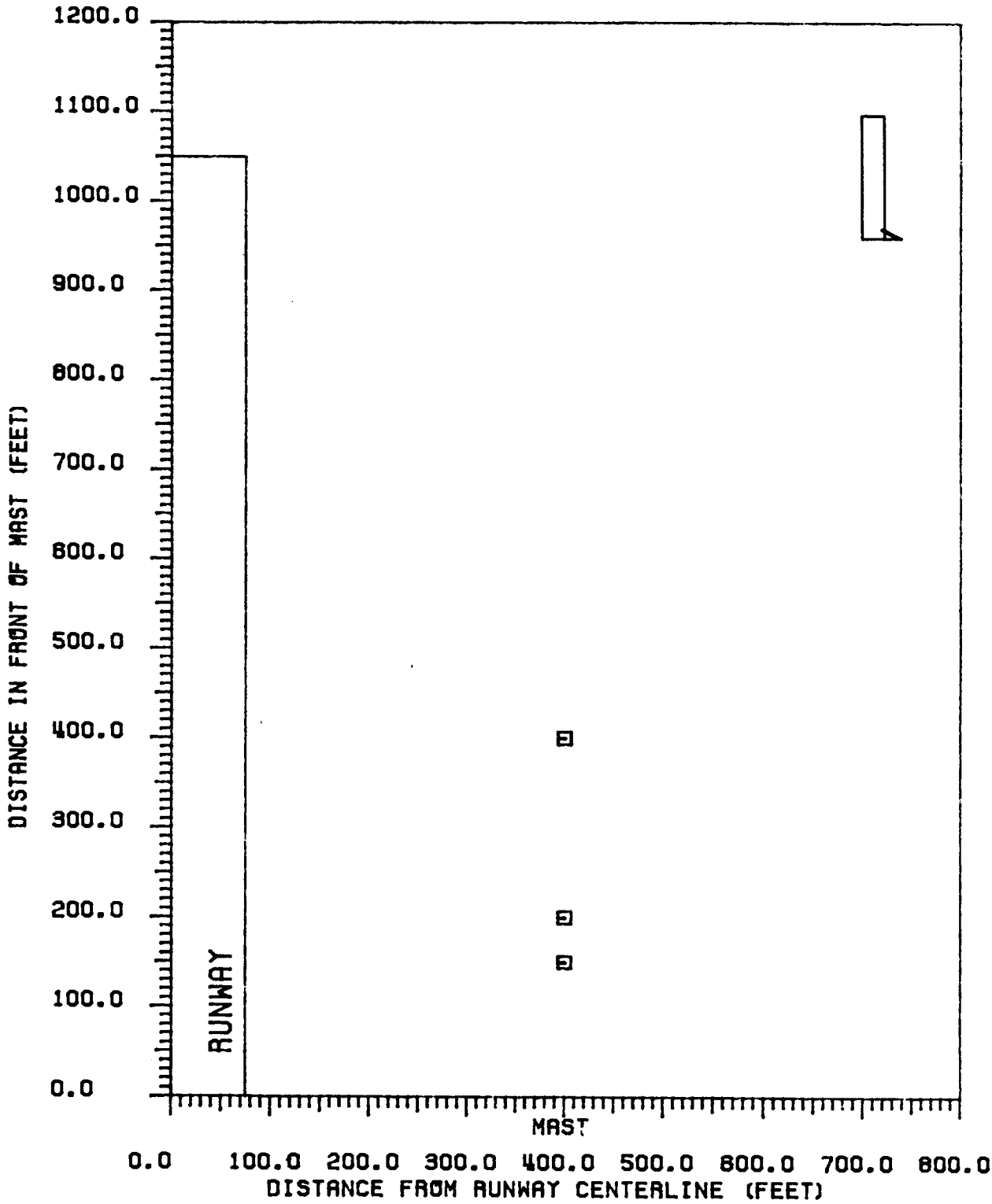

Figure 2-131. Critical area map for CAT I tolerances relating to C-440 aircraft. C-440 fuselage is parallel to runway centerline with tail towards the mast. Capture effect glide slope, directional antennas.

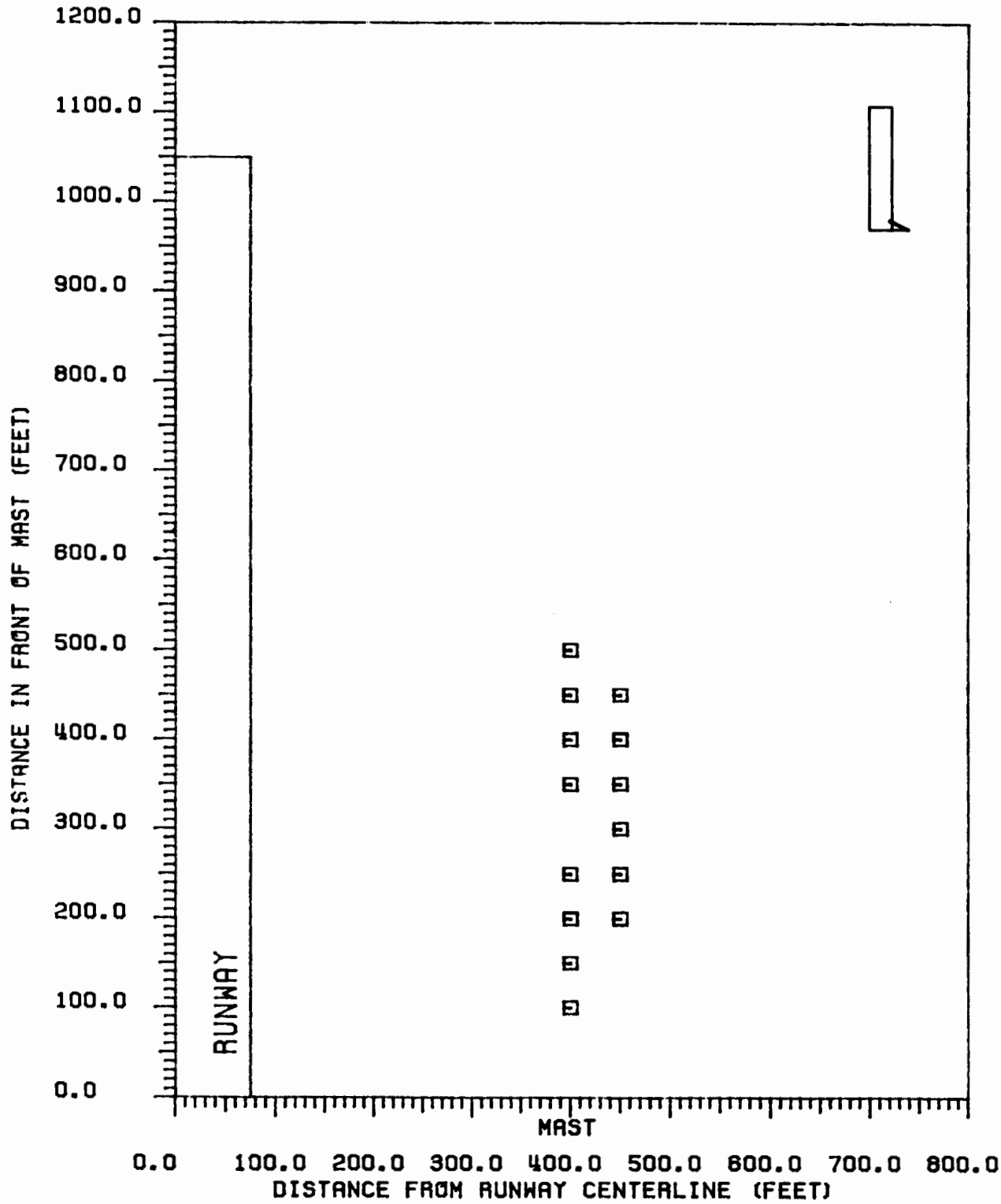

Figure 2-132. Critical area map for CAT II/III tolerances relating to C-440 aircraft. C-440 fuselage is parallel to runway centerline with tail towards the mast. Capture effect glide slope, directional antennas.

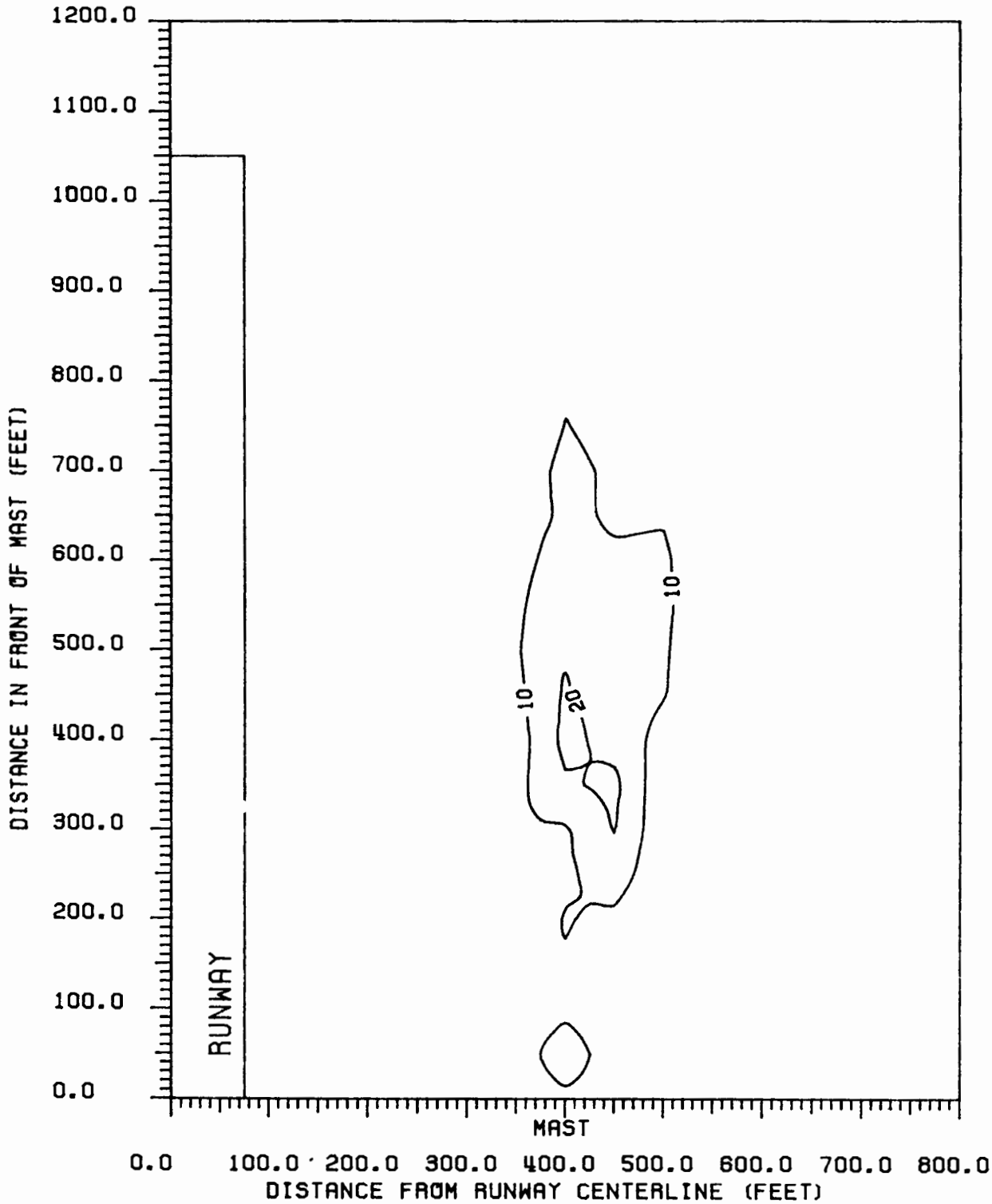

Figure 2-133. Contours of peak CDI values produced in ILS Zone 2 for a C-440. C-440 fuselage is parallel to runway centerline, with tail towards the mast. Capture effect glide slope, directional antennas.

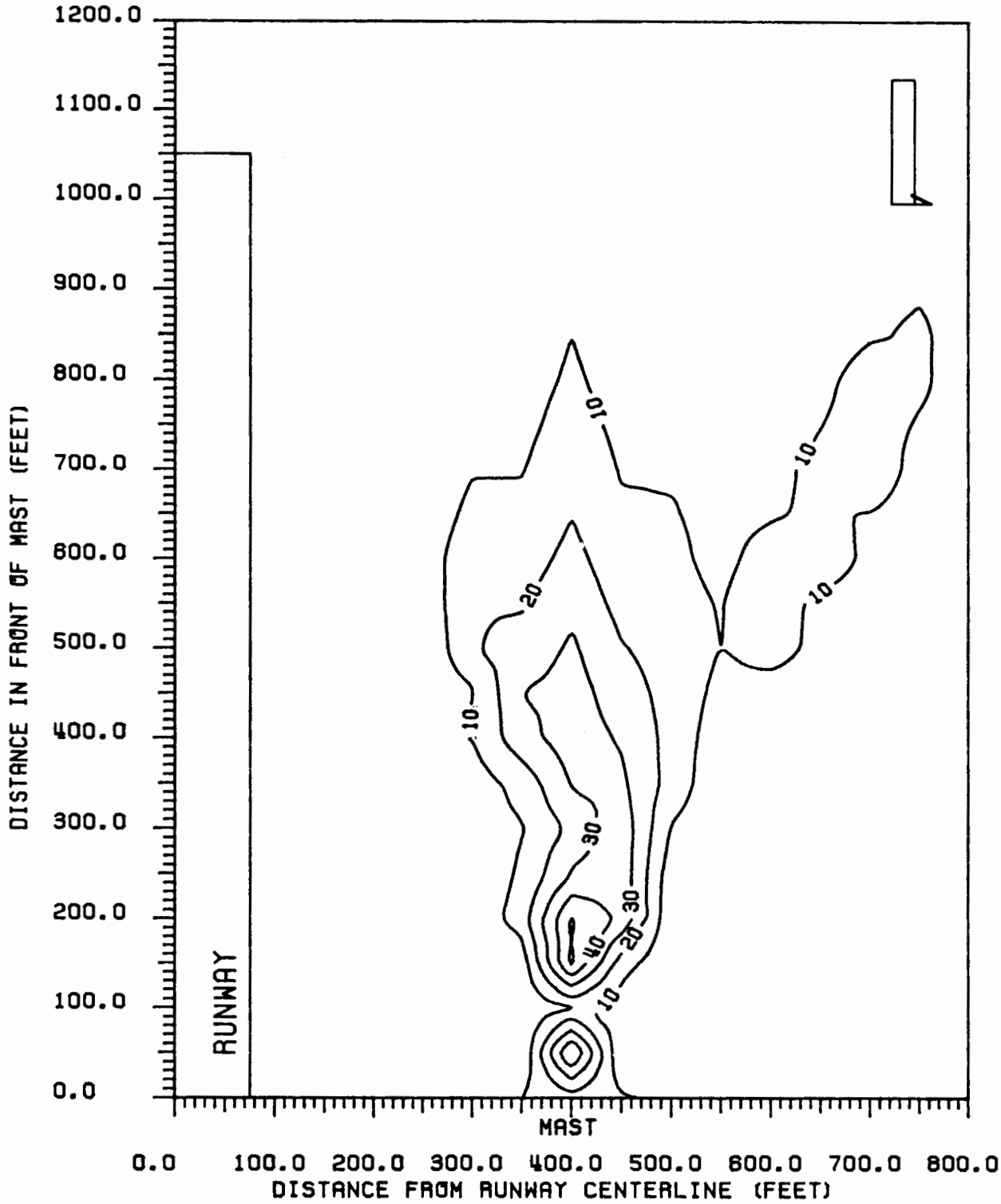

Figure 2-134. Contours of peak CDI values produced between ILS Point B and ILS Point C for a C-440. C-440 fuselage is parallel to runway centerline, with tail towards the mast. Capture effect glide slope, directional antennas.

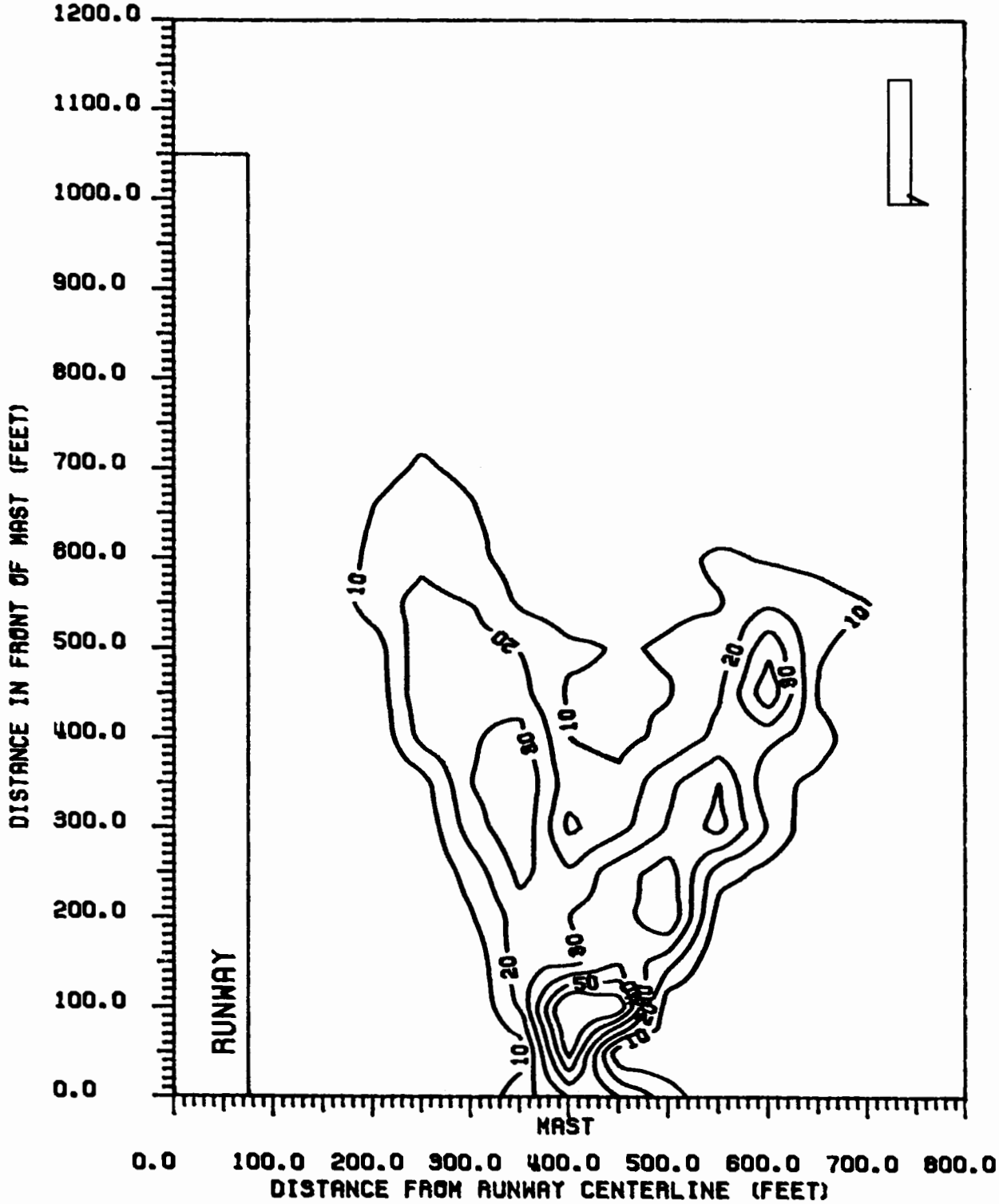

Figure 2-135. Contours of peak CDI values produced between ILS Point C and threshold for a C-440. C-440 fuselage is parallel to runway centerline, with tail towards the mast. Capture effect glide slope, directional antennas.

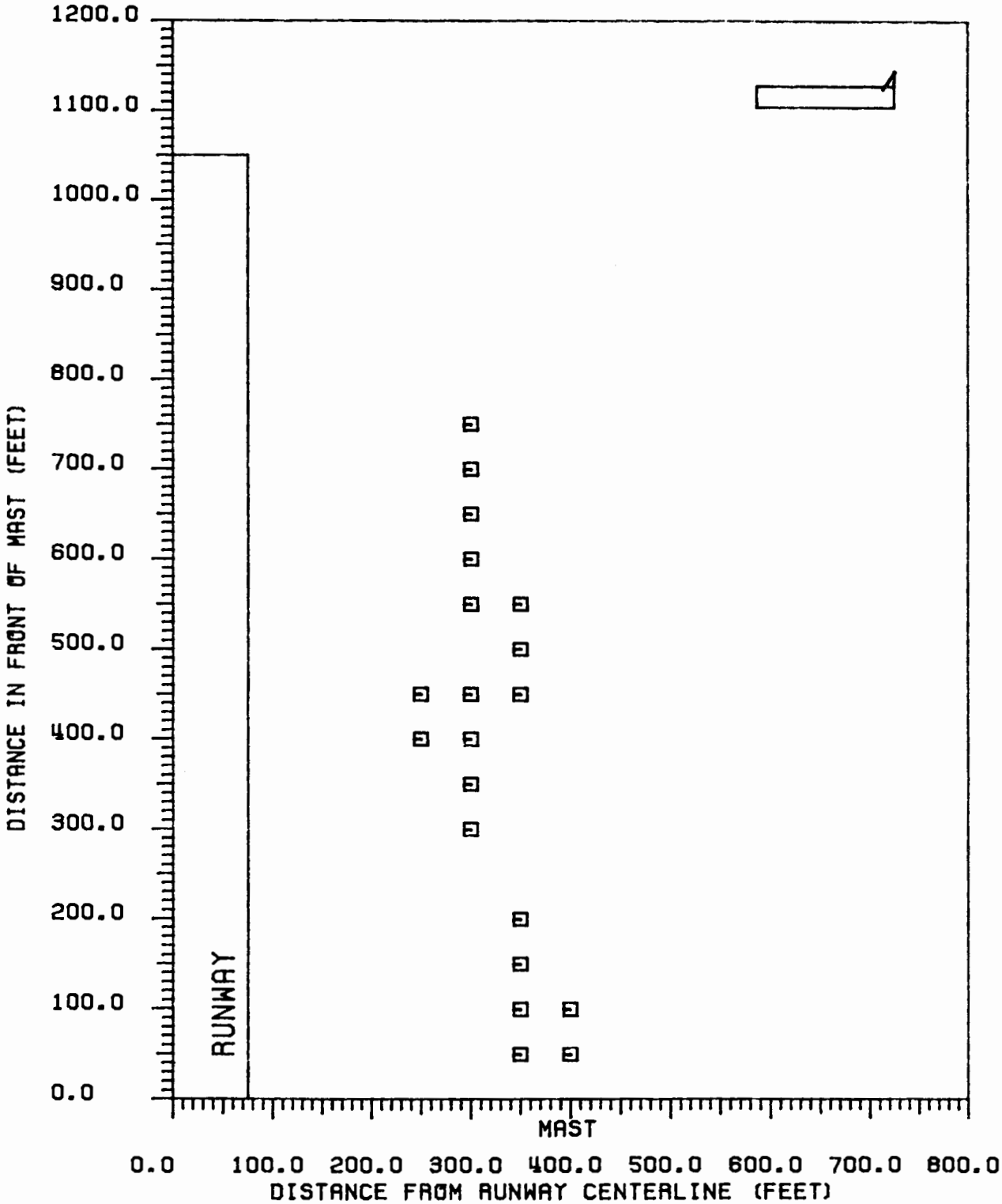

Figure 2-136. Critical area map for CAT II/III tolerances relating to DC-9 aircraft. DC-9 fuselage is perpendicular to runway centerline with tail away from the runway. Capture effect glide slope, directional antennas.

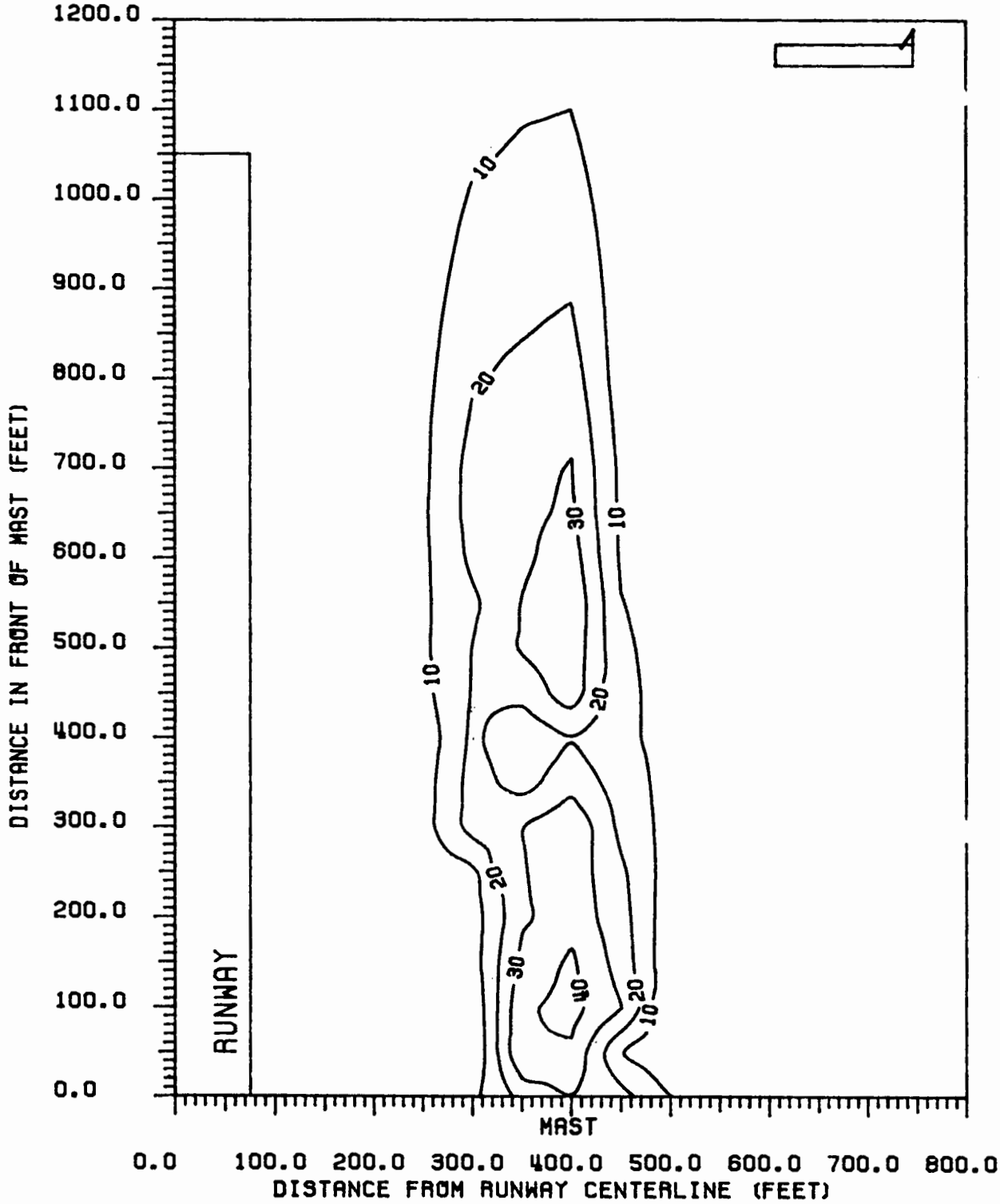

Figure 2-137. Contours of peak CDI values produced in ILS Zone 2 for a DC-9. DC-9 fuselage is perpendicular to runway centerline, with tail away from the runway. Capture effect glide slope, directional antennas.

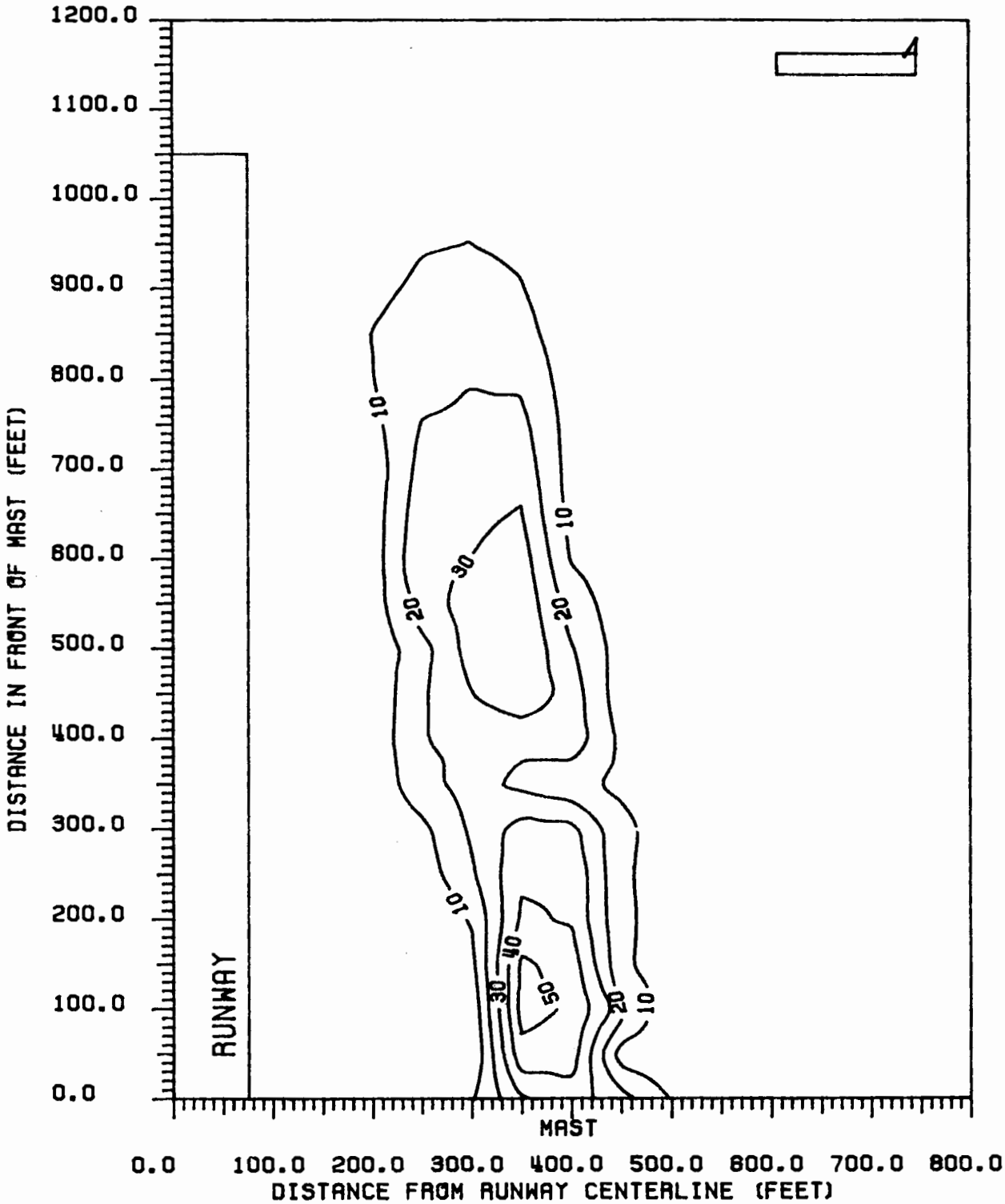

Figure 2-138. Contours of peak CDI values produced between ILS Point B and ILS Point C for a DC-9. DC-9 fuselage is perpendicular to runway centerline, with tail away from runway. Capture effect glide slope, directional antennas.

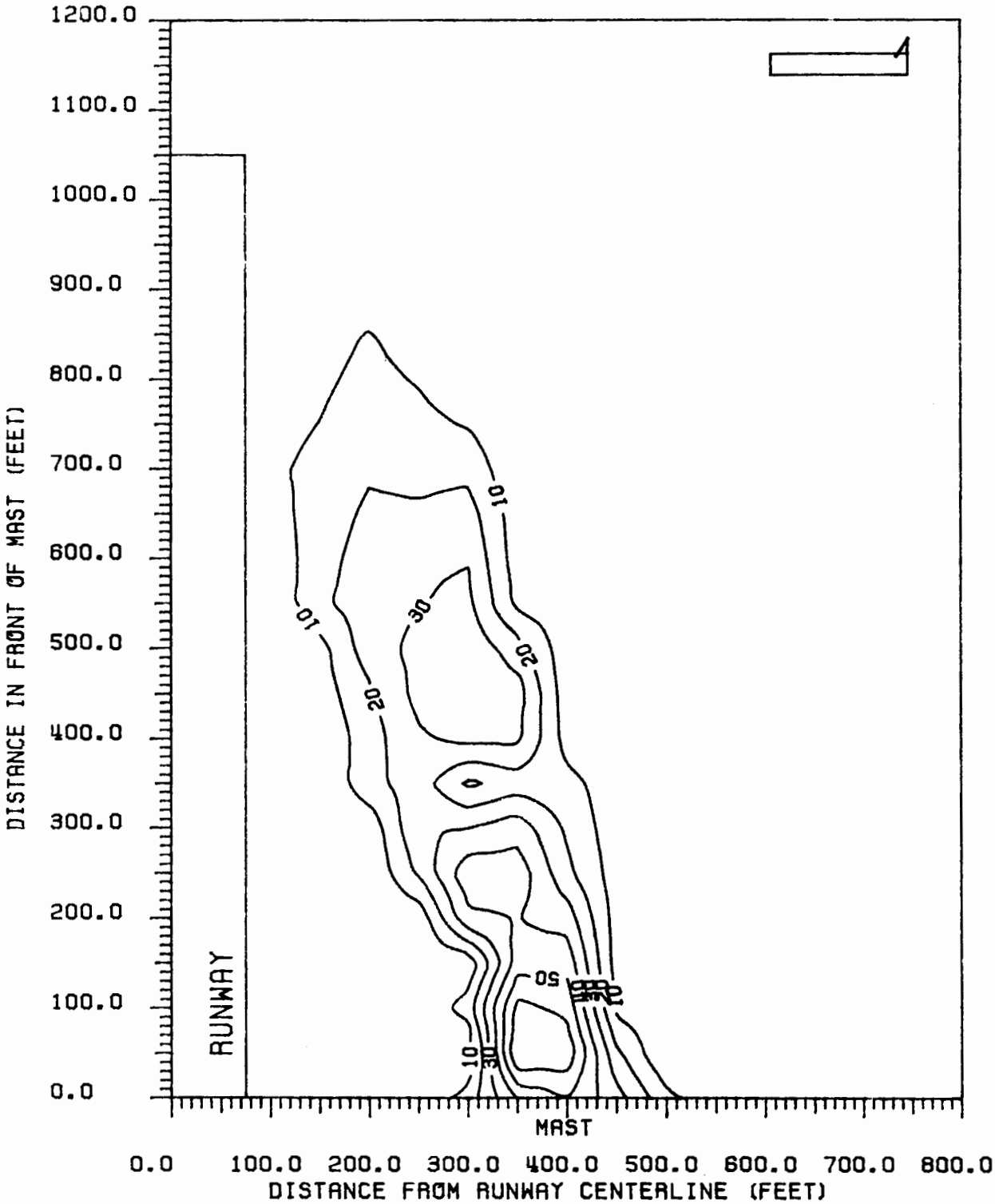

Figure 2-139. Contours of peak CDI values produced between ILS Point C and threshold for a DC-9. DC-9 fuselage is perpendicular to runway centerline, with tail away from runway. Capture effect glide slope, directional antennas.

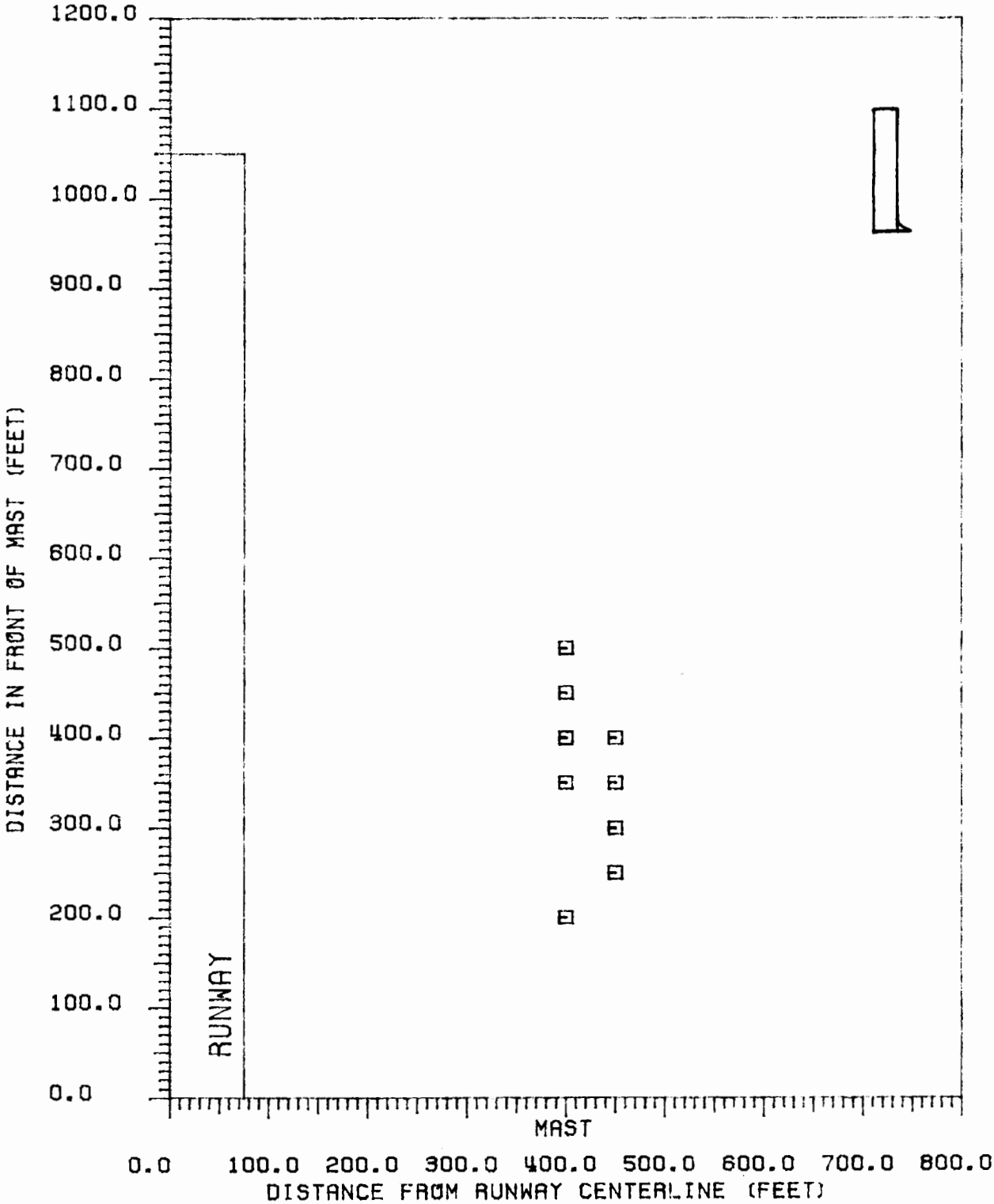

Figure 2-140. Critical area map for CAT I tolerances relating to DC-9 aircraft. DC-9 fuselage is parallel to runway centerline with tail towards the mast. Capture effect glide slope, directional antennas.

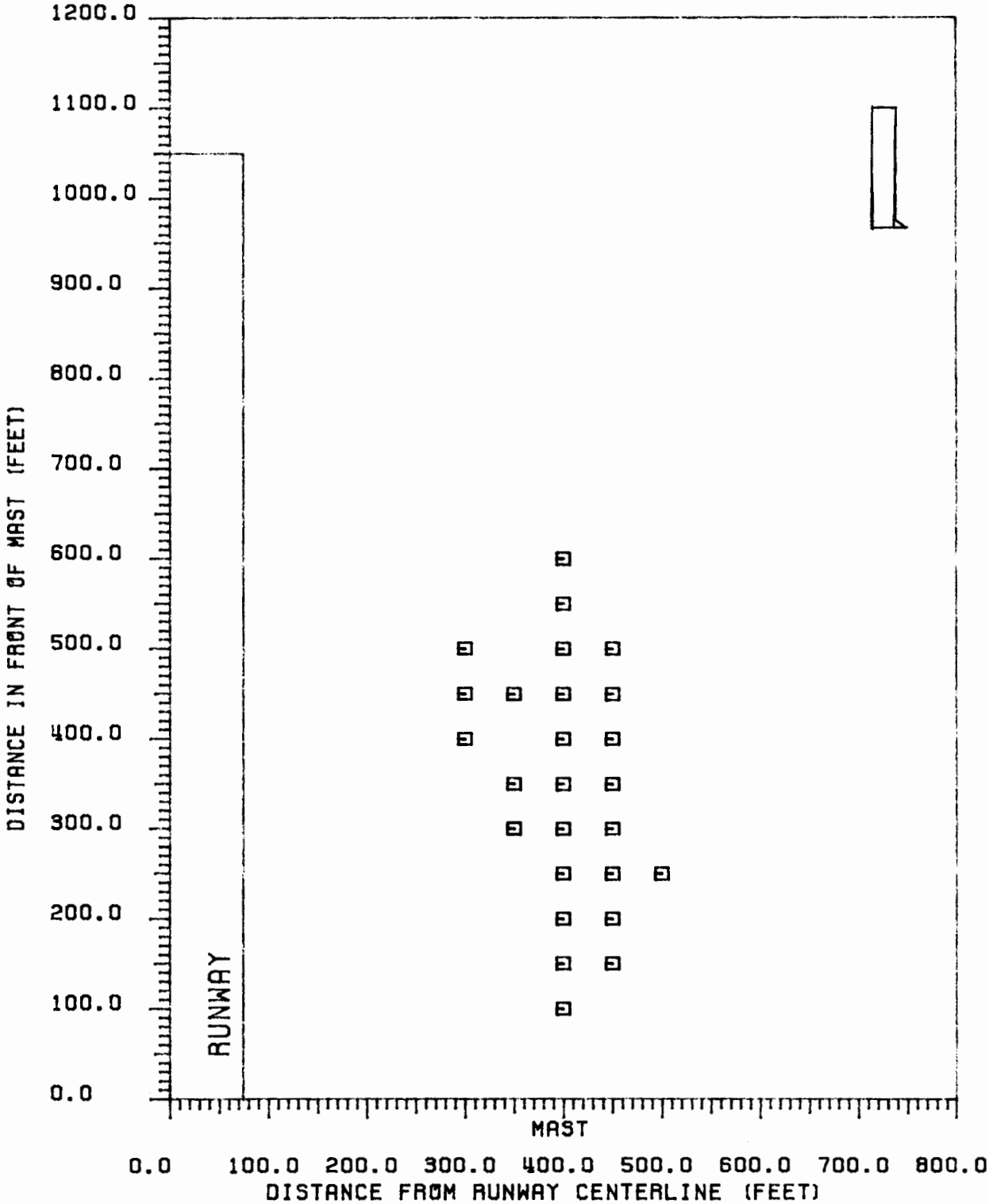

Figure 2-141. Critical area map for CAT II/III tolerances relating to DC-9 aircraft. DC-9 fuselage is parallel to runway centerline with tail towards the mast. Capture effect glide slope, directional antennas.

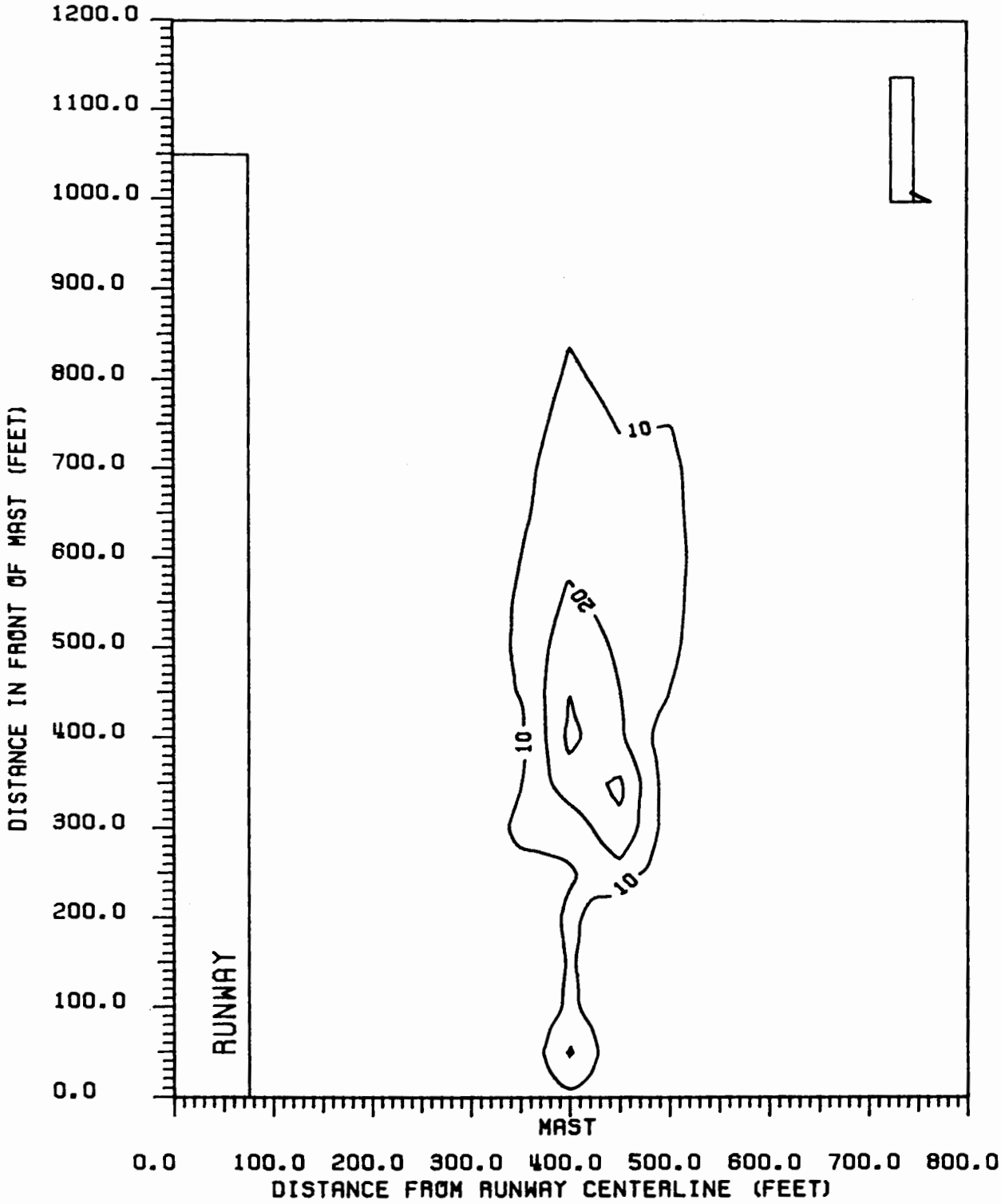

Figure 2-142. Contours of peak CDI values produced in ILS Zone 2 for a DC-9. DC-9 fuselage is parallel to runway centerline, with tail towards the mast. Capture effect glide slope, directional antennas.

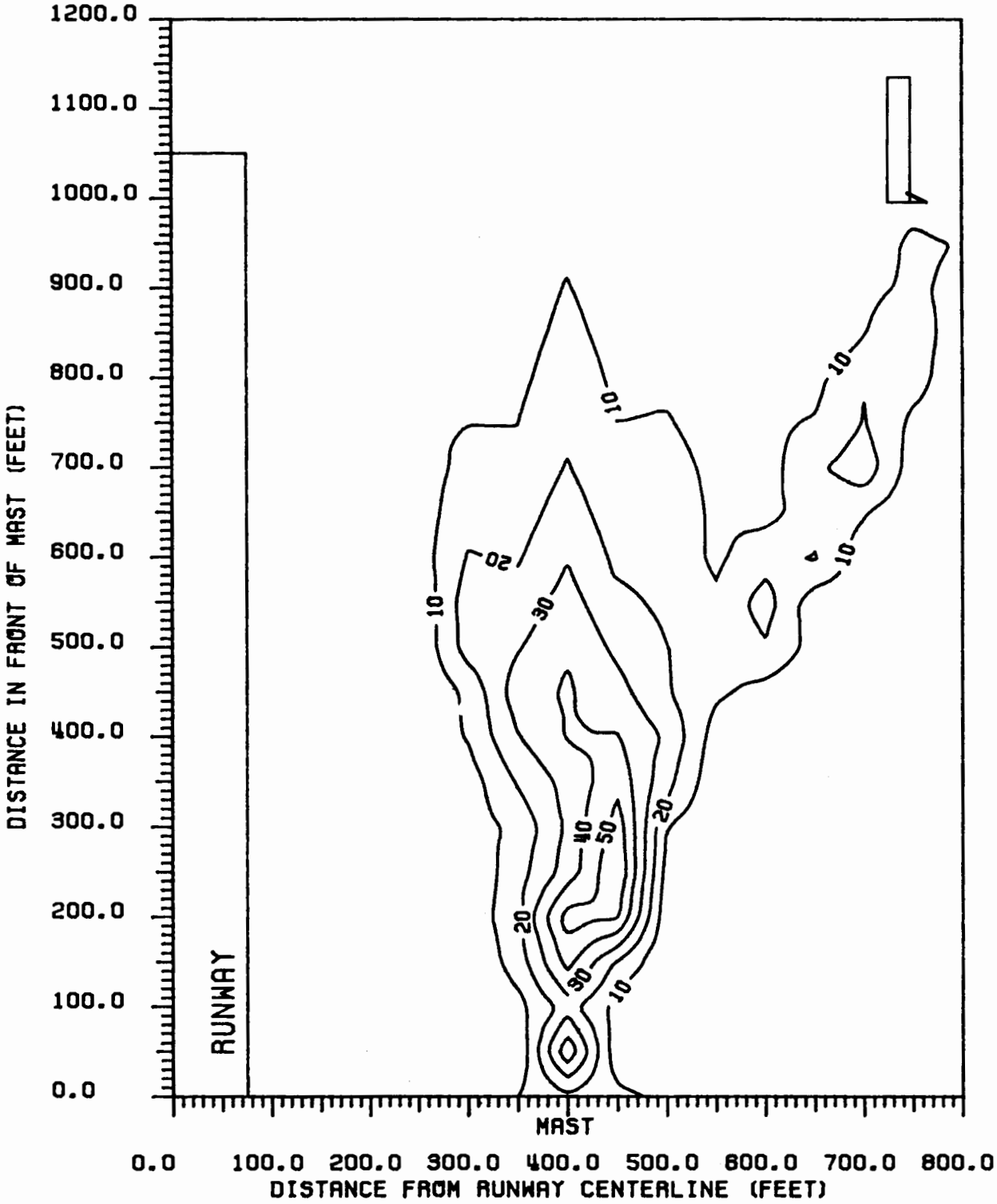

Figure 2-143. Contours of peak CDI values produced between ILS Point B and ILS Point C for a DC-9. DC-9 fuselage is parallel to runway centerline, with tail towards the mast. Capture effect glide slope, directional antennas.

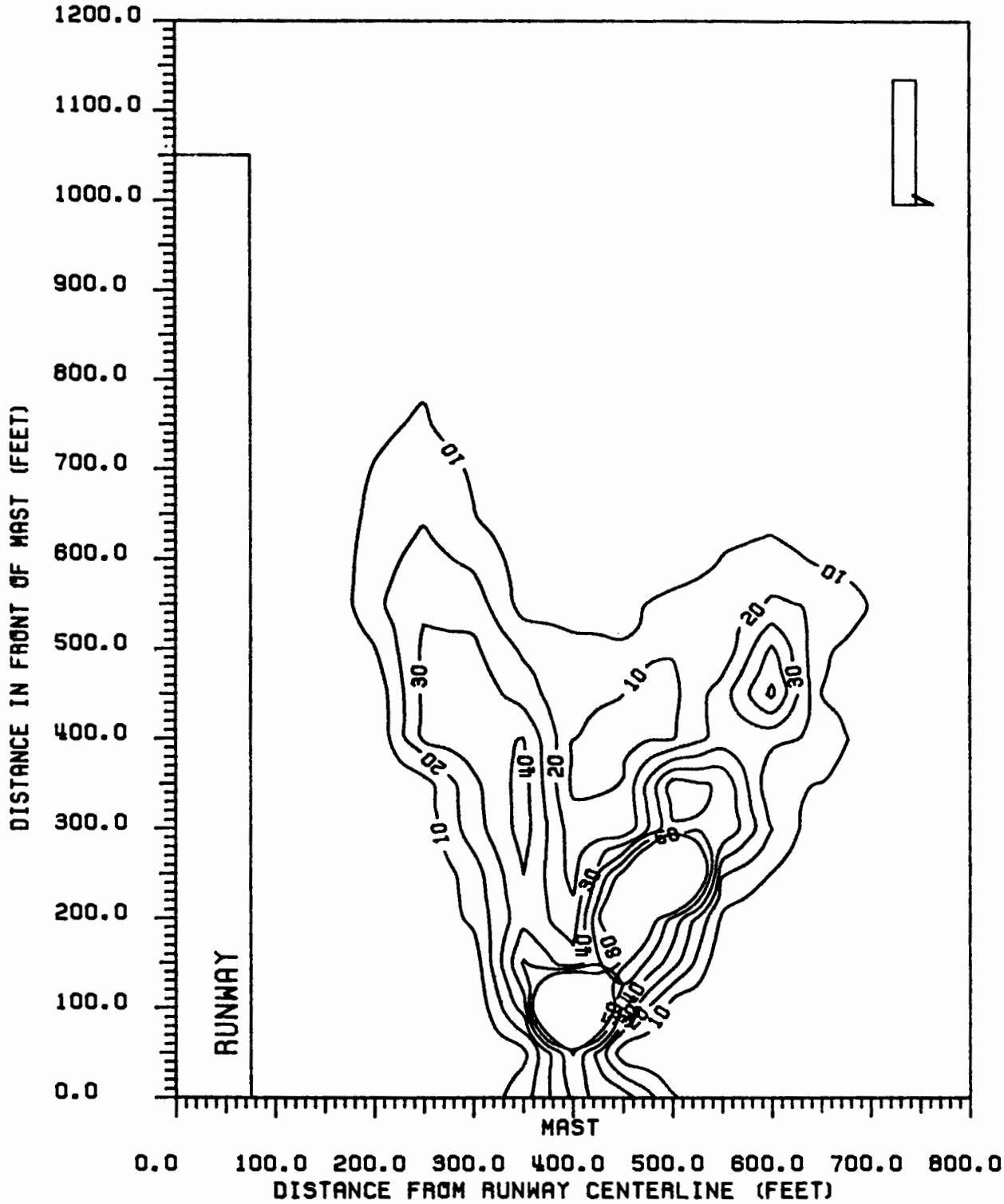

Figure 2-144. Contours of peak CDI values produced between ILS Point C and threshold for a DC-9. DC-9 fuselage is parallel to runway centerline, with tail towards the mast. Capture effect glide slope, directional antennas.

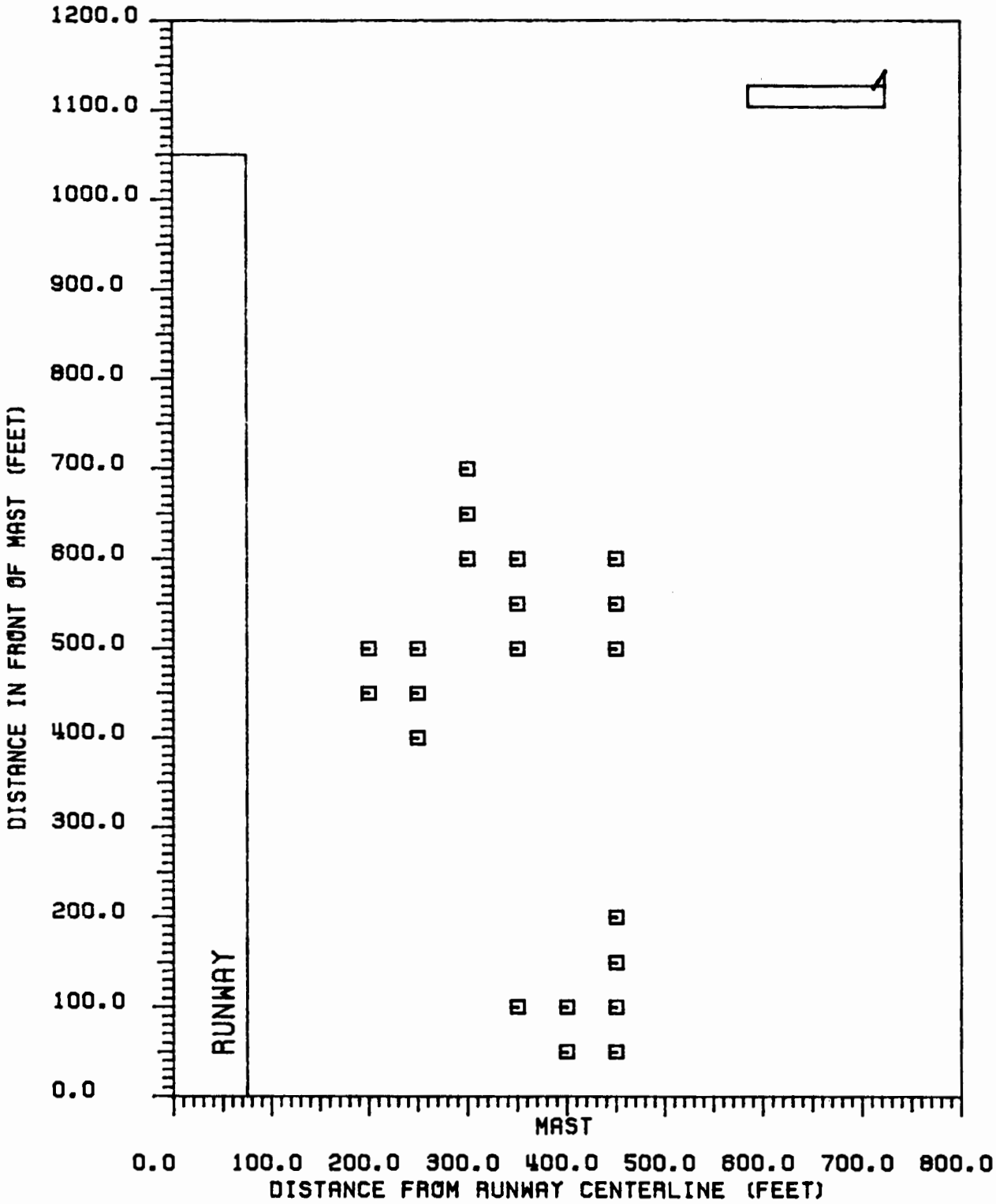

Figure 2-145. Critical area map for CAT II/III tolerances relating to B-727 aircraft. B-727 fuselage is perpendicular to runway centerline with tail away from the runway. Capture effect glide slope, directional antennas.

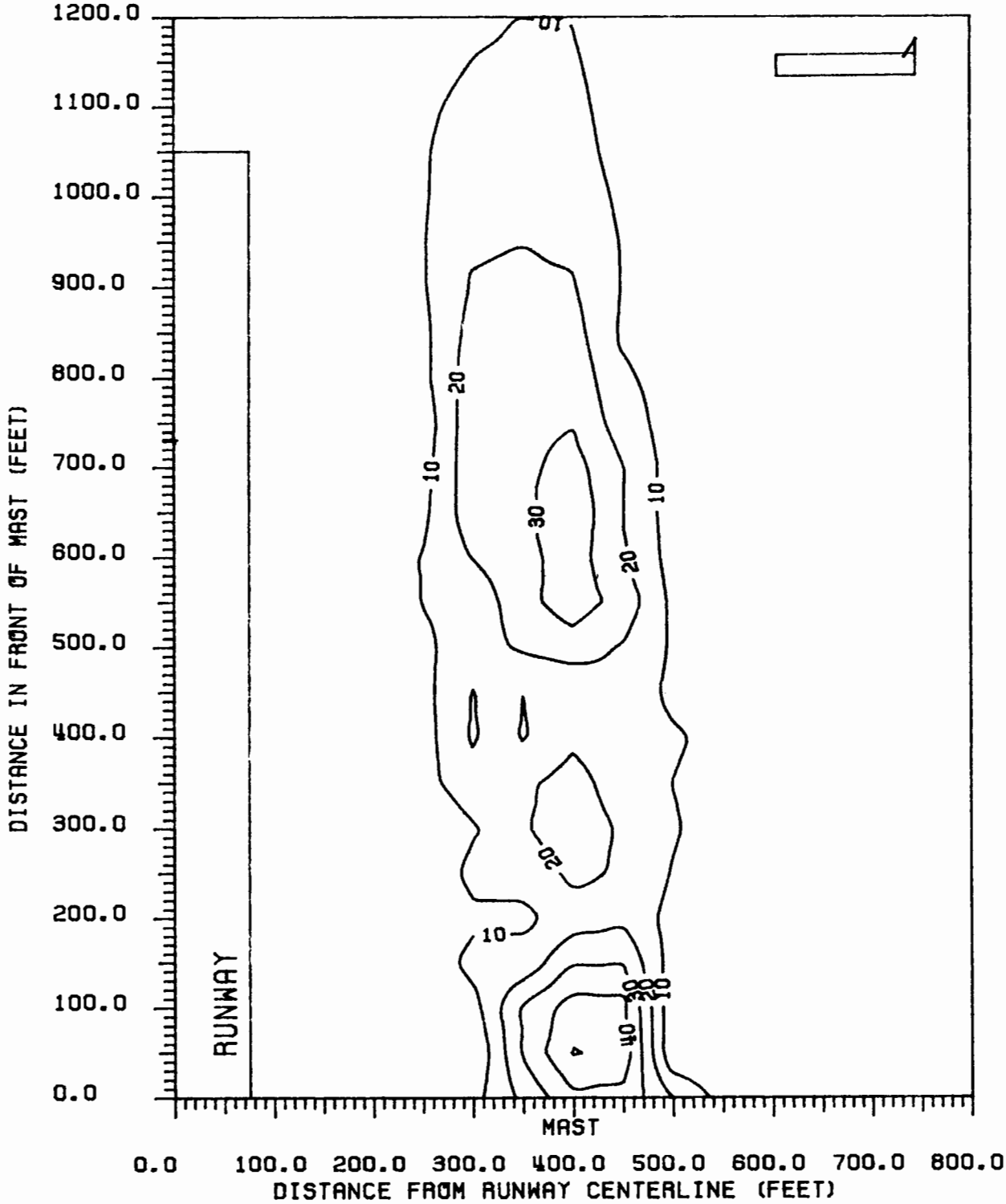

Figure 2-146. Contours of peak CDI values produced in ILS Zone 2 for a B-727. B-727 fuselage is perpendicular to runway centerline, with tail away from the runway. Capture effect glide slope, directional antennas.

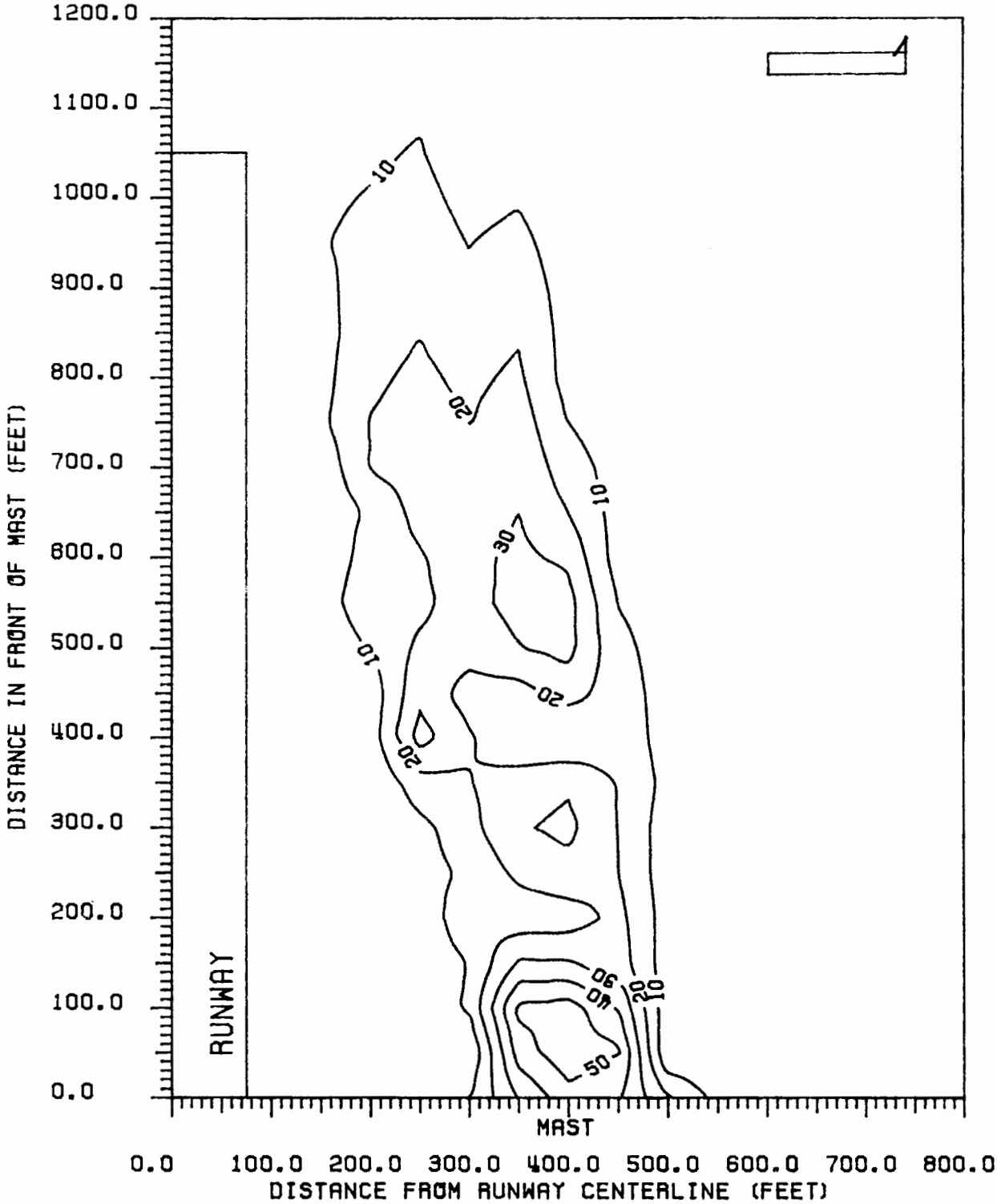

Figure 2-147. Contours of peak CDI values produced between ILS Point B and ILS Point C for a B-727. B-727 fuselage is perpendicular to runway centerline, with tail away from runway. Capture effect glide slope, directional antennas.

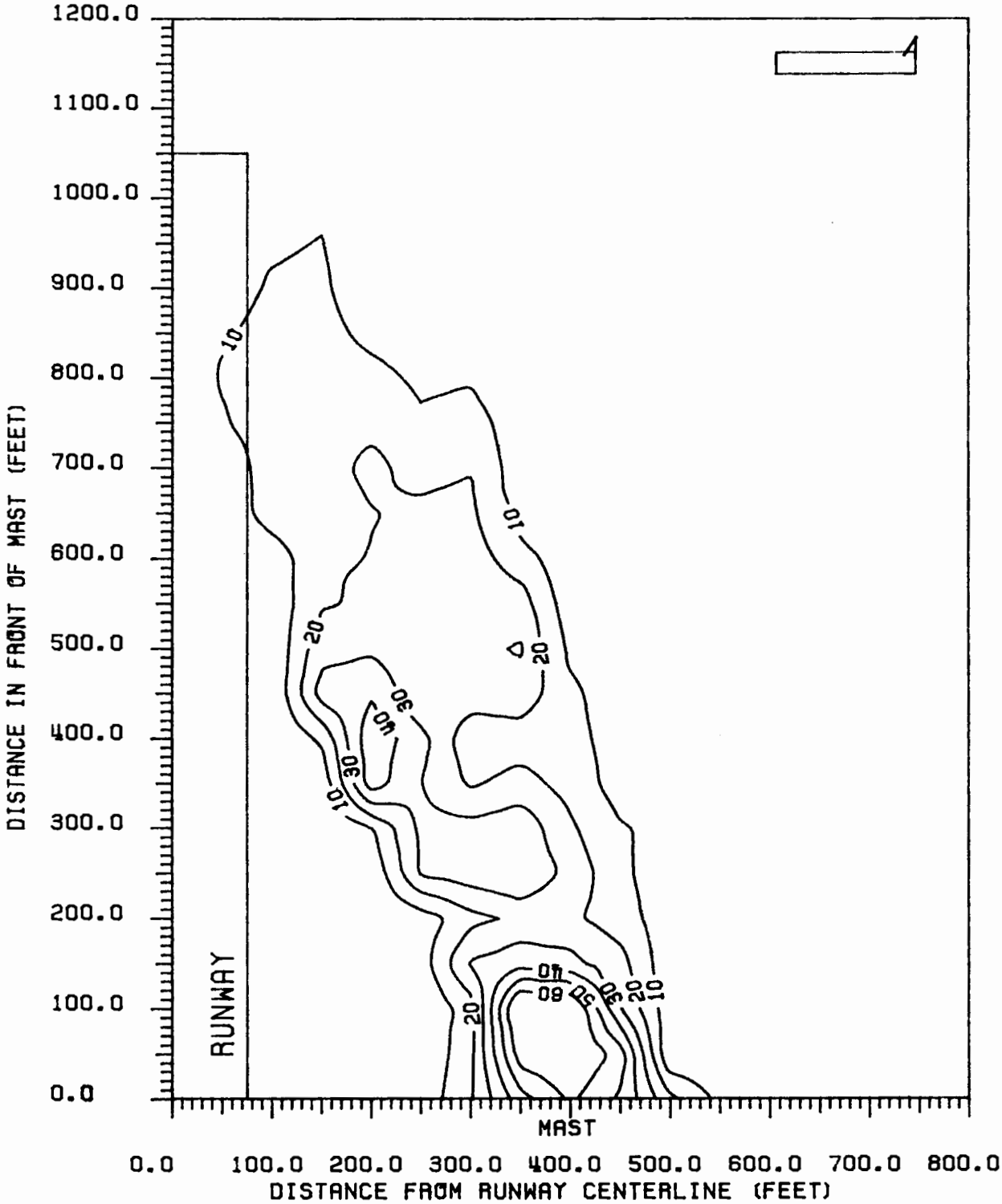

Figure 2-148. Contours of peak CDI values produced between ILS Point C and threshold for a B-727. B-727 fuselage is perpendicular to runway centerline, with tail away from runway. Capture effect glide slope, directional antennas.

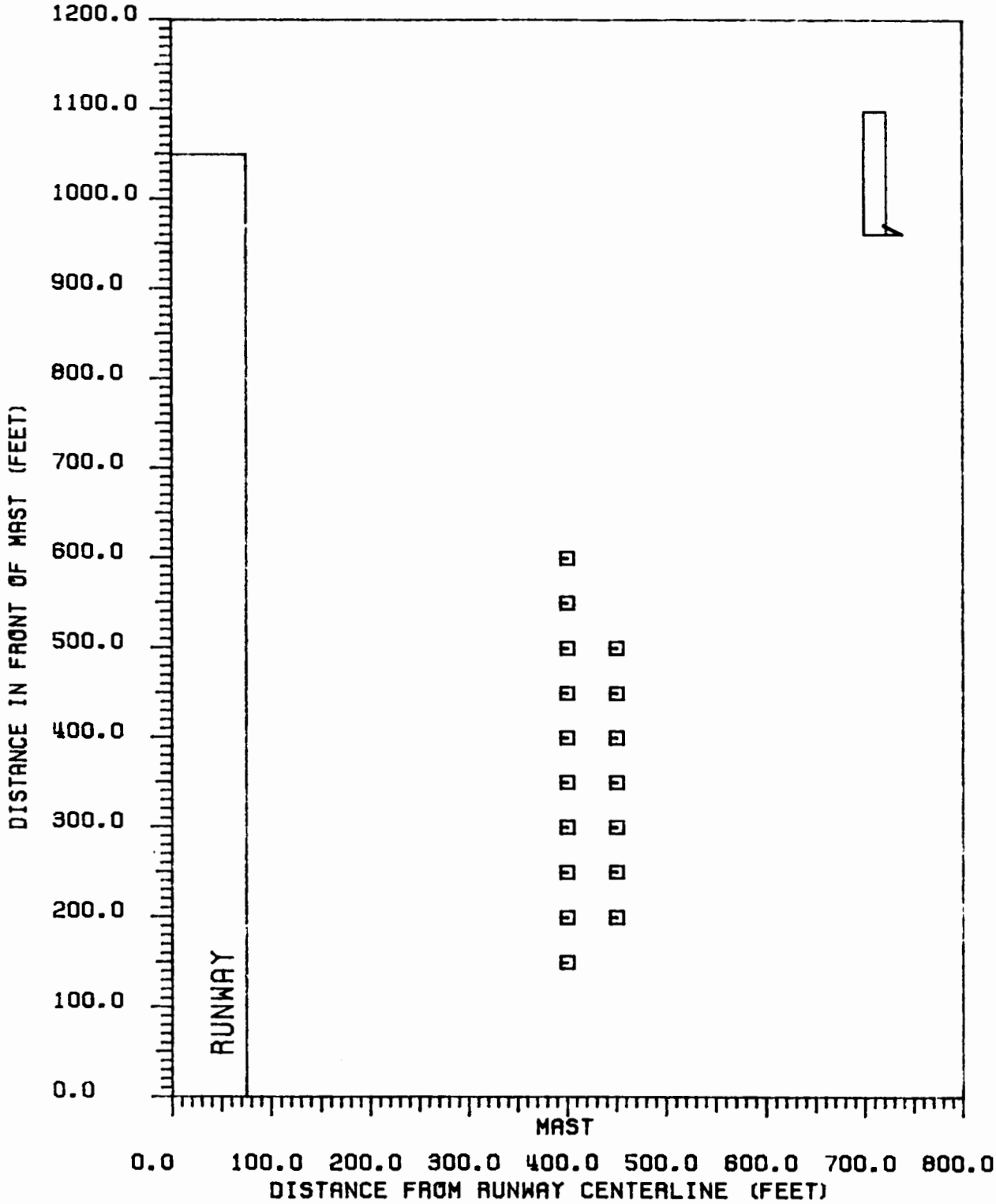

Figure 2-149. Critical area map for CAT I tolerances relating to B-727 aircraft. B-727 fuselage is parallel to runway centerline with tail towards the mast. Capture effect glide slope, directional antennas.

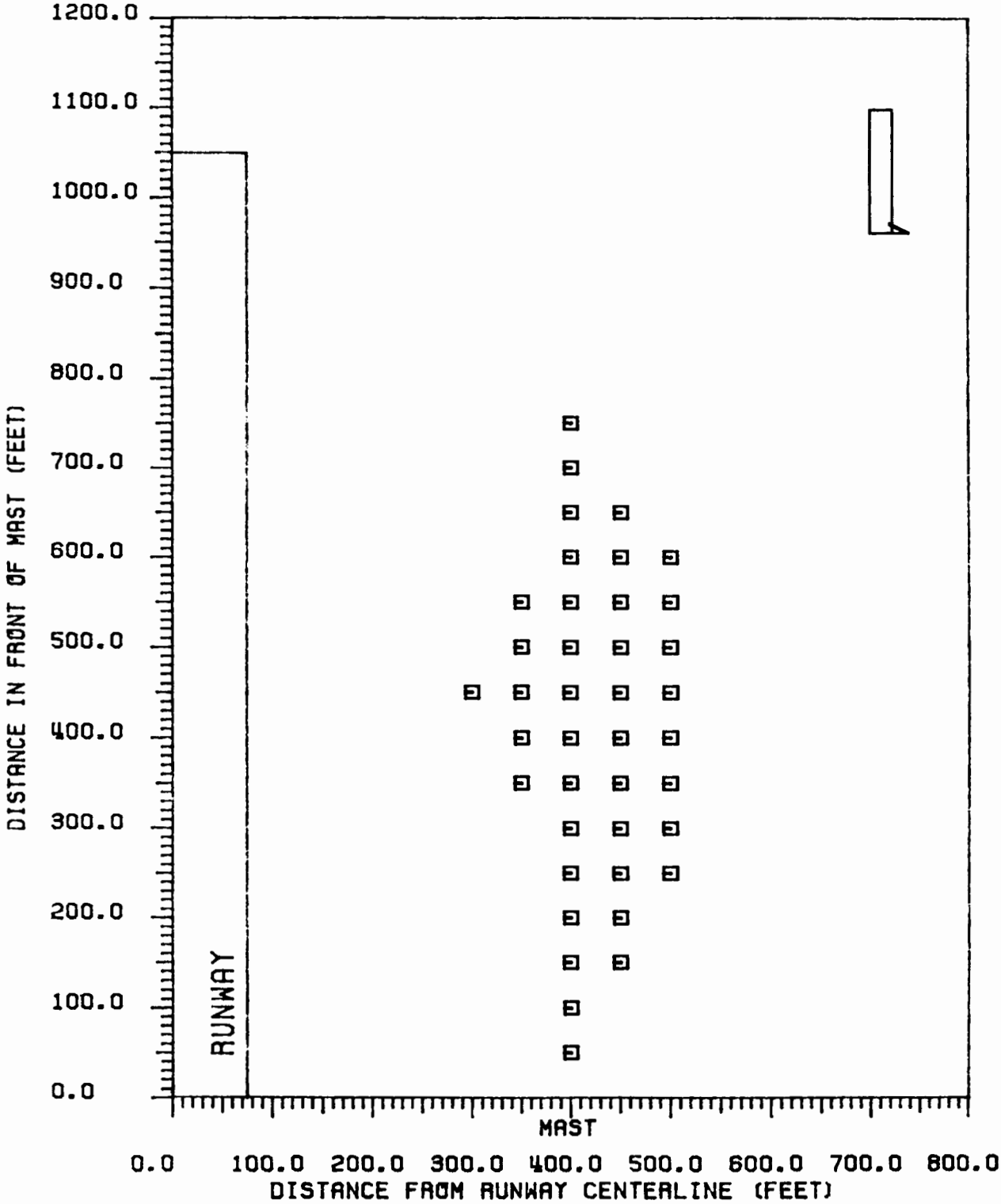

Figure 2-150. Critical area map for CAT II/III tolerances relating to B-727 aircraft. B-727 fuselage is parallel to runway centerline with tail towards the mast. Capture effect glide slope, directional antennas.

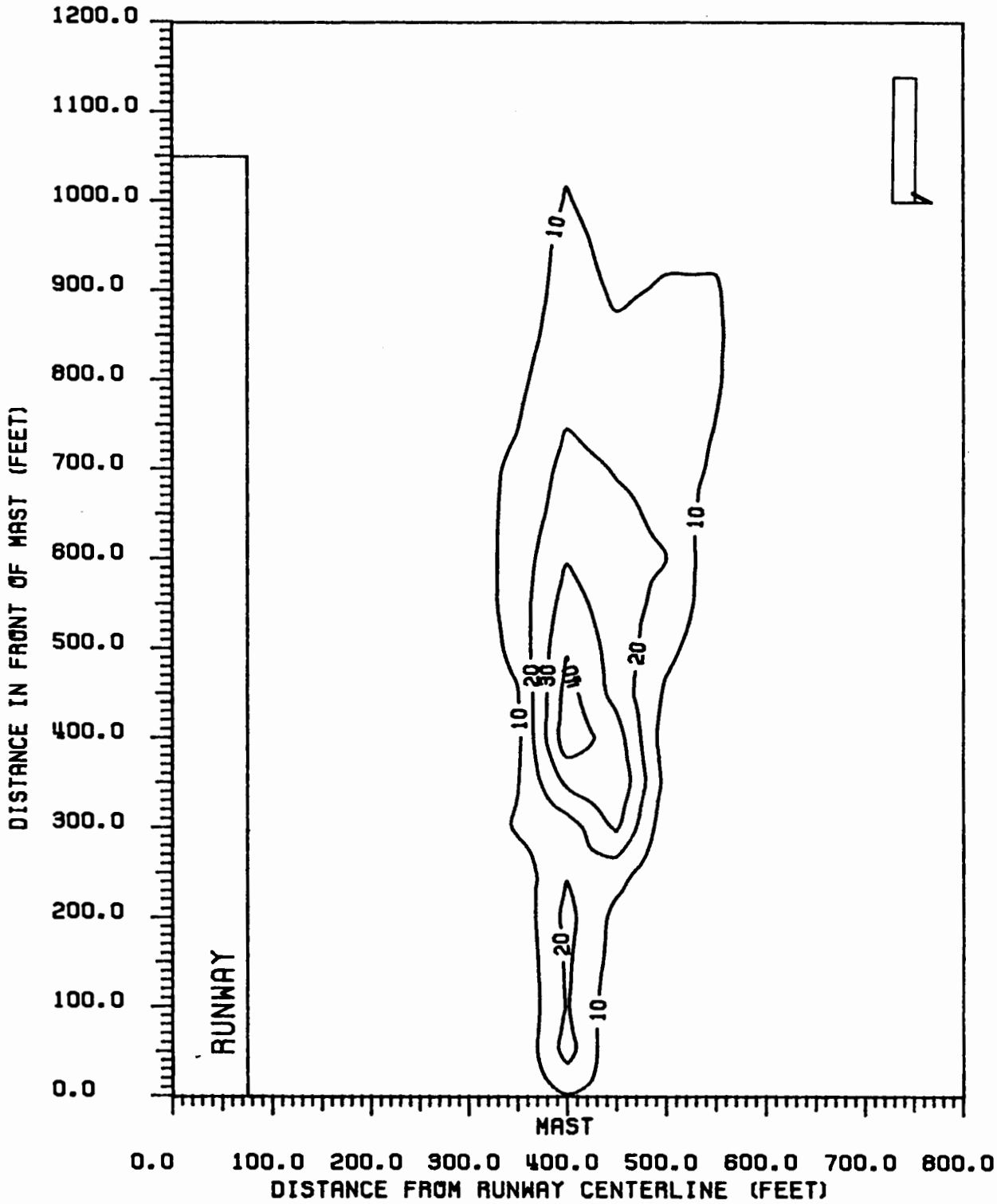

Figure 2-151. Contours of peak CDI values produced in ILS Zone 2 for a B-727. B-727 fuselage is parallel to runway centerline, with tail towards the mast. Capture effect glide slope, directional antennas.

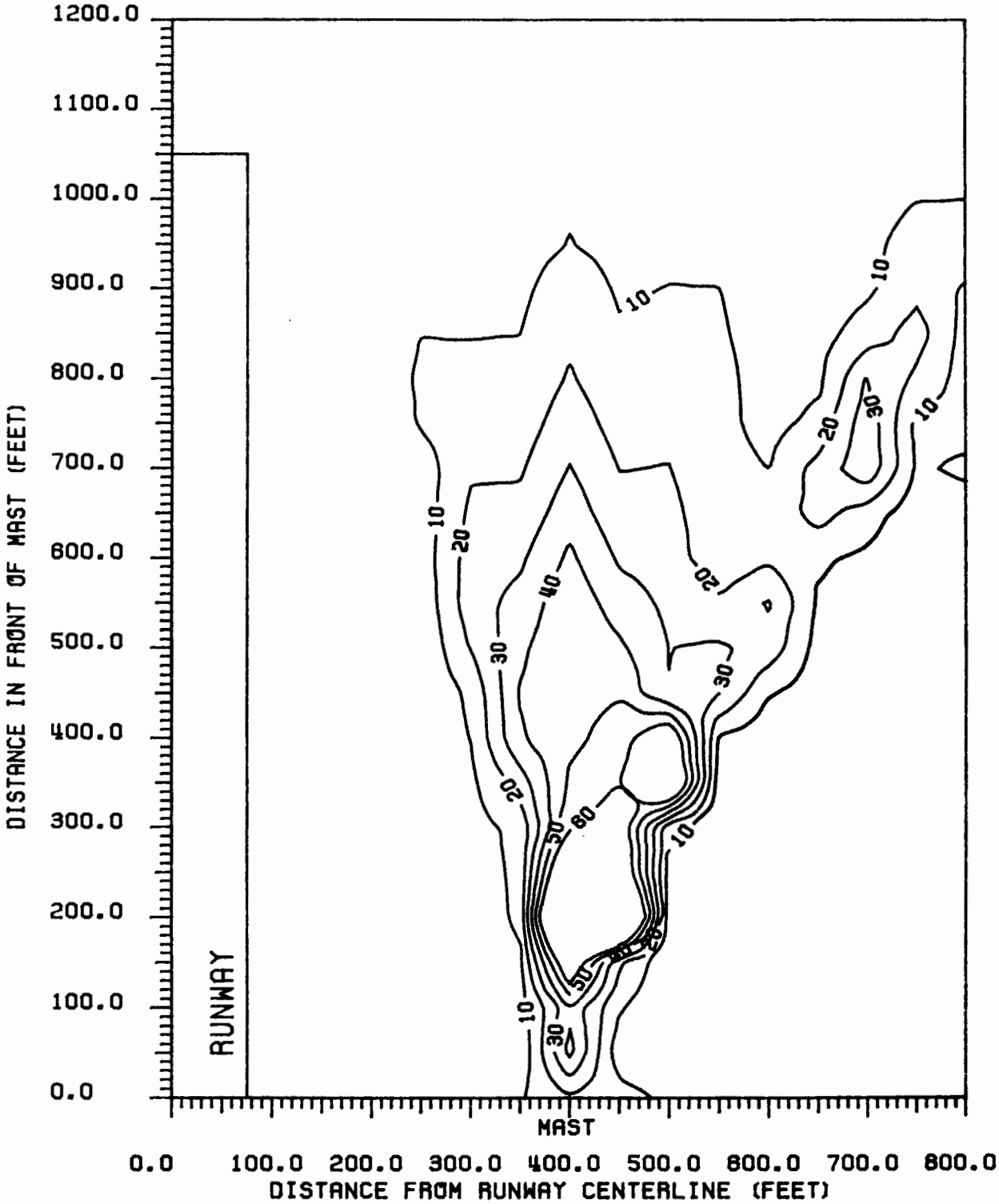

Figure 2-152. Contours of peak CDI values produced between ILS Point B and ILS Point C for a B-727. B-727 fuselage is parallel to runway centerline, with tail towards the mast. Capture effect glide slope, directional antennas.

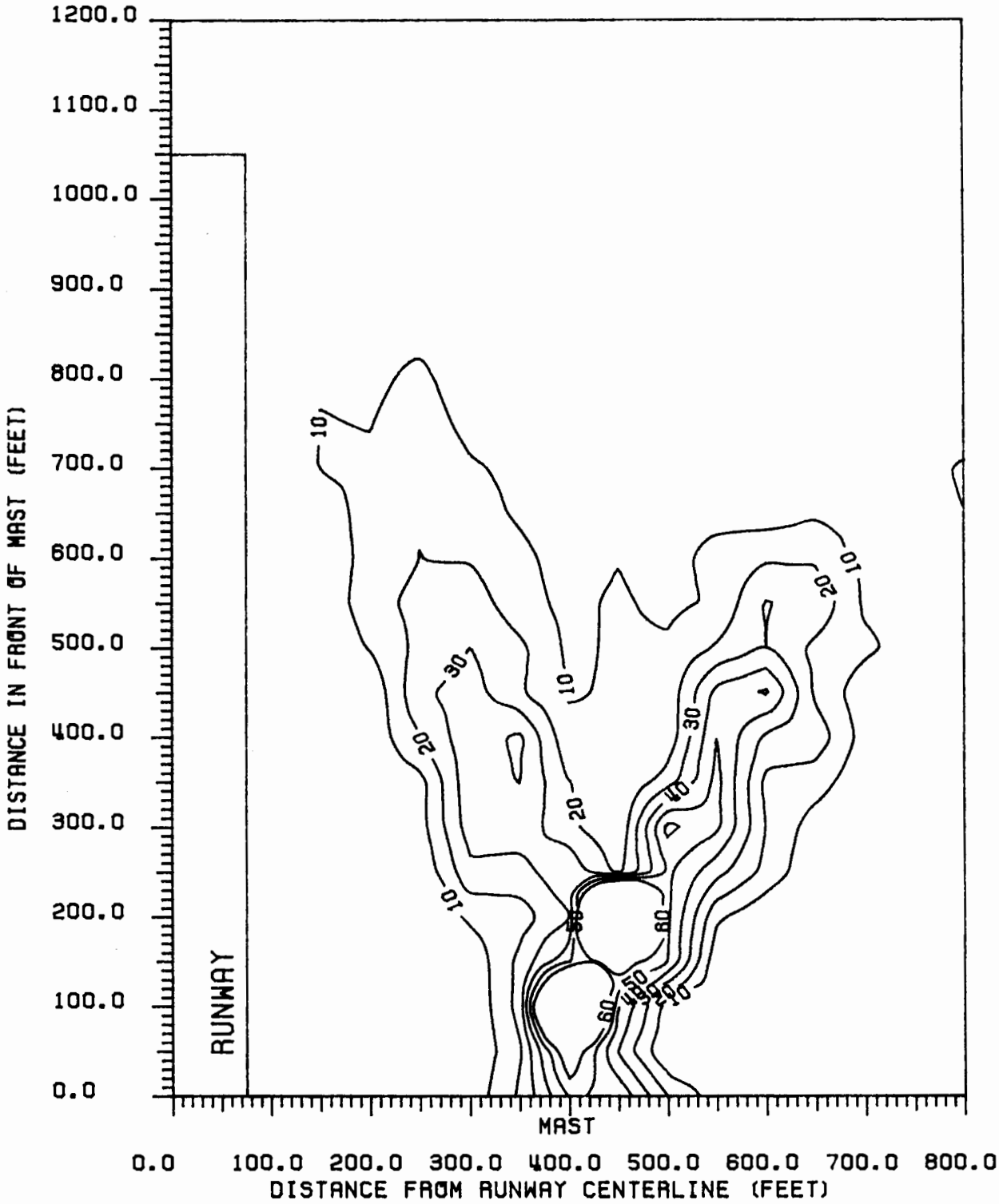

Figure 2-153. Contours of peak CDI values produced between ILS Point C and threshold for a B-727. B-727 fuselage is parallel to runway centerline, with tail towards the mast. Capture effect glide slope, directional antennas.

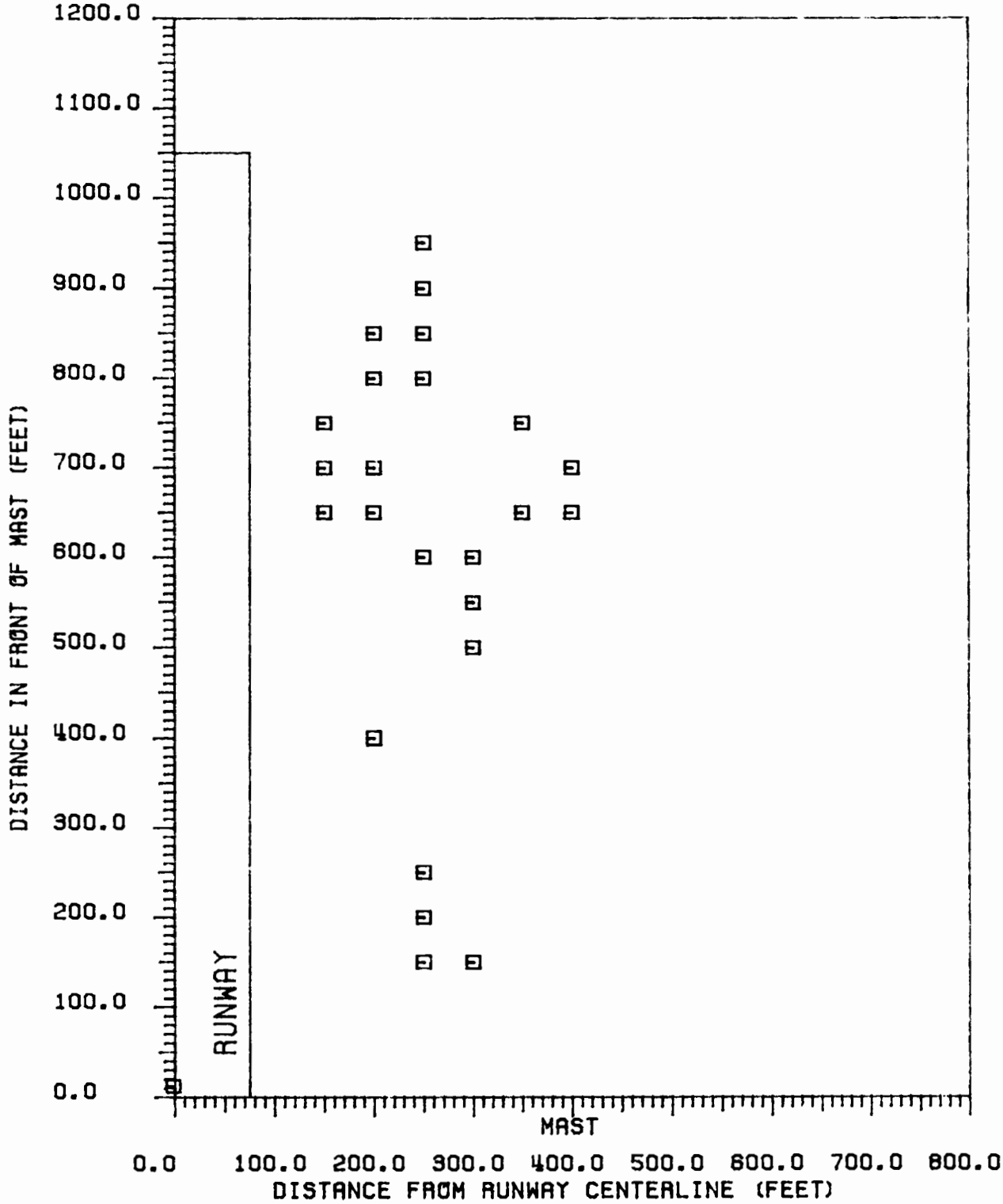

Figure 2-154. Critical area map for CAT II/III tolerances relating to B-747 aircraft. B-747 fuselage is perpendicular to runway centerline with tail away from the runway. Capture effect glide slope, directional antennas.

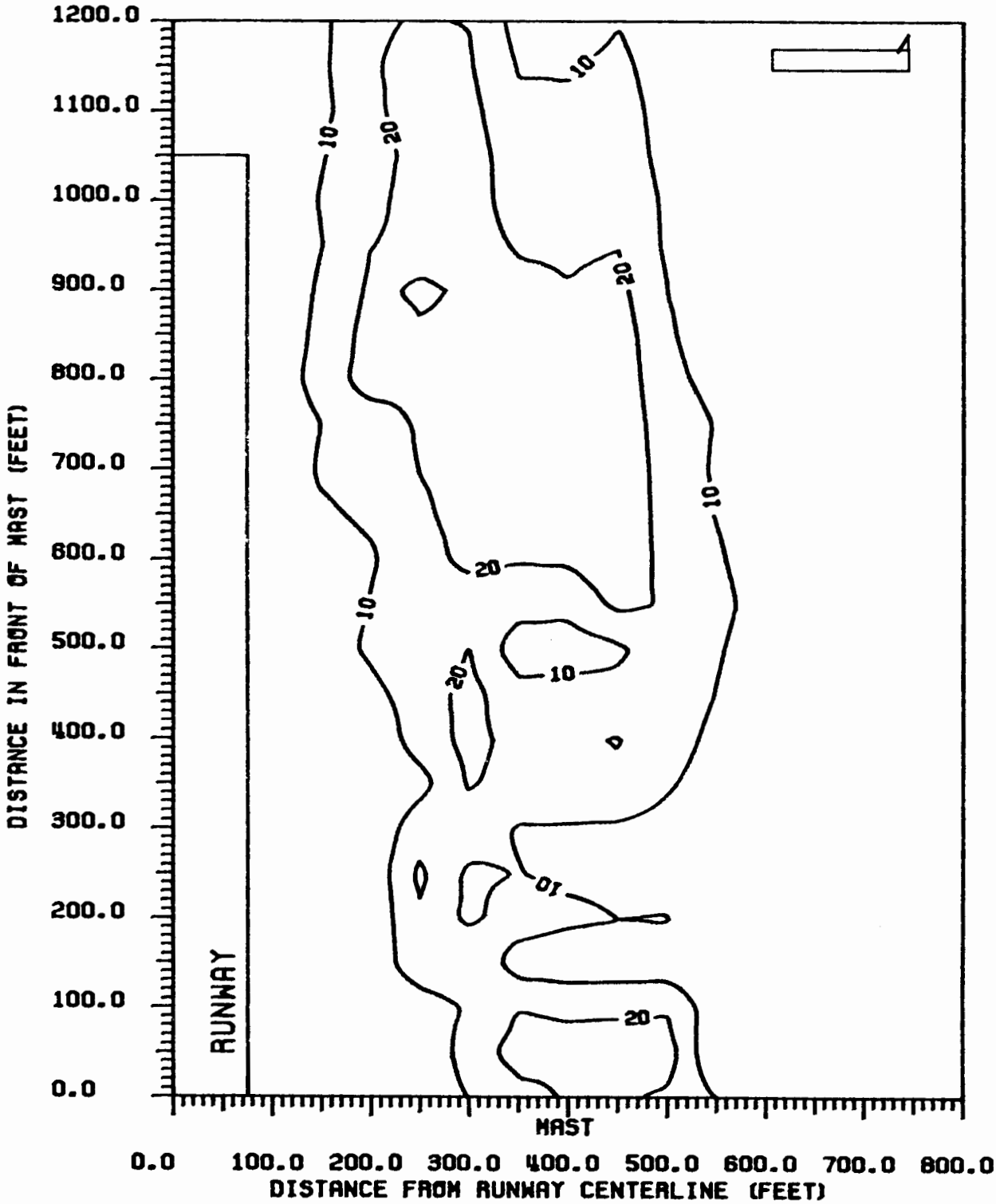

Figure 2-155. Contours of peak CDI values produced in ILS Zone 2 for a B-747. B-747 fuselage is perpendicular to runway centerline, with tail away from the runway. Capture effect glide slope, directional antennas.

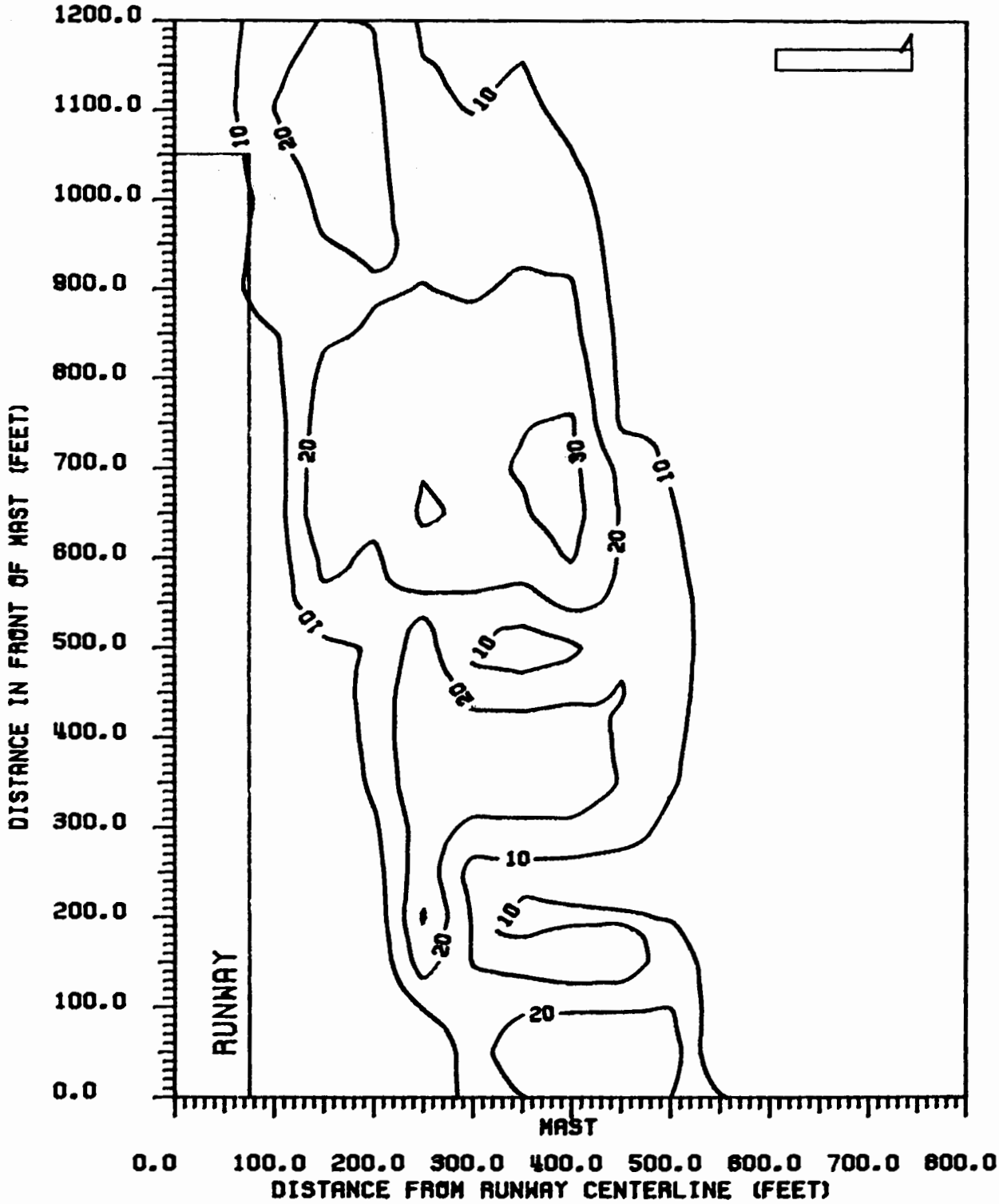

Figure 2-156. Contours of peak CDI values produced between ILS Point B and ILS Point C for a B-747. B-747 fuselage is perpendicular to runway centerline, with tail away from runway. Capture effect glide slope, directional antennas.

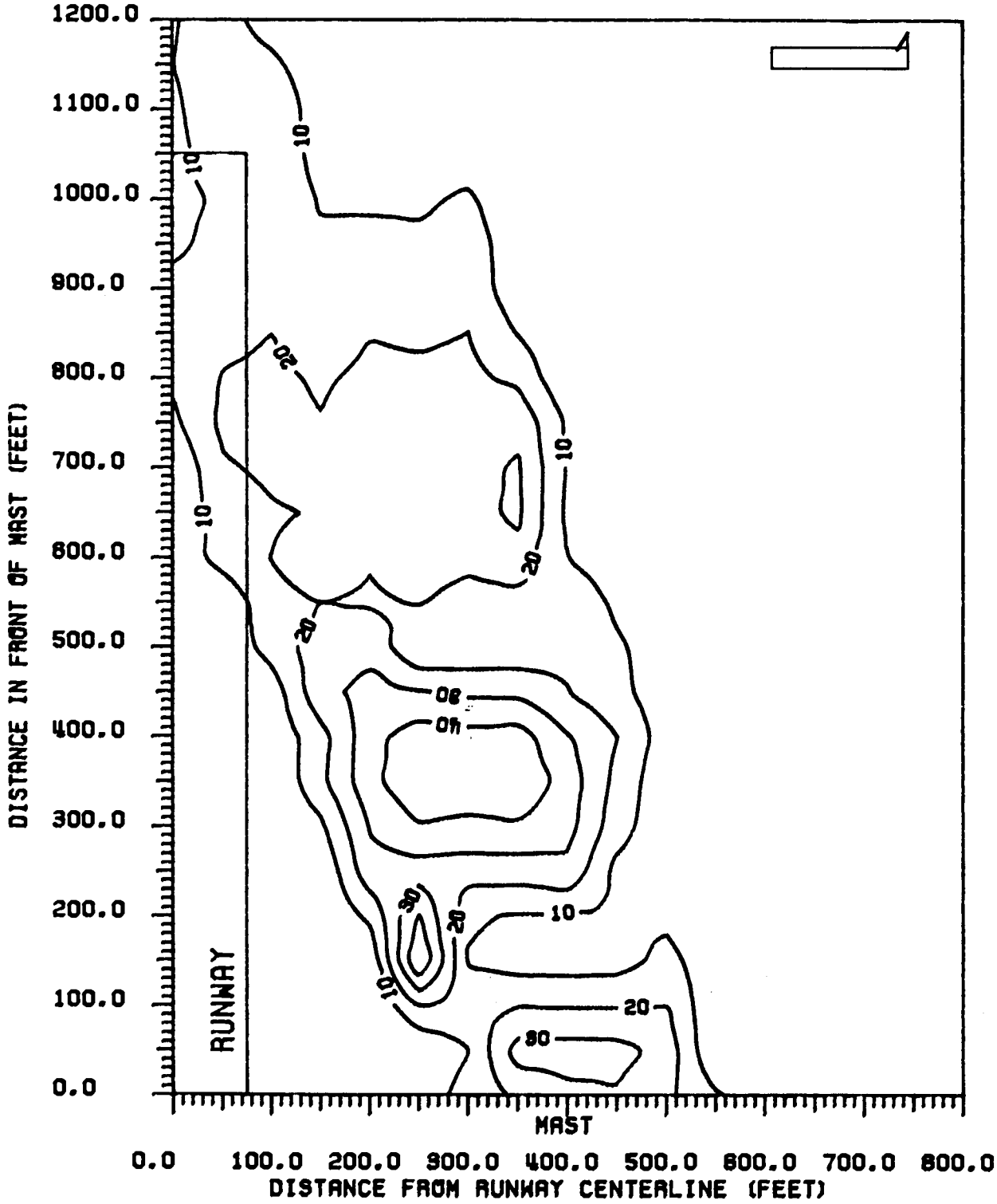

Figure 2-157. Contours of peak CDI values produced between ILS Point C and threshold for a B-747. B-747 fuselage is perpendicular to runway centerline, with tail away from runway. Capture effect glide slope, directional antennas.

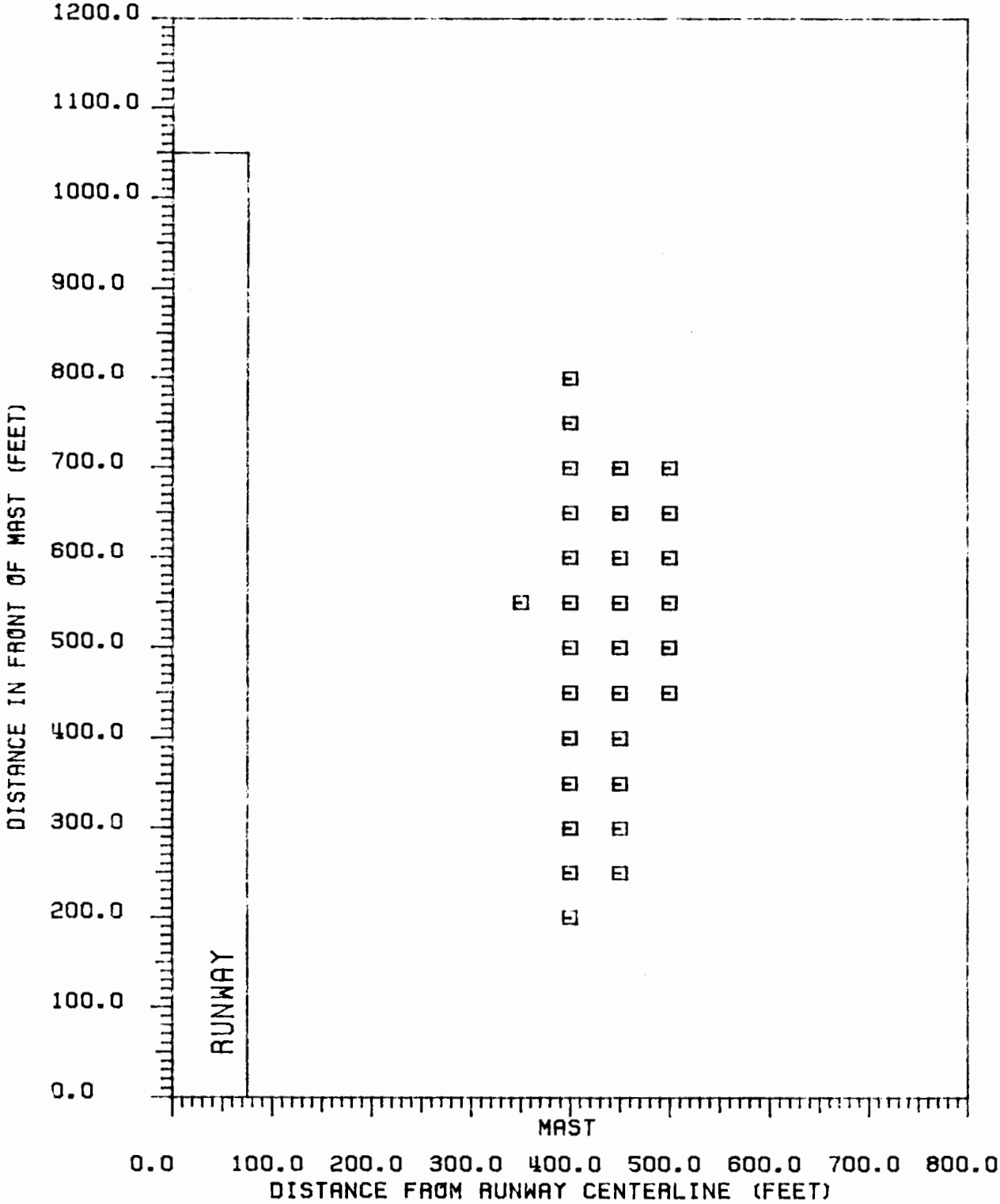

Figure 2-158. Critical area map for CAT I tolerances relating to B-747 aircraft. B-747 fuselage is parallel to runway centerline with tail towards the mast. Capture effect glide slope, directional antennas.

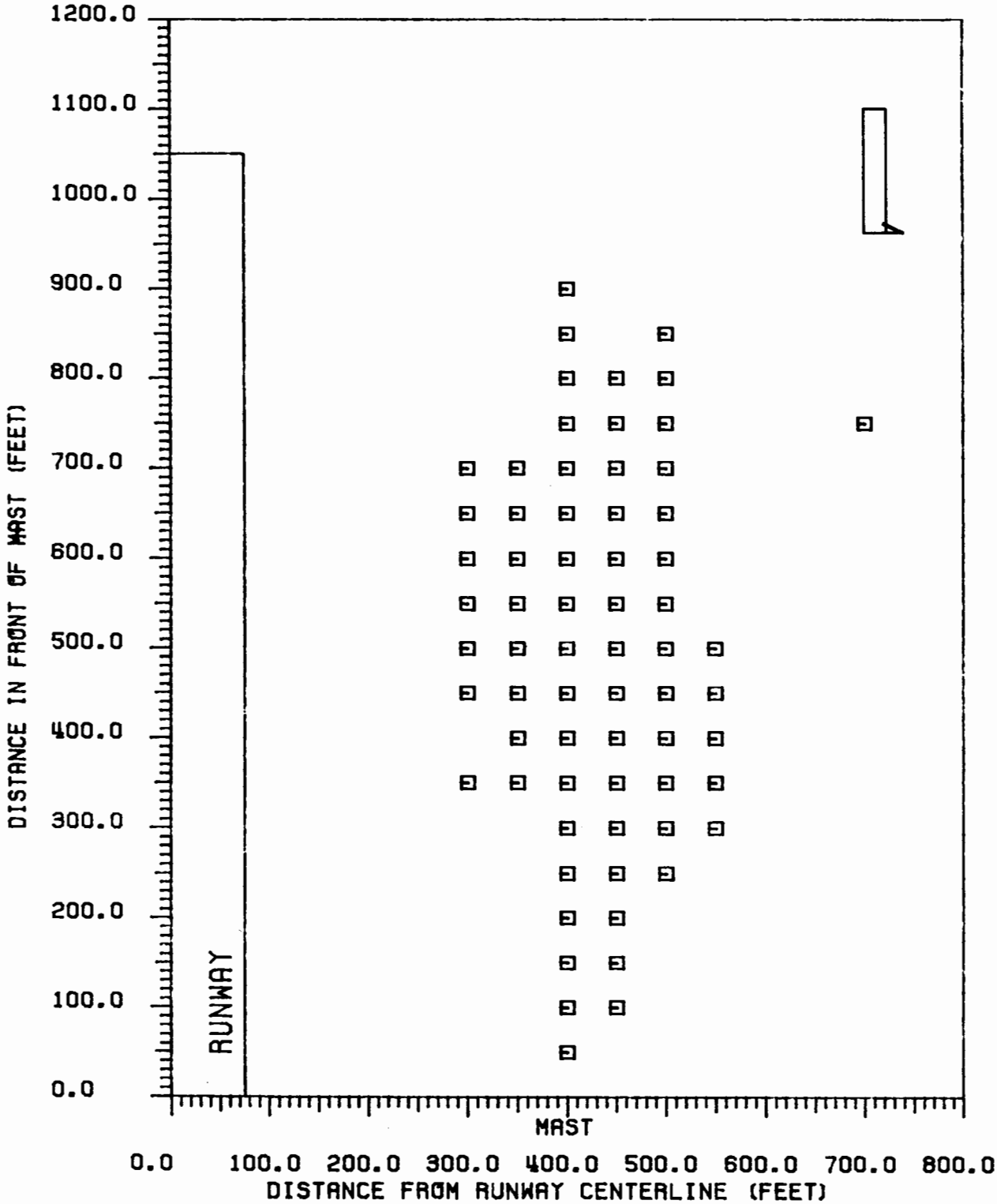

Figure 2-159. Critical area map for CAT II/III tolerances relating to B-747 aircraft. B-747 fuselage is parallel to runway centerline with tail towards the mast. Capture effect glide slope, directional antennas.

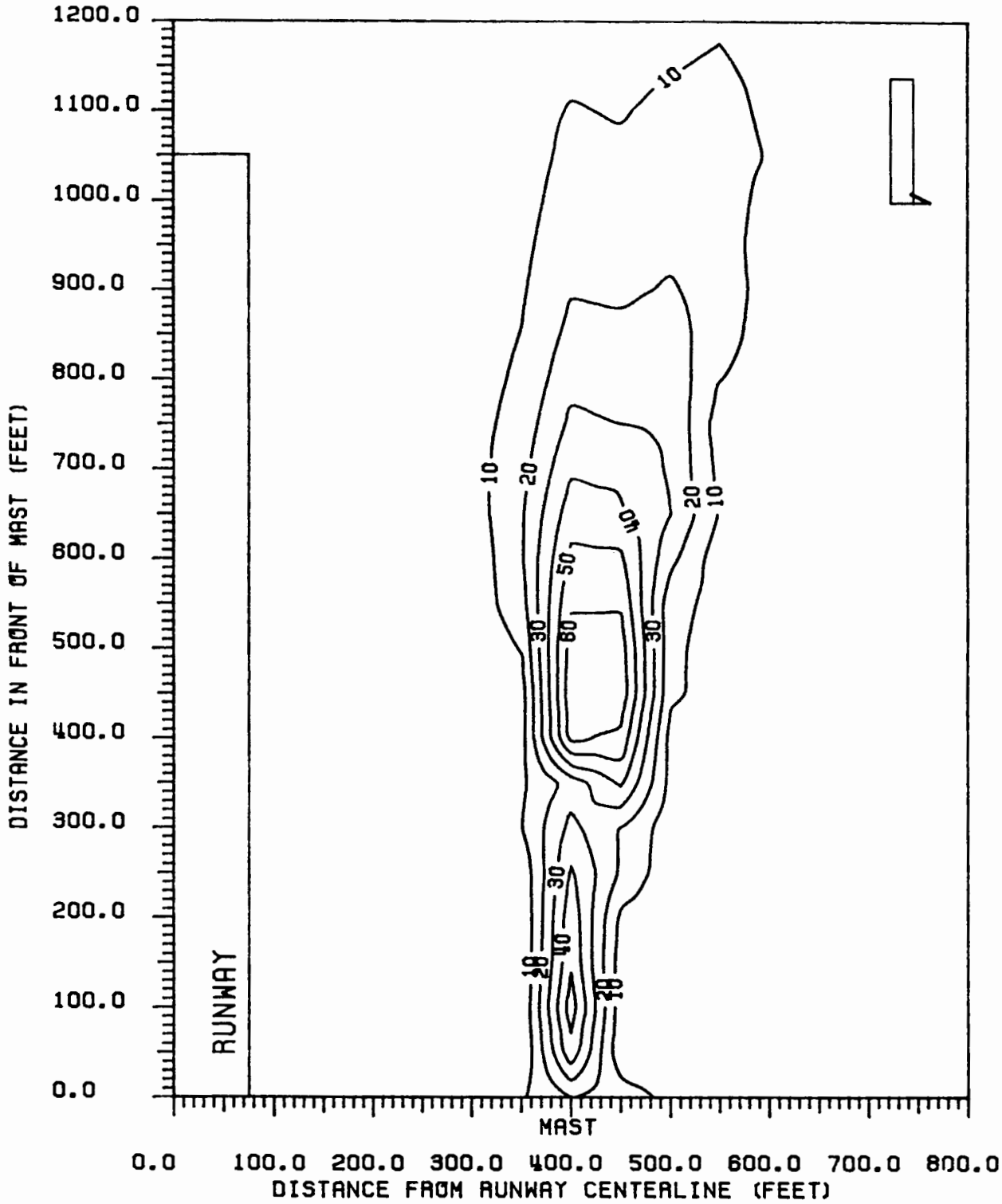

Figure 2-160. Contours of peak CDI values produced in ILS Zone 2 for a B-747. B-747 fuselage is parallel to runway centerline, with tail towards the mast. Capture effect glide slope, directional antennas.

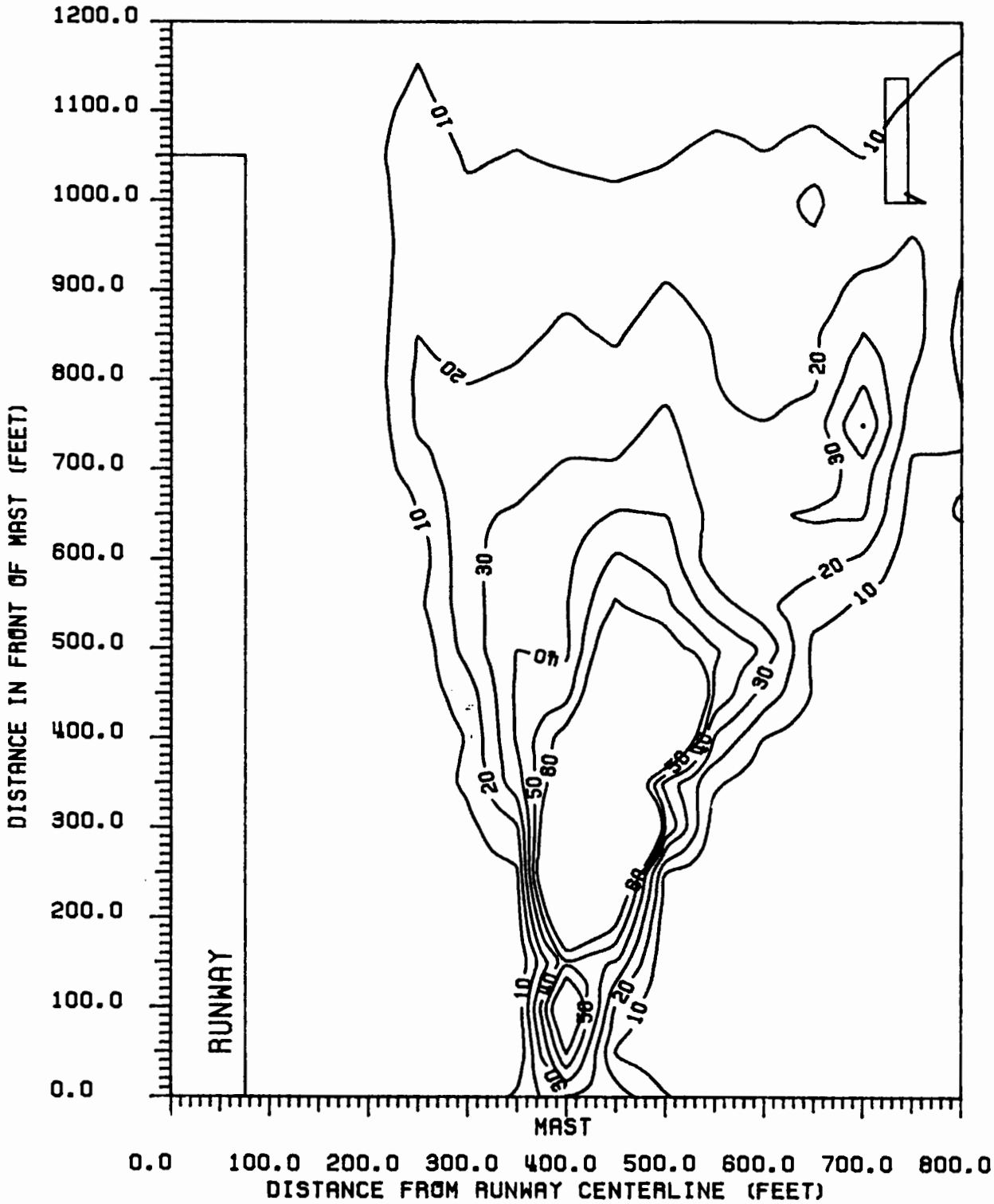

Figure 2-161. Contours of peak CDI values produced between ILS Point B and ILS Point C for a B-747. B-747 fuselage is parallel to runway centerline, with tail towards the mast. Capture effect glide slope, directional antennas.

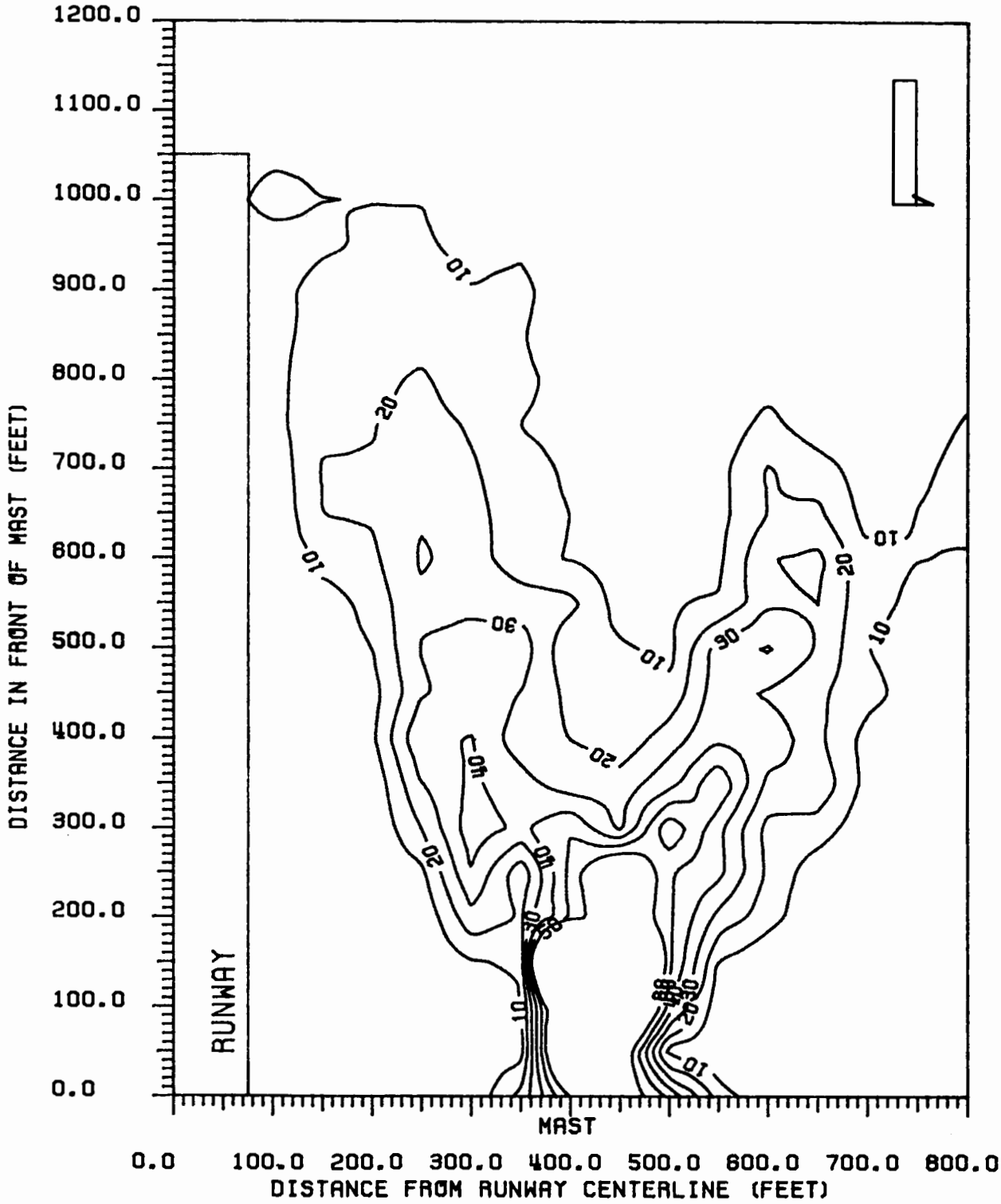

Figure 2-162. Contours of peak CDI values produced between ILS Point C and threshold for a B-747. B-747 fuselage is parallel to runway centerline, with tail towards the mast. Capture effect glide slope, directional antennas.

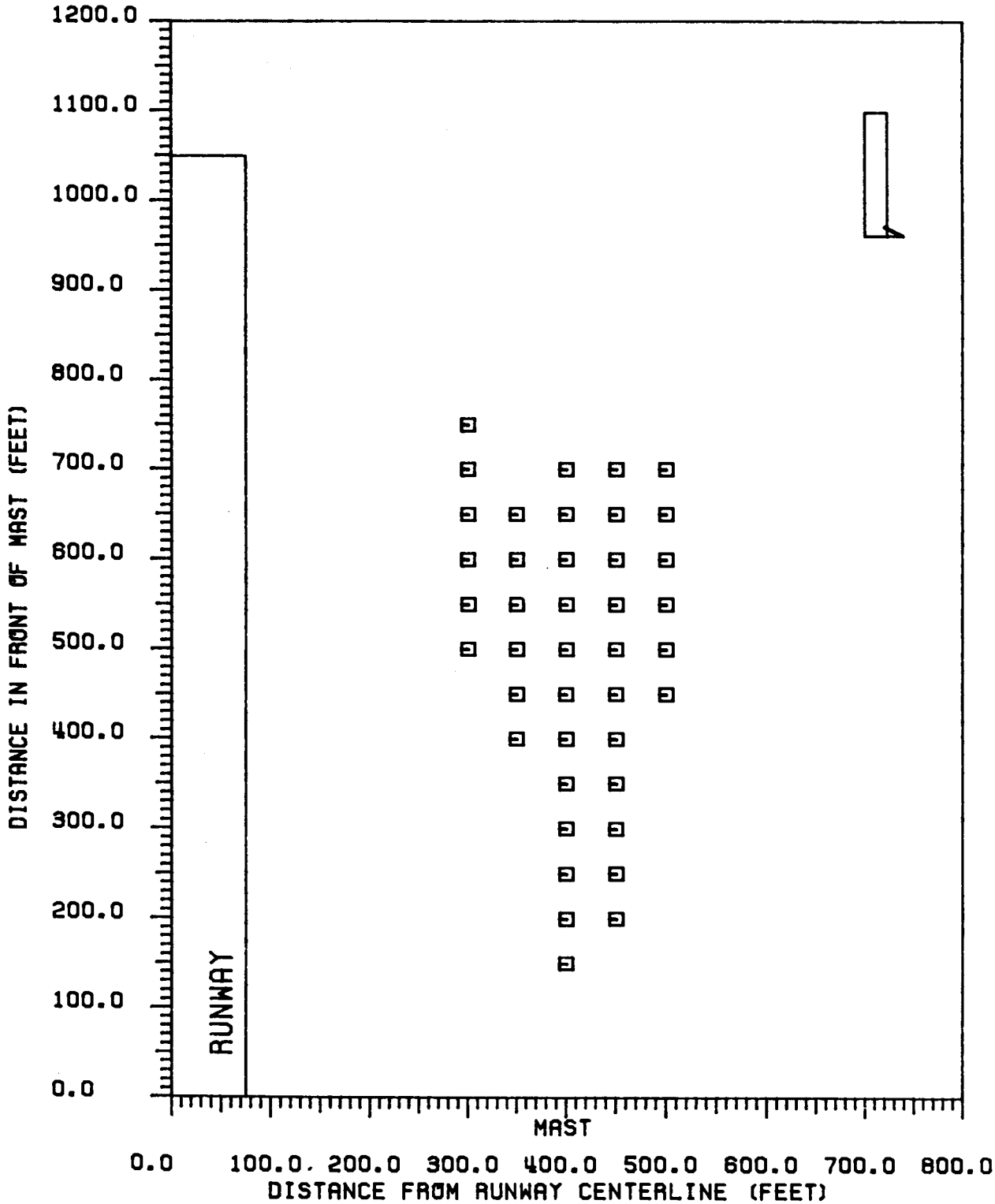

Figure 2-163. Critical area map for CAT I tolerances relating to B-727 aircraft. B-727 fuselage is parallel to runway centerline with tail towards the mast. Null reference glide slope, dipole antennas.

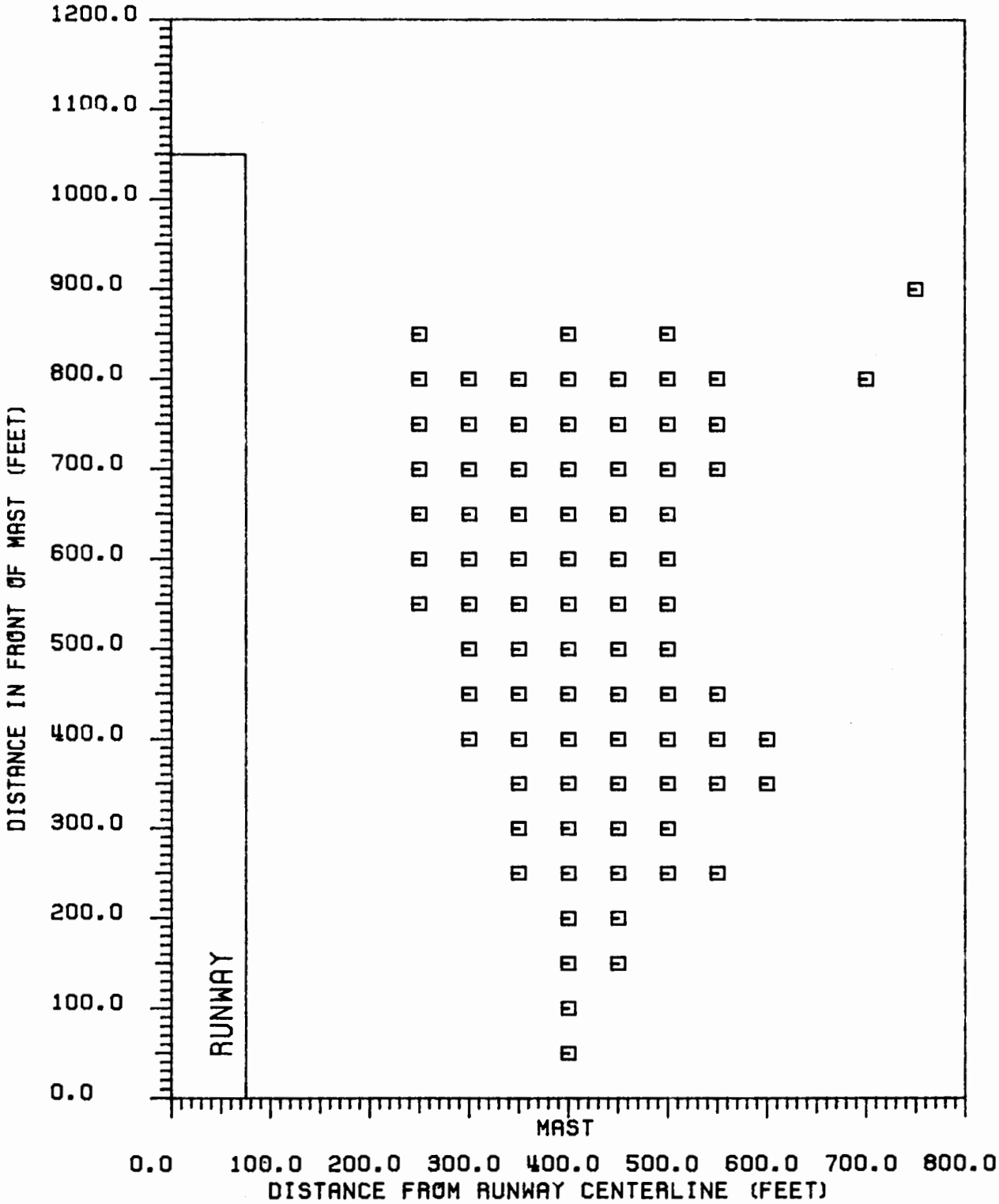

Figure 2-164. Critical area map for CAT II/III tolerances relating to B-727 aircraft. B-727 fuselage is parallel to runway centerline with tail towards the mast. Null reference glide slope, dipole antennas.

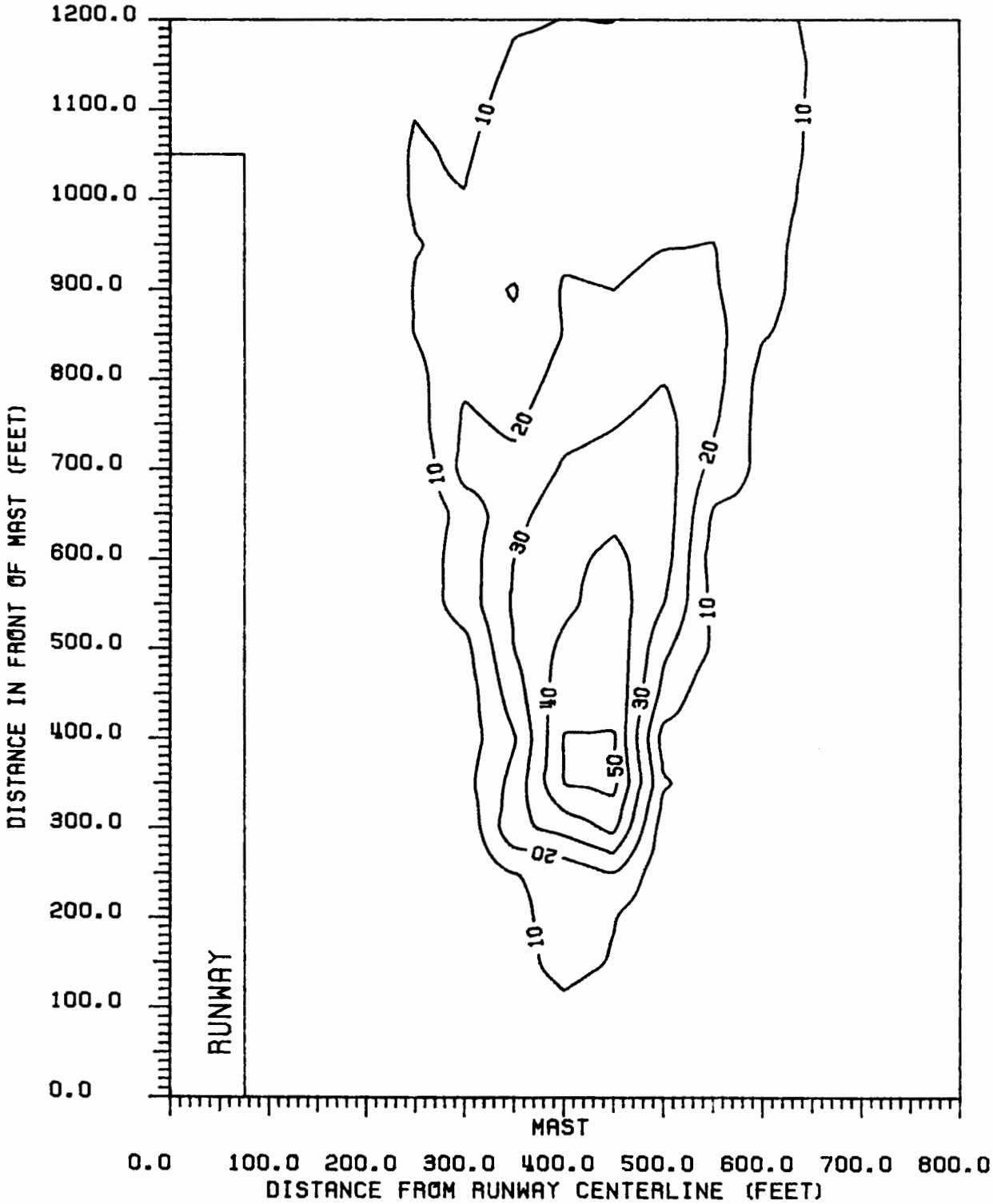

Figure 2-165. Contours of peak CDI values produced in ILS Zone 2 for a B-727. B-727 fuselage is parallel to runway centerline, with tail towards the mast. Null reference glide slope, dipole antennas.

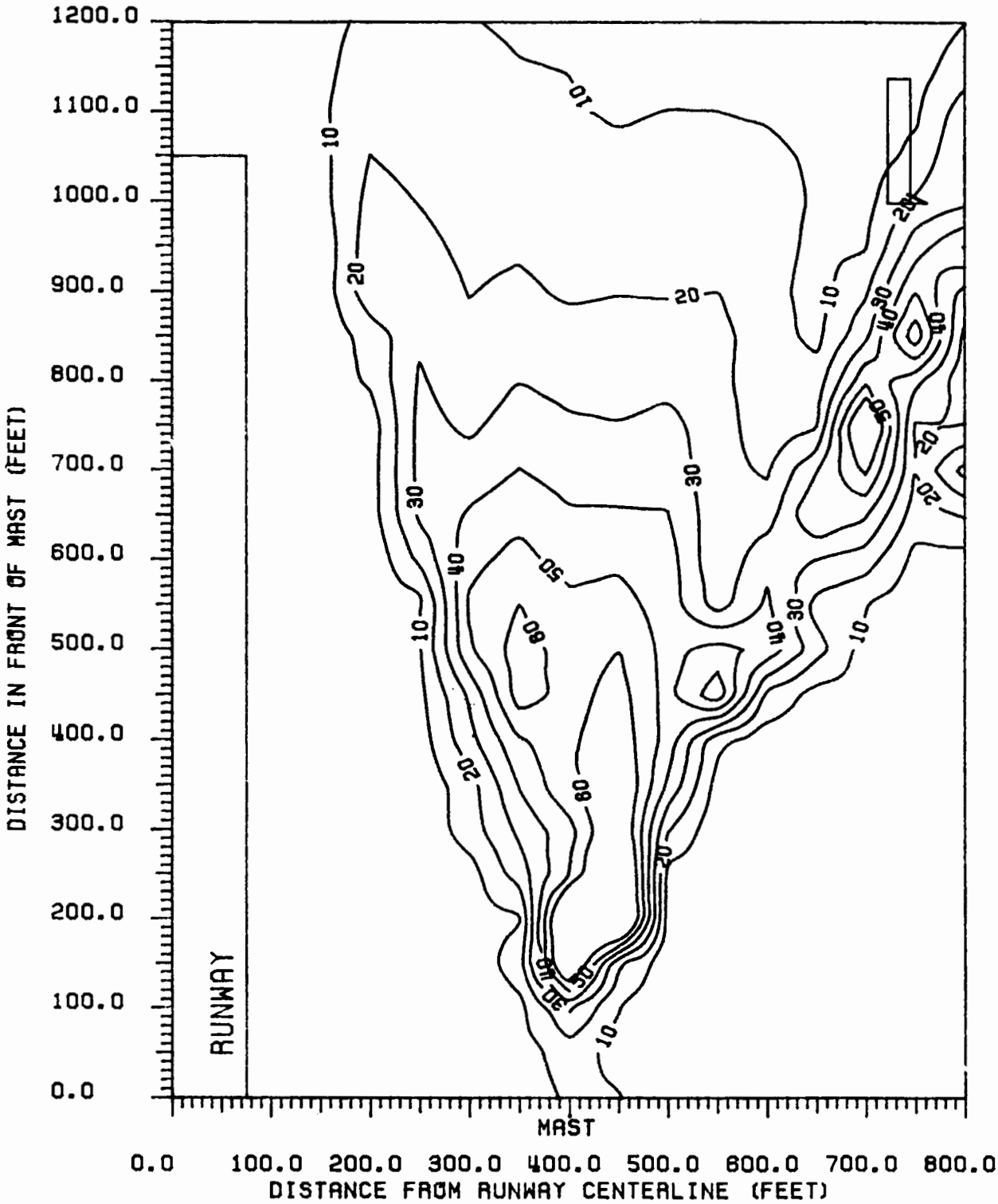

Figure 2-166. Contours of peak CDI values produced between ILS Point B and ILS Point C for a B-727. B-727 fuselage is parallel to runway centerline, with tail towards the mast. Null reference glide slope, dipole antennas.

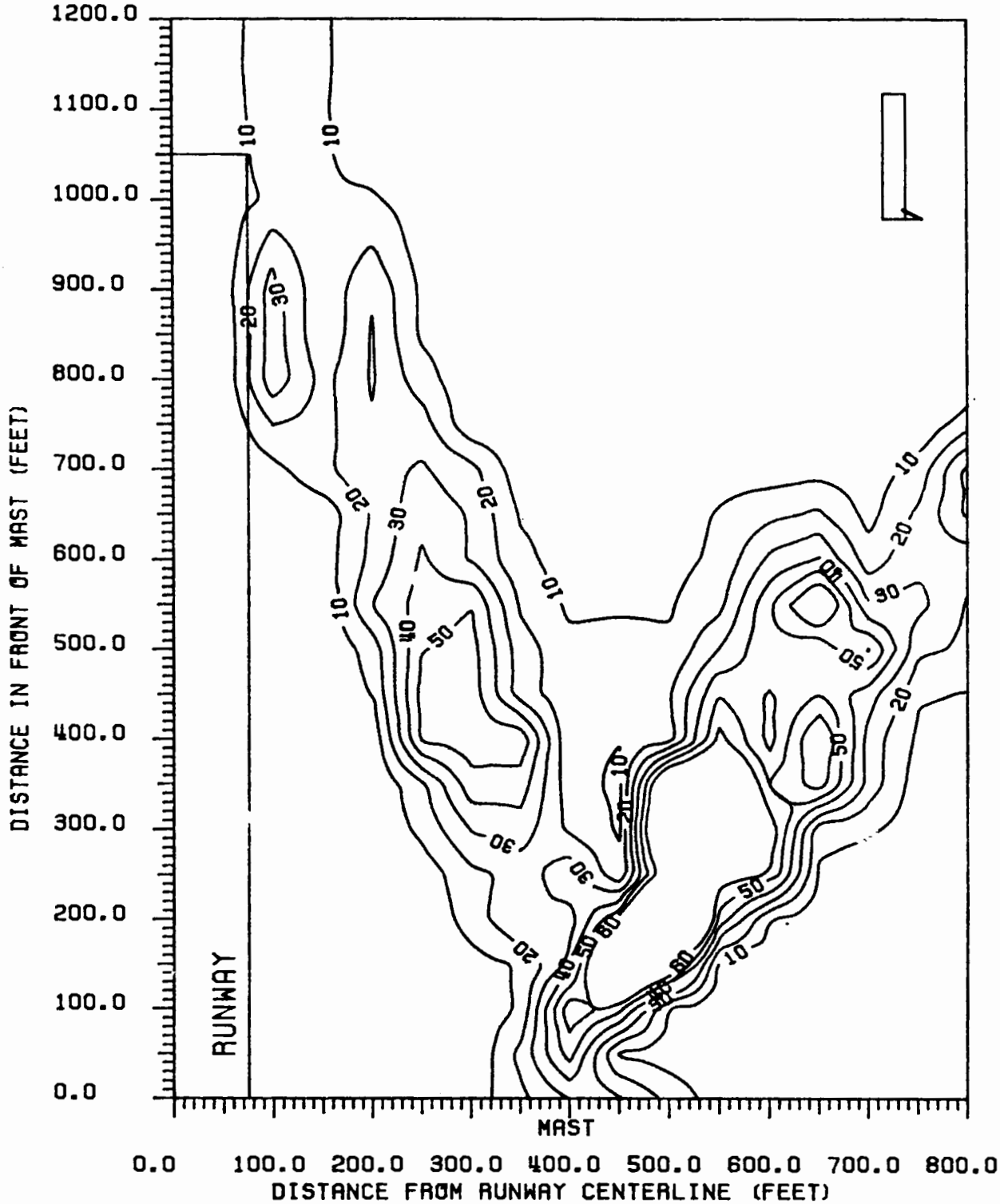

Figure 2-167. Contours of peak CDI values produced between ILS Point C and threshold for a B-727. B-727 fuselage is parallel to runway centerline, with tail towards the mast. Null reference glide slope, dipole antennas.

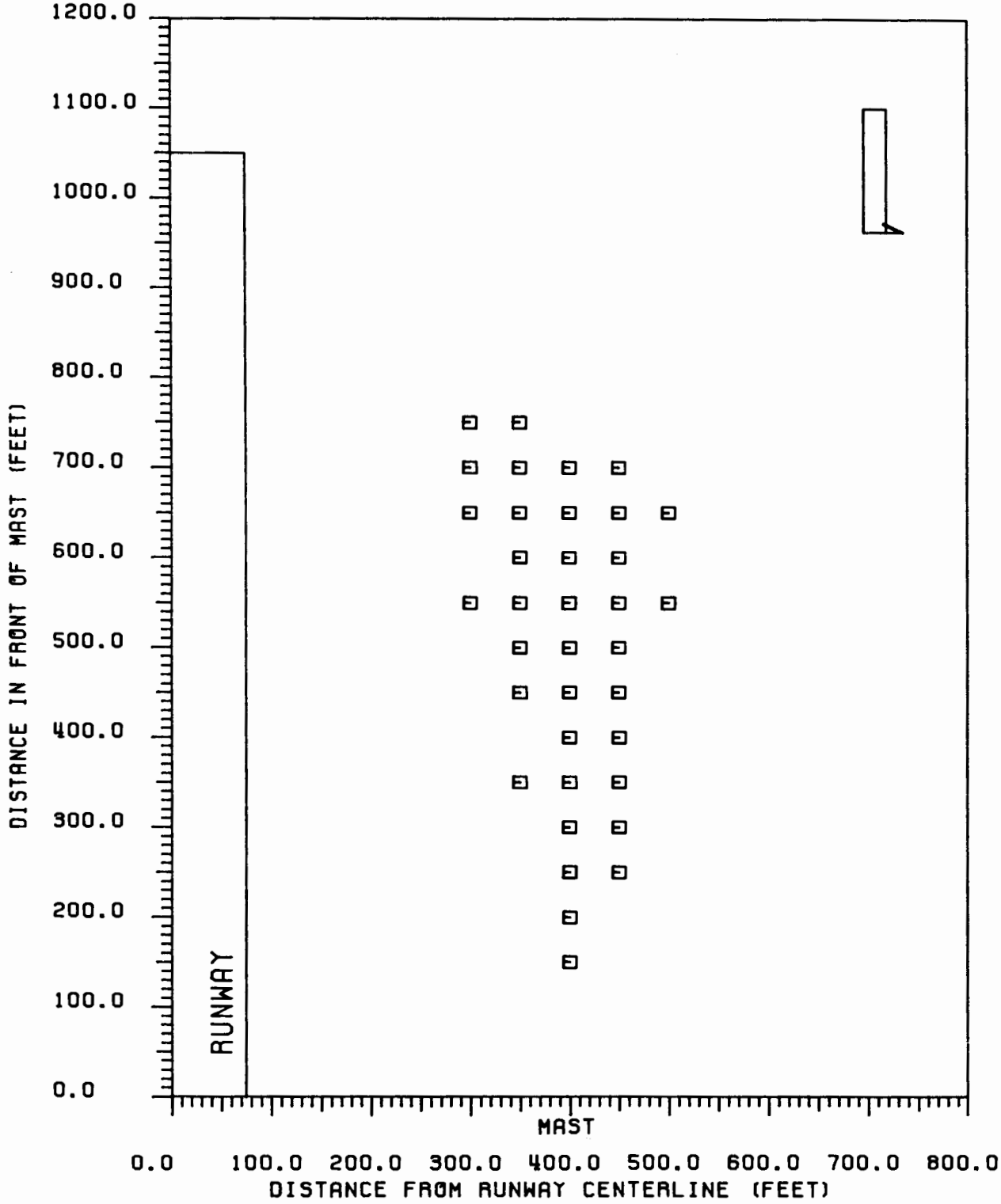

Figure 2-168. Critical area map for CAT I tolerances relating to B-727 aircraft. B-727 fuselage is parallel to runway centerline with tail towards the mast. Null reference glide slope, 2-lambda antennas.

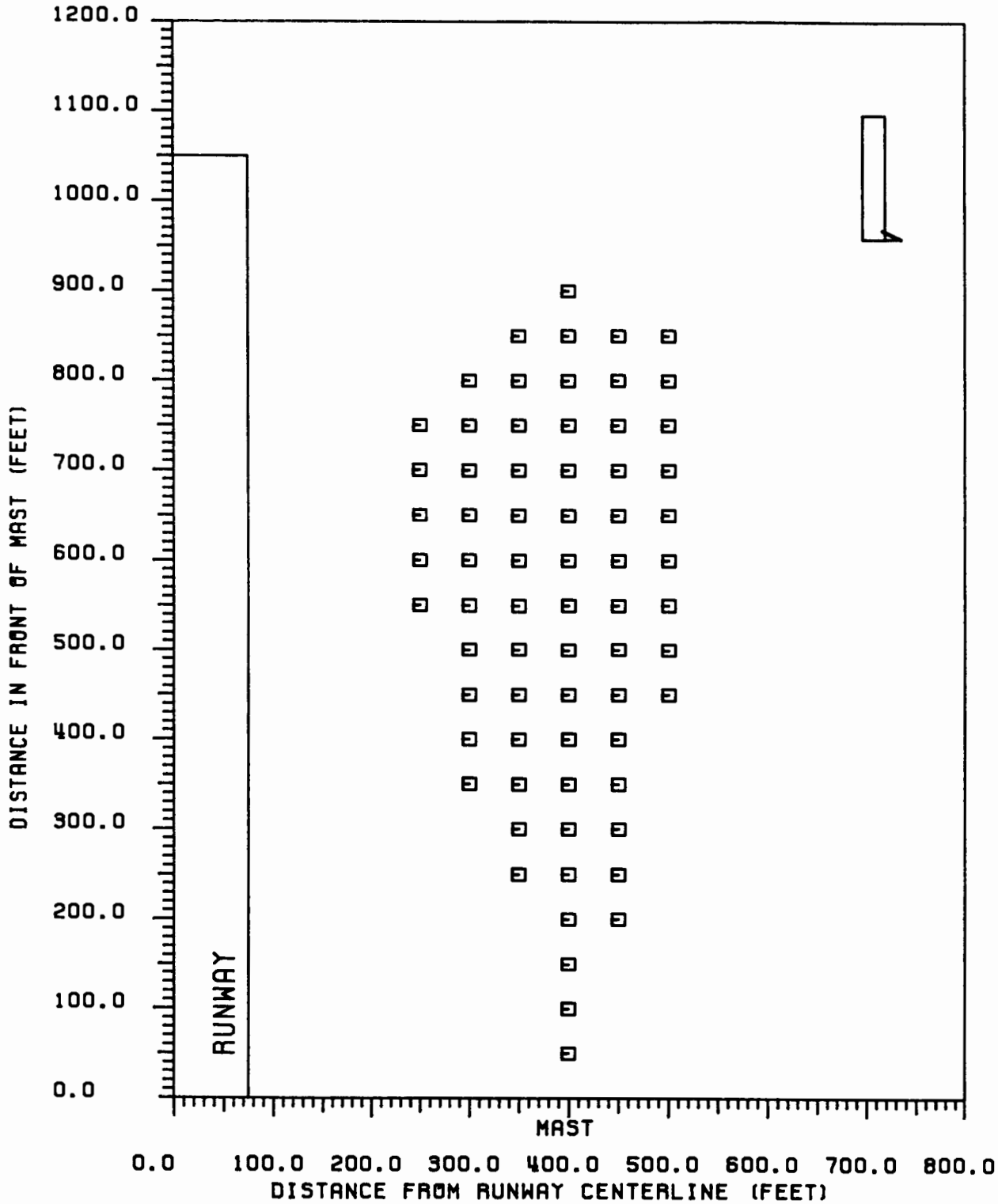

Figure 2-169. Critical area map for CAT II/III tolerances relating to B-727 aircraft. B-727 fuselage is parallel to runway centerline with tail towards the mast. Null reference glide slope, 2-lambda antennas.

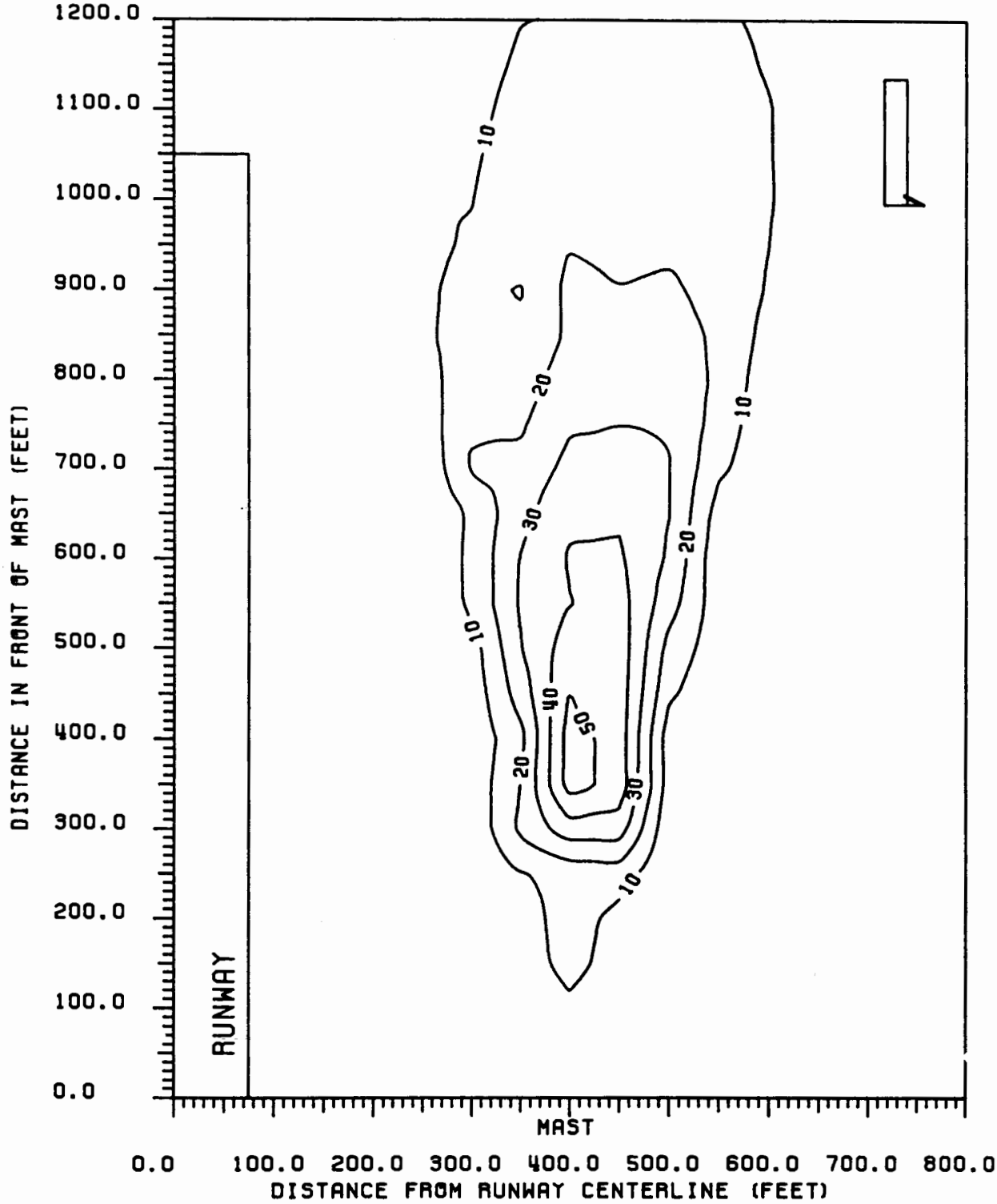

Figure 2-170. Contours of peak CDI values produced in ILS Zone 2 for a B-727. B-727 fuselage is parallel to runway centerline, with tail towards the mast. Null reference glide slope, 2-lambda antennas.

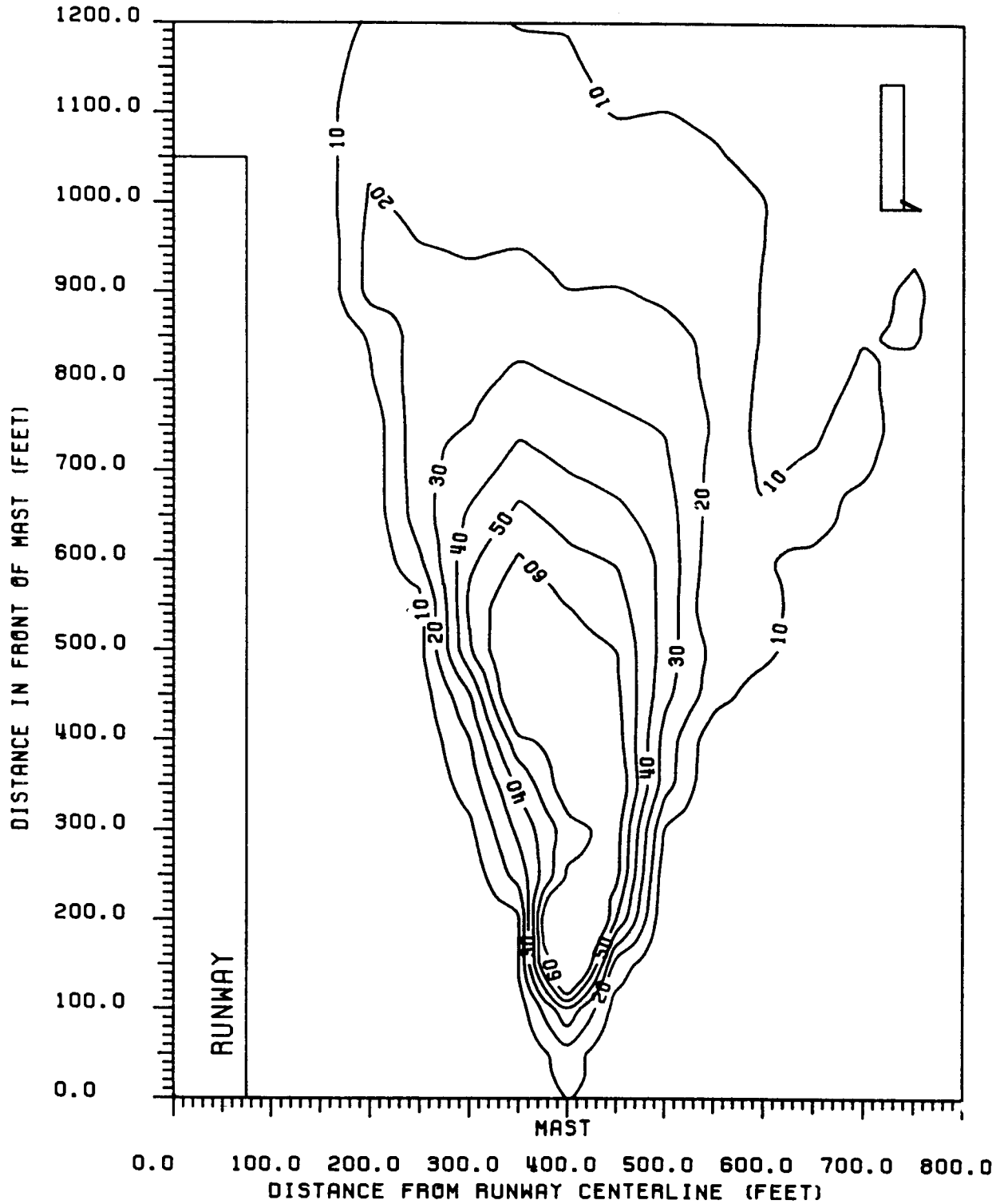

Figure 2-171. Contours of peak CDI values produced between ILS Point B and ILS Point C for a B-727. B-727 fuselage is parallel to runway centerline, with tail towards the mast. Null reference glide slope, 2-lambda antennas.

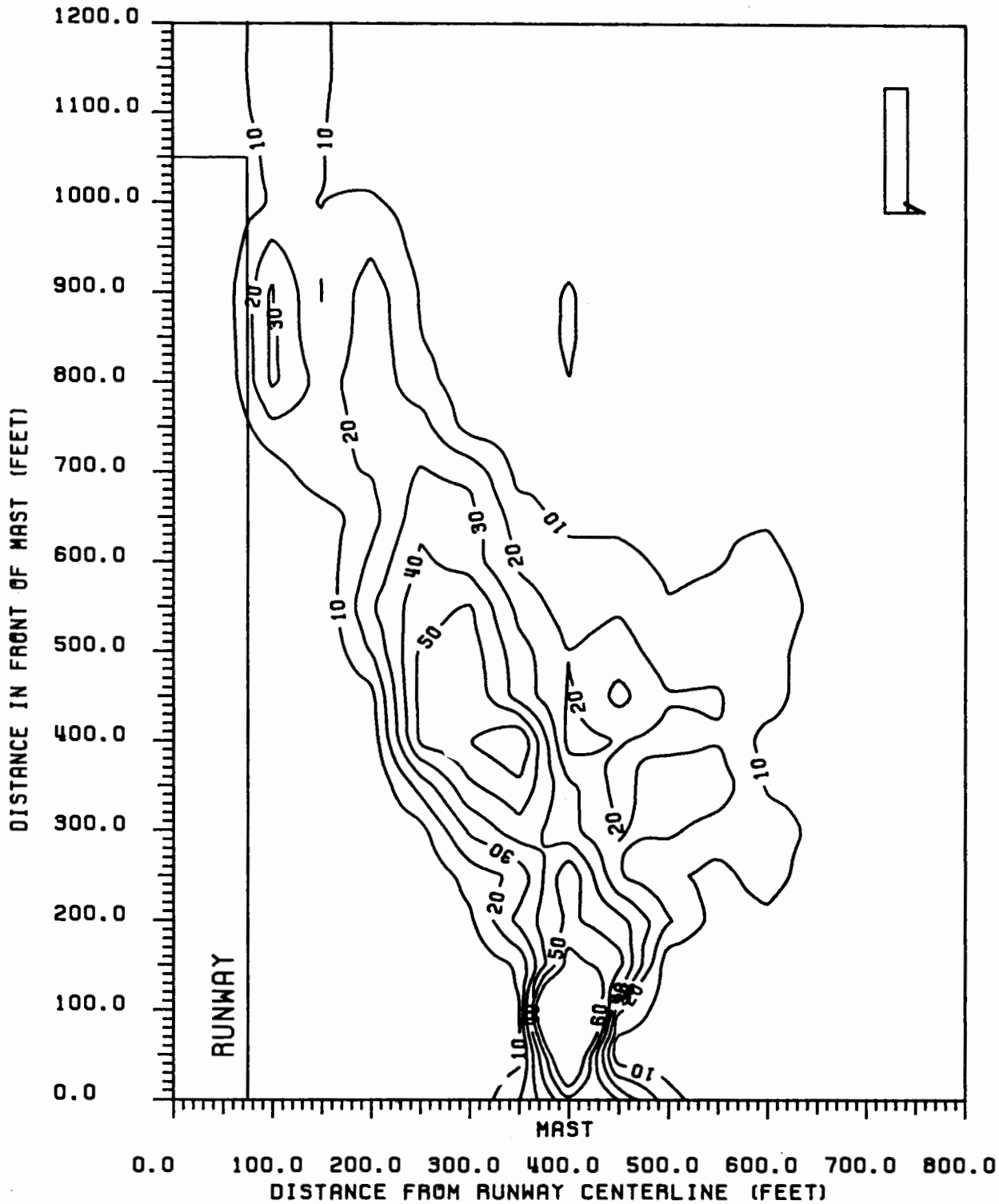

Figure 2-172. Contours of peak CDI values produced between ILS Point C and threshold for a B-727. B-727 fuselage is parallel to runway centerline, with tail towards the mast. Null reference glide slope, 2-lambda antennas.

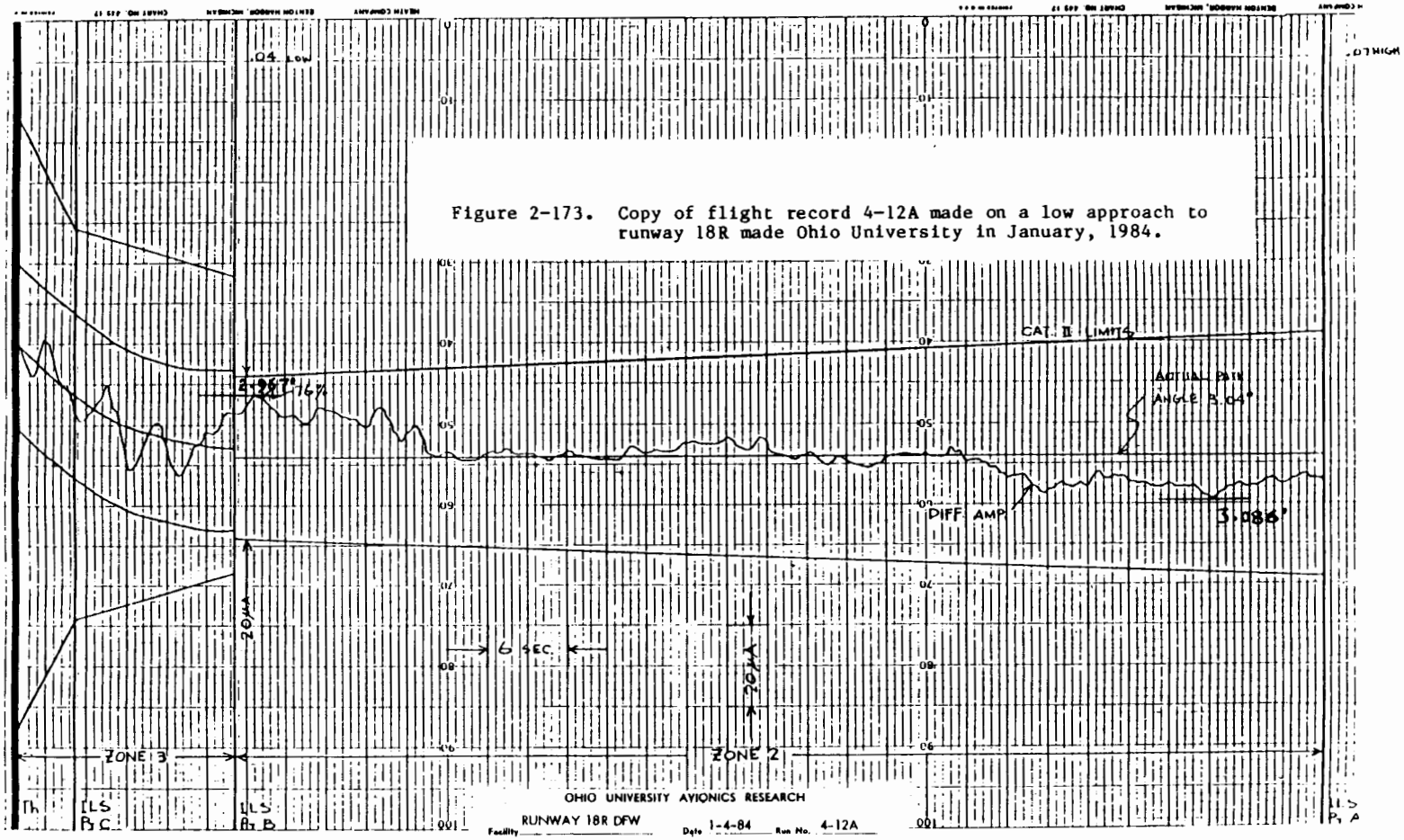

Figure 2-173. Copy of flight record 4-12A made on a low approach to runway 18R made Ohio University in January, 1984.

OHIO UNIVERSITY AVIONICS RESEARCH

Facility: RUNWAY 18R DFW
Date: 1-4-84 Run No.: 4-12A
Type: Null Glide Slope
Parameter of Interest: structure
Aircraft: N25688
Chart Speed: 10 in./min.
Crew: Hille, McFarland, Phipps
Cal/Scale:
Theodolite Oper.: NORD
Red = ± 100 uAFS
Theodolite Ref.: 3°
Blue = ± 100 uAFS
Remarks:
Red: diff. Amp Blue: CDI
A/S: 140 Knots Alt. - ft.
Time: 11:30 CST

This chart recording has been produced by the Ohio University Avionics Engineering Center with equipment calibrated and maintained in FAA Repair Station CO7-10.

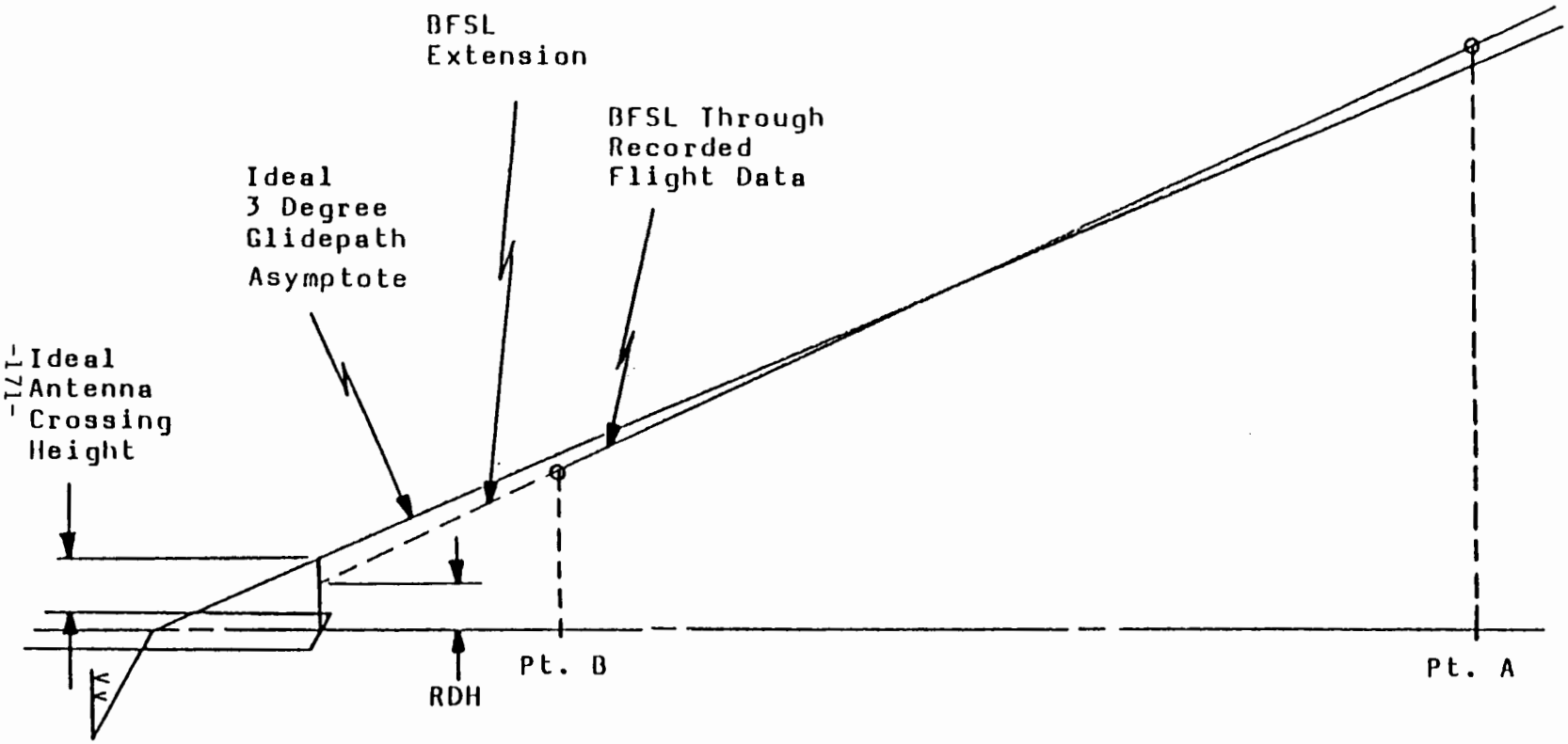

Figure 2-174. Example of how a low RDH is produced by a decrease of the path angle in ILS Zone 2.

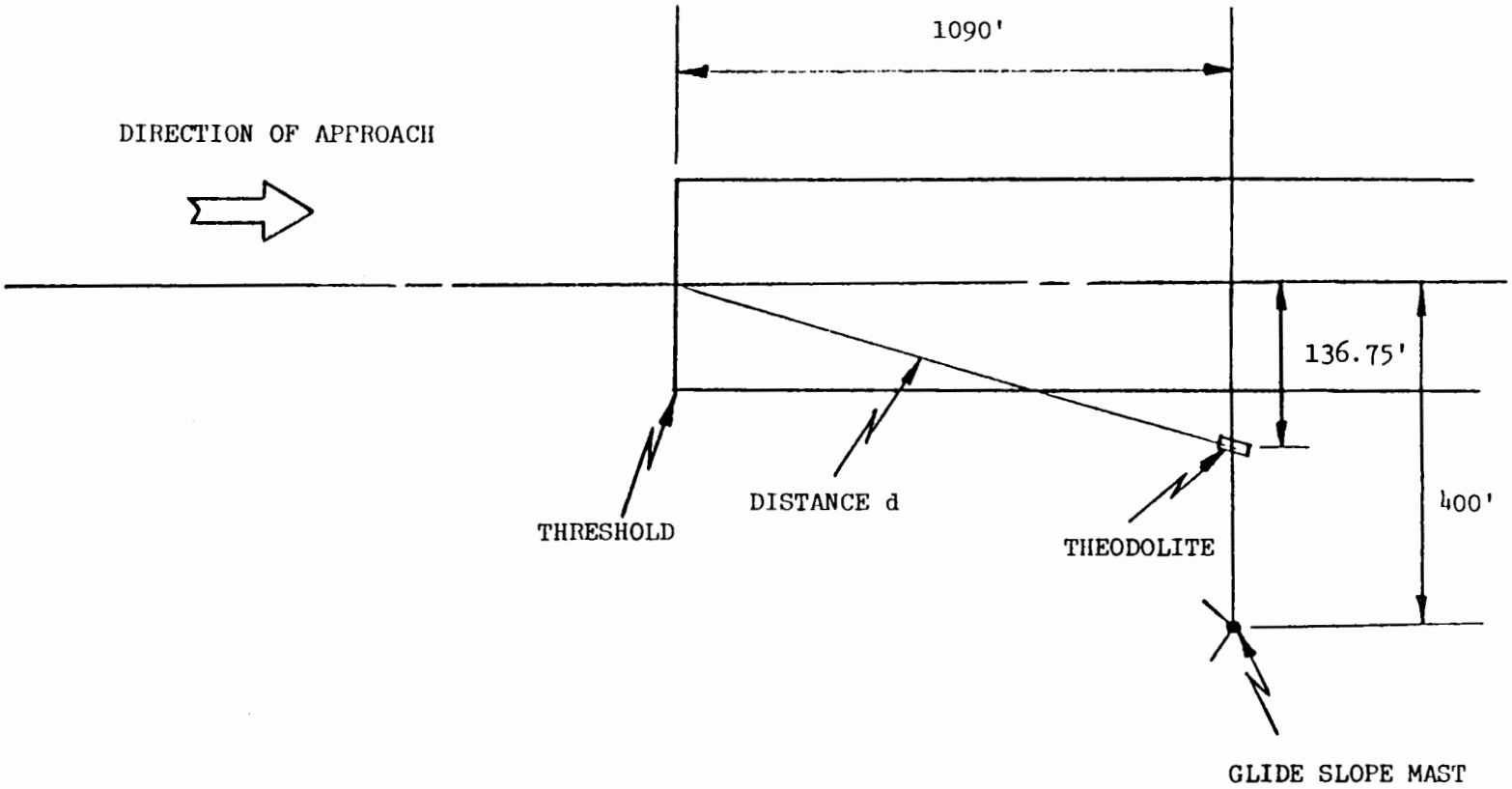

Figure 2-175. Positioning of theodolite.

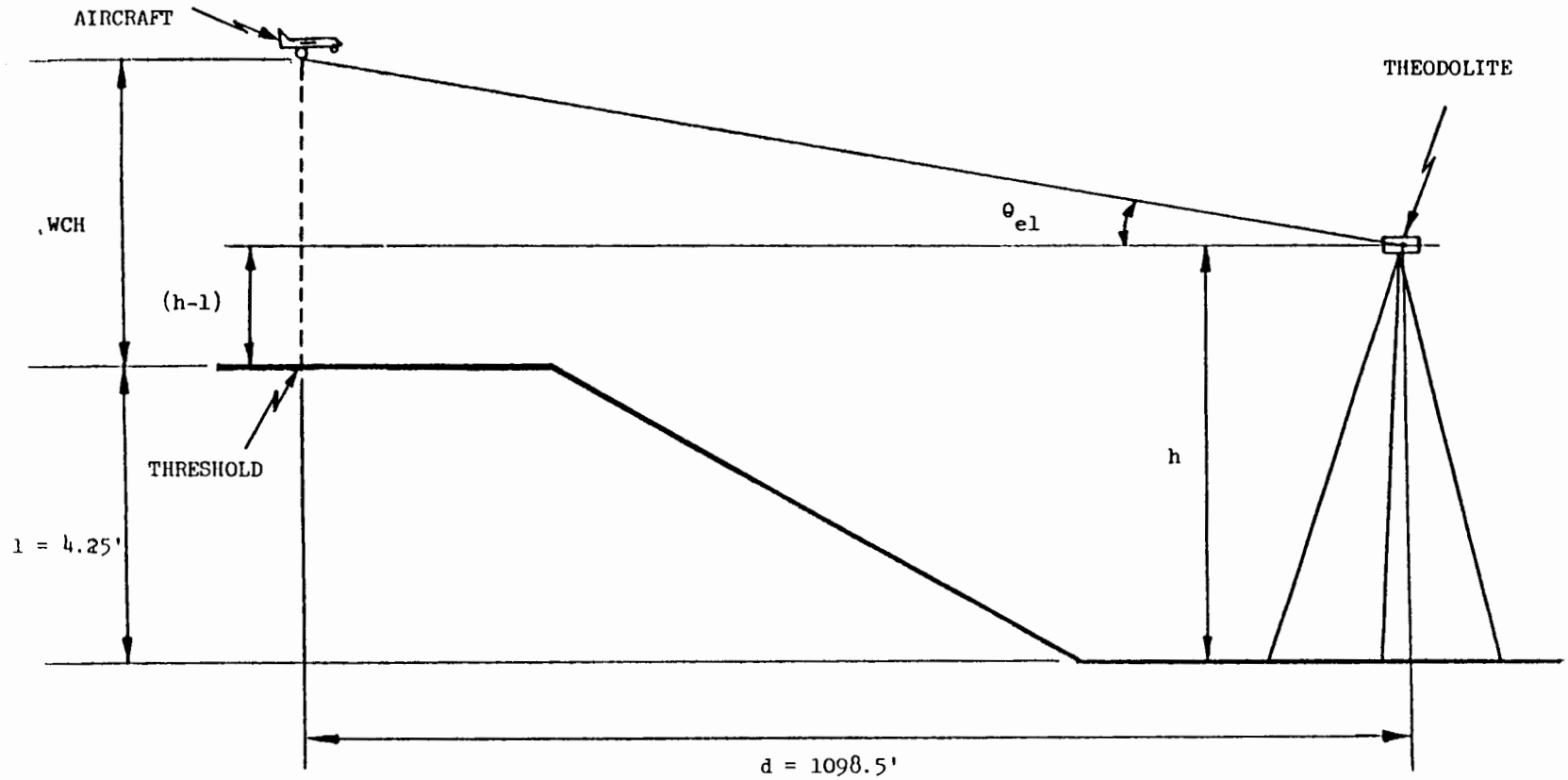

$$WCH = d \tan(\theta_{el}) + (h-1)$$

Figure 2-176. Test geometry for calculations.

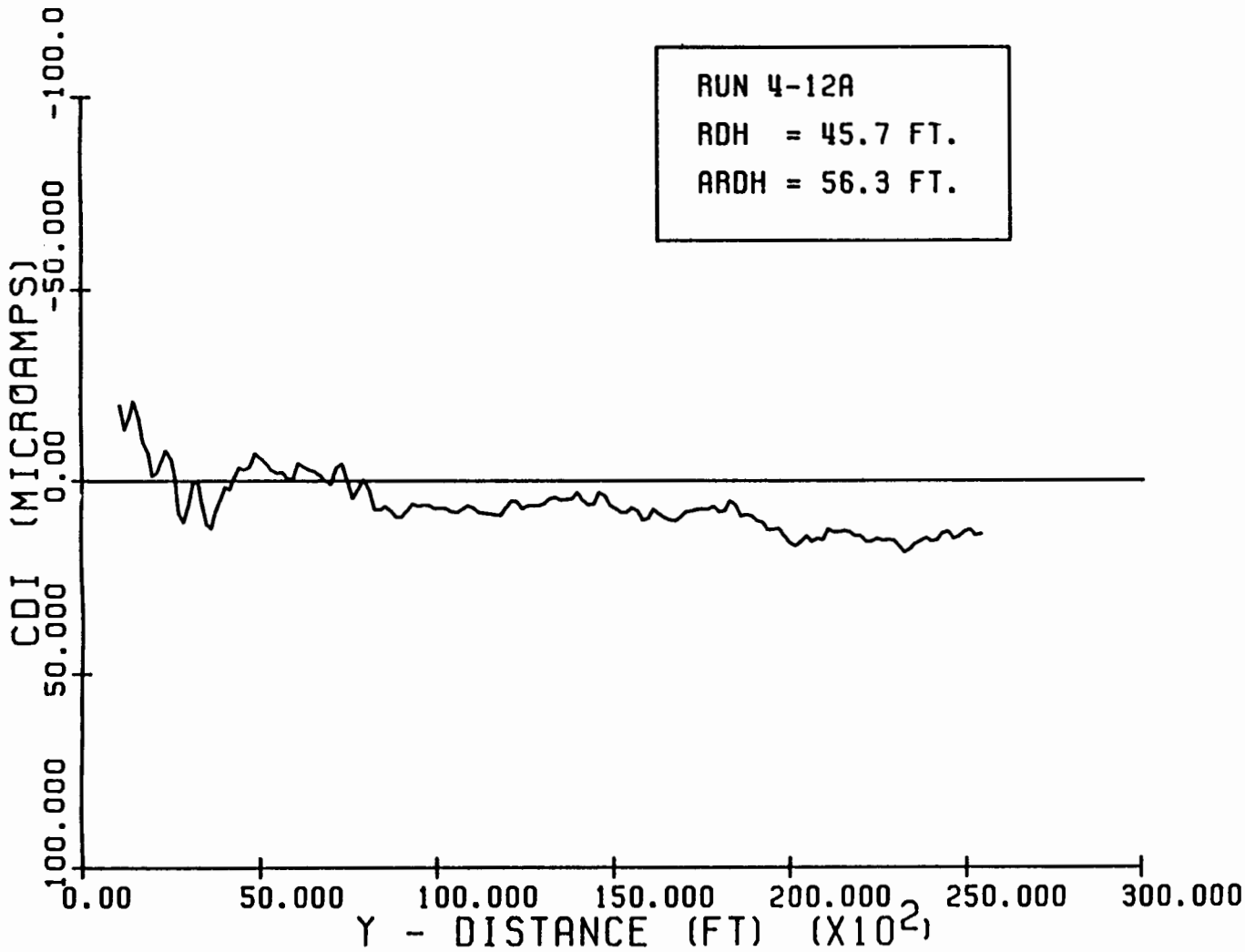

Figure 2-177. Digitized flight recording for a low approach to runway 18R. Data taken by Ohio University, January 4, 1984, Run No. 4-12A.

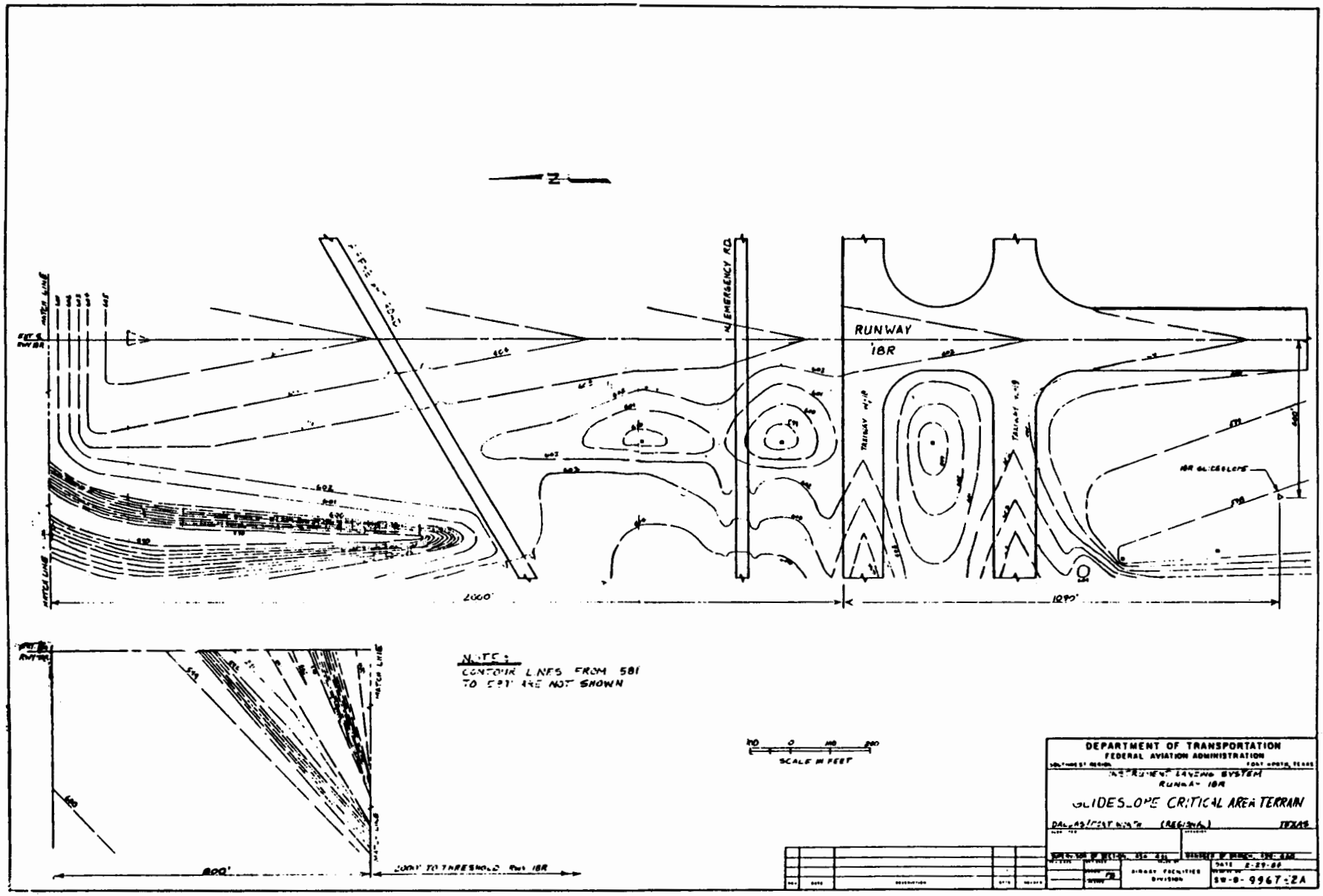

Figure 2-178. Topographic map of glide slope critical area terrain for DFW runway 18R.

X	Y	Z
-10000.0	0.0	3.04
0.0	0.0	3.04
400.0	0.0	0.00
500.0	0.0	0.00
-10000.0	580.0	4.06
0.0	580.0	4.06
250.0	580.0	0.00
500.0	580.0	0.00
-10000.0	650.0	4.18
0.0	650.0	4.18
300.0	650.0	3.20
500.0	650.0	5.00
-10000.0	900.0	4.65
0.0	900.0	4.65
150.0	900.0	0.70
500.0	900.0	0.70
-10000.0	1000.0	5.81
0.0	1000.0	5.81
400.0	1000.0	4.00
500.0	1000.0	4.00
-10000.0	1242.0	5.26
0.0	1242.0	5.26
260.0	1242.0	1.15
500.0	1242.0	5.65
-10000.0	1500.0	5.70
0.0	1500.0	5.79
300.0	1500.0	5.00
500.0	1500.0	6.00
-10000.0	1600.0	5.95
0.0	1600.0	5.95
300.0	1600.0	0.00
500.0	1600.0	5.00
-10000.0	1800.0	6.25
0.0	1800.0	6.25
300.0	1800.0	2.30
500.0	1800.0	6.00
-10000.0	3050.0	7.15
0.0	3050.0	7.15
400.0	3050.0	7.15
500.0	3050.0	7.15
-10000.0	3150.0	2.00
0.0	3150.0	2.00
400.0	3150.0	2.00
500.0	3150.0	2.00

Figure 2-179. Coordinates of terrain profile system.

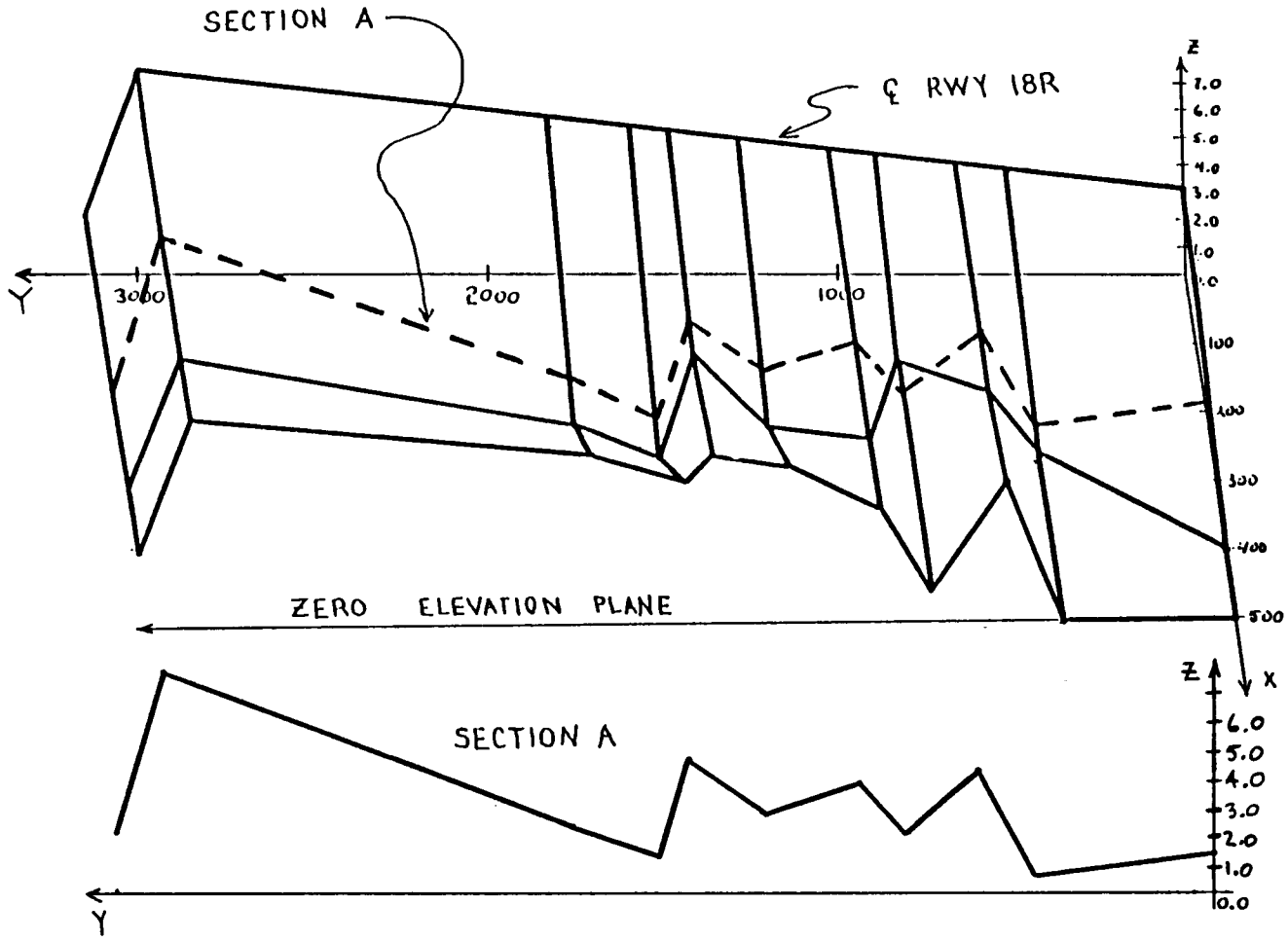

Figure 2-180. Isometric drawing of the three-dimensional terrain profile showing the three depressions in the first Fresnel zone.

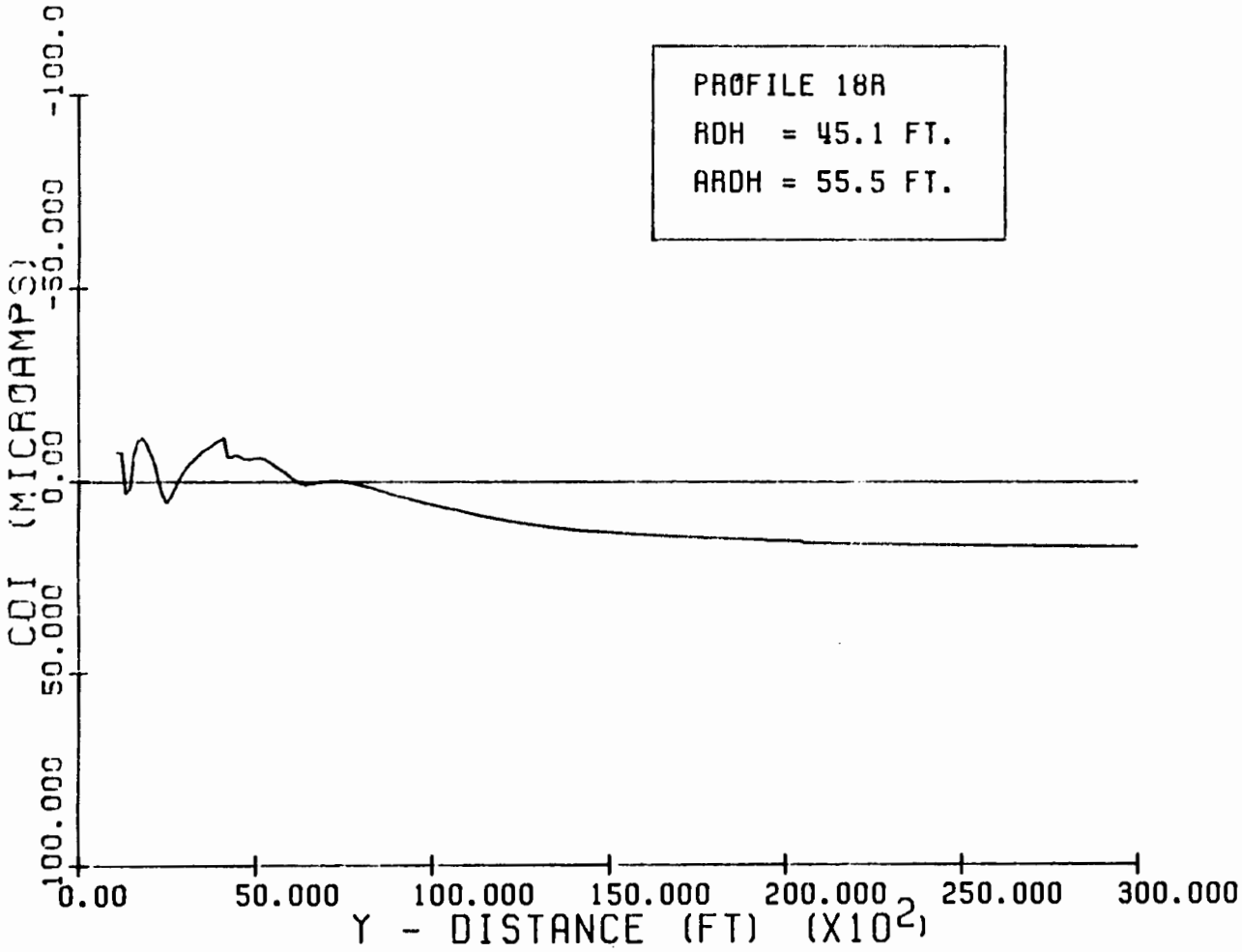

Figure 2-181. Simulated differential amplifier trace for the terrain profile in figure 2-180.

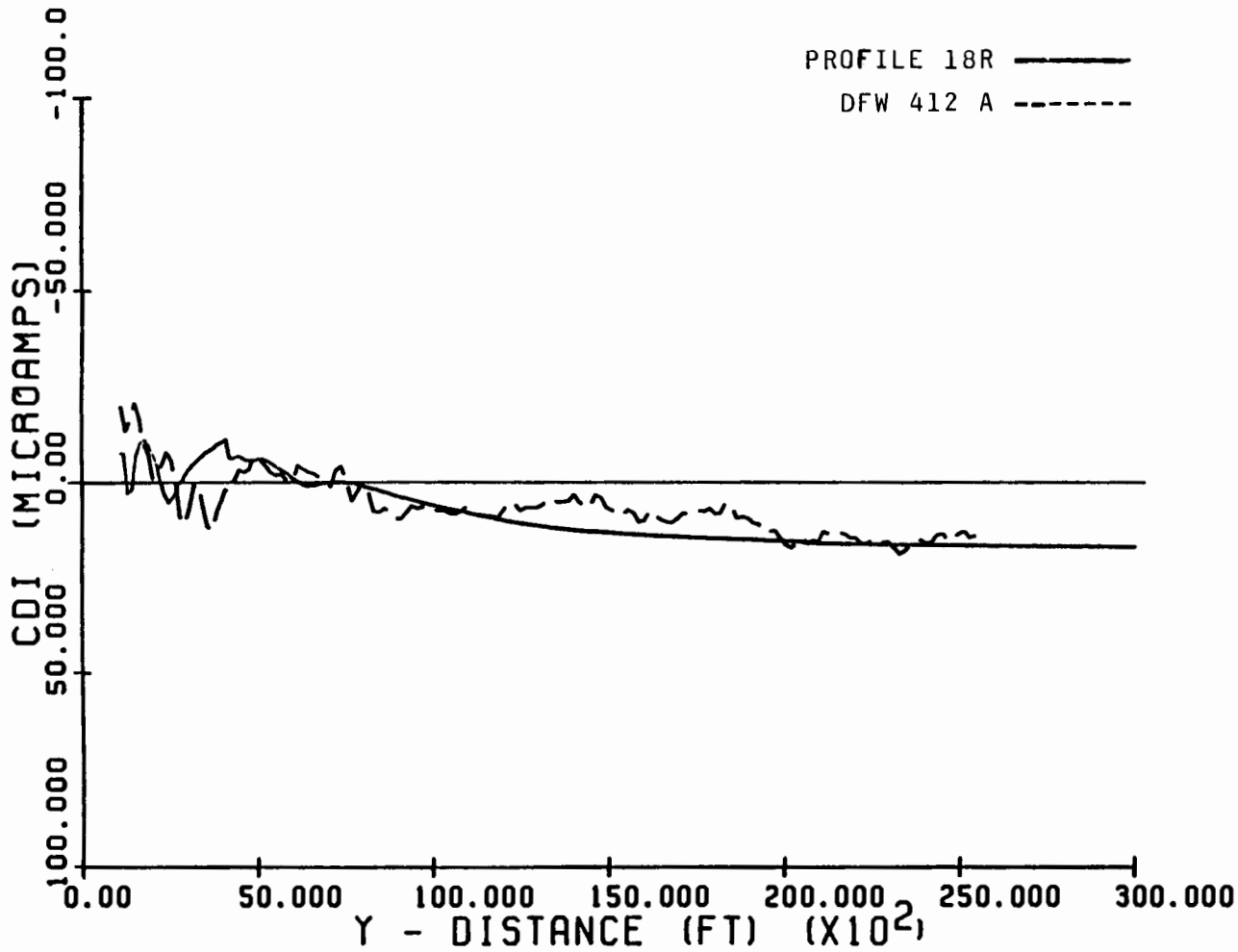

Figure 2-182. Comparison of actual and simulated differential amplifier recordings. The actual data is taken from Run 4-12A by Ohio University. The simulated trace is for the terrain profile shown in figure 2-180.

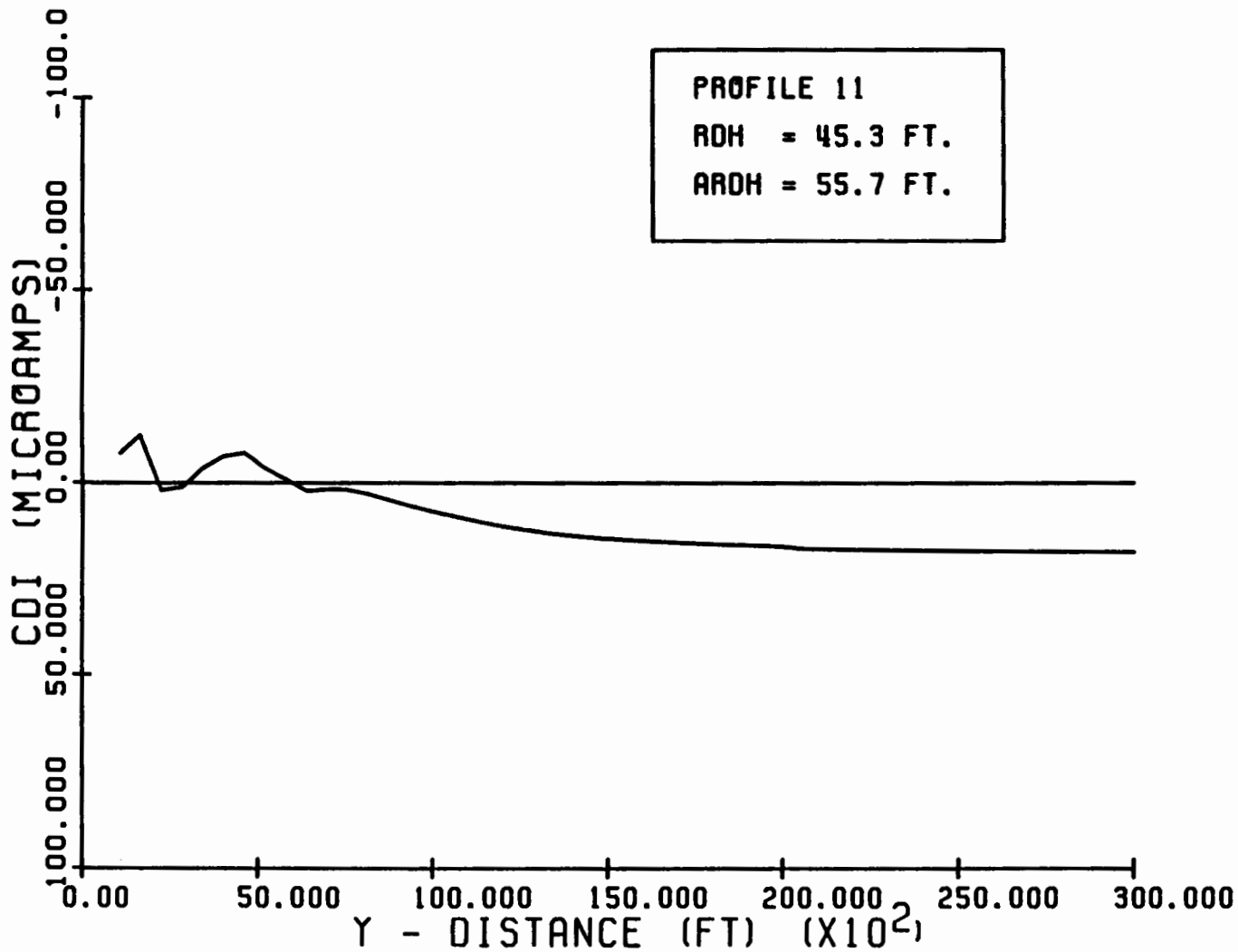

Figure 2-183. CDI trace showing the effect of decreasing depth of depression at Y=900' to 598.85' MSL.

Depth of Depression at Y=900' to 598.85' MSL.

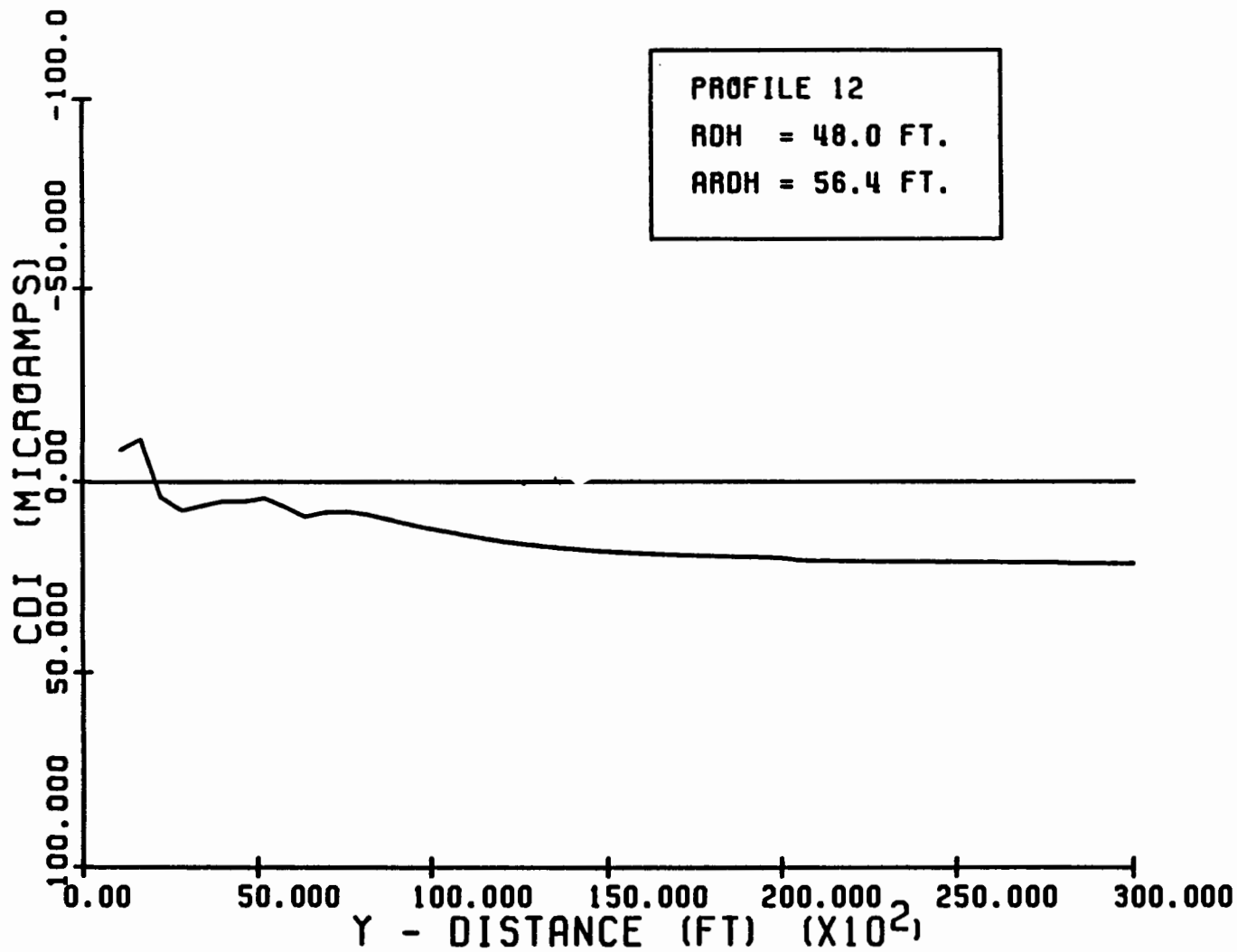

Figure 2-184. CDI trace showing the effect of decreasing depth of depression at Y=900' to 599.85' MSL.

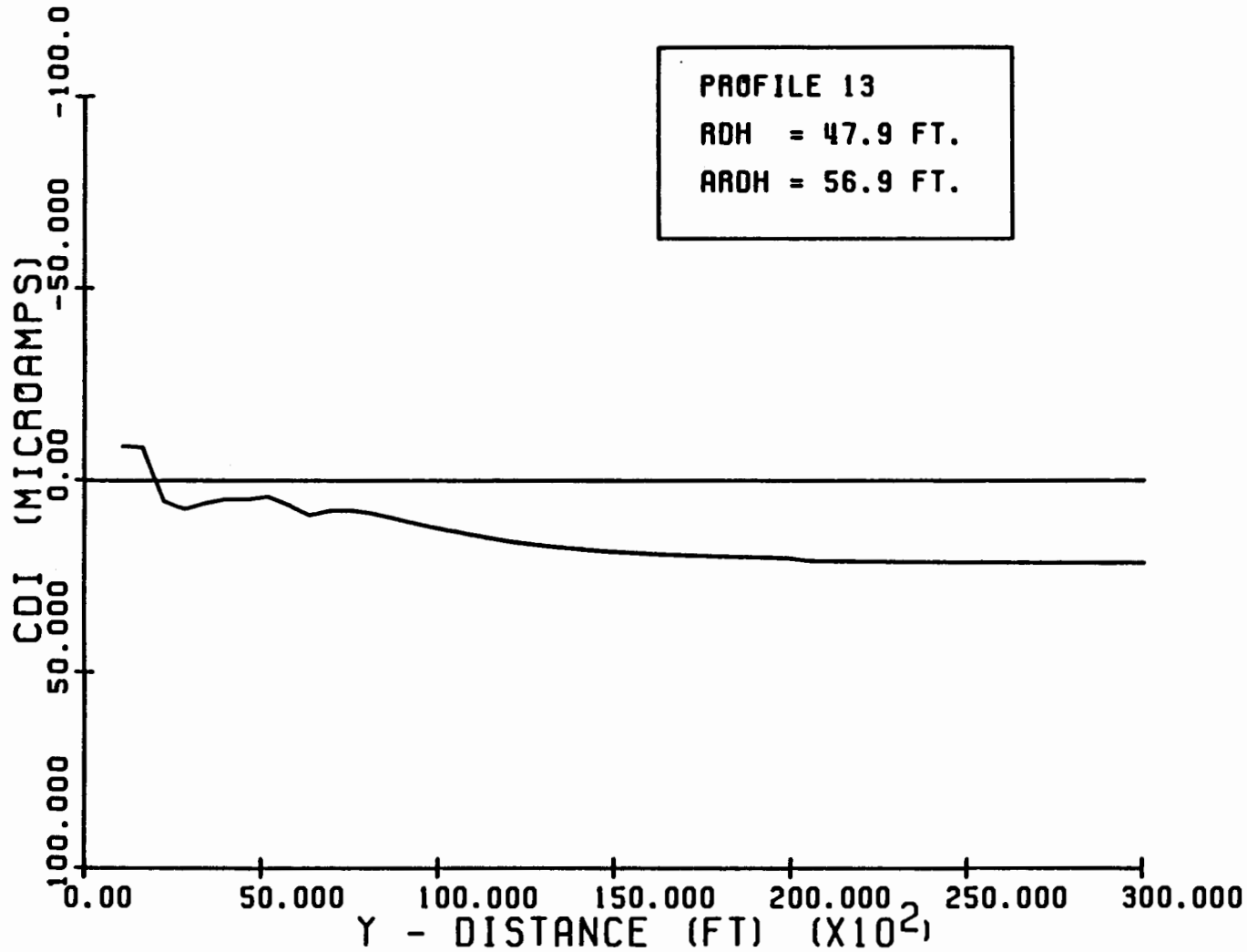

Figure 2-185. CDI trace showing the effect of decreasing depth of depression at Y=900' to 600.85' MSL.

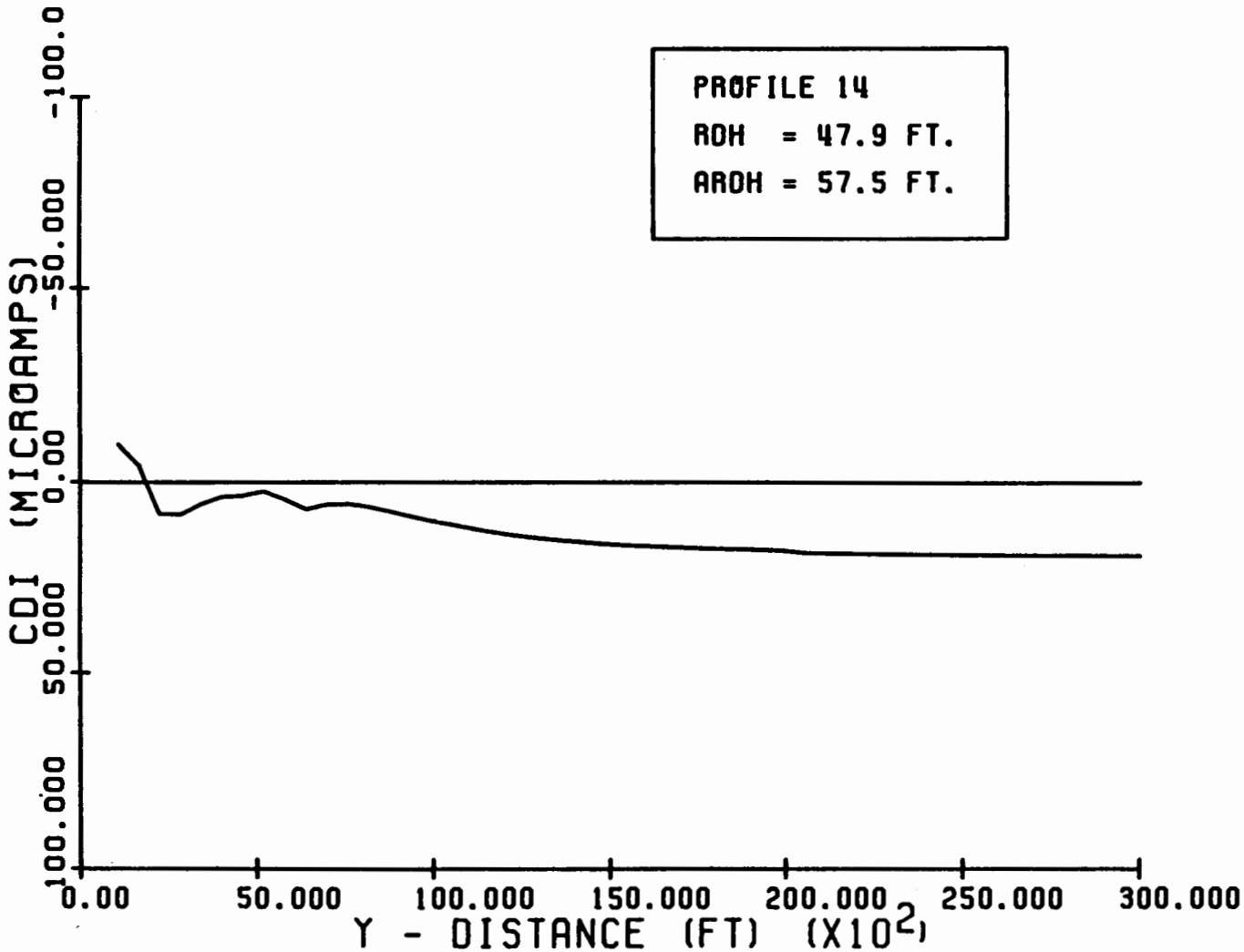

Figure 2-186. CDI trace showing the effect of decreasing depth of depression at Y=900' to 601.85' MSL.

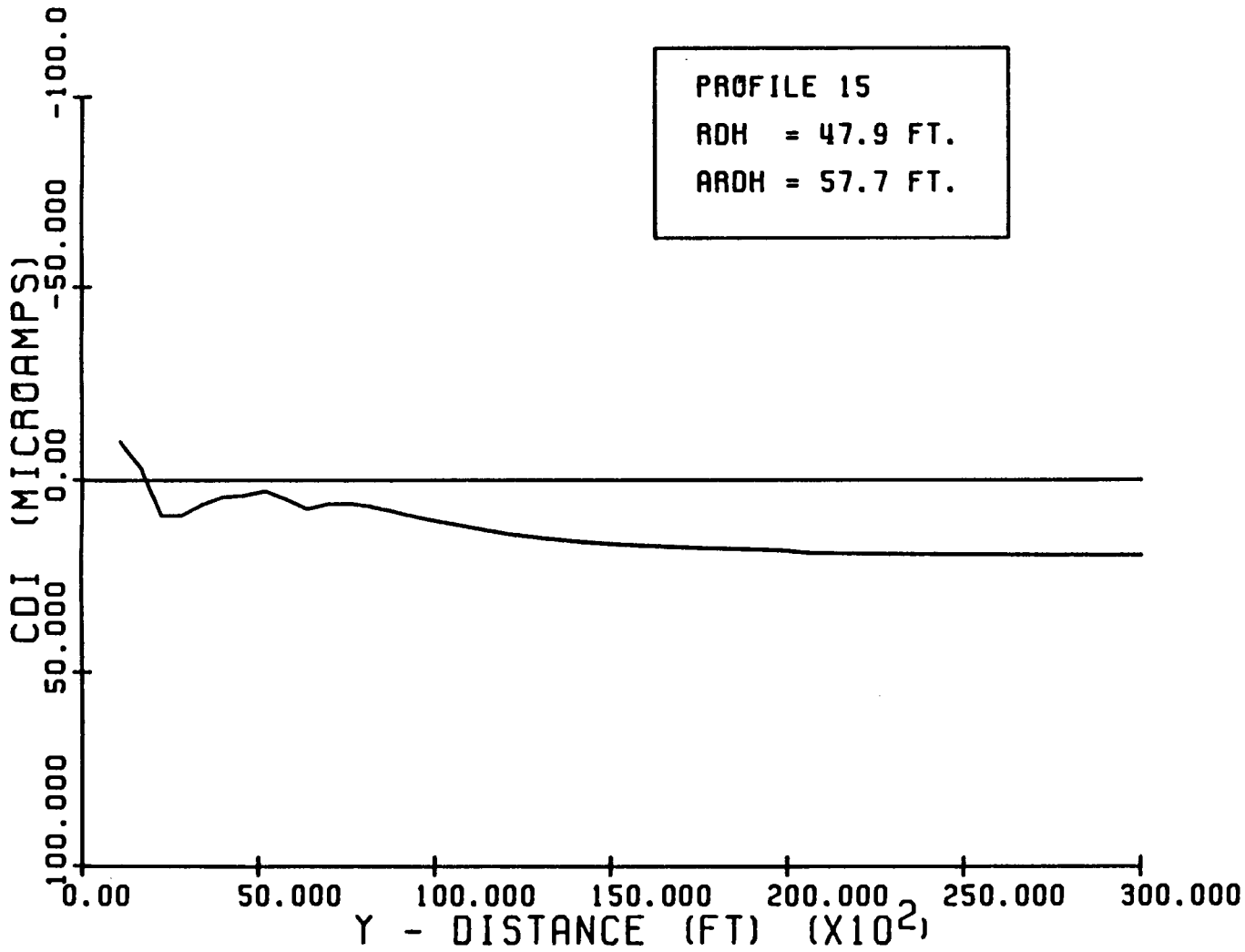

Figure 2-187. CDI trace showing the effect of decreasing depth of depression at Y=900' to 602.85' MSL.

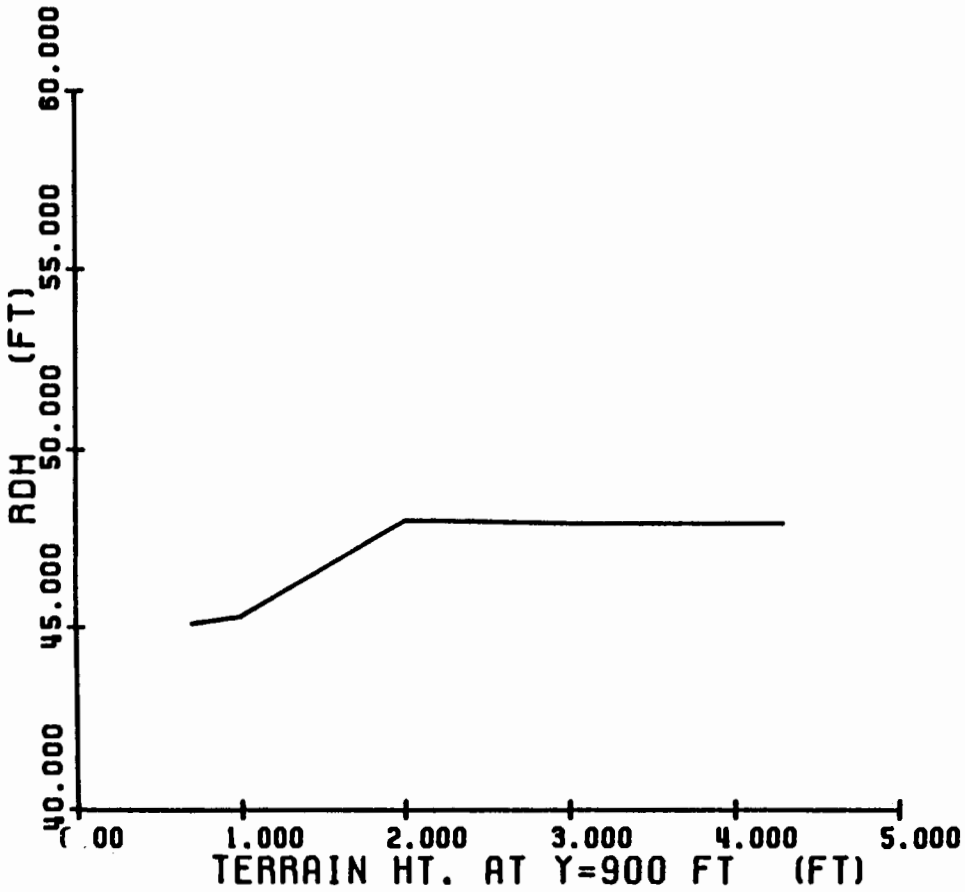

Figure 2-188. Sensitivity of RDH to depth of depression at Y=900'.

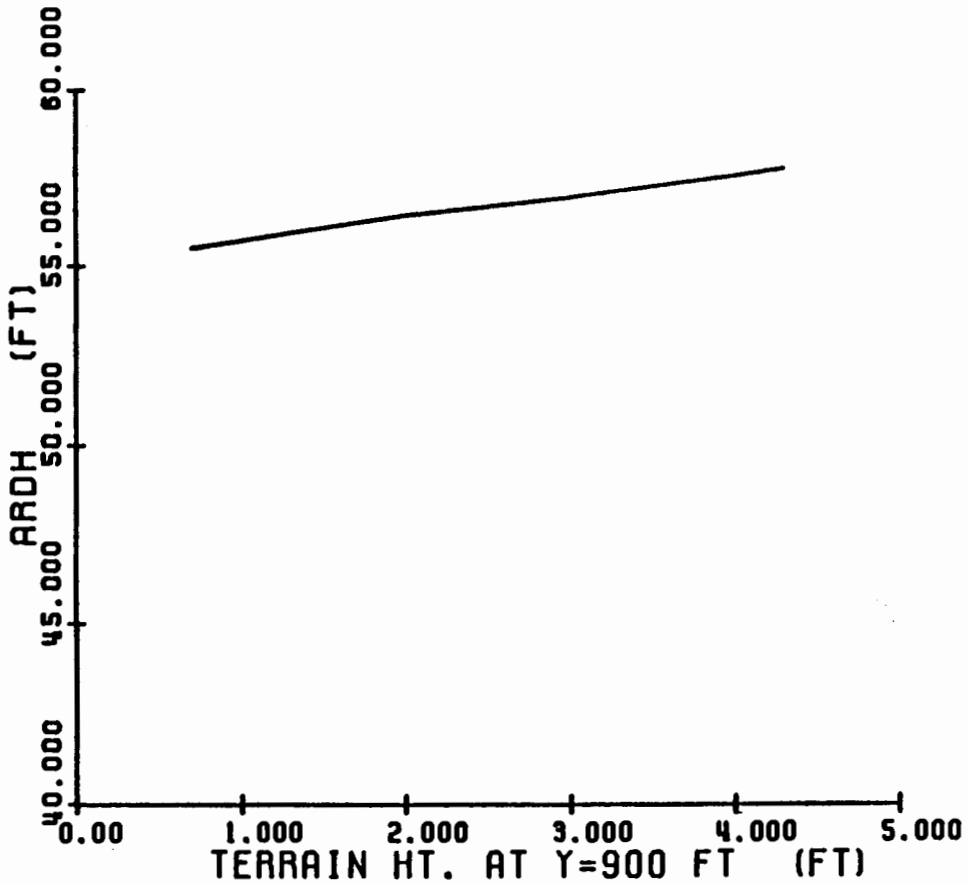

Figure 2-189. Sensitivity of ARDH to depth of depression at Y=900'.

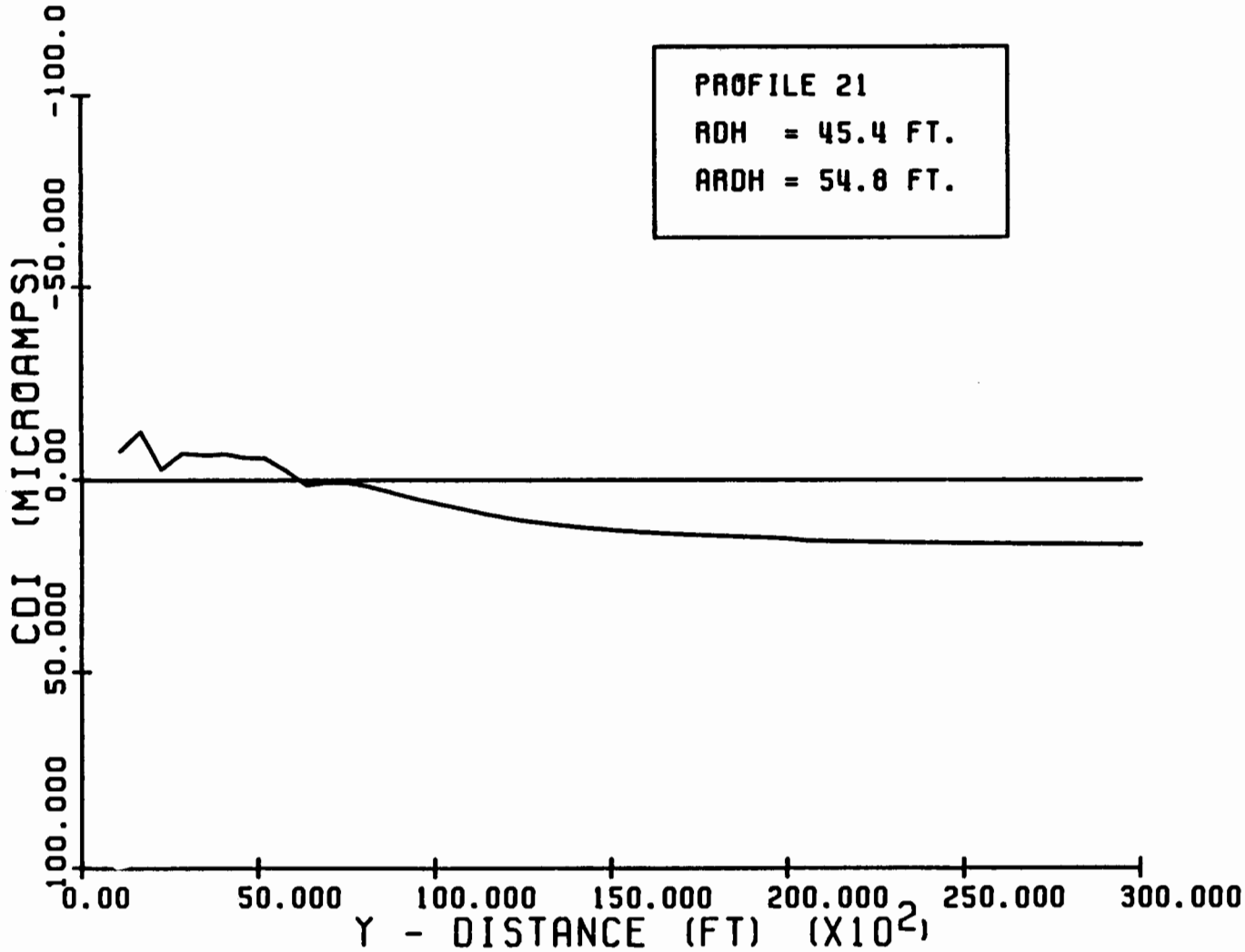

Figure 2-190. CDI trace showing the effect of decreasing depth of depression at Y=1242' to 599.85' MSL.

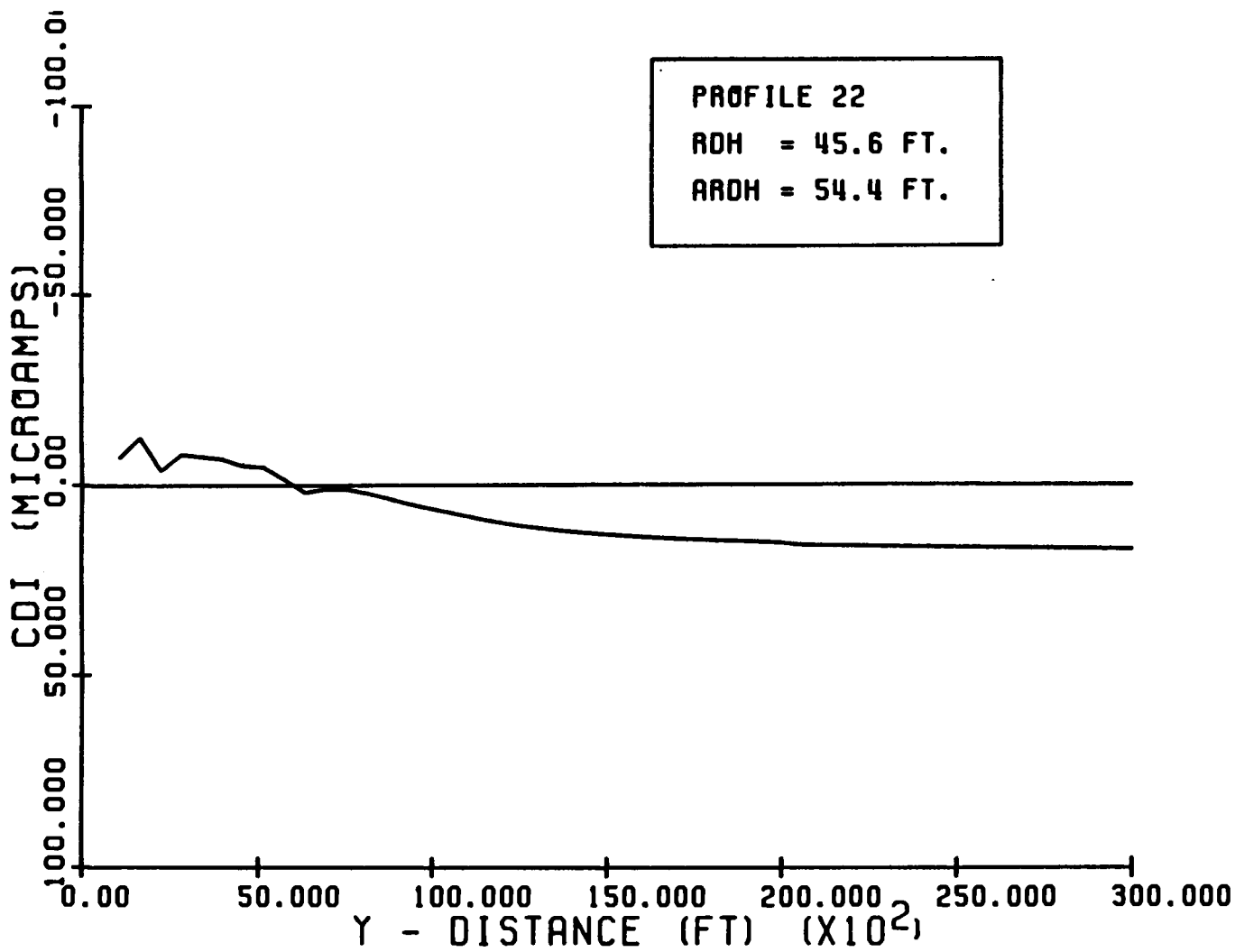

Figure 2-191. CDI trace showing the effect of decreasing depth of depression at Y=1242' to 600.85' MSL.

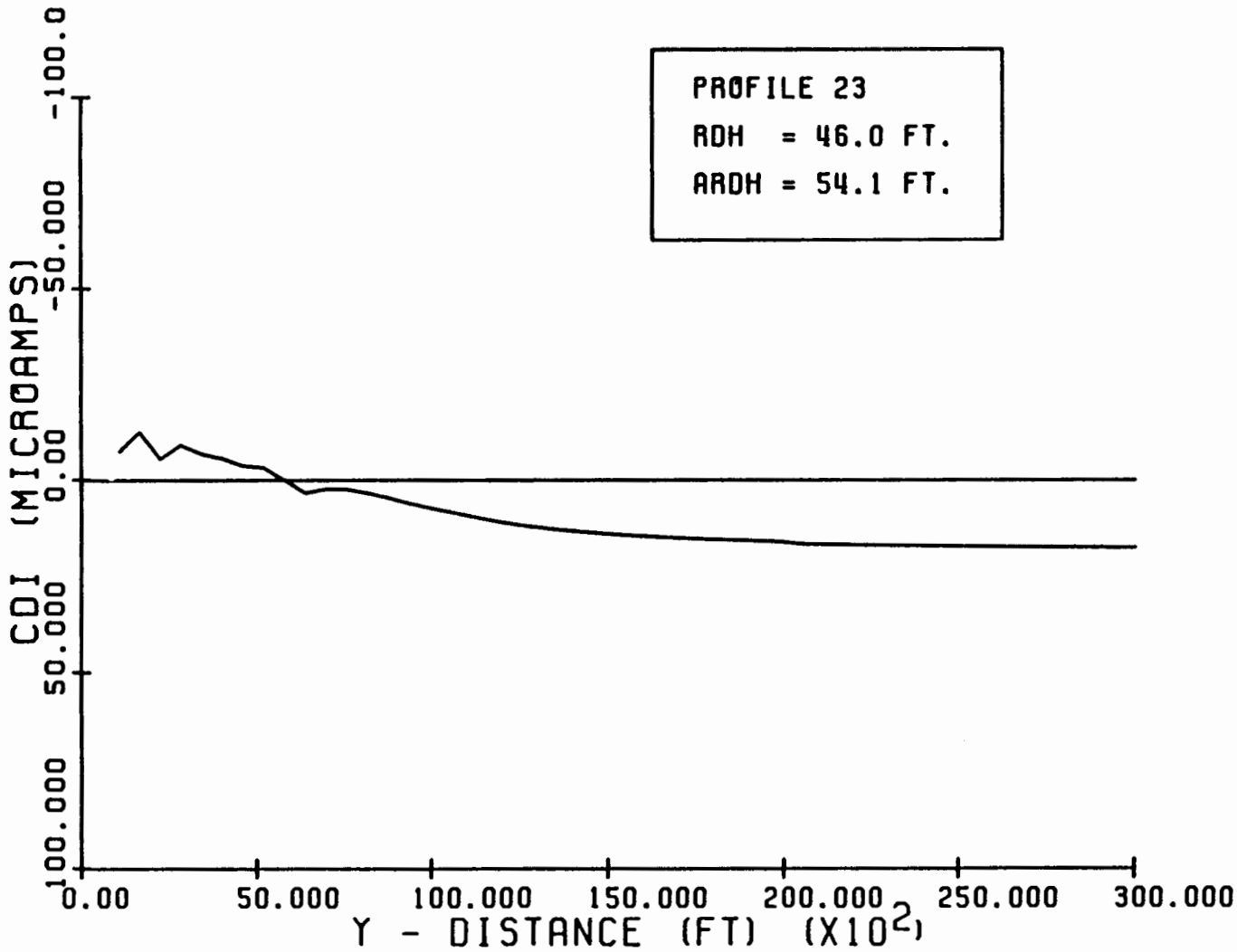

Figure 2-192. CDI trace showing the effect of decreasing depth of depression at Y=1242' to 601.85' MSL.

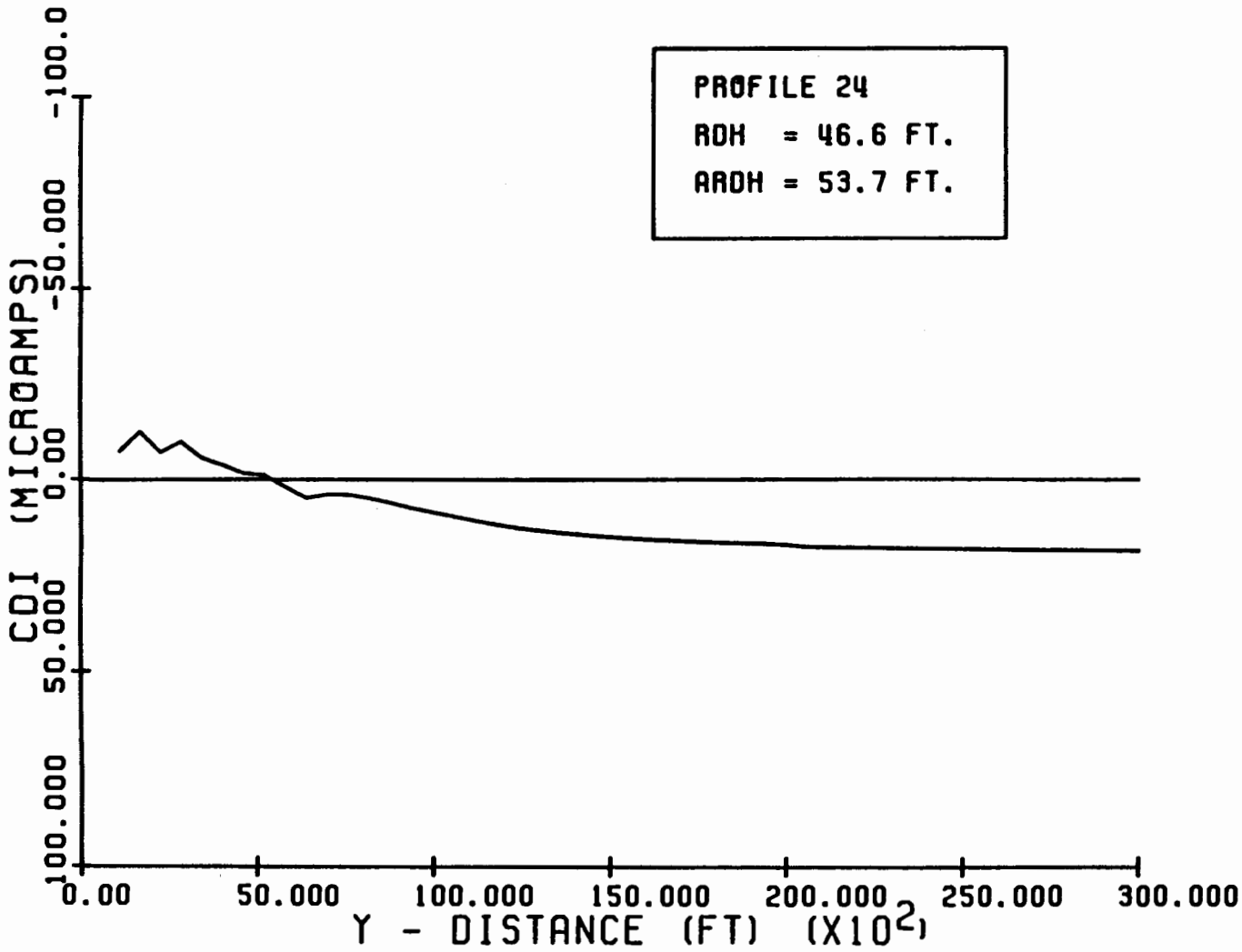

Figure 2-193. CDI trace showing the effect of decreasing depth of depression at Y=1242' to 602.85' MSL.

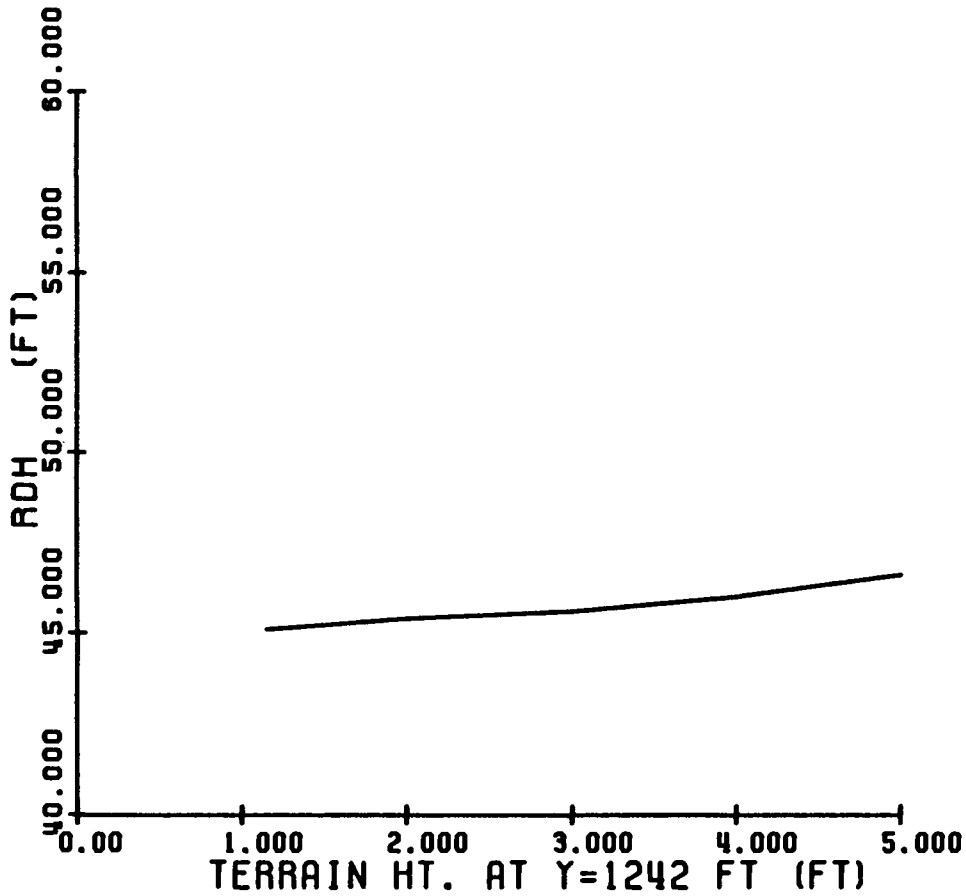

Figure 2-194. Sensitivity of RDH to depth of depression at Y=1242'.

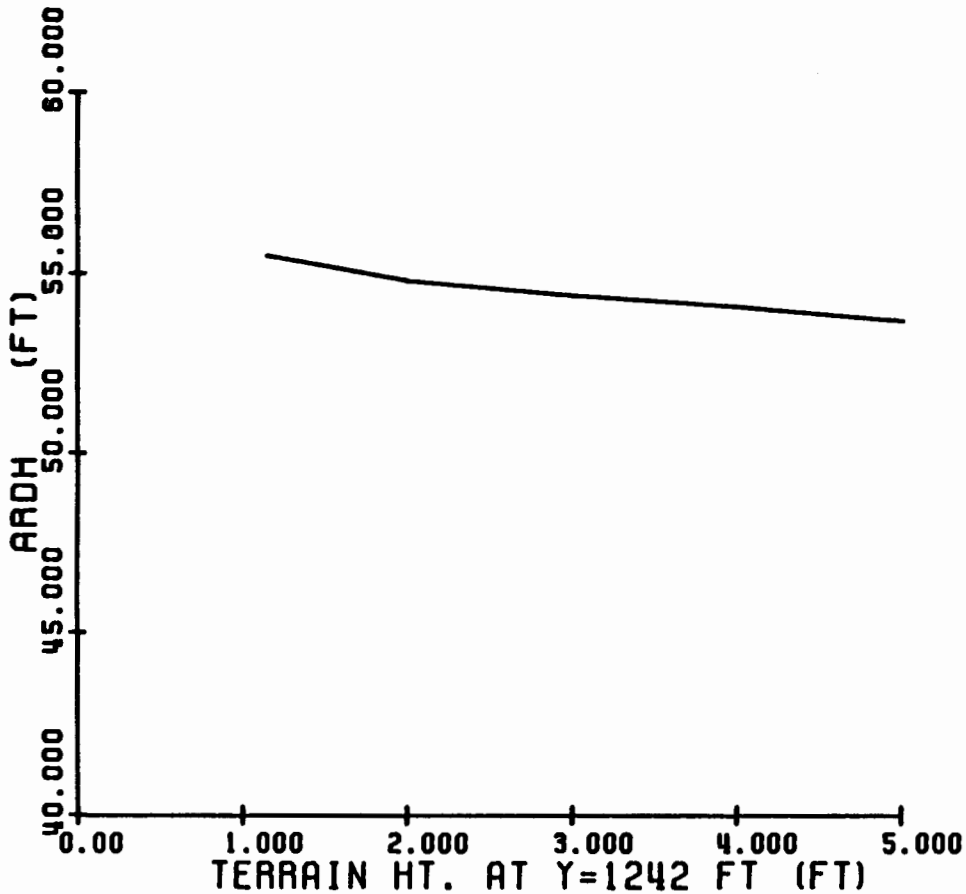

Figure 2-195. Sensitivity of ARDH to depth of depression at Y=1242'.

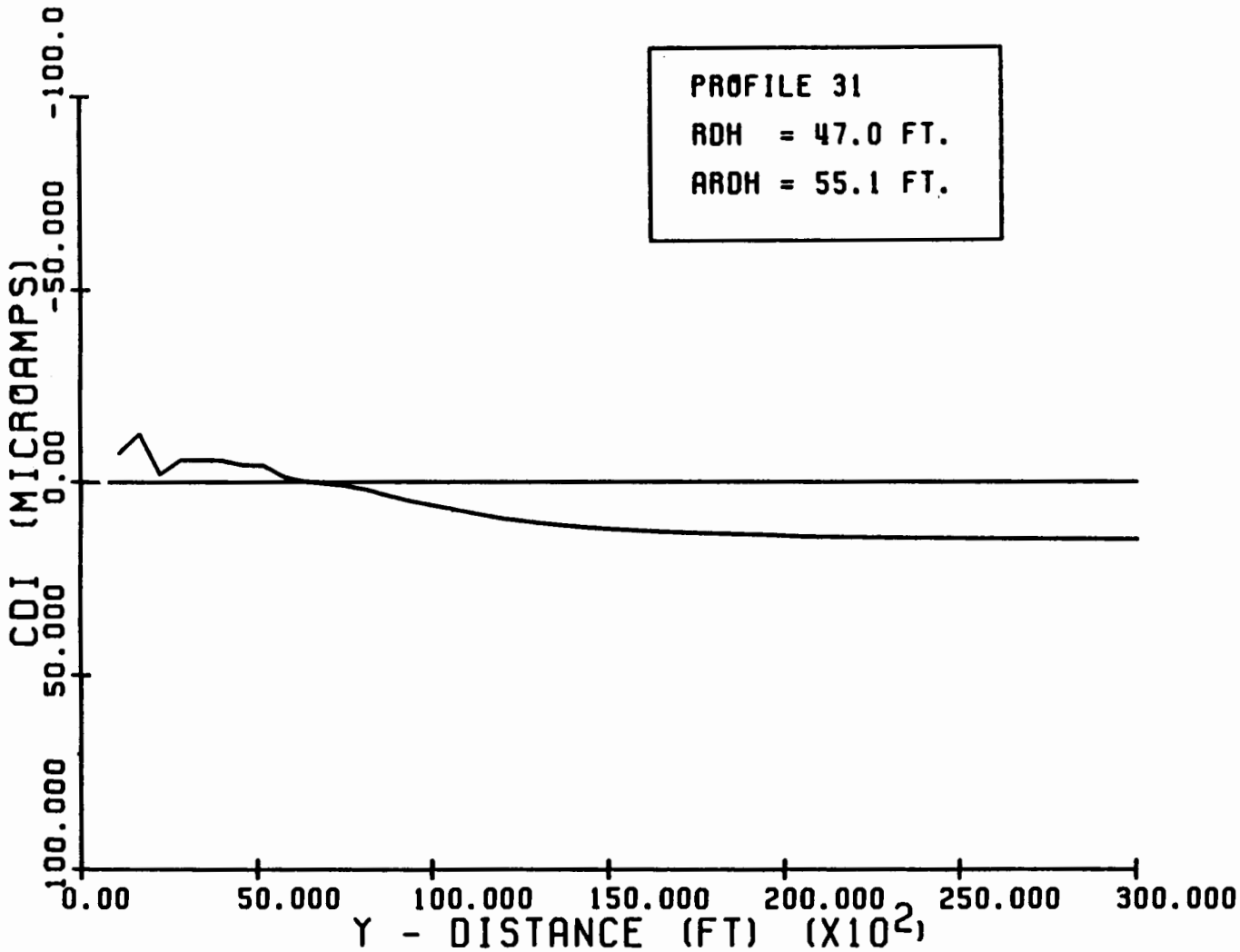

Figure 2-196. CDI trace showing the effect of decreasing depth of depression at Y=1600' to 598.85' MSL.

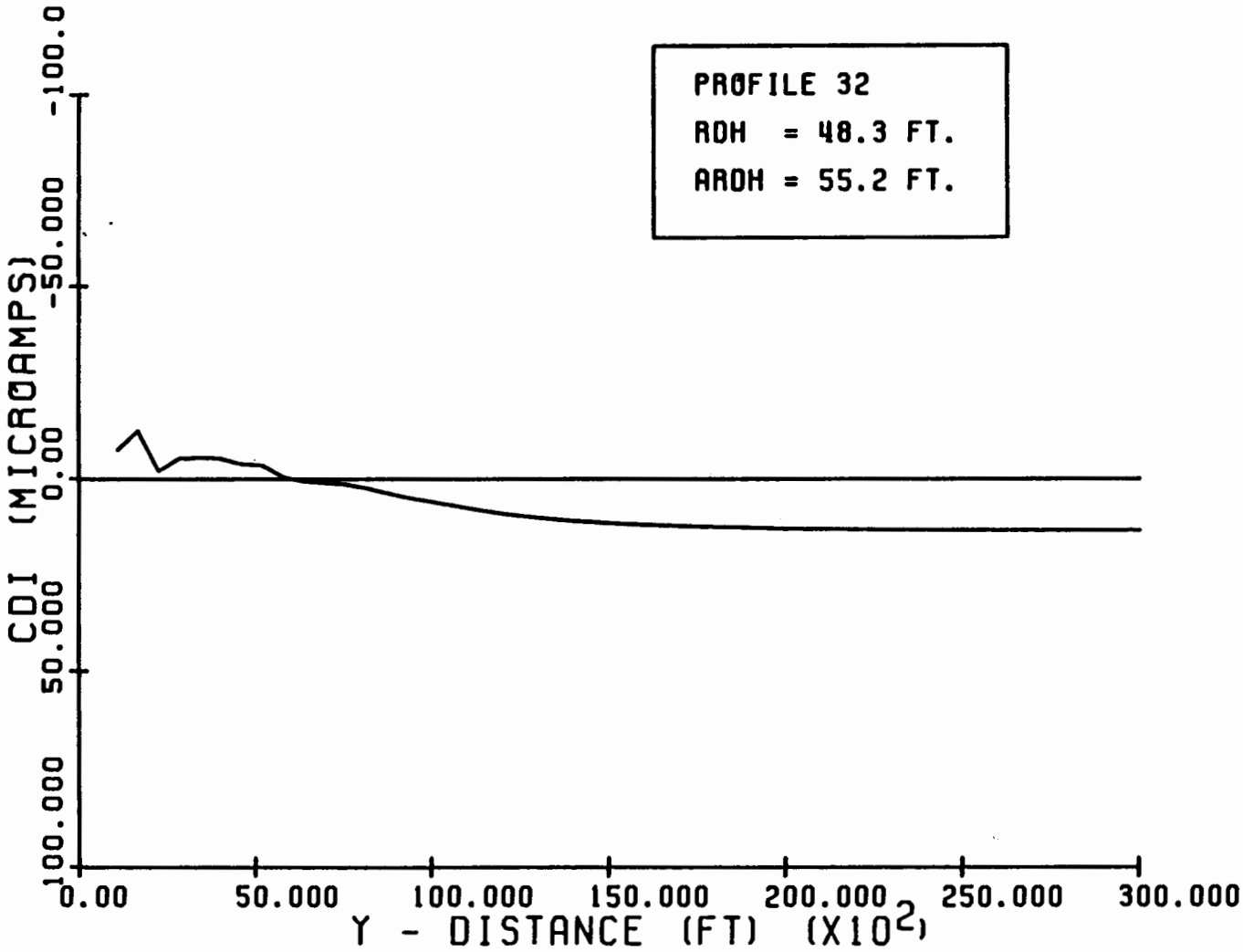

Figure 2-197. CDI trace showing the effect of decreasing depth of depression at Y=1600' to 599.85' MSL.

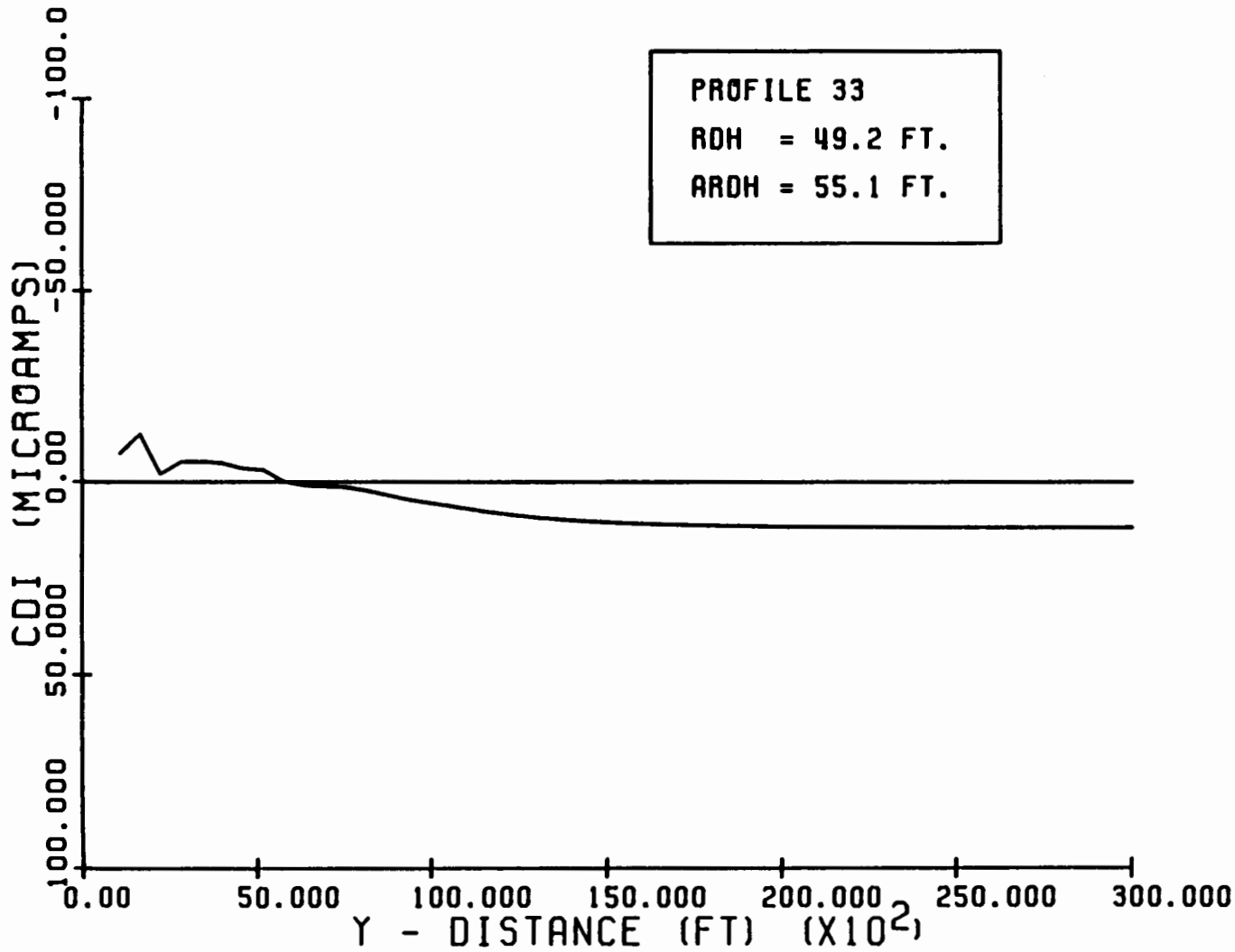

Figure 2-198. CDI trace showing the effect of decreasing depth of depression at Y=1600' to 600.85' MSL.

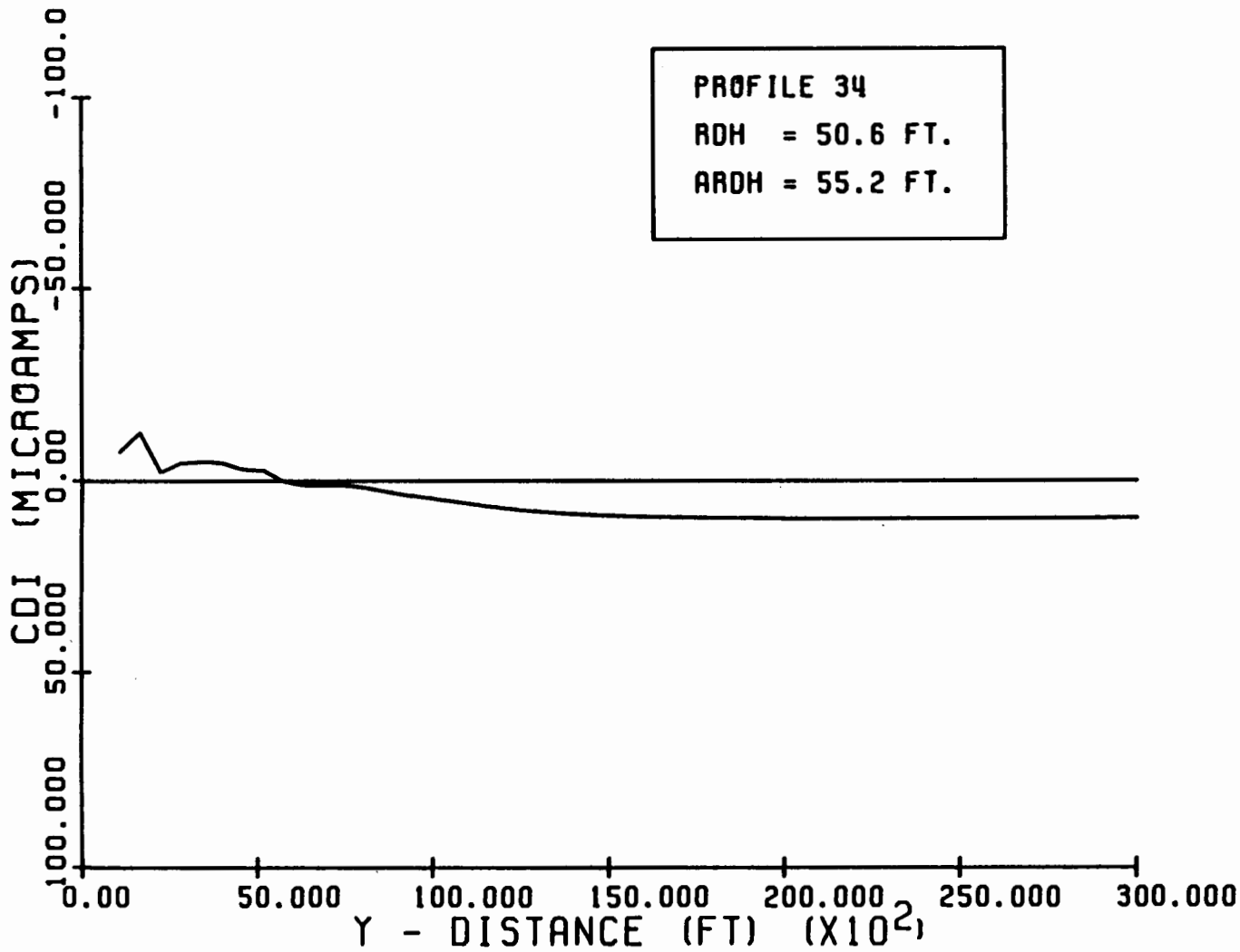

Figure 2-199. CDI trace showing the effect of decreasing depth of depression at Y=1600' to 601.85' MSL.

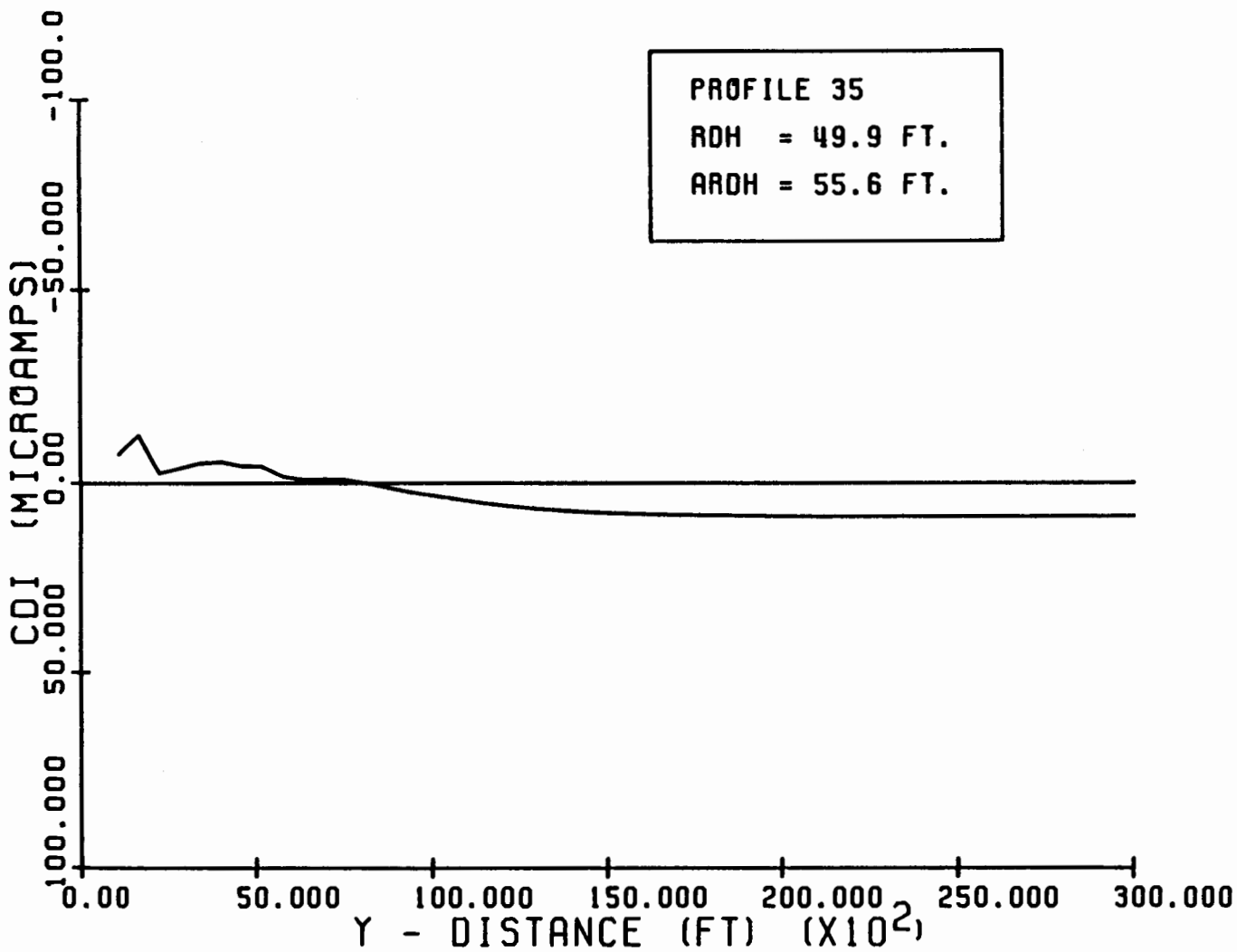

Figure 2-200. CDI trace showing the effect of decreasing depth of depression at Y=1600' to 602.85' MSL.

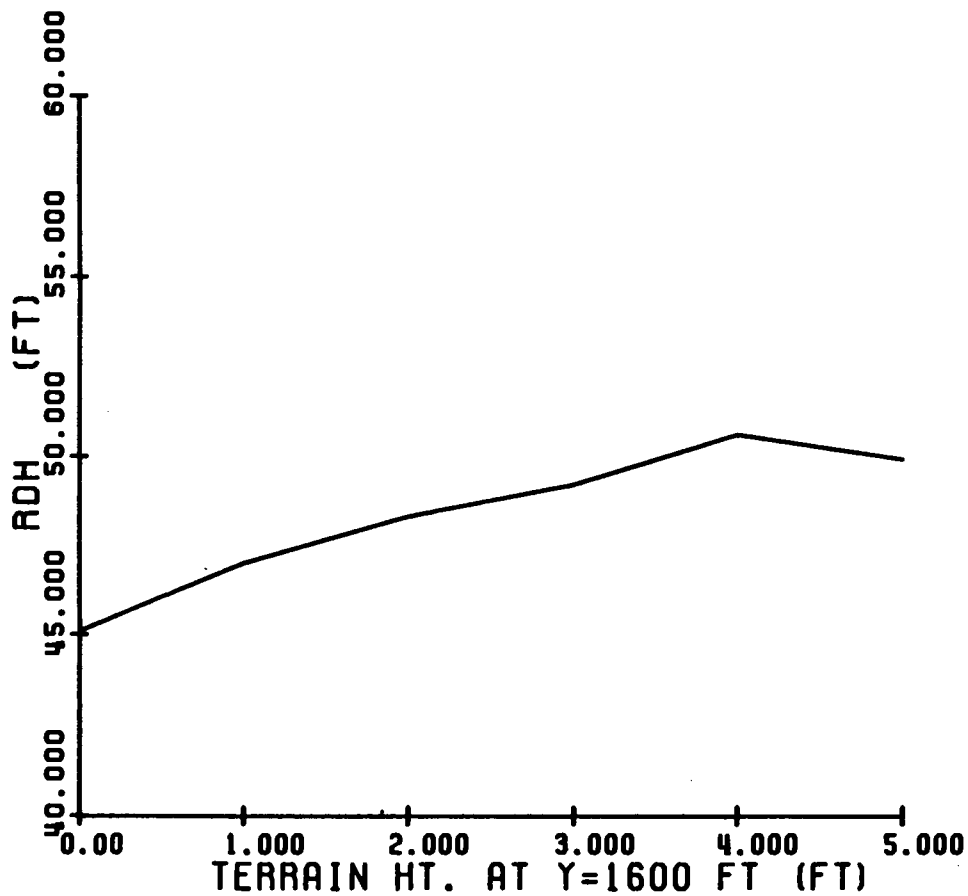

Figure 2-201. Sensitivity of RDH to depth of depression at Y=1600'.

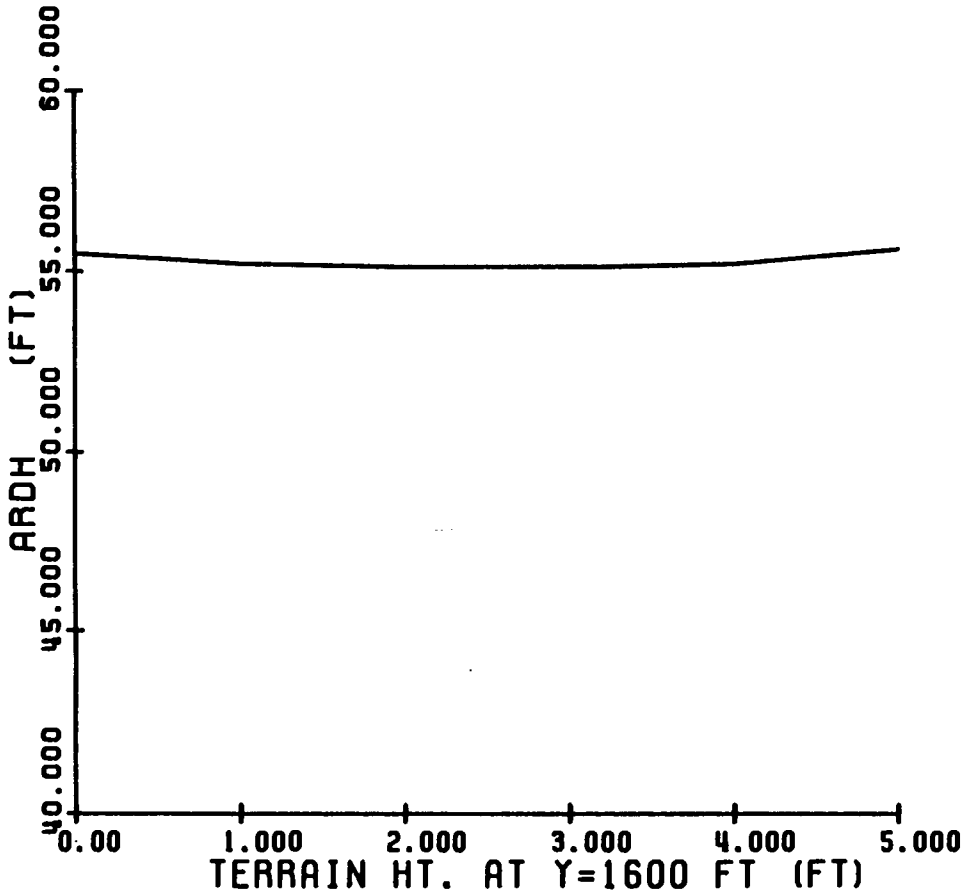

Figure 2-202. Sensitivity of ARDH to depth of depression at Y=1600'.

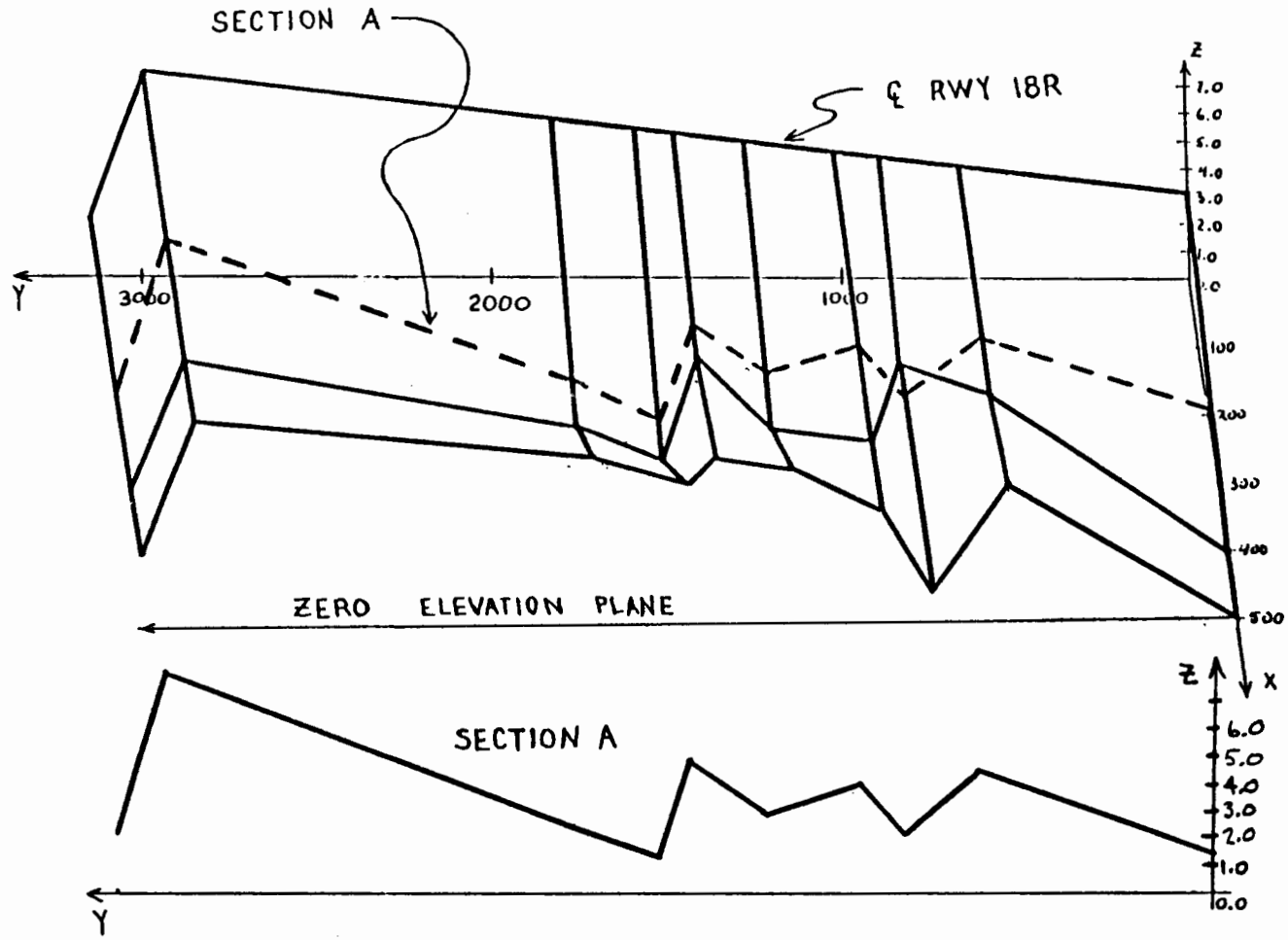

Figure 2-203. Isometric drawing of the modified terrain profile simulating grading of area between antennas and taxiway W-19.

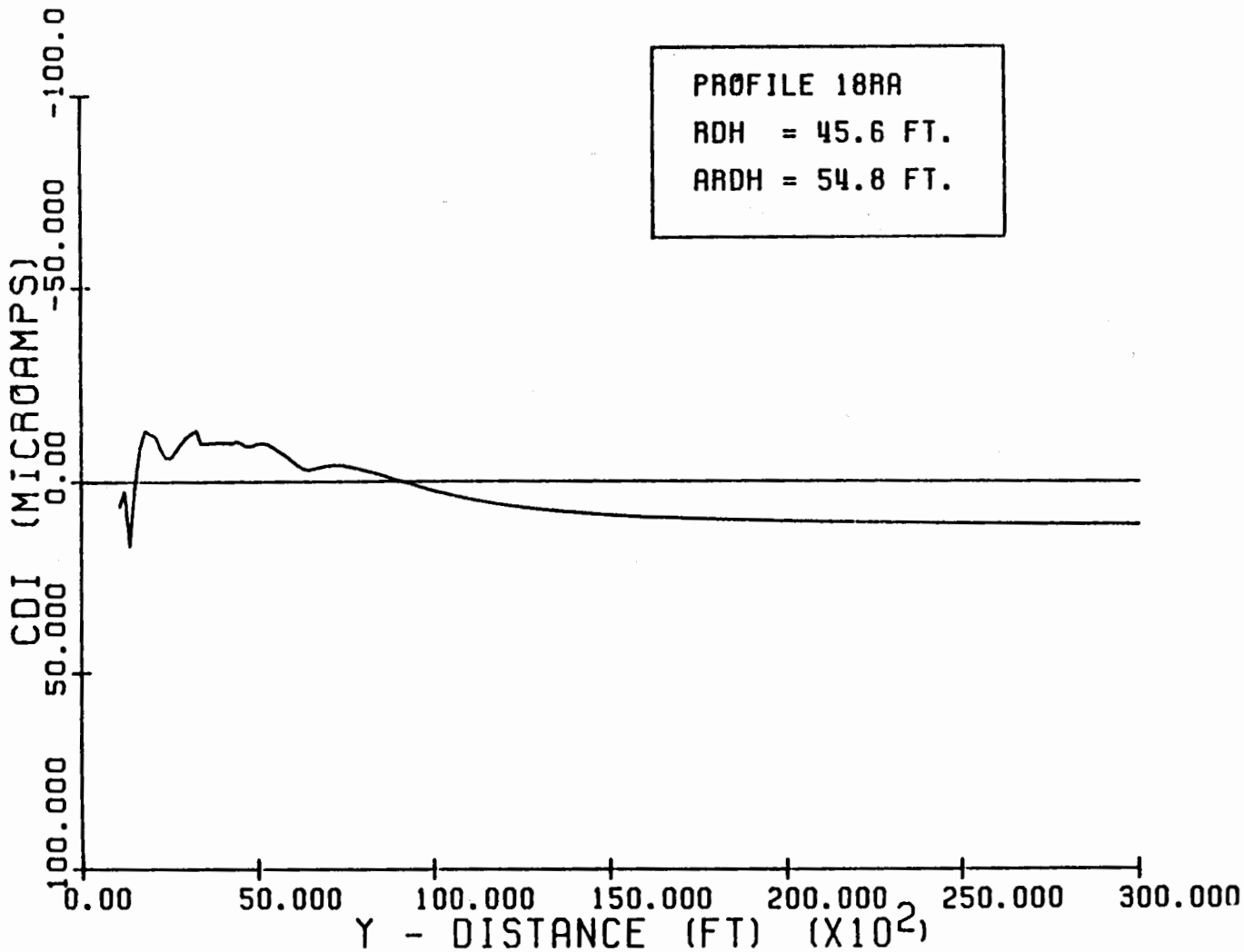

Figure 2-204. Differential amplifier recording for the terrain profile in figure 27. Antenna heights adjusted for 3 degree path angle.

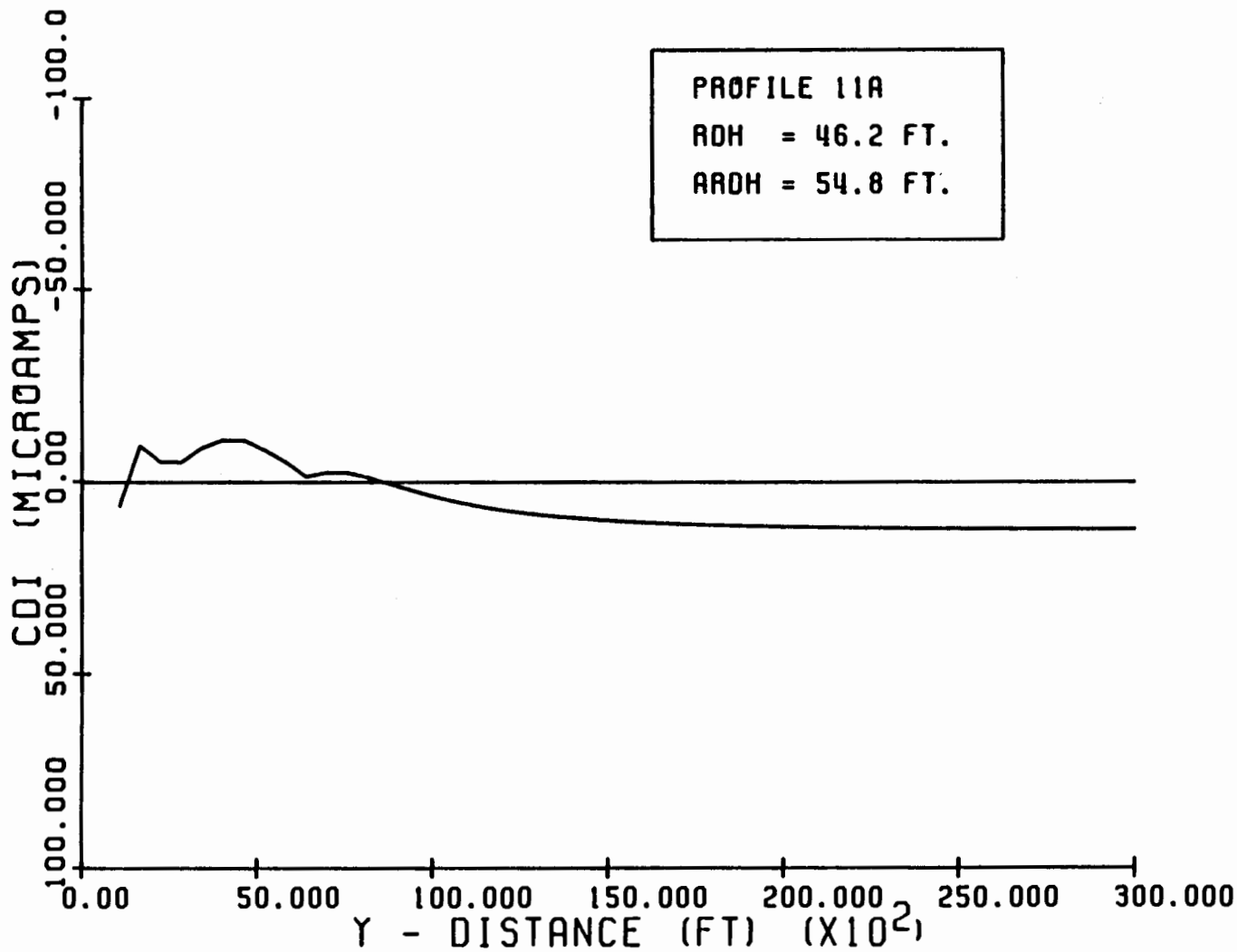

Figure 2-205. CDI trace showing the effect of decreasing depth of depression at Y=900' to 598.85' MSL for modified profile.

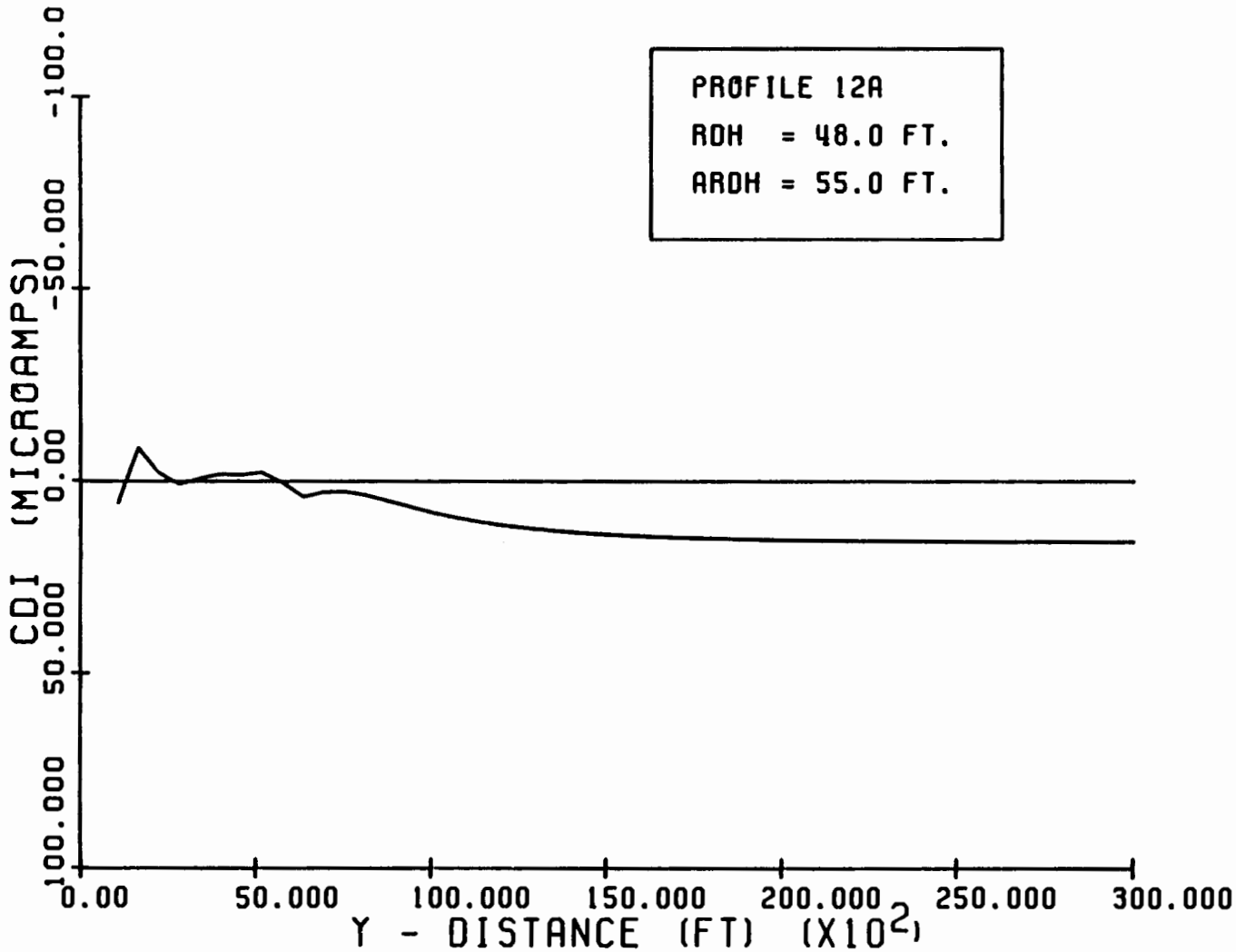

Figure 2-206. CDI trace showing the effect of decreasing depth of depression at Y=900' to 599.85' MSL for modified profile.

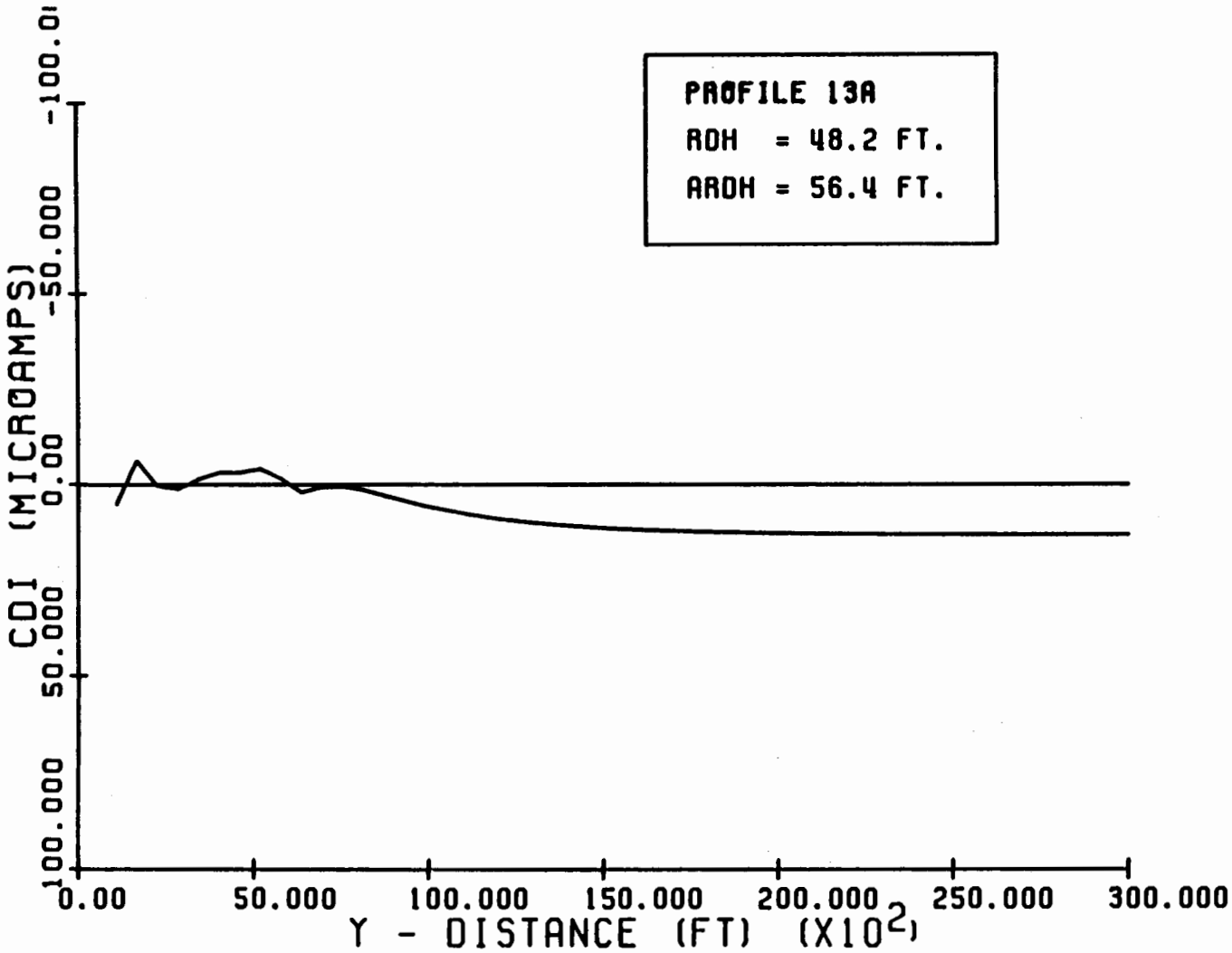

Figure 2-207. CDI trace showing the effect of decreasing depth of depression at Y=900' to 600.85' MSL for modified profile.

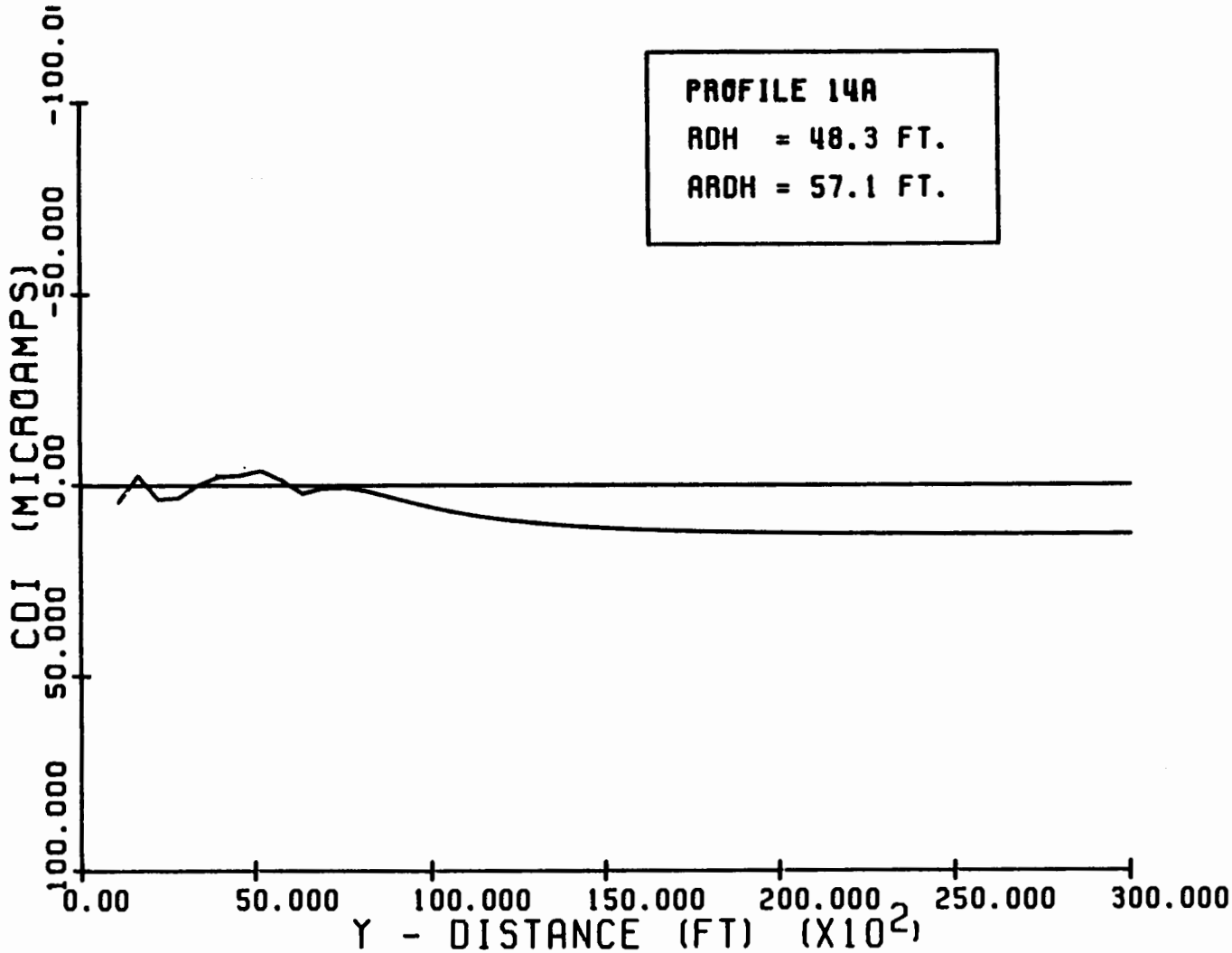

Figure 2-208. CDI trace showing the effect of decreasing depth of depression at Y=900' to 601.85' MSL for modified profile.

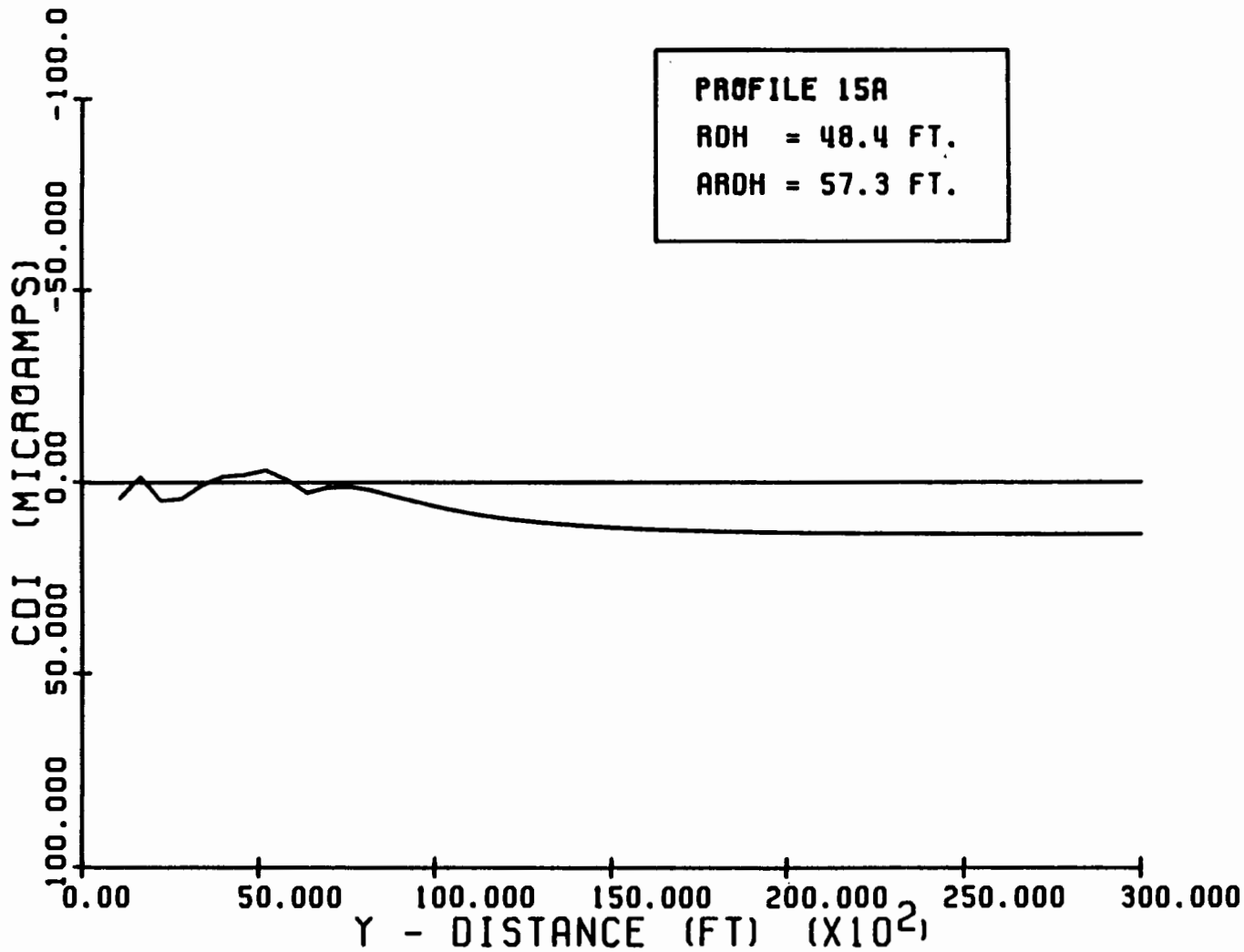

Figure 2-209. CDI trace showing the effect of decreasing depth of depression at Y=900' to 602.85' MSL for modified profile.

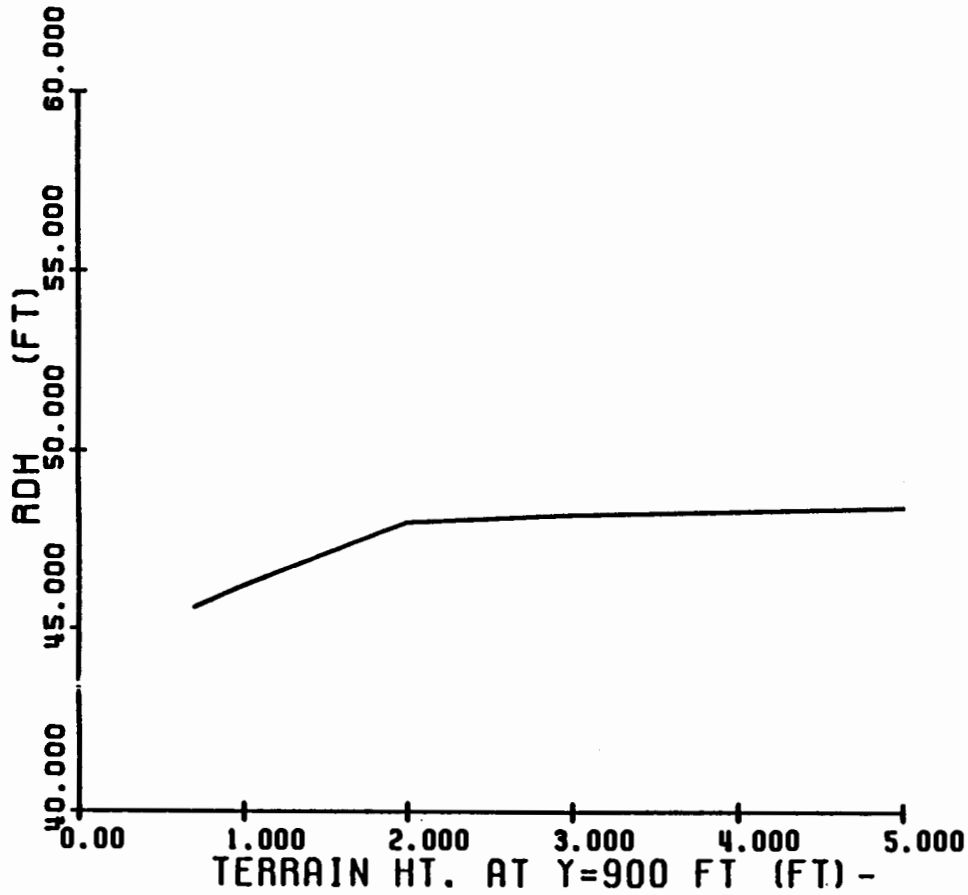

Figure 2-210. Sensitivity of RDH to depth of depression at Y=900' for modified profile.

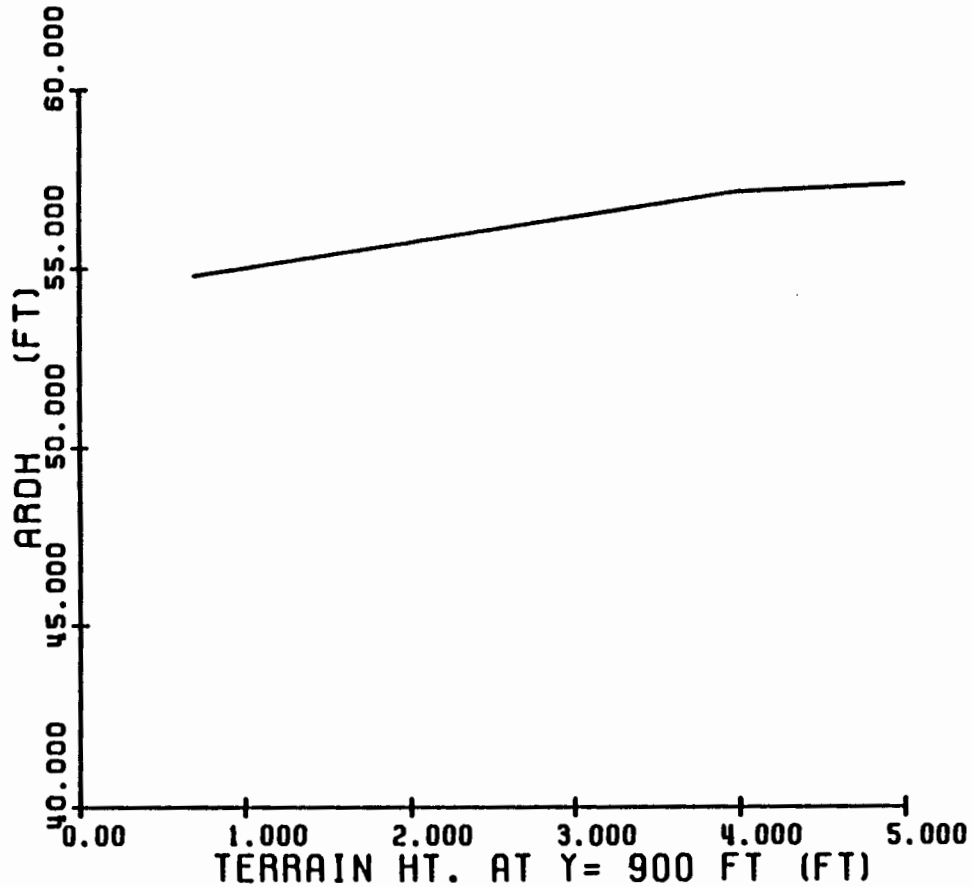

Figure 2-211. Sensitivity of ARDH to depth of depression at Y=900' for modified profile.

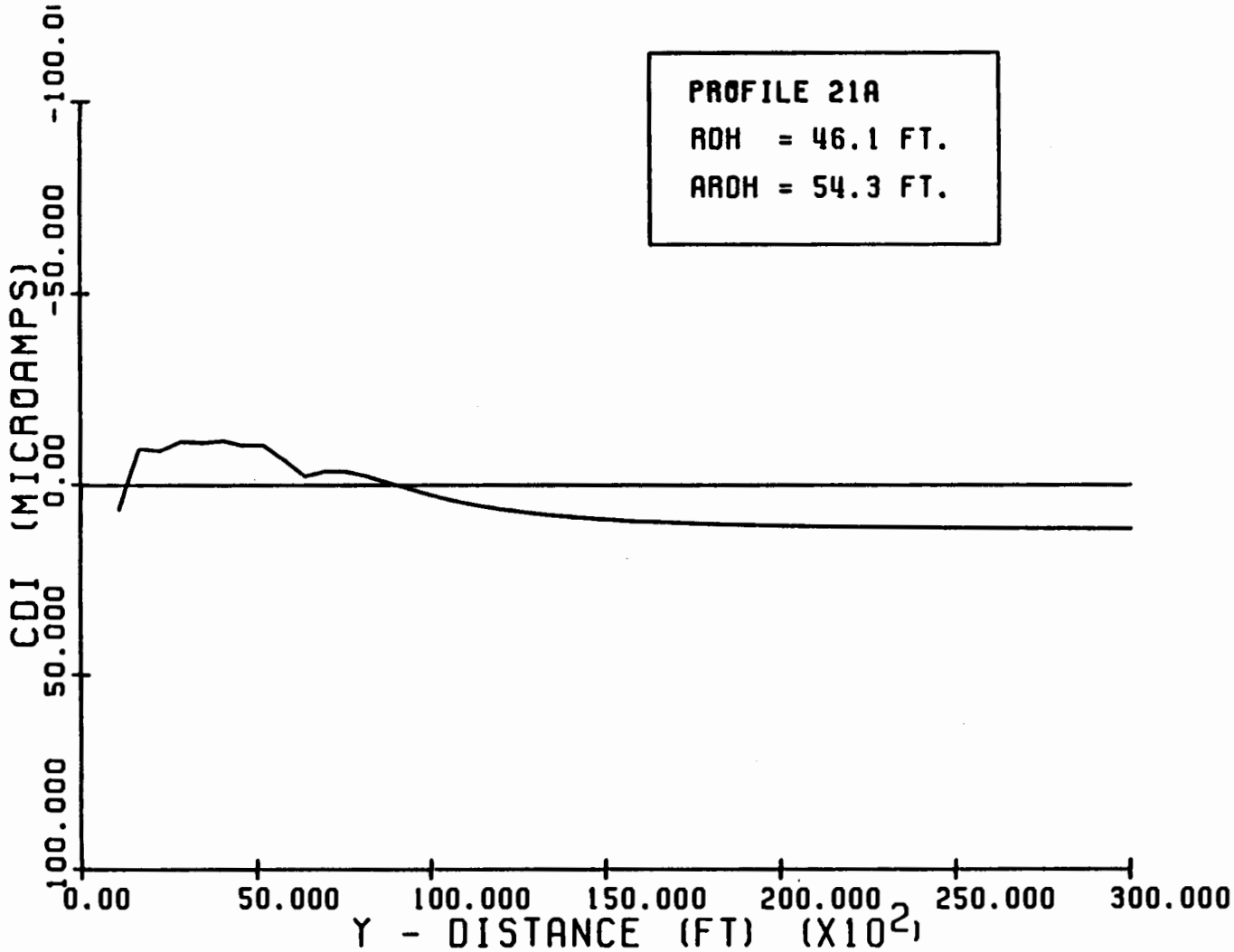

Figure 2-212. CDI trace showing the effect of decreasing depth of depression at Y=1242' to 599.85' MSL for modified profile.

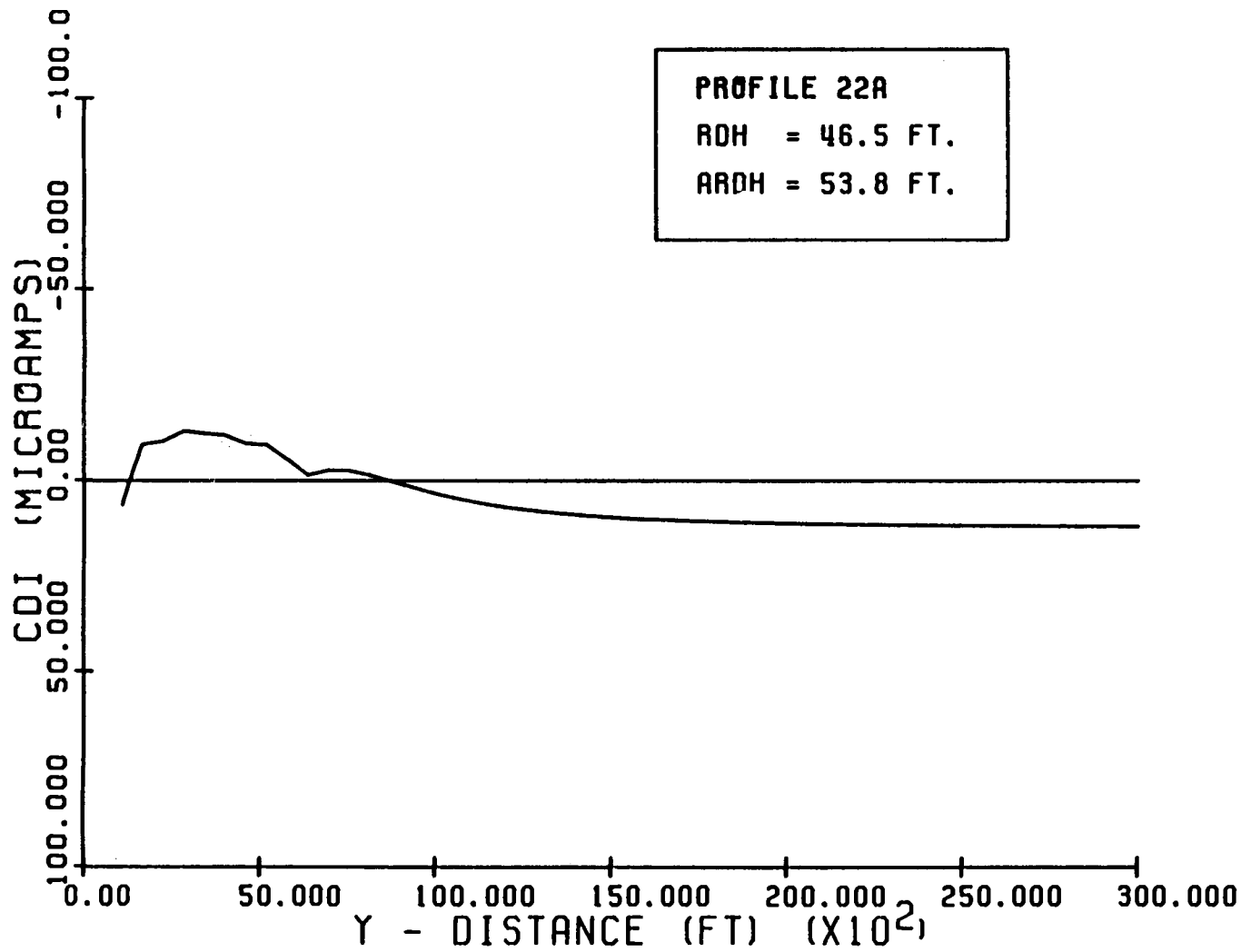

Figure 2-213. CDI trace snowing the effect of decreasing depth of depression at Y=1242' to 600.85' MSL for modified profile.

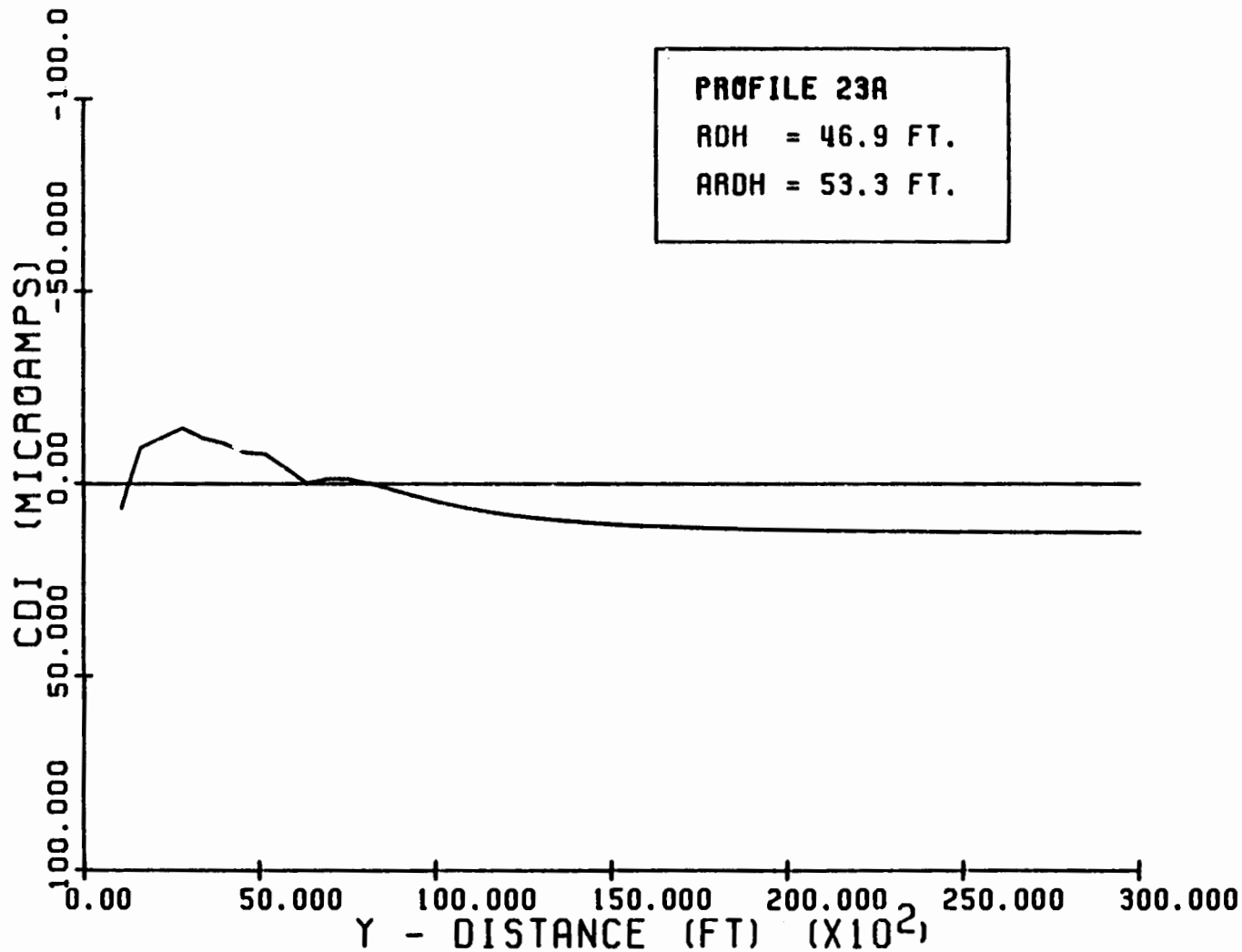

Figure 2-214. CDI trace showing the effect of decreasing depth of depression at Y=1242' to 601.85' MSL for modified profile.

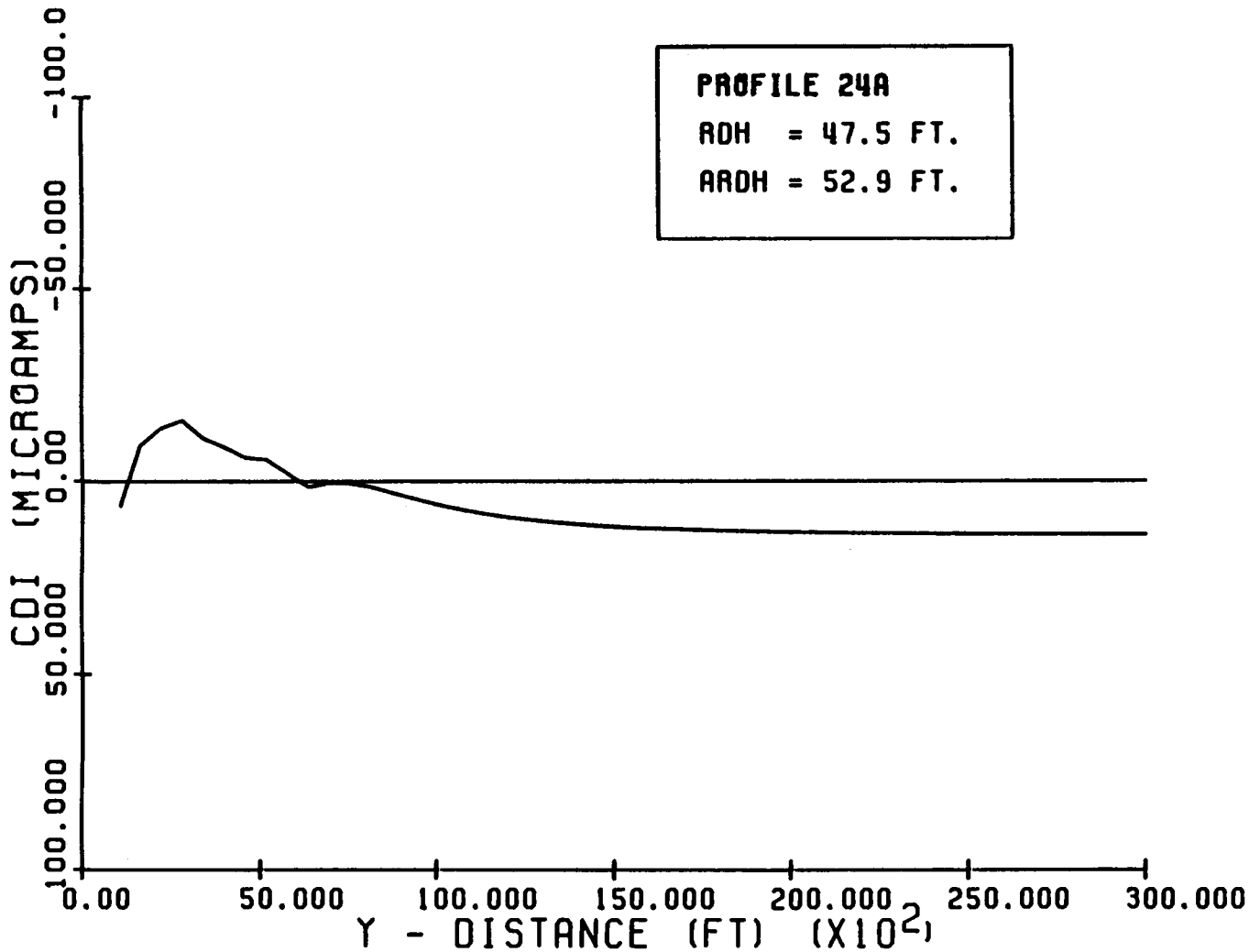

Figure 2-215. CDI trace showing the effect of decreasing depth of depression at Y=1242' to 602.85' MSL for modified profile.

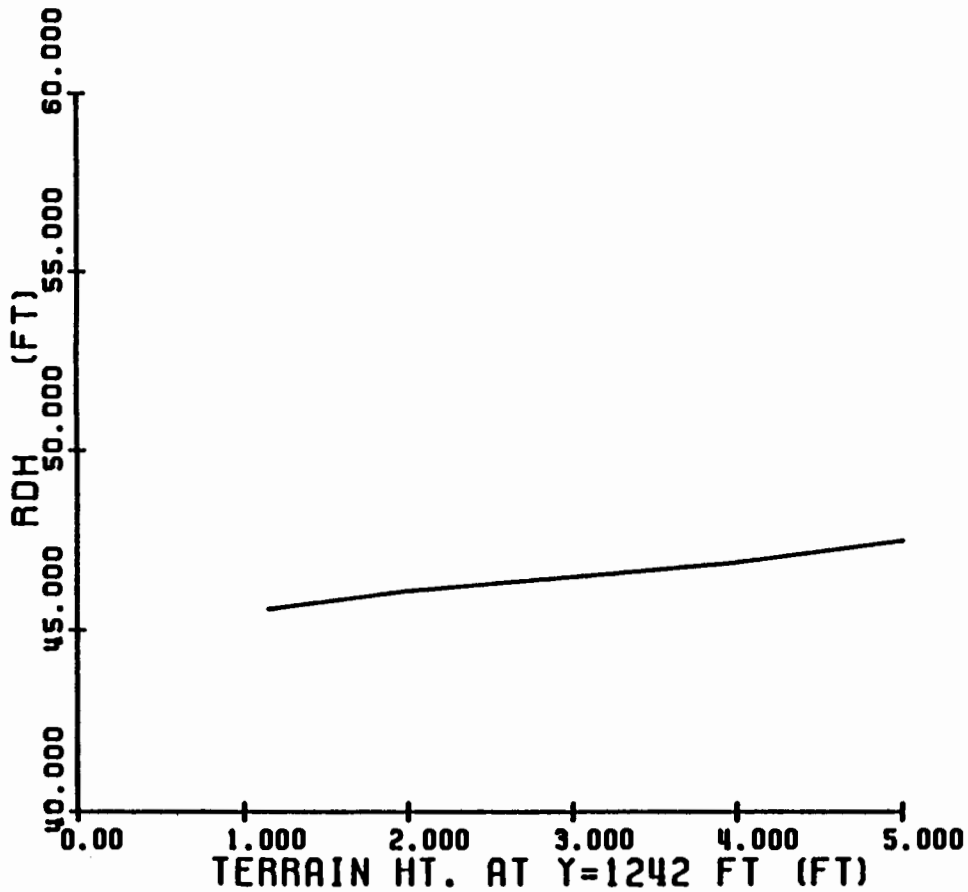

Figure 2-216. Sensitivity of RDH to depth of depression at Y=1242' for modified profile.

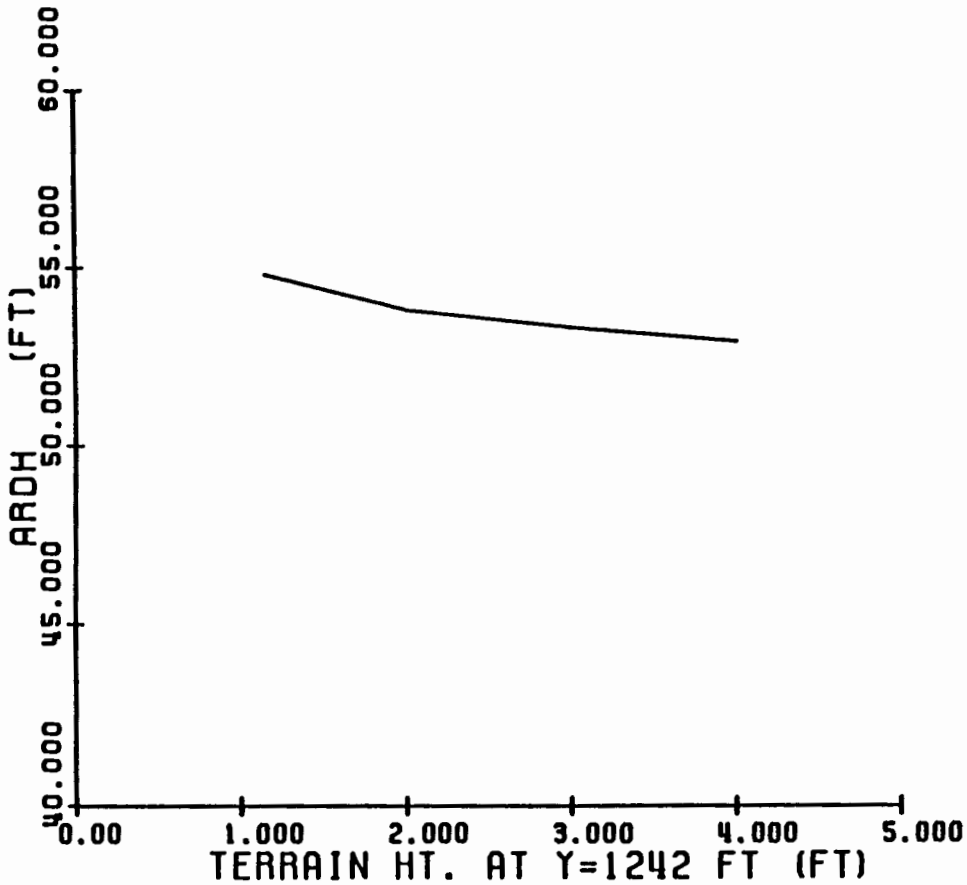

Figure 2-217. Sensitivity of ARDH to depth of depression at Y=1242' for modified profile.

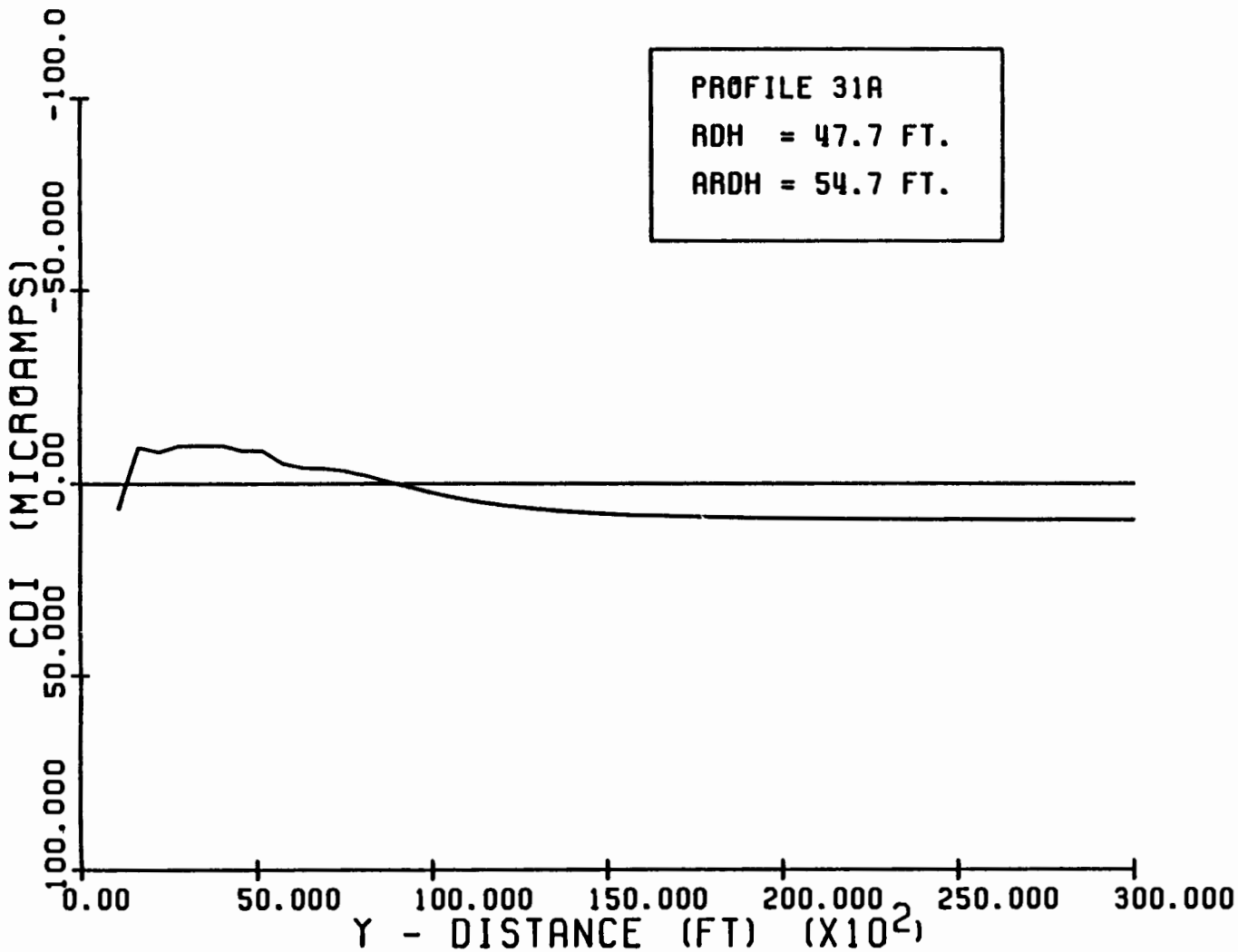

Figure 2-218. CDI trace showing the effect of decreasing depth of depression at Y=1600' to 598.85' MSL for modified profile.

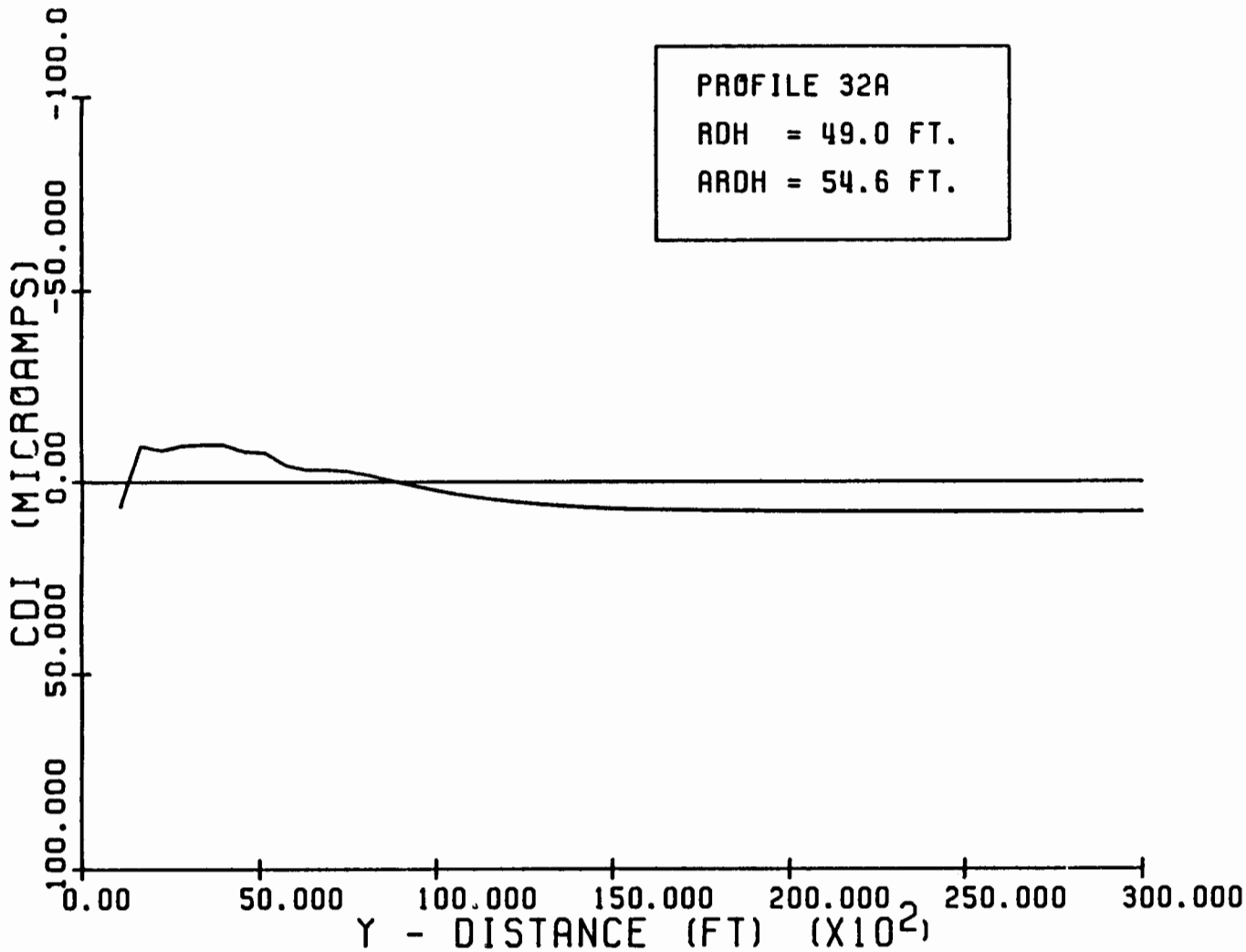

Figure 2-219. CDI trace showing the effect of decreasing depth of depression at Y=1600' to 599.85' MSL for modified profile.

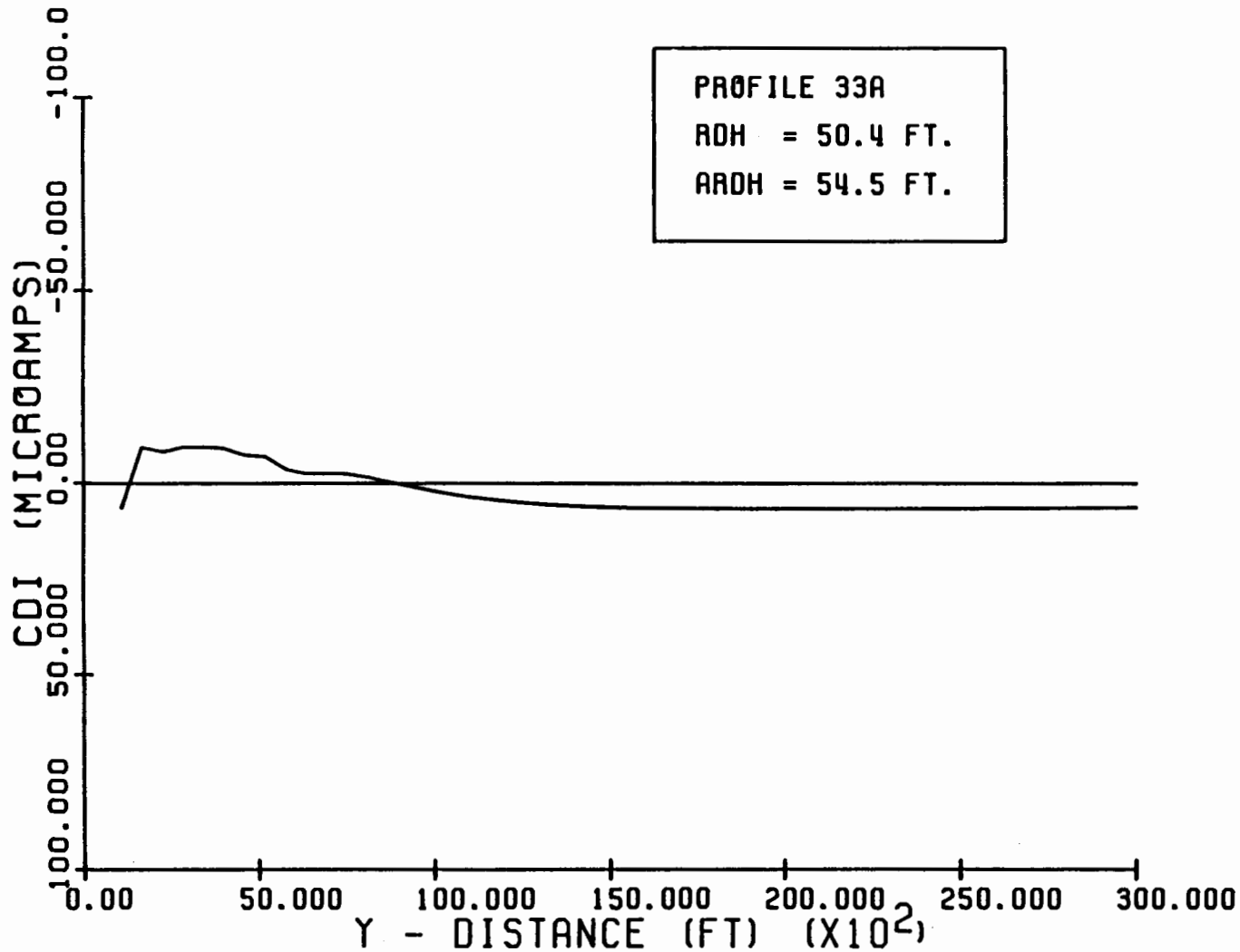

Figure 2-220. CDI trace showing the effect of decreasing depth of depression at Y=1600' to 600.85' MSL for modified profile.

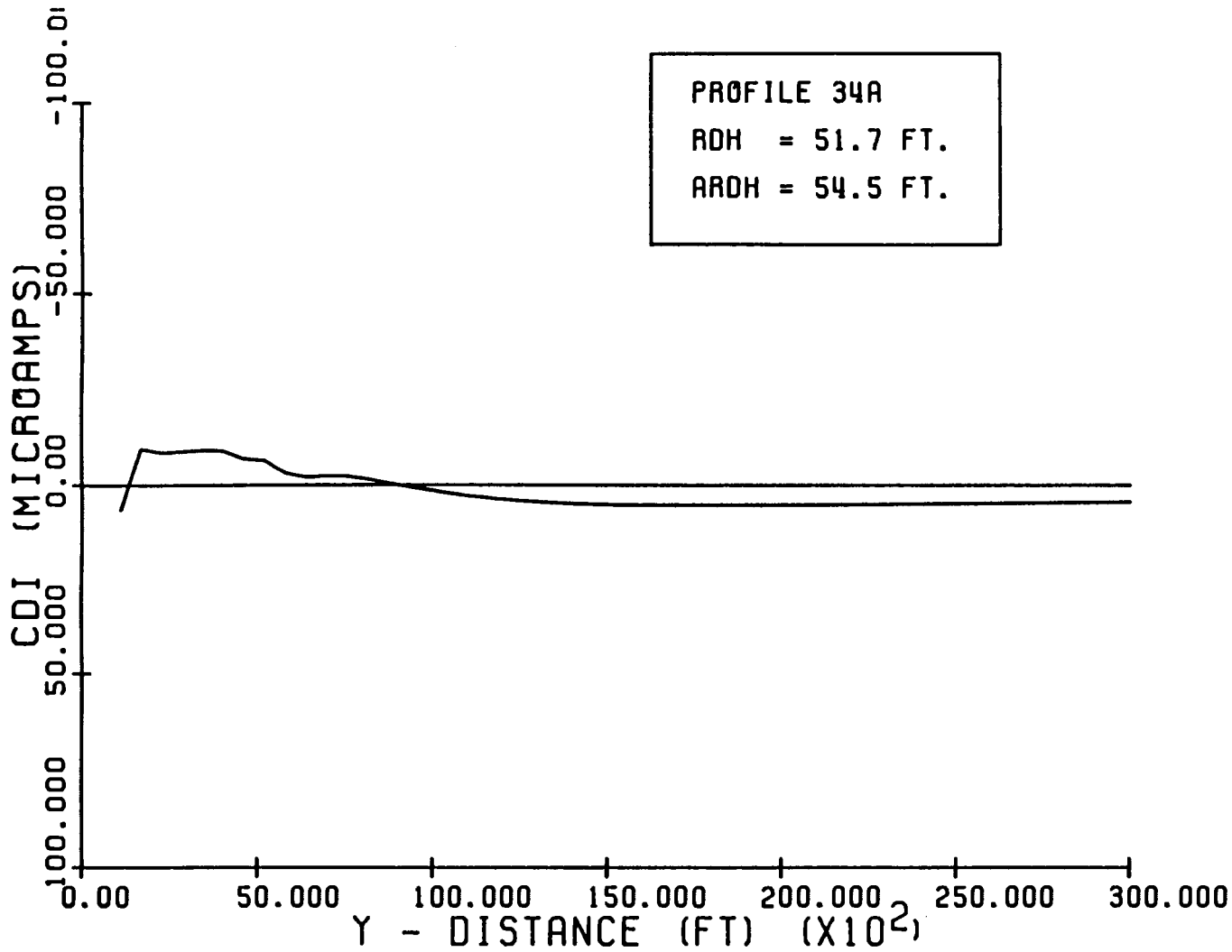

Figure 2-221. CDI trace showing the effect of decreasing depth of depression at Y=1600' to 601.85' MSL for modified profile.

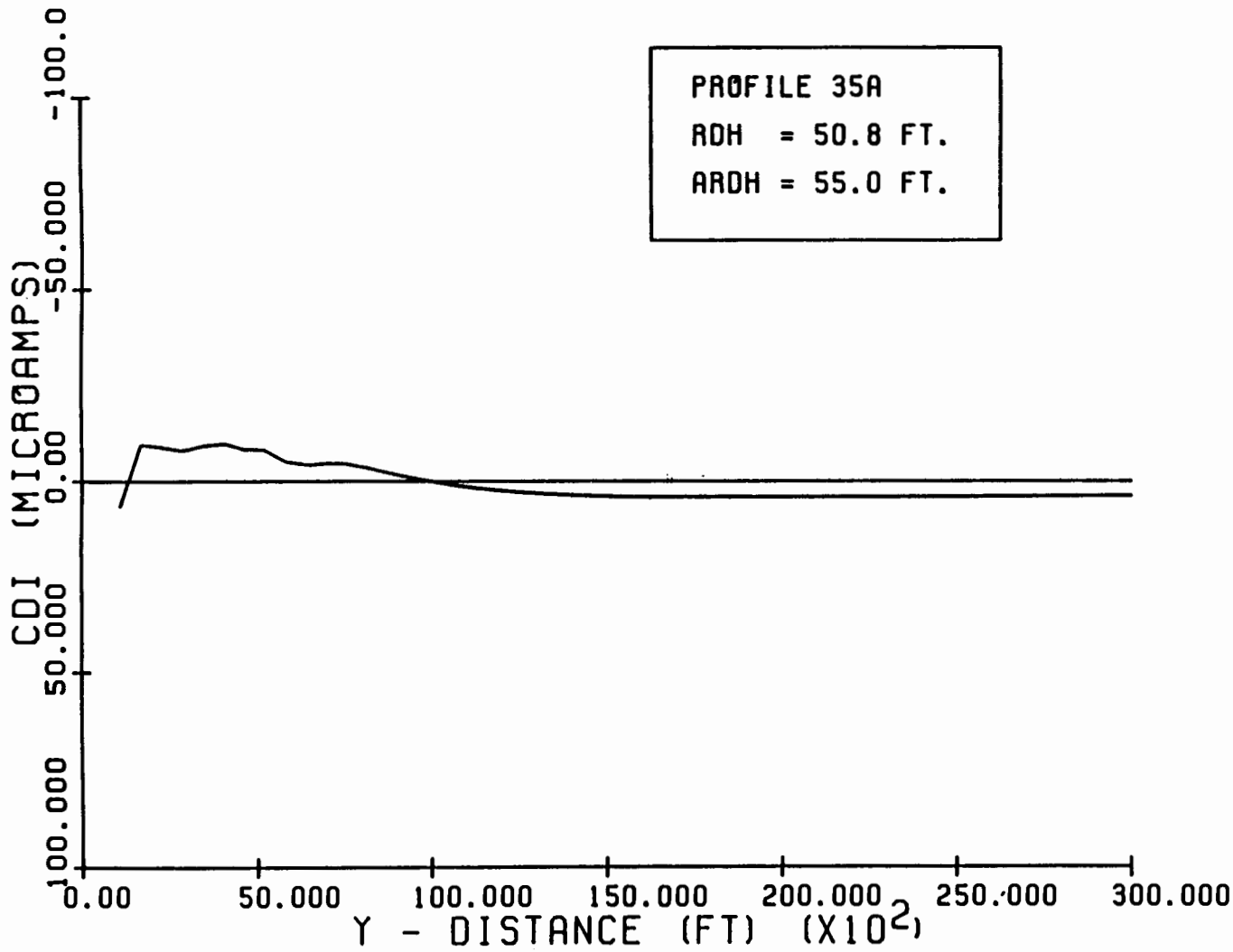

Figure 2-222. CDI trace showing the effect of decreasing depth of depression at Y=1600' to 602.85' MSL for modified profile.

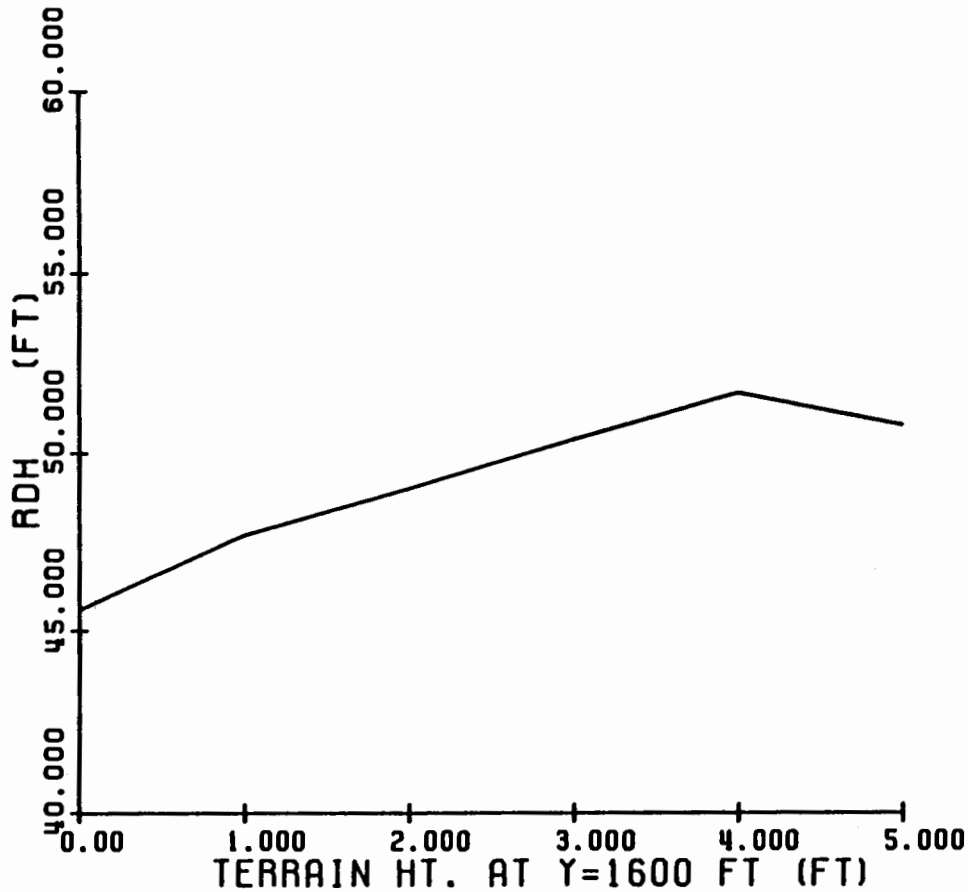

Figure 2-223. Sensitivity of RDH to depth of depression at Y=1600' for modified profile.

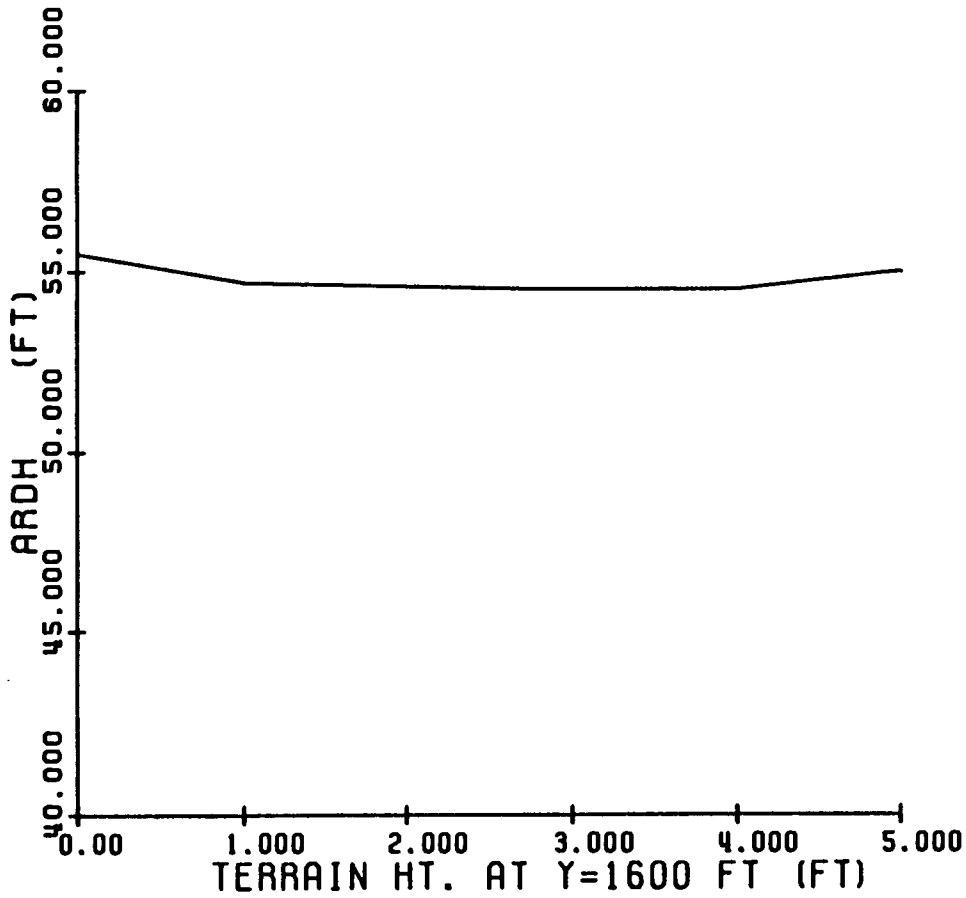

Figure 2-224. Sensitivity of ARDH to depth of depression at Y=1600' for modified profile.

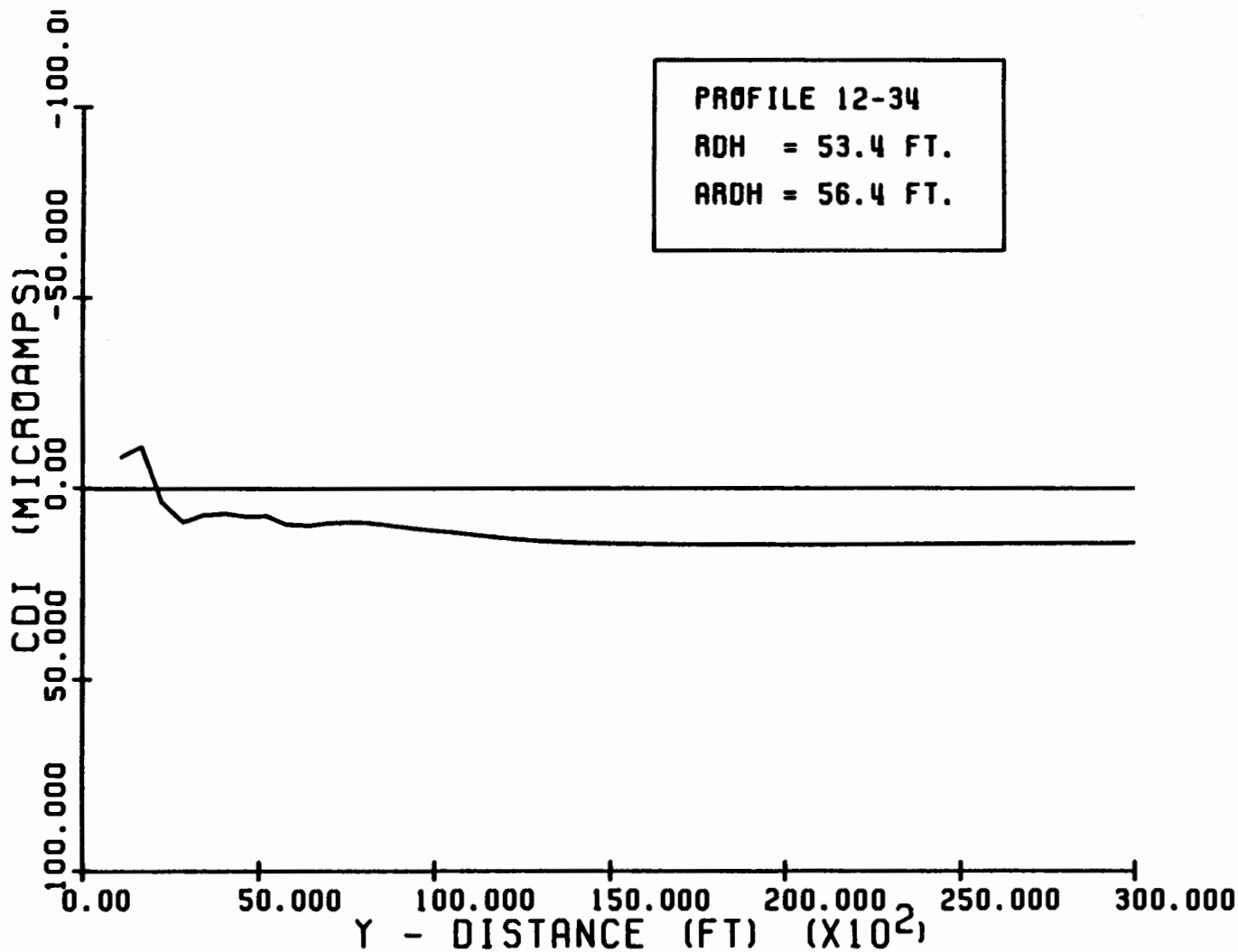

Figure 2-225. CDI trace showing the effects of decreasing the depth of the depression at Y=900' to 599.85' MSL and the depth of the depression at Y=1600' to 602.85' MSL.

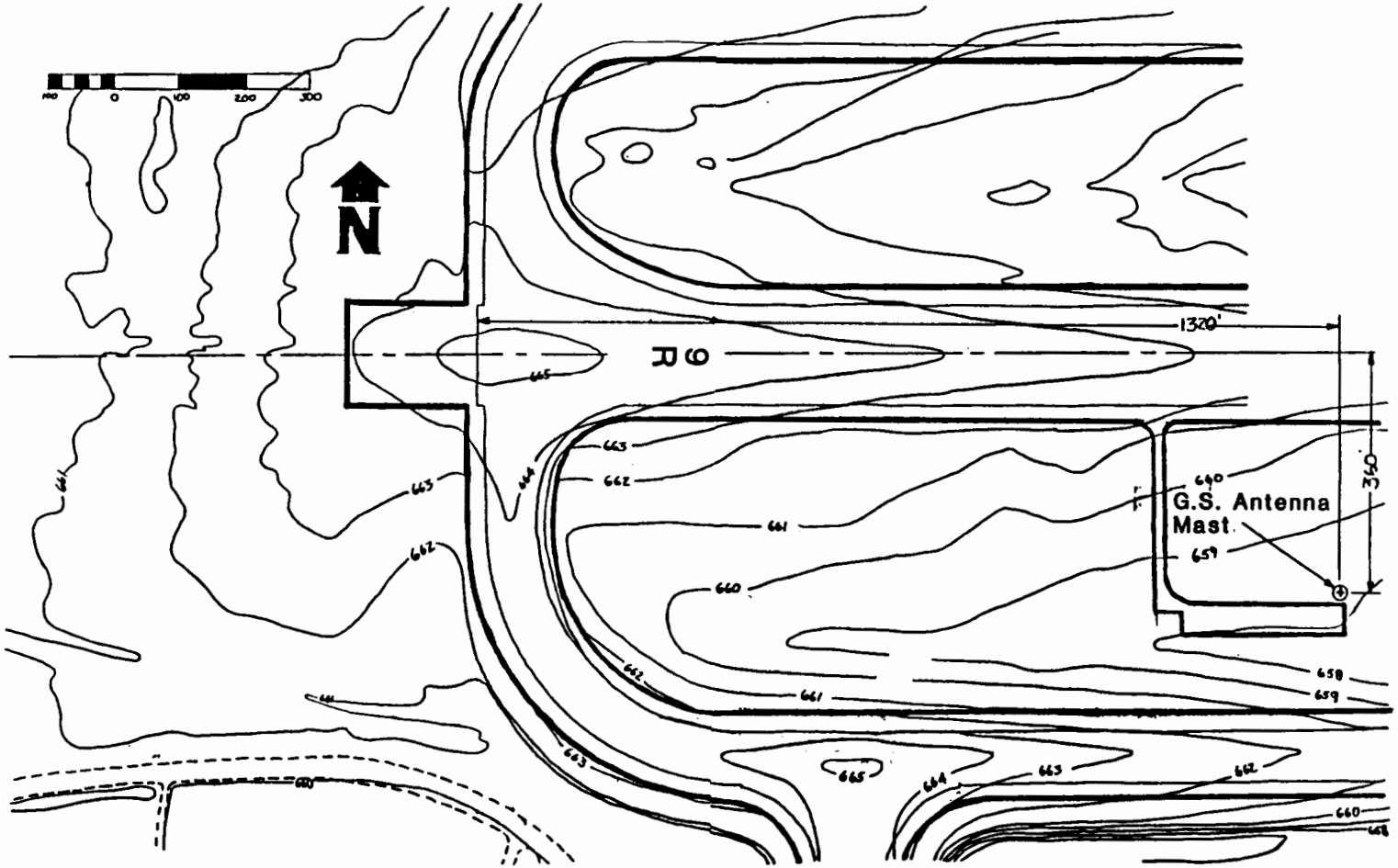

Figure 2-226. Topographic map of proposed glide slope critical area terrain at runway 9R, Chicago O'Hare International Airport.

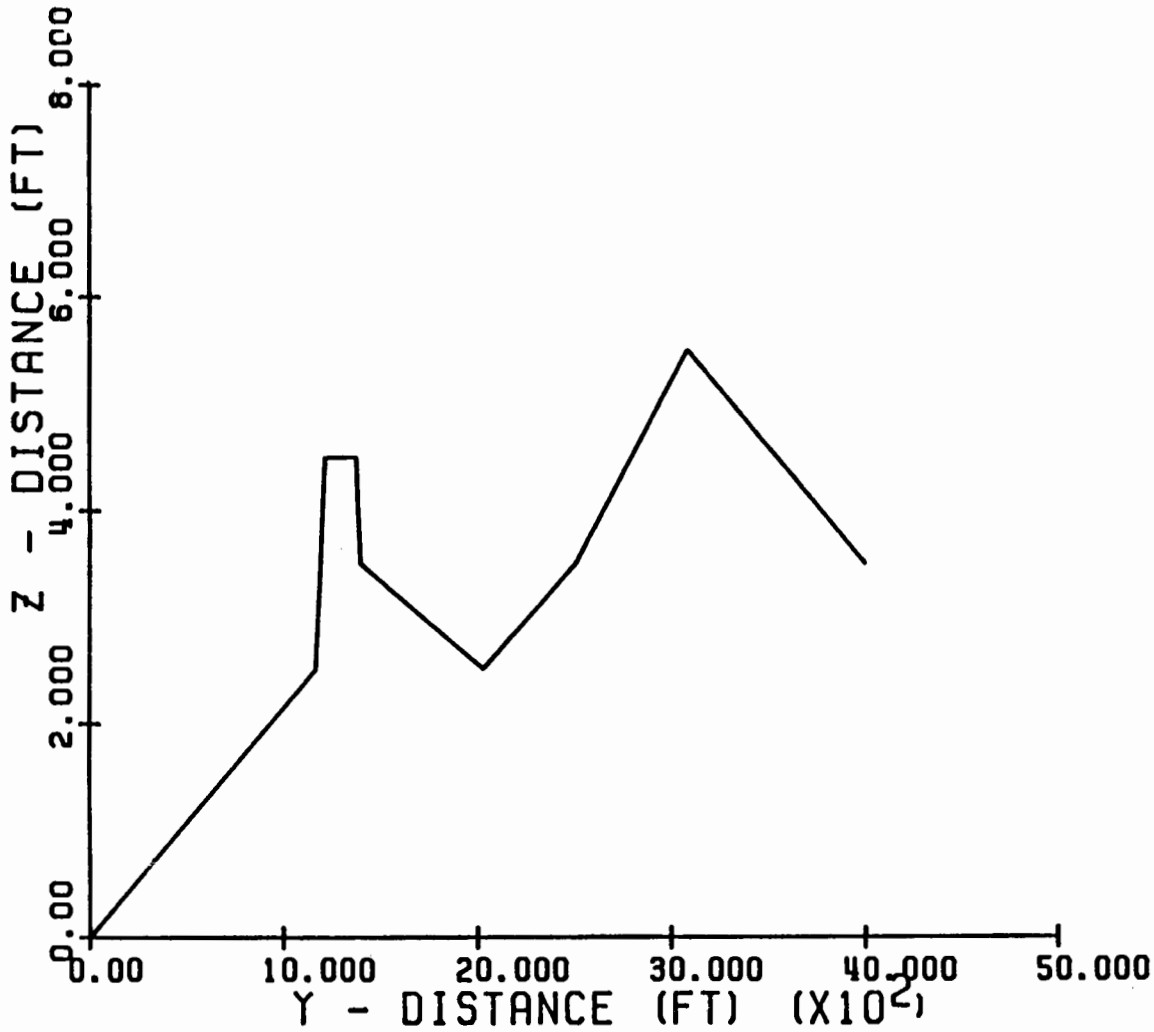

Figure 2-227. Two-dimensional terrain profile representing the critical area terrain shown in figure 2-226.

```
*        O'HARE RUNWAY 9R GLIDE SLOPE TERRAIN MODEL
SECTION        1
NO OF PTS     10     1
COORD.          0.0        0.0        0.0
                0.0     1170.0        2.5
                0.0     1220.0        4.5
                0.0     1380.0        4.5
                0.0     1400.0        3.5
                0.0     2030.0        2.5
                0.0     2510.0        3.5
                0.0     3090.0        5.5
                0.0     4000.0        3.5
                0.0    20000.0        1.5
SECTION        2
THEODOLITE                360.00      0.0        0.00       3.00       0.7
SECTION        3
ANT DATA       2          331.7       0.400      0.300      0.900
POSITION       1          360.860     0.000     15.15
                0.0        0.0        1.0        0.0        0.0        0.0
POSITION       2          359.140     0.000     30.30
               1.0         0.0        0.0        0.0        0.0        0.0
SECTION        4
PATTERN        3    50     1           0.0    30000.0       3.0
                                       0.0     1000.0
SECTION        5
OUTPUT         3     1     2       30000.0       0.0      100.0     -100.000000000000
...

R!
```

Figure 2-228. Sample of input data file for mathematical model OUGS.

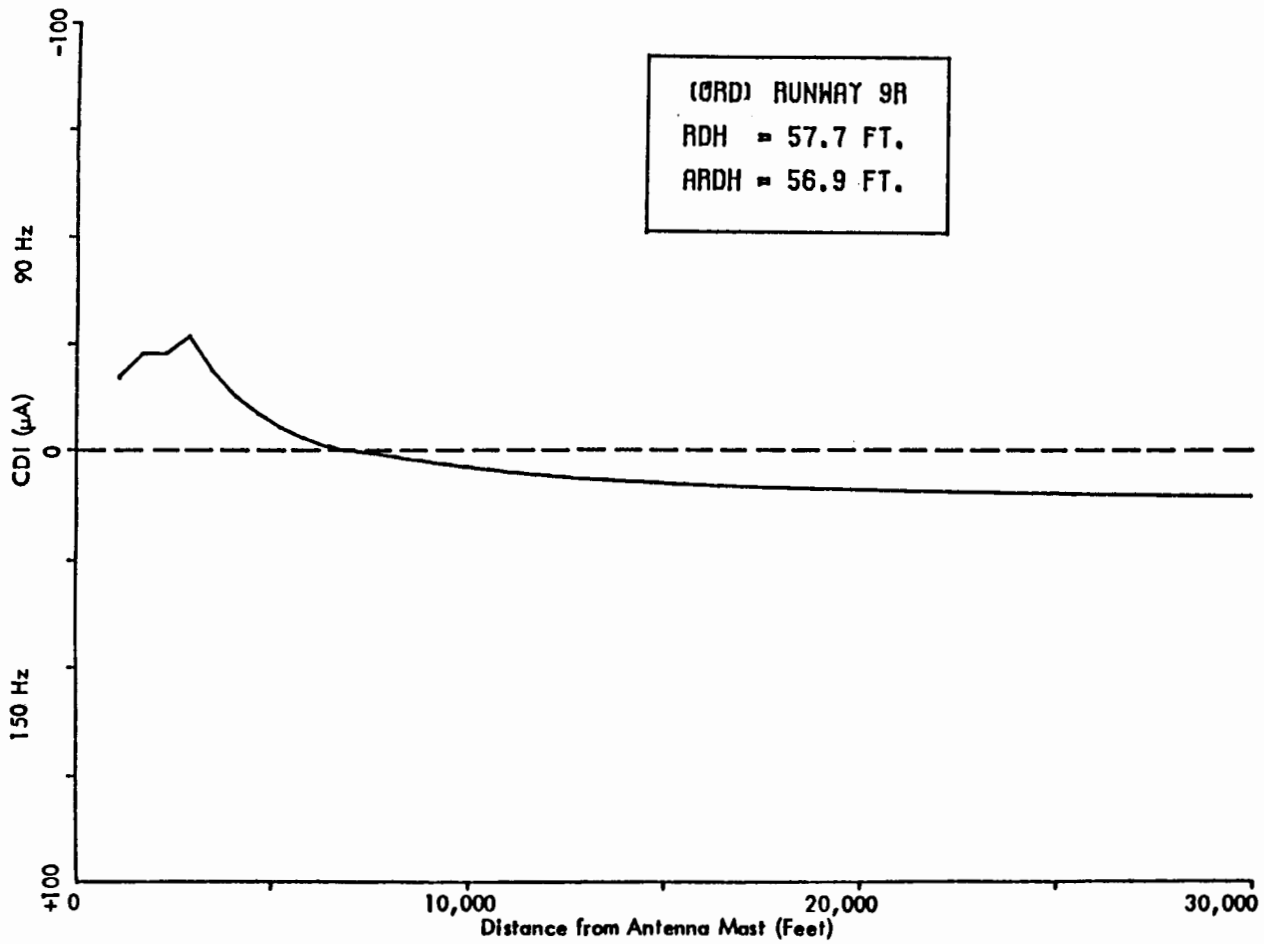

Figure 2-229. Simulated differential amplifier recording for the terrain profile shown in figure 2-227.

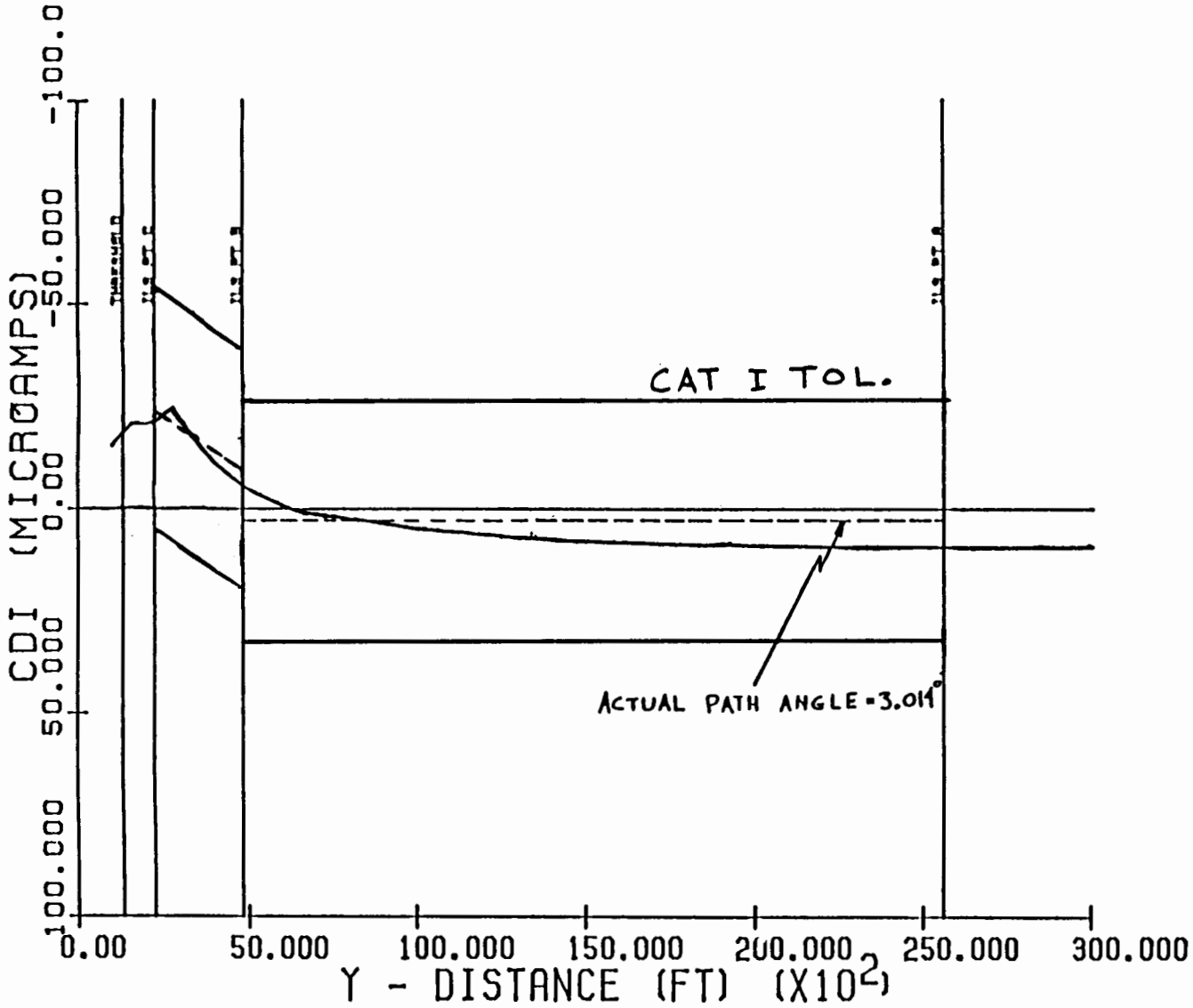

Figure 2-230. Simulated differential amplifier recording for the terrain profile shown in figure 2-227, with Category I tolerances applied.

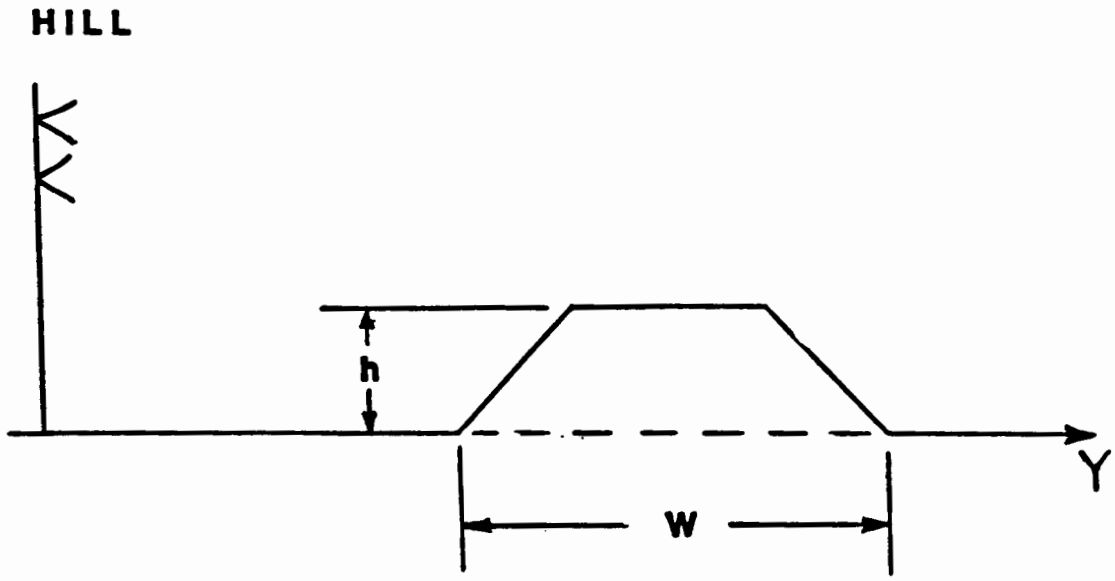

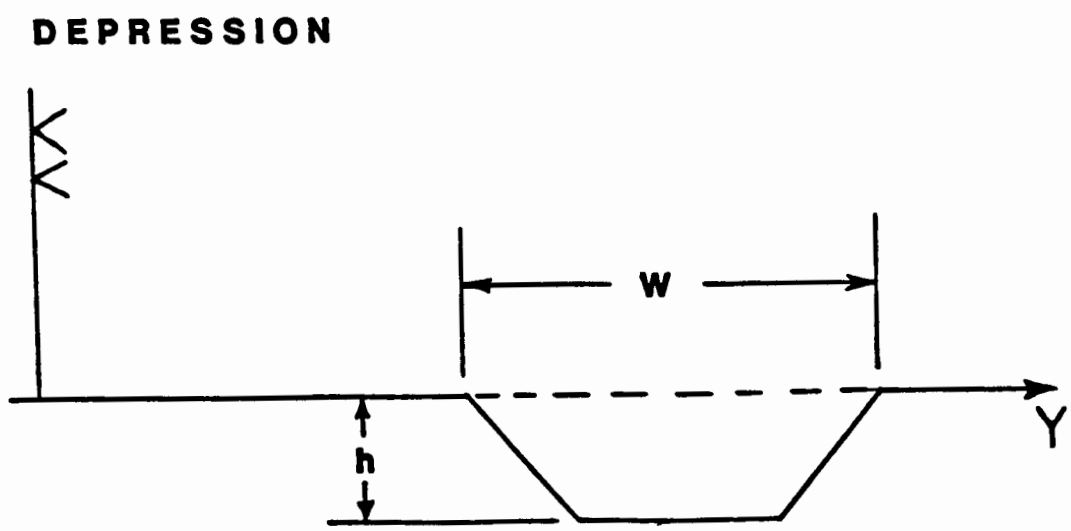

Figure 2-231. Examples of the shapes of irregular terrain considered.

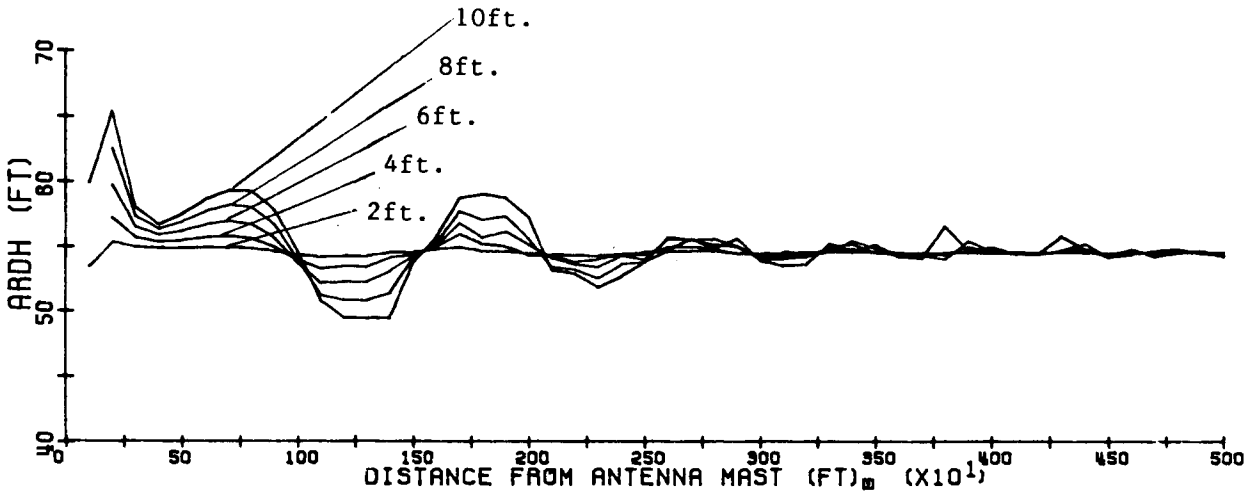

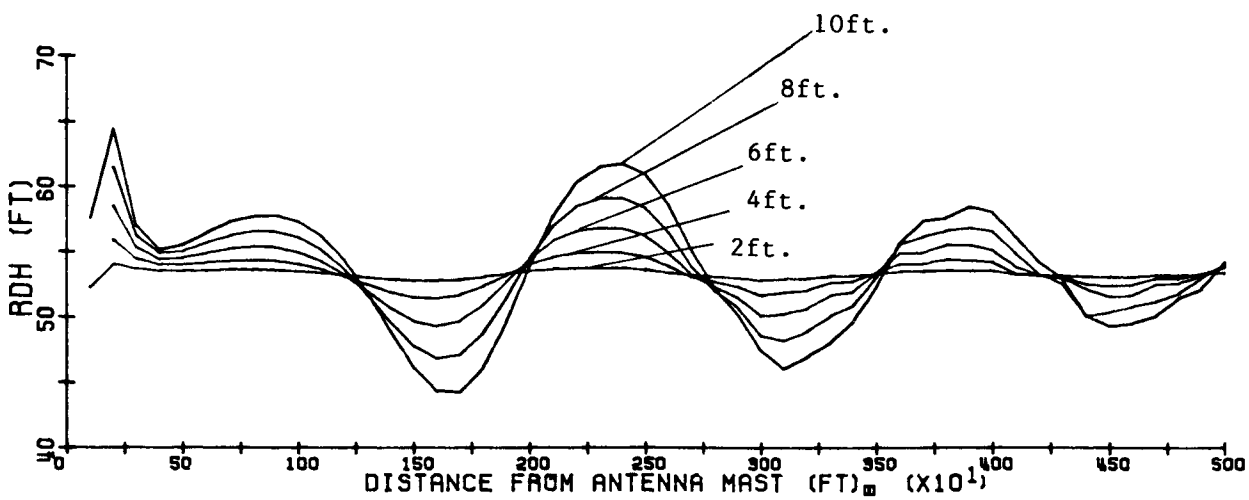

Figure 2-232. Example of a sensitivity curve produced by varying location of a hill 10 feet in duration (w) and 10 feet high (h).

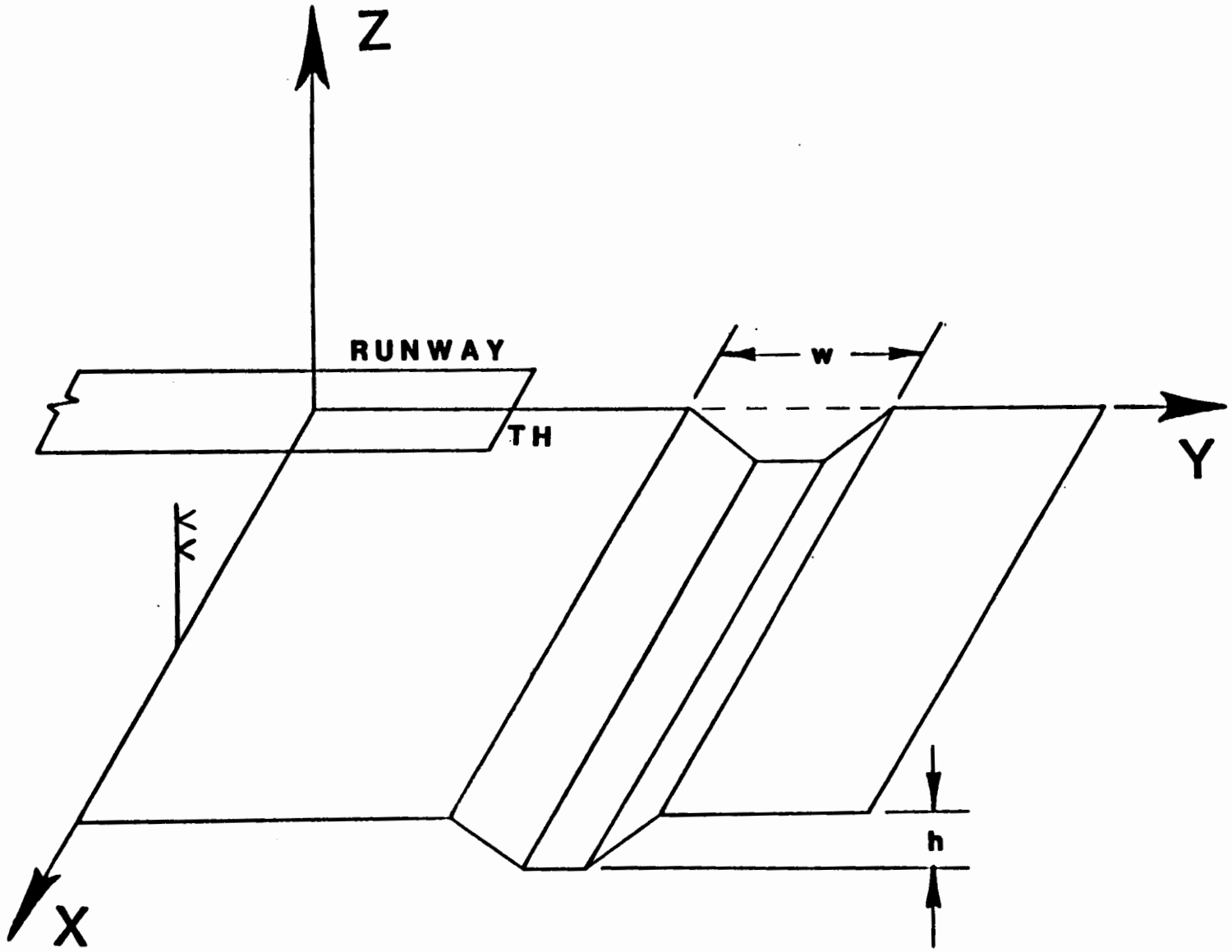

Figure 2-233. Three-dimensional approximation of a terrain depression formed by two-dimensional reflecting plates.

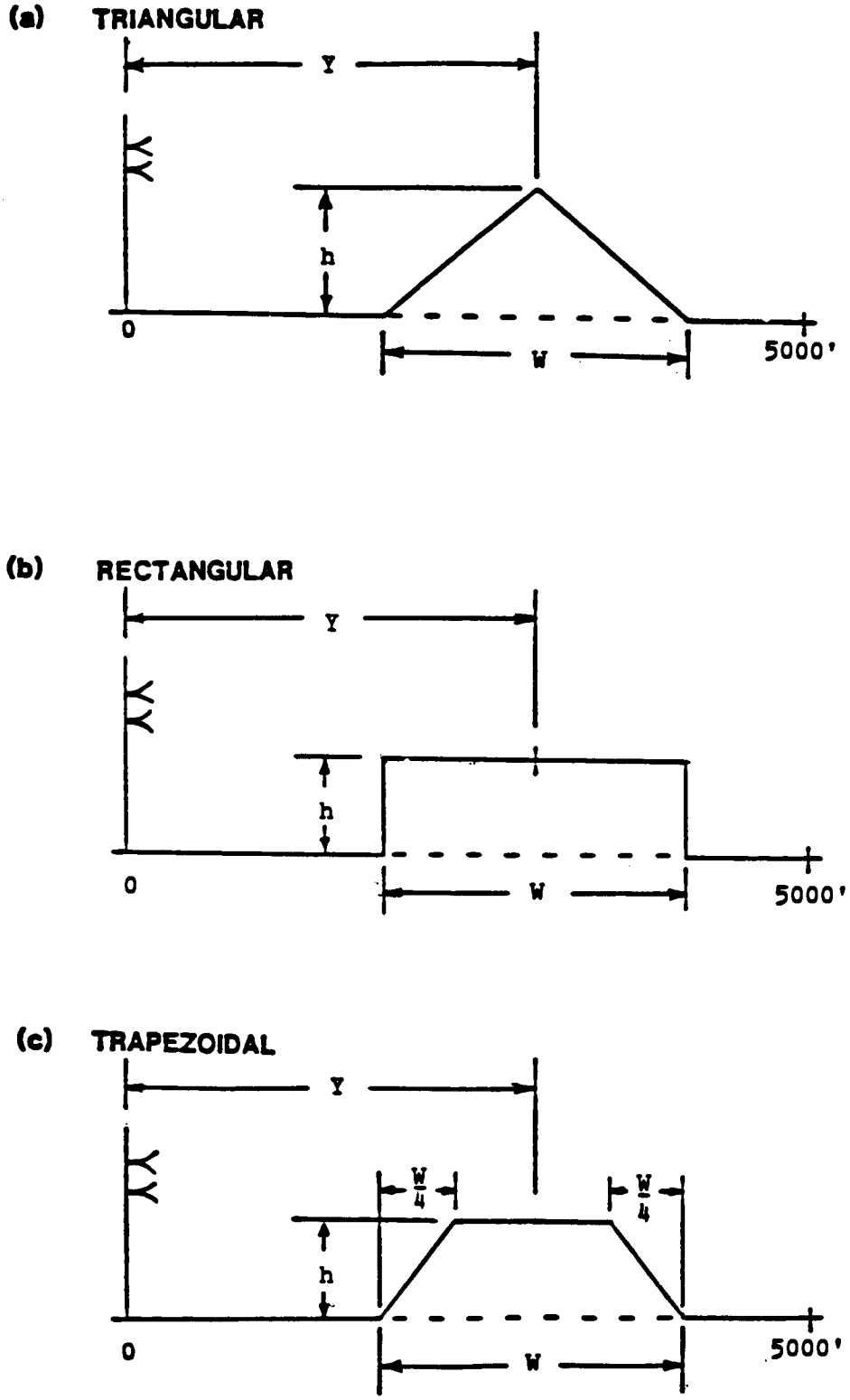

Figure 2-234. Profiles of the shapes of irregular terrain considered initially for sensitivity analysis.

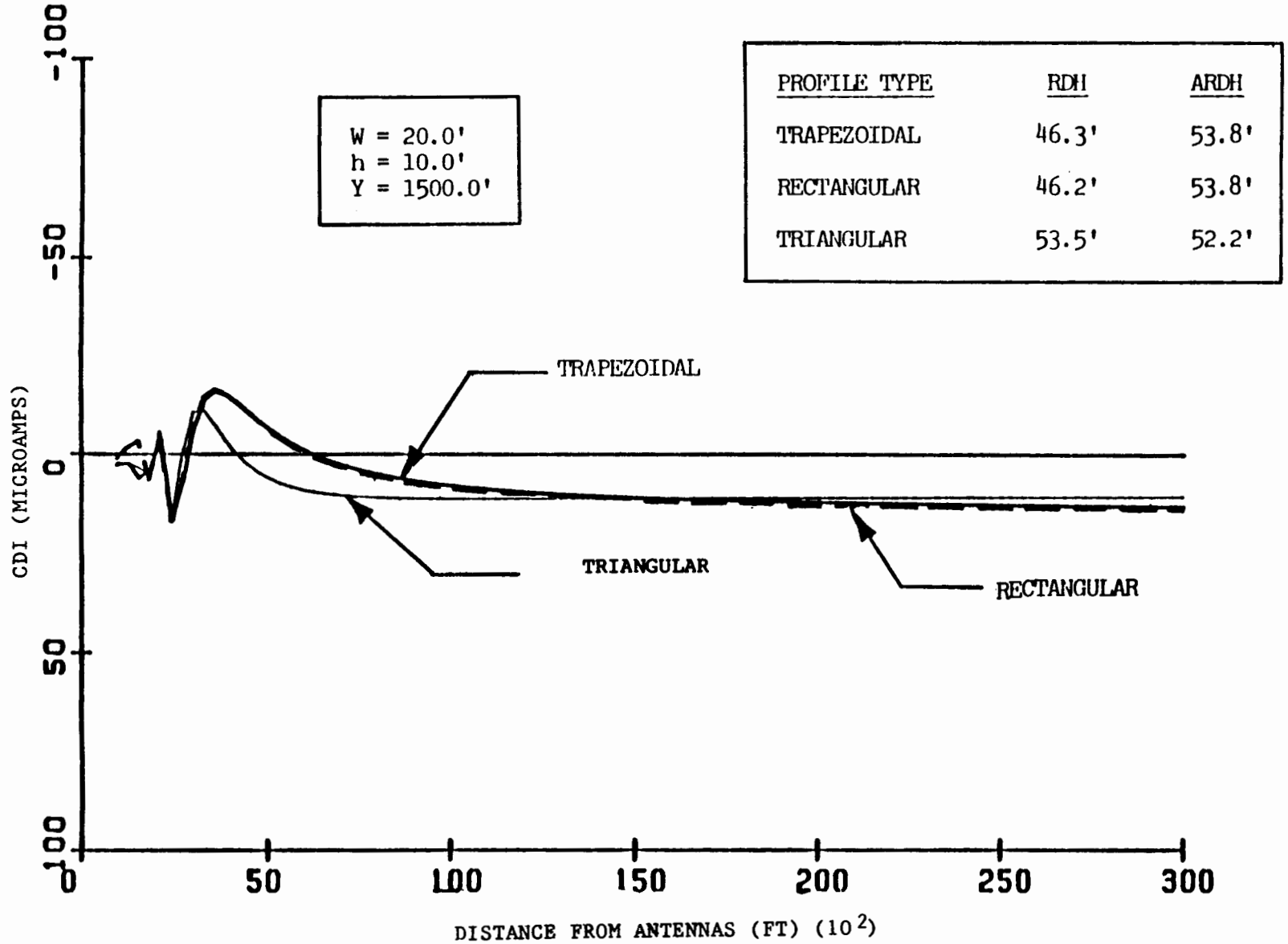

Figure 2-235. Simulated differential amplifier recordings for the shapes of irregular terrain shown in figure 2-234 and of the dimensions shown, for a null-reference glide slope.

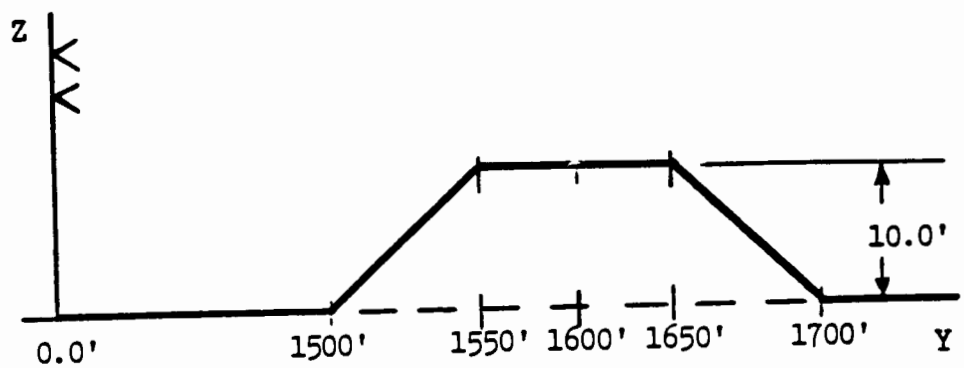

X(ft)	Y(ft)	Z(ft)
0.0	0.0	0.0
0.0	1500	0.0
0.0	1550	10.0
0.0	1600	10.0
0.0	1650	10.0
0.0	1700	0.0

Figure 2-236. Example of a terrain profile which is used as an input to the simulation.

```
*          RDH SENSITIVITY
SECTION        1
NO OF PTS      6     1
COORD.          0.0        0.0        0.0
                0.0     1400.0        0.0
                0.0     1450.0       10.0
                0.0     1550.0       10.0
                0.0     1600.0        0.0
                0.0     5000.0       10.0
SECTION        2
THEODOLITE              400.00       0.0        0.00       3.00       0.7
SECTION        3
ANT DATA       2        331.1        0.400      0.300      0.900
POSITION       1        400.333      0.000     14.13
                0.0       0.0         1.0        0.0        0.0        0.0
POSITION       2        399.667      0.000     28.26
               1.0        0.0        0.0        0.0        0.0        0.0
SECTION        4
PATTERN        3   21     1           0.0    25300.0       3.0
                                      0.0     4500.0
SECTION        5
OUTPUT         3    1     2       30000.0       0.0      100.0     -100.000000000000
...
```

Figure 2-237. Example of an input for the mathematical model OUGS.

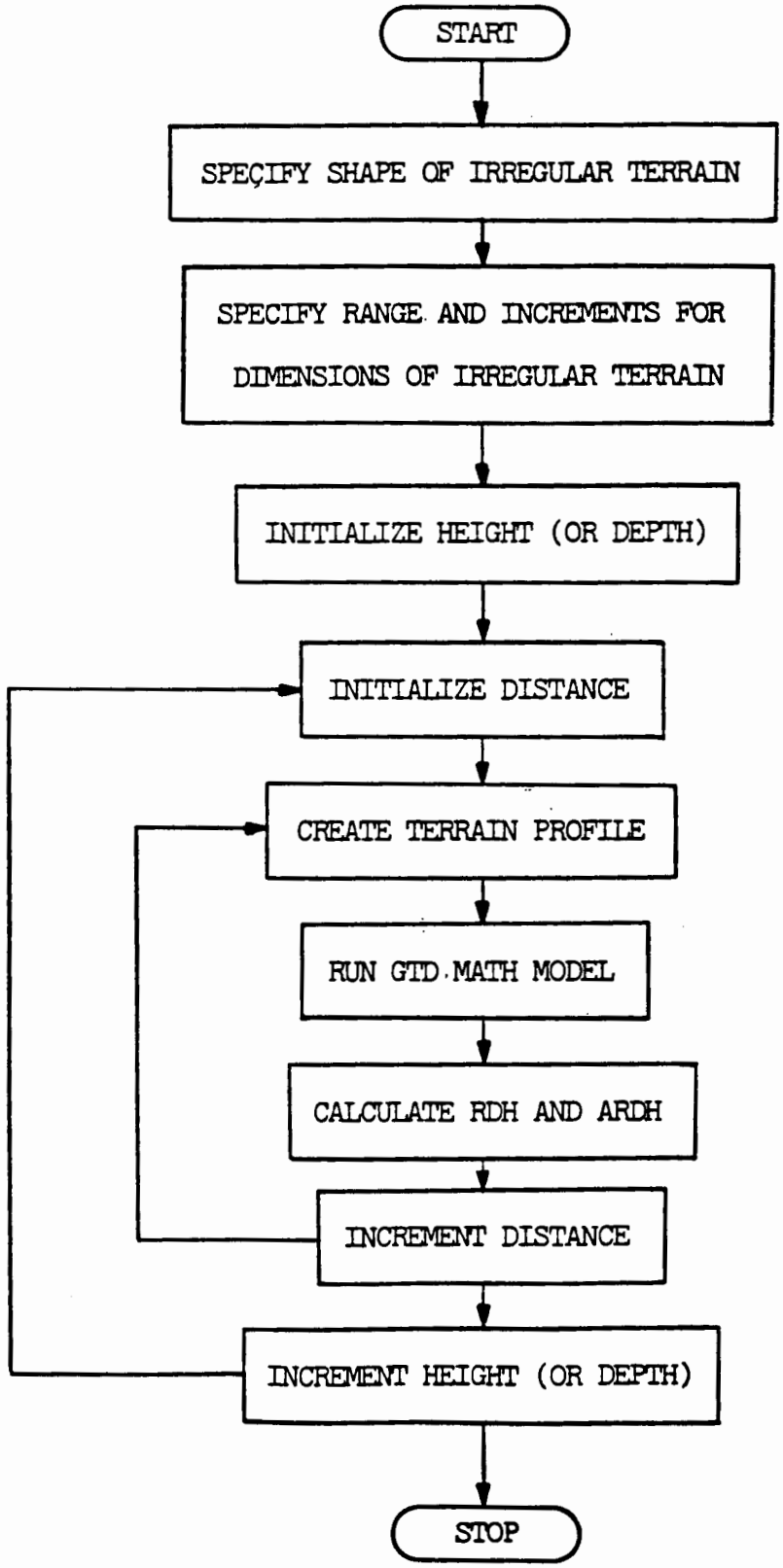

Figure 2-238. Flow chart of the procedure used in the sensitivity analysis.

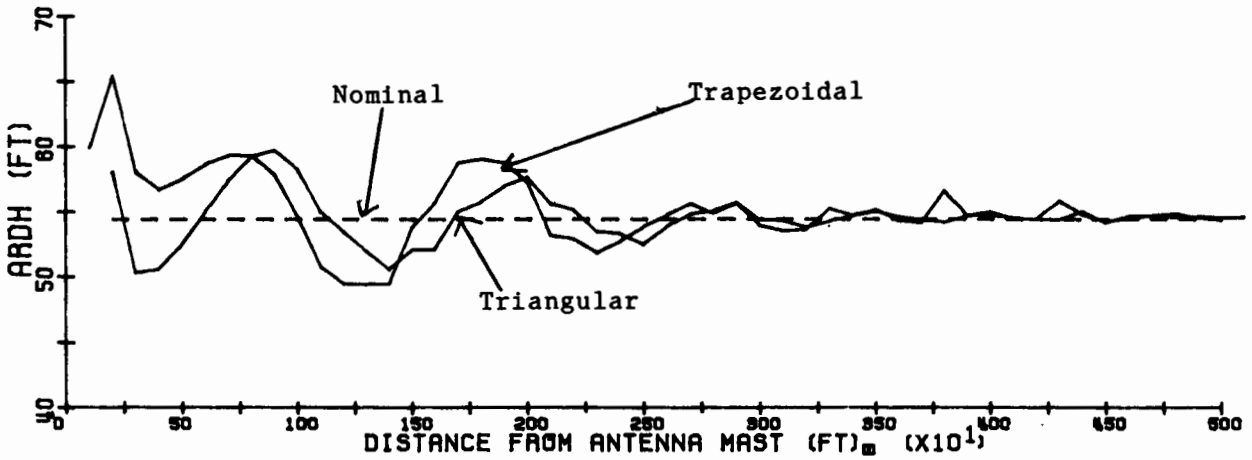

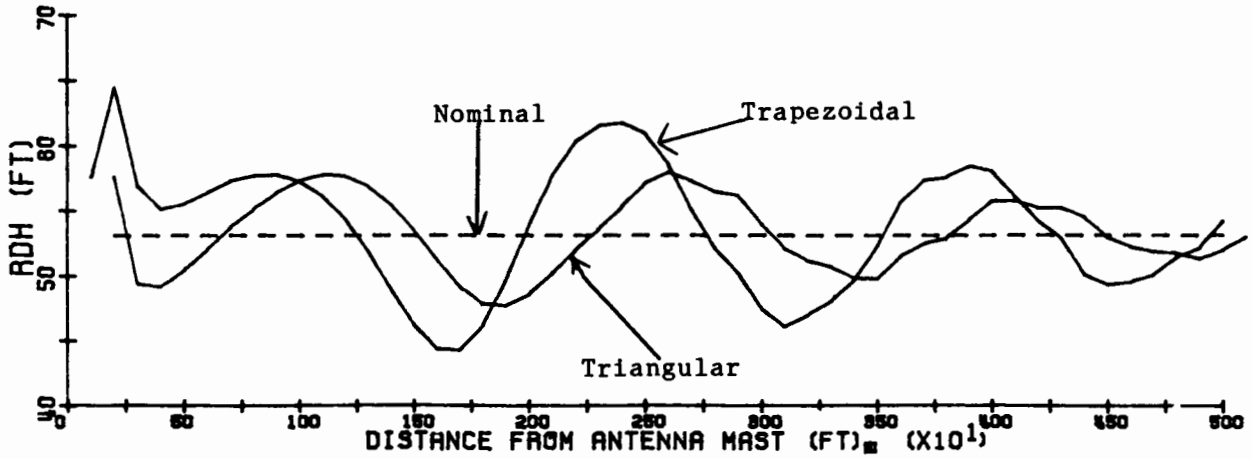

Figure 2-239. Comparison of sensitivity curves for triangular- and trapezoidal-shaped profiles of irregular terrain.

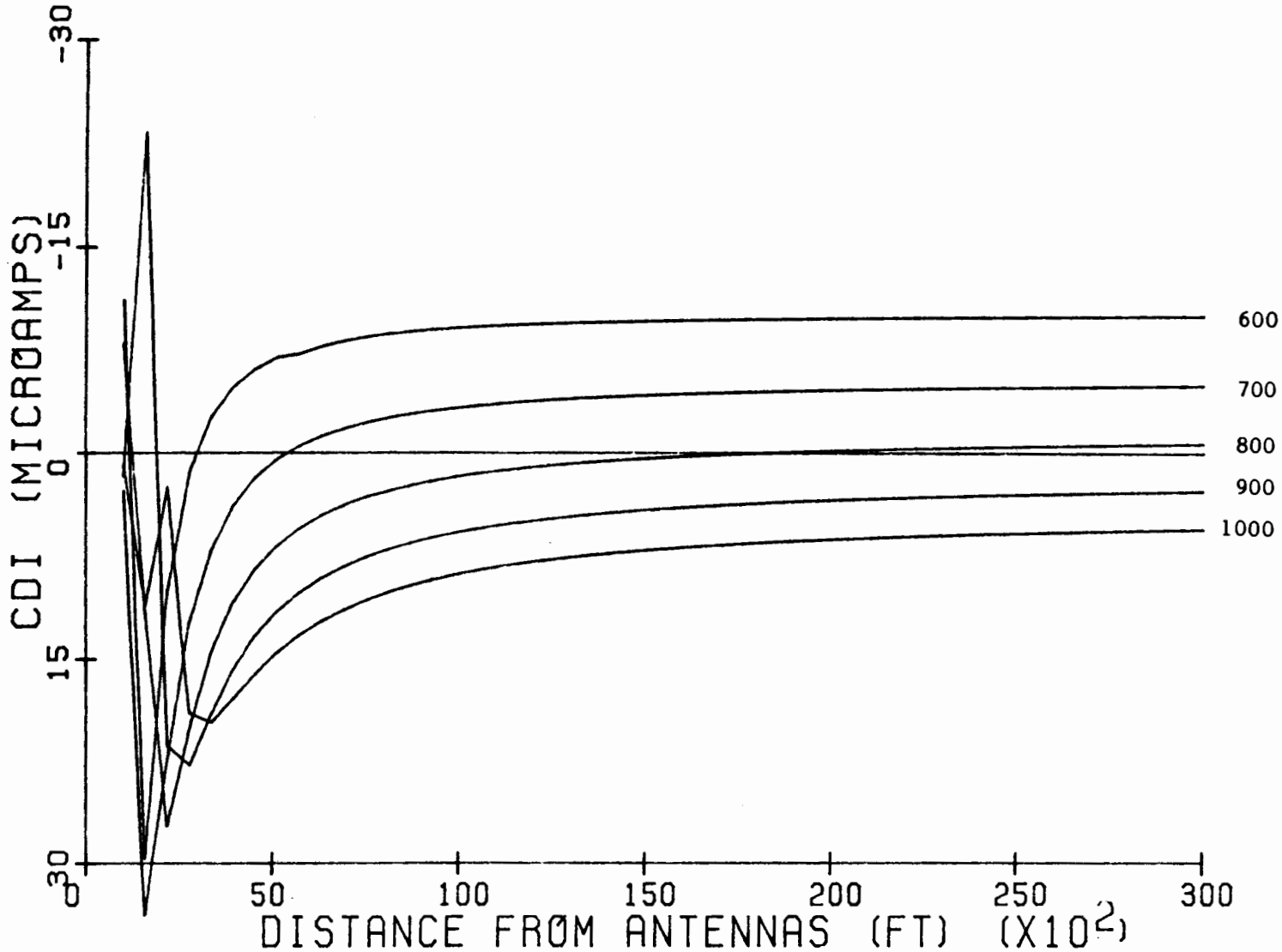

Figure 2-240. Simulated differential amplifier recordings for a triangular-shaped elevation of 10' duration and 10' high, located at 600' to 1000' from the antenna mast.

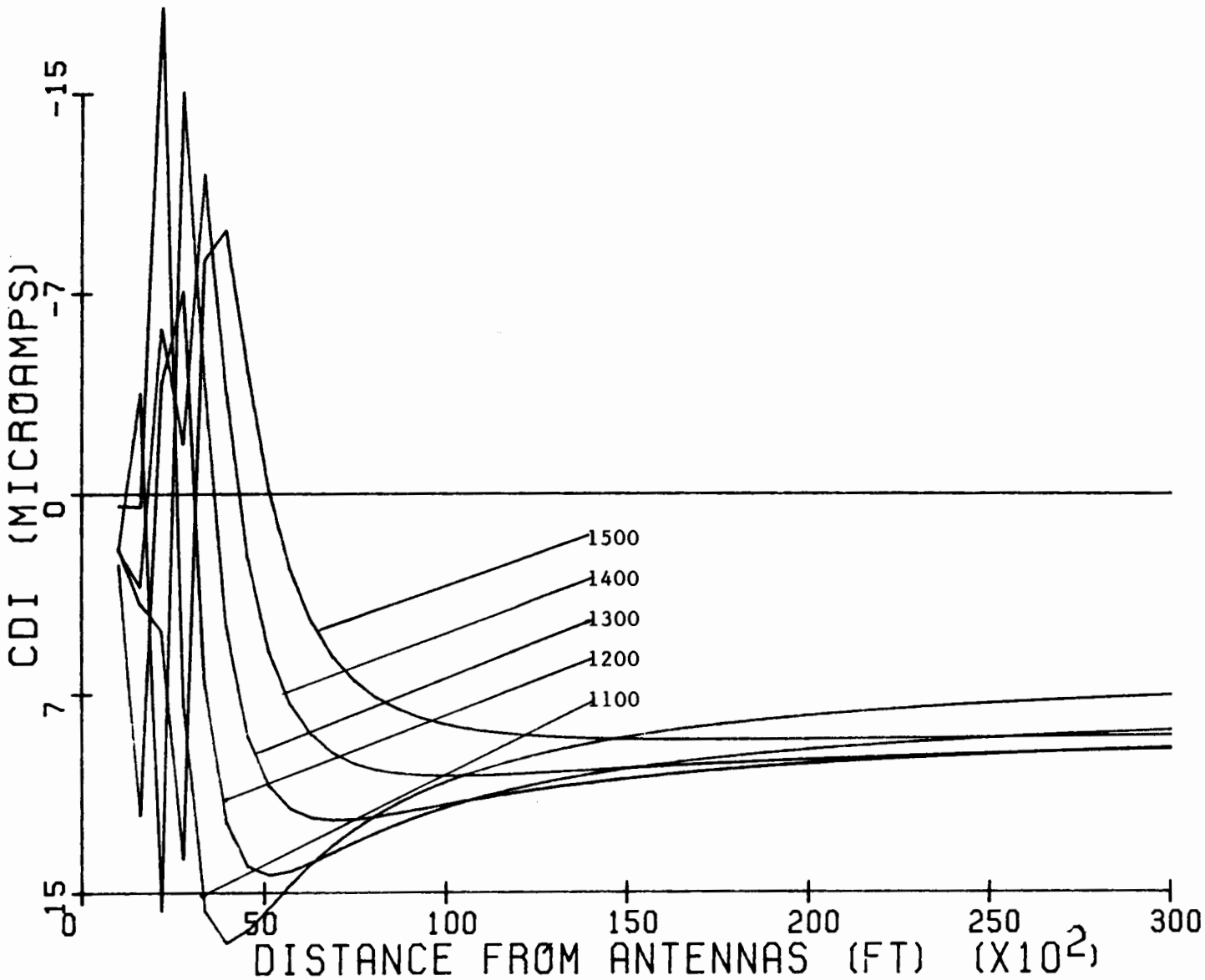

Figure 2-241. Simulated differential amplifier recordings for a triangular-shaped elevation of 10' duration and 10' high, located at 1100' to 1500' from the antenna mast.

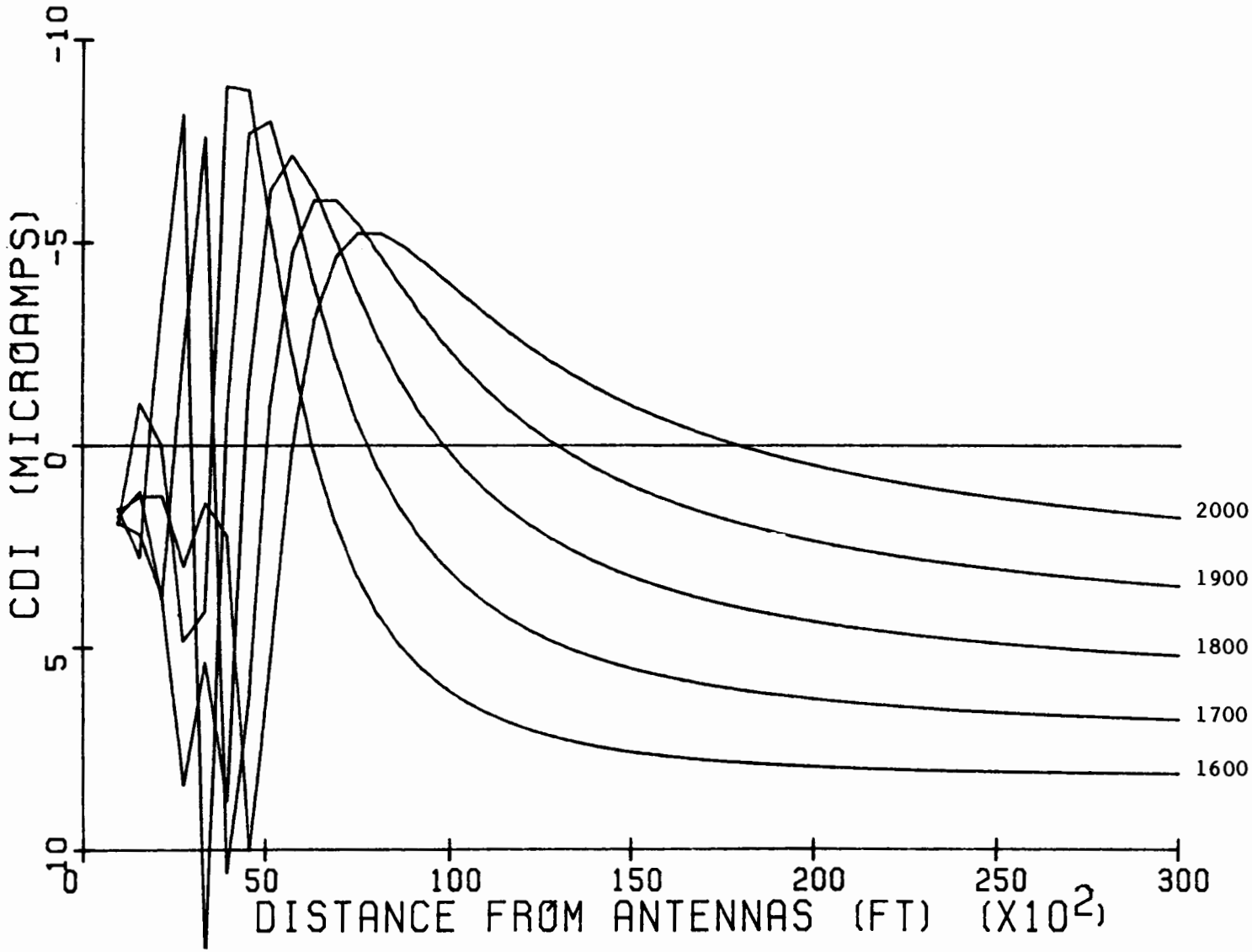

Figure 2-242. Simulated differential amplifier recordings for a triangular-shaped elevation of 10' duration and 10' high, located at 1600' to 2000' from the antenna mast.

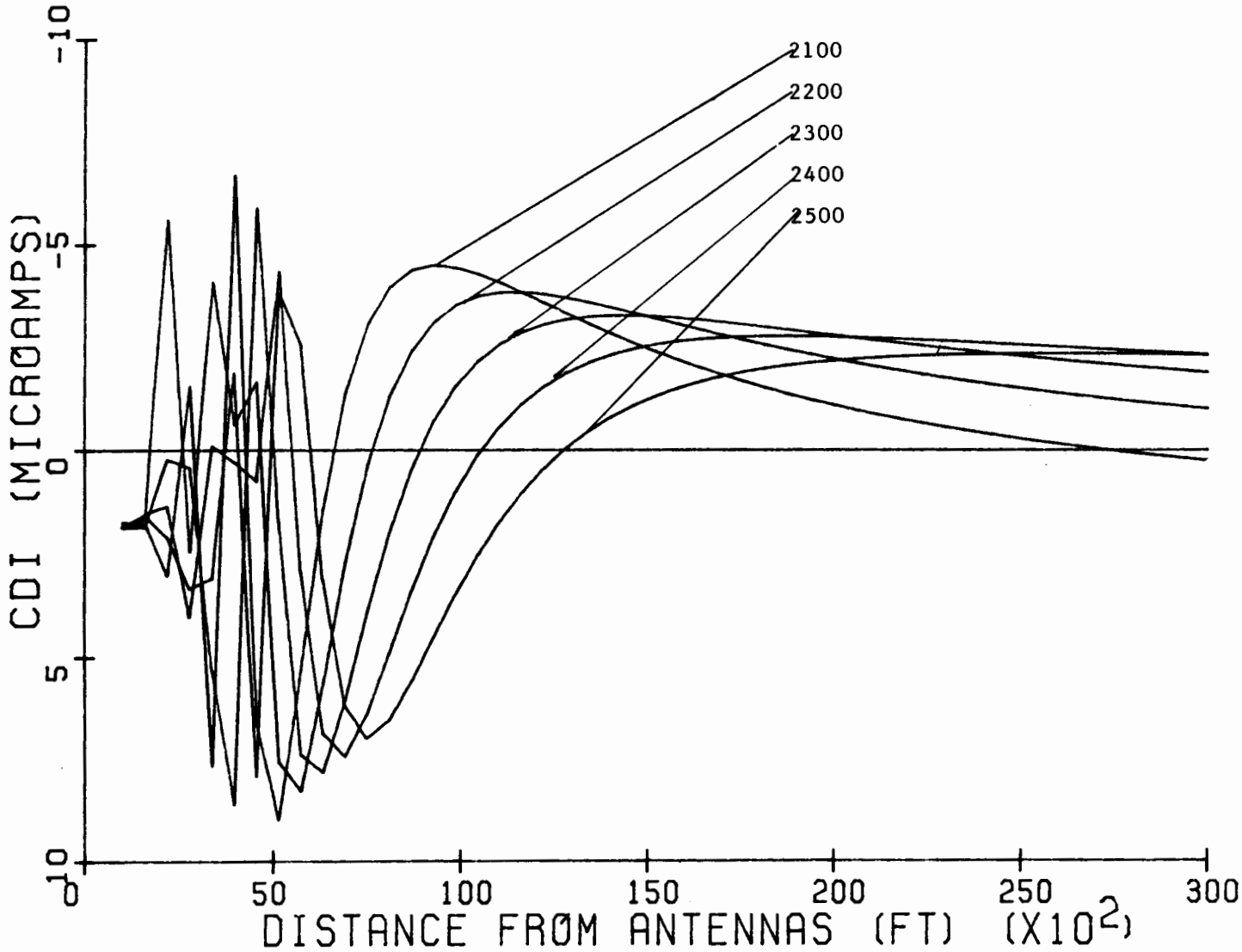

Figure 2-243. Simulated differential amplifier recordings for a triangular-shaped elevation of 10' duration and 10' high, located at 2100' to 2500' from the antenna mast.

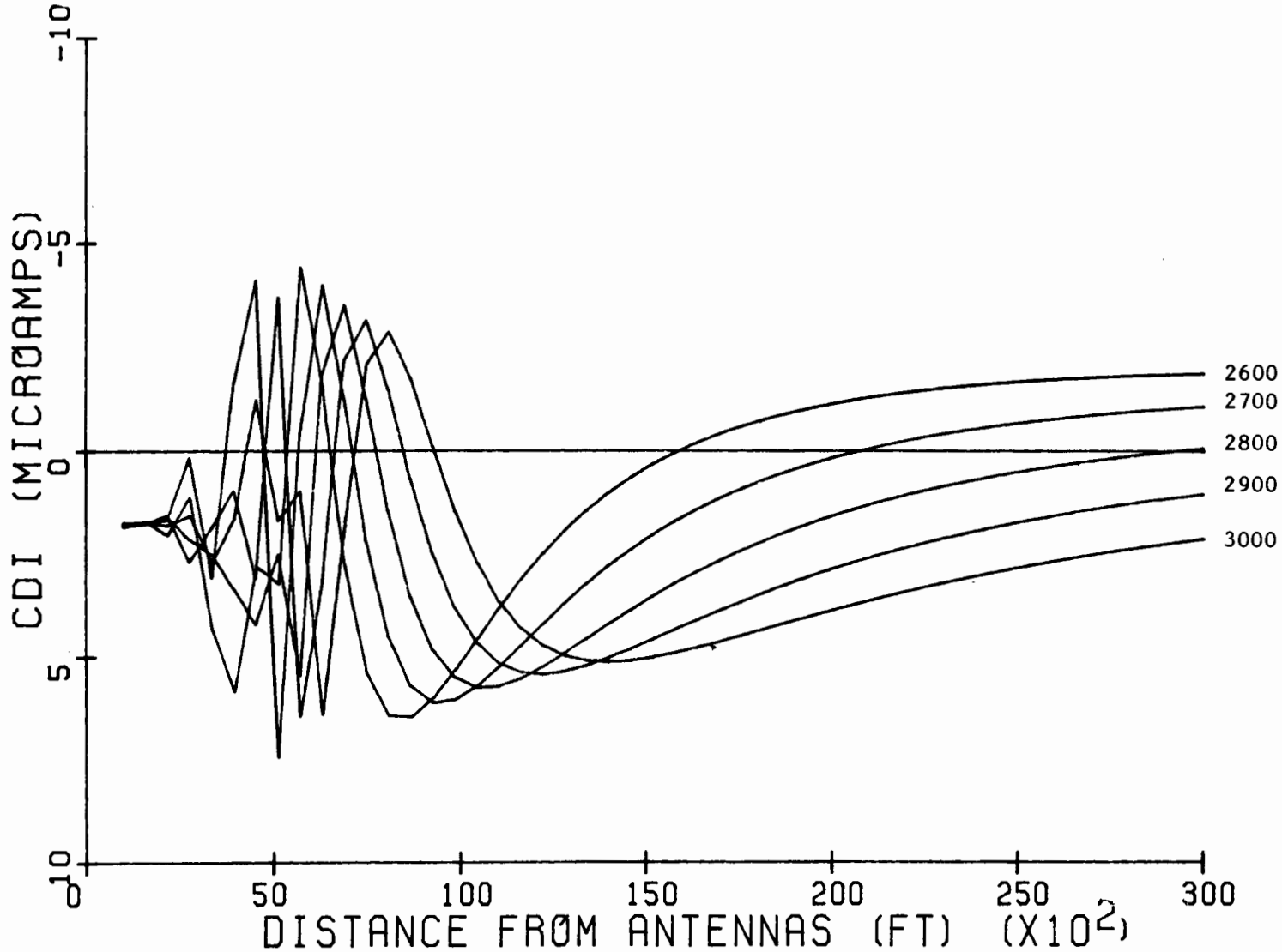

Figure 2-244. Simulated differential amplifier recordings for a triangular-shaped elevation of 10' duration and 10' high, located at 2600' to 3000' from the antenna mast.

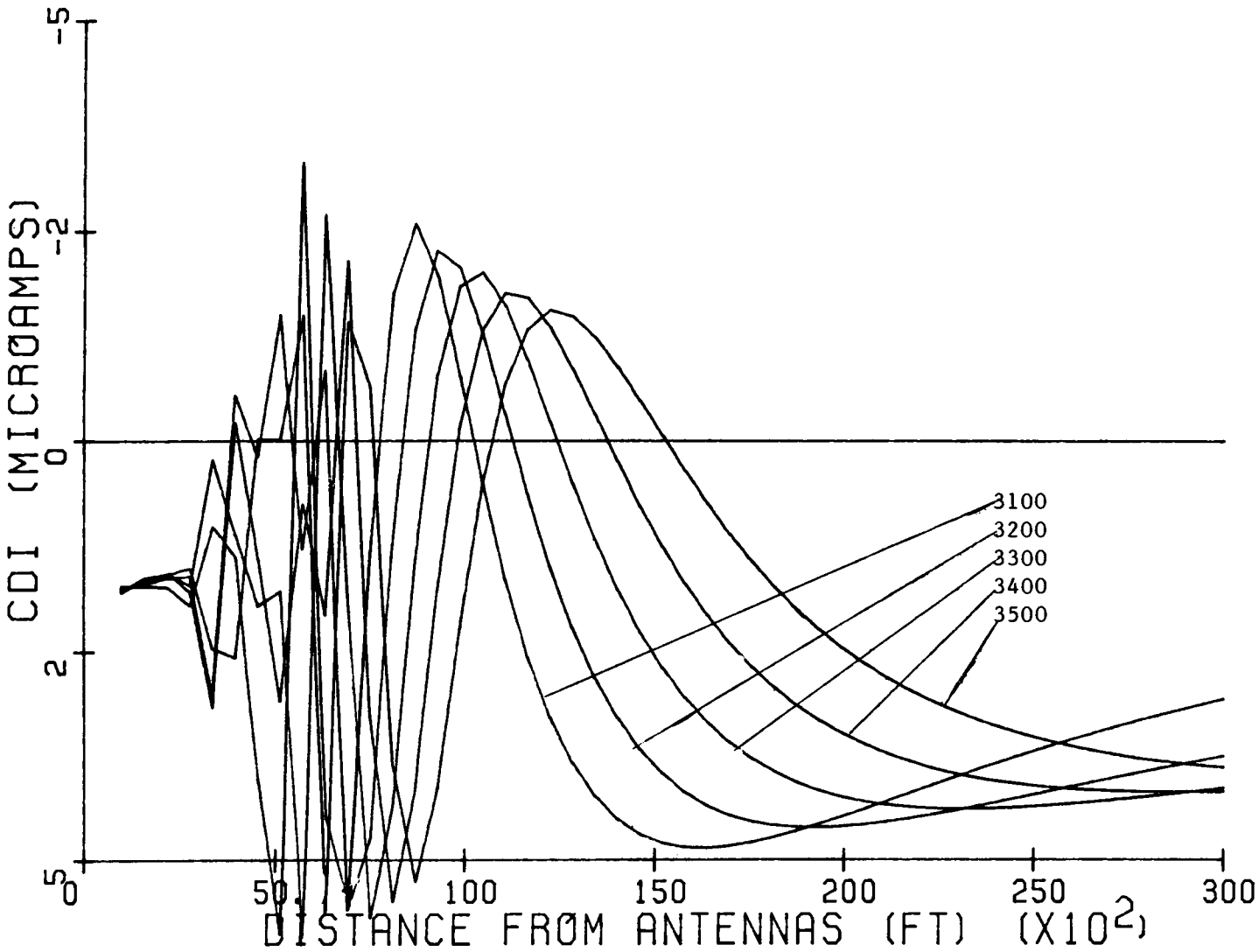

Figure 2-245. Simulated differential amplifier recordings for a triangular-shaped elevation of 10' duration and 10' high, located at 3100' to 3500' from the antenna mast.

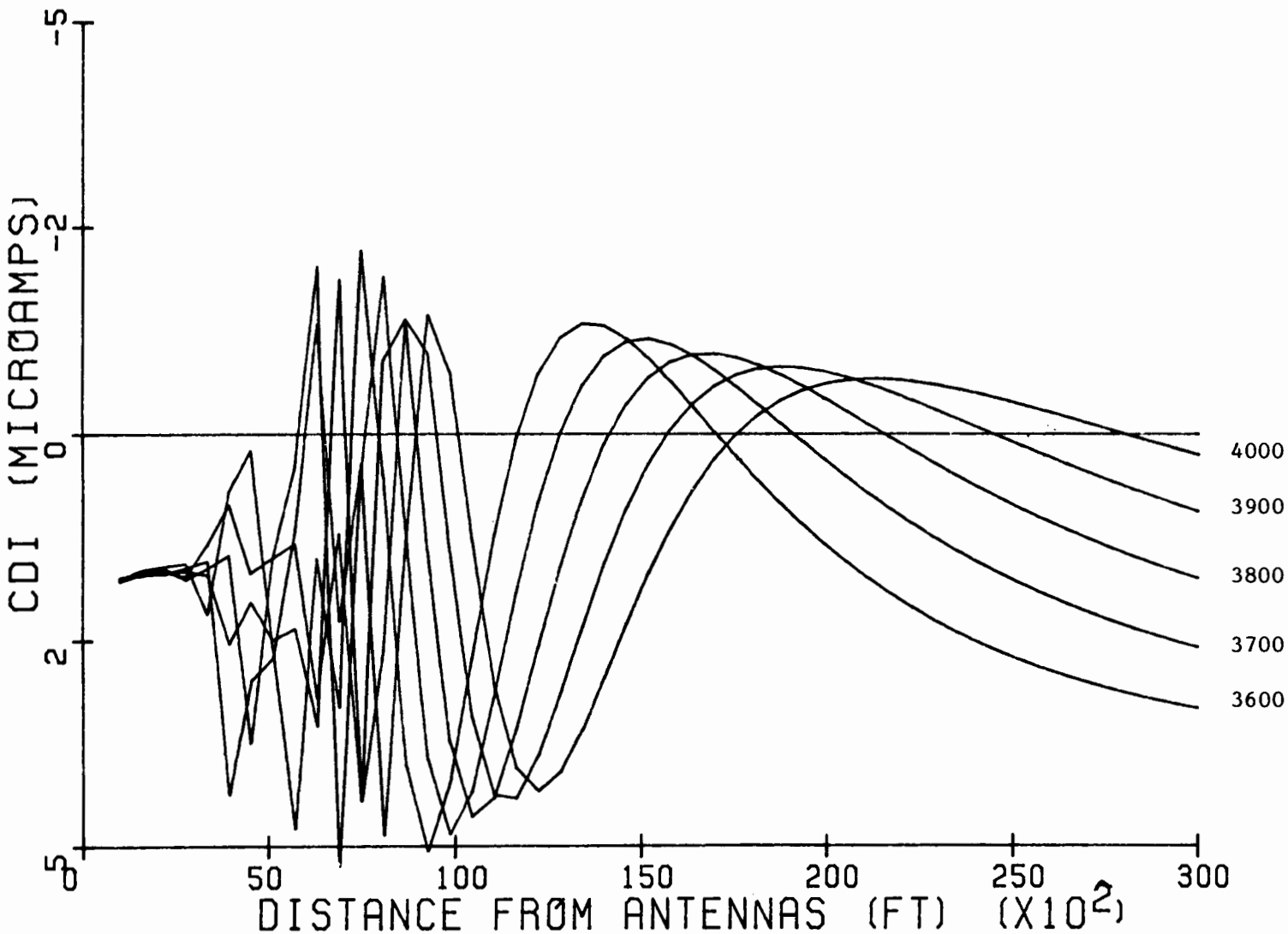

Figure 2-246. Simulated differential amplifier recordings for a triangular-shaped elevation of 10' duration and 10' high, located at 3600' to 4000' from the antenna mast.

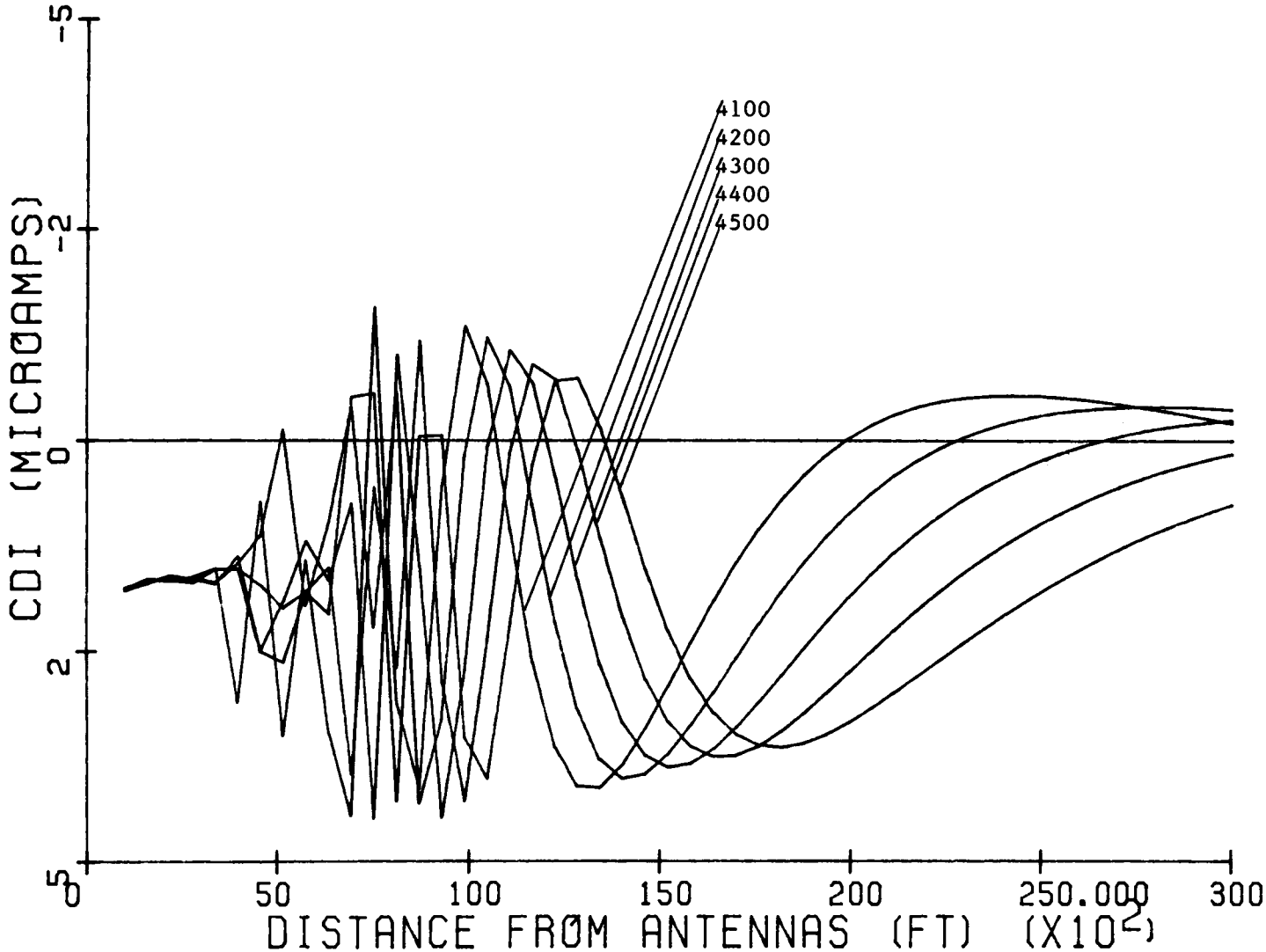

Figure 2-247. Simulated differential amplifier recordings for a triangular-shaped elevation of 10' duration and 10' high, located at 4100' to 4500' from the antenna mast.

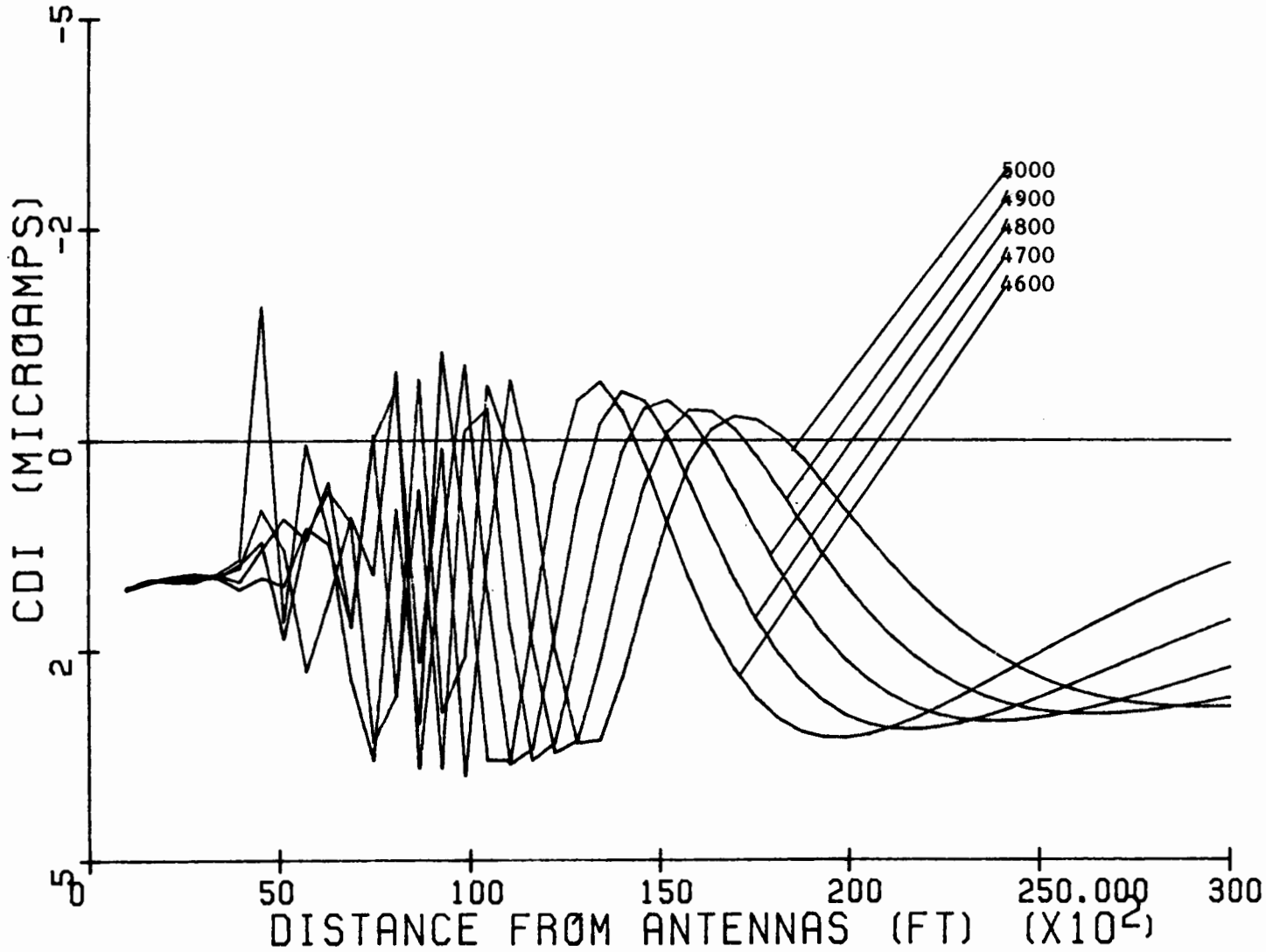

Figure 2-248. Simulated differential amplifier recordings for a triangular-shaped elevation of 10' duration and 10' high, located at 4600' to 5000' from the antenna mast.

RDH AND ARDH FOR VARYING ANTENNA BACKSETS

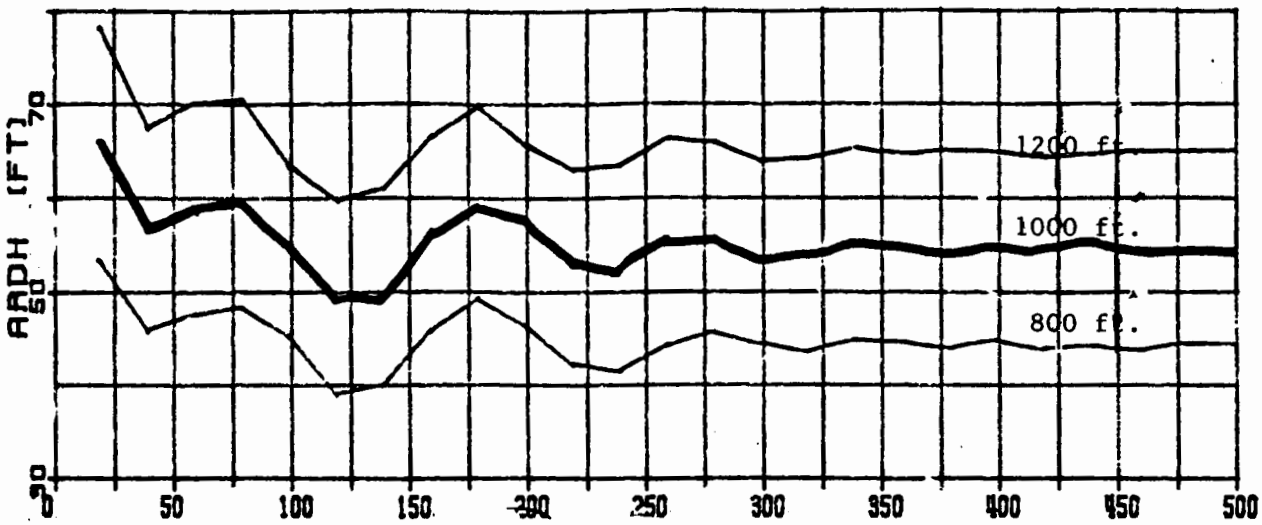

DISTANCE FROM ANTENNAS (FT) (X10)

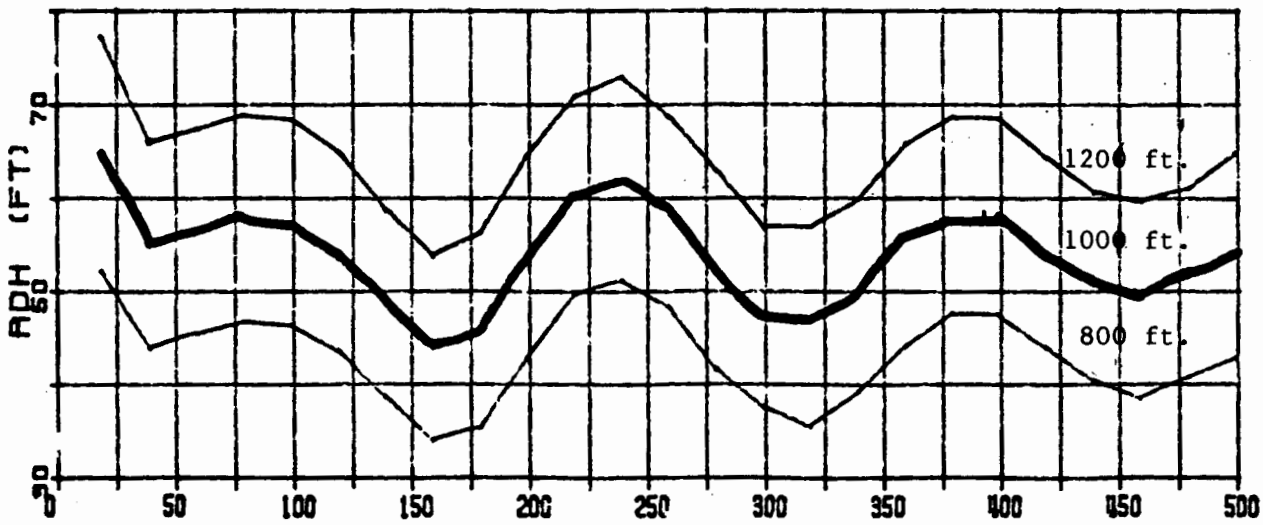

DISTANCE FROM ANTENNAS (FT) (X10)

Figure 2-249. Comparison of sensitivity curves produced by a trapezoidal-shaped elevation, 10' in duration and 10' high, for distances of the antenna mast along centerline from threshold of 800', 1000', an 1200'.

RDH AND ARDH FOR VARYING PATH ANGLE

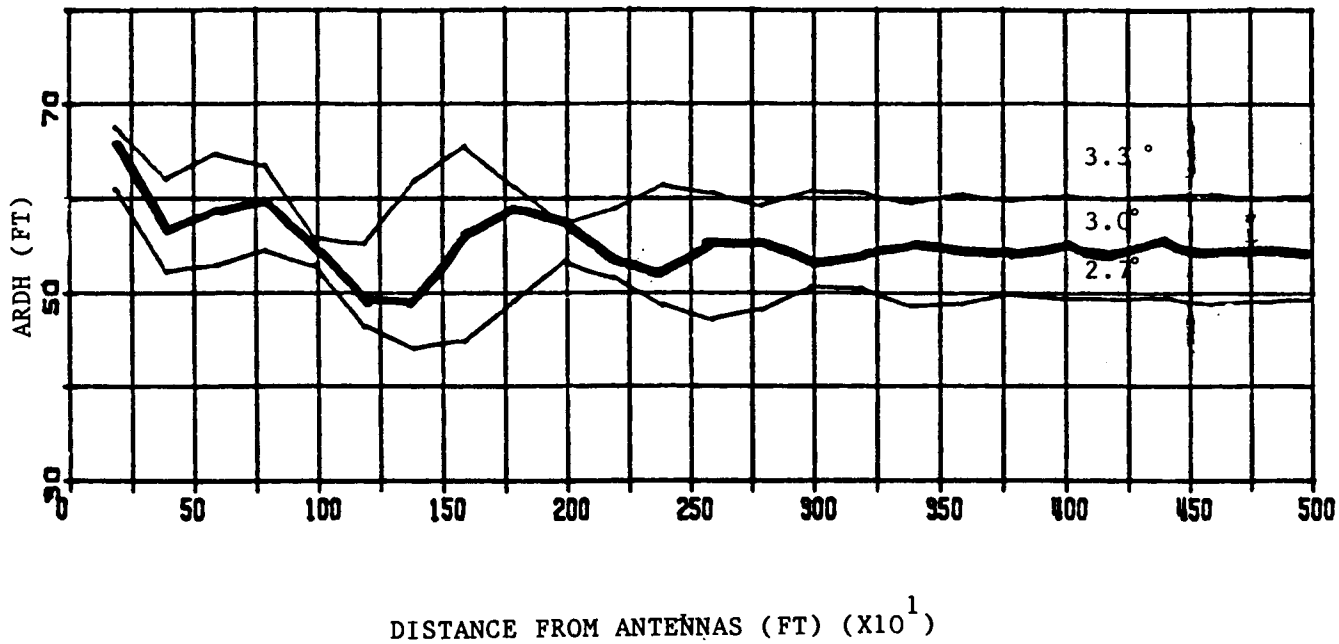

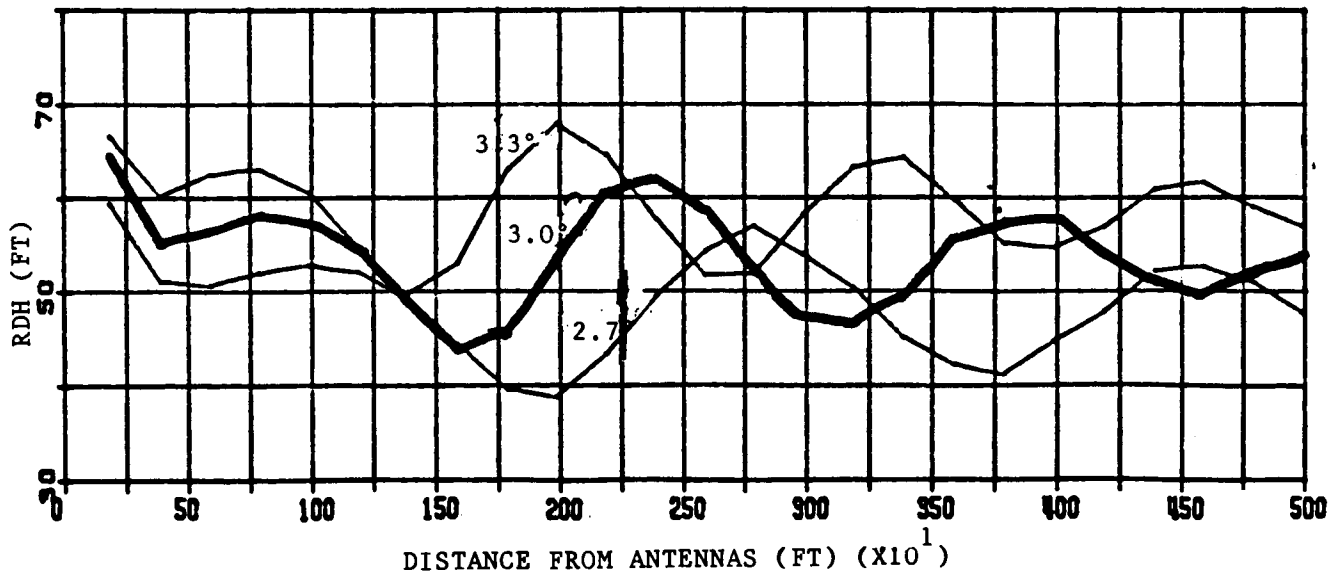

Figure 2-250. Comparison of sensitivity curves produced by a trapezoidal-shaped elevation, 10' in duration and 10' high, for path angles of 2.7, 3.0, and 3.3 degrees.

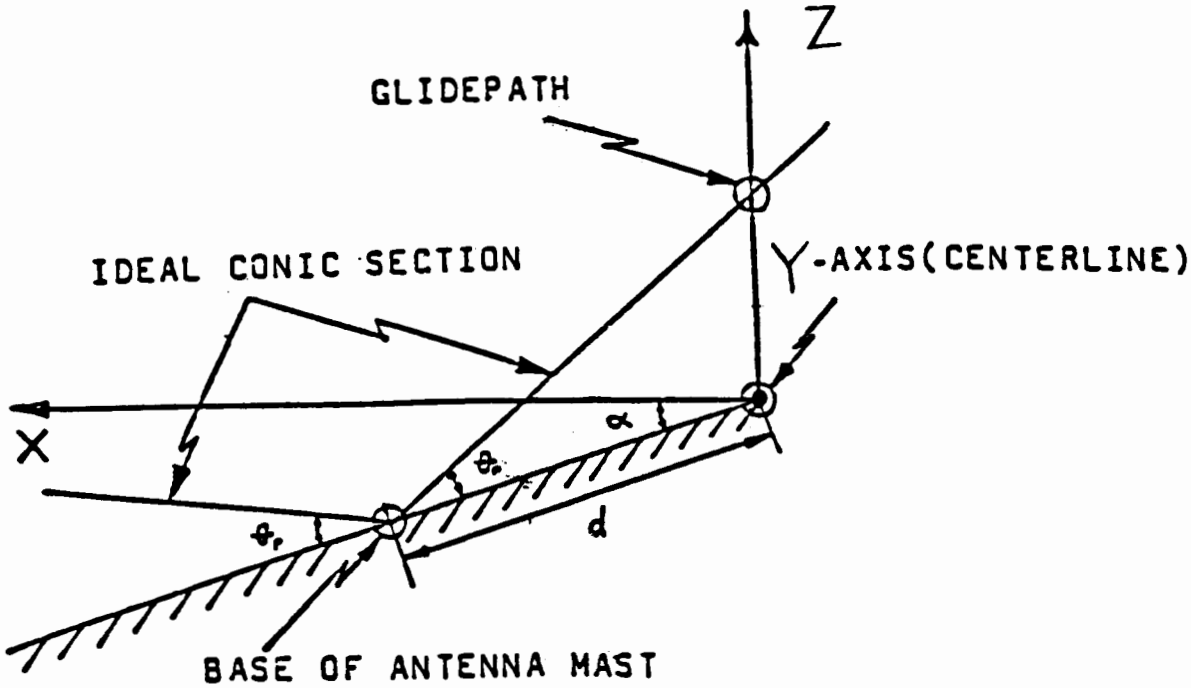

Figure 2-251. Illustration of the uniform, laterally sloping terrain in the plane containing the glide slope antenna mast.

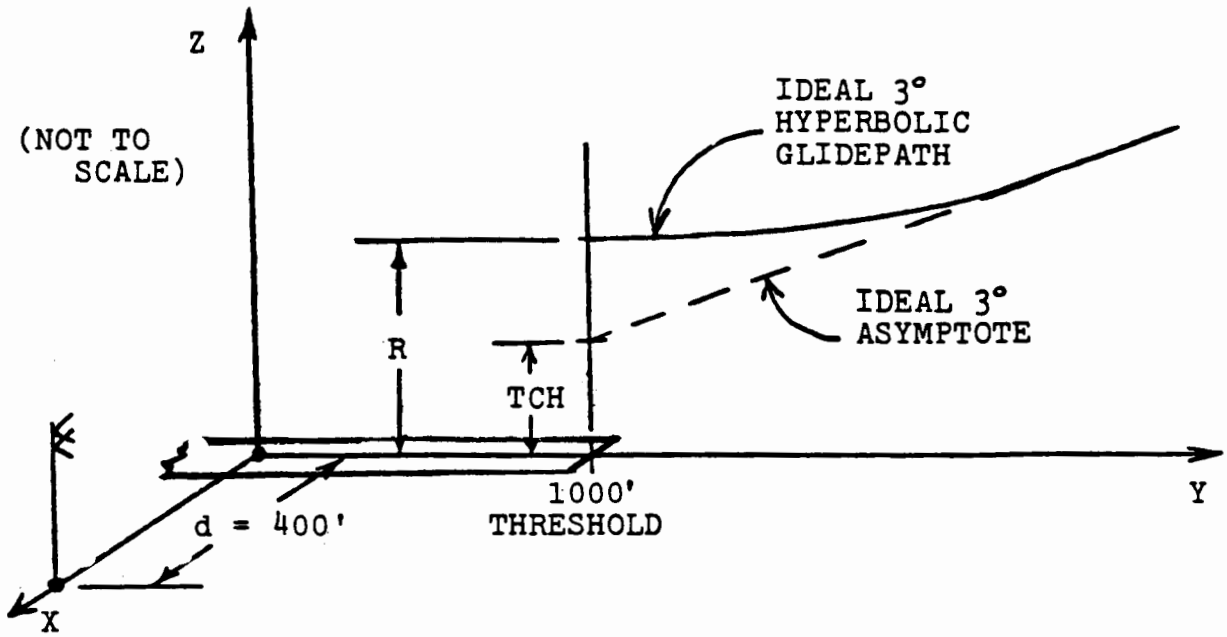

R = 56.4′

TCH = 52.4′

RDH = 53.1′

ARDH = 54.4′

Figure 2-252. Comparison of various heights at threshold for an ideal glide slope site, with the antennas located as shown, for a path angle of 3.0 degrees.

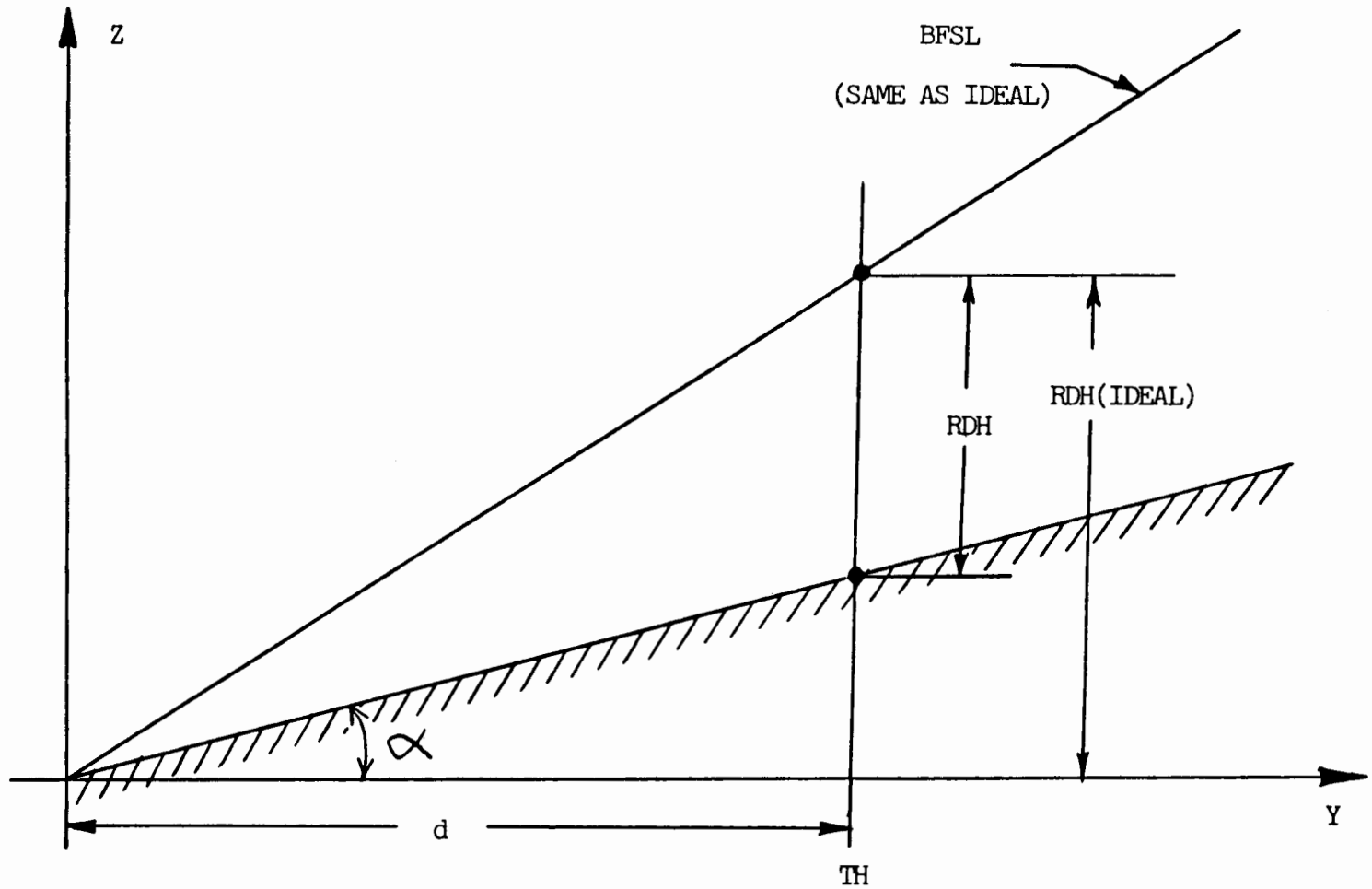

$$RDH = RDH(IDEAL) - d \tan \alpha$$

Figure 2-253. Illustration of the effects of uniform, longitudinally upsloping terrain on the reference datum heights.

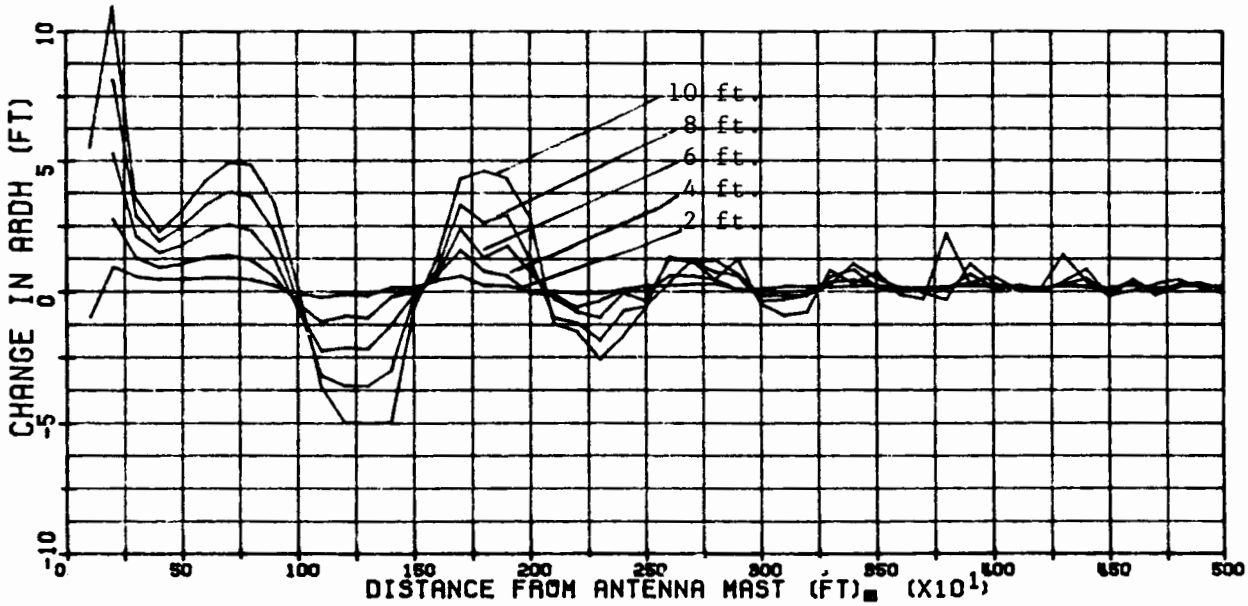

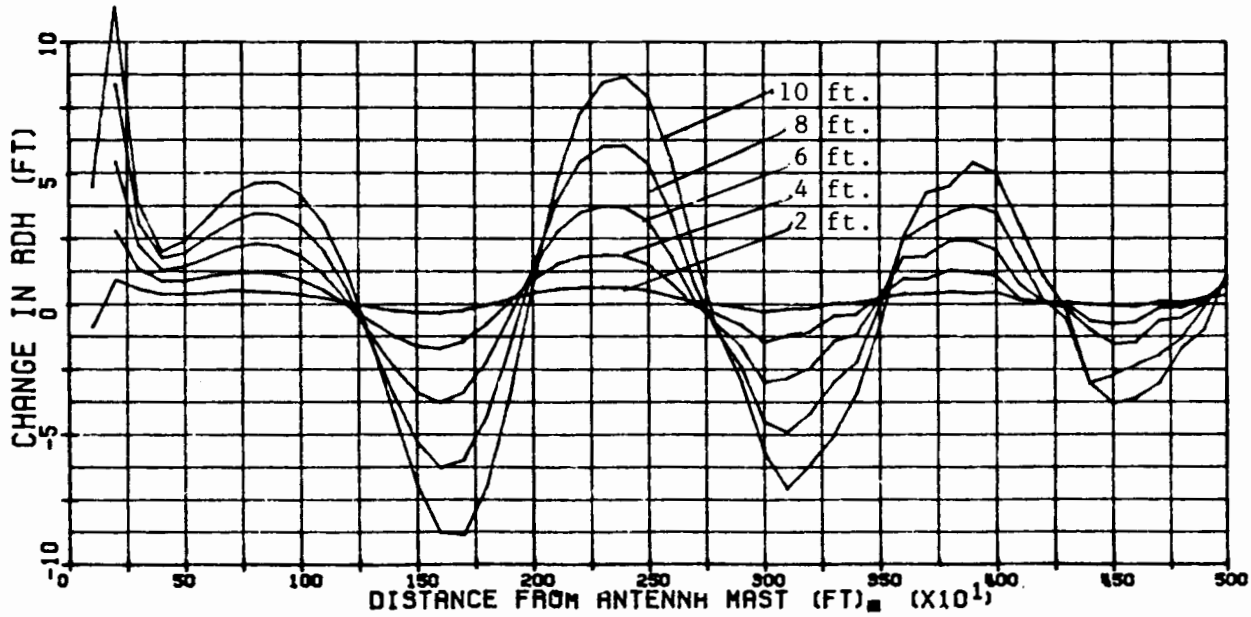

Figure 2-254. Sensitivity curves for deviation of RDH and ARDH from the ideal values, for an elevation with a duration of 10' and a height of 2, 4, 6, 8, and 10'.

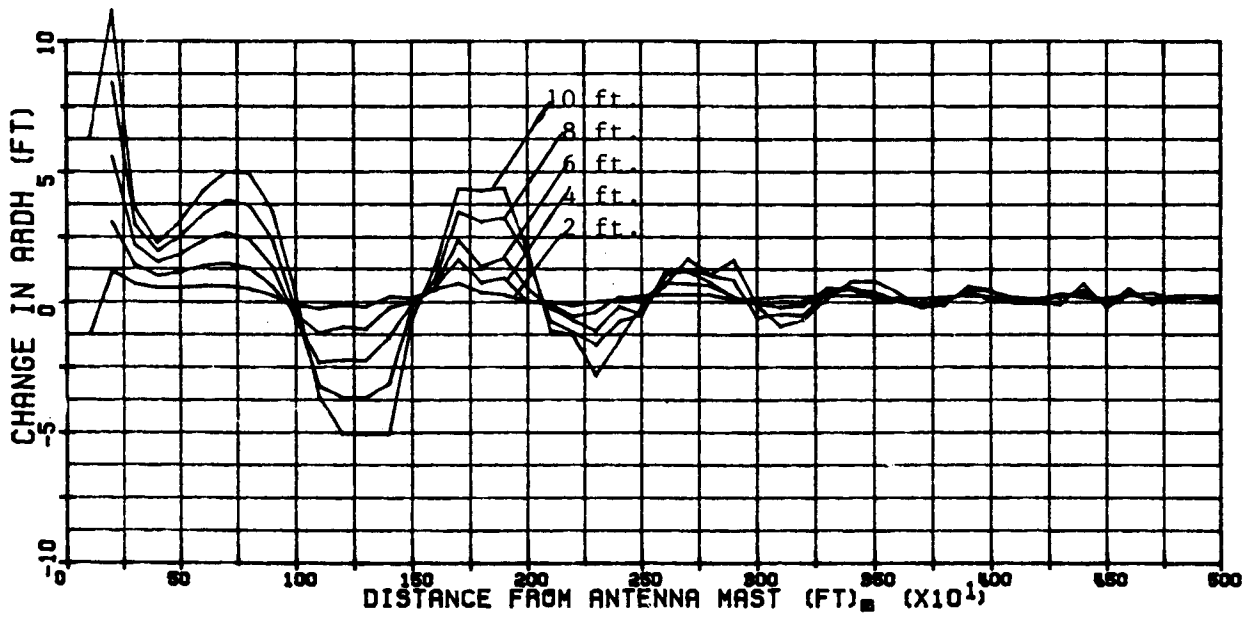

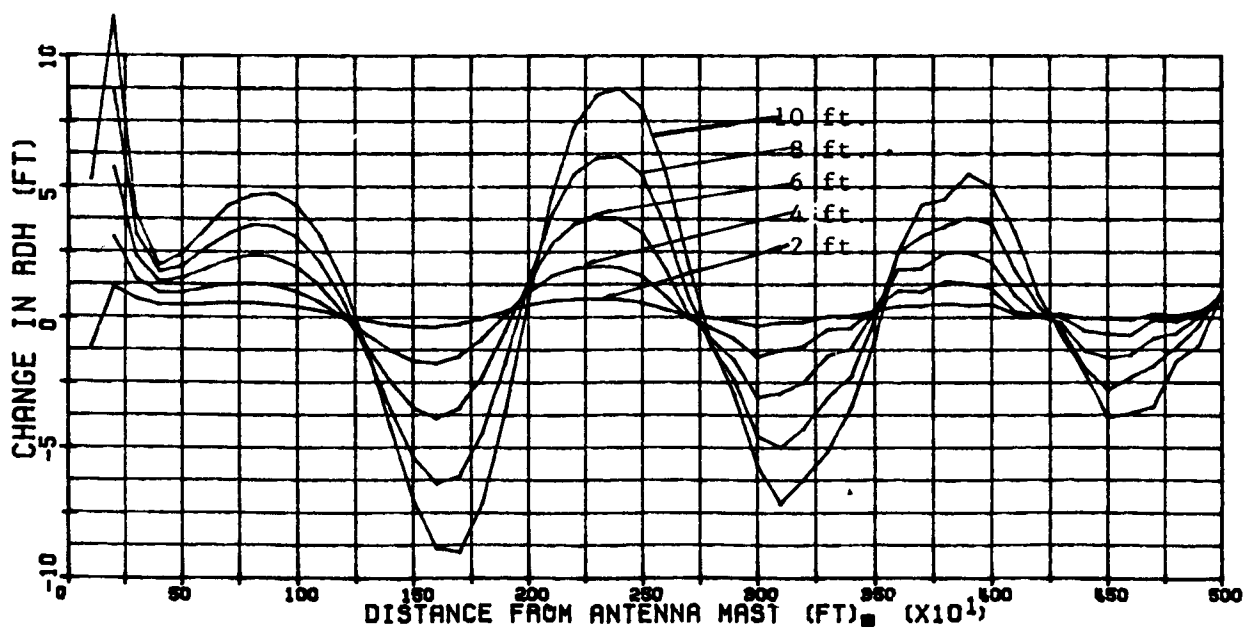

Figure 2-255. Sensitivity curves for deviation of RDH and ARDH from the ideal values, for an elevation with a duration of 20' and a height of 2, 4, 6, 8, and 10'.

CHANGE FROM IDEAL RDH AND ARDH

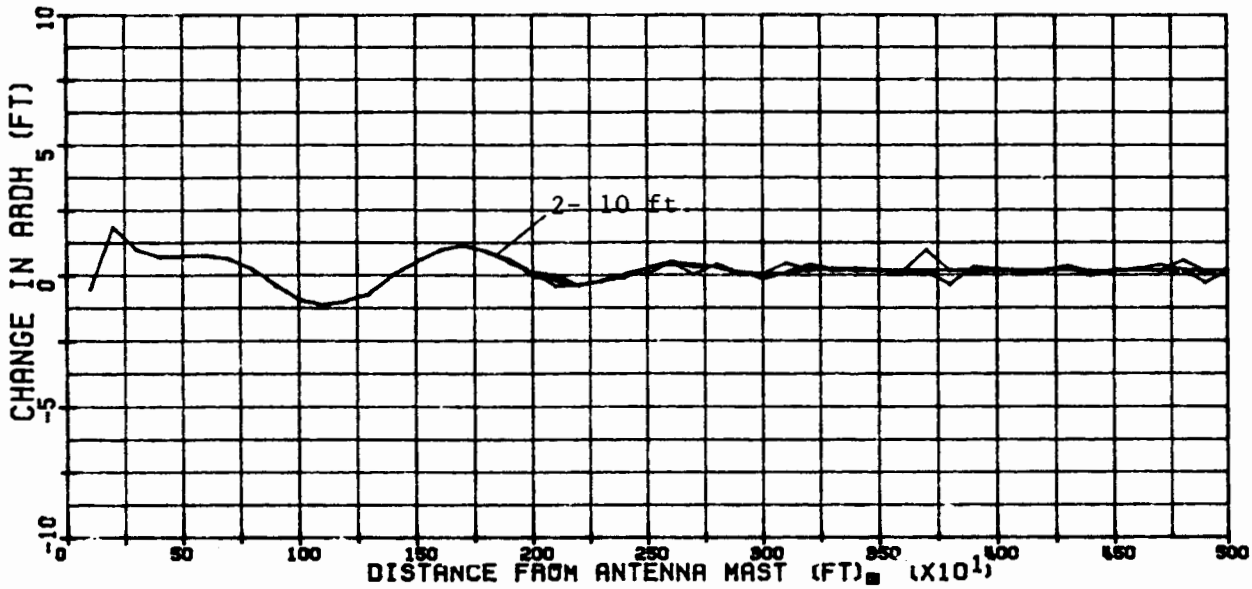

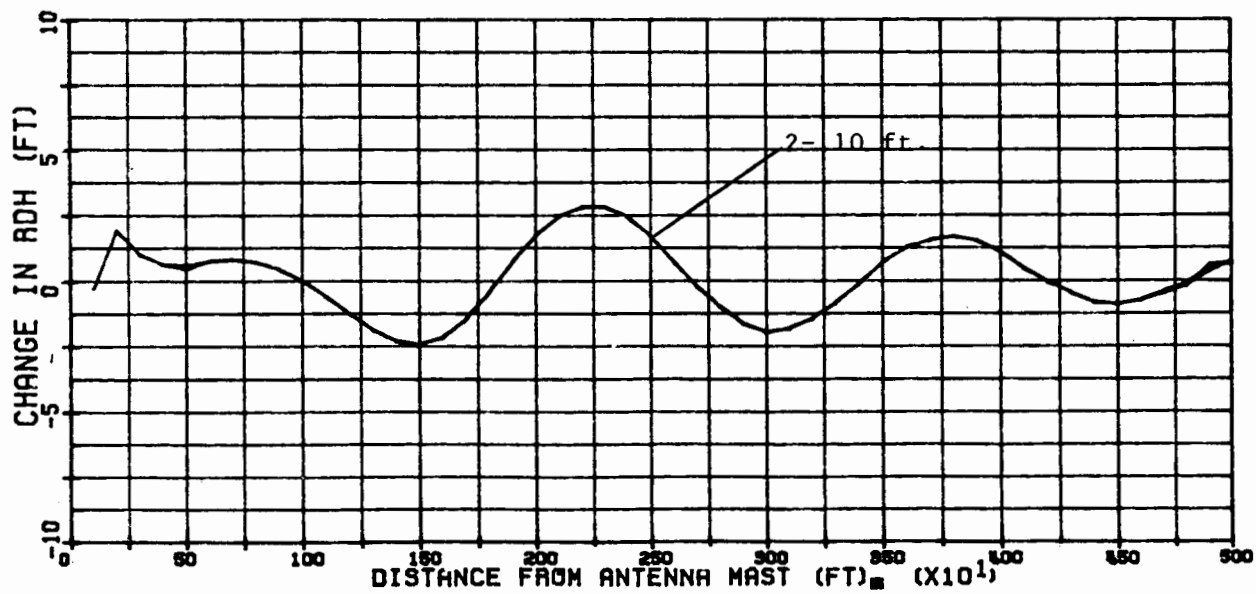

Figure 2-256. Sensitivity curves for deviation of RDH and ARDH from the ideal values, for a depression with a duration of 10' and a height of 2, 4, 6, 8, and 10'.

CHANGE FROM IDEAL RDH AND ARDH

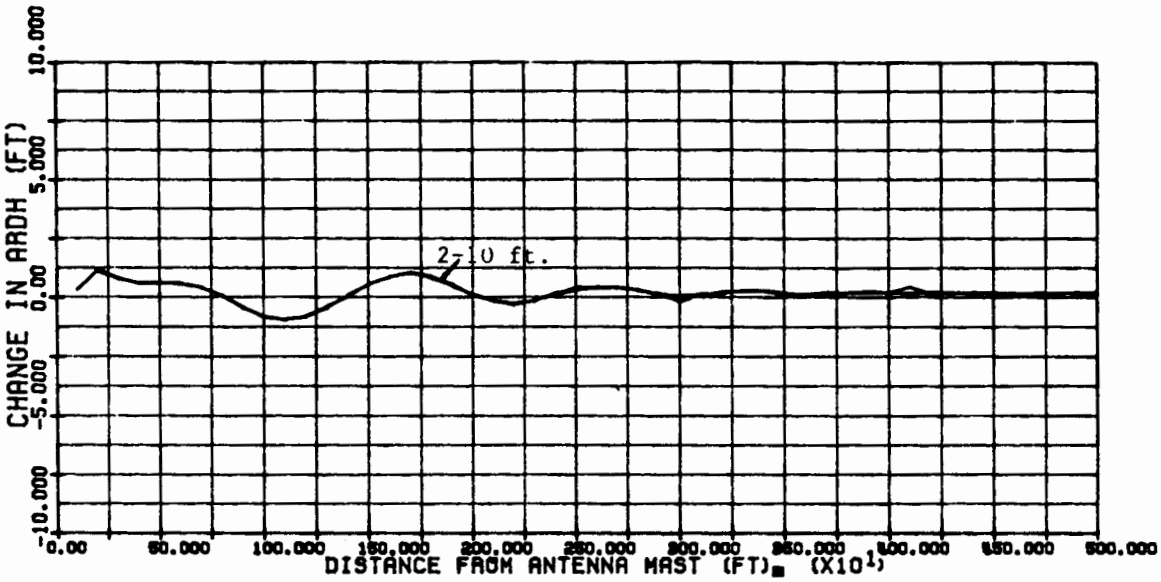

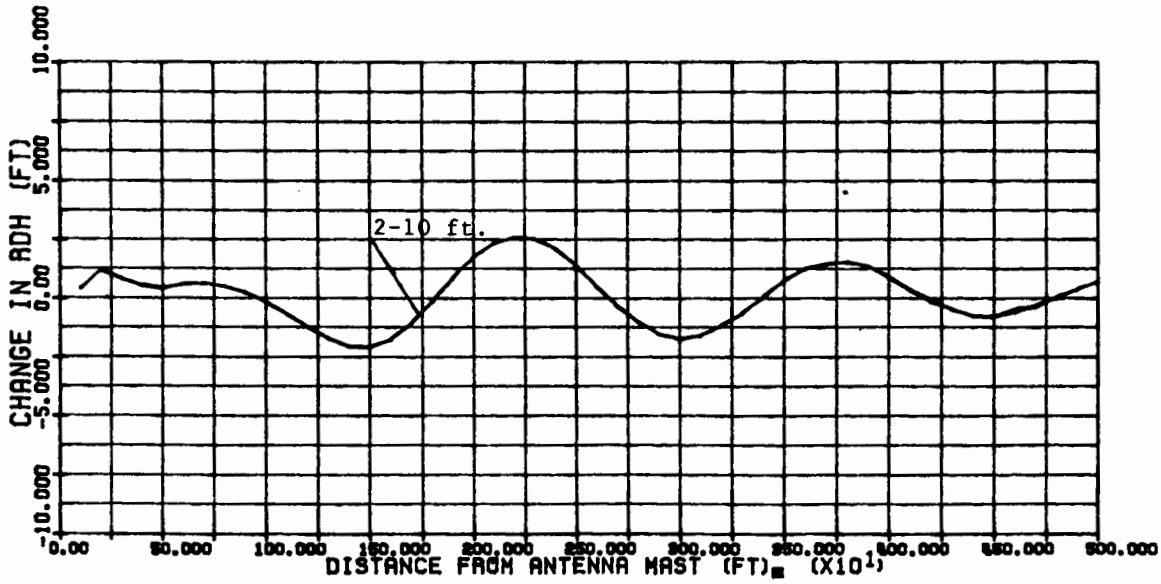

Figure 2-257. Sensitivity curves for deviation of RDH and ARDH from the ideal values, for a depression with a duration of 20' and a height of 2, 4, 6, 8, and 10'.

FINITE-DURATION IRREGULARITY

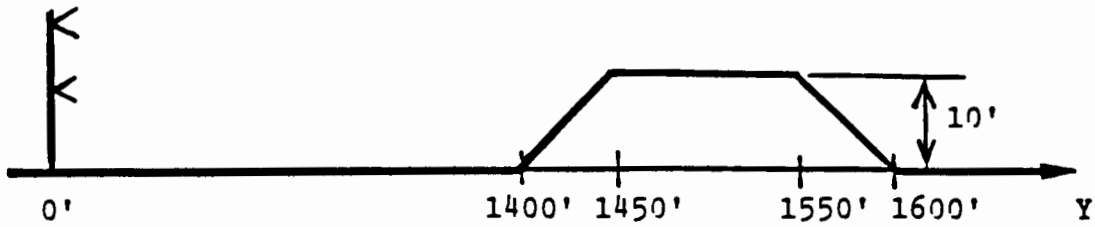

INFINITE-DURATION IRREGULARITY

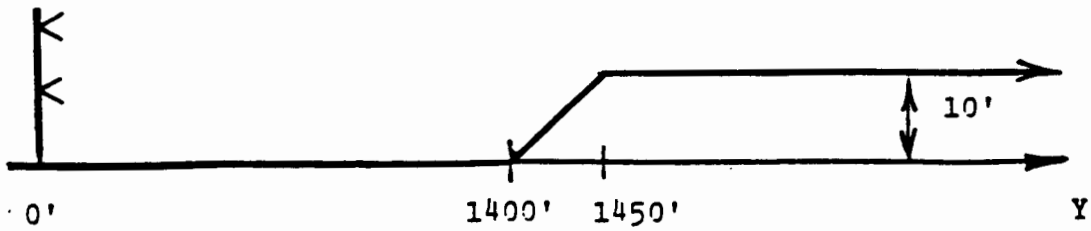

Figure 2-258. Two terrain profiles of a finite region of upsloping terrain considered to examine the effects of terrain following the upslope.

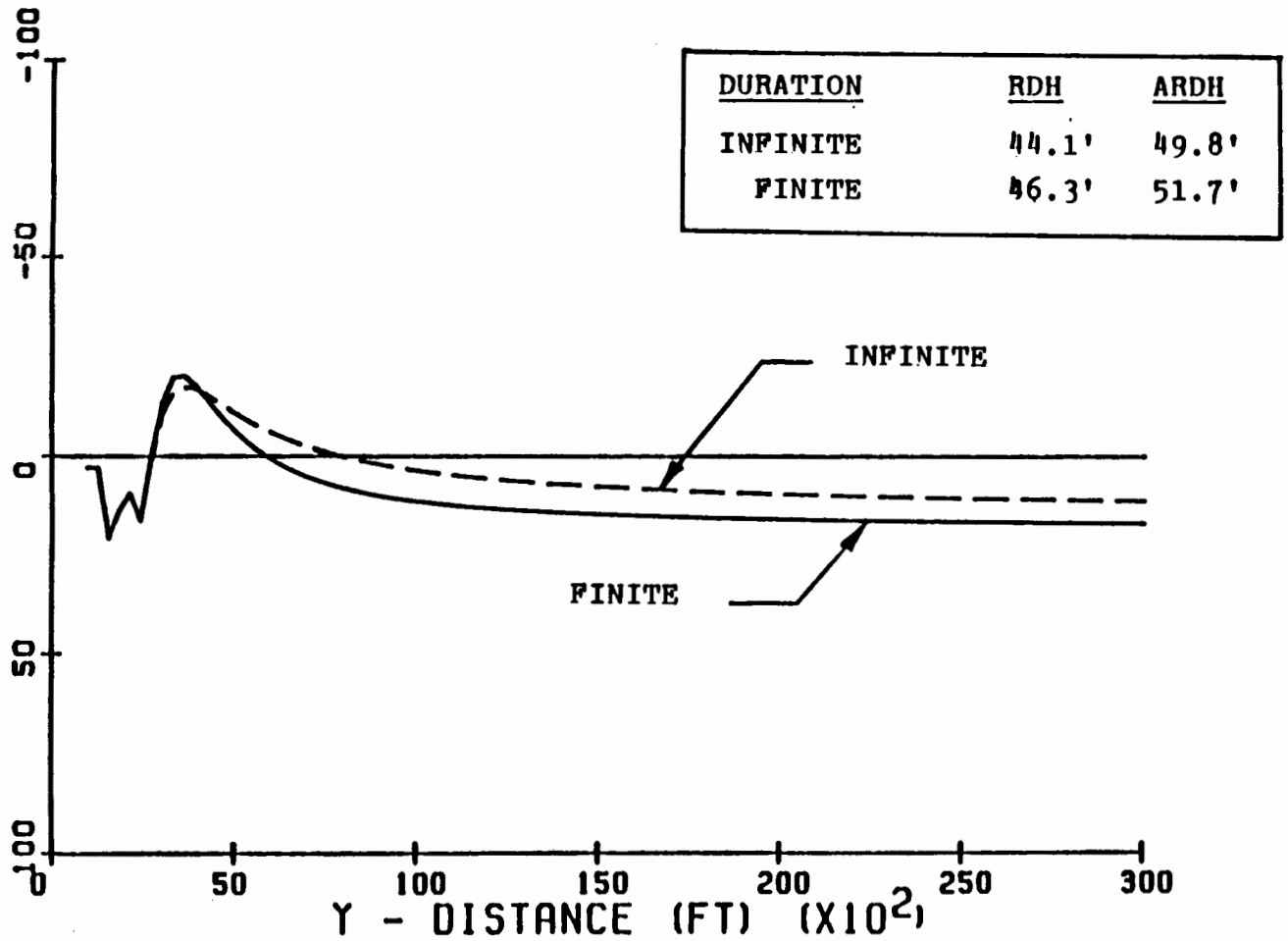

Figure 2-259. Simulated differential amplifier recordings for terrain profiles shown in figure 2-258, showing the independence of the trace (and reference datum heights) on the terrain following the upslope.

CHANGE FROM IDEAL RDH AND ARDH

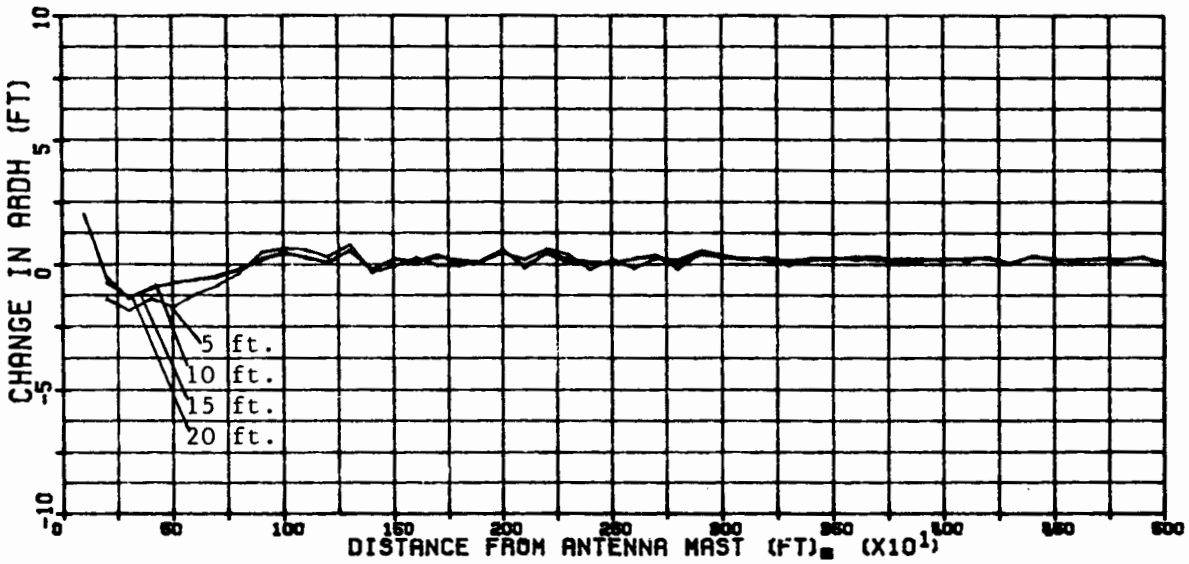

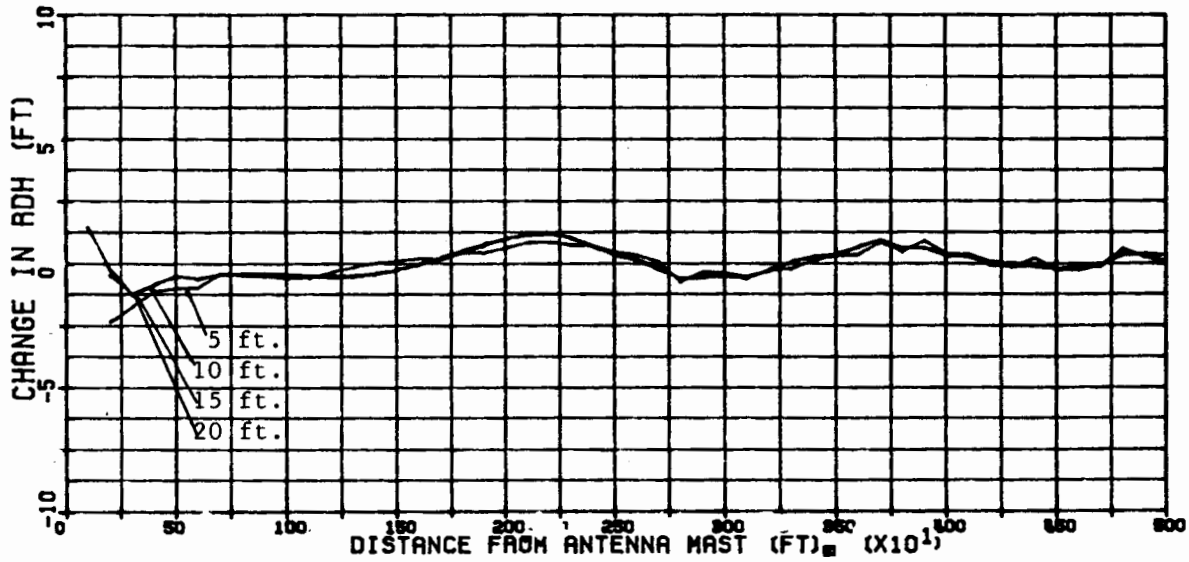

Figure 2-260. Sensitivity curves for deviation of RDH and ARDH from the ideal values, for a depression with a duration of 100' and a height of 5, 10, 15, and 20'.

CHANGE FROM IDEAL RDH AND ARDH

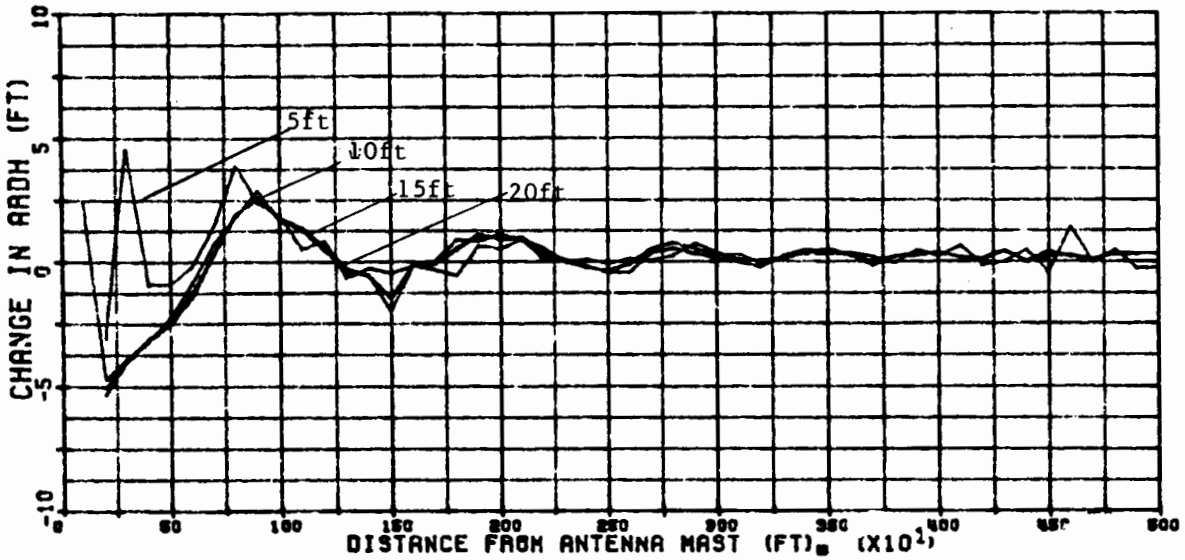

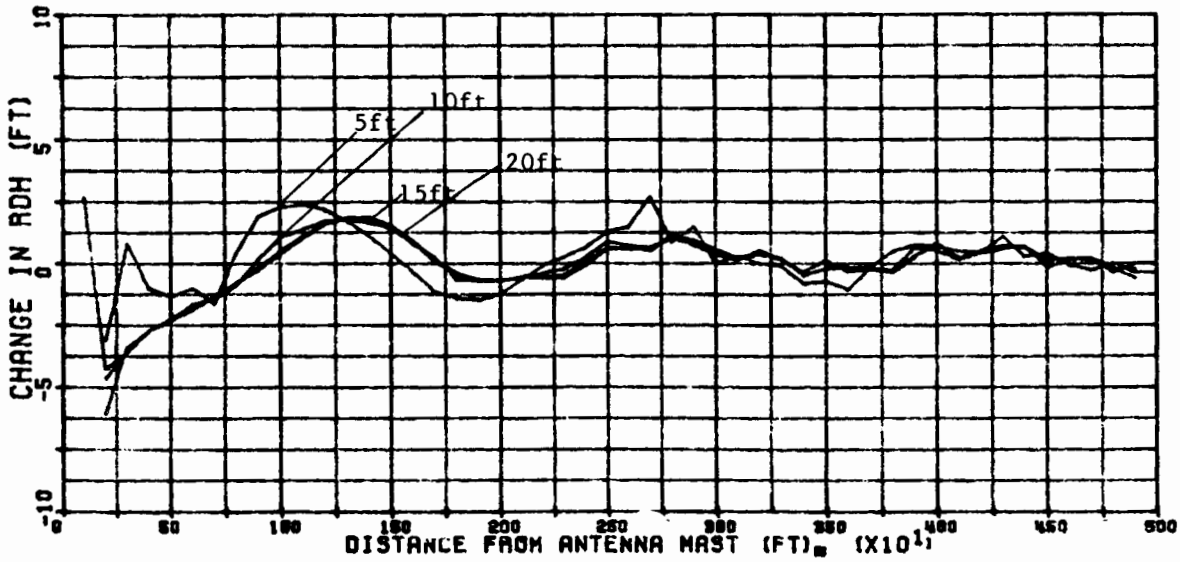

Figure 2-261. Sensitivity curves for deviation of RDH and ARDH from the ideal values, for a depression with a duration of 200' and a height of 5, 10, 15, and 20'.

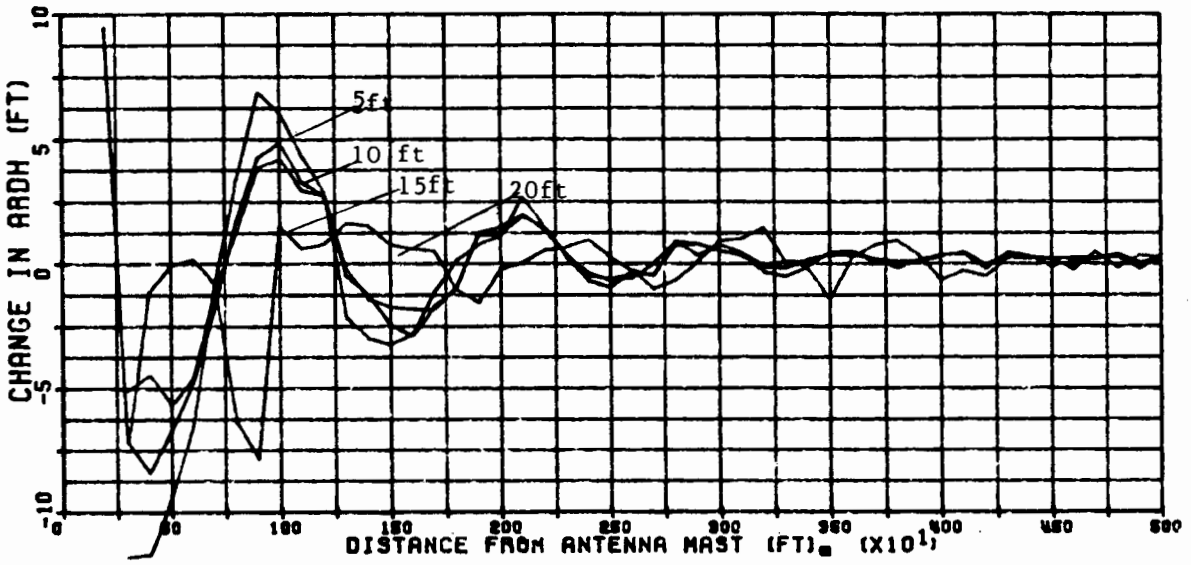

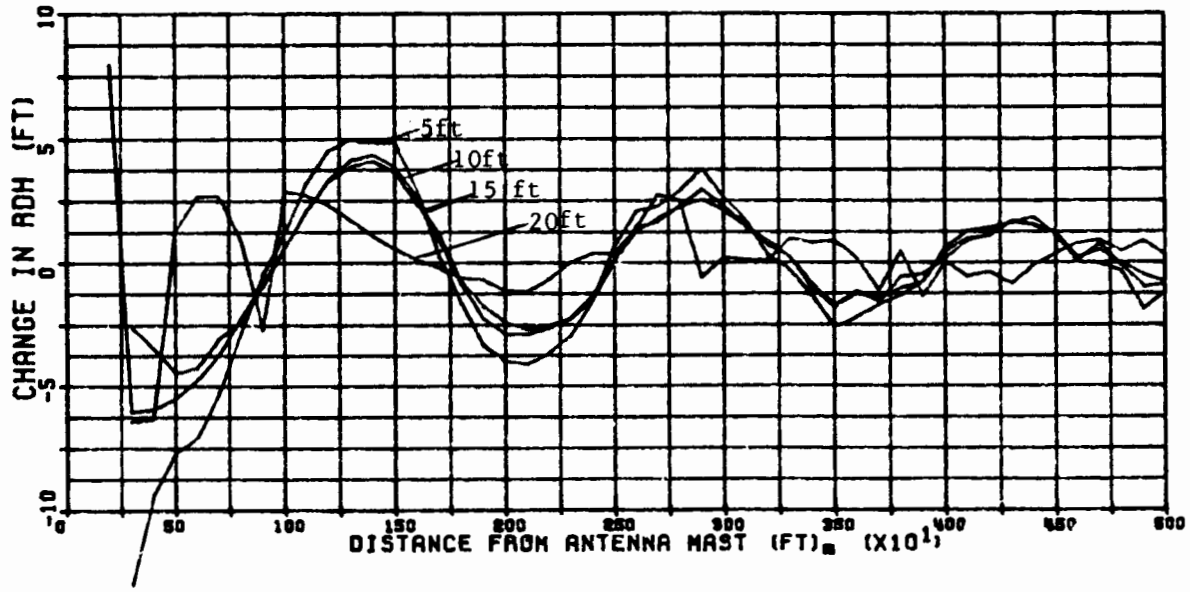

Figure 2-262. Sensitivity curves for deviation of RDH and ARDH from the ideal values, for a depression with a duration of 300' and a height of 5, 10, 15, and 20'.

CHANGE FROM IDEAL RDH AND ARDH

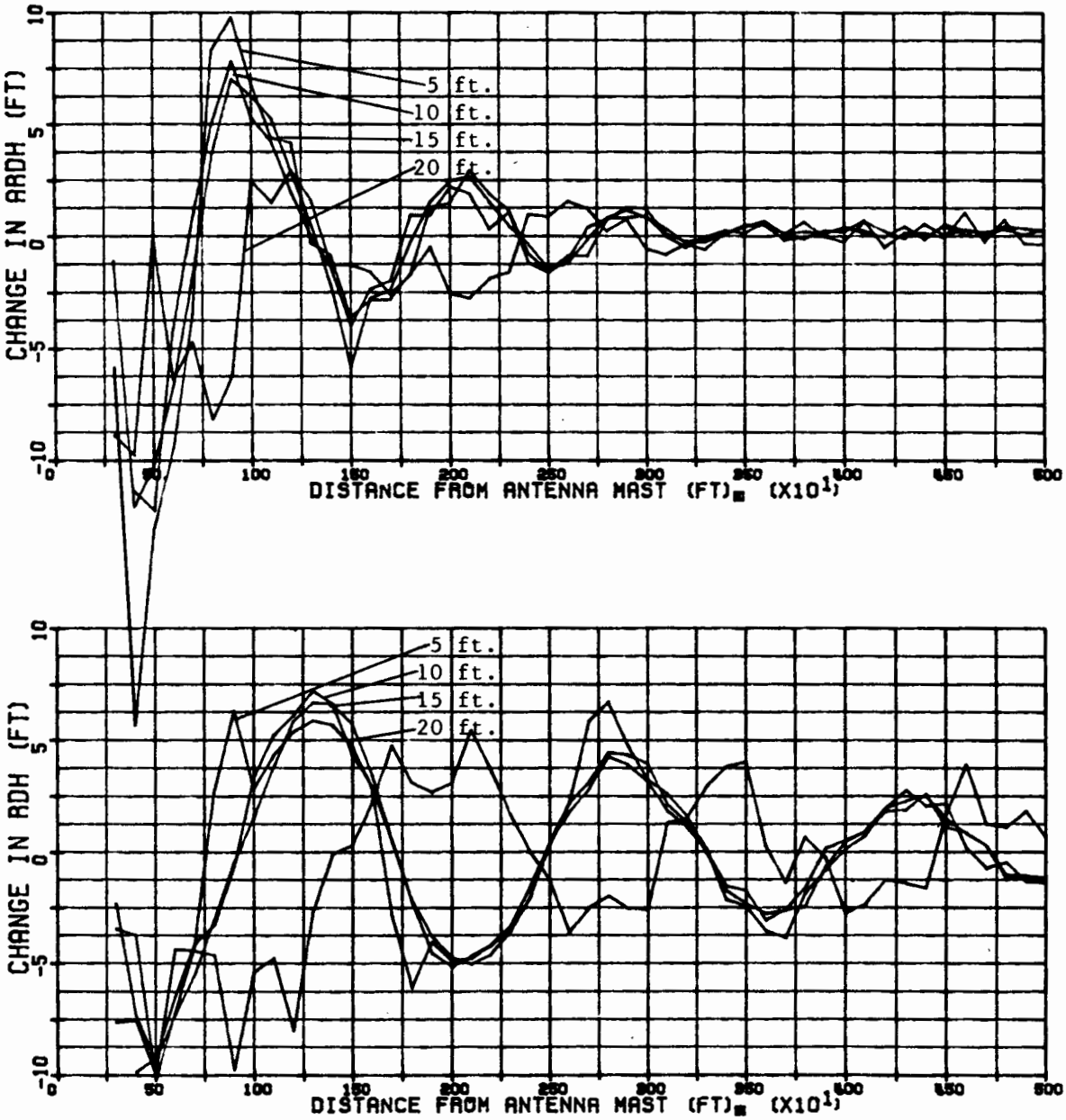

Figure 2-263. Sensitivity curves for deviation of RDH and ARDH from the ideal values, for a depression with a duration of 400' and a height of 5, 10, 15, and 20'.

CHANGE FROM IDEAL RDH AND ARDH

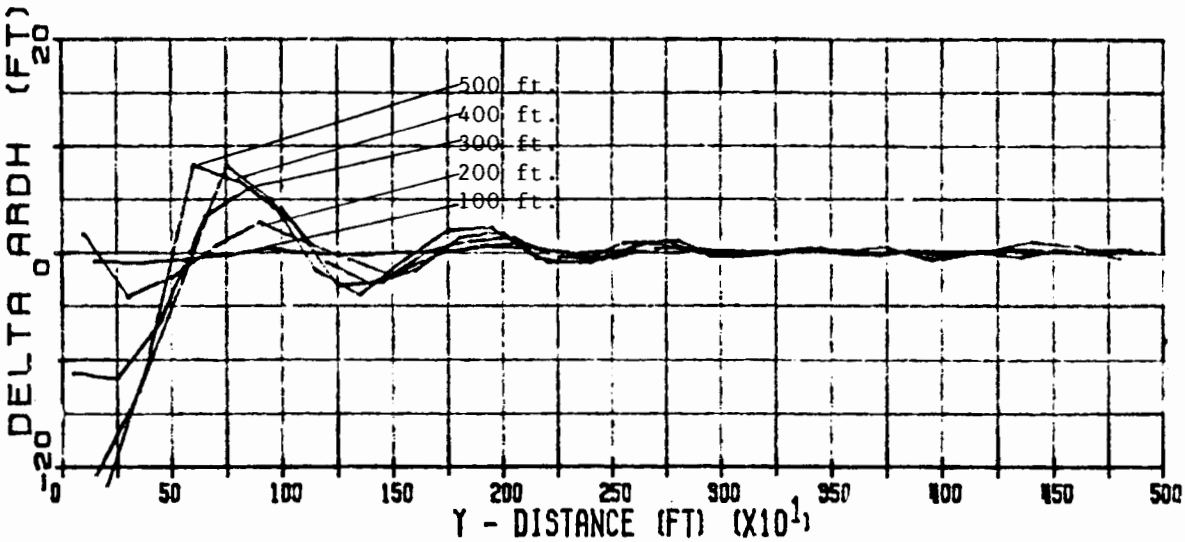

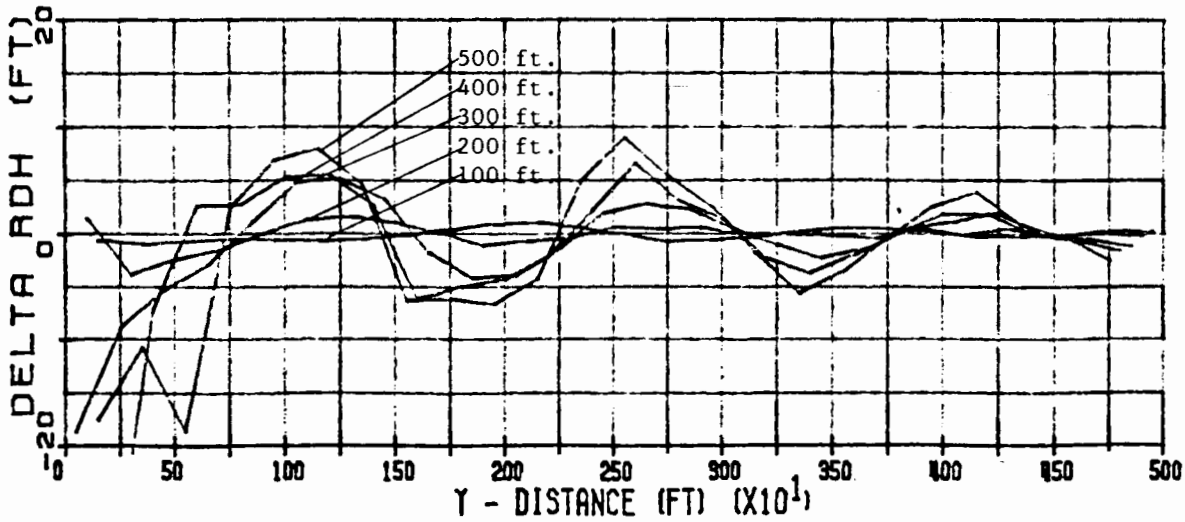

Figure 2-264. Sensitivity curves for deviation of RDH and ARDH from the ideal values, for depressions with durations of 100, 200, 300, 400 and 500', showing how increasing durations of terrain depressions affect the reference datum heights.

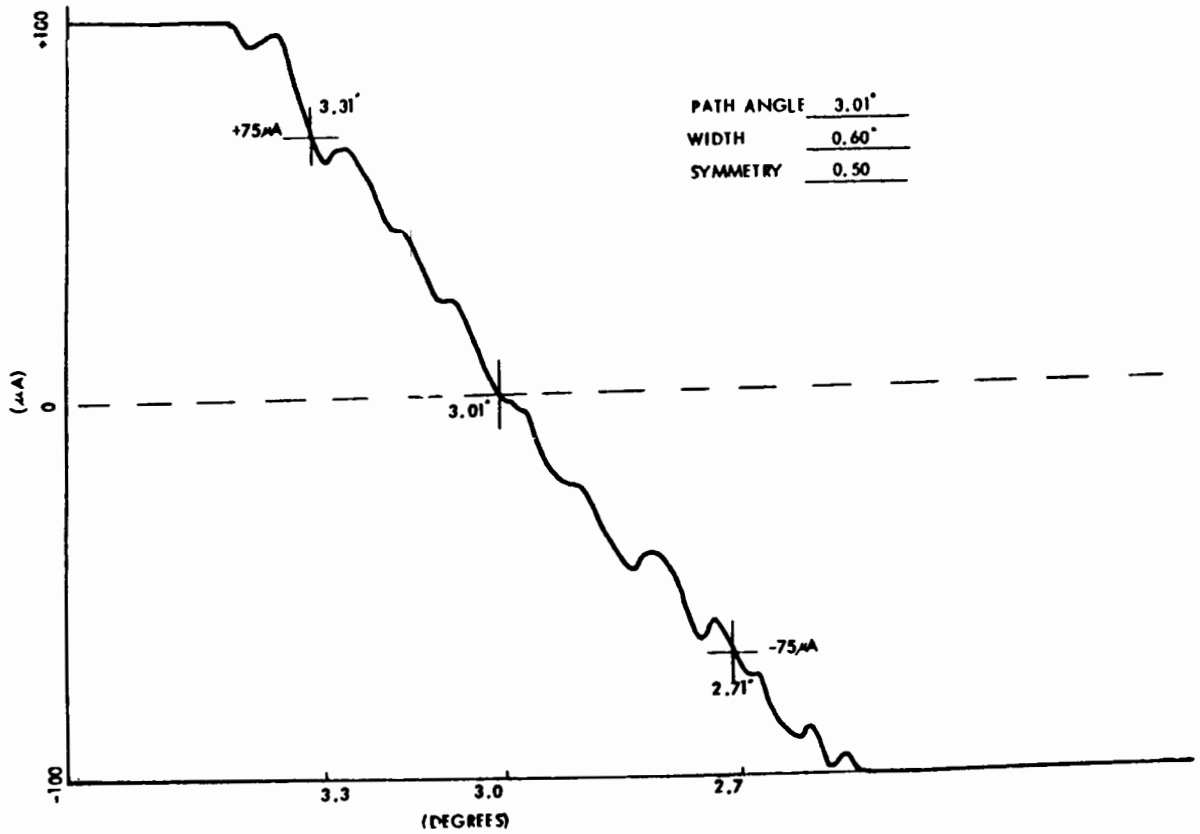

Figure 2-265. Flight recording made on a level run at Wheeling, WV before removal of trees.

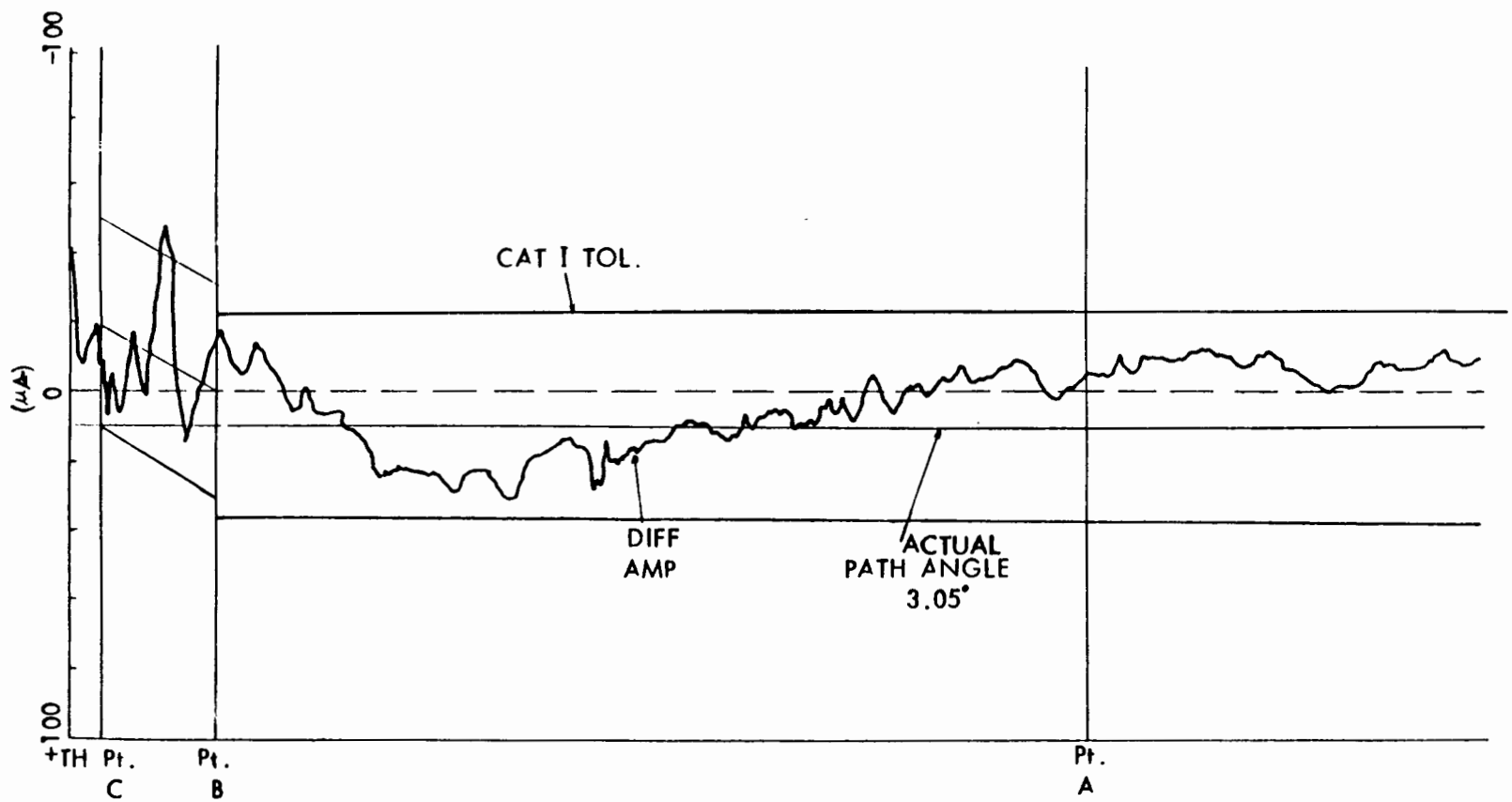

Figure 2-266. Differential amplifier recording made on a low approach at Wheeling, WV before removal of trees, showing marginal CAT I tolerance and an RDH of 76'.

Figure 2-267. Picture of the tree line after cutting at Wheeling, WV. The sideband reference glide slope is located 250' off centerline and the row of trees is located approximately 300' off centerline. This is the condition for the measurements shown in Figure 2-269.

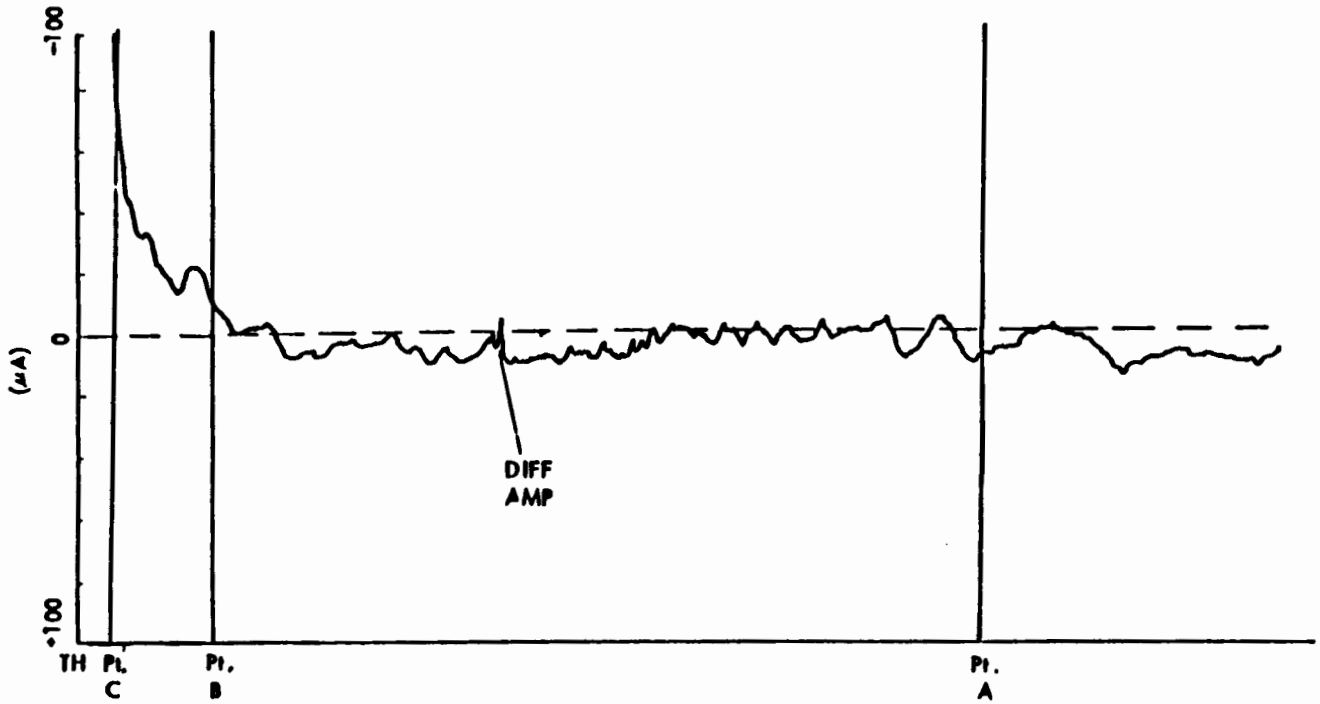

Figure 2-268. Differential amplifier recording made on a low approach at Wheeling, WV in line with the long row of trees to the east of the runway centerline.

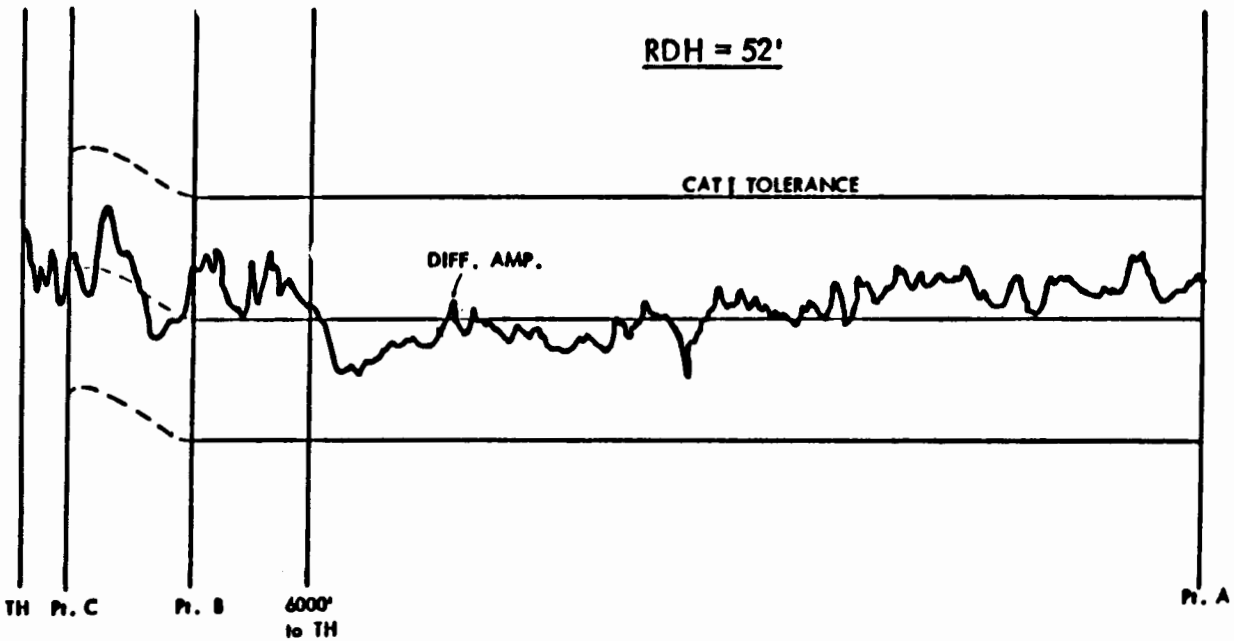

Figure 2-269. Differential amplifier recording made on a low approach at Wheeling, WV after removal of the row of trees. The structure is clearly improved (see figure 2-266) and the RDH of 52' is within applicable tolerances.

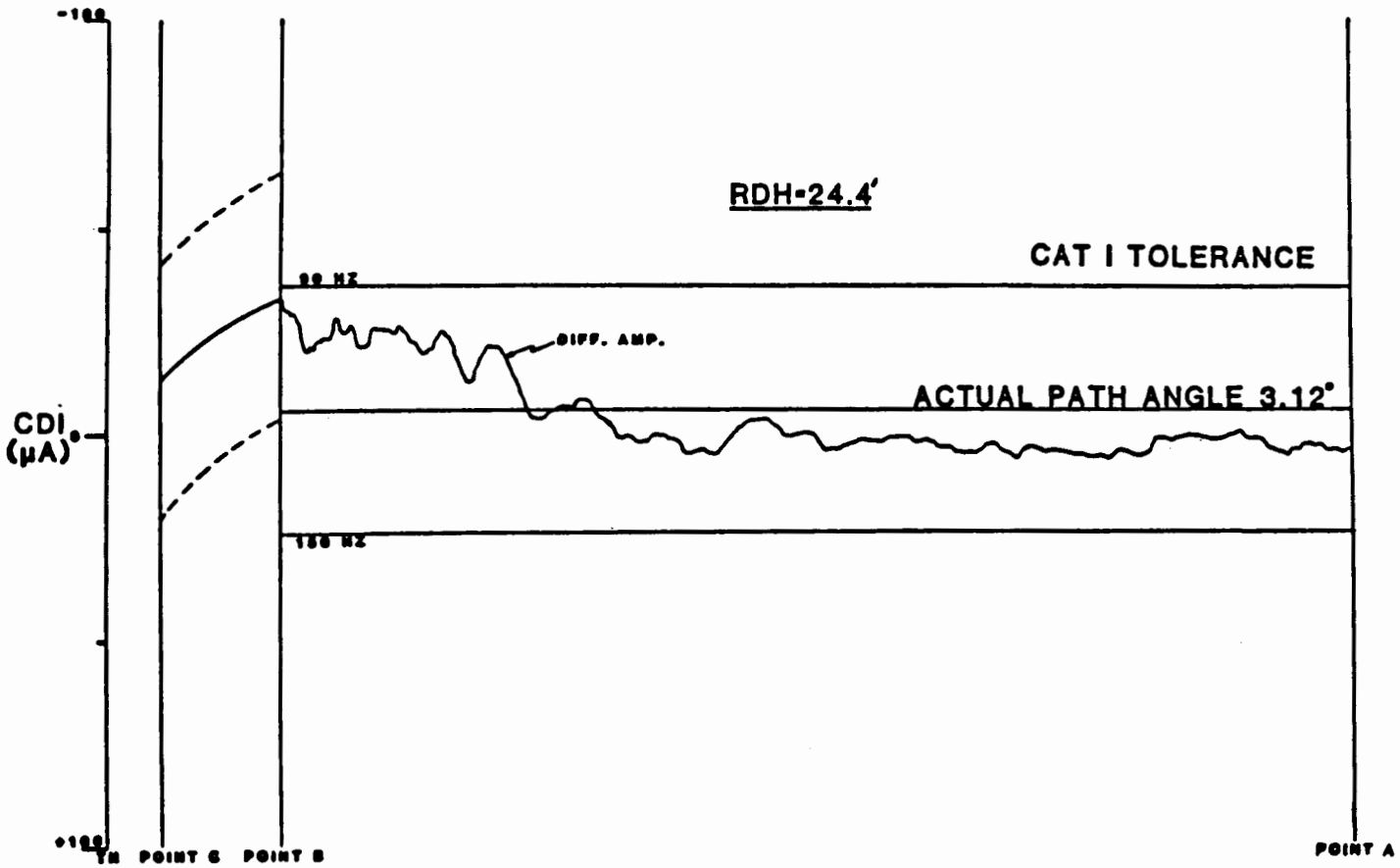

Figure 2-270. Differential amplifier recording made on a low approach to Runway 18 at the Greenville, SC, Downtown Airport.

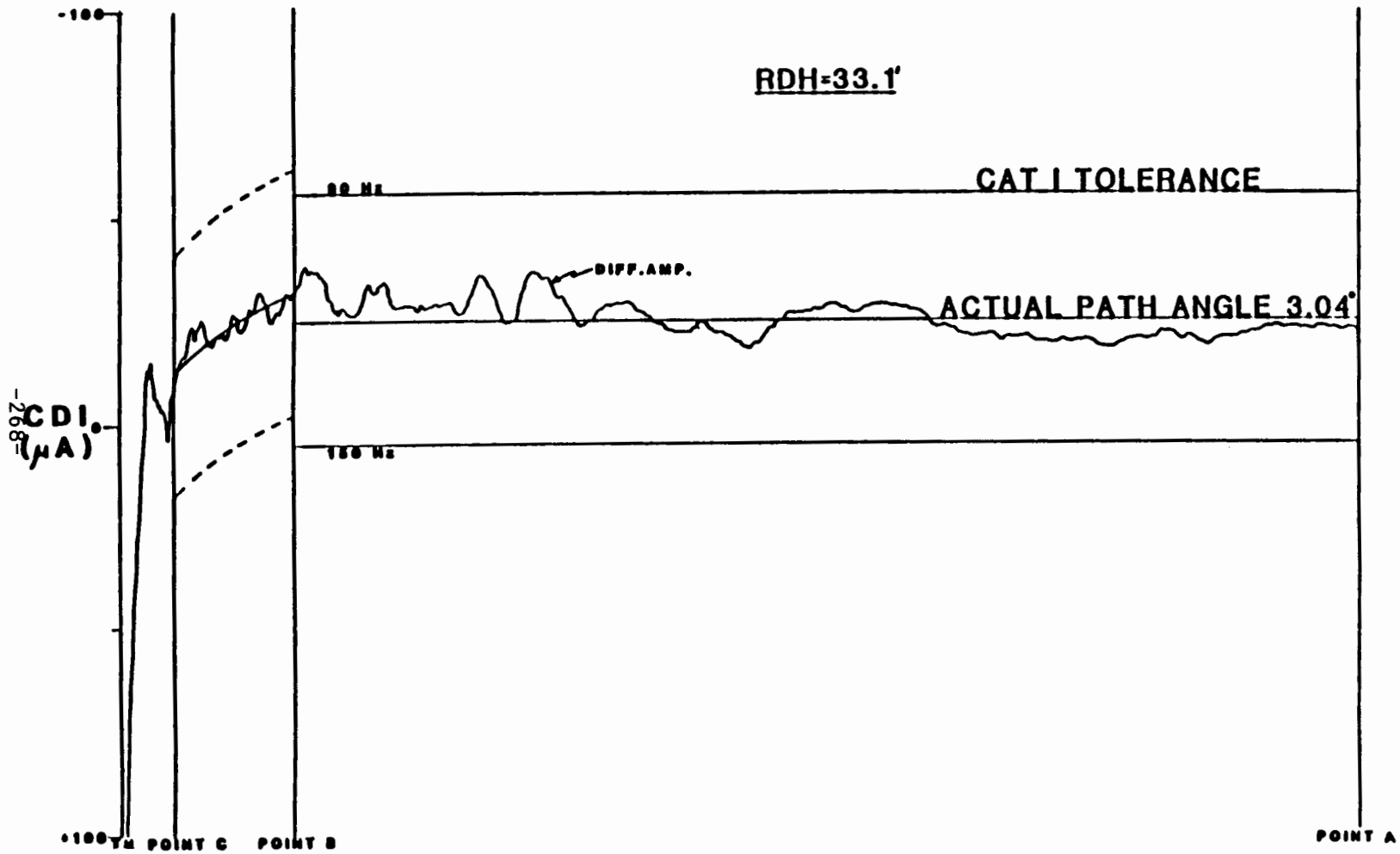

Figure 2-271. Differential amplifier recording made on a low approach after advancing the phase of the upper antenna by 20 degrees.

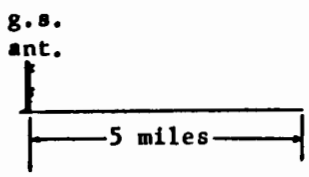

SITE #1: IDEAL.

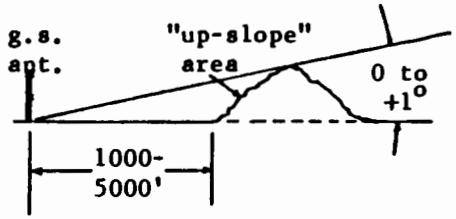

SITE #2: TERRAIN SLOPES UP-WARDS ABOVE INITIAL TERRAIN-PROJECTED.

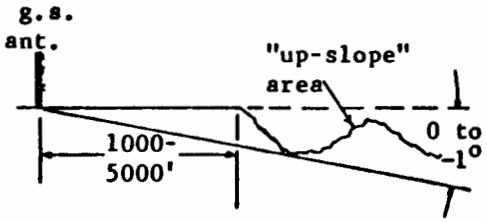

SITE #3: TERRAIN SLOPES UP-WARDS BELOW INITIAL TERRAIN-PROJECTED.

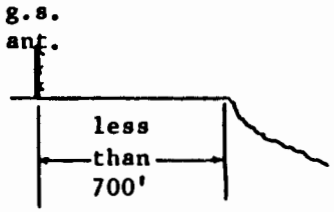

SITE #4: NO UP-SLOPE AREA; LIMITED TERRAIN IN FRONT OF ARRAY.

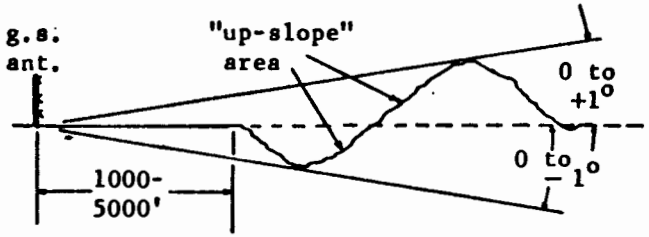

SITE #5: COMBINATION OF SITES #2 AND 3.

	SITE #1	SITE #2	SITE #3	SITE #4	SITE #5
PER CENT OF TOTAL SITES	5%	20%	15%	15%	45%
NULL REFERENCE	all	very few	few	none	very few
SIDEBAND REFERENCE	all	few	many	very few	few
CAPTURE EFFECT	all	most	most	none	most
END FIRE	all	many	all	all	many

Figure 2-272. Types of sites encountered in U.S.

Type of Sites

Type of Facilities	#1	#2	#3	#4	#5
NULL REFERENCE				NA	
SIDEBAND REFERENCE					
CAPTURE EFFECT				NA	

Figure 2-273. Matrix of mean RMS values.

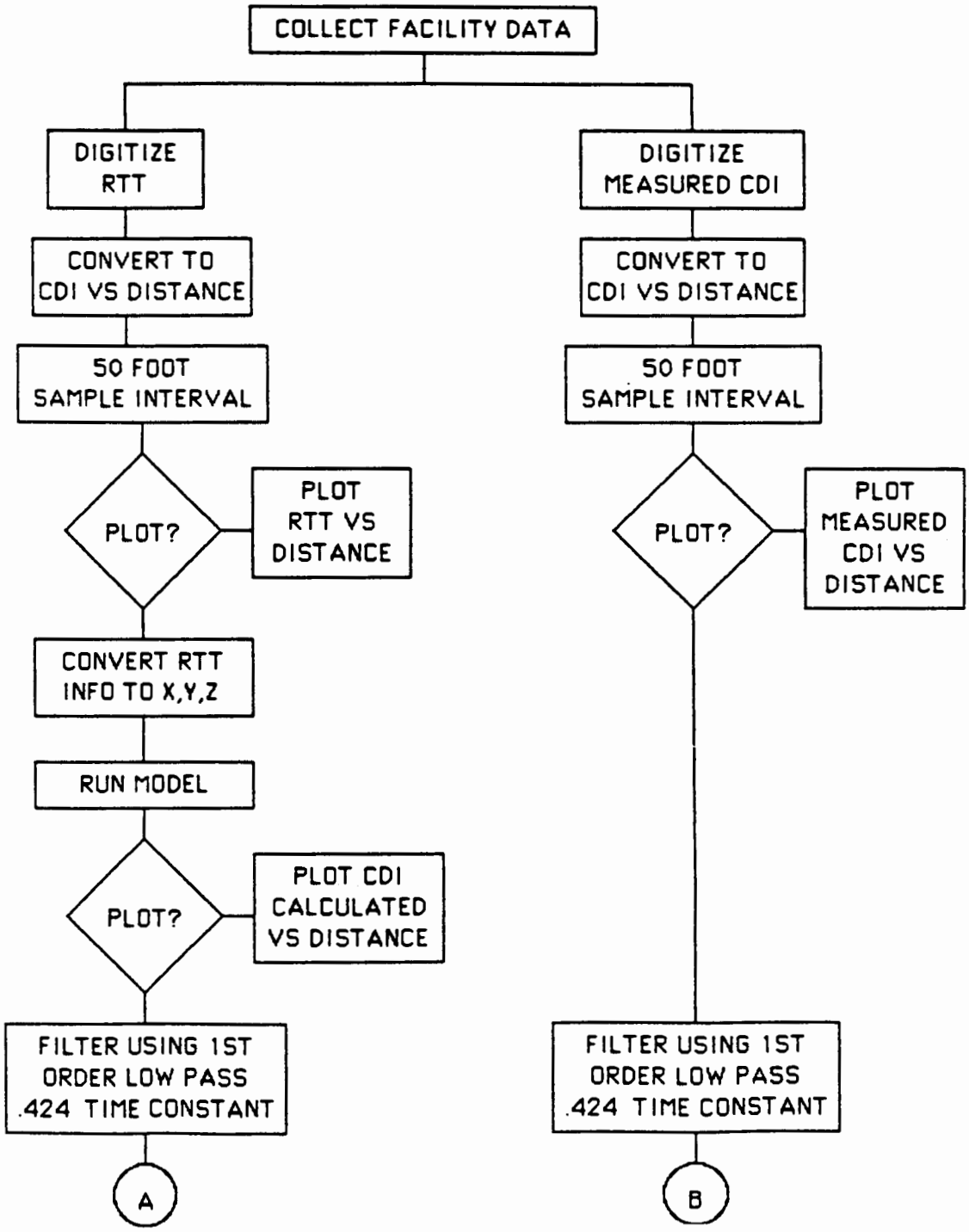

Figure 2-274. Flowchart of math model validation procedure (2 sheets).

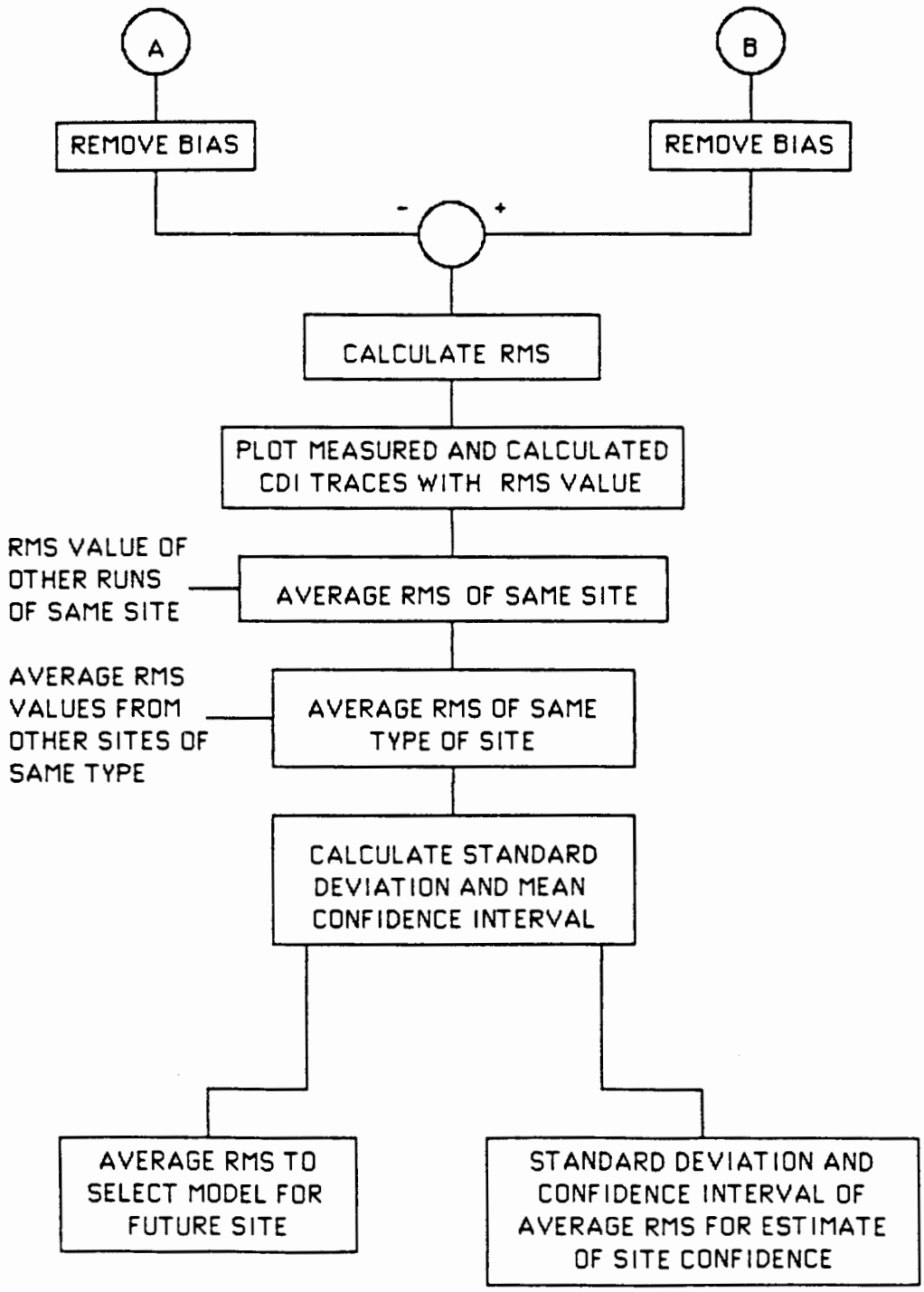
A
B
REMOVE BIAS
REMOVE BIAS
-
+
CALCULATE RMS
PLOT MEASURED AND CALCULATED CDI TRACES WITH RMS VALUE
RMS VALUE OF OTHER RUNS OF SAME SITE
AVERAGE RMS OF SAME SITE
AVERAGE RMS VALUES FROM OTHER SITES OF SAME TYPE
AVERAGE RMS OF SAME TYPE OF SITE
CALCULATE STANDARD DEVIATION AND MEAN CONFIDENCE INTERVAL
AVERAGE RMS TO SELECT MODEL FOR FUTURE SITE
STANDARD DEVIATION AND CONFIDENCE INTERVAL OF AVERAGE RMS FOR ESTIMATE OF SITE CONFIDENCE

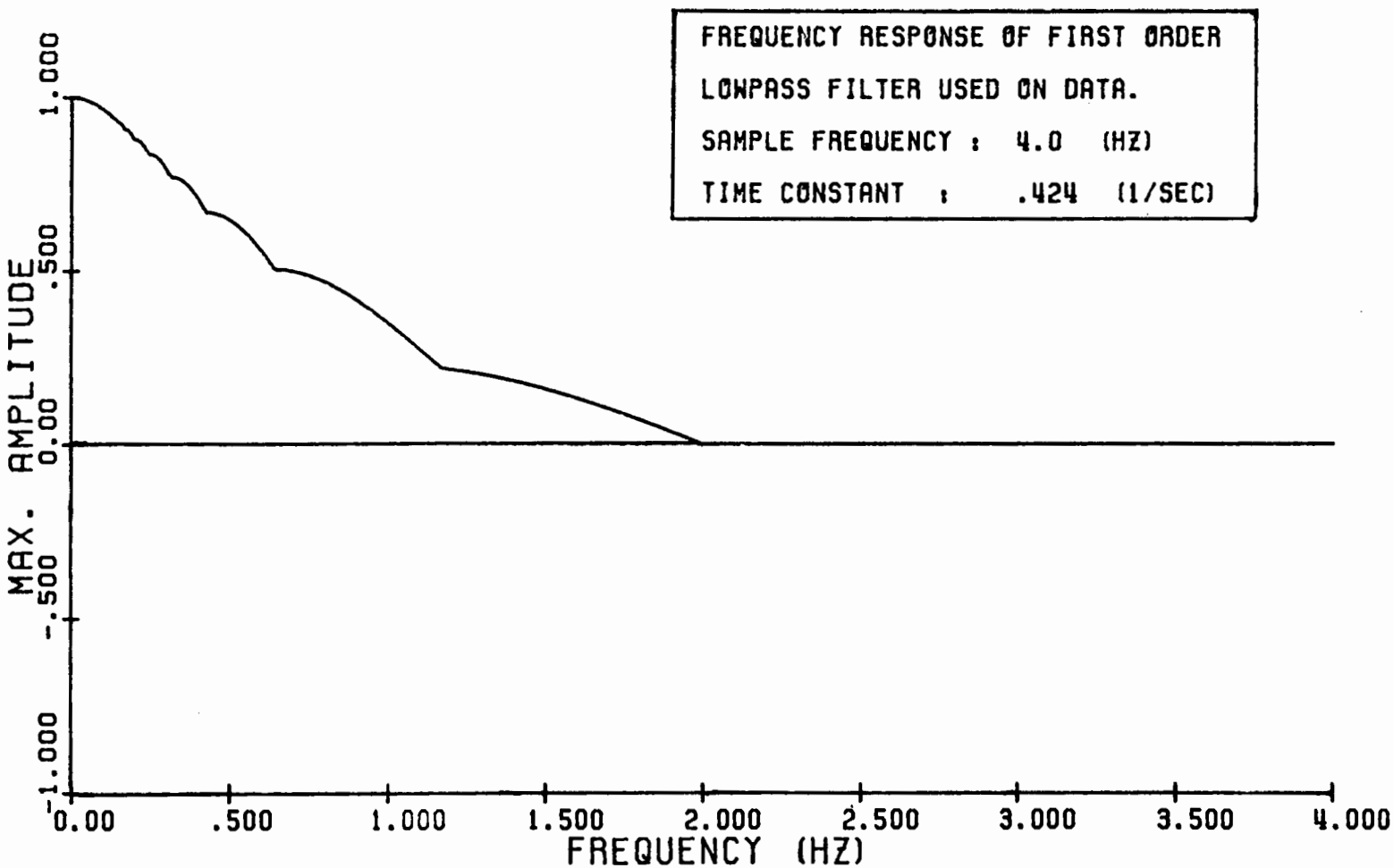

Figure 2-275. Frequency response of filter used on measured and calculated data.

X	Y	Z
4 5		
-10000.0	0.0	0.00
0.0	0.0	0.00
200.0	0.0	0.00
450.0	0.0	0.00
-10000.0	590.0	0.05
0.0	590.0	0.05
200.0	590.0	0.05
450.0	590.0	0.05
-10000.0	1590.0	0.25
0.0	1590.0	0.25
200.0	1590.0	0.25
450.0	1590.0	-0.35
-10000.0	2090.0	0.25
0.0	2090.0	0.25
200.0	2090.0	0.25
450.0	2090.0	0.25
-10000.0	4590.0	0.00
0.0	4590.0	0.00
200.0	4590.0	0.00
450.0	4590.0	0.00

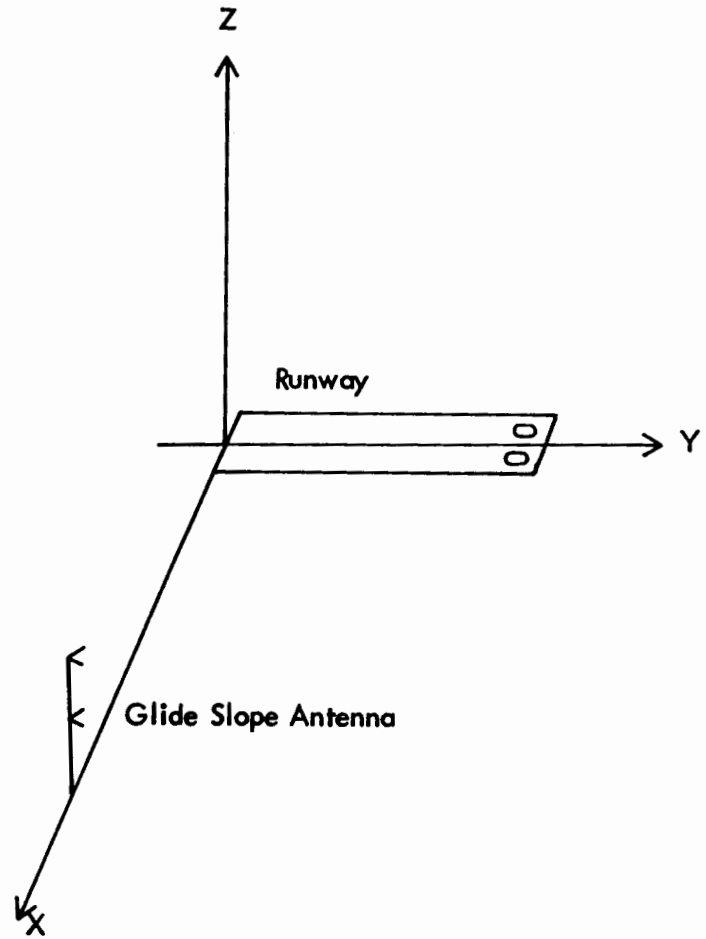

Figure 2-276. Sample terrain profile for Tamiami test site.

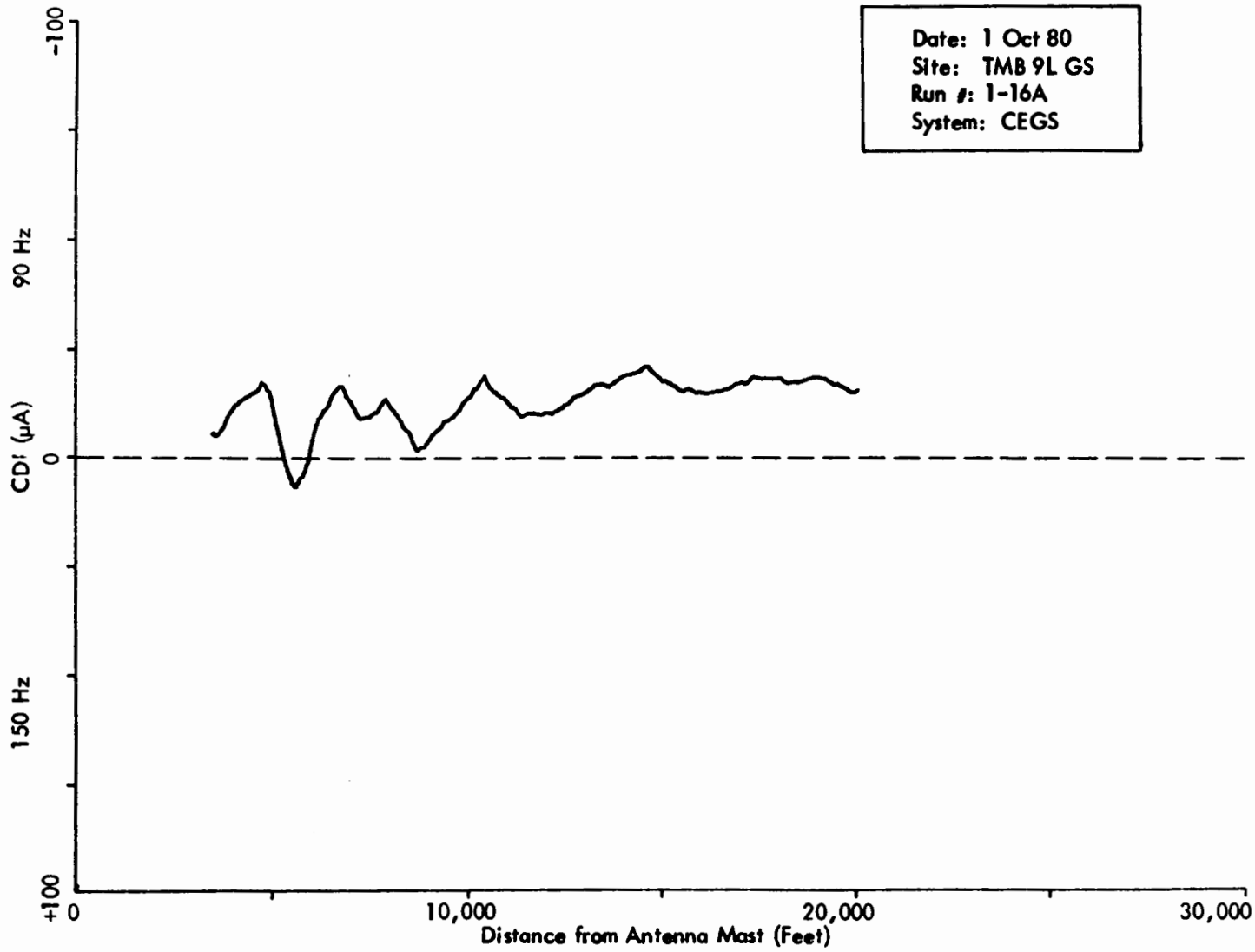

Figure 2-277. Sample of digitized RTT information recorded at TMB.

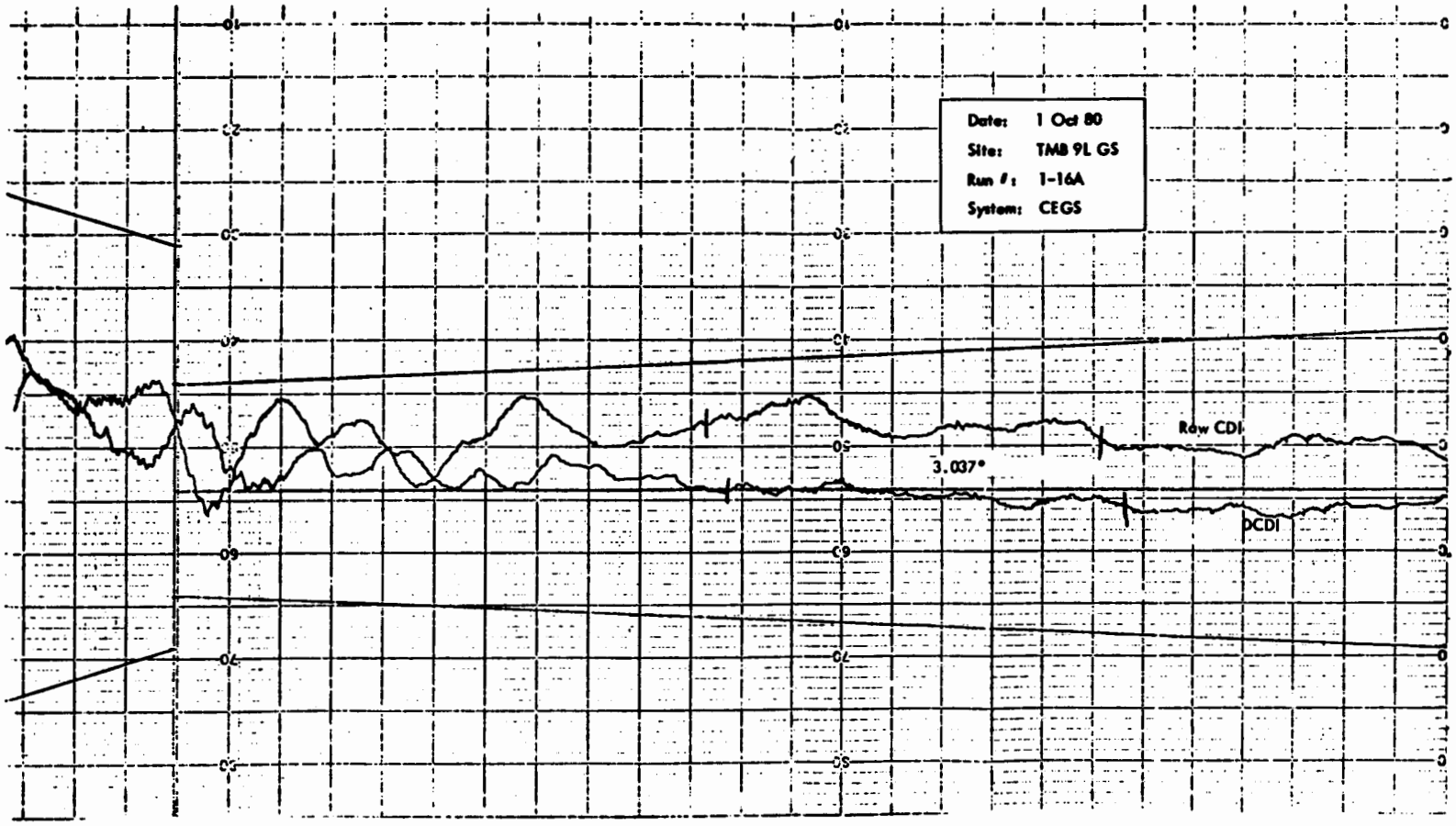

Figure 2-278. Measured raw CDI and differential CDI traces from aircraft recorder.

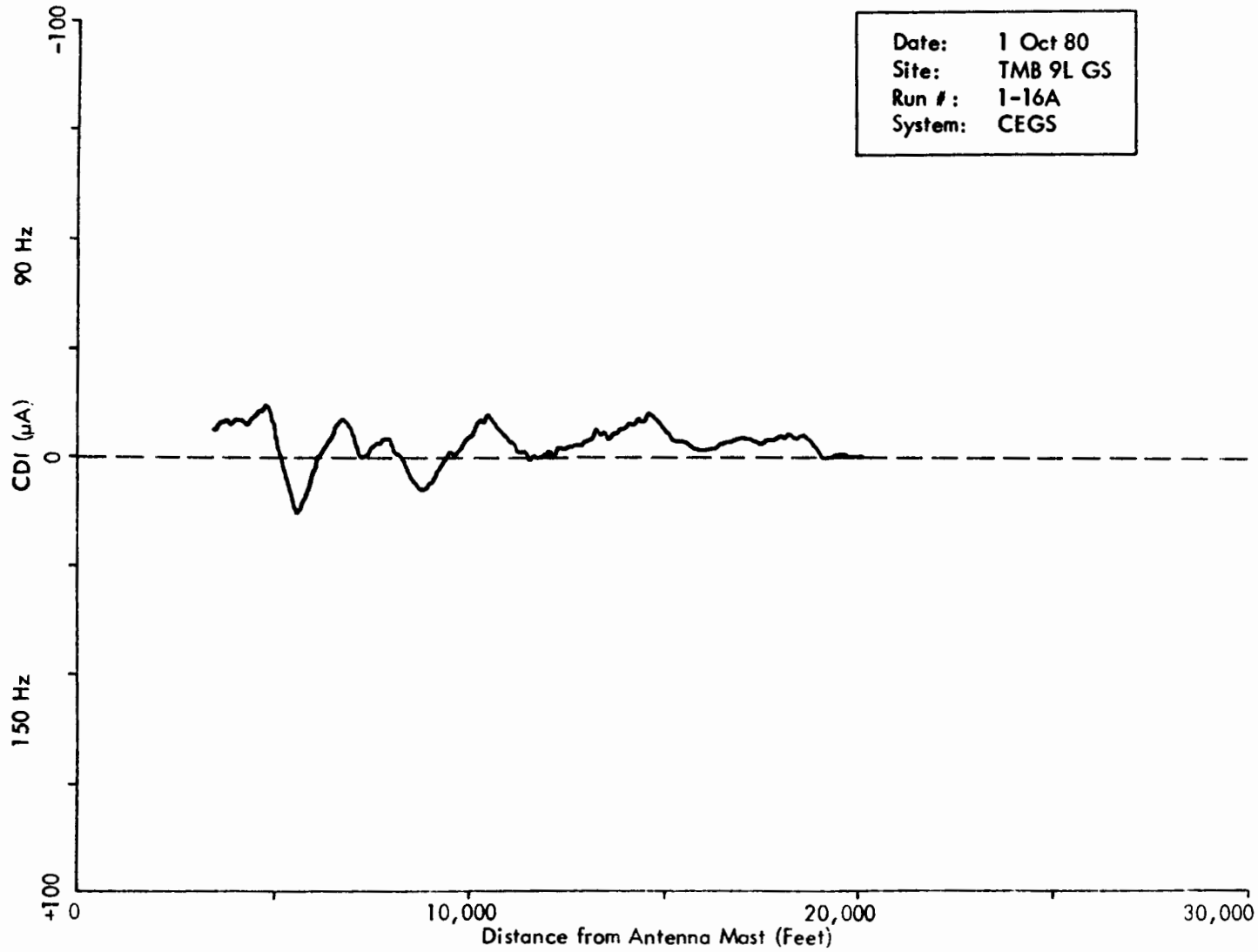

Figure 2-279. Measured CDI trace after digitization and sampling process.

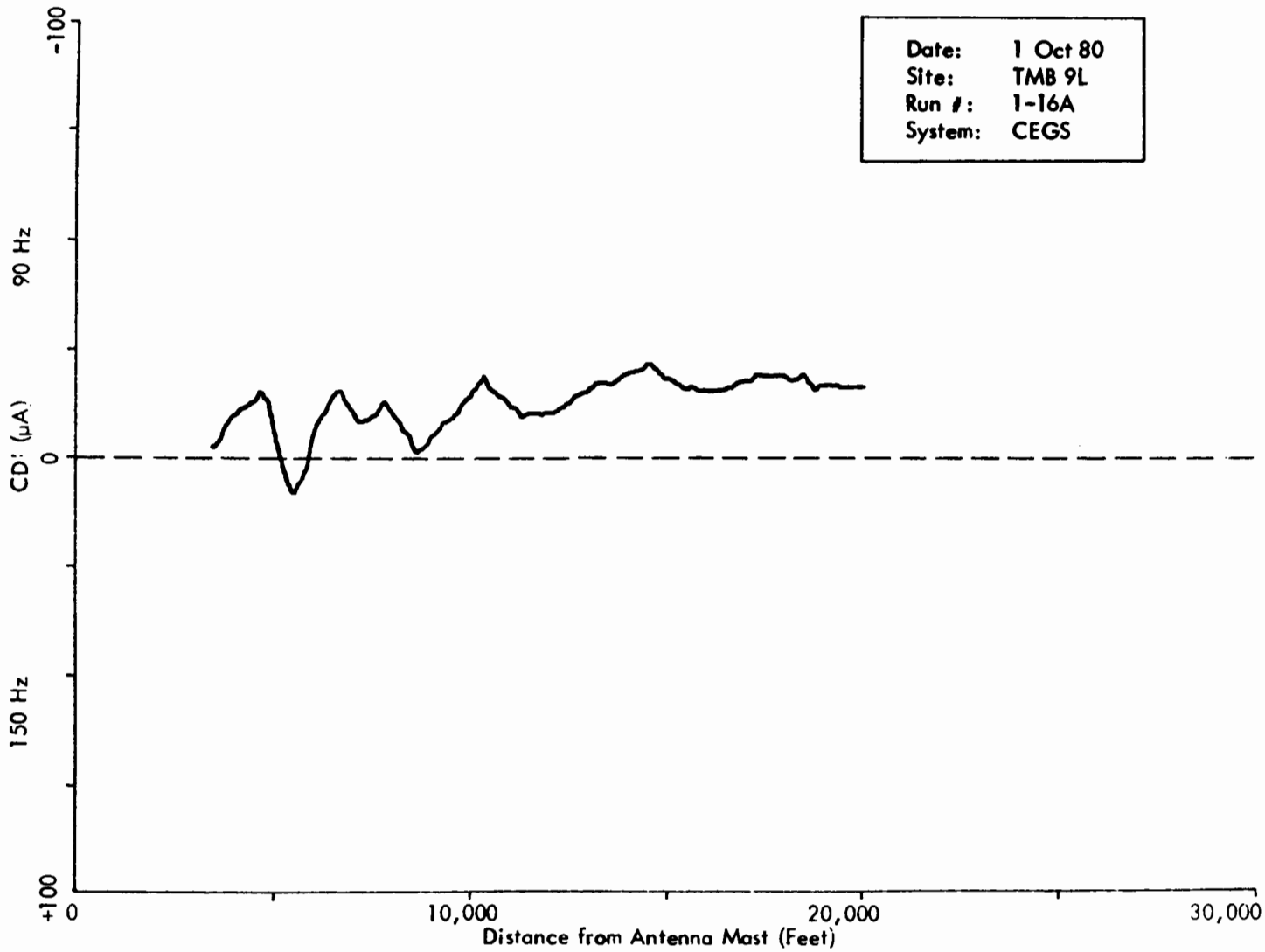

Figure 2-280. Model calculation.

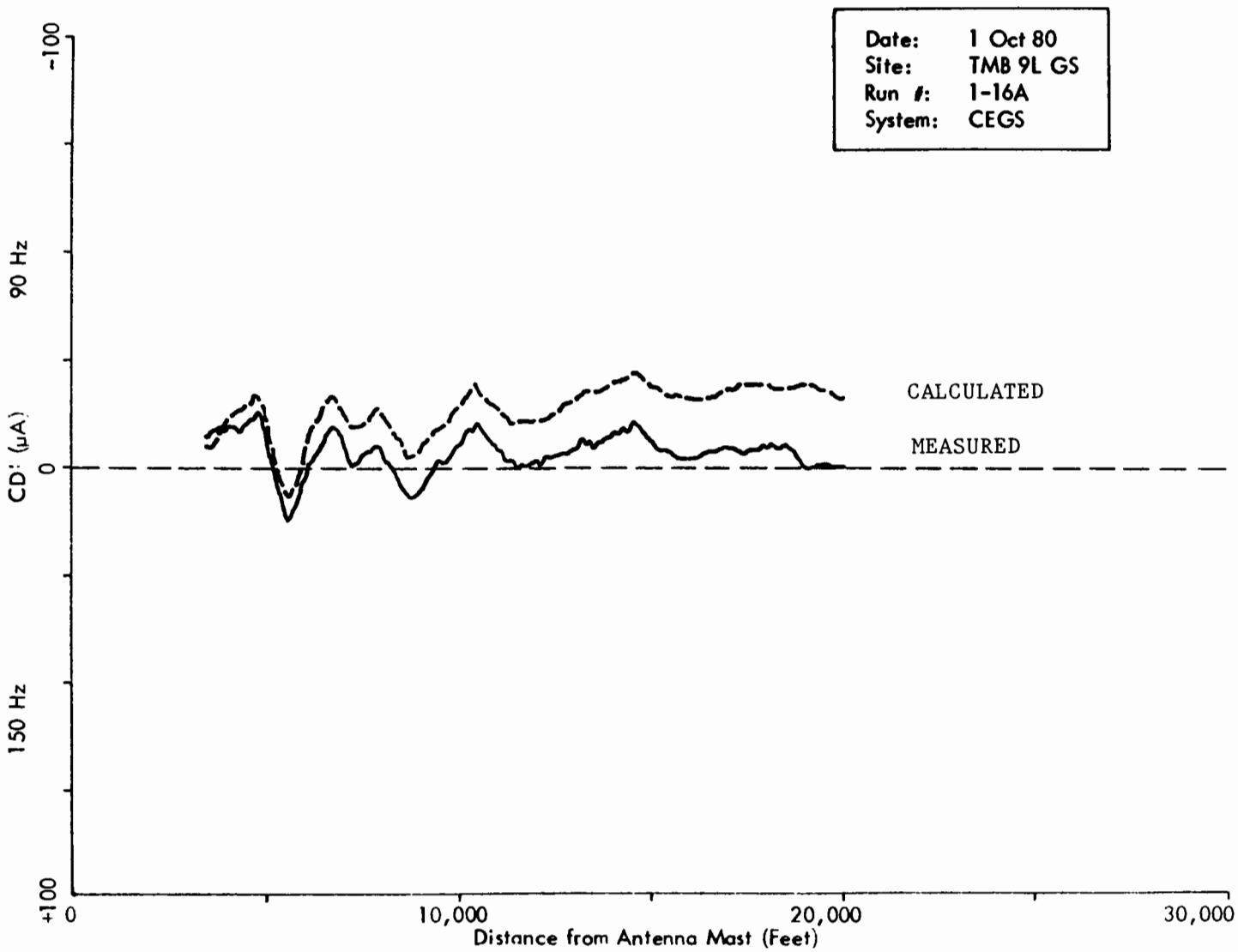

Figure 2-281. Digitized measured raw CDI and model output traces.

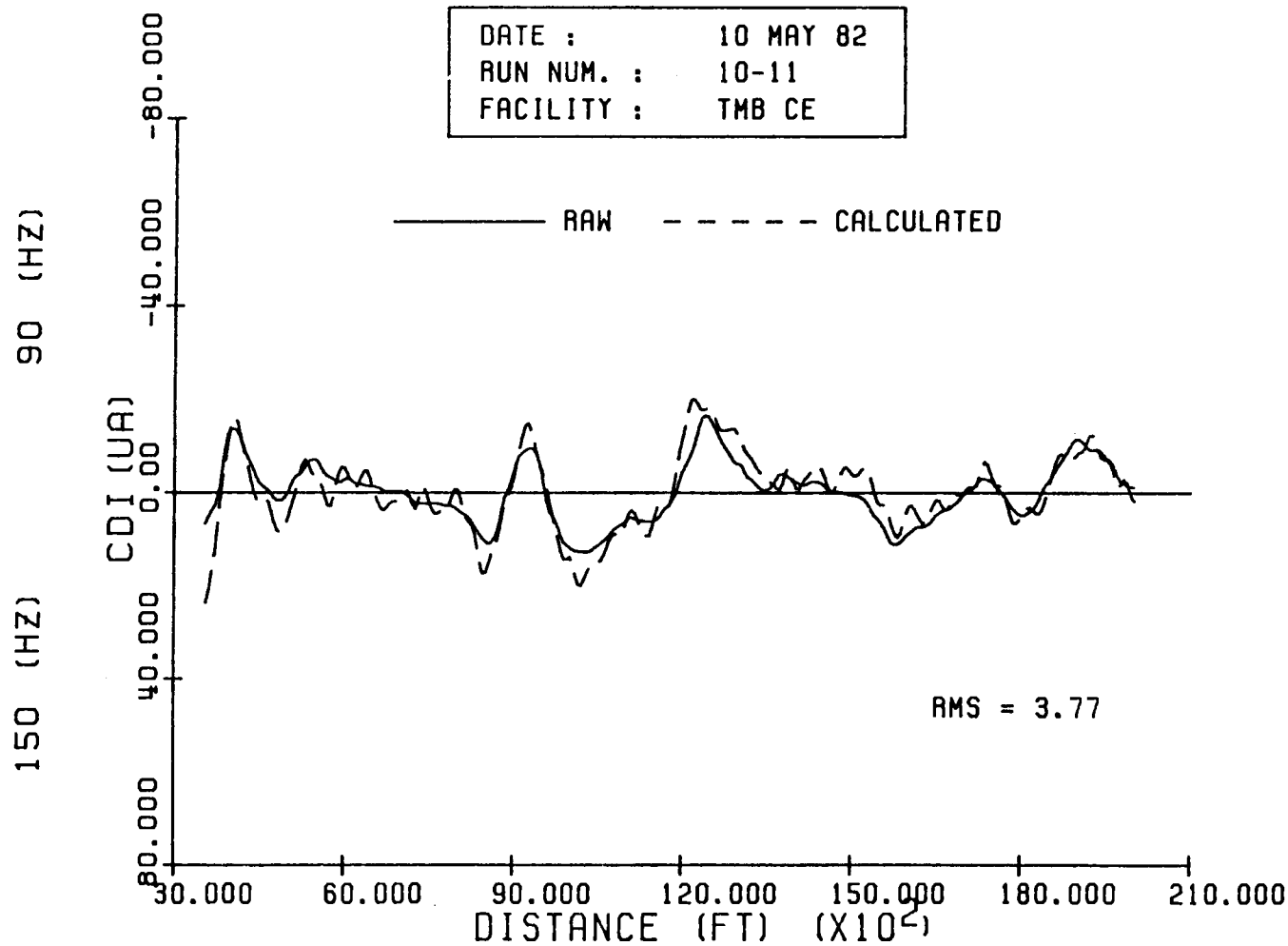

Figure 2-282. Filtered, zero-mean, CDI traces; TMB 10-11.

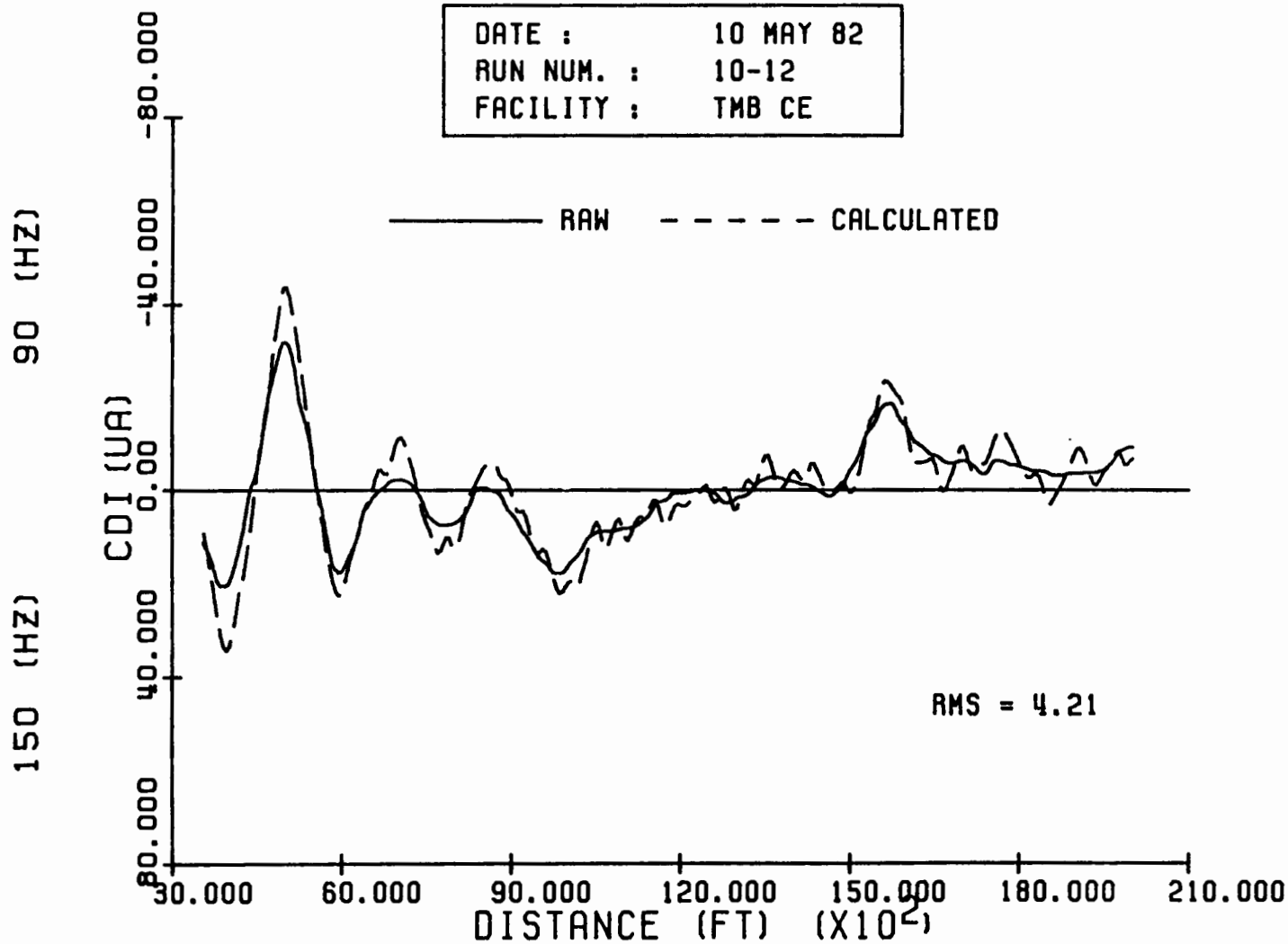

Figure 2-283. Filtered, zero-mean, CDI traces; TMB 10-12.

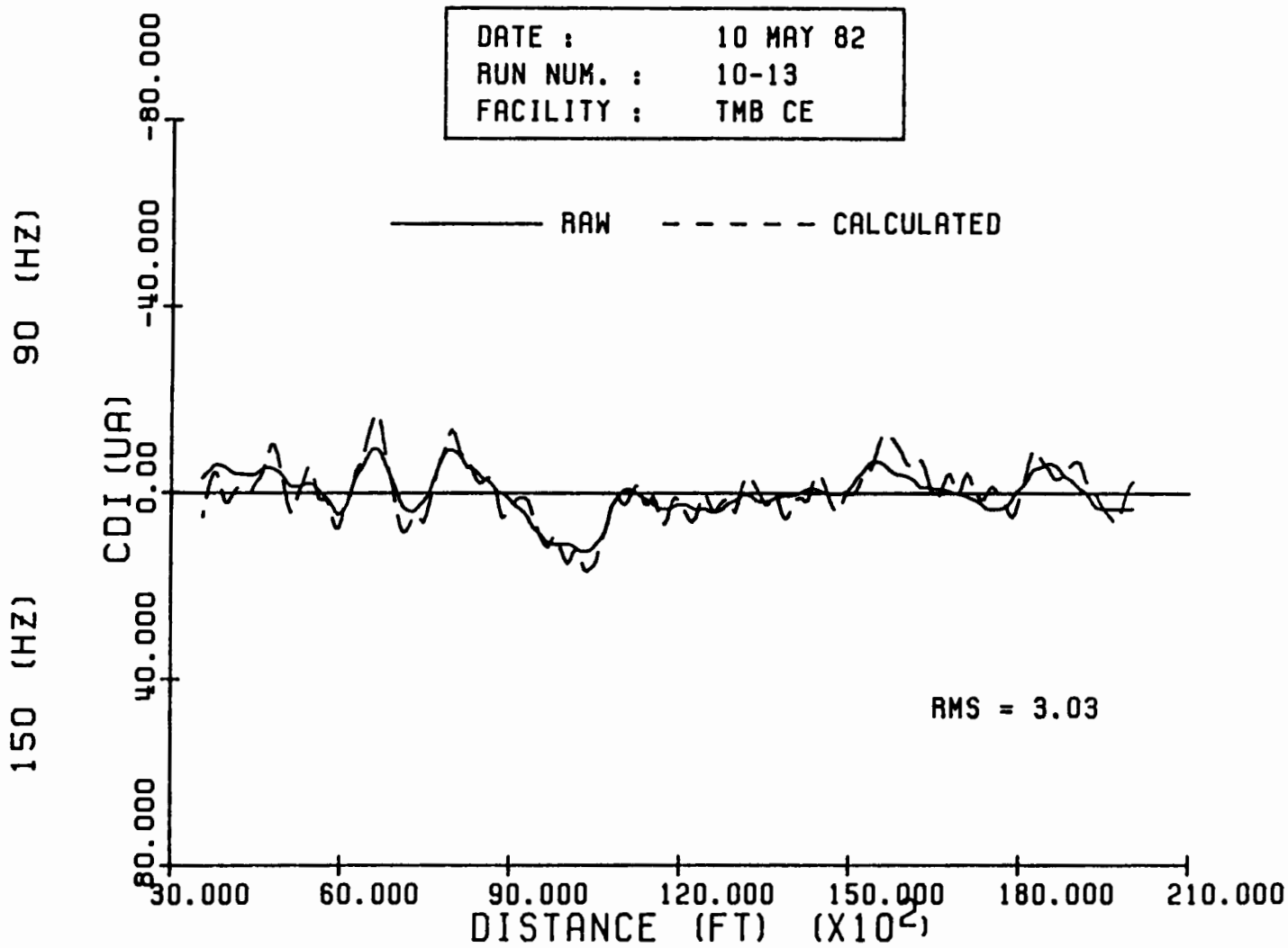

Figure 2-284. Filtered, zero-mean, CDI traces; TMB 10-13.

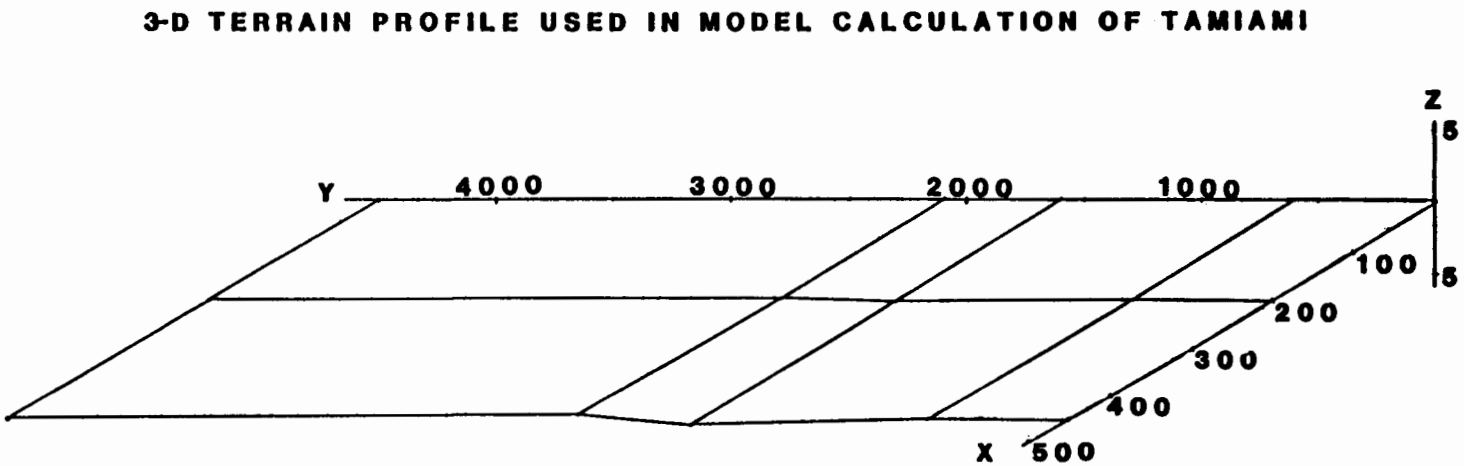

Figure 2-285. TMB terrain profile.

3-D TERRAIN PROFILE USED IN MODEL CALCULATION OF LAWTON

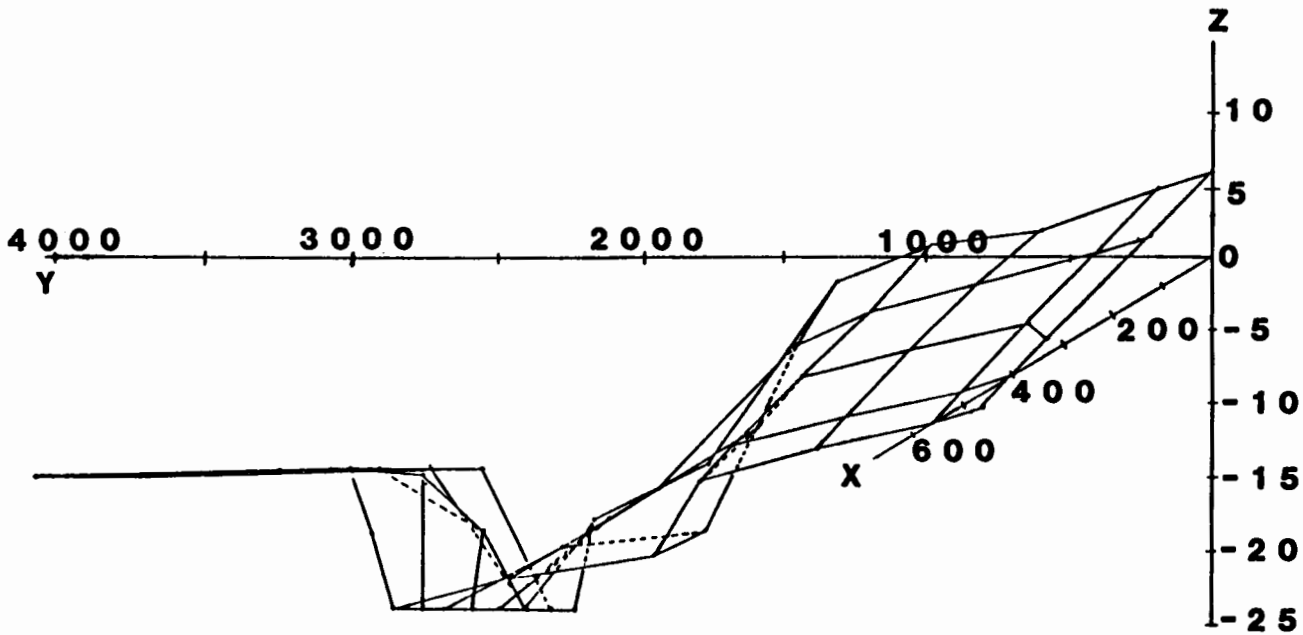

Figure 2-286. LAW terrain profile.

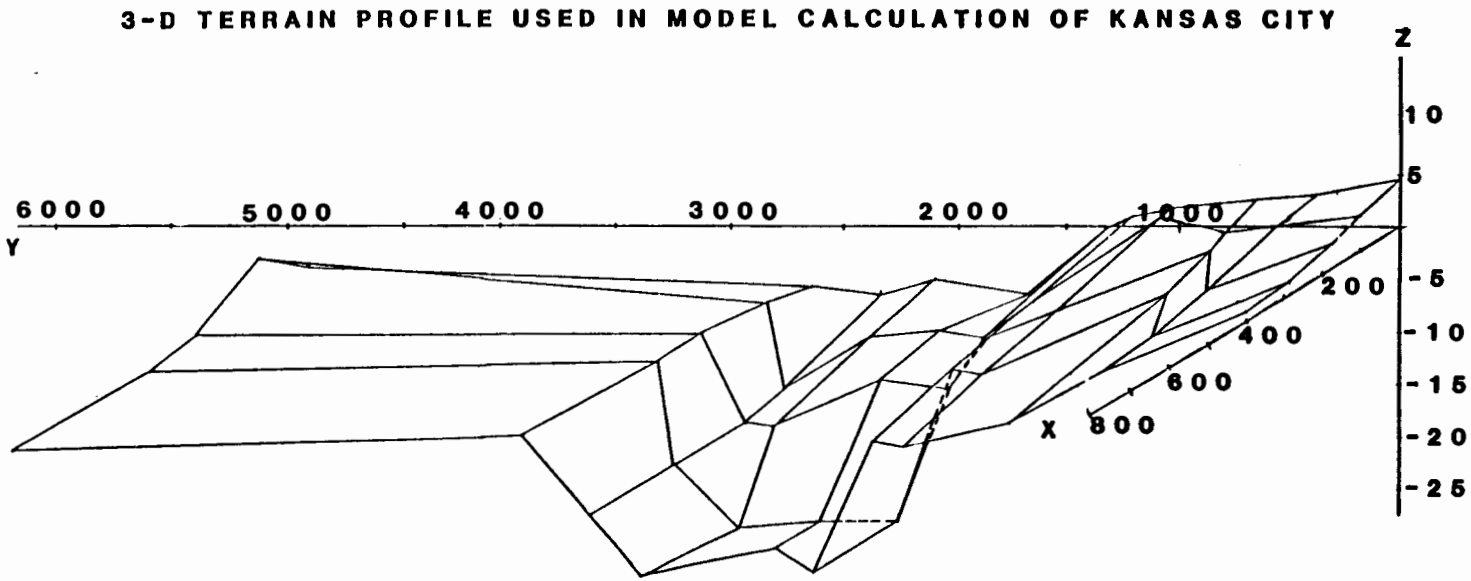

Figure 2-287. PAJ terrain profile.

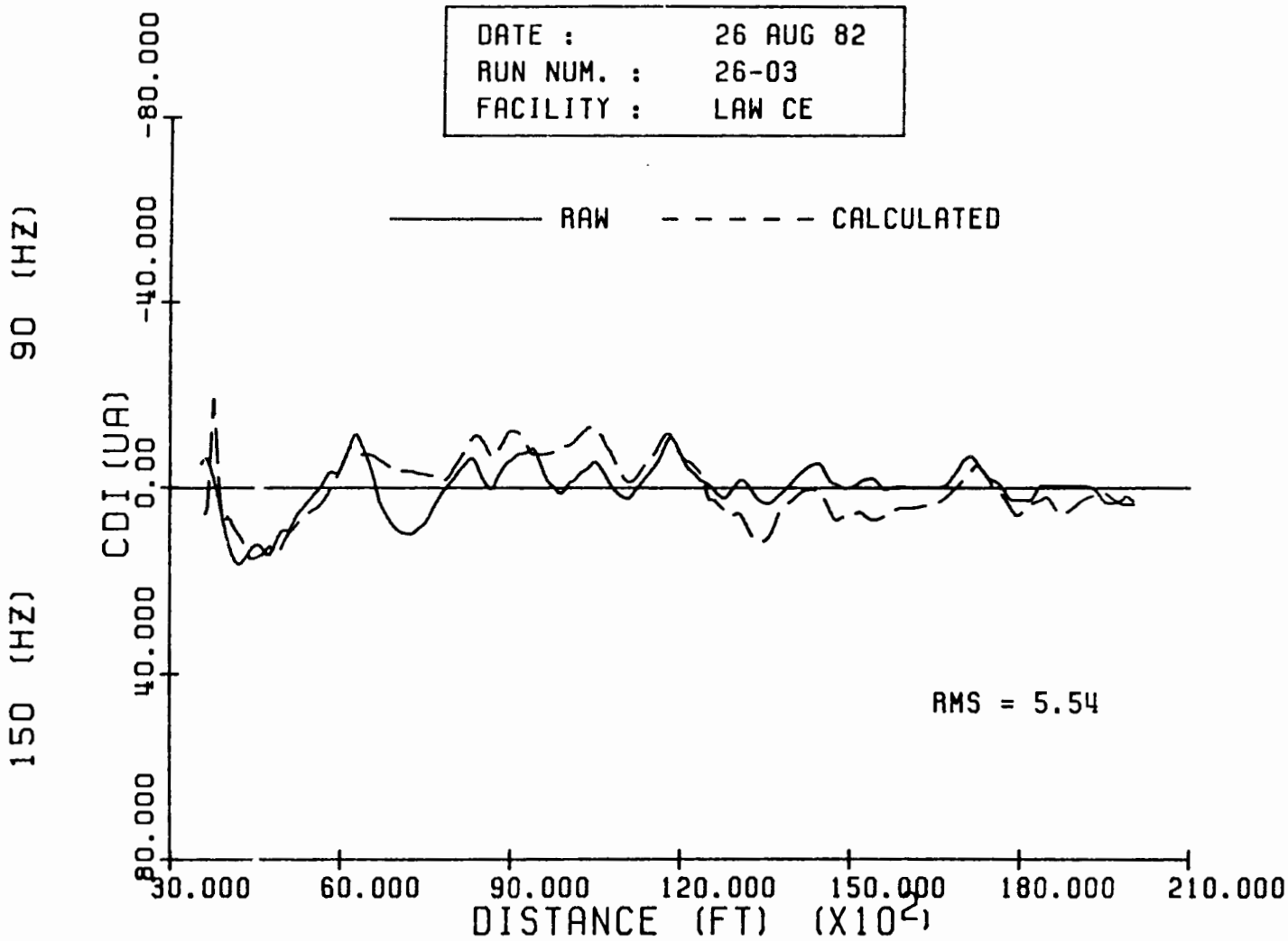

Figure 2-288. Filtered, zero-mean, CDI traces; LAW 26-03.

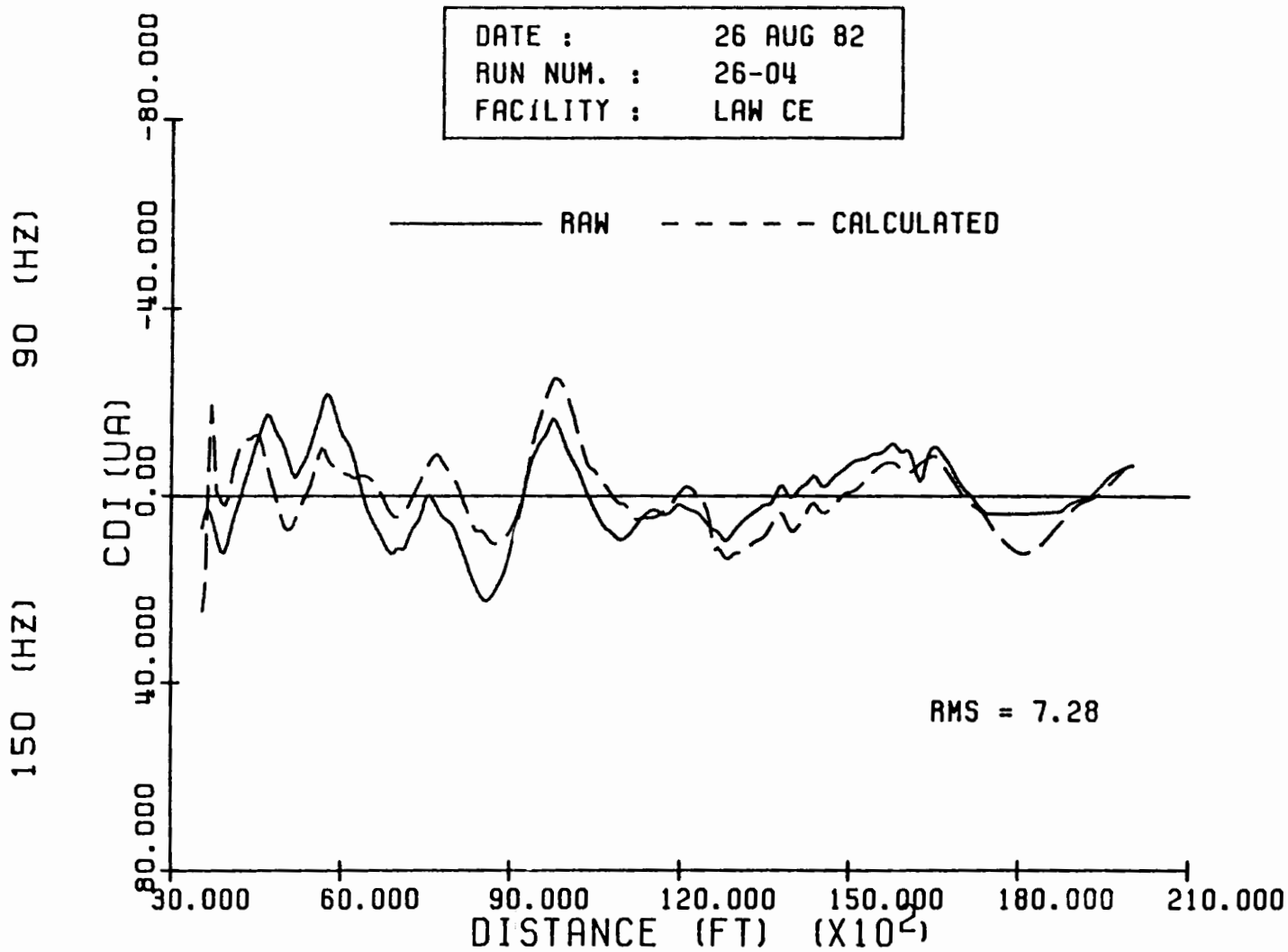

Figure 2-289. Filtered, zero-mean, CDI traces; LAW 26-04.

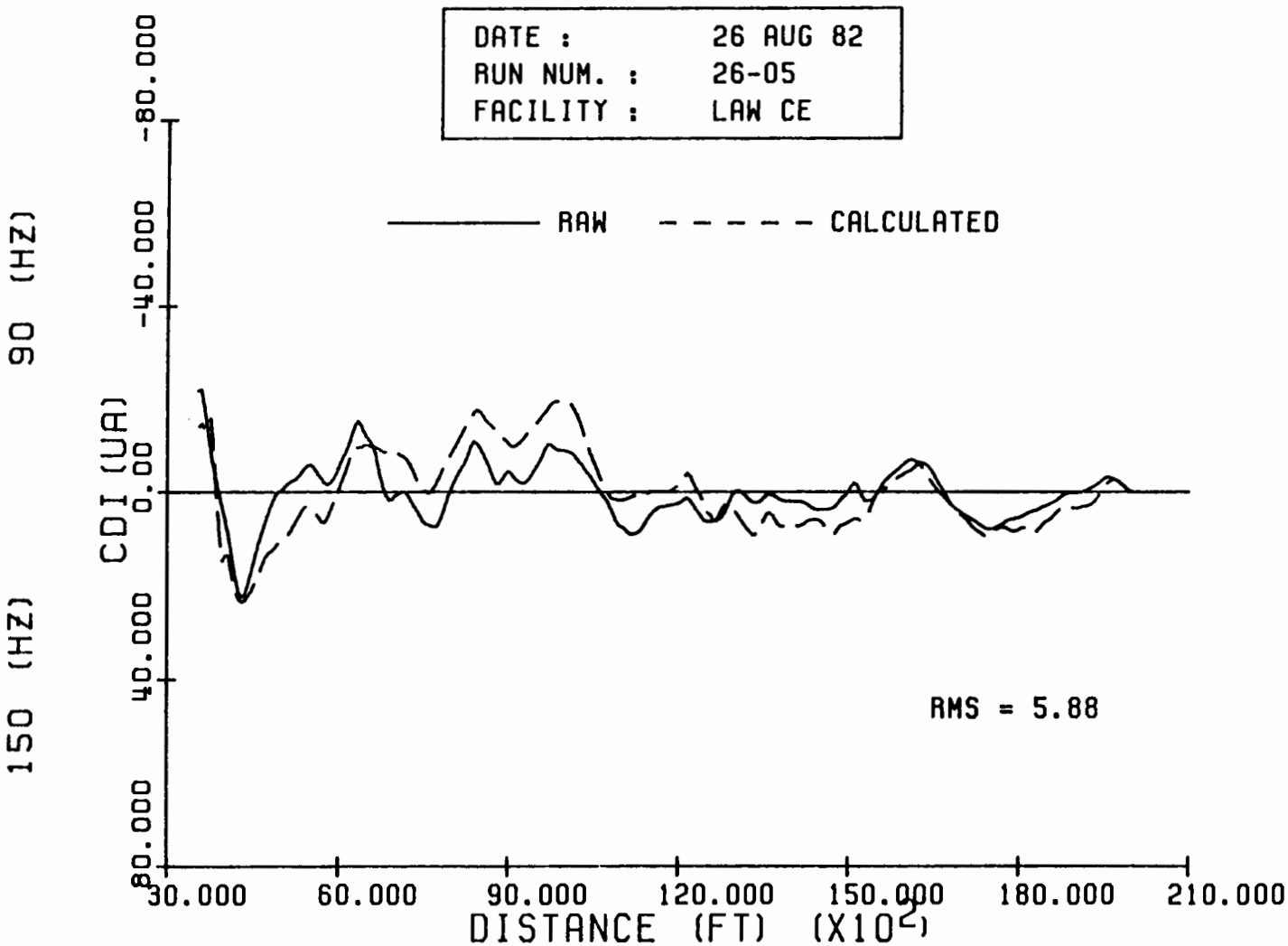

Figure 2-290. Filtered, zero-mean, CDI traces; LAW 26-05.

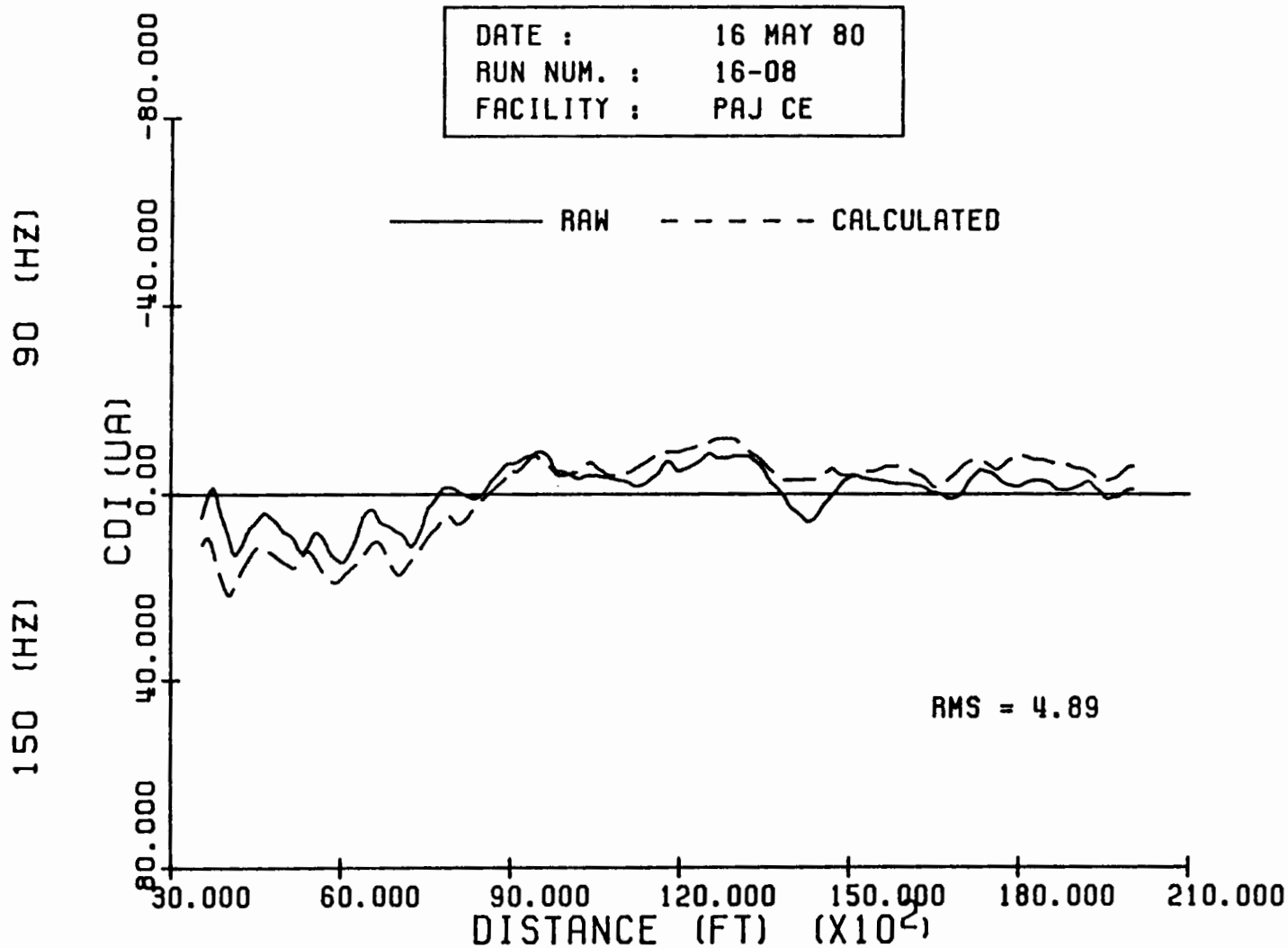

Figure 2-291. Filtered, zero-mean, CDI traces; PAJ 16-08.

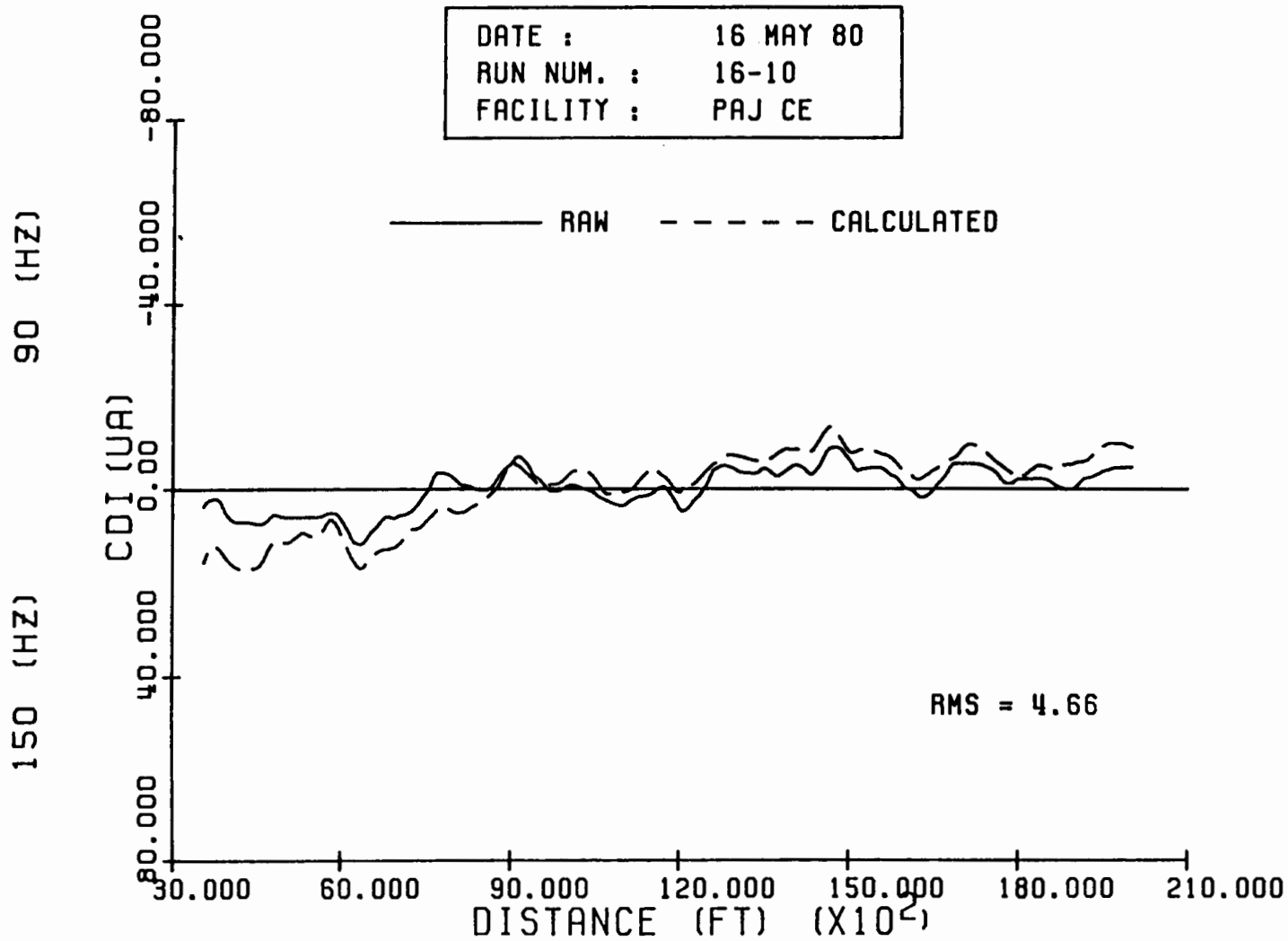

Figure 2-292. Filtered, zero-mean, CDI traces; PAJ 16-10.

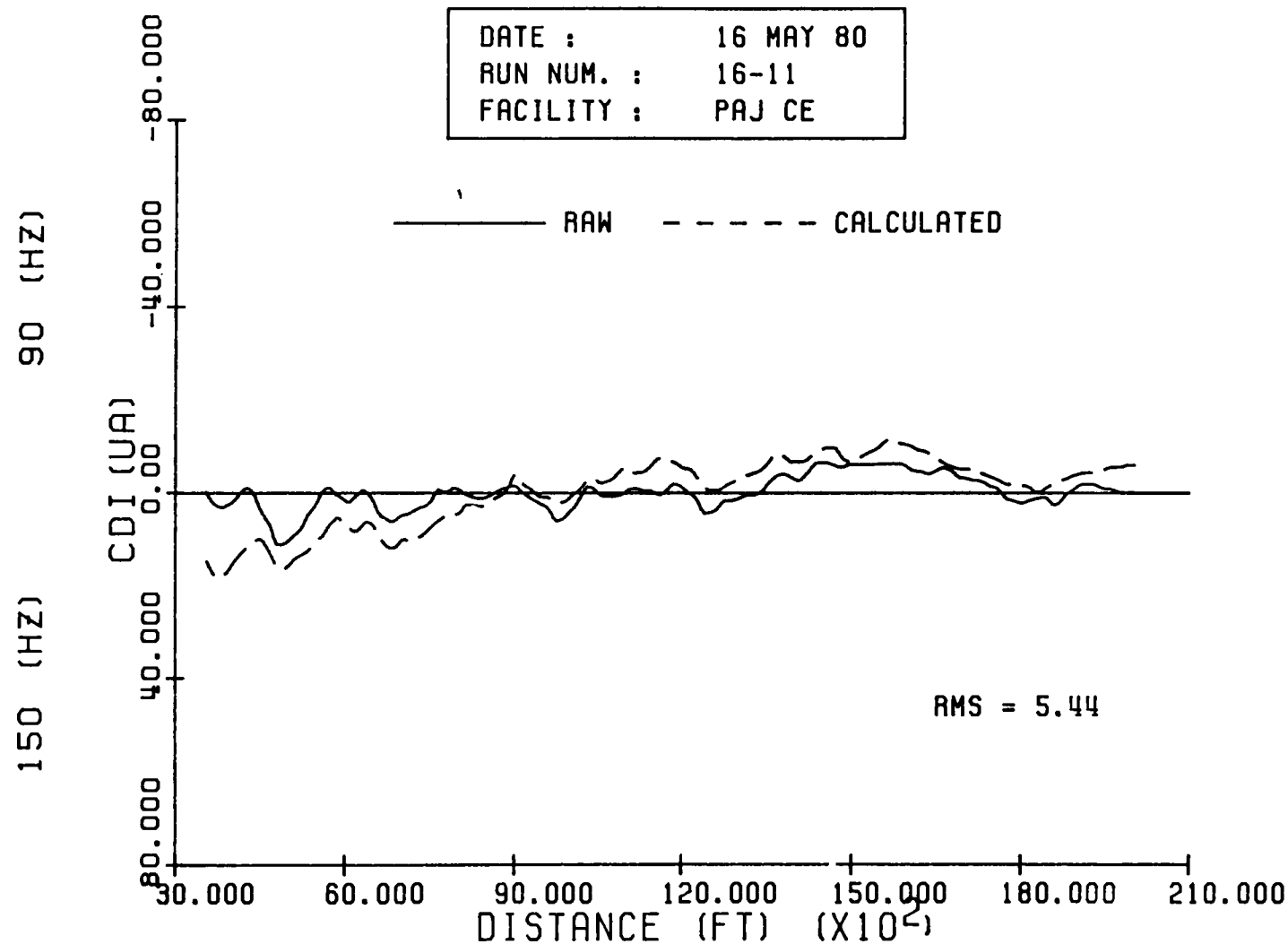

Figure 2-293. Filtered, zero-mean, CDI traces; PAJ 16-11.

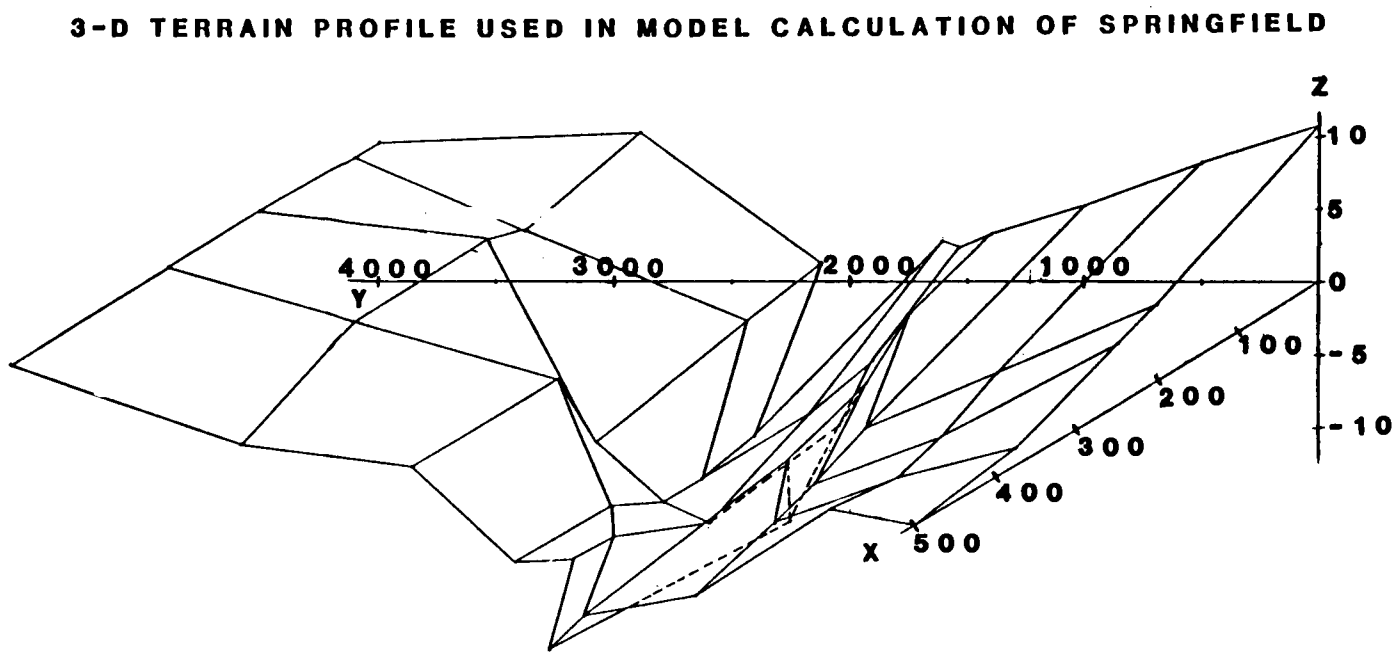

Figure 2-294. SGH terrain profile.

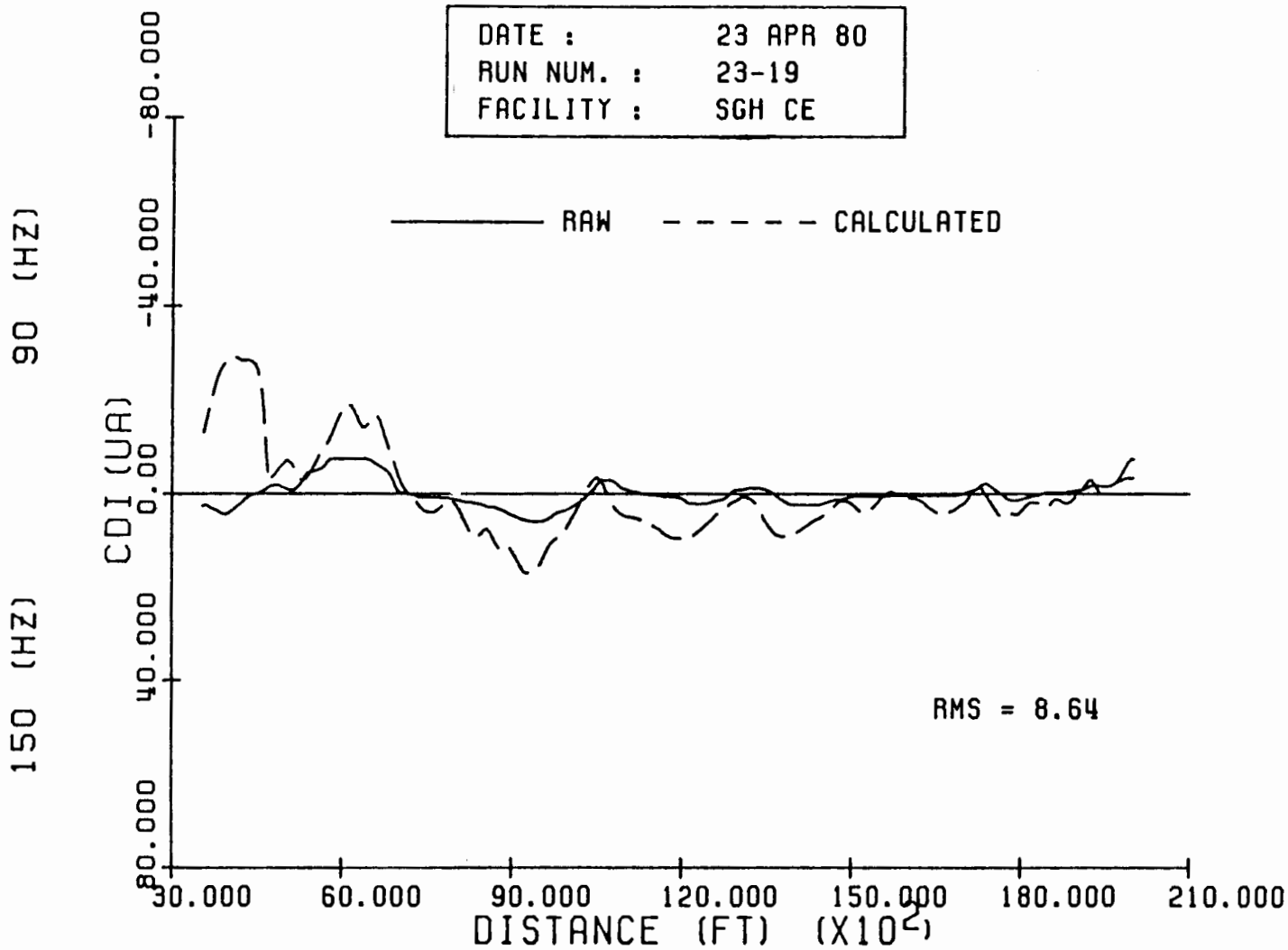

Figure 2-295. Filtered, zero-mean, CDI traces; SGH 23-19.

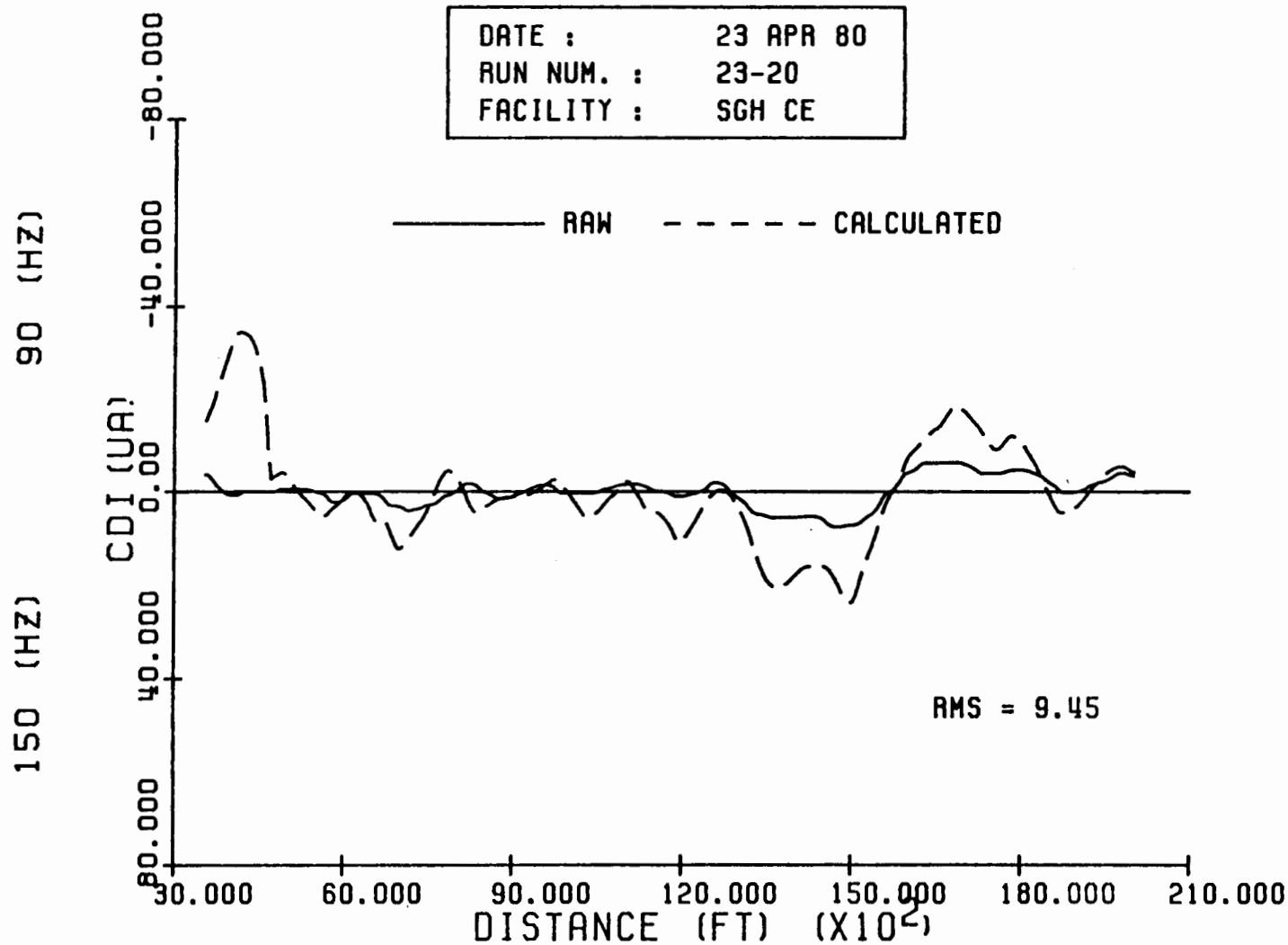

Figure 2-296. Filtered, zero-mean, CDI traces; SGH 23-20.

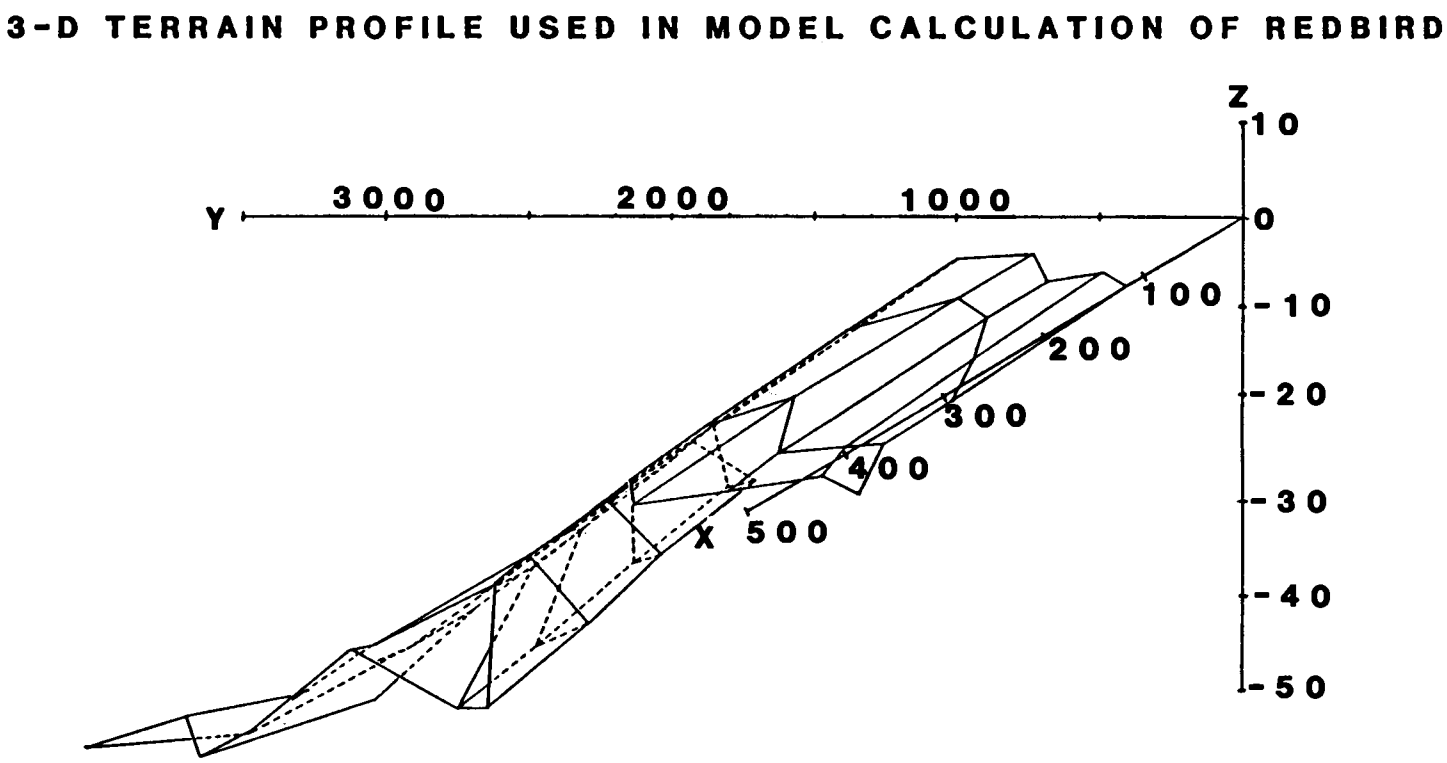

Figure 2-297. RDB terrain profile.

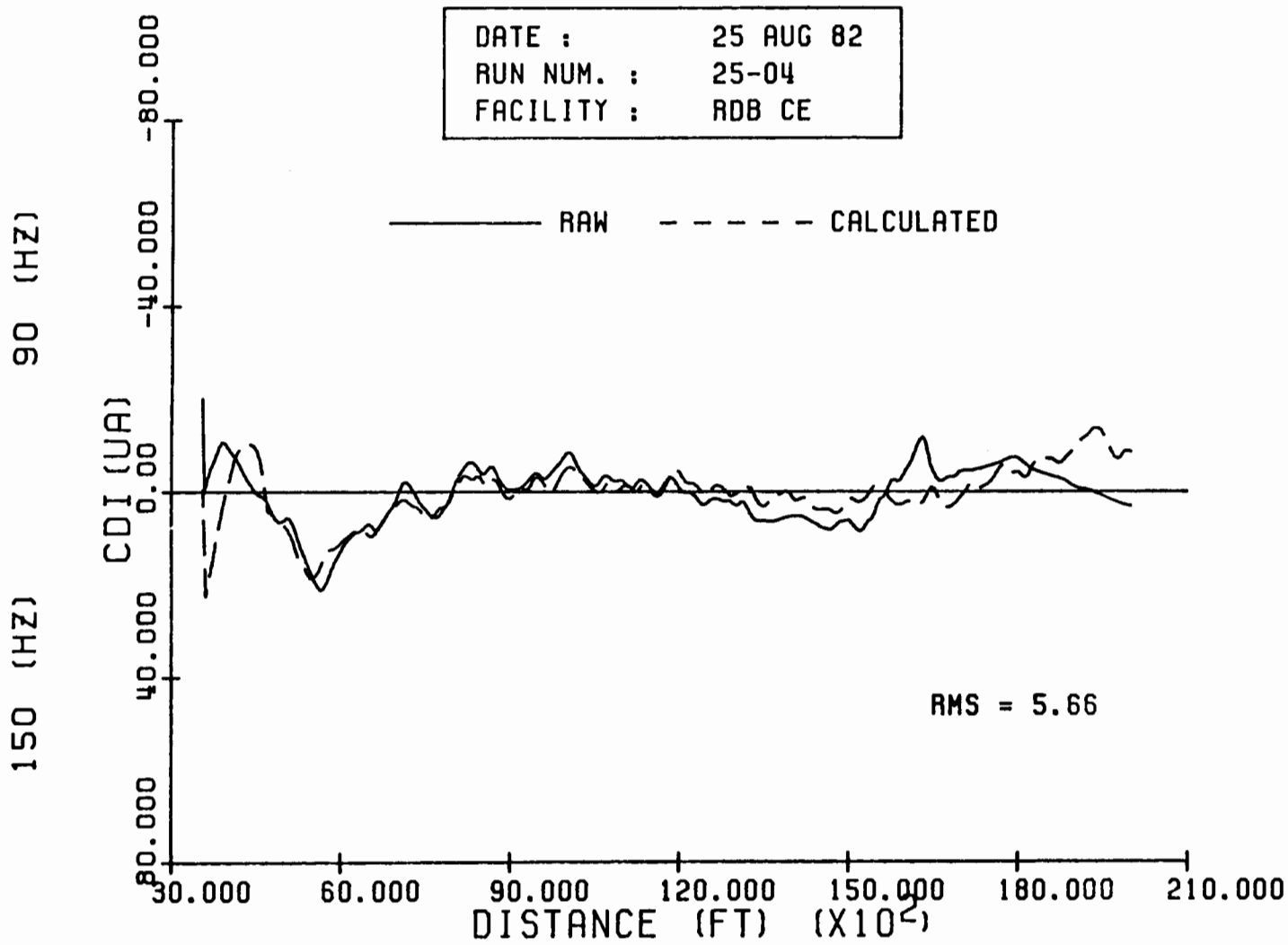

Figure 2-298. Filtered, zero-mean, CDI traces; RDB 25-04.

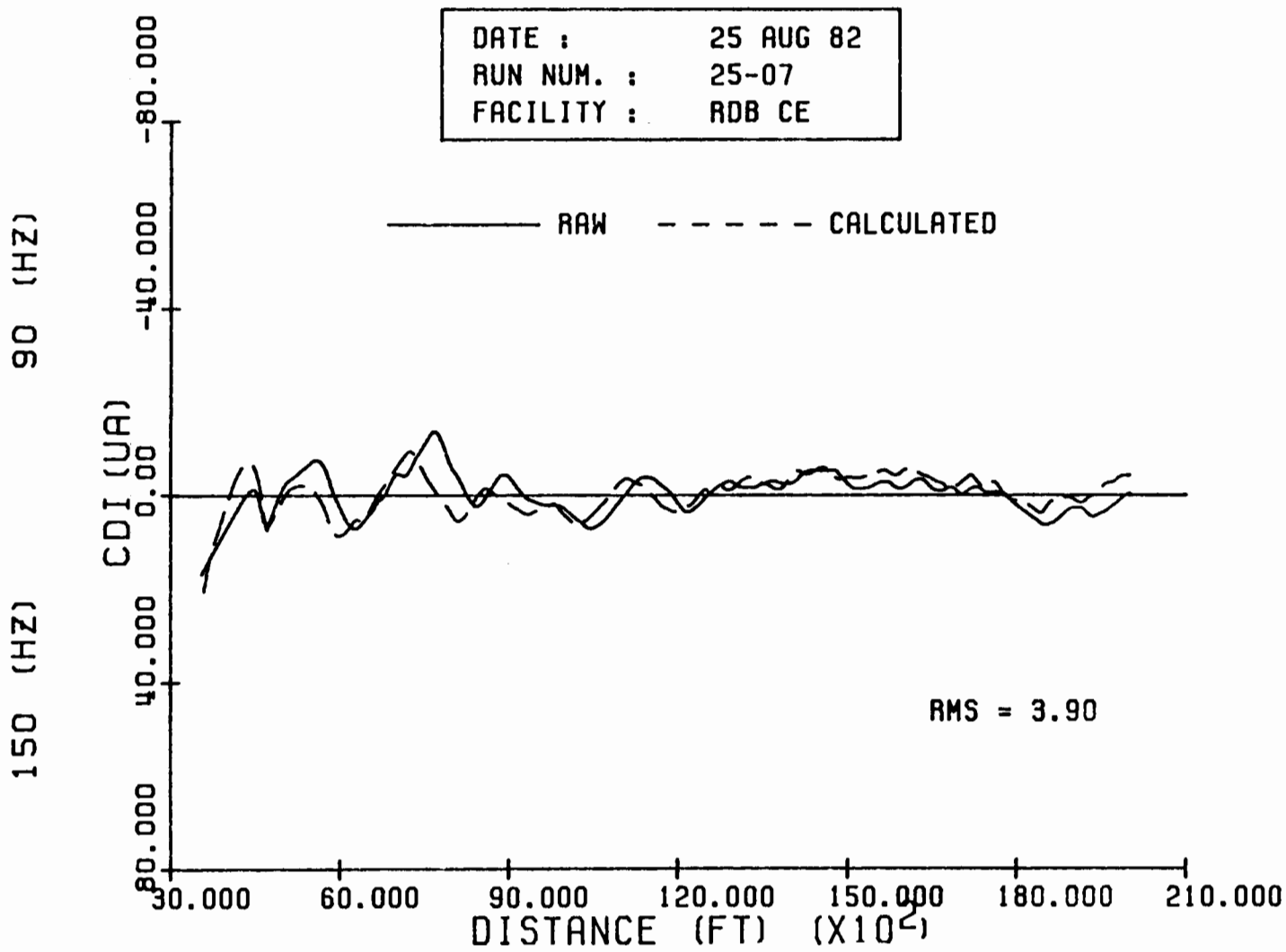

Figure 2-299. Filtered, zero-mean, CDI traces; RDB 25-07.

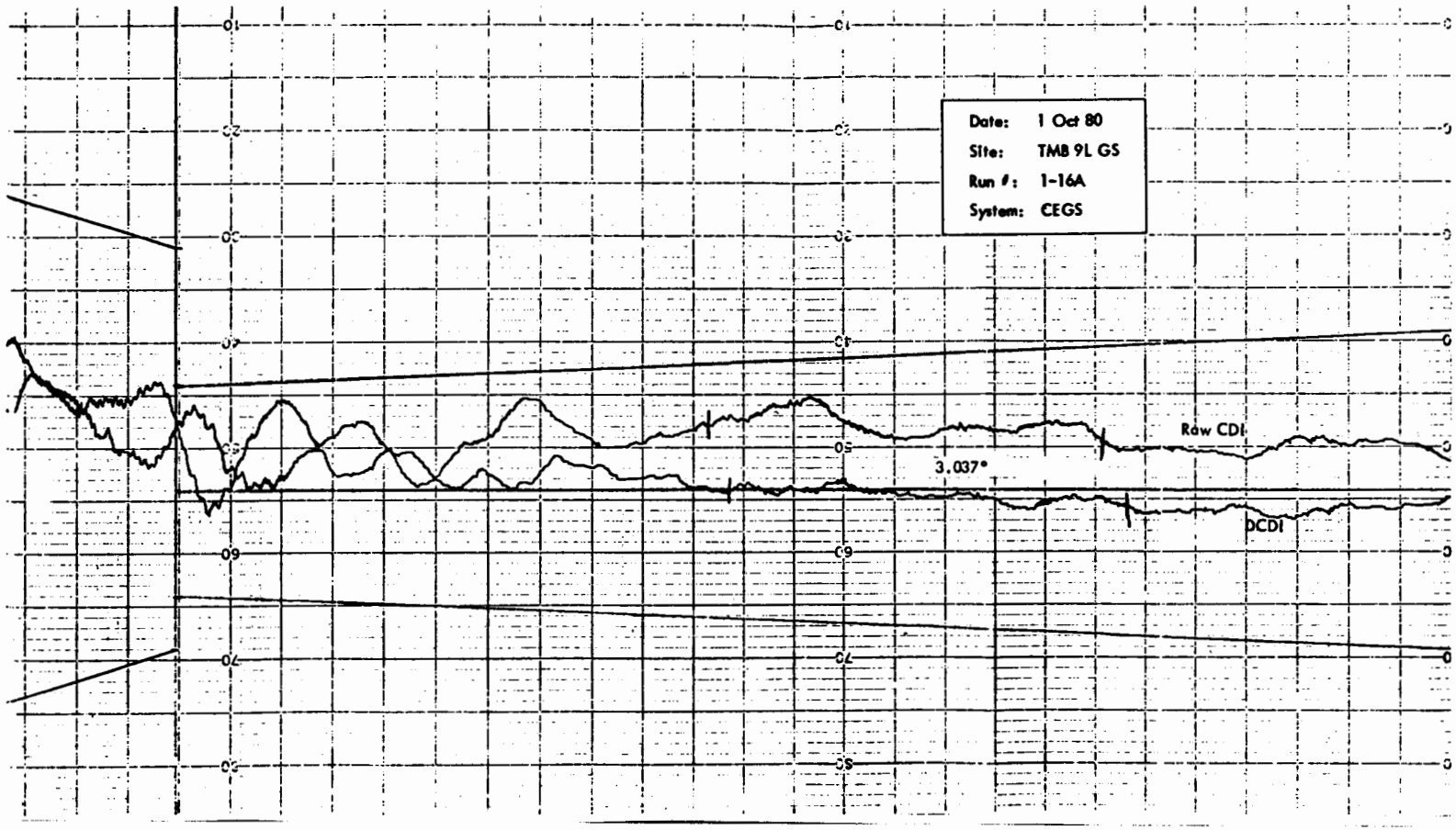

Figure 2-300. Measured raw CDI and differential CDI traces from aircraft recorder.

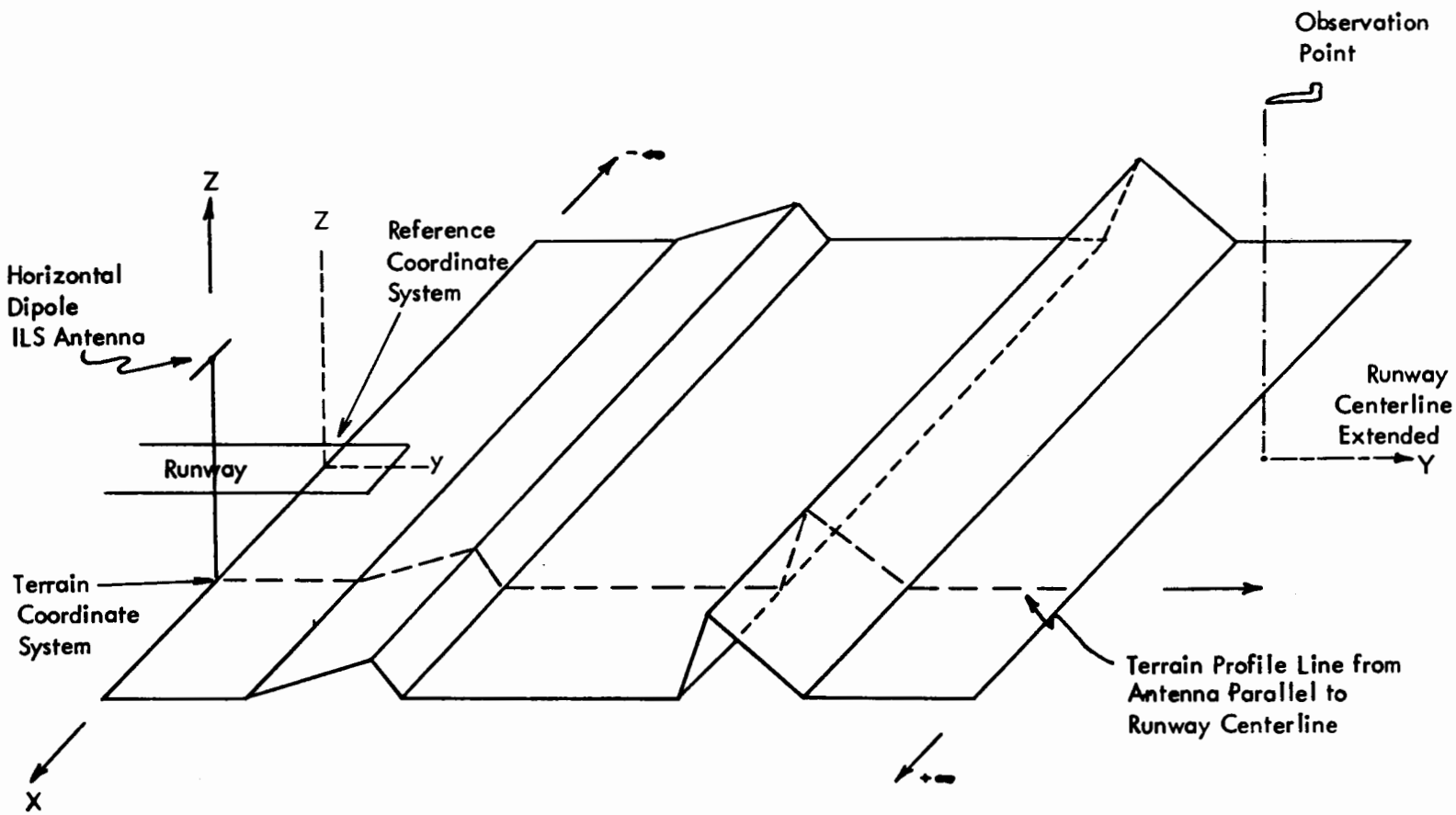

Figure 2-301. Two-dimensional conducting plate approximation to reflecting terrain.

X	Y	Z
4 5		
-10000.0	0.0	0.00
0.0	0.0	0.00
200.0	0.0	0.00
450.0	0.0	0.00
-10000.0	590.0	0.05
0.0	590.0	0.05
200.0	590.0	0.05
450.0	590.0	0.05
-10000.0	1590.0	0.25
0.0	1590.0	0.25
200.0	1590.0	0.25
450.0	1590.0	-0.35
-10000.0	2090.0	0.25
0.0	2090.0	0.25
200.0	2090.0	0.25
450.0	2090.0	0.25
-10000.0	4590.0	0.00
0.0	4590.0	0.00
200.0	4590.0	0.00
450.0	4590.0	0.00

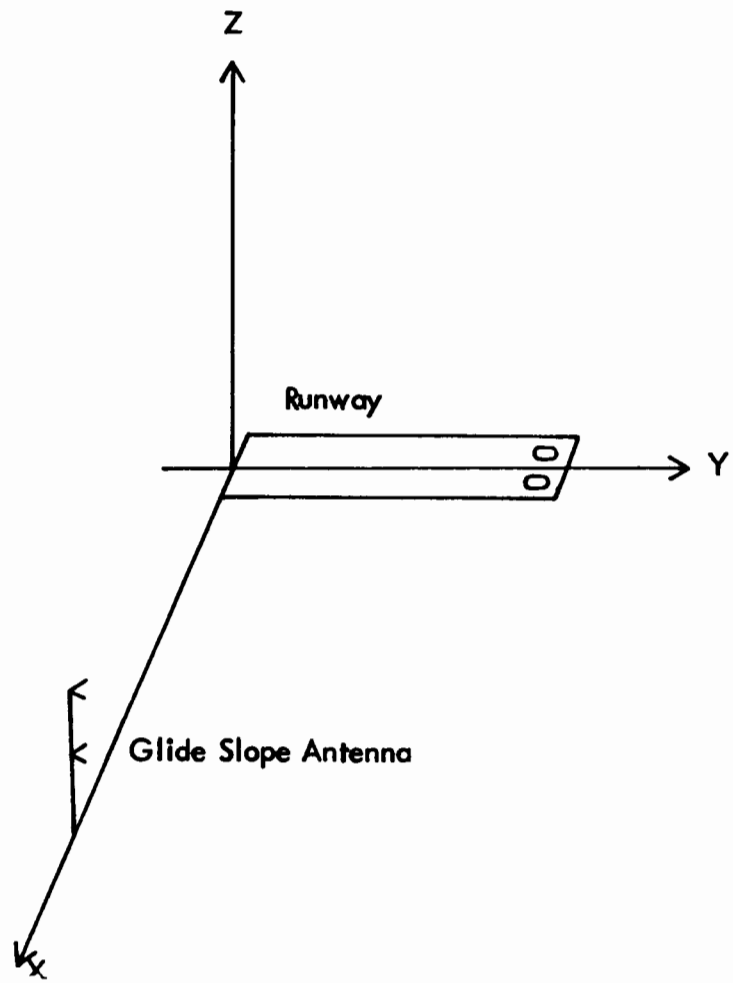

Figure 2-302. Sample terrain profile.

```
*   MODEL INPUT SAMPLE
SECTION       1
NO. OF PTS    0     1     0                                                  Terrain Section
SECTION       2
THEOD                     424.000    82.280     5.167     3.000     0.700    Theodolite Section
SECTION       3
ANT. DATA     3           332.000     0.400     0.300     0.900     0
POSITION      1           452.670     0.0      14.130
CURR & PHS    -0.500       0.0        1.000     0.0       0.484     0.0      Antenna
POSITION      2           451.920     0.0      28.260                        Section
CURR & PHS     1.000       0.0       -0.500     0.0       0.0       0.0
POSITION      3           450.930     0.0      42.390
CURR & PHS    -0.500       0.0        0.0       0.0       0.484     0.0
SECTION       4
PATTERN       3   331     1           0.0   20000.000     3.000              Pattern Selection
PATTERN                               0.0    3500.000                        Section
SECTION       5
OUTPUT        2     1     1      30000.000     0.0     100.000 -100.00000000000000  Output Control Section
...
```

Figure 2-303. Example of model input data.

The following control points were used in digitizing flight check recordings.

1.	Second road	33,075 FT.
2.	Canal	18,787 FT.
3.	Krome avenue	12,950 FT.
4.	Boundary fence	1,979 FT.
5.	Threshold	1,044 FT.

Numbers to be entered when executing DATACON are:

33075.0
14288.0
5837.0
10971.0
935.0

The theodolite location used in the validation is:

X = 424.0 FEET
Y = 82.28 FEET
Z = 5.167 FEET

The glide slope reference angle is 3 degrees.

These traces were taken from 10 in. recordings.

Figure 2-304. Sample memo file containing data used in validation procedure.

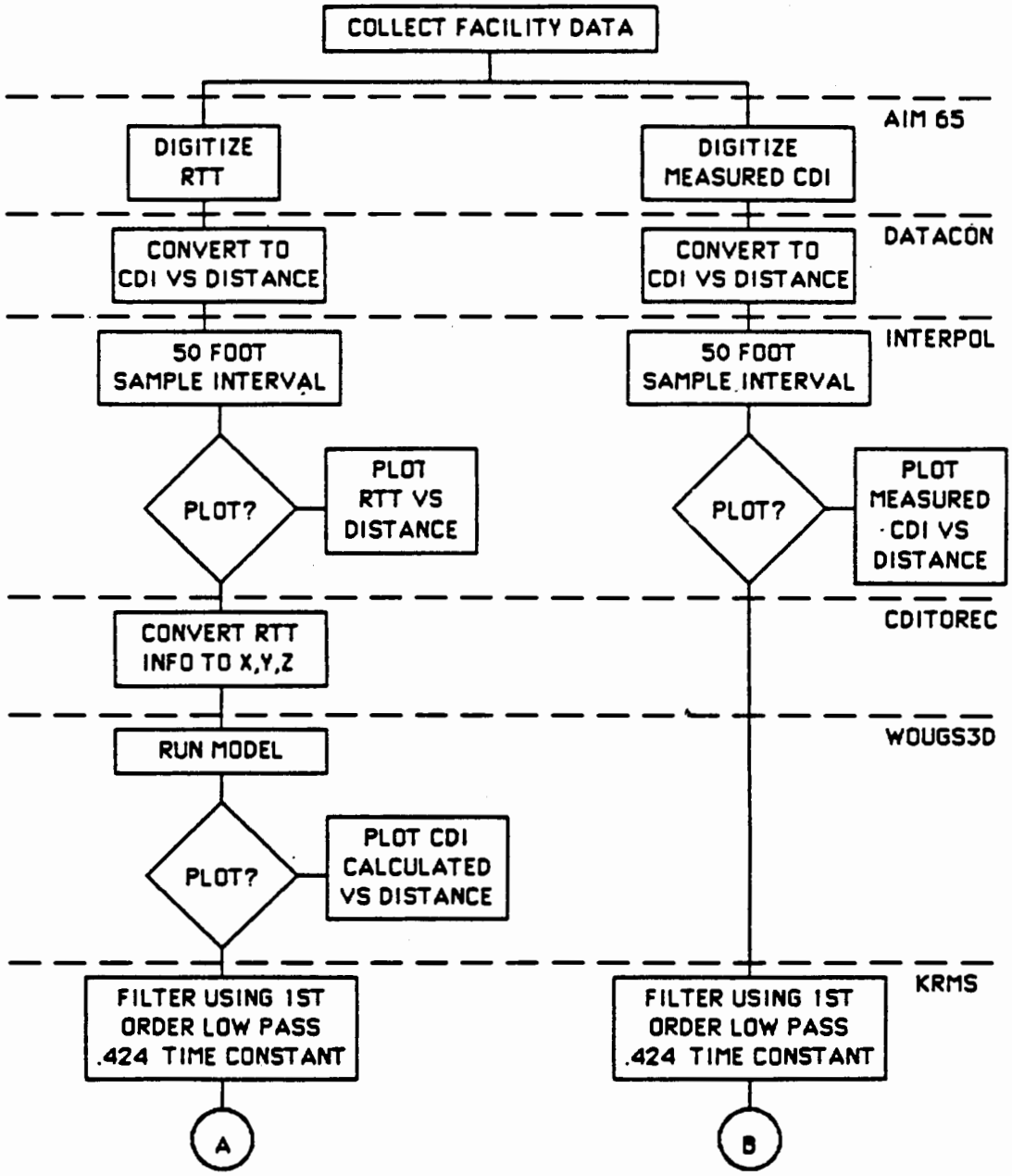

Figure 2-305. Flowchart of math model validation procedure (2 sheets).

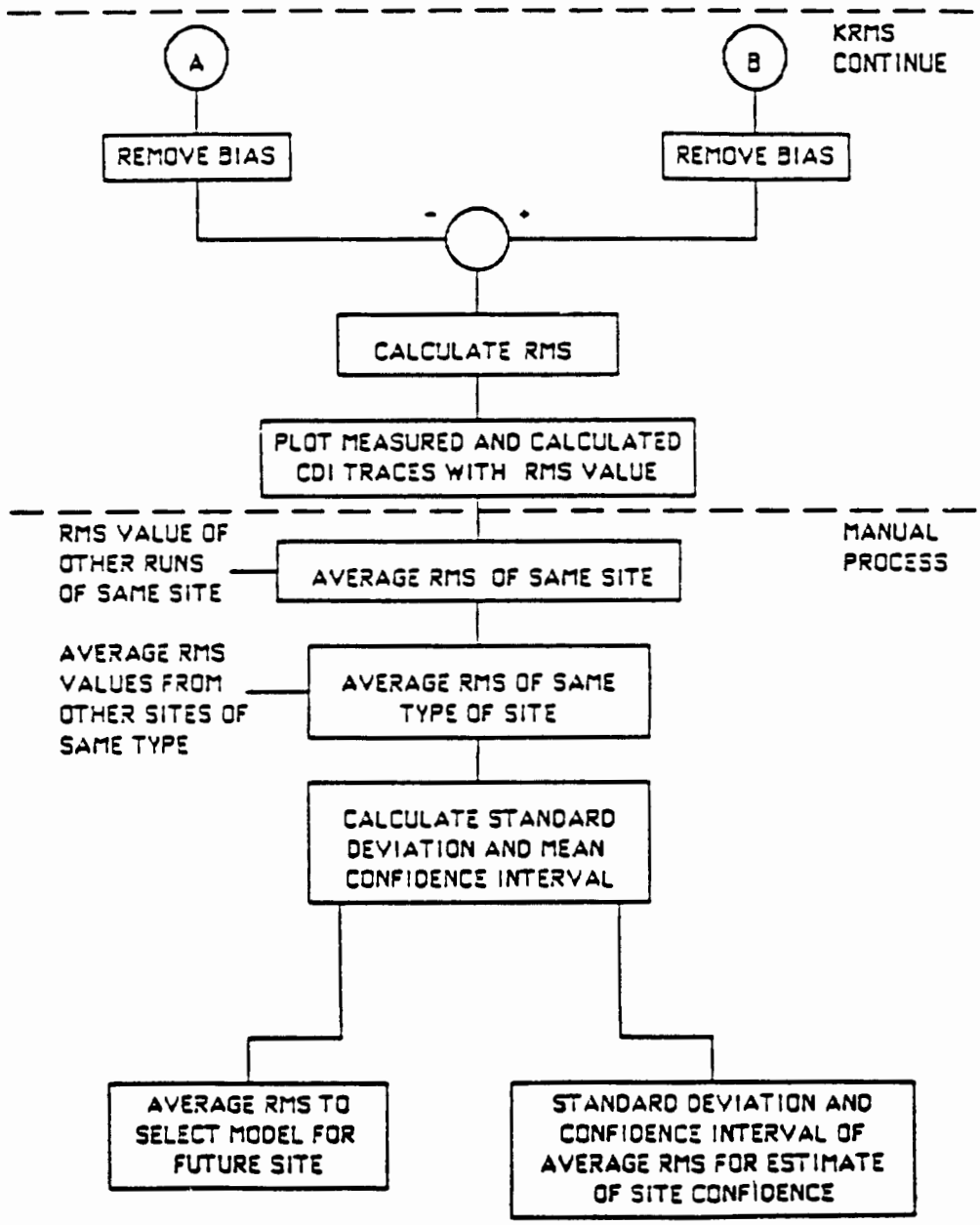
KRMS
CONTINUE
A
B
REMOVE BIAS
REMOVE BIAS
-
+
CALCULATE RMS
PLOT MEASURED AND CALCULATED
CDI TRACES WITH RMS VALUE
MANUAL
PROCESS
RMS VALUE OF
OTHER RUNS
OF SAME SITE
AVERAGE RMS OF SAME SITE
AVERAGE RMS
VALUES FROM
OTHER SITES OF
SAME TYPE
AVERAGE RMS OF SAME
TYPE OF SITE
CALCULATE STANDARD
DEVIATION AND MEAN
CONFIDENCE INTERVAL
AVERAGE RMS TO
SELECT MODEL FOR
FUTURE SITE
STANDARD DEVIATION AND
CONFIDENCE INTERVAL OF
AVERAGE RMS FOR ESTIMATE
OF SITE CONFIDENCE

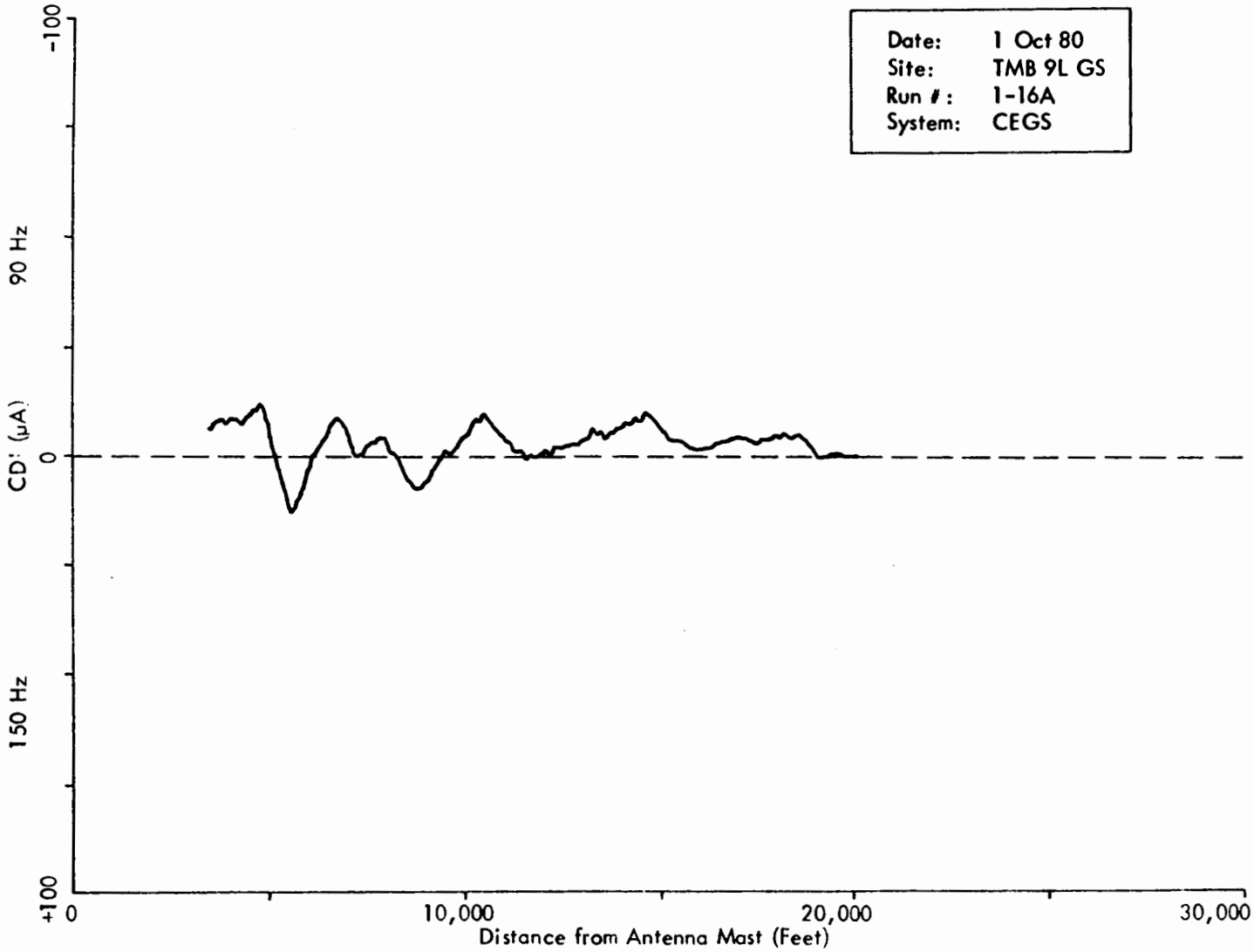

Figure 2-306. Measured CDI trace after digitization and sampling process.

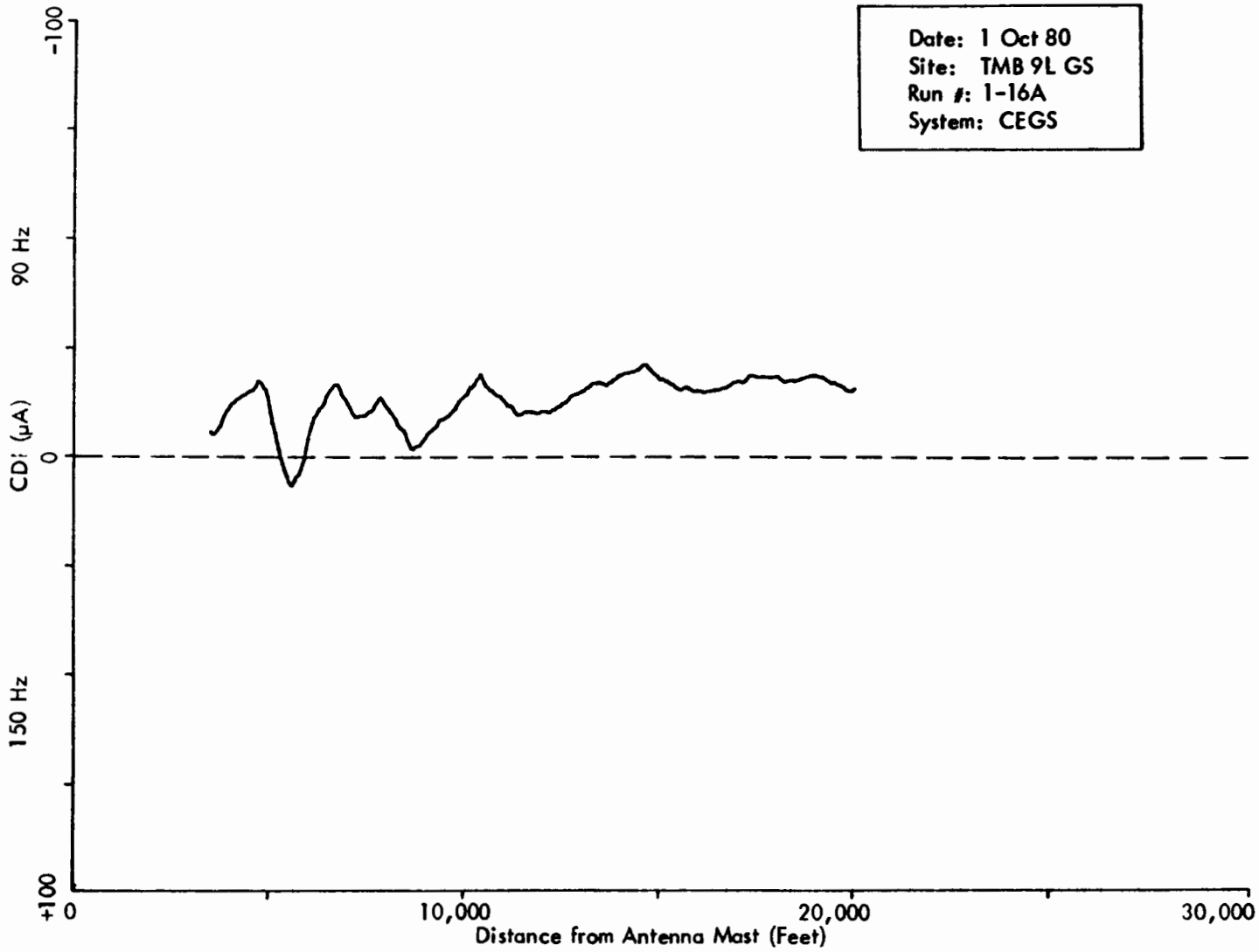

Figure 2-307. Sample of digitized RTT information recorded at TMB.

```
*   SAMPLE OF MODEL INPUT FOR VALIDATION OF GLIDE SLOPE
SECTION        1
NO. OF PTS     0     1     0
SECTION        2
THEOD                  424.000    82.280      5.167      3.000      0.700
SECTION        3
ANT. DATA      3       332.000      0.400      0.300      0.900     0
POSITION       1       452.670      0.0       14.130
CURR & PHS    -0.500     0.0        1.000      0.0        0.484      0.0
POSITION       2       451.920      0.0       28.260
CURR & PHS     1.000     0.0       -0.500      0.0        0.0        0.0
POSITION       3       450.930      0.0       42.390
CURR & PHS    -0.500     0.0        0.0        0.0        0.484      0.0
SECTION        4
PATTERN        3  331     1          0.0    20000.000      3.000
PATTERN                              0.0     3500.000
SECTION        5
OUTPUT         2     1     1      30000.000      0.0      100.000 -100.00000000000000

      0.0      20000.0000    1076.2549
      0.0      19950.0000    1073.2639
      0.0      19900.0000    1071.1345
      0.0      19850.0000    1068.7878
      0.0      19800.0000    1066.6580

      --------------*---------------

      0.0       3700.0000     198.1818
      0.0       3650.0000     195.8096
      0.0       3600.0000     193.2879
      0.0       3550.0000     190.7264
      0.0       3500.0000     188.2540
```

Figure 2-308. Sample of model input for validation of glide slope.

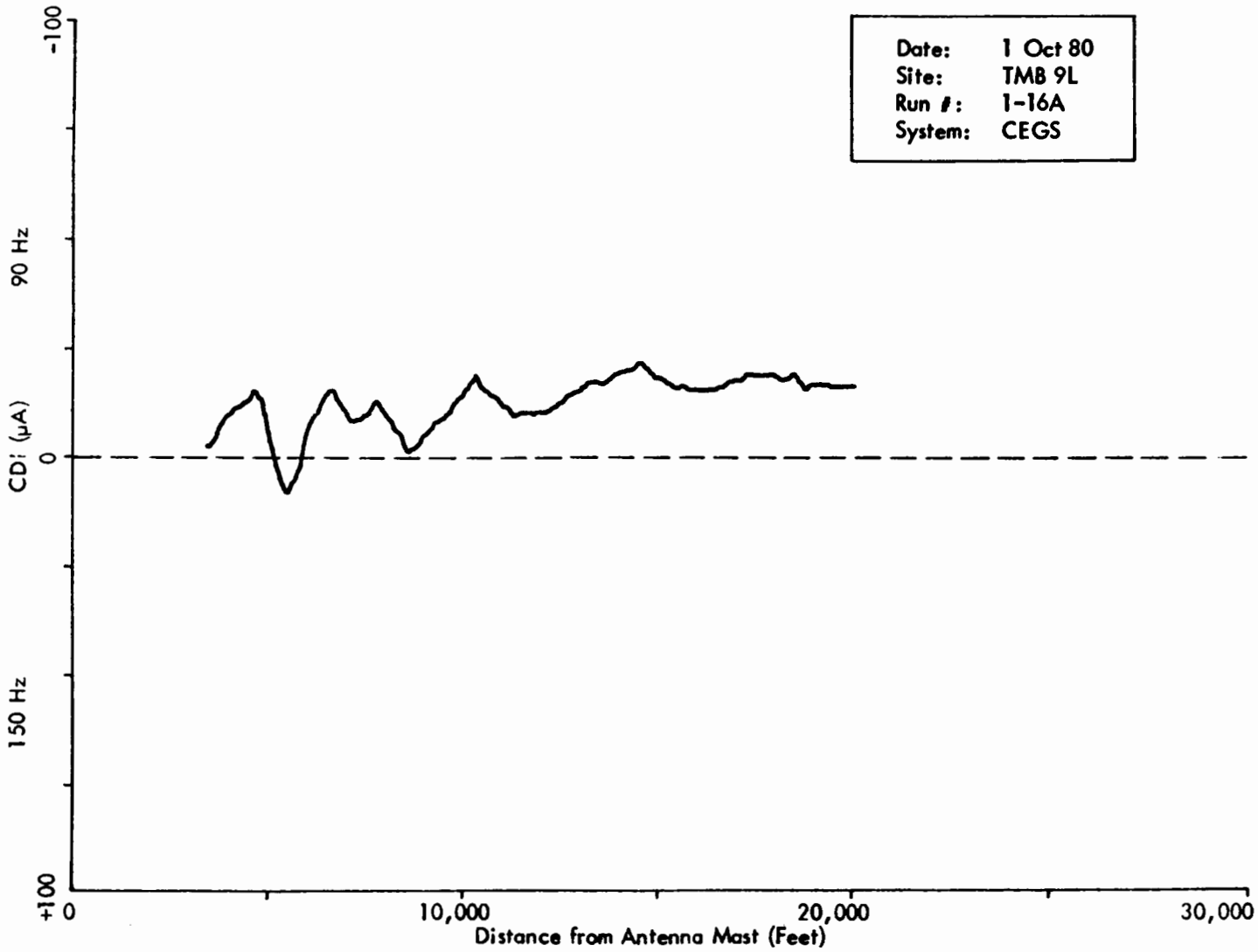

Figure 2-309. Model calculation.

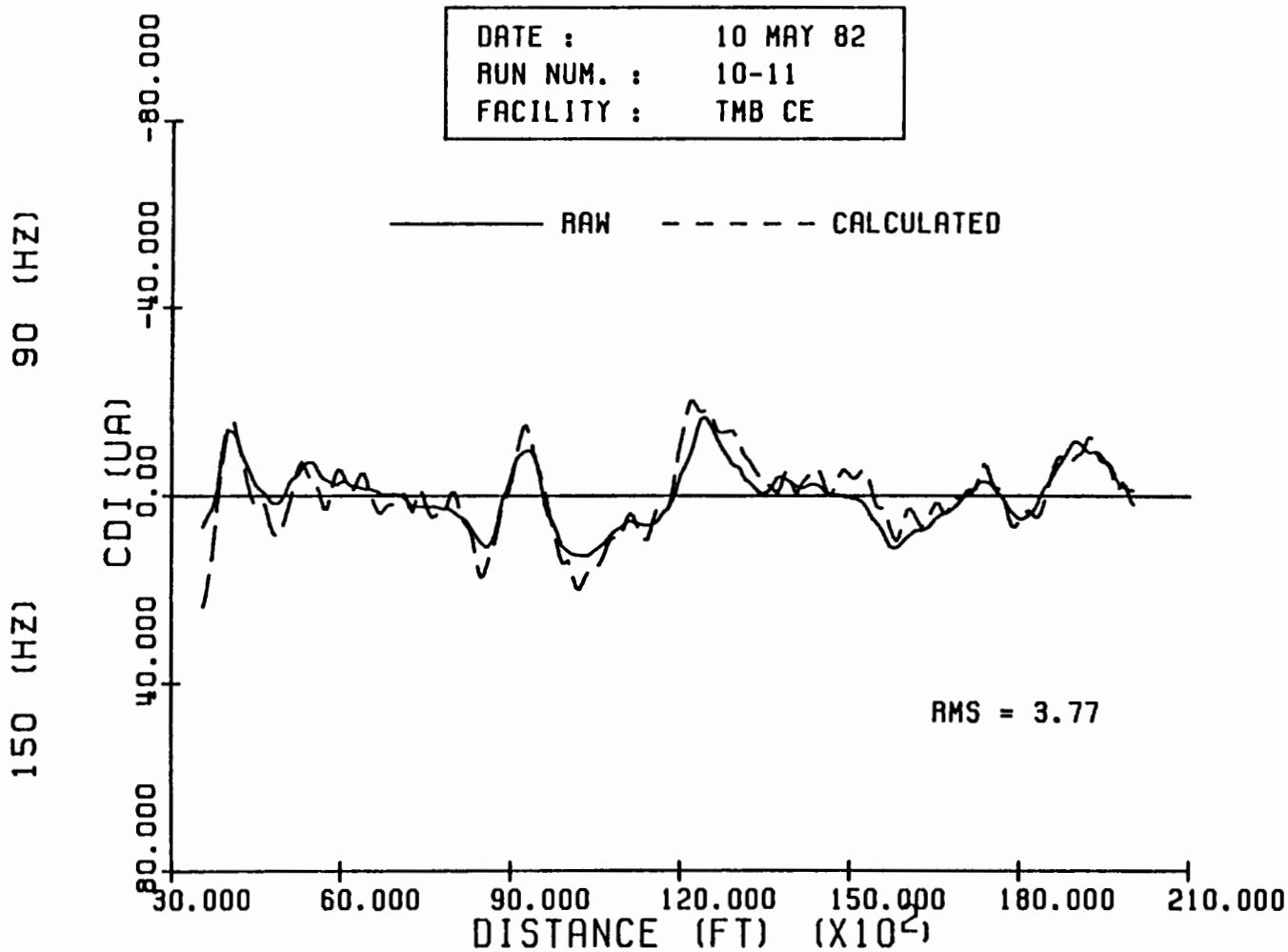

Figure 2-310. Filtered, zero-mean, CDI traces used for model validation.

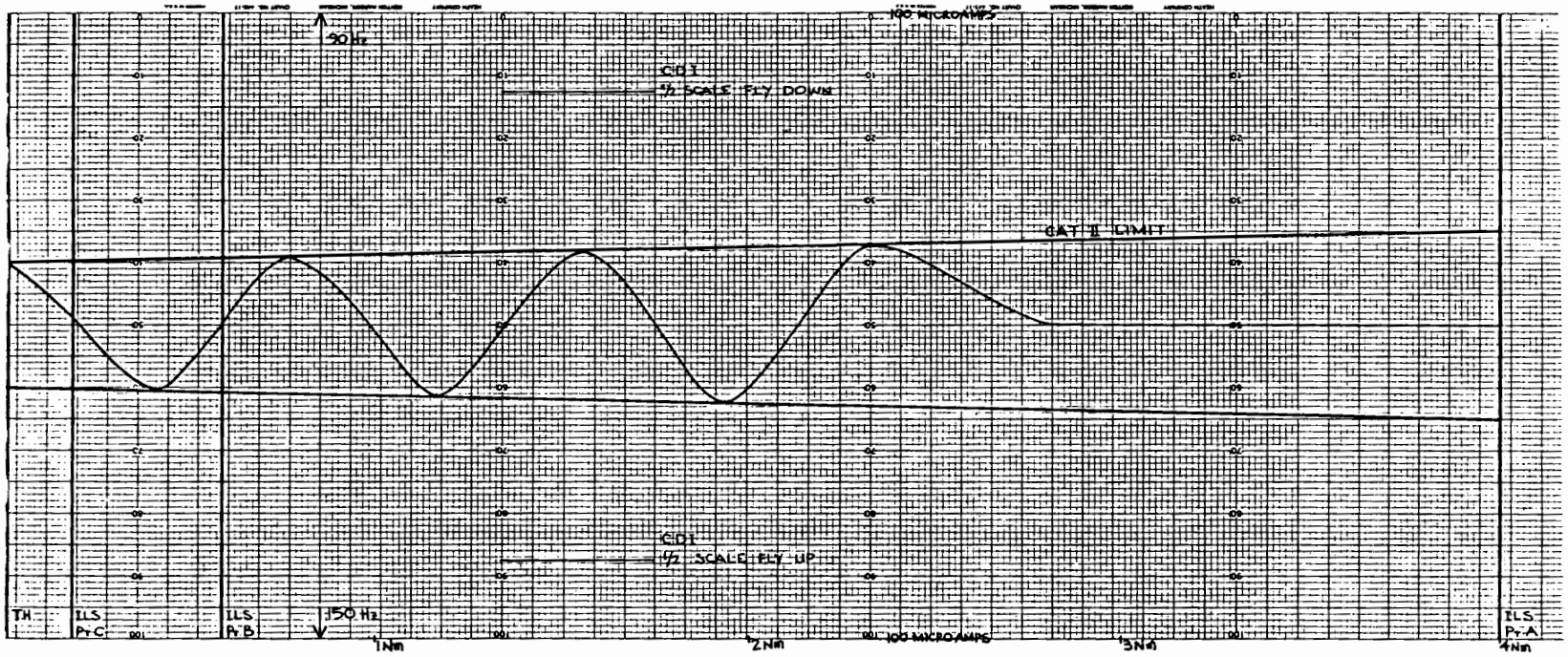

Figure 4-1. Test Path 1 (Case 1), glide slope structure for flight simulation which provided a uniform spatial frequency existing throughout ILS Zones 2 and 3. The magnitude shown was that for which Category II limits would be reached.

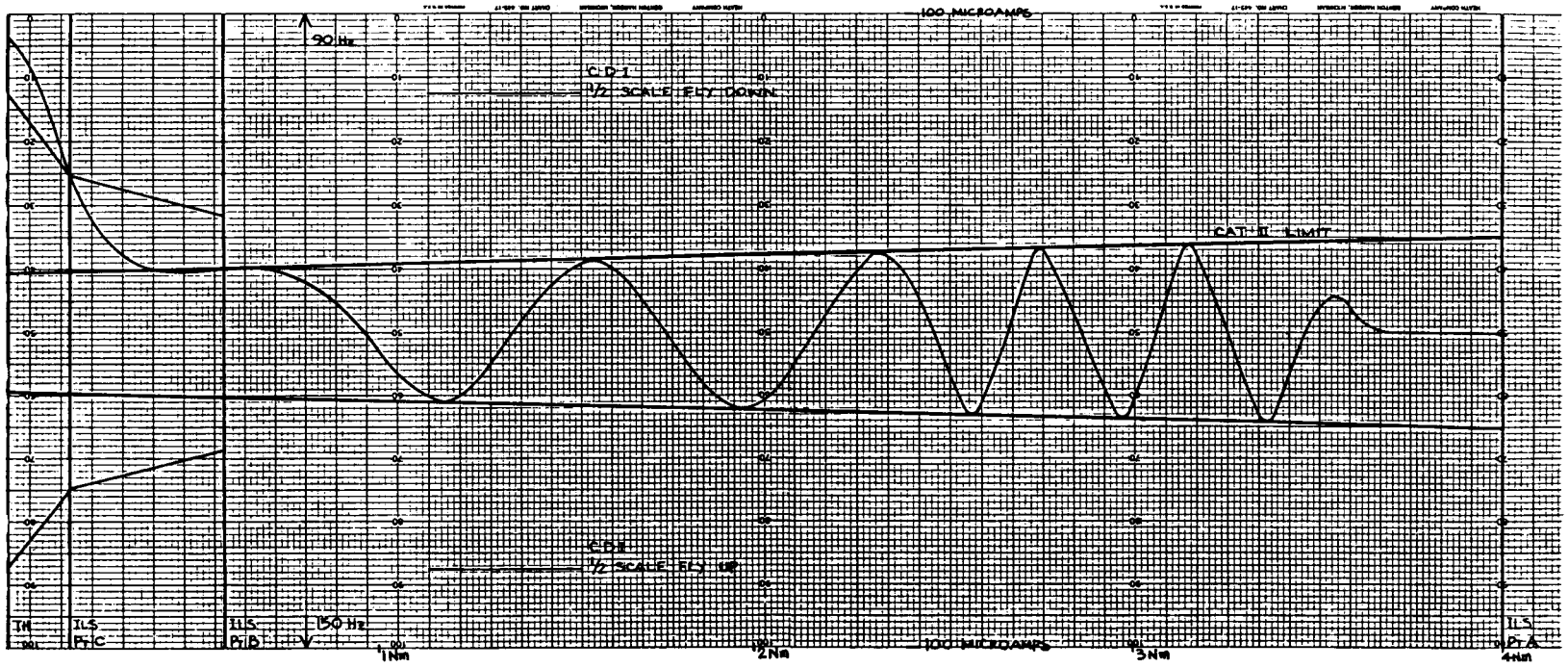

Figure 4-2. Test Path 2 (Case 2), the glide slope structure was constructed to provide a slowly decreasing spatial frequency with a maximum fly-down occurring as the threshold of the runway is approached.

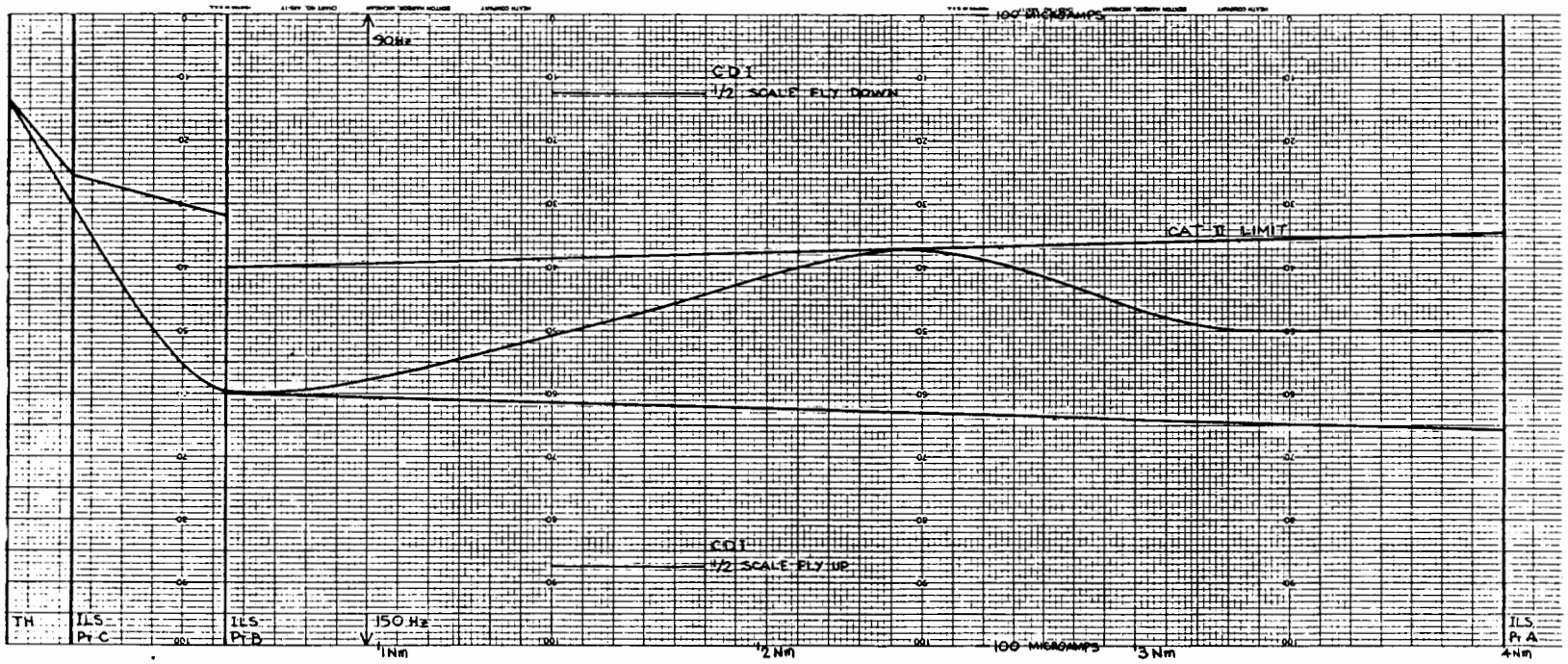

Figure 4-3. Test Path 3 (Case 3), the glide slope structure was constructed to provide a slowly varying path, one which the pilot could be expected to fly ending in a maximum fly-down condition at the runway threshold.

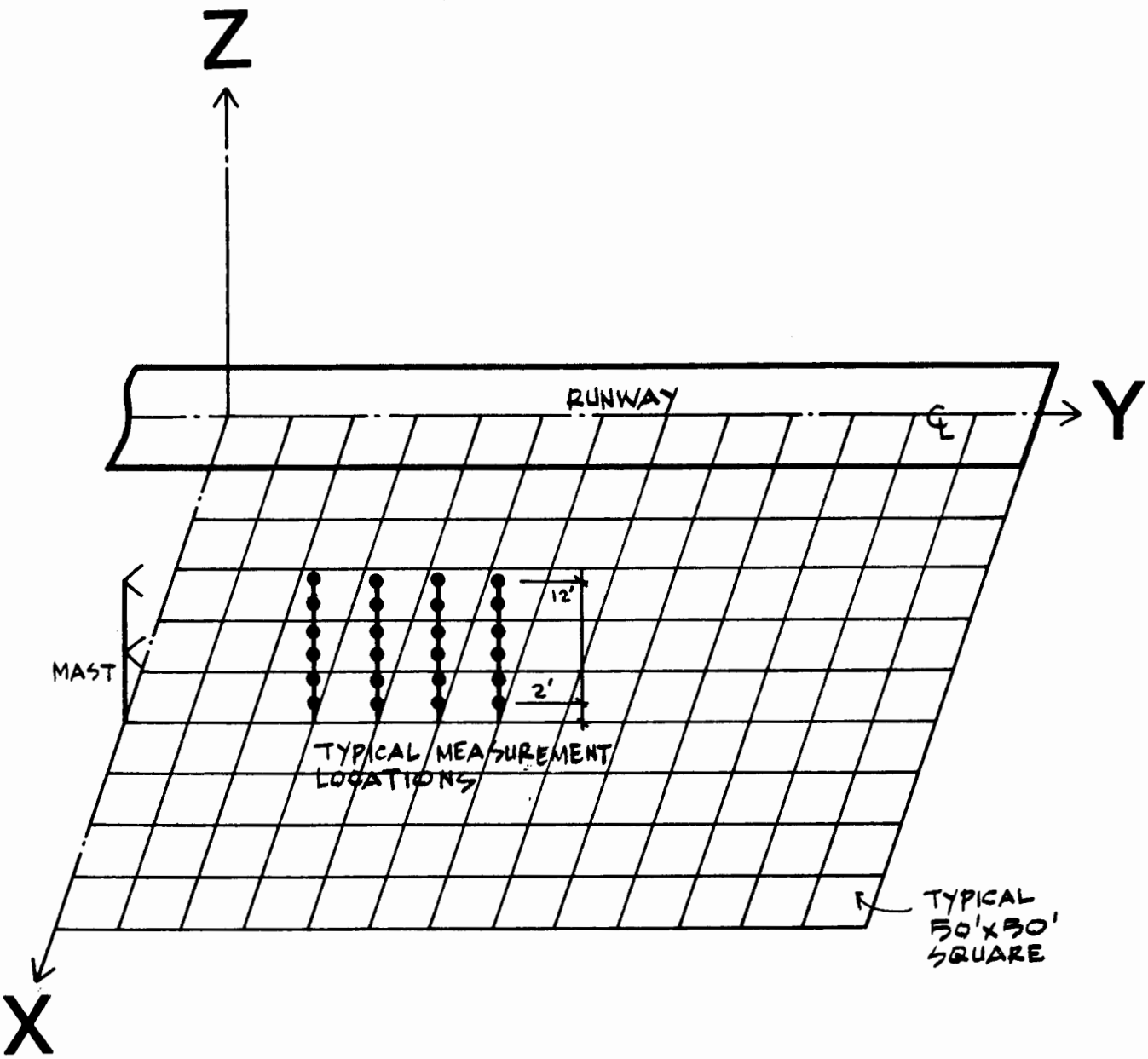

Figure 5-1. Coordinate system description.

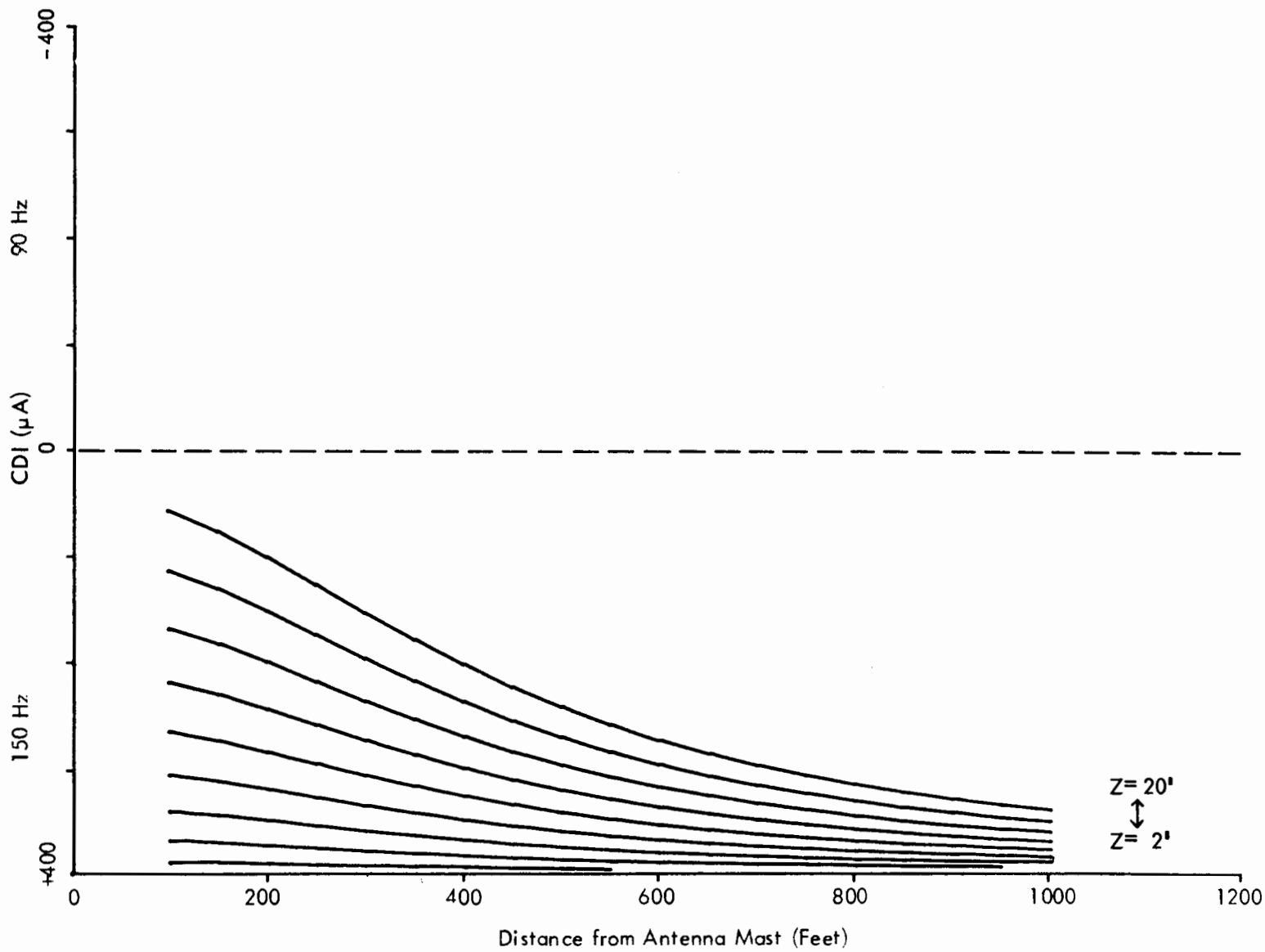

Figure 5-2. TMB predicted data, normal SBR, X=50', Z=2' to Z=12'.

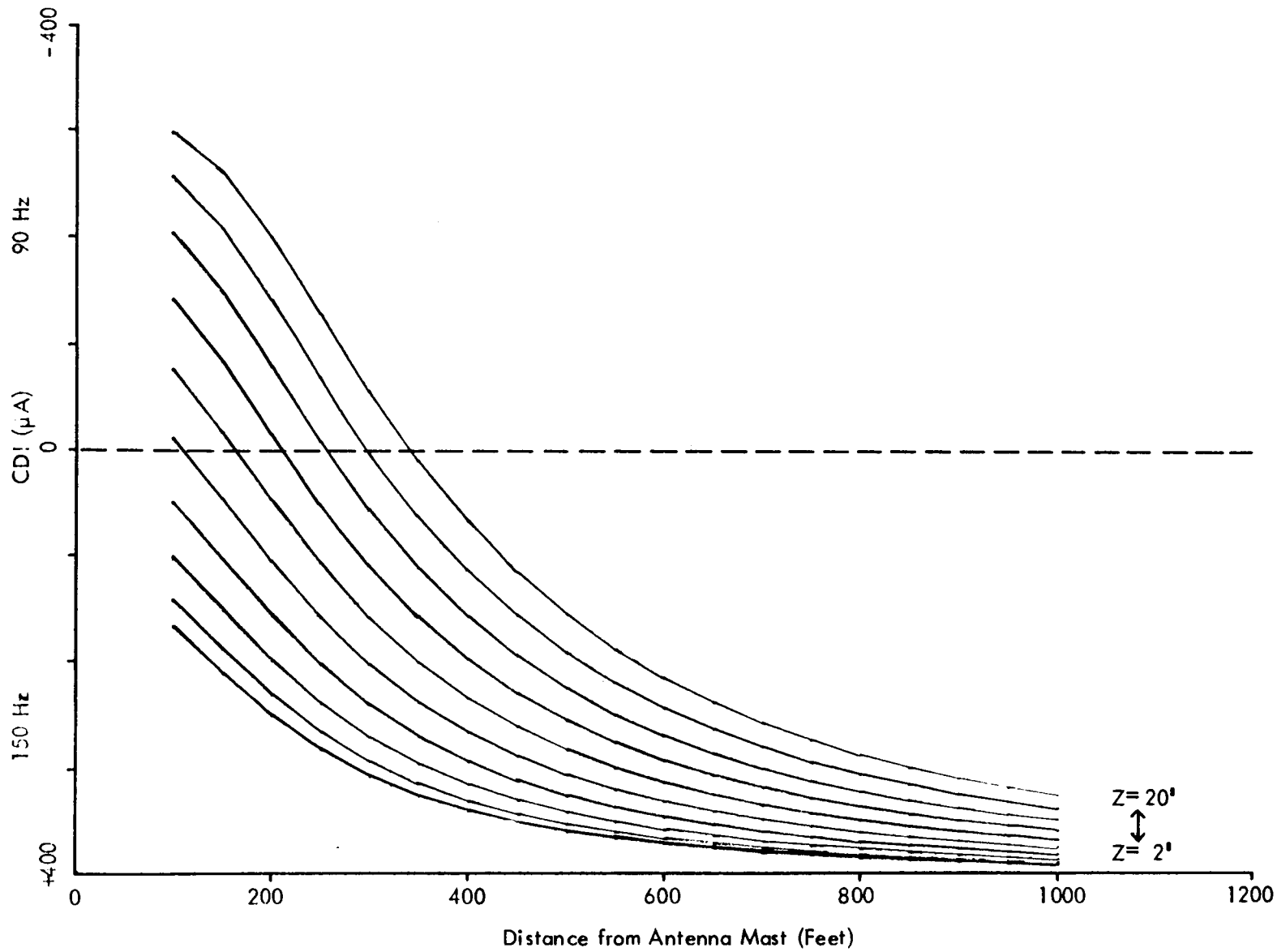

Figure 5-3. TMB predicted data, normal SBR, X=250', Z=2' to Z=12'.

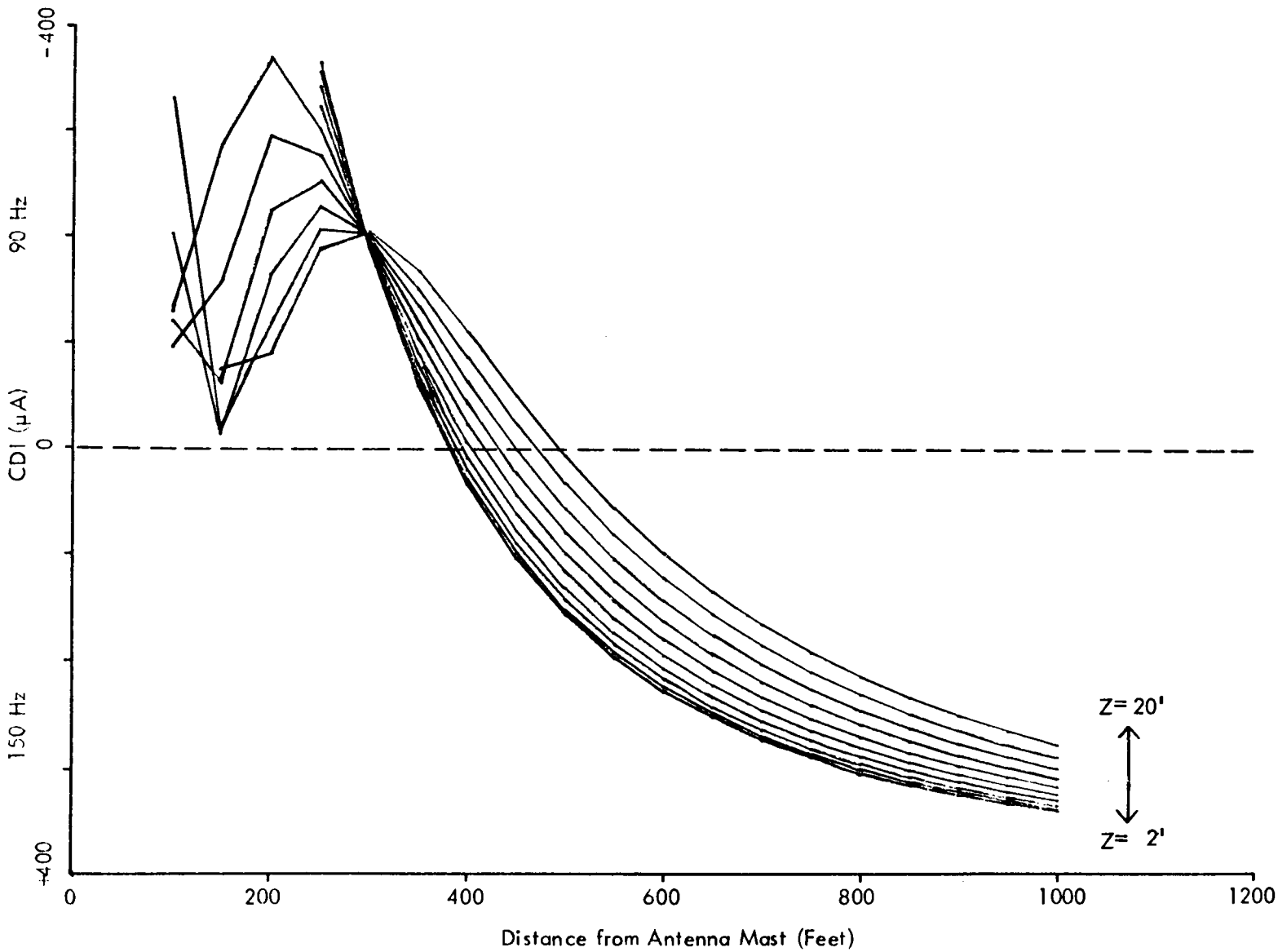

Figure 5-4. TMB predicted data, normal SBR, X=500', Z=2' to Z=12'.

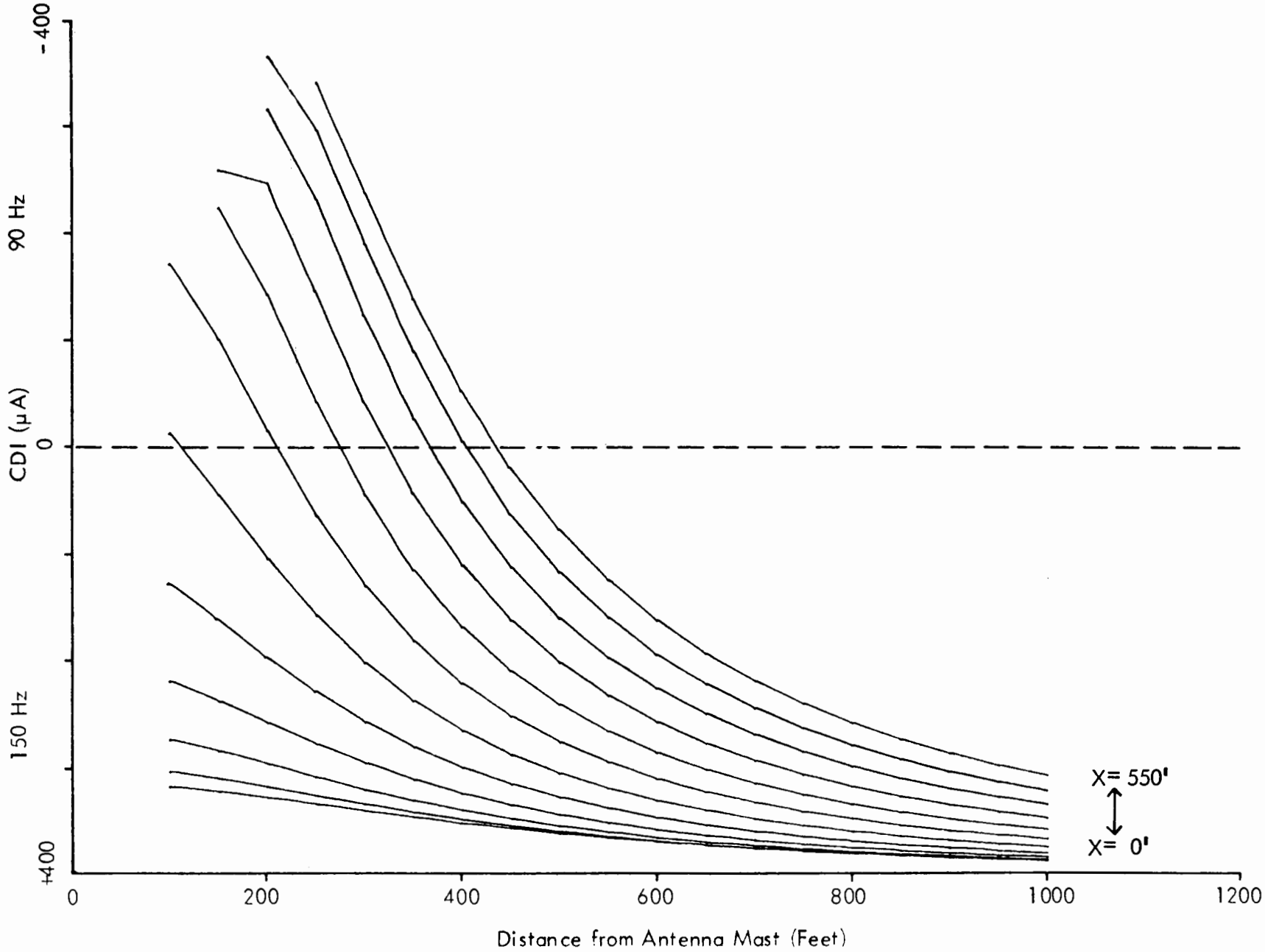

Figure 5-5. TMB predicted data, normal SBR, X=0' to X=550', Z=10'.

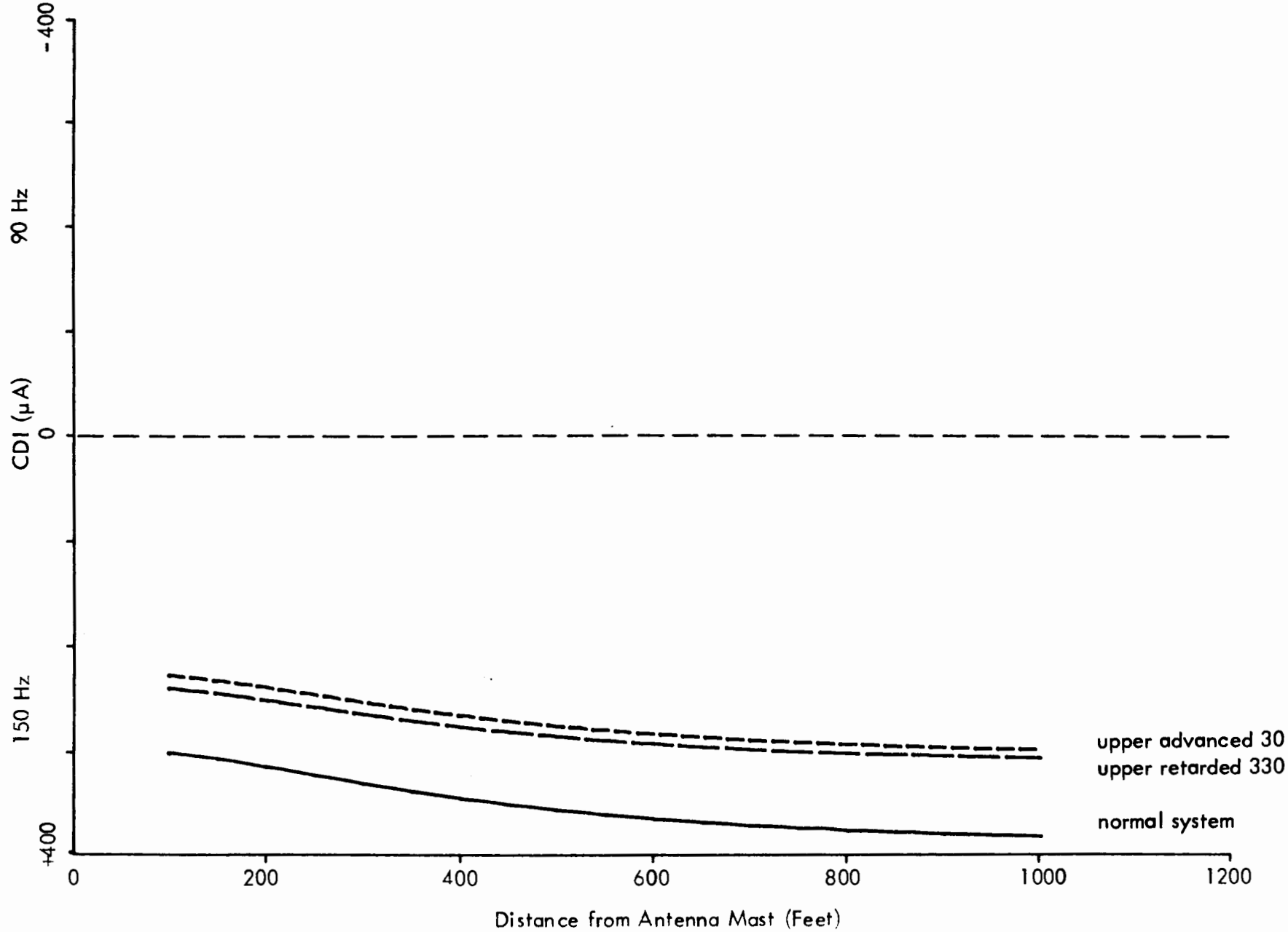

Figure 5-6. TMB predicted data, dephase U/L , X=50', Z=10'.

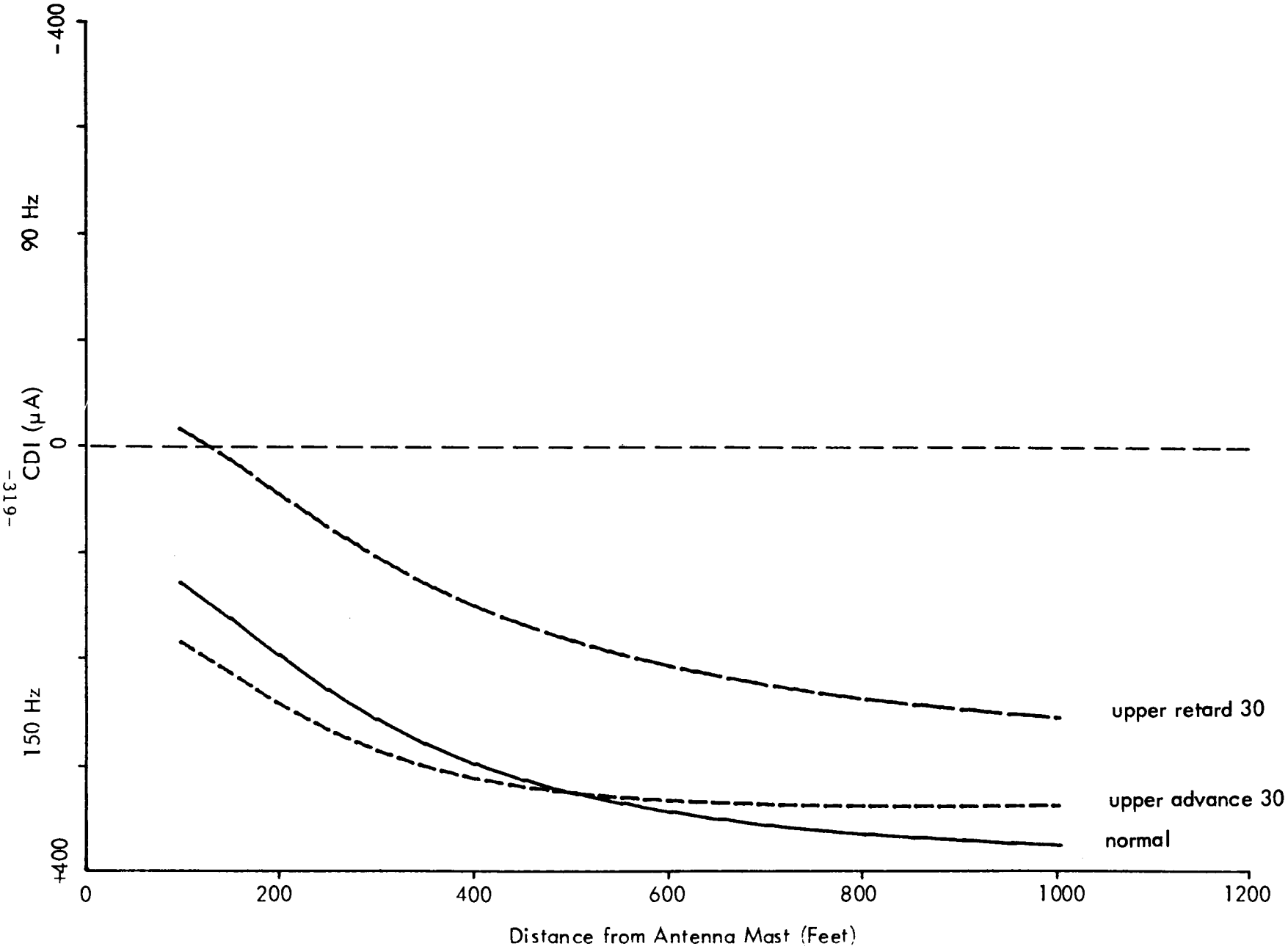

Figure 5-7. TMB predicted data, dephase $\dot{U}/L$, X=200', Z=10'.

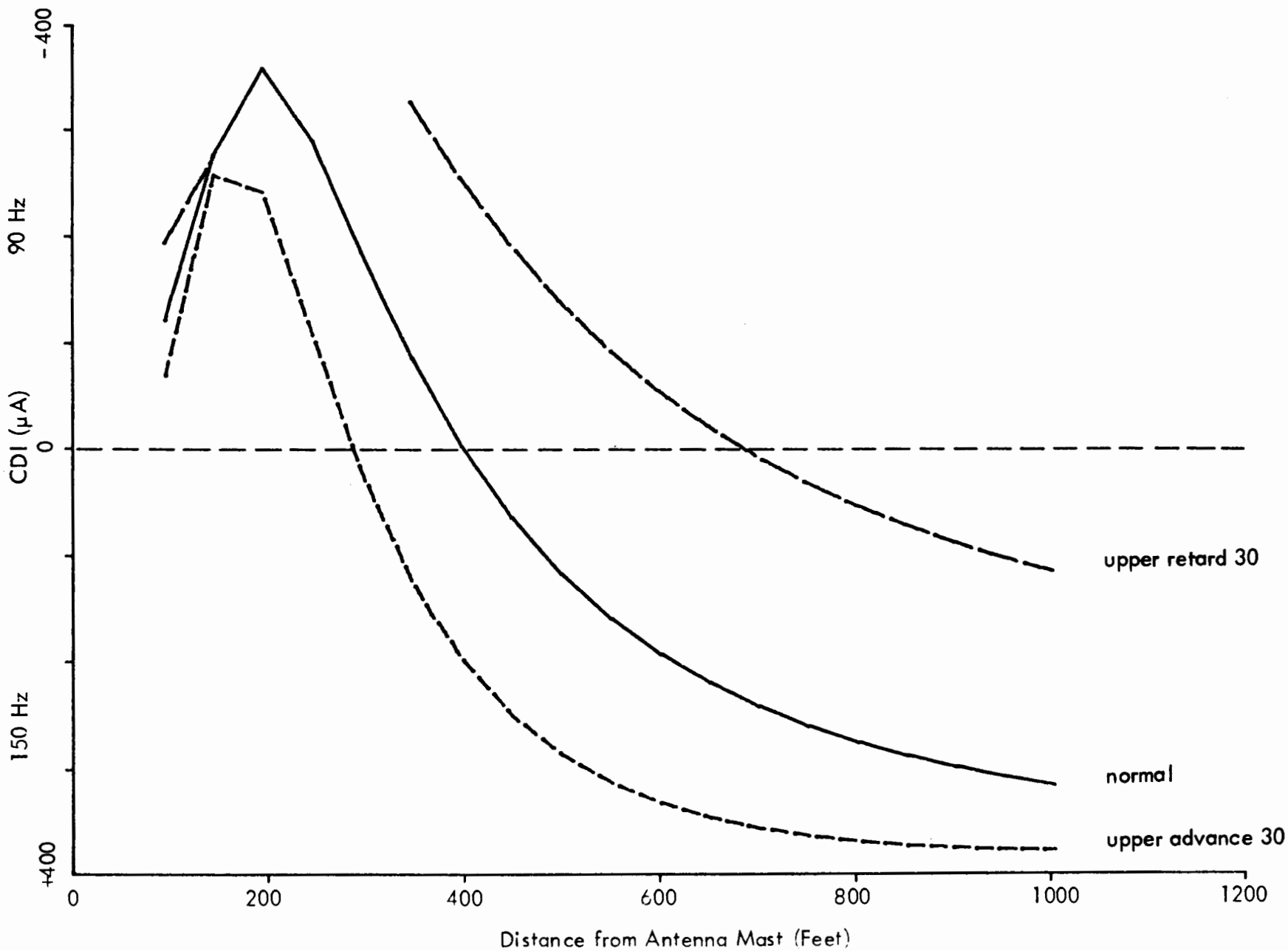

Figure 5-8. TMB predicted data, dephase U/L , X=500', Z=10'.

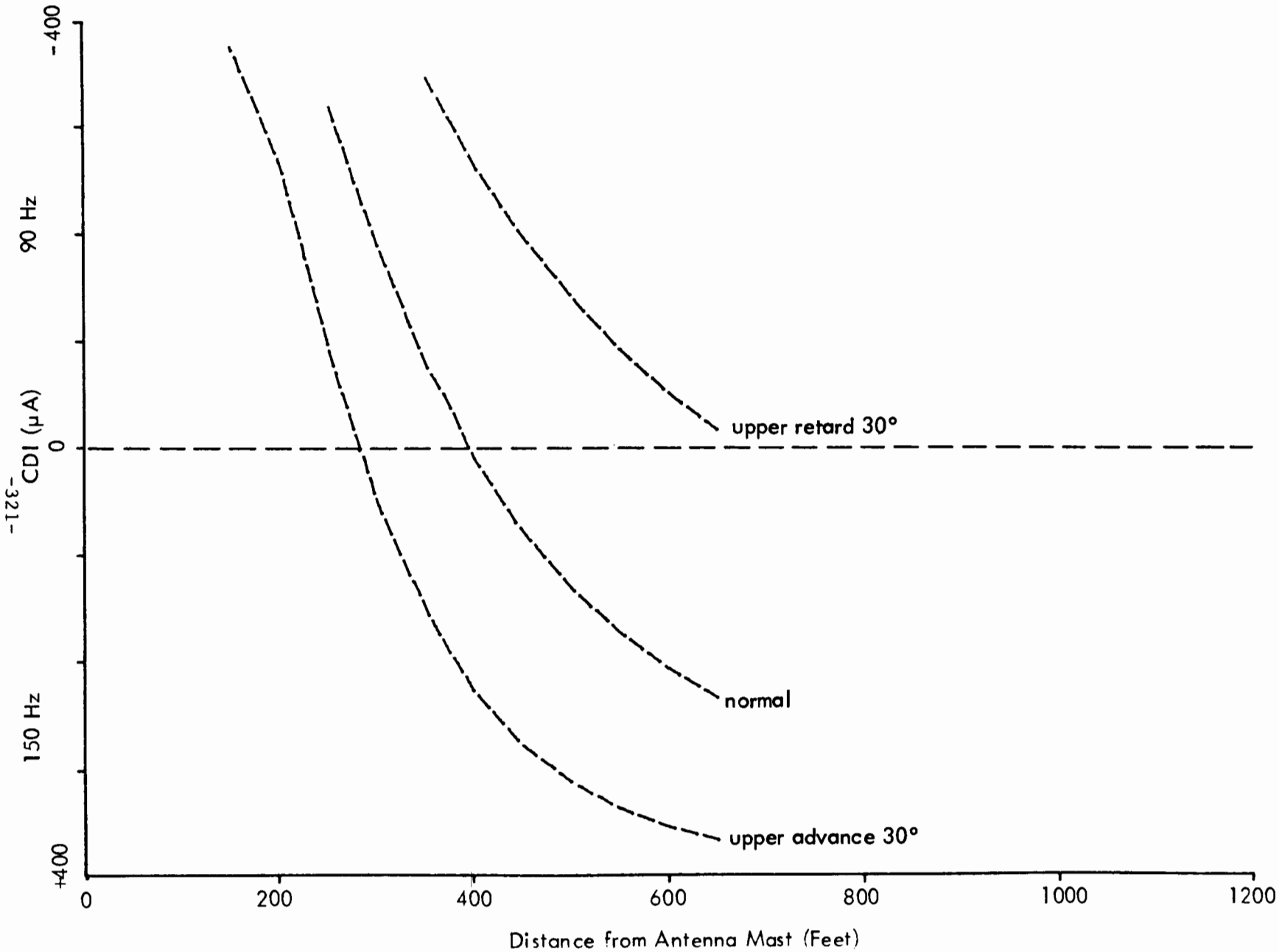

Figure 5-9. TMB predicted data, dephase U/L , X=500', Z=8'.

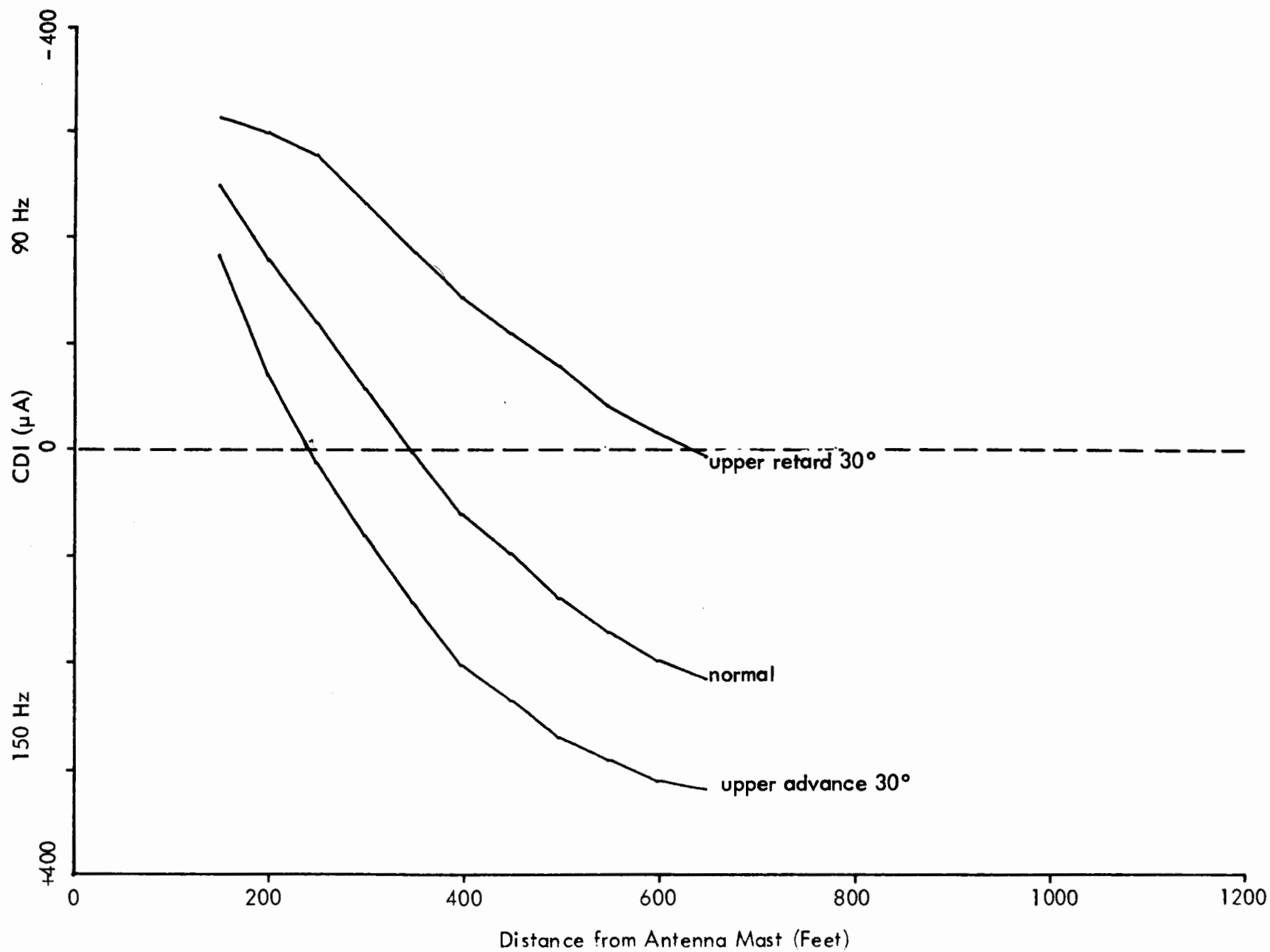

Figure 5-10. TMB measured data, dephase U/L , X=500' Z=8'.

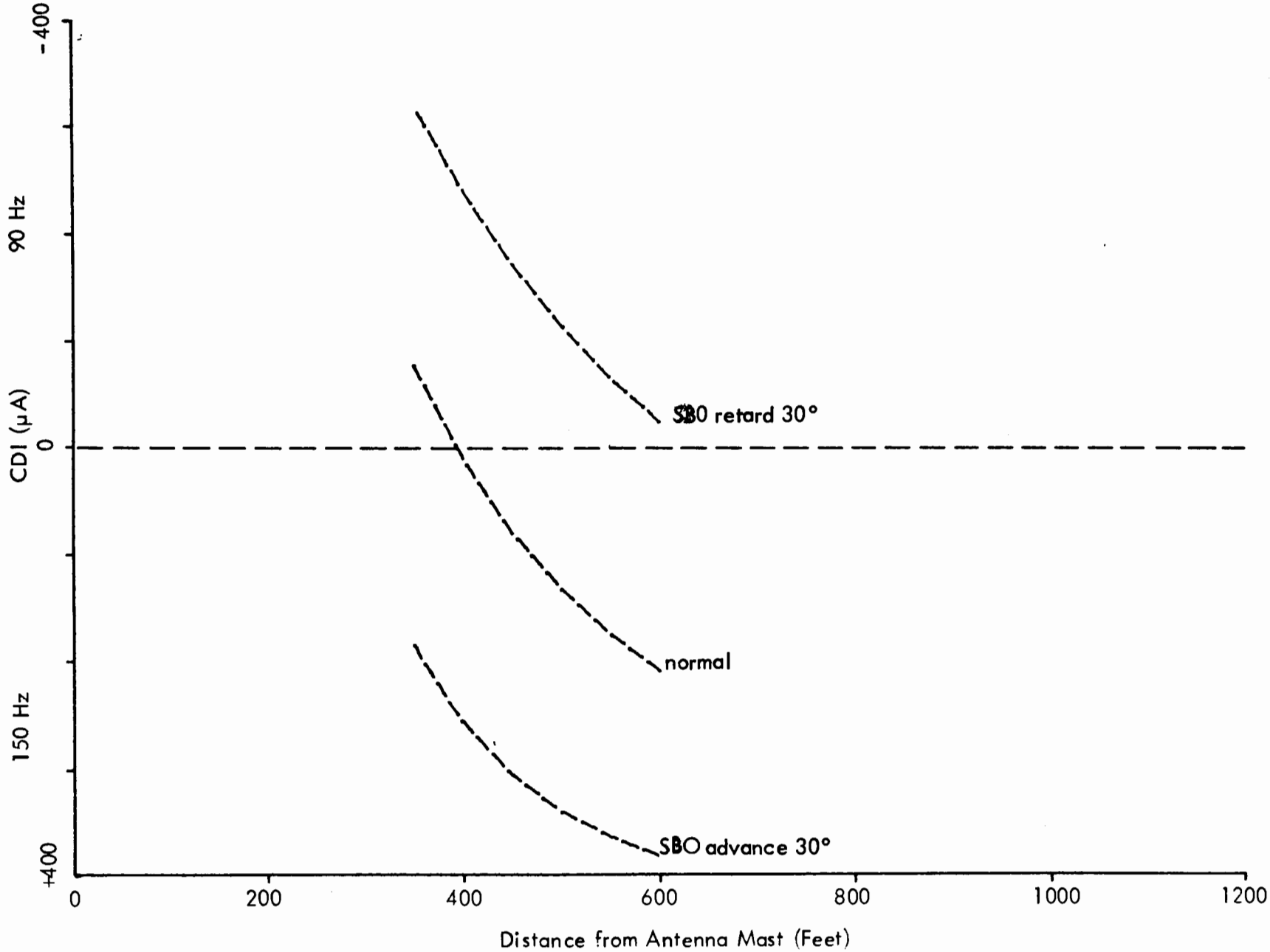

Figure 5-11. TMB predicted data, dephase CSB/SBO, X=500', Z=8'.

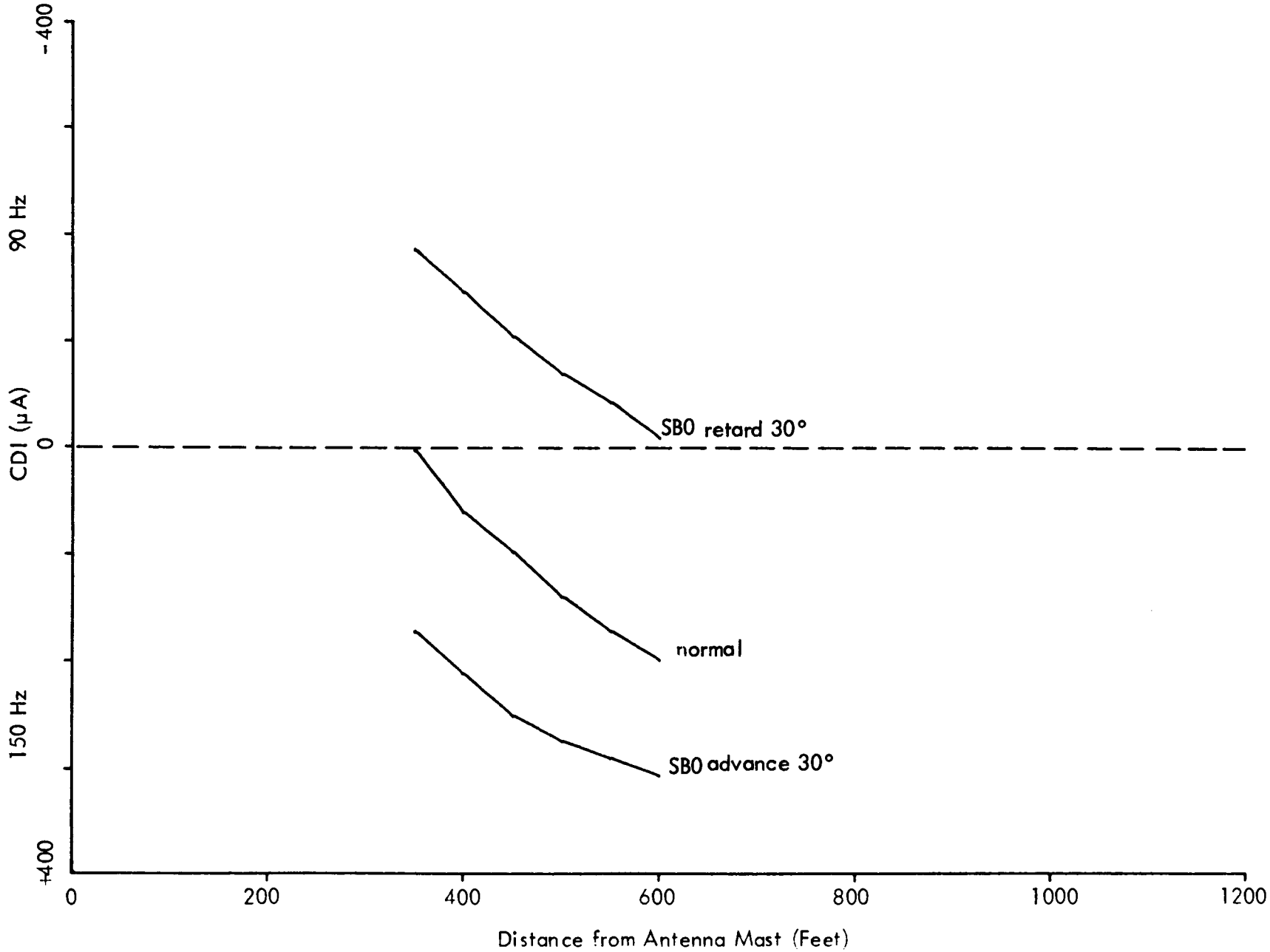

Figure 5-12. TMB measured data, dephase CSB/SBO, X=500', Z=8'.

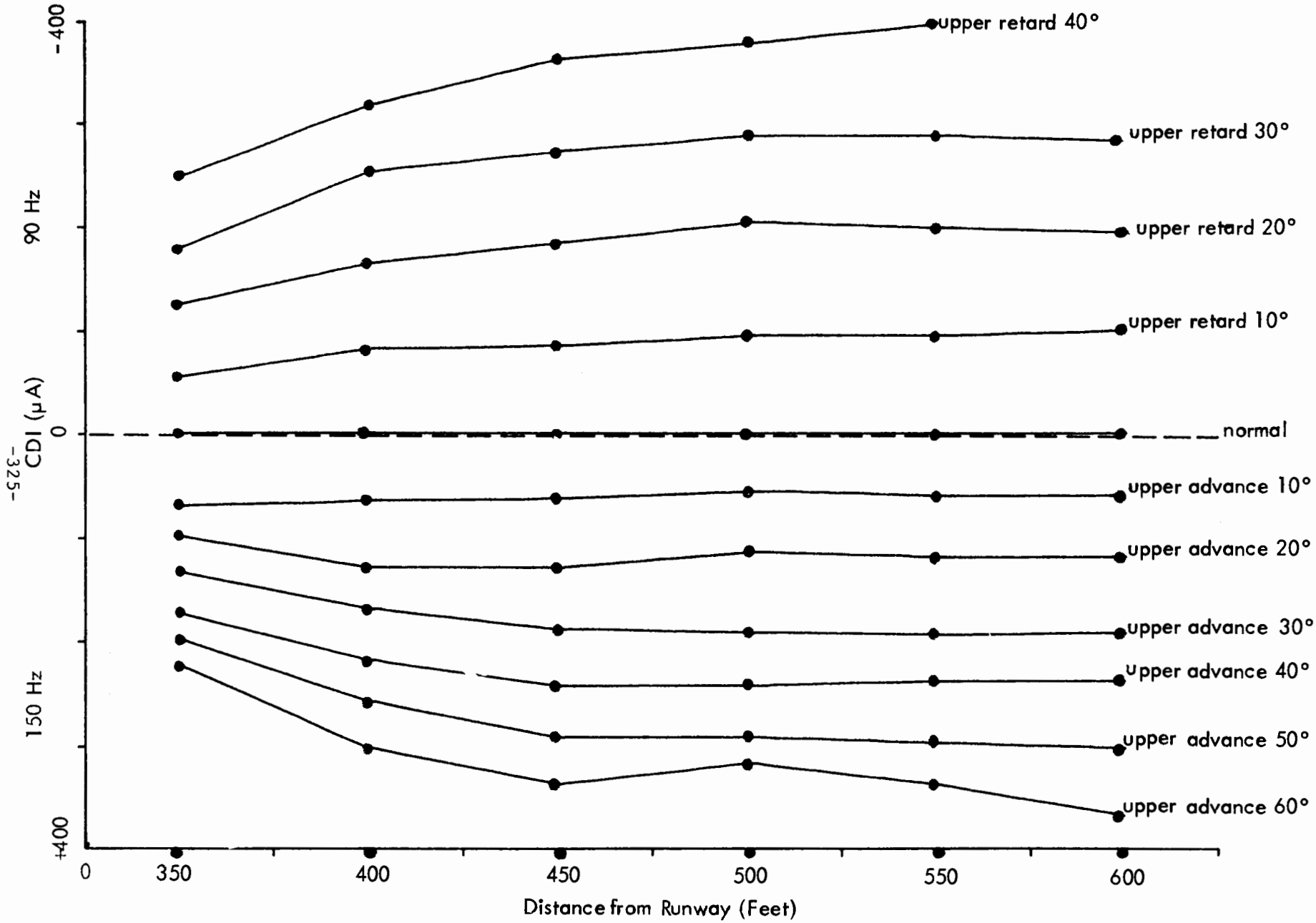

Figure 5-13. TMB measured data, U/L dephase, probe locations.

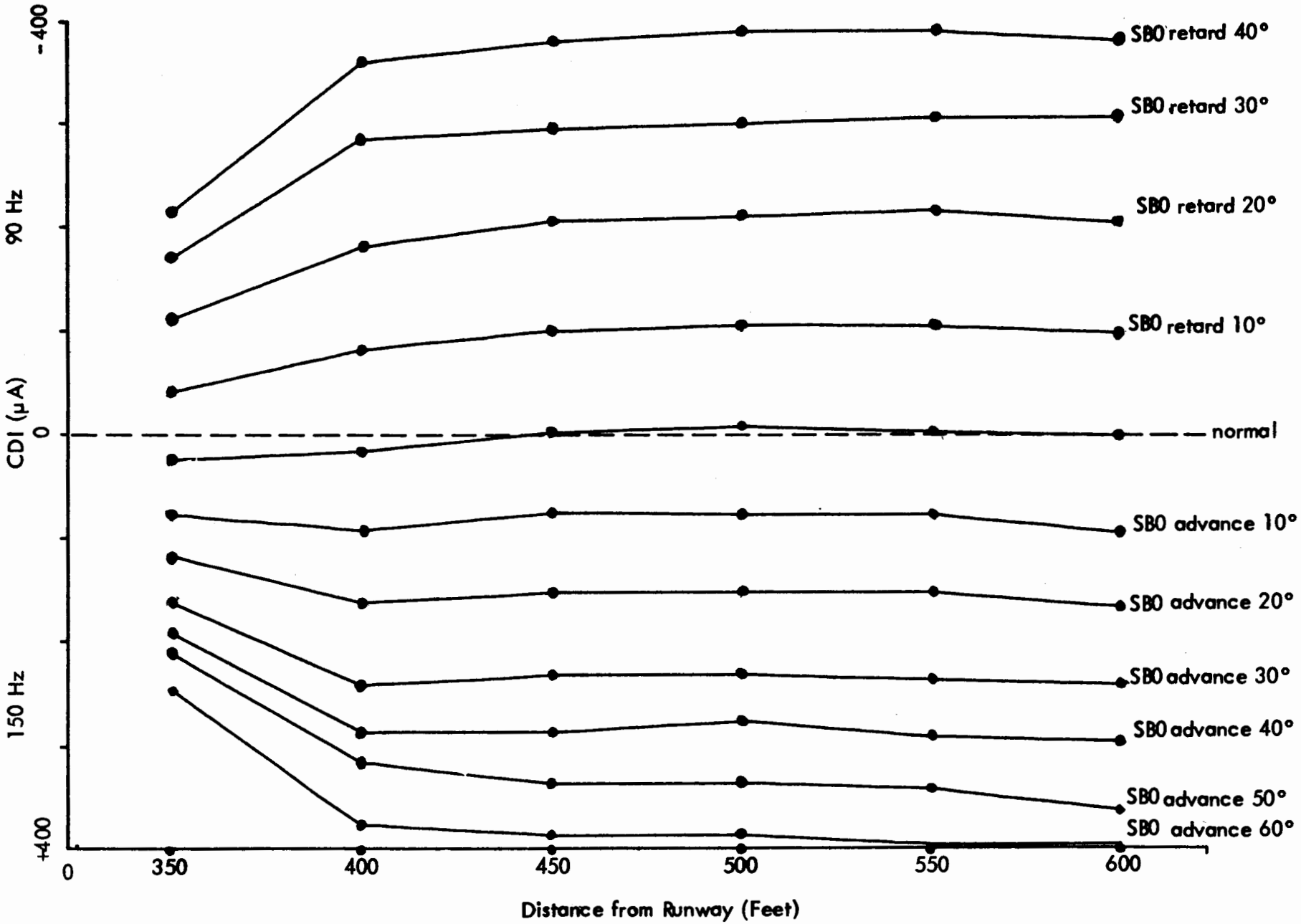

Figure 5-14. TMB measured data, CSB/SBO dephase, probe locations.

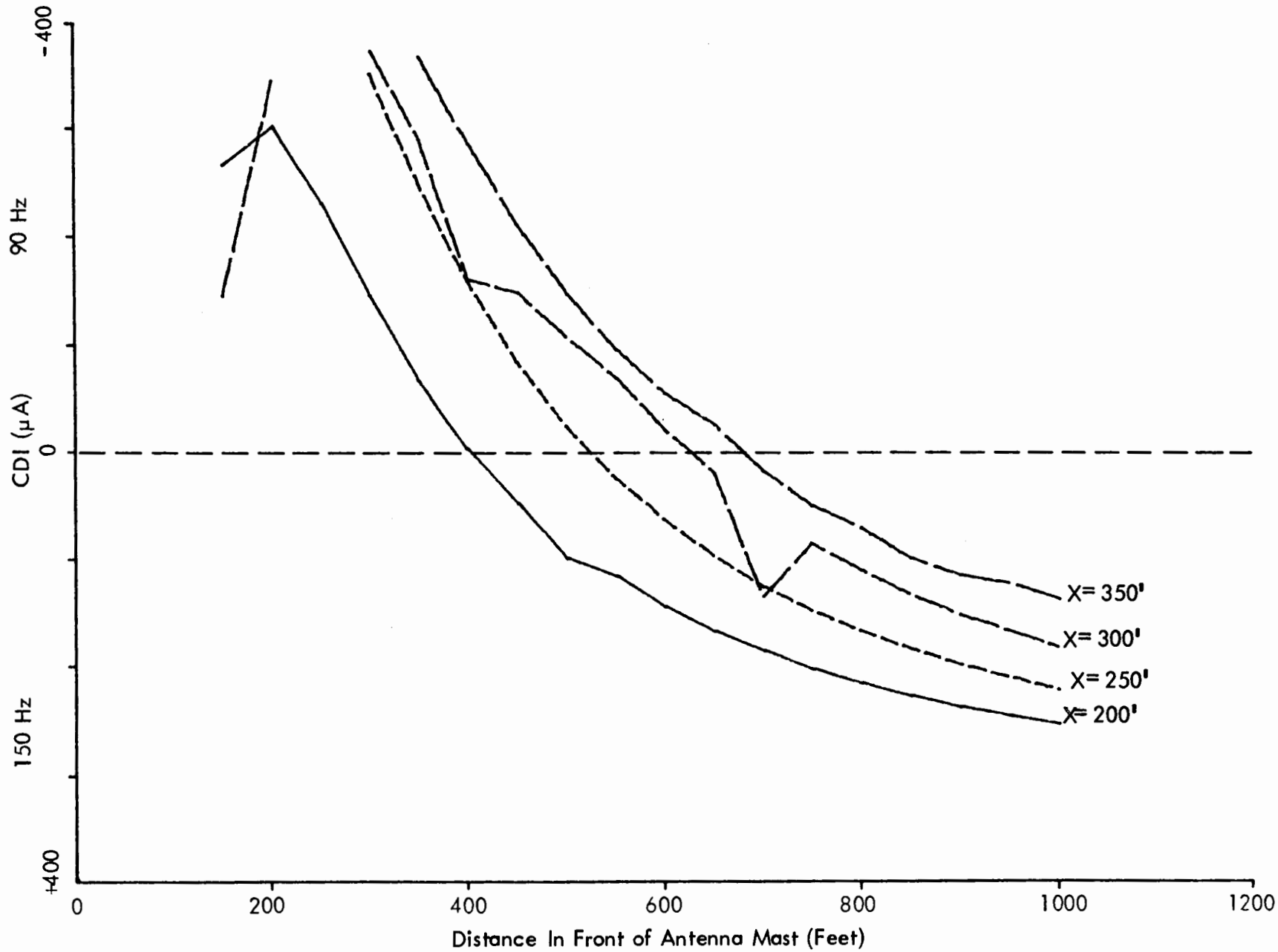

Figure 5-15. MGW predicted data, normal SBR, X=200' to X=350',Z=8'.

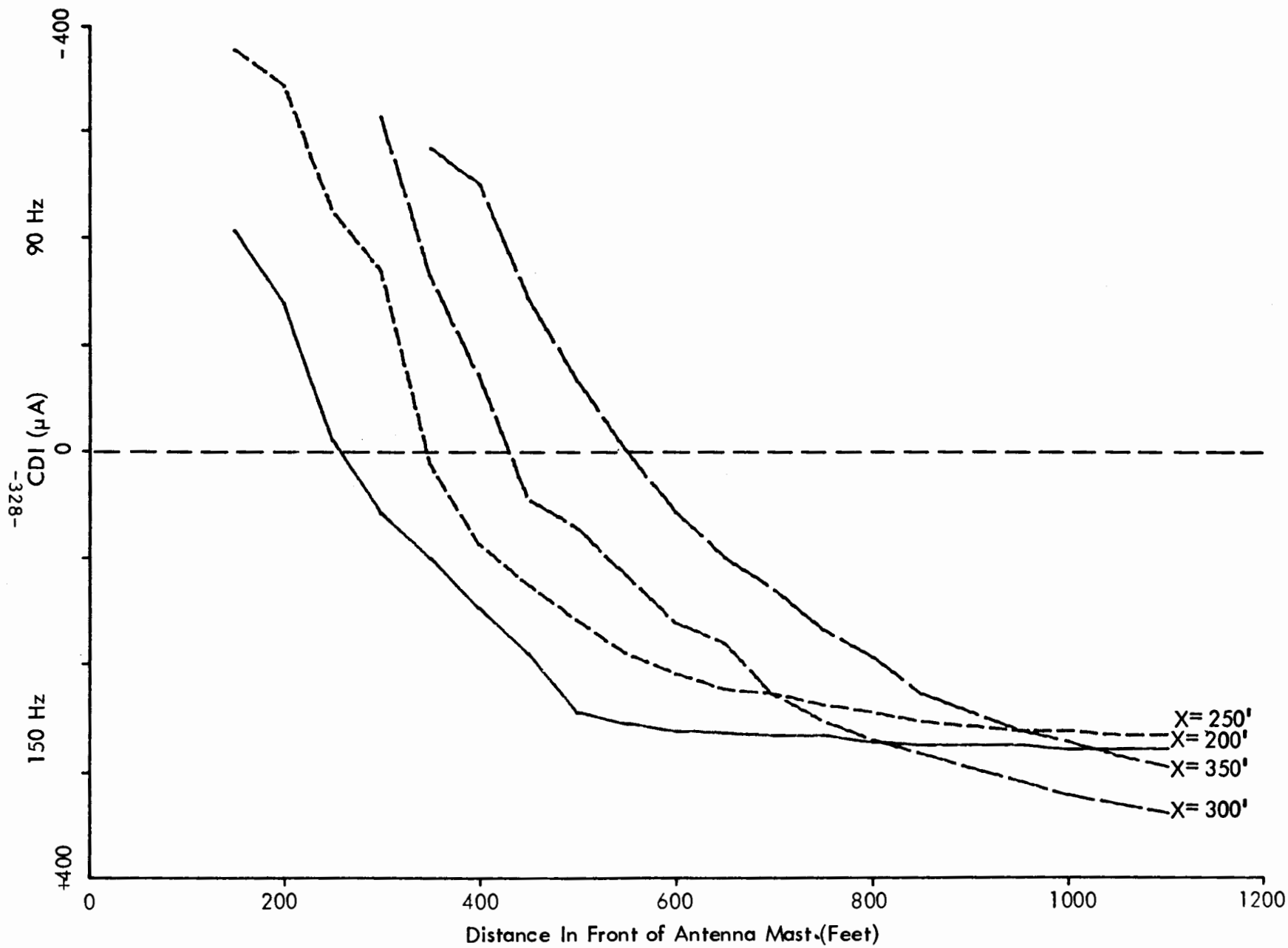

Figure 5-16. MGW measured data, normal SBR, X=200' to X=350'. Z=8'.

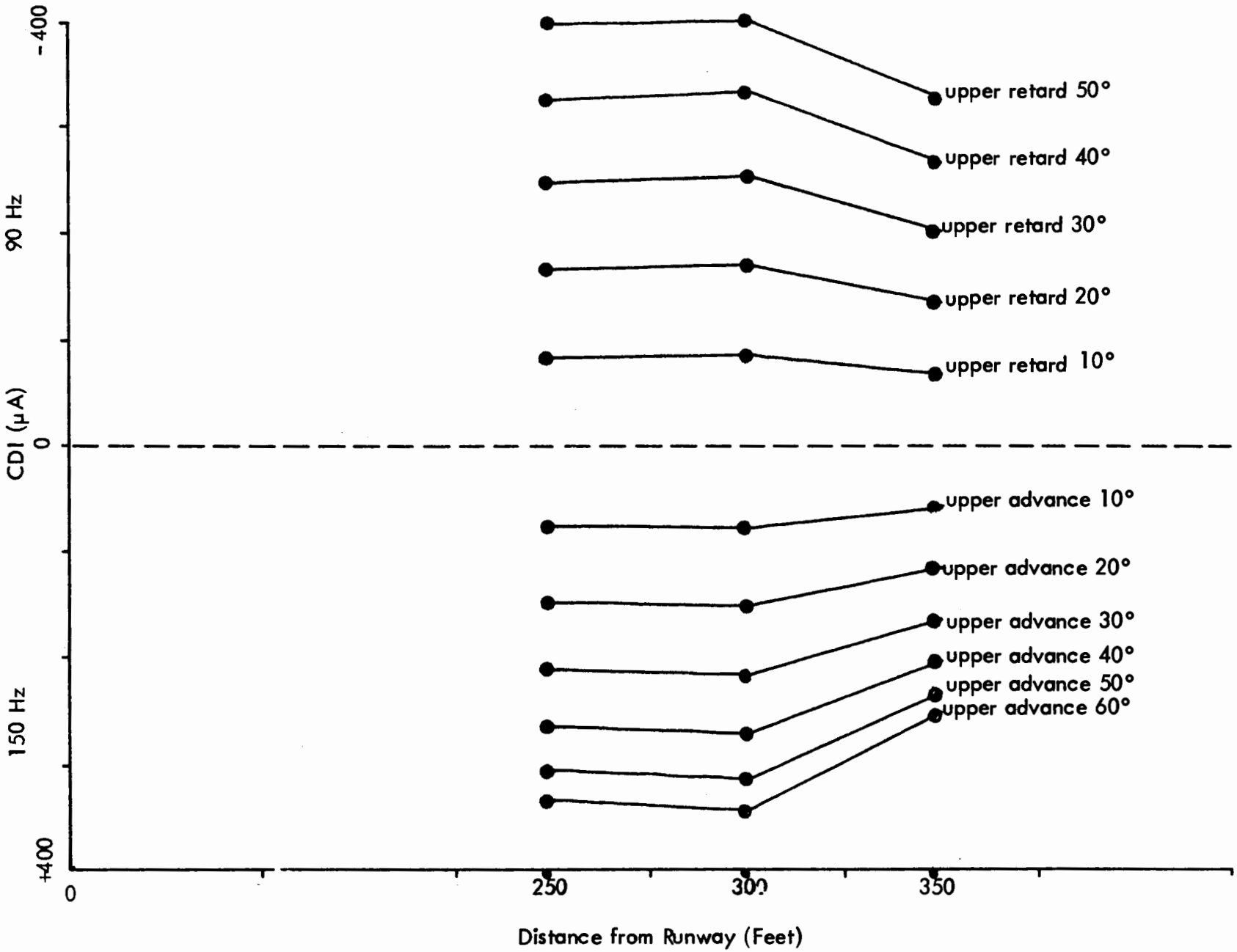

Figure 5-17. MGW predicted data, dephase U/L, 0 μA locations.

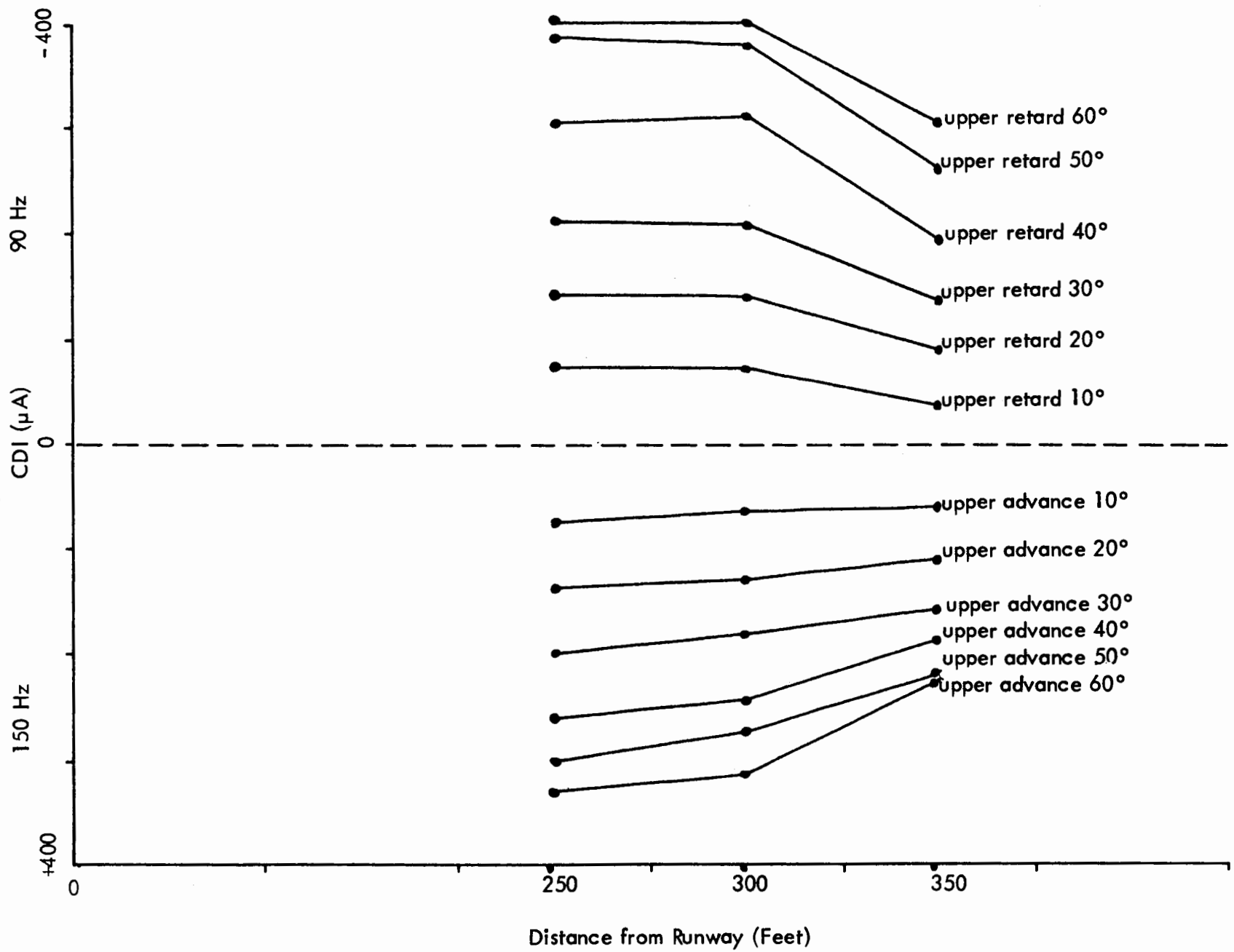

Figure 5-18. MGW measured data, dephase U/L, probe locations.

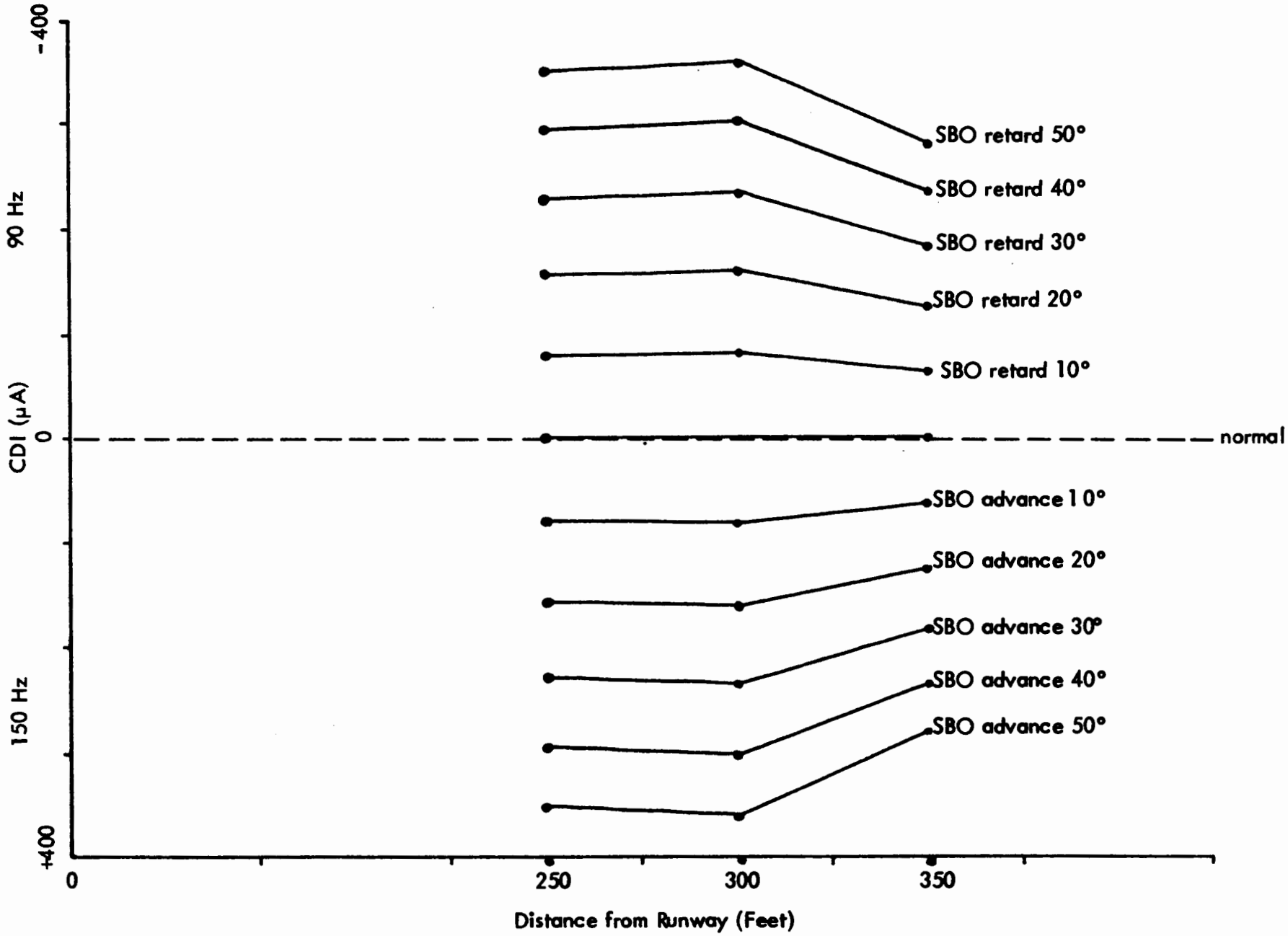

Figure 5-19. MGW predicted data, dephase CSB/SBO, 0 μA locations.

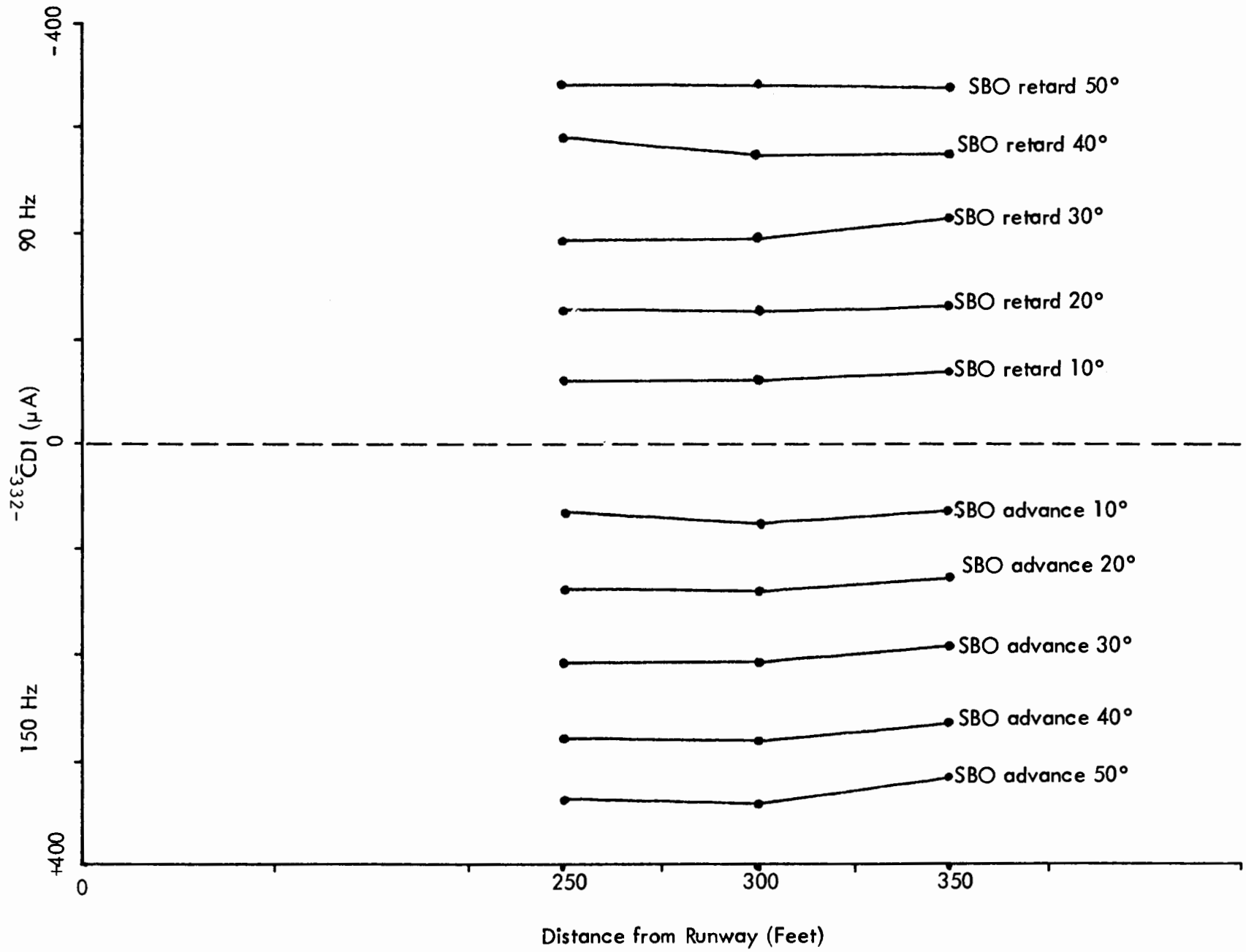

Figure 5-20. MGW measured data, dephase CSB/SBO, probe locations.

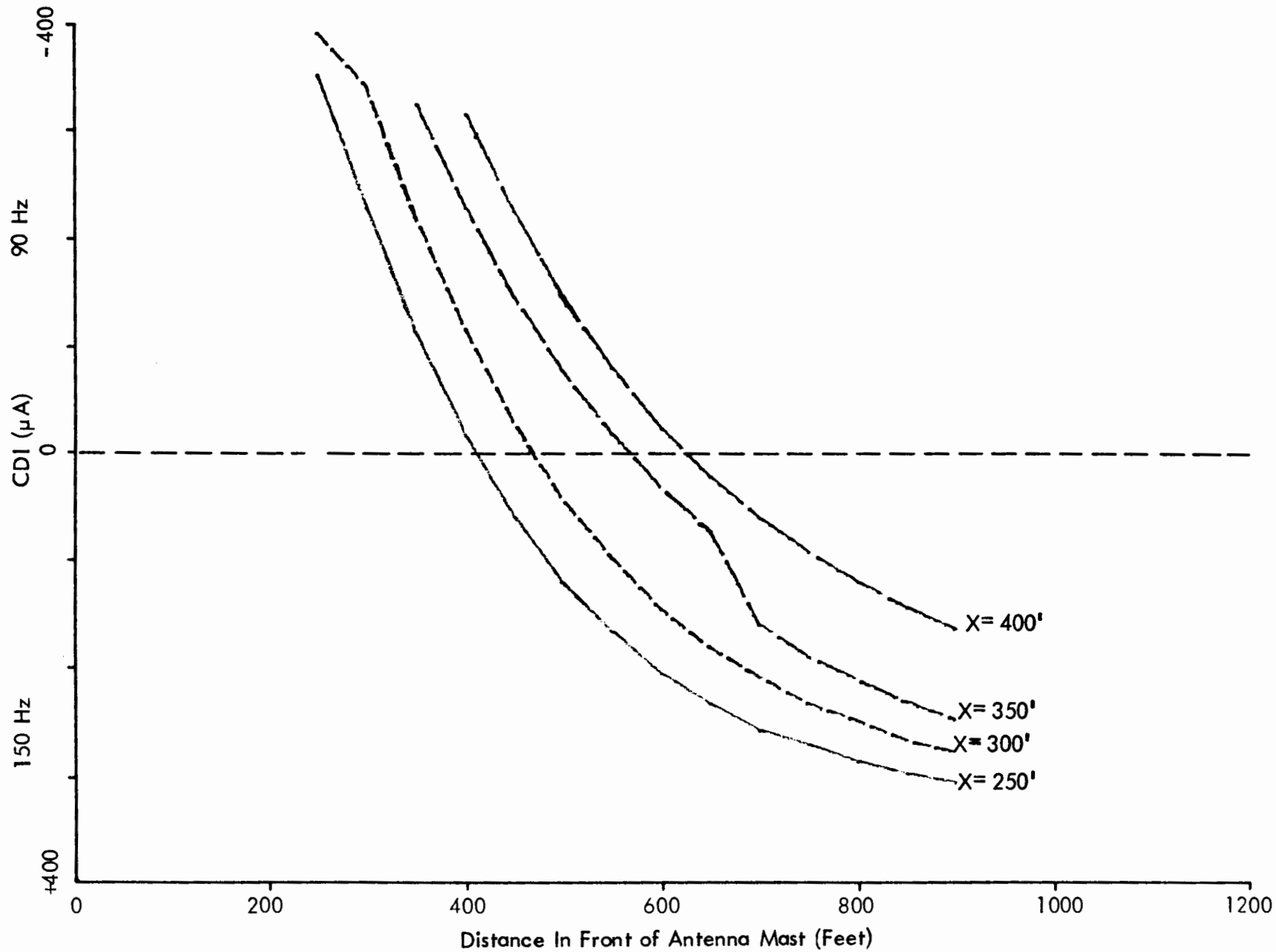

Figure 5-21. CKB predicted data, normal SBR, X=250' to X=400',Z=8'.

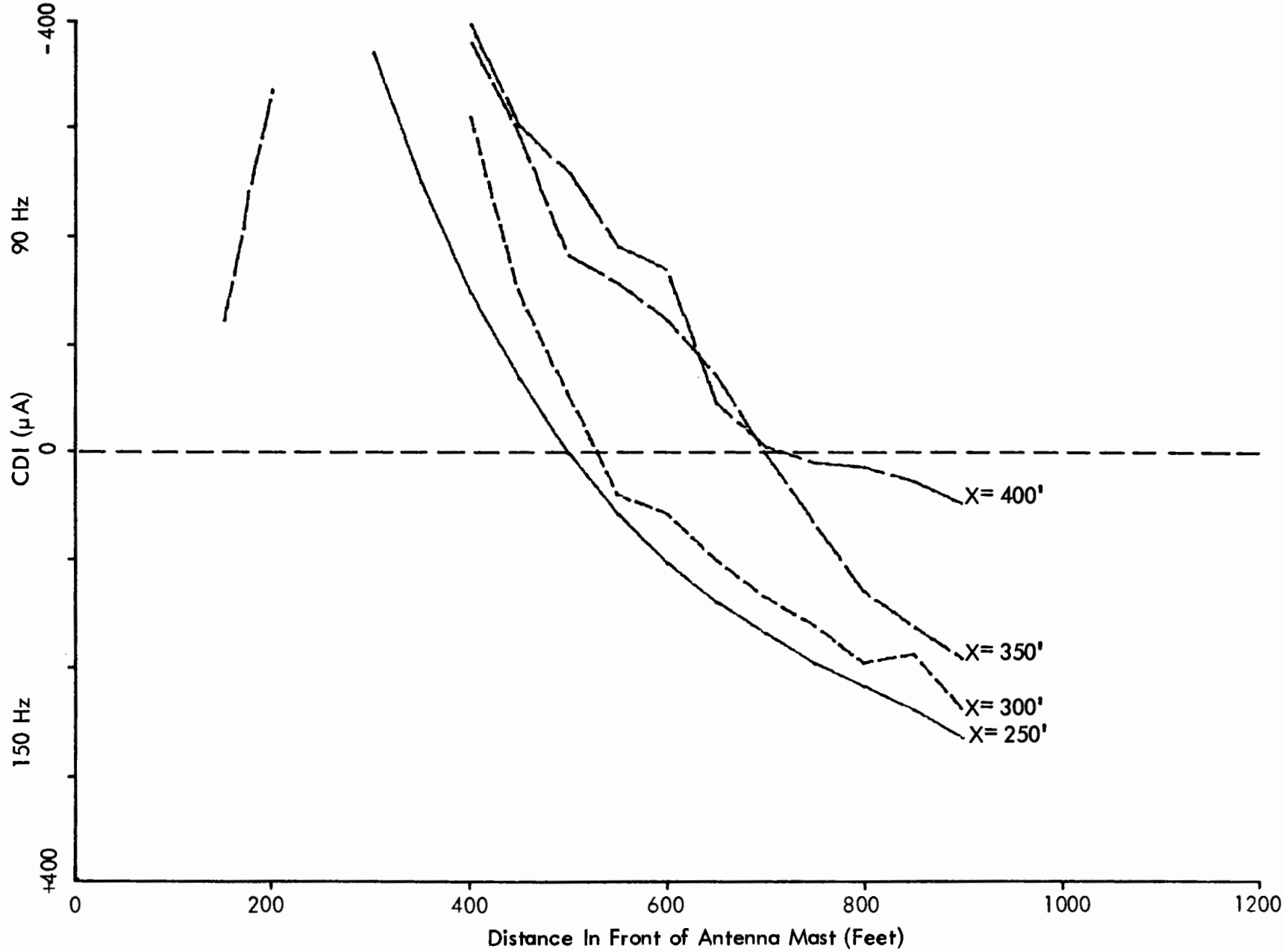

Figure 5-22. CKB measured data, normal SBR, X=250' to X=400', Z=8'.

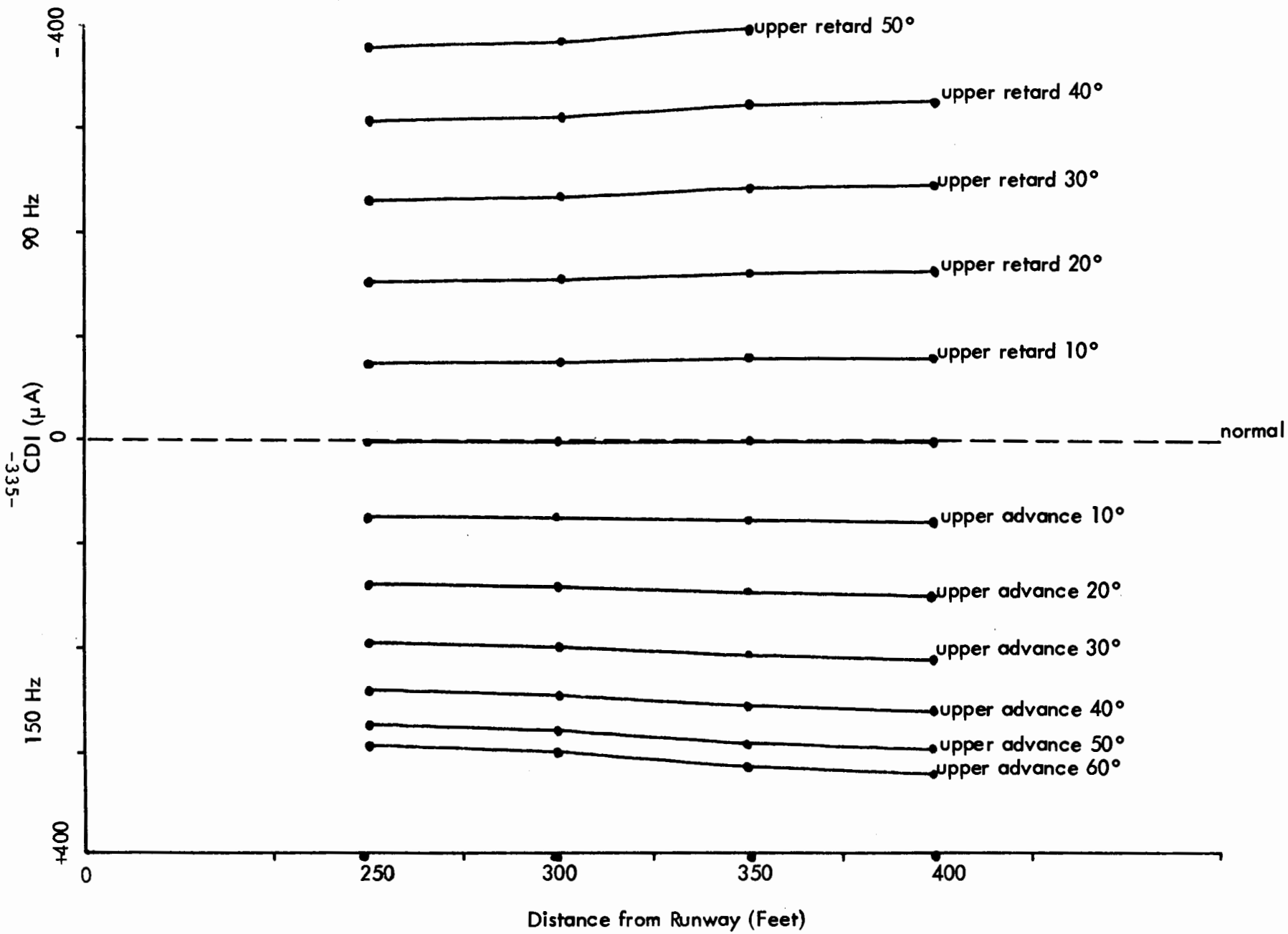

Figure 5-23. CKB predicted data, dephase U/L, 0 μA locations.

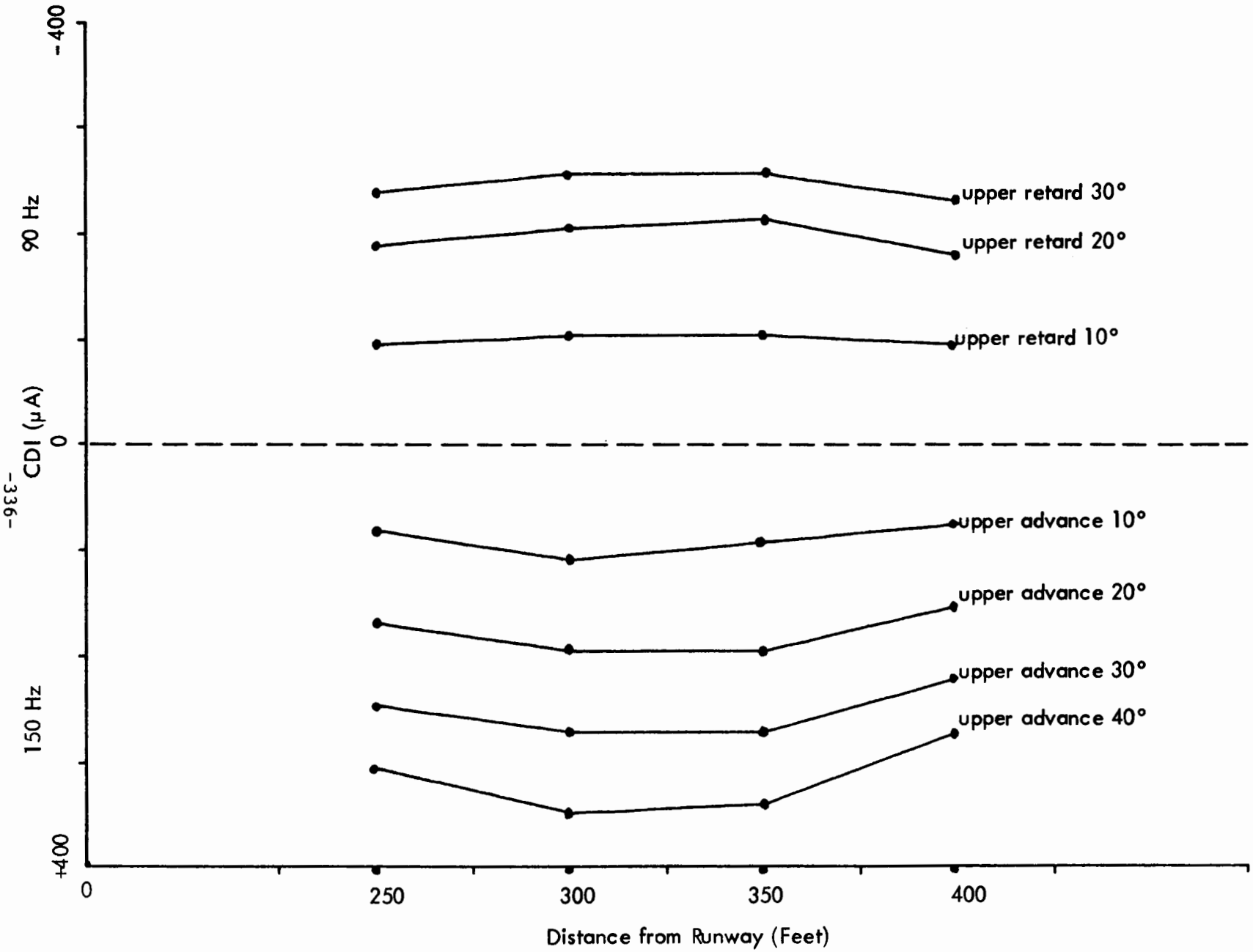

Figure 5-24. CKB measured data, dephase U/L, probe locations.

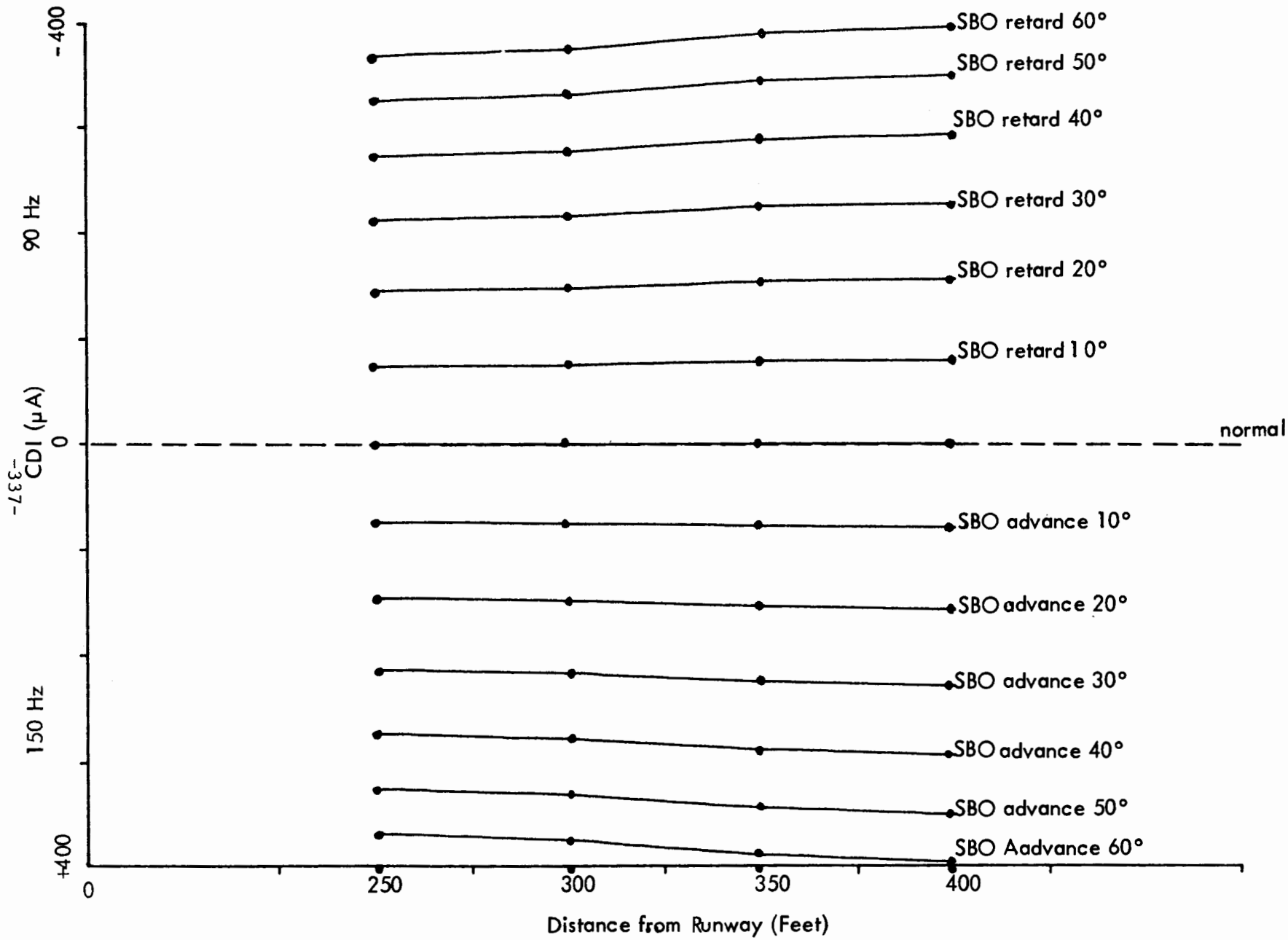

Figure 5-25. CKB predicted data, dephase CSB/SBO, 0 μA locations.

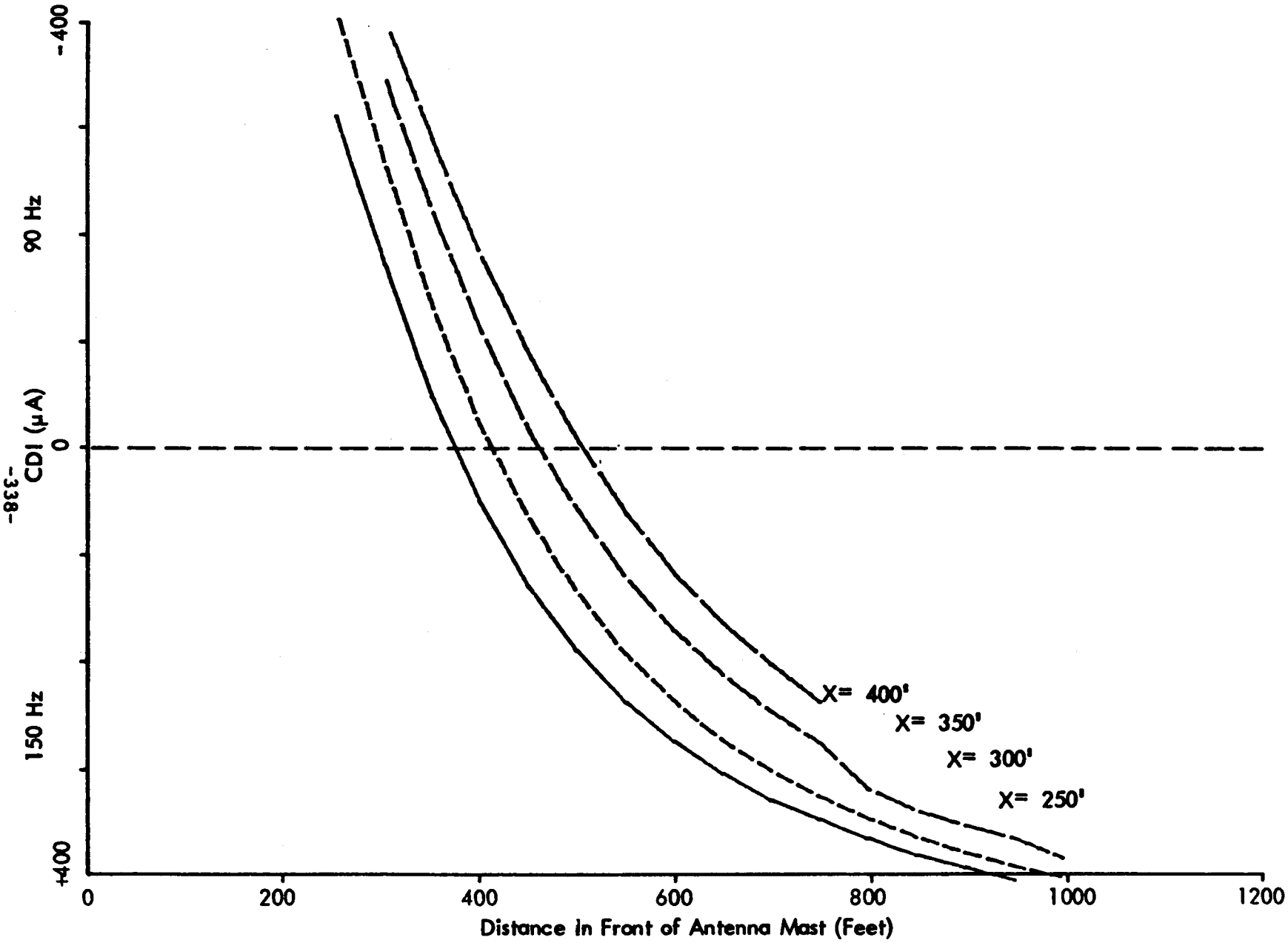

Figure 5-26. BLF predicted data, normal SBR, X=250' to X=400',Z=8'.

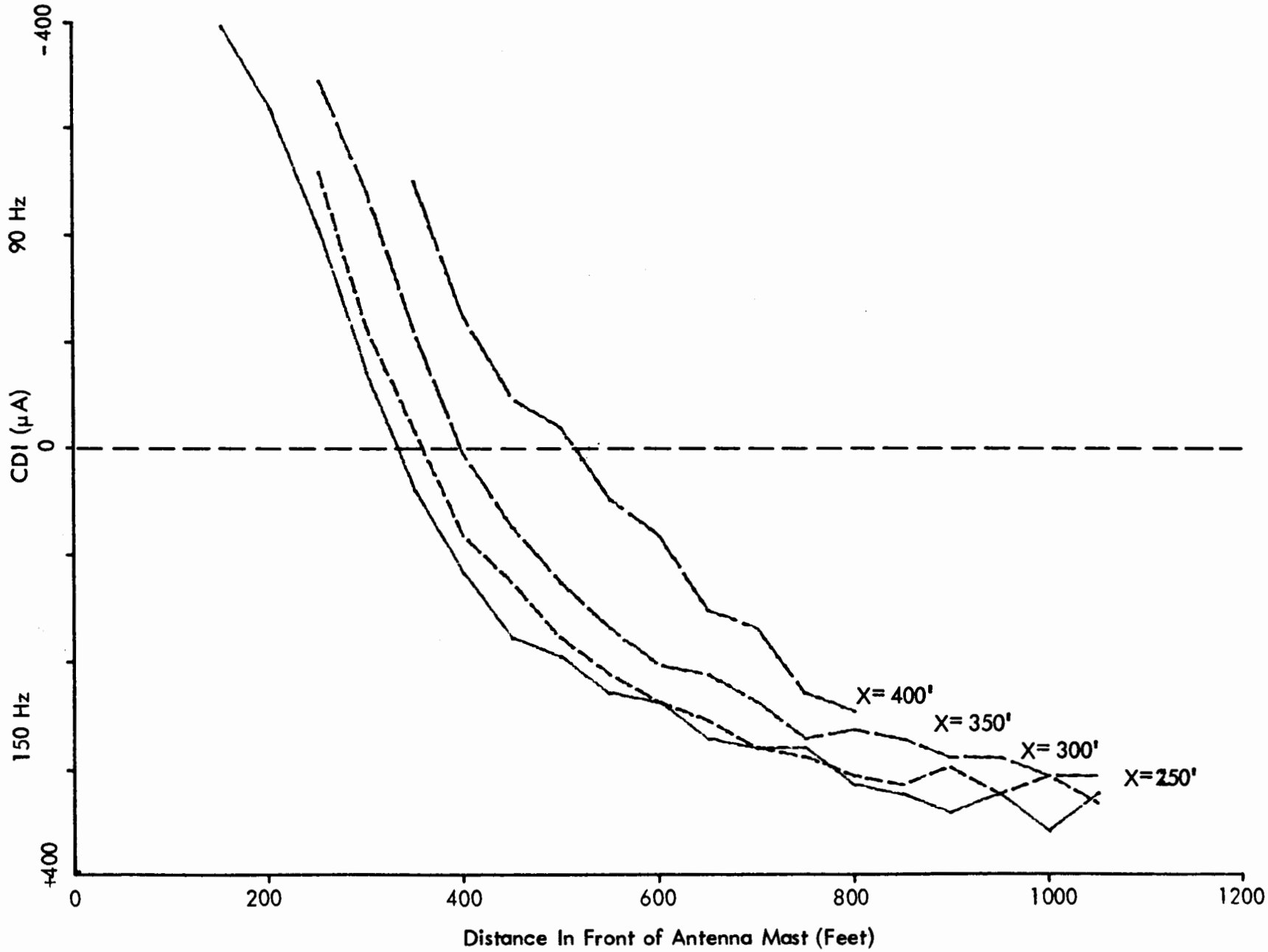

Figure 5-27. BLF measured data, normal SBR, X=250' to X=400', Z=8'.

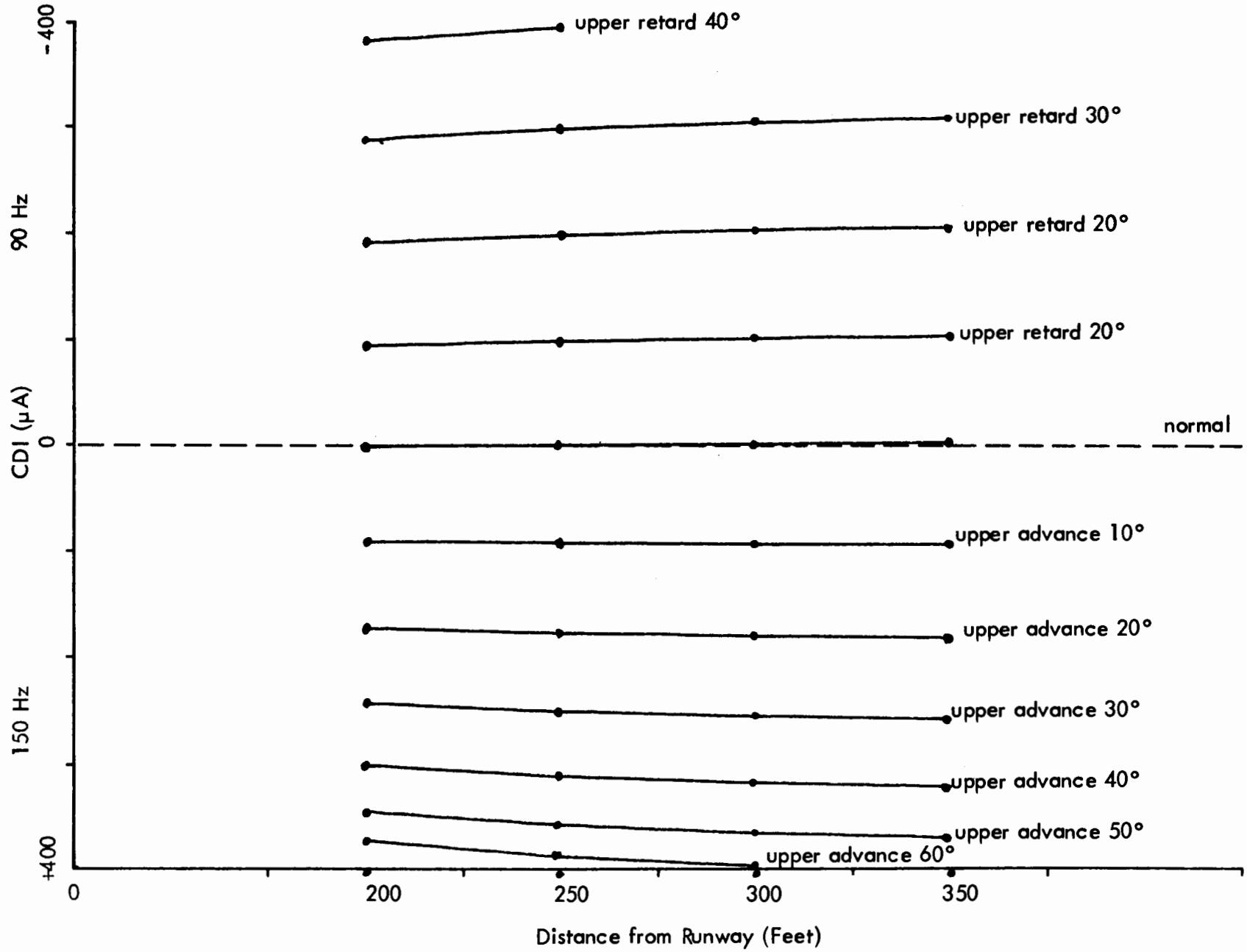

Figure 5-28. BLF predicted data, dephase U/L, 0 μA locations.

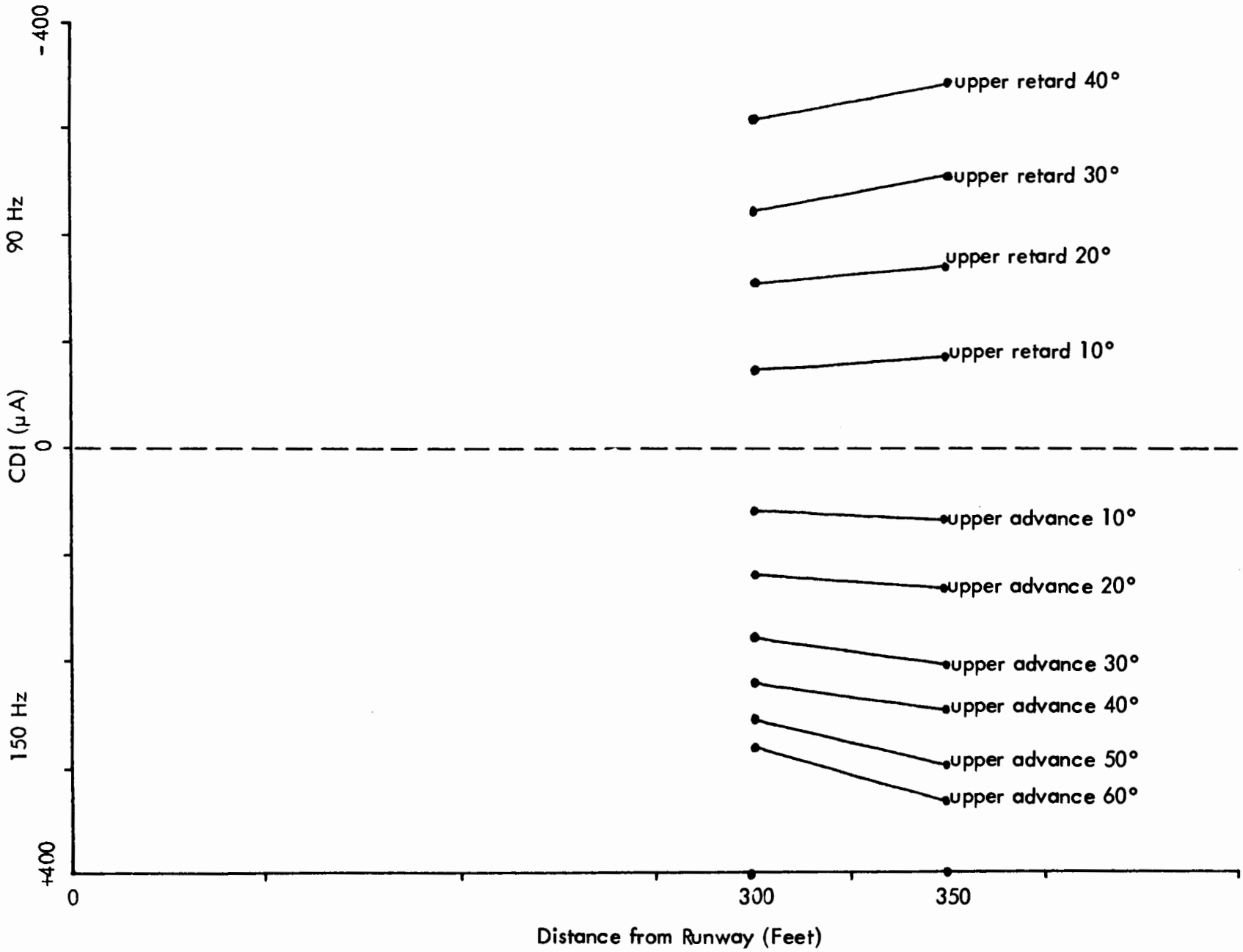

Figure 5-29. BLF measured data, dephase U/L, probe locations.

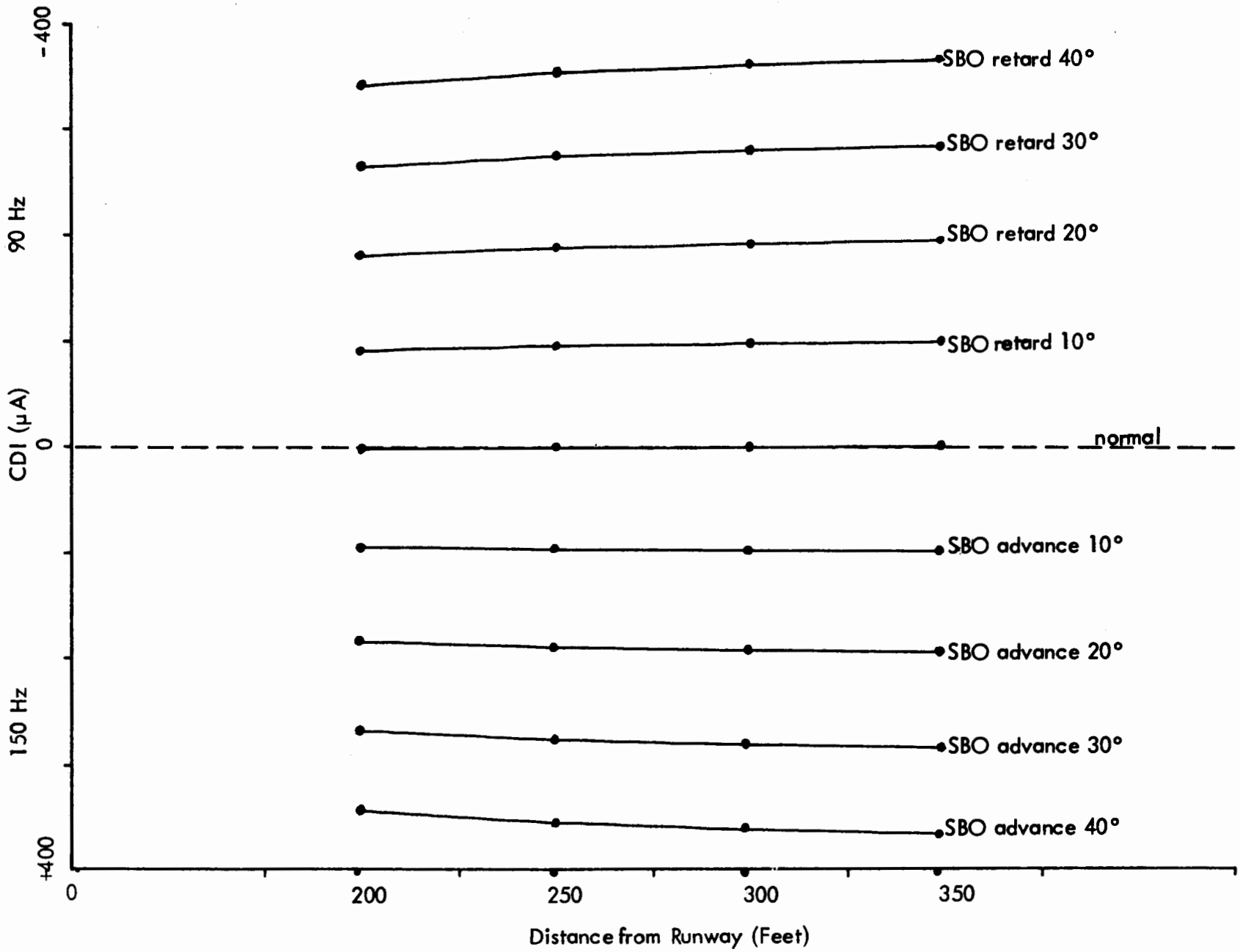

Figure 5-30. BLF predicted data, dephase CSB/SBO, 0 μA locations.

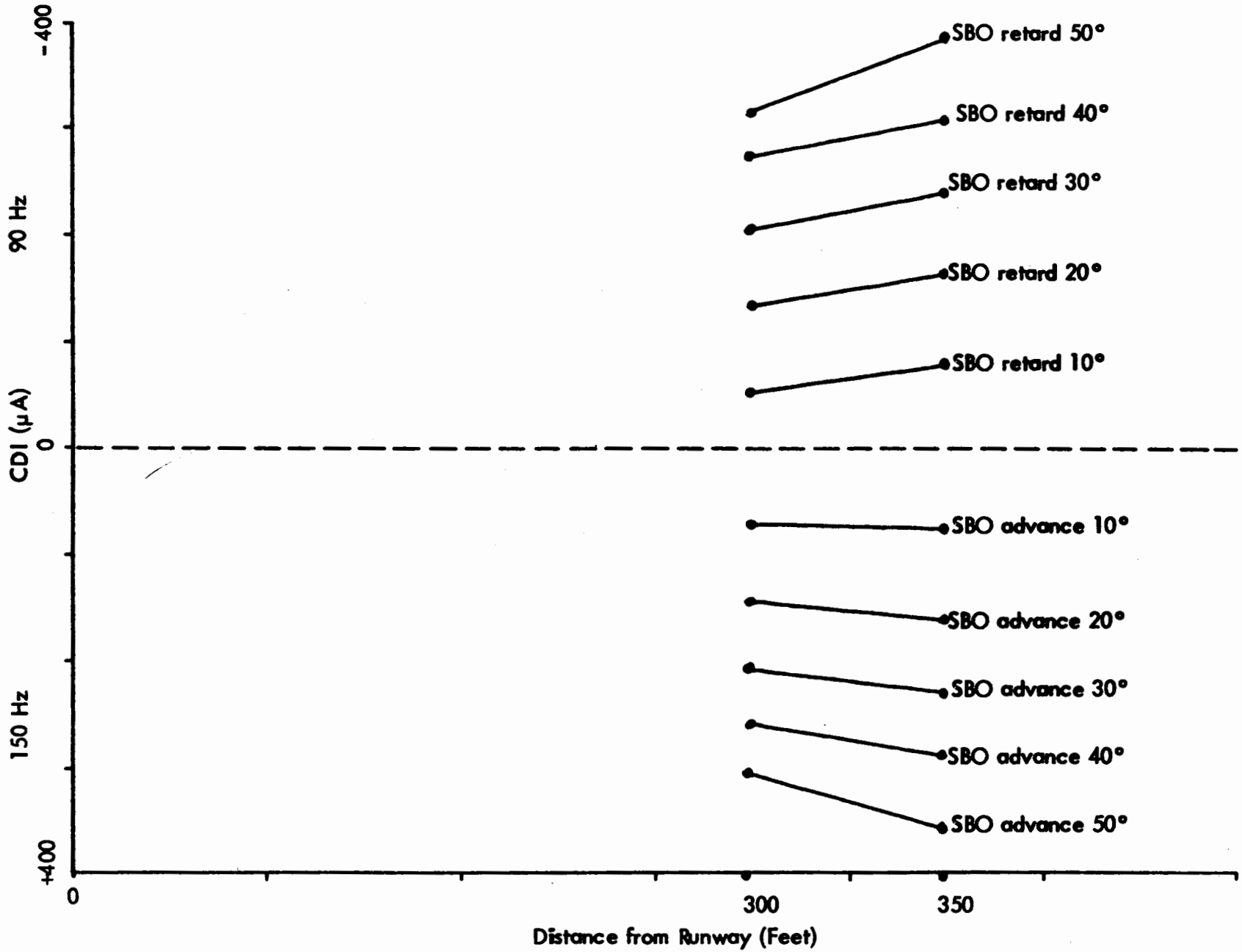

Figure 5-31. BLF measured data, dephase CSB/SBO, probe locations.

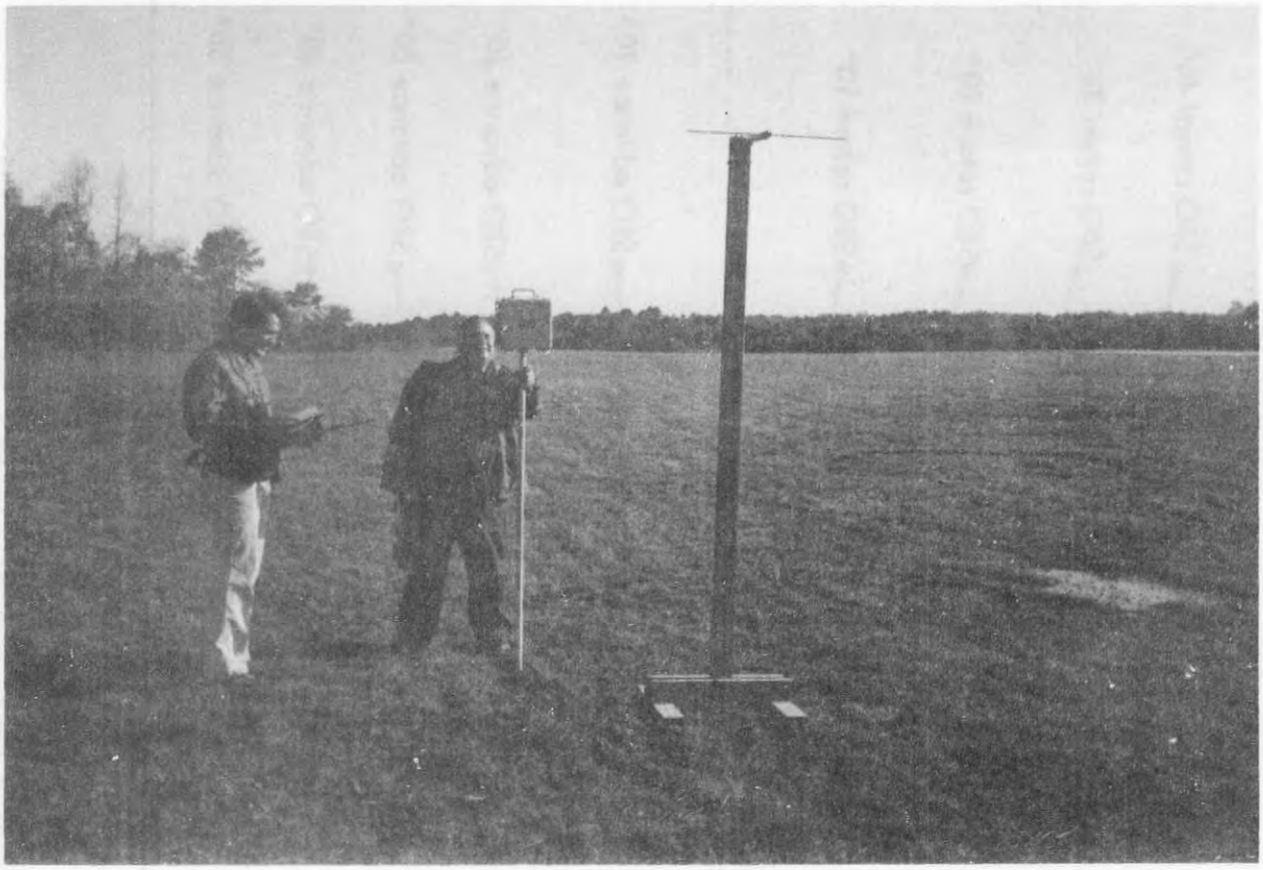

Figure 5-32. Photograph of wooden mast used in measurements.

*U.S. GOVERNMENT PRINTING OFFICE: 1986--491-810/20805